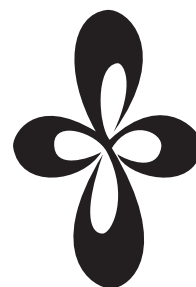


ANNUAL REVIEW

***INSTITUTE
FOR
MOLECULAR
SCIENCE***



2002

Published by

Institute for Molecular Science

Okazaki National Research Institutes

Myodaiji, Okazaki 444-8585, Japan

Phone: +81-564-55-7418 (Secretary Room)

Facsimile: +81-564-54-2254 (Secretary Room)

URL: <http://www.ims.ac.jp/>

Editorial Committee 2002

Chairperson

FUJII, Hiroshi

Vice-Chairperson

NAGATA, Toshi

SUZUKI, Yoko

FURUKAWA, Ko

NEGISHI, Yuichi

YAMADA, Ryo

HOSOKOSHI, Yuko

INOUE, Katsuya

HATSUI, Takaki

MATSUO, Tsukasa

TAIRA, Takunori

TANAKA, Shoji

TAKAHASHI, Kazutoshi

TAKAMI, Toshiya

NAGASONO, Hisayo

NAKAMURA, Rie

IMS 2002

First of all, I wish to announce that Emeritus Professor Hiro-o Inokuchi received the Order of Cultural Merits last year for his great contribution to the establishment of the new area of science, Molecular Electronics. Since the foundation of the Institute for Molecular Science in 1975, more than a quarter of century has passed. Professor Inokuchi who joined IMS from the first stage of IMS history has devoted to the development of novel electronic properties of organic molecular solids and many new materials which have interesting electronic and magnetic properties have been synthesized under the influence of Professor Inokuchi. The Research Center for Molecular-scale Nanoscience newly established from April, 2002 at IMS is positioned to be the center of the excellence of post-nanotechnology research on the basis of the remarkable scientific achievements of Inokuchi group.



In this annual review, recent development of researches at six departments and five research facilities are reported in addition to the report on the joint study programs of IMS 2001. This is my sincere wish as a director of IMS that the reader may enjoy reading this annual review into which great efforts and ideas of IMS research staff beautifully crystallize.

October, 2002

A handwritten signature in black ink, appearing to read 'Kaya Koji'. The signature is written in a cursive, flowing style.

KAYA, Koji
Director General, Institute for Molecular Science

CONTENT

IMS 2002	iii
CONTENT	v
ORGANIZATION AND STAFF	1
COUNCIL	13
BUILDINGS AND CAMPUS	15
RESEARCH ACTIVITIES I	17

Department of Theoretical Studies

I-A Theoretical Study and Design of New Bonding, Structures, and Reactions	17
I-A-1 A Silicon-Silicon Triple Bond Surrounded by Bulky Terphenyl Groups	17
I-A-2 The Quest of Stable Silanones: Substituent Effects	17
I-A-3 Substituent Effects on Germanium-Germanium and Tin-Tin Triple Bonds	17
I-A-4 Theoretical Study of an Isolable Compound with a Short Silicon-Silicon Triple Bond; (<i>t</i> Bu ₃ Si) ₂ MeSiSi≡SiSiMe(Si <i>t</i> Bu ₃) ₂	17
I-A-5 Interesting Compounds Featuring Double Bonding between Heavier Group 15 Elements	17
I-A-6 The First Halogen-Substituted Cyclotrigermenes: A Unique Halogen Walk over the Three-Membered Skeleton and Facial Stereoselectivity in the Diels-Alder Reaction	18
I-A-7 Effects of the σ* Orbital of C-Apical O-Equatorial Spirophosphoranes on the Structure, Stereomutation, and Reactivity	18
I-A-8 Theoretical Calculations of Vibrational Modes in Endohedral Metallofullerenes: La@C ₈₂ and Sc ₂ @C ₈₄	18
I-A-9 A Stable Unconventional Structure of Sc ₂ @C ₆₆ Found by Density Functional Calculations	18
I-A-10 Theoretical Study of the Cations and Anions of La ₂ @C ₈₀ and Sc ₃ N@C ₈₀	18
I-A-11 Theoretical Identification of the Structures of C ₂₀ : Prevalence of the Monocyclic Isomer and Existences of the Smallest Fullerene and Bowl Isomers	18
I-A-12 The Size of Silicon Clusters Suitable for Endohedral Metal-Doping	19
I-A-13 What is the Smallest Metal-Encapsulated Germanium Clusters?	19
I-A-14 Host-Guest Interaction in Molecular Capsule Formation	19
I-A-15 Does the Axial Ligand of Iron (IV)-Oxo-Porphyrin Affect the Reactivity of Cytochrome P450?	19
I-A-16 A Nonspectroscopic Method to Determine the Photolytic Decomposition Pathways of 3-Chloro-3-Alkyldiazirine; Carbene, Diazo and Rearrangement in Excited State	19
I-A-17 Prediction of Molecular Crystal Structures by an Ab Initio Pair Potential Method	19
I-B Prediction of Protein Tertiary Structures from the First Principles	21
I-B-1 Replica-Exchange Monte Carlo Simulation of a Small Peptide in Aqueous Solution Based on the RISM Theory	21
I-B-2 Comparison of AMBER, CHARMM, OPLS, and GROMOS Force Fields by Generalized-Ensemble Simulations	21
I-C Development of Simulation Algorithms for Complex Systems	21
I-C-1 An Application of the Multicanonical Monte Carlo Method to the Bulk Water System	21
I-D Applications of the Zhu-Nakamura Theory to Electronically Nonadiabatic Chemical Reactions	23
I-D-1 Significant Improvement of the Trajectory Surface Hopping Method by the Zhu-Nakamura Theory	23
I-D-2 New Implementation of the Trajectory Surface Hopping Method with Use of the Zhu-Nakamura Theory. II. Application to the Charge Transfer Processes in the 3D DH ₂ ⁺ System	23
I-D-3 Elucidations of Nonadiabatic Tunneling Type and Conical Intersection Type Reactions with Use of the Zhu-Nakamura Theory	23
I-E Theory of Nonadiabatic Transitions	23
I-E-1 Nonadiabatic Transition: Concepts, Basic Theories and Applications	23
I-E-2 Semiclassical Theory of Nonadiabatic Transition and Tunneling	24
I-E-3 Analytical Solutions to Wave Packet Dynamics in a Laser Field	24
I-F Quantum Dynamics of Chemical Reactions	24
I-F-1 Accurate Quantum Dynamics of Electronically Nonadiabatic Chemical Reaction in the DH ₂ ⁺ System	24

I-F-2	Chemical Reactions in the $O(^1D) + HCl$ System I. Ab Initio Global Potential Energy Surfaces for the $1^1A'$, $2^1A'$, and $1^1A''$ States	24
I-F-3	Chemical Reactions in the $O(^1D) + HCl$ System II. Dynamics on the Ground $1^1A'$ State and Contributions of the Excited ($1^1A''$ and $2^1A'$) States	25
I-F-4	Chemical Reactions in the $O(^1D) + HCl$ System III. Quantum Dynamics on the Excited ($1^1A''$ and $2^1A'$) Potential Energy Surfaces	25
I-F-5	Use of Diabatic Basis in the Adiabatic-by-Sector R-Matrix Propagation Method in Time-Independent Reactive Scattering Calculations	25
I-G	Laser Control of Molecular Processes	25
I-G-1	Control of Photodissociation Branching Using the Complete Reflection Phenomenon: Application to HI Molecule	25
I-G-2	Control of Molecular Processes by a Sequence of Linearly Chirped Pulses	25
I-G-3	Selective Excitation among Closely Lying Multi-Levels	26
I-G-4	Photodissociation of H_2^+ and HD^+ in an Intense Laser Field	26
I-H	Theory of Multi-Dimensional Tunneling	26
I-H-1	Practical Implementation of the Instanton Theory for the Ground-State Tunneling Splitting	26
I-H-2	Instanton Theory for Multi-Dimension Decay through Tunneling	26
I-I	New Methods for Scattering Calculations	27
I-I-1	Regularization of Scattering Calculations at R-Matrix Poles	27
I-I-2	Calculation of Resonances <i>via</i> the R-Matrix Method	27
I-J	Theoretical Studies of Dissociative Attachment and Dissociative Recombination	27
I-J-1	Study of Dissociative Electron Attachment to HI Molecule by Using R-Matrix Representation for Green's Function	27
I-J-2	Analytical Treatment of the K-Matrix Integral Equation in the Dynamics of Superexcited Molecules	27
I-K	Theoretical Studies of Ultrafast Nonlinear Optical Spectroscopy of Molecules in Condensed Phases	29
I-K-1	Probing a Colored-Noise Induced Peak of a Strongly Damped Brownian System by One- and Two-Dimensional Spectroscopy	29
I-K-2	Vibrational Spectroscopy of a Harmonic Oscillator System Nonlinearly Coupled to a Heat Bath	29
I-K-3	Two-Dimensional Raman and Infrared Vibrational Spectroscopy for a Harmonic Oscillator System Nonlinearly Coupled with a Colored Noise Bath	29
I-K-4	Two-Time Correlation Function of a Two-Dimensional Quantal Rotator in a Colored Noise	29
I-K-5	Energy-Level Diagrams and Their Contribution to Two-Dimensional Spectroscopic Signal: Distinction between Relaxation Mechanisms by Two-Dimensional Spectroscopy	30
I-K-6	Two-Dimensional Spectroscopy for a Two-Dimensional Rotator Coupled to a Gaussian-Markoffian Noise Bath	30
I-K-7	Absorption Spectra for Two-Dimensional Rotator with Nonlinear System-Bath Coupling	30
I-L	The Condensed Phase Quantum Dynamics of Molecules and Atoms	31
I-L-1	The Energy Landscape for Solvent Dynamics in Electron Transfer Reactions: A Minimalist Model	31
I-L-2	A Quantum Master Equation with a Langevin Force; a Realization of a Real-Time Quantum Monte-Carlo Simulation in a Dissipative Environment	31
I-M	Theoretical Studies of Correlated Electron Systems	31
I-M-1	Biorthogonal Approach for Explicitly Correlated Calculations Using the Transcorrelated Hamiltonian	31
I-M-2	Application of the Transcorrelated Hamiltonian to the Linearized Coupled Cluster Singles and Doubles Model	31
I-N	Electronic Properties of Nanostructured Materials	33
I-N-1	Carbon Foam: Spanning the Phase Space between Graphite and Diamond	33
I-N-2	Electronic Structure of Ba_4C_{60} and Cs_4C_{60}	33
I-N-3	Geometric and Electronic Structure of New Carbon-Network Materials: Nanotube Array on Graphite Sheet	33
I-N-4	First Principles Study of H_2 and CH_4 Physisorption on Carbon Nanotubes	33
I-O	Simulation and Dynamics of Chemical Systems	34
I-O-1	Quasi-Degenerate Perturbation Theory with General Multiconfiguration Self-Consistent Field Reference Functions	34
I-O-2	A Highly Efficient Algorithm for Electron Repulsion Integrals over Relativistic Four-Component Gaussian-Type Spinors	34
I-O-3	Accurate Relativistic Gaussian Basis Sets Determined by the Third-Order Douglas-Kroll Approximation with a Finite-Nucleus Model	34
I-O-4	A Density Functional Study of van der Waals Interactions	34

I-P Theoretical Studies of Quantum Effects in Chemical Reactions	35
I-P-1 Quantum Scattering Calculations of the $O(^1D) + N_2(X^1\Sigma_g^+) \rightarrow O(^3P) + N_2(X^1\Sigma_g^+)$ Spin-Forbidden Electronic Quenching Collision	35
I-P-2 Translational Energy Dependence of $NO + NO / N_2 + O_2$ Product Branching in the $O(^1D) + N_2O$ Reaction: a Classical Trajectory Study on a New Global Potential Energy Surface for the Lowest $^1A'$ State	35
I-P-3 A CASPT2 Study of the Doublet Potential Energy Surface for the $CH(X^2\Pi) + N_2(X^1\Sigma_g^+)$ Reaction	35
I-Q Electronic Structure of a Molecule in Solution	36
I-Q-1 Equilibrium and Nonequilibrium Solvation Structure of Hexaamineruthenium (II,III) in Aqueous Solution: Ab Initio RISM-SCF Study	36
I-R Solvation Thermodynamics of Protein and Related Molecules	36
I-R-1 Partial Molar Volumes and Compressibilities of Alkali-Halide Ions in Aqueous Solution: Hydration Shell Analysis with an Integral Equation Theory of Molecular Liquids	37
I-S Collective Density Fluctuations in Polar Liquids and Their Response to Ion Dynamics	37
I-S-1 Translational Diffusion and Reorientational Relaxation of Water Analyzed by Site-Site Generalized Langevin Theory	38
I-S-2 Interaction-Site Model Description of the Reorientational Relaxation of Molecular Liquids: Incorporation of the Interaxial Coupling into the Site-Site Generalized Langevin/Mode-Coupling Theory	38
I-S-3 Collective Density Fluctuations and Dynamics of Ions in Water Studied by the Interaction-Site Model of Liquids	38
I-T Developing Theories of Liquids and Liquid Mixtures	38
I-T-1 Buthanol-Water Mixture, Structure of <i>tert</i> -Butyl Alcohol-Water Mixtures Studied by the RISM Theory	39
I-T-2 Improvement of the Reference Interaction Site Model Theory for Calculating the Partial Molar Volume of Amino Acids and Polypeptides	39
I-T-3 Description of a Polar Molecular Liquid in a Disordered Microporous Material with Activating Chemical Groups by a Replica RISM Theory	39
I-T-4 Toward a Molecular Theory for the van der Waals-Maxwell Description of Fluid Phase Transitions	39
I-U Neutral-Ionic, Dimerization and Photoinduced Phase Transitions and Their Dynamics in Mixed-Stack Organic Charge-Transfer Complexes	41
I-U-1 Finite-Temperature Phase Diagram of Mixed-Stack Charge-Transfer Complexes	41
I-U-2 Lattice and Magnetic Instabilities near the Neutral-Ionic Phase Transition of the One-Dimensional Extended Hubbard Model with Alternating Potentials in the Thermodynamic Limit	41
I-U-3 Variation of Excitation Spectra in Mixed-Stack Charge-Transfer Complexes	41
I-U-4 Dynamic Spin Correlations near Neutral-Ionic Phase Transitions	42
I-U-5 Thermodynamics of Neutral-Ionic and Ferroelectric Phase Transitions in the Two-Chain System	42
I-U-6 Domain-Wall Dynamics after Photoexcitations near Neutral-Ionic Phase Transitions	42
I-U-7 Variation Mechanisms of Ground-State and Optical-Excitation Properties in Quasi-One-Dimensional Two-Band Electron Systems	42
I-U-8 Photoinduced Dynamics of Ionicity near the Neutral-Ionic Phase Boundary in a One-Dimensional Extended Peierls-Hubbard Model	42
I-V Self-Doping, Nonlinear Excitations and Photoinduced Transitions between Charge and Lattice Ordered Phases of Metal Complexes	43
I-V-1 Self-Doping Effect on the Mott Transition Accompanied with Three-Fold Charge Ordering in $(DCNQI)_2Cu$	43
I-V-2 Spin Solitons in the Alternate Charge Polarization Background of MMX Chains	43
I-V-3 Photoexcited States and Photoinduced Dynamics in Electronic Phases of MMX-Chain Systems	43
I-V-4 Electromodulation Spectra of Optical Absorption in One-Dimensional Strongly Correlated Systems	43
I-W Dimensional Crossovers in Electronic Phases and Their Excitation Spectra of Quasi-One-Dimensional Organic Conductors	44
I-W-1 Dimensional Crossovers and Phase Transitions in Strongly Correlated Low-Dimensional Electron Systems: Renormalization-Group Study	44
I-W-2 Correlation-Induced Dimensional Crossovers of Charge-Transfer Excitations in Quasi-One-Dimensional Organic Conductors	44

I-X Underlying Gauge Structure and Competing Orders in Underdoped Cuprate Superconductors	44
I-X-1 Signature of the Staggered Flux State around a Superconducting Vortex in Underdoped Cuprates	45
I-X-2 Underlying SU(2) Gauge Structure and Hidden Staggered Flux State in the Lightly Doped Spin Liquid	45
I-X-3 Coexistence of Staggered Flux and Antiferromagnetic States in Superconducting Vortices in the Lightly Doped Mott Insulator	45
RESEARCH ACTIVITIES II	47

Department of Molecular Structure

II-A Development of Near-Field Dynamic Spectroscopy and Application to Mesophase Systems	47
II-A-1 Development of an Ultrafast Near-Field Spectroscopy and Observation of Dynamic Processes in GaAs Crystal	47
II-A-2 Near-Field Autocorrelation Measurements of Femtosecond Light Pulses at a Tip of a 100-nm Apertured Probe by Two-Photon-Induced Photoconductivity	48
II-A-3 Structure and Photophysics of PIC J-Aggregates Studied by Scanning Near-Field Optical Microscopy	48
II-B Laser Cooling and Trapping of Metastable Helium Atoms	50
II-B-1 New Design for Efficient Magneto-Optical Trapping of Metastable Helium Atoms	50
II-C Spectroscopic Studies on Atoms and Ions in Liquid Helium	50
II-C-1 Laser Spectroscopy of Eu Atoms in Liquid ³ He and ⁴ He	50
II-D Electron Transfer Regulation in Tetraheme Cytochromes <i>c</i>	52
II-D-1 Redox-Coupled Conformational Alternations in Cytochrome <i>c</i> ₃ from <i>D. vulgaris</i> Miyazaki F on the Basis of its Reduced Solution Structure	52
II-D-2 A Role of the Aromatic Ring of Tyr43 in Tetraheme Cytochrome <i>c</i> ₃ from <i>Desulfovibrio vulgaris</i> Miyazaki F	52
II-D-3 A Directional Redox-Regulator Based on the Heme-Chain Architecture in the Small Tetraheme Cytochrome <i>c</i> from <i>Shewanella oneidensis</i>	52
II-E Studies on Higher-Order Gaussian Light Beams	54
II-E-1 Simple Generation of Higher-Order Gaussian Beams and the Application to Spectroscopy	54
II-F Ultrafast Dynamics of Surface Adsorbed Species	55
II-F-1 Time-Resolved Study of Formate on Ni(111) by Picosecond SFG Spectroscopy	55
II-F-2 SFG Spectroscopy of CO/Ni(111): UV Pumping and Transient Hot Band Transition of Adsorbed CO	55
II-F-3 Surface Hydroxyl Group and Adsorbed Water on γ -Al ₂ O ₃ Studied by Picosecond Infrared Pump-Probe Experiment	55
II-G Spin Reorientation Transitions of Ultrathin Magnetic Films Induced by Chemisorption	56
II-G-1 Perpendicular Magnetic Anisotropy in Co/Pd(111) Stabilized by Chemisorption of CO and NO	56
II-H Local Structures in Photoinduced States of Molecular-Based Magnetic Materials	57
II-H-1 Photoinduced Phase Transition of RbMnFe(CN) ₆ Studied by X-Ray-Absorption Fine Structure Spectroscopy	57
II-I Molecular and Electronic Structures of Metallofullerenes	58
II-I-1 Spin Dynamics of Lanthanum Metallofullerenes	58
II-I-2 Electronic State of Scandium Trimer Encapsulated in C ₈₂ Cage	58
II-I-3 Efficient Reduction of Metallofullerenes by Solvation of Pyridine and Dimethylformamide	59
II-J High Field and Pulsed Electron Spin Resonance Spectroscopy	59
II-J-1 High-Field/High-Frequency ESR Study of Gadolinium Metallofullerenes	59
II-J-2 A Bindschedler's Green-Based Arylamine: Its Polycations with High-Spin Multiplicity	60
II-K State Correlated Raman Spectroscopy	61
II-K-1 Molecular Ordering Deformation Induced by Externally Applied Electric Field in an Antiferroelectric Liquid Crystal	61

RESEARCH ACTIVITIES III	63
--------------------------------------	-----------

Department of Electronic Structure

III-A Synthesis and Characterization of Exotic Molecule-Based Nano-Clusters with Transition Metals : Behavior as Single Domain Magnets	63
III-A-1 Magnetic Behavior of Crude CoC ₂ Solid Synthesized in Acetonitrile Solution	63
III-A-2 Electron Microscope and EXAFS Study of Matrix Embedded (Co-C ₂) _n Nano-Cluster Magnets	63

III-A-3	Magnetic Behavior of Matrix Embedded (Co-C ₂) _n Nano-Clusters as Single Domain Room-Temperature Magnets	64
III-A-4	Construction of Vacuum Apparatus for Mass-Resolved Spectroscopies of Non-Volatile Solid Samples	64
III-B	States of Neutral and Ionic Molecular Associates in Solutions	65
III-B-1	States of Molecular Associates in Binary Mixtures of Acetic Acid with Protic and Aprotic Polar Solvents: A Raman Spectroscopic Study	65
III-C	Ultrafast Dynamics and Scanning Tunneling Microscopy	66
III-C-1	Construction of an Apparatus for Direct Observation of Reactions Induced by Ultrafast Laser Pulses Using a Low Temperature STM	66
III-C-2	Construction of a Femtosecond Time-Resolved Ionization Detected Spectrometer	66
III-C-3	Picosecond Time-Resolved Raman Studies on the Photochromic Reactions of Diarylethenes	67
III-D	Spectroscopic and Dynamical Studies of Molecular Cluster Ions	67
III-D-1	Intermolecular Interactions in Aniline/Benzene Hetero-Trimer and Aniline Homo-Trimer Ions	68
III-D-2	Infrared Photodissociation Spectroscopy of Protonated Formic Acid-Water Binary Clusters, H ⁺ ·(HCOOH) _n ·H ₂ O (<i>n</i> = 1–5). Spectroscopic Study of Ion Core Switch Model and Magic Number	68
III-D-3	Infrared Photodissociation Spectroscopy of Aniline ⁺ -(Water) _{1,2} and Aniline ⁺ -(Methanol) _{1,2}	68
III-D-4	Intracluster Proton Transfer in Aniline-Amine Complex Ions	68
III-D-5	LIF and IR Dip Spectra of Jet-Cooled <i>p</i> -Aminophenol- <i>M</i> (<i>M</i> = CO, N ₂): Hydrogen-Bonded or van der Waals-Bonded Structure?	68
III-D-6	Structure and Intermolecular Hydrogen Bond of Jet-Cooled <i>p</i> -Aminophenol-(H ₂ O) ₁ Studied by Electronic and IR-Dip Spectroscopy and Density Functional Theory Calculations	69
III-D-7	Positive Charge Distribution in (Benzene) ₁ (toluene) ₂ ⁺ and (Benzene) ₂ (toluene) ₁ ⁺ Studied by Photodissociation Spectroscopy	69
III-D-8	Infrared Photodissociation Spectroscopy of [Aniline-(Water) _n] ⁺ (<i>n</i> = 1–8)	69
III-E	Spectroscopy and Dynamics of Vibrationally Excited Molecules and Clusters	70
III-E-1	Hydrogen Transfer in Photo-Excited Phenol/Ammonia Clusters by UV-IR-UV Ion Dip Spectroscopy and Ab Initio MO Calculations I: Electronic Transitions	72
III-E-2	Hydrogen Transfer in Photo-Excited Phenol/Ammonia Clusters by UV-IR-UV Ion Dip Spectroscopy and Ab Initio MO Calculations II: Vibrational Transitions	72
III-E-3	Picosecond Time-Resolved Infrared Spectra of Photo-Excited Phenol-(NH ₃) ₃ Cluster	72
III-E-4	Picosecond Time-Resolved Nonresonant Ionization Detected IR Spectroscopy on 7-Azaindole Dimer	73
III-E-5	Structure of Hydrogen-Bonded Clusters of 7-Azaindole Studied by IR Dip Spectroscopy and Ab Initio Molecular Orbital Calculation	73
III-E-6	Structures of Carbazole-(H ₂ O) _n (<i>n</i> = 1–3) Clusters Studied by IR Dip Spectroscopy and a Quantum Chemical Calculation	73
III-E-7	Structure of 1-Naphthol/Alcohol Clusters Studied by IR Dip Spectroscopy and Ab Initio Molecular Orbital Calculations	73
III-E-8	Pulsed Field Ionization Zero Kinetic Energy Photoelectron Study on Methylanisole Molecules in a Supersonic Jet	73
III-E-9	The PFI-ZEKE Photoelectron Spectrum of <i>m</i> -Fluorophenol and its Aqueous Complexes: Comparing Intermolecular Vibrations in Rotational Isomers	74
III-E-10	OH- and CH-Stretching Overtone Spectra of Catechol	74
III-F	Ultrafast Molecular Dynamics Studied by Time-Resolved Photoelectron Imaging	75
III-F-1	Ionization Dynamics of NO A (2Σ ⁺) State Studied by Time-Resolved Photoelectron Imaging	75
III-F-2	Theoretical Analysis of Rotational Revivals in Intersystem Crossing in Pyrazine	75
III-F-3	Femtosecond Photoelectron Imaging on Pyridazine: S ₁ Decay Rate and 3s and 3p Rydberg State Energetics	76
III-G	Non-Adiabatic Photodissociation Dynamics of Fundamental Molecules	76
III-G-1	Non-Adiabatic Bending Dissociation of OCS: The Effect of Bending Excitation on the Transition Probability	76
III-G-2	Velocity Map Fragment Imaging on 205 nm Photodissociation of Nitrous Oxide	77
III-H	Development of New Devices for Molecular Dynamics Experiments	77
III-H-1	Three Dimensional Photofragment Imaging Using a Fast Response Imager	77
III-H-2	High Repetition Rate Two Dimensional Imaging Using C-MOS Imager	77
III-H-3	Construction of a Rotating-Source Crossed Beam Apparatus	77

III-I Structure and Properties of Polyoxometalates with a Magnetic, Electronic, or Biological Significance	78
III-I-1 Synthesis and Crystal Structure of a Novel Vanadium-Containing Tungstobismutate(III) $K_{12}[(VO)_3(BiW_9O_{33})_2] \cdot 30H_2O$	78
III-I-2 Crystallization and Structural Characterization of Two Europium Molybdates, $Eu_4Mo_7O_{27}$ and $Eu_6Mo_{10}O_{39}$	78
III-I-3 Nanocluster Crystals of Lacunary Polyoxometalates as Structure-Design-Flexible, Inorganic Nonlinear Materials	78
III-I-4 A Three-Dimensional Inorganic/Organic Hybrid Vanadium Oxide Complex with Pentacoordinate Co^{II} , $[CoV_2O_6(4,4'-bipy)]$	78
III-I-5 $Tb_2Mo_4O_{15}$	79
III-I-6 H_2O_2 -Based Epoxidation of Bridged Cyclic Alkenes with $[P\{Ti(O_2)\}_2W_{10}O_{38}]^{7-}$ in Monophasic Systems: Active Site and Kinetics	79
III-I-7 Photochemical Formation of a Lacunary Tire-Shaped Anion, $[Mo_{142}O_{432}H_{26}(H_2O)_{58}]^{14-}$, through Degradative Self-Assembly of $[Mo_{36}O_{112}(H_2O)_{16}]^{8-}$: Topology of Ring-Structural Molybdenum Blues	79
III-I-8 Size-Dependent Population of Trivalent Rare Earth Cations (RE^{3+}) in $[(RE)_2(H_2O)_2(SbW_9O_{33})(W_5O_{18})_2]^{15-}$, and Structural Characterization of a Lutetium-Polyoxotungstate Complex $[Lu_3(H_2O)_4(SbW_9O_{33})_2(W_5O_{18})_2]^{21-}$	79
III-I-9 $Gd_4Mo_7O_{27}$, a Novel Phase in the Gd_2O_3 - MoO_3 System	79
III-I-10 Time-Resolved ESR-Spectroscopic Investigation of Polyoxometalate Photochemistry	79
III-J Electronic Spectroscopy and Excited-State Dynamics of Aromatics Clusters	81
III-J-1 S_1 - S_0 Vibronic Spectrum of the Benzene Tetramer	81
III-J-2 S_1 - S_0 Vibronic Spectrum of the Benzene Trimer	81
III-K Electronic Spectroscopy of Molecules in Pendular States	81
III-K-1 Construction of an Apparatus for Measurements of Fluorescence Excitation Spectra in a Strong DC Electric Field	82
III-K-2 Laser-Induced Fluorescence Spectra of Pendular-State Aromatics in a Strong DC Electric Field	82
III-L Wave Packet Engineering Using a Phase-Programmable Femtosecond Optical Source	83
III-L-1 Single Molecular Phase-to-Amplitude Converter	83

RESEARCH ACTIVITIES IV -----85

Department of Molecular Assemblies

IV-A Spectroscopic Study of Charge Carriers in Organic Conductors	85
IV-A-1 Raman Study of the Charge Ordering in α -(BEDT-TTF) $_2I_3$ at High Pressure	85
IV-A-2 Raman Study of the Charge Ordering in α' -(BEDT-TTF) $_2IBr_2$ at High Pressure	86
IV-A-3 Charge Ordering in θ -(BEDT-TTF) $_2TIM(SCN)_4$ ($M = Co$ and Zn) Studied by Vibrational Spectroscopy	86
IV-A-4 High-Pressure Raman Study on a 1/3-Filled System (BEDT-TTF) $_3CuBr_4$	87
IV-A-5 Infrared and Raman Studies of the Charge Ordering in the Organic Semiconductor κ - $[(Et)_4N](ET)_4Co(CN)_6 \cdot 3H_2O$	87
IV-A-6 Charge-Ordering and Magnetic Phase Transitions in θ -(BDT-TTP) $_2Cu(NCS)_2$	87
IV-A-7 Spectroscopic Studies of Charge-Ordering System in Organic Conductors	88
IV-A-8 Charge and Molecular Arrangement in (DI-DCNQI) $_2Ag$ Studied by Vibrational Spectra	88
IV-A-9 Charge Distribution and Molecular Arrangement in the Pressure-Induced Metallic Phase of (DI-DCNQI) $_2Ag$	89
IV-A-10 Study of the Phase Transitions of (DI-DCNQI) $_2M$ ($M = Ag, Li, Cu$) through the Analysis of the Temperature Dependent Vibronic and Vibrational Infrared Absorptions	89
IV-A-11 Development of a High-Pressure Cell for Raman Measurement Using Sapphire Anvil	90
IV-A-12 Optical Study of Two-Dimensional Organic Metal (EO-TTP) $_2AsF_6$ (EO-TTP=2-(4,5-ethylenedioxy-1,3-dithiol-2-ylidene)-5-(1,3-dithiol-2-ylidene)-1,3,4,6-tetrathiapentalene)	90
IV-B Microscopic Investigation of Molecular-Based Conductors	91
IV-B-1 EPR Investigation of the Electronic States in β' -type $[Pd(dmit)_2]_2$ Compounds (where dmit is the 1,3-dithia-2-thione-4,5-dithiolato)	91
IV-B-2 NMR Study of Charge Localized States of (TMTTF) $_2Br$	91
IV-B-3 Magnetic Investigation of Possible Quasi-One-Dimensional Two-Leg Ladder Systems, (BDTFP) $_2X(PhCl)_{0.5}$ ($X = PF_6, AsF_6$)	92
IV-B-4 Microscopic Investigation of a New Two-Component Organic Conductor with Itinerant and Localized Spins: (CHTM-TTP) $_2TCNQ$	92
IV-B-5 ESR Study of the Charge Ordering States in (TMTTF) $_2X$	93

IV-C Magnetic Organic Superconductors and Related Systems	94
IV-C-1 An Indication of Magnetic-Field-Induced Superconductivity in a Bi-Functional Layered Organic Conductor, κ -(BETS) ₂ FeBr ₄	94
IV-C-2 Dual-Action Molecular Superconductors with Magnetic Anions	94
IV-C-3 A Series of Organic Conductors κ -(BETS) ₂ FeBr _x Cl _{4-x} (0 ≤ x ≤ 4) Exhibiting Successive Antiferromagnetic and Superconducting Transitions	95
IV-C-4 Magnetic Molecular Conductors Based on BETS Molecules and Divalent Magnetic Anions [BETS = Bis(ethylenedithio)tetraselenafulvalene]	95
IV-C-5 Crystal Structure of BETS ²⁺ Dication Salt (BETS)TlCl ₅ and Formal Charge Dependence of Bond Lengths of BETS ^{+Q} (Q = 0–2)	96
IV-C-6 Charge-Transfer Salt of [C ₁₂ H ₈ S ₄ Se ₄ Cl ₂]FeCl ₄ ·C ₆ H ₅ Cl	96
IV-C-7 A New Charge-Transfer Salt of (BETS) ₄ Fe ₂ (C ₂ O ₄) ₅	97
IV-D Development of New Conducting Molecular Materials	97
IV-D-1 Development of Conducting Crystals Based on Single-Component Transition Metal Complex Molecules with Extended-TTF Ligands	97
IV-D-2 A Conducting Crystal Based on a Single-Component Paramagnetic Molecule [Cu(dmdt) ₂] (dmdt = dimethyltetrathiafulvalenedithiolate)	98
IV-D-3 Novel π -Electron Donors for Magnetic Conductors Containing a PROXYL Radical	98
IV-D-4 Novel TTP Donors Containing a PROXYL Radical for Magnetic Molecular Conductors	99
IV-D-5 Synthesis and Physical Properties of New Molecular Conductors Based on Lanthanoid Nitrate Complex Anions	99
IV-E Control of Intermolecular Interactions with Chemical and Physical Methods	100
IV-E-1 Unique Structural and Physical Properties of Ni(dmit) ₂ Anion Radical Salts Characterized by Short Te...S Contacts, where dmit = 1,3-dithiole-2-thione-4,5-dithiolate	100
IV-E-2 Uniaxial Strain Effect in the Two-Dimensional Strongly Correlated System, β^{\prime} -(CH ₃) ₄ As[Pd(dmit) ₂] ₂ (dmit = 1,3-dithiol-2-thione-4,5-dithiolate)	100
IV-F Synthetic Approach Toward Single Molecular Transistors	102
IV-F-1 Synthesis of Novel Ruthenium Complexes Optimized for Molecular Single Electron Transistor	102
IV-F-2 Preparation of Porphyrin Wires Optimized for Molecular Field Effect Transistors	102
IV-F-3 Synthesis of Octopus Shaped Self Standing Molecular Jacks	102

RESEARCH ACTIVITIES V -----103

Department of Applied Molecular Science

V-A Synthesis of Chiral Molecule-Based Magnets	103
V-A-1 Structure and Magnetic Properties of a Chiral Two-dimensional Ferrimagnet with T_C of 38 K	103
V-B Hydrothermal Synthesis of Molecule-Based Magnets	104
V-B-1 Self-Organized Metallo-Helicates and –Ladder with 2,2'-Biphenyldicarboxylate (C ₁₄ H ₈ O ₄) ²⁻ : Synthesis, Crystal Structures, and Magnetic Properties	104
V-C Synthesis and Characterization of Quantum-Spin Systems	104
V-C-1 Magnetic Properties of Organic Two-Leg Spin Ladder Systems with $S = 1/2$ and $S = 1$	104
V-C-2 Low Dimensionality Observed by ESR Measurements in $S = 1$ Spin Ladder Substance BIP-TENO	105
V-D Organic Ferrimagnetism	105
V-D-1 Magnetic Properties on an Organic Ferrimagnetic Compound and Related Materials	105
V-E Pressure Effects on Molecular Magnetism	106
V-E-1 Pressure Effects on Molecular Magnets of Mn Complexes with Bisaminoxylbenzene Derivatives	106
V-E-2 Pressure-Induced Metamagnetic Behavior in a Quasi-One-Dimensional Molecule-Based Ferrimagnet	106
V-F Bioinorganic Studies on Structures and Functions of Non-Heme Metalloenzymes Using Model Complexes	107
V-F-1 Novel Phosphate Bond Formation in a Cobalt(III) Complex System	107
V-F-2 Syntheses and Structures of Tetrakis(1-methyluracilato)palladium Complexes Capturing Alkali Metal Ions. A New Type of Metallo-Podand	107
V-F-3 Investigations of the Effects of Intramolecular Hydrogen Bonding Networks on Tripodal Trihydroxamate-Type Artificial Siderophores	107
V-F-4 The Role of the Zn(II) Site in Cu,Zn SOD (1). Synthesis and Characterization of Novel Hydroperoxo-Zinc(II) Intermediates	108
V-F-5 Epoxidation Activities of Mononuclear Ruthenium-oxo Complexes with a Square Planar 6,6'-Bis(benzoylamino)-2,2'-bipyridine and Axial Ligands	108
V-F-6 Reactivity of Hydroperoxide Bound to a Mononuclear Non-Heme Iron Site	108

V-F-7	Reactivity Control for Epoxidation of Olefins and Dehydrogenation of Alcohols Catalyzed by Ruthenium-oxo Complexes	108
V-F-8	Crystal Structure and Solution Behavior of the Iron(III) Complex of the Artificial Trihydroxamate Siderophore with Tris(3-aminopropyl)amine Backbone	109
V-F-9	Reverse Reactivity in Hydroxylation of Adamantane and Epoxidation of Cyclohexene Catalyzed by the Mononuclear Ruthenium-oxo Complexes with 6-Substituted Tripodal Polypyridine Ligands	109
V-F-10	Characterization of an NH- π Interaction in Co(III) Ternary Complexes with Aromatic Amino Acids	109
V-F-11	The Role of the Zn(II) Site in Cu,Zn SOD. (2) Evidence of Superoxide Disproportionation Catalyzed by Sterically- and Electrostatically-Controlled Zinc(II) Complexes	110
V-F-12	SOD Activities of the Copper Complexes with Tripodal Polypyridylamine Ligands Having a Hydrogen Bonding Site	110
V-F-13	Site-Selective Recognition of Amino Acids by Co(III) Complexes Containing a (N)(O) ₃ -Type Tripodal Tetradentate Ligand	110
V-G	Probing Time-Dependent Processes in Solution with Time-Resolved Spectroscopic Methods	111
V-G-1	Femtosecond Time-Resolved Anisotropy Measurement of Biphenyl Fluorescence	111
V-G-2	Effect of Pump and Probe Light Field on Picosecond Time-Resolved Resonance Raman Spectra of <i>S</i> ₁ <i>trans</i> -Stilbene. Disagreement between Stokes- and Anti-Stokes Scattering Frequencies	111
V-G-3	Photoinduced Cl Transfer Reaction between Biphenyl and Carbon Tetrachloride Studied by Nanosecond Time-Resolved Infrared Spectroscopy and Picosecond Time-Resolved Fluorescence Spectroscopy	112
V-G-4	Analysis of the Solvent- and Temperature-Dependent Raman Spectral Changes of <i>S</i> ₁ <i>trans</i> -Stilbene and the Mechanism of the <i>Trans</i> to <i>Cis</i> Isomerization: Dynamic Polarization Model of Vibrational Dephasing and the C=C Double-Bond Rotation	112
V-G-5	Picosecond Dynamics of Stepwise Double Proton-Transfer Reaction in the Excited State of the 2-Aminopyridine/Acetic Acid System	113
V-H	Structures and Properties of Lanthanoid-Metallofullerenes	114
V-H-1	Spectroscopic Studies of Endohedral Metallofullerenes	114
V-H-2	Structural Study of Three Isomers of Tm@C ₈₂ by ¹³ C NMR Spectroscopy	114
V-I	Development of Organic Superconductors	114
V-I-1	New Organic Superconductors Consisting of an Unprecedented π -Electron Donor	114
V-I-2	Tetrachloroferrate (III) Salts of BDH-TTP and BDA-TTP: Crystal Structures and Physical Properties	115
V-J	Stereodynamics of Crossed Beam Reactions	116
V-J-1	Stereo-Selectivity in the Penning Ionization Reaction of CH ₃ X (X = Cl, Br, I) + Ar(³ P) \rightarrow CH ₃ X ⁺ + Ar + e ⁻	116
V-J-2	Evidence for the HCl ⁺ (A) Formation in the Reaction of Ne(³ P) with the Size-Selected HCl Dimer Using an Electrostatic Hexapole Field	116
V-K	Photodissociation Dynamics	116
V-K-1	Photodissociation of DCI Dimer Selected by an Electrostatic Hexapole Field Combined with Doppler-Selected TOF Technique: Observation of [CIDCI] Transient Species	117
V-K-2	A New Channel of Hydrogen Elimination in the 121.6-nm Photodissociation of Formic Acid Detected by a Doppler-Selected TOF Mass Spectrometry	117
V-L	Non-Destructive Structure Determination of Neural Clusters	117
V-L-1	Focusing and Selecting the Linear Type HBr-N ₂ O by Using a 2 m Long Electrostatic Hexapole Field	117
V-M	Reaction Dynamics at Surfaces	118
V-M-1	Hydrogen-Exchange Reactions <i>via</i> Hot Hydrogen Atoms Produced in the Dissociation Process of Molecular Hydrogen on Ir{100}	118
V-N	Simulation of Molecular Clusters	119
V-N-1	Characterization of Gel Using Modeled Radical Polymerization with Cross Linkers Performed by Monte Carlo Method	119
V-N-2	Analysis of Intra- and Inter-Linkers in Gels by Brownian Dynamics Simulation	119
V-N-3	Self-Assembly of Amphiphiles into Vesicles: a Brownian Dynamics Simulation	119
V-N-4	Fusion Pathways of Vesicles, a Brownian Dynamics Simulation	119
V-N-5	Adhesion of Nanoparticles to Vesicles: a Brownian Dynamics Simulation	119
V-N-6	Structural Changes of Pulled Vesicles: a Brownian Dynamics Simulation	119
V-O	Development of Broadband Solid-State NMR Spectroscopy	121
V-O-1	Numerical Simulations and Experiments on the Transmission Line Probe	121
V-O-2	Developments of Fast Digital RF Frequency Modulator	122

RESEARCH ACTIVITIES VI -----123**Department of Vacuum UV PhotoScience**

VI-A Electronic Structure and Decay Mechanism of Inner-Shell Excited Molecules -----	123
VI-A-1 Spin-Forbidden Shake-Up States in the Valence Ionization of CS ₂ -----	123
VI-A-2 Spin- and Symmetry Forbidden Ionized States of OCS Molecule -----	123
VI-A-3 Measurements of Sulfur 2 <i>p</i> Photoelectron and Sulfur L-emission of SF ₆ at Sulfur 2 <i>p</i> Resonances -----	124
VI-A-4 N 1 <i>s</i> Photoabsorption of N ₂ Trapped in Rare Gas Matrices -----	124
VI-A-5 Ab Initio CI Calculation for O1 <i>s</i> → σ* Core-Excited States of Ozone: Difference in Direction between Transition Dipole Moment and Photodissociation -----	125
VI-B Soft X-Ray Photoelectron-Photoabsorption Spectroscopy and Electronic Structure of Transition Metal Compounds -----	126
VI-B-1 B 1 <i>s</i> - and La 4 <i>d</i> -Edge Photoabsorption and Resonant Photoelectron Spectroscopy of Rare-Earth Borocarbide LaB ₂ C ₂ -----	126
VI-C Observation of Vibrational Coherence (Wavepacket Motion) in Solution-Phase Molecules Using Ultrashort Pulses -----	127
VI-C-1 Excited-State Vibrational Coherence of Solution-Phase Molecules Observed in the Third-Order Optical Process Using Extremely Short Pulses -----	127
VI-D Studies of Primary Photochemical/Physical Processes Using Femtosecond Electronic Spectroscopy -----	127
VI-D-1 Femtosecond/Picosecond Time-Resolved Spectroscopy of Trans-Azobenzene: Isomerization Mechanism Following S ₂ (ππ*) ← S ₀ Photoexcitation -----	128
VI-D-2 Ultrafast Fluorescence of the Chromophore of the Green Fluorescent Protein in Alcohol Solutions -----	128
VI-D-3 Femtosecond Study of Solvation Dynamics of DCM in Micelles -----	128
VI-E Studies of Photochemical Reactions Using Picosecond Time-Resolved Vibrational Spectroscopy -----	129
VI-E-1 Picosecond Time-Resolved Raman Study of the Solvated Electron in Water -----	129
VI-E-2 Observation of Resonance Hyper-Raman Scattering from all-trans-Retinal -----	129
VI-F Synchrotron Radiation Stimulated Surface Reaction and Nanoscience -----	131
VI-F-1 Patterning SiO ₂ Thin Films Using Synchrotron Radiation Stimulated Etching with a Co Contact Mask -----	131
VI-G Noble Semiconductor Surface Vibration Spectroscopy -----	131
VI-G-1 Infrared Reflection Absorption Spectroscopy Using CoSi ₂ Buried Metal Layer Substrate Made by Wafer-Bonding -----	132
VI-G-2 Hydrogen Diffusion and Chemical Reactivity with Water on Nearly Ideally H-Terminated Si(100) Surface -----	132
VI-G-3 Atomic Hydrogen-Induced Oxidation on Water-Adsorbed Si(100)-(2×1) Surfaces -----	132
VI-H Integration of Bio-Functional Materials on Silicon -----	133
VI-H-1 Hydrophobic/Hydrophilic Interactions of Cytochrome <i>c</i> with Functionalized Self-Assembled Monolayers on Silicon -----	133
VI-H-2 Influence of Substrate Roughness on the Formation of Self-Assembled Monolayers (SAM) on Silicon(100) -----	134
VI-I Photoionization and Photodissociation Dynamics Studied by Electron and Fluorescence Spectroscopy -----	135
VI-I-1 Formation and Autoionization of a Dipole-Forbidden Superexcited State of CS ₂ -----	135
VI-I-2 Autoionization and Neutral Dissociation of Superexcited HI Studied by Two-Dimensional Photoelectron Spectroscopy -----	135
VI-I-3 Development of the Apparatus for High-Resolution Dispersed Spectroscopy and Fluorescence Excitation Spectroscopy at BL3A2 -----	135
VI-I-4 UV and Visible Dispersed Spectroscopy for the Photofragments Produced from H ₂ O in the Extreme Ultraviolet -----	136
VI-J Vacuum UV Spectroscopy Making Use of a Combination of Synchrotron Radiation and a Mode-Locked or Pulsed UV Laser -----	137
VI-J-1 Partial Photoionization Cross Sections for N ₂ ⁺ (X ² Σ _g ⁺ , <i>v</i> _X = 0, 1) Measured by a Laser Synchrotron Radiation Combination Technique -----	137
VI-K Extreme UV Photoionization Studies by Employing a Dragon-Type Grazing-Incidence Monochromator -----	138
VI-K-1 Anisotropy of Fragment Ions from SF ₆ by Photoexcitation of a Valence- or Sulfur 2 <i>p</i> - Electron between 23 and 210 eV -----	138
VI-K-2 Construction of the Photoionization Spectrometer for Fullerenes and Metallofullerenes --	139
VI-K-3 Photoion Yield Spectra of C ₆₀ in the Region of 23–210 eV -----	139

RESEARCH ACTIVITIES VII -----141

Coordination Chemistry Laboratories

VII-A Development of Novel Transition Metal Complex Catalysts Having MOP Ligands -----	141
VII-A-1 Asymmetric Hydrosilylation of Styrenes Catalyzed by Palladium-MOP Complexes: Ligand Modification and Mechanistic Studies -----	141
VII-A-2 Modification of Chiral Monodentate Phosphine Ligands (MOP) for Palladium-Catalyzed Asymmetric Hydrosilylation of Cyclic 1,3-Dienes -----	141
VII-A-3 (<i>R</i>)-2-Diphenylphosphino-2'-methoxy-1,1'-binaphthyl -----	141
VII-B Green and Risk-Free Catalysis -----	142
VII-B-1 Amphiphilic Resin-Supported Rhodium-Phosphine Catalysts for C-C Bond Forming Reactions in Water -----	142
VII-B-2 Double Carbonylation of Aryl Iodides with Primary Amines under Atmospheric Pressure Conditions Using Pd/PPh ₃ /DABCO/THF System -----	142
VII-C Electrochemical Analysis of Biological Functions of Metalloproteins and their Mutated Molecules and its Applications to Coordination Chemistry for Catalysis -----	143
VII-C-1 Effects of Alkyl Chain as a Spacer on Electrochemical Reaction and SEIRA Spectra for Self-Assembled Monolayer Having Anthraquinone Redox Center -----	143
VII-C-2 Analysis of Biological Functions of Metalloproteins Using Biocompatible Modified Electrodes -----	143
VII-C-3 Interfacial Structures of Self-Assembled Monolayers of 2-Pyridinethiol on Au(111) Studied by In Situ Tunneling Microscopy -----	143
VII-C-4 NADP ⁺ Sensor on <i>Chrorella</i> Ferredoxin/Ferredoxin-NADP ⁺ -Reductase Modified Indium Oxides -----	143
VII-C-5 Surface pK _a of Amine-Terminated Self-Assembled Monolayers Evaluated by Direct Observation of Counter Anion by FT-Surface Enhanced Raman Spectroscopy -----	144
VII-C-6 Ion Selectivity for Electrode Reactions on Functionalized Monolayer Modified Electrode -----	144
VII-C-7 In-Situ STM Observation of Coronene Epitaxial Adlayers on Au(111) Surfaces Prepared by the Transfer of Langmuir Films -----	144
VII-C-8 New Route to Protoporphyrins III and XIII from Common Starting Pyrroles -----	144
VII-D Nano-Sciences of Advanced Metal Complexes -----	145
VII-D-1 Tuning of Electronic Structures of Quasi-One-Dimensional Bromo-Bridged Ni(III) Complexes with Strong Electron-Correlation by Doping of Co(III) Ions, [Ni _{1-x} Co _x (chxn) ₂ Br]Br ₂ -----	145
VII-D-2 Angle-Resolved Photoemission Study of the MX-Chain Compound [Ni(chxn) ₂ Br]Br ₂ : Spin-Charge Separation in Hybridized <i>d-p</i> Chains -----	145
VII-D-3 ESR Detection of Induced Spin Moments in Halogen-Bridged Mixed-Metal Complexes Ni _{1-x} Pd _x (chxn) ₂ Br ₃ -----	146
VII-D-4 A Chemical Modification of a Mn ₁₂ Single-Molecule Magnet by Replacing Carboxylate Anions with Diphenylphosphate Anions -----	146
VII-D-5 Construction of a One-Dimensional Chain Composed of Mn ₆ Clusters and 4,4'-Bipyridine Linker: The First Step for Creation of "Nano-Dots-Wires" -----	147
VII-D-6 Framework Engineering by Anions and Porous Functionalities Cu(II)/4,4'-bpy Coordination Polymers -----	147
VII-D-7 New Microporous Coordination Polymer Affording Guest-Coordination Sites at Channel Walls -----	147
VII-E Large Macrocyclic Formation Assisted by Coordination Bonds -----	148
VII-E-1 Solution and Solid-State Characterization of a Dicationic Receptor for Large Substrates --	148
VII-F Development of New Carbonylation Reactions -----	149
VII-F-1 Ru ₃ (CO) ₁₂ -Catalyzed Coupling Reaction of <i>sp</i> ³ C-H Bonds Adjacent to a Nitrogen Atom in Alkylamines with Alkenes -----	149
VII-F-2 Catalytic Carbonylation Reactions of Benzyne Derivatives -----	149
VII-G Development of Cycloisomerization Reactions -----	149
VII-G-1 Cycloisomerization of ω-Aryl-1-Alkynes: GaCl ₃ as a Highly Electrophilic Catalyst for Alkyne Activation -----	149
VII-H Multi-Electron Reduction of Carbon Dioxide through Metal-Carbonyl and Oxidative Activation of Water via Metal-Oxo Complexes -----	151
VII-H-1 Syntheses of New Ruthenium Carbonyl Terpyridine <i>o</i> -Phenylene Complexes: Strong Interaction between Carbonyl and <i>o</i> -Phenylene Ligands -----	151
VII-H-2 Synthesis and Redox Properties of Bis(ruthenium-hydroxo)complexes with Quinone and Bipyridine Ligand as a Water-Oxidation Catalysts -----	151
VII-H-3 Ruthenium Terpyridine Complexes with Mono- and Bi-Dentate Dithiolene Ligands -----	152

VII-H-4 A Ru-Carbene Complex with a Metallacycle Involving a 1,8-Naphthylidene Framework	152
VII-H-5 Ruthenium Oxyl Radical Complex Containing <i>o</i> -Quinone Ligand Detected by ESR Measurements of Spin Trapping Technique	152
VII-H-6 Multi-Electron Reduction of CO ₂ via Ru-CO ₂ -C(O)OH, -CO, -CHO, and -CH ₂ OH Species	153
VII-I Silanechalcogenolato Complexes	154
VII-I-1 Palladium Dimethylsilanedithiolato Complex: a Precursor for Ti-Pd and Ti-Pd ₂ Heterometallic Complexes	154
VII-I-2 Synthesis and Reactions of Triphenylsilanethiolato Complexes of Manganese(II), Iron(II), Cobalt(II), and Nickel(II)	154
VII-J Coordination Chemistry of New Multidentate Ligands and Activation of Small Molecules ---	155
VII-J-1 Binuclear Iron(II) Complex from a Linked-bis(amidinate) Ligand: Synthesis and its Reaction with Carbon Monoxide	155
VII-J-2 Synthesis and Structures of Ti(III) and Ti(IV) Complexes Supported by a Tridentate Aryloxy Ligand	155
VII-J-3 Dinitrogen-Bond Cleavage in a Niobium Complex Supported by a Tridentate Aryloxy Ligand	155
VII-K Synthesis of Compounds Having a Novel Bonding Containing Heavier Main Group Elements	156
VII-K-1 Syntheses and Crystal Structures of the First Disulfur and Diselenium Complexes of Platinum	156
VII-K-2 Synthesis and Structure of the First Stable Phosphabismuthene	156
VII-K-3 Synthesis of Kineically Stabilized Silaneselone and Silanetellone	157
VII-K-4 The First Stable 9-Silaanthracene	157
VII-K-5 Synthesis and Characterization of an Extremely Hindered Tetraaryl-Substituted Digermene and its Unique Properties in the Solid State and in Solution ..	158
VII-K-6 Syntheses, Structures and Properties of Kinetically Stabilized Distibenes and Dibismuthenes, Novel Doubly Bonded Systems between Heavier Group 15 Elements	158
VII-K-7 Synthesis and Properties of the First Stable Germabenzene	159
VII-K-8 Reactions of 2-Germanaphthalene with Elemental Sulfur and Selenium: Synthesis of Novel Cyclic Polychalcogenides Containing a Germanium, Trichalcogenagermolanes	159
VII-K-9 Synthesis and Properties of the First Stable 1-Silanaphthalene	160
VII-K-10 Synthesis and Isolation of the First Germacyclopropabenzene: A Study to Elucidate the Intrinsic Factor for the Ring Deformation of Cyclopropabenzene Skeletons	160
VII-L Precise Synthesis of Functional Macromolecules Using Organometallic Complexes	162
VII-L-1 Helical Poly(aryl isocyanide)s Possessing Chiral Alkoxy carbonyl Groups	162
VII-L-2 Formation of an Optically Active Helical Polyisocyanide Langmuir-Blodgett Film	162
VII-L-3 Helical Chiral Polyisocyanides Possessing Porphyrin Pendants: Determination of Helicity by Exciton Coupled Circular Dichroism	162

RESEARCH ACTIVITIES VIII

Laser Research Center for Molecular Science

VIII-A Developments and Researches of New Laser Materials	163
VIII-A-1 Ce ³⁺ :LiCaAlF ₆ Crystal for High-Gain or High-Peak-Power Amplification of Ultraviolet Femtosecond Pulses and New Potential Ultraviolet Gain Medium: Ce ³⁺ :LiSr _{0.8} Ca _{0.2} AlF ₆	163
VIII-A-2 Optical Fiber for Deep Ultraviolet Light	163
VIII-A-3 Crystal Growth of Fluorides for Optical Applications	163
VIII-A-4 Growth of Ce-Doped Colquirite- and Scheelite-Type Single Crystals for UV Laser Applications	164
VIII-A-5 High-Energy Pulse Generation from Solid-State Ultraviolet Lasers Using Large Ce:Fluoride Crystals	164
VIII-A-6 New Adjustment Technique for Time Coincidence of Femtosecond Laser Pulses Using Third Harmonic Generation in Air and its Application to Holograph Encoding System	165
VIII-A-7 Hybrid Time-Resolved Spectroscopic System for Evaluating Laser Material Using a Table-Top-Sized, Low-Jitter, 3-MeV Picosecond Electron-Beam Source with a Photocathode	165
VIII-A-8 Simultaneous Measurement of Thickness and Water Content of Thin Black Ink Films for the Printing Using THz Radiation	165
VIII-A-9 Far-Infrared Absorption Measurements of Polypeptides and Cytochrome <i>c</i> by THz Radiation	166

VIII-A-10	0.43 J, 10 Hz Fourth Harmonic Generation of Nd:YAG Laser Using Large $\text{Li}_2\text{B}_4\text{O}_7$ Crystals	166
VIII-A-11	Electron-Beam Excitation of a $\text{Ce}^{3+}:\text{LiCaAlF}_6$ Crystal for Future High-Peak-Power UV Lasers	166
VIII-B	Development and Research of Advanced Tunable Solid State Lasers	168
VIII-B-1	Thermal-Birefringence-Induced Depolarization in Nd:YAG Ceramics	168
VIII-B-2	Intrinsic Reduction of the Depolarization Loss in Solid-State Lasers by Use of a (110)-Cut $\text{Y}_3\text{Al}_5\text{O}_{12}$ Crystal	169
VIII-B-3	The Effect of Nd Concentration on the Spectroscopic and Emission Decay Properties of Highly-Doped Nd:YAG Ceramics	169
VIII-B-4	Spectroscopy and Laser Emission under Hot Band Resonant Pumping in Highly Doped Nd:YAG Ceramics	171
VIII-B-5	Efficient Laser Emission in Concentrated Nd Laser Materials under Pumping into the Emitting Level	172
VIII-B-6	1064-nm Laser Emission of Highly Doped Nd:Yttrium Aluminium Garnet under 885-nm Diode Laser Pumping	174
VIII-B-7	Diode Edge-Pumped Microchip Composite Yb:YAG Laser	175
Research Center for Molecular-Scale Nanoscience		
VIII-C	Development of Organic Semiconductors for Molecular Thin-Film Devices	177
VIII-C-1	Perfluoro-1,3,5-tris(<i>p</i> -Oligophenyl)benzenes: Amorphous Electron-Transport Materials with High Glass-Transition Temperature and High Electron Mobility	177
VIII-C-2	Synthesis and Properties of Iridium Complexes Bearing Perfluoroaryl-Substituted 2-Phenylpyridine	177
VIII-D	Field Effect Transistors with Organic Semiconductors	179
VIII-D-1	Electrical Characteristics of Phthalocyanine Films Prepared by Electrophoretic Deposition	179
VIII-D-2	BTQBT (bis-(1,2,5-thiadiazolo)- <i>p</i> -Quinobis(1,3-dithiole)) Thin Films; A Promising Candidate for High Mobility Organic Transistors	179
VIII-D-3	Field Effect Transistors of BTQBT and Its Derivatives	179
VIII-D-4	Preparation of Nanometer-Gap Electrodes for Field Effect Transistors by Electroplating	180
VIII-E	Preparation and Characterization of Highly Ordered Molecular Films on Silicon Bound with Si-C Covalent Bond	180
VIII-E-1	Force Curve Measurement of Self-Assembled Organic Monolayers Bound Covalently on Silicon(111)	180
VIII-E-2	Atomic Force Microscope Anodization of Si(111) Covered with Alkyl Monolayers	180
VIII-E-3	Nanopatterning of Alkyl Monolayers Covalently Bound to Si(111) with an Atomic Force Microscope	181
VIII-F	Development of Precisely-Defined Macromolecules and their Organization on Substrate Surfaces for Molecular-Scale Electronics Circuits	182
VIII-F-1	Design and Synthesis of Molecular Junction and Anchor Modules for Multi-Function Integrated Macromolecules	182
VIII-G	Development of Novel Heterocyclic Compounds and their Molecular Assemblies for Advanced Materials	182
VIII-G-1	Crystal Engineering Using Anilic Acids and Dipyrindyl Compounds through a New Supramolecular Synthone	182
VIII-G-2	Bis(tetra- <i>n</i> -butylammonium) Bis(2-dicyanomethylene-4,5-dimercapto-1,3- dithiole)nickel(II)	183
VIII-G-3	^1H NMR Analysis and Crystal Structures of 1,1',3,3'-Tetramethyl-2,2'-bi-1 <i>H</i> - Imidazolium Bis(tetraphenylborate): Ion-Associative Interactions Containing Ketone, Aldehyde, and Nitrile	183
VIII-G-4	4,7-Diiodo-2,1,3-Benzothiadiazole and 7,7'-Diiodo-4,4'-bis(2,1,3-benzothiadiazole)	184
VIII-G-5	Synthesis and Properties of π -Extended TTF Analogues and Their Cation Radical and Dication Salts	184
VIII-G-6	Synthesis and Structure of Bi- and Terthiophene Derivatives Having 4-Pyridylethynyl Substituents	184
VIII-H	Designing Artificial Photosynthesis at Molecular Dimensions	185
VIII-H-1	Photoinduced Oxidation of Alcohols Catalyzed by Porphyrins and TEMPO	185
VIII-I	Development of New Metal Complexes as Redox Catalysts	186
VIII-I-1	Syntheses of a 6-(2-Pyrrolyl)-2,2'-Bipyridine Derivative and Its Ruthenium Complex	186
VIII-J	Electronic Properties of Monolayer-Protected Metal Clusters	187
VIII-J-1	Development of Mass Spectrometer for Clusters	187

VIII-J-2	Formation of Pd _n (SR) _m Clusters (<i>n</i> < 60) in the Reactions of PdCl ₂ and RSH (R = <i>n</i> -C ₁₈ H ₃₇ , <i>n</i> -C ₁₂ H ₂₅)	187
VIII-J-3	Size-Selective Preparation of Water-Soluble Gold Clusters	188
VIII-J-4	Characterization and Purification of Pd:SR Nanoparticles by Gel Permeation Chromatography	188
VIII-K	Structures and Dynamics of Molecular Cluster Ions	189
VIII-K-1	Structural Evolution of Large (CO ₂) _{<i>n</i>} ⁻ Clusters as Studied by Mass Spectrometry	189
VIII-K-2	Photochemistry of (NO) _{<i>n</i>} ⁻ as Studied by Photofragment Mass Spectrometry	190
VIII-L	Rotational Echo Double Resonance (REDOR) Experiments with Overtone Adiabatic Inversion Pulses	191
VIII-L-1	The Observation of REDOR Phenomena for Solid-State ¹³ C- ¹⁴ N Spin Systems with the Help of Overtone Adiabatic Inversion Pulses	191
VIII-M	Nanoscale Characterization of Heterogeneous Catalyst Surfaces	192
VIII-M-1	Determination of Extra-Framework Cation Positions and Their Occupancies on Heulandite(010) by Atomic Force Microscopy	192
VIII-M-2	Molecular Orbital Interpretation of Thymine/Graphite NC-AFM Images	192
VIII-M-3	Partial Reduction of Si(IV) in SiO ₂ Thin Film by Deposited Metal Particles —An XPS Study	192
VIII-M-4	Apparent Local Structural Change Caused by Ultraviolet Light on a TiO ₂ Surface Observed by Scanning Tunneling Microscopy	192
VIII-M-5	Various Phases on Natural Stilbite (010) Surface Observed by Atomic Force Microscopy under Aqueous Conditions	192
VIII-N	Studies of Electronic Structure of Organic Thin Films and Organic/Inorganic Interfaces by Electron Spectroscopies	194
VIII-N-1	Low Energy Electron Diffraction of the System In-[perylene-3,4,9,10-tetracarboxylic Dianhydride] on MoS ₂	194
VIII-N-2	Electronic Structure and Molecular Orientation at Thin Film Surfaces of Pendant-Group Polymers Studied by Outermost Surface Spectroscopy Using Metastable Atoms	194
VIII-N-3	Photodegradation of Poly(tetrafluoroethylene) and Poly(vinylidene fluoride) Thin Films by Inner Shell Excitation	195
VIII-N-4	Intramolecular Energy-Band Dispersion in Oriented Thin Film of <i>n</i> -CF ₃ (CF ₂) ₂₂ CF ₃ Observed by Angle-Resolved UV Photoemission and its Theoretical Simulation	195
VIII-O	Study on Compact X-Ray Sources	196
VIII-O-1	Study on Radiation Shielding for Small Synchrotron Radiation Facilities	196
VIII-P	Syntheses of Fullerene-Based New Materials with Novel Physical Properties	197
VIII-P-1	Pressure and Temperature Dependences of the Structural Properties of Dy@C ₈₂ Isomer I	197
VIII-P-2	Ferromagnetism and Giant Magnetoresistance in the Rare-Earth Fullerides Eu _{6-x} Sr _x C ₆₀	197
VIII-P-3	Bridging Fullerenes with Metals	197
VIII-P-4	Structure and Physical Properties of Cs _{3+α} C ₆₀ (α = 0.0–1.0) under Ambient and High Pressures	197
VIII-P-5	Complex-Plane Impedance Study on a Hydrogen-Doped Copper Coordination Polymer: <i>N,N'</i> -bis(2-hydroxyethyl)dithiooxamidatocopper(II)	198
VIII-P-6	Crystal Structure and Electronic Transport of Dy@C ₈₂	198
VIII-P-7	<i>N</i> -Channel Field-Transistors with Thin Films of Fullerenes	198
VIII-P-8	STM Study of Dy@C ₈₂ on Si(111)-(7×7) Surface	198
VIII-Q	Effects of High Magnetic Field on Chemical Process	199
VIII-Q-1	Magnetic Field Effects on Anodic Oxidation of Potassium Iodide	199
VIII-Q-2	High Magnetic Field Effect on the Growth of 3-Dimensional Silver Dendrites	199
VIII-R	Theoretical and Computational Study on Gas Phase Reactions and Chromic Molecules	200
VIII-R-1	Polycyano–Polycadmate Host Clathrates Including a Methylviologen Dication. Syntheses, Crystal Structures and Photo-Induced Reduction of Methylviologen Dication	200
VIII-R-2	IR Absorption Spectra of Electrochromic WO ₃ Films	200
VIII-R-3	A Local Interpolation Scheme Using No Derivatives in Potential Sampling: Application to O(¹ <i>D</i>) + H ₂ System	200
VIII-R-4	Theoretical Study on Photoinduced Color Change and Charge Transfer of Methylviologen	200
VIII-R-5	Potential Energy Surface Generation Using Ab Initio Calculations and IMLS/Shepard Interpolation for the LiH + H ⇌ Li + H ₂ Reactions	201
VIII-S	Macromolecular Self-Assembly Opens a Way to the Development of Novel Materials that Have Characteristics of Cellular Systems	202
VIII-S-1	Fabrication of “Entropy-Saving” Nano-Solar-Cells	202

VIII-S-2 Model Study on Signaling Behaviors of Scaffold Proteins —Toward its Application to Novel Computing Devices—	202
VIII-S-3 Physicochemical Studies on the Molecular Mechanism of Photosynthesis	202

Equipment Development Center

VIII-T Development of “Special Machine”	204
VIII-T-1 Development of Twin-Probe Scanning Tunneling Microscope	204

Ultraviolet Synchrotron Orbital Radiation Facility

VIII-U Development of the UVSOR Light Source	205
VIII-U-1 Development of Lattice Components for UVSOR Upgrade Project	205
VIII-U-2 Storage Ring Free Electron Laser	205
VIII-U-3 Ion Trapping at UVSOR	205
VIII-U-4 Design Study of Vacuum System Improvement	205
VIII-V Researches by the USE of UVSOR	206
VIII-V-1 Non-Radiative Decay of the Core Excitons in Auger-Free Luminescence Materials, CsCl and BaF ₂	206
VIII-V-2 Photoelectron Spectroscopic Study on Photo-Induced Phase Transition of Spin-Crossover Complex	206
VIII-V-3 Surface-Photovoltage Effect in GaAs-GaAsP Super-Lattice Studied with Combination of Synchrotron Radiation and the Laser	206
VIII-V-4 Pump/Probe Experiments with FEL and SR Pulses at UVSOR	206
VIII-V-5 Angle-Resolved Photoion Spectra of SO ₂	207
VIII-V-6 The Measurement of Absorption Spectra of Trifluoromethyl Sulfur Pentafluoride in VUV Region	207
VIII-V-7 Symmetry-Resolved Cl 2 <i>p</i> Photoabsorption Spectra of Cl ₂	208
VIII-V-8 Dynamical Angular Correlation in Molecular Auger Decay	208
VIII-V-9 Nondipolar Electron Angular Distributions from Fixed-in-Space Molecules	209
VIII-V-10 Double and Triple Excitations Near the K-Shell Ionization Threshold of N ₂ Revealed by Symmetry-Resolved Spectroscopy	209
VIII-V-11 Optical and Magneto-Optical Studies on Electronic Structure of CeSb in the Magnetically Ordered States	209
VIII-V-12 Low Energy Electronic Structure of Ce _{1-x} La _x Sb (<i>x</i> = 0, 0.1) in the Magnetically Ordered States	209
VIII-V-13 Temperature Dependence of Low-Energy Optical Conductivity of Yb ₄ (As _{1-x} P _x) ₃ (<i>x</i> = 0, 0.05, 0.15)	209
VIII-V-14 Charge Ordering Effect of Electronic Structure of Yb ₄ (As _{1-x} Sb _x) ₃	210
VIII-V-15 Temperature-Induced Valence Transition of EuNi ₂ (Si _{0.25} Ge _{0.75}) ₂ Studied by Eu 4 <i>d-4f</i> Resonant Photoemission and Optical Conductivity	210
VIII-V-16 Optical Gap in the Diluted Kondo Semiconductors Yb _{1-x} Lu _x B ₁₂ : Lattice and Single-Site Effects	210
VIII-V-17 Magneto-Optical Study of the Colossal Magnetoresistance Pyrochlore Tl ₂ Mn ₂ O ₇	210
VIII-V-18 Influence of Electronic Structure of CeSbNi _{0.15} on its Optical Conductivity	210

Computer Center

VIII-W Computer Simulation of Quantum Systems in Condensed Phase	211
VIII-W-1 Vibrational Energy Transfer from Solute to Solvent: An Analysis Based upon Path Integral Influence Functional Theory and Mixed Quantum-Classical Molecular Dynamics Method	211
VIII-X Molecular Dynamics Study of Classical Complex Systems	211
VIII-X-1 A Molecular Dynamics Study of Water Penetration into Biomembrane	211
VIII-X-2 Molecular Dynamics Study of Mechanical Extension of Polyaniline by AFM Cantilever	211
VIII-Y Theoretical Studies on Electronic Structure and Dynamics of Electronically Excited States	212
VIII-Y-1 Chemical Reactions in the O(¹ D) + HCl System I. <i>Ab Initio</i> Global Potential Energy Surfaces for the 1 ¹ A', 2 ¹ A', and 1 ¹ A'' States	212
VIII-Y-2 Millimeter-Wave Spectroscopy of the Internal-Rotation Band of the He–HCN Complex and the Intermolecular Potential Energy Surface	212
VIII-Y-3 Determination of the Global Potential Energy Surfaces and Transition Wave Packet Dynamics for Polyatomic Systems	212
VIII-Y-4 <i>Ab Initio</i> Study of Conformers of <i>p-tert</i> -Butylcalix [4] Crown-6-Ether Complexed with Alkyl Ammonium Cations	213

VIII-Y-5 <i>Ab Initio</i> Study of the Complexation Behavior of Calix[5]arene Derivative toward Alkyl Ammonium Cations	213
VIII-Y-6 Formation of $\text{HCl}^+(\text{A}^2\Sigma^+)$ and $\text{HBr}^+(\text{A}^2\Sigma^+)$ Resulting from $\text{He}(2^3\text{S})$ Penning Ionization of HCl and HBr	213
VIII-Y-7 Theoretical Study of Vibrational States for AINC/AICN	213
VIII-Y-8 Boundary Expansion in Time-Dependent Nonadiabatic Problems	213
VIII-Y-9 Optimal Control of Random Matrix Systems with a Parameter	214

RESEARCH ACTIVITIES IX

Center for Integrative Bioscience

IX-A Molecular Mechanisms of Oxygen Activation by Heme Enzymes	215
IX-A-1 Asymmetric Sulfoxidation and Amine Binding by H64D/V68A and H64D/V68S Mb: Mechanistic Insight into the Chiral Discrimination Step	215
IX-A-2 Molecular Mechanism of the Catalase Reaction Studied by Myoglobin Mutants	215
IX-B Model Studies of Non-Heme Proteins	216
IX-B-1 Reactivity of Hydrogenperoxide Bound to a Mononuclear Non-Heme Iron Site	216
IX-B-2 Synthesis, Structure, and Properties of A Novel Mononuclear Iron(III) Complex Containing Peroxocarbonate Ligand	216
IX-B-3 Structural and Spectroscopic Features of a <i>cis</i> (Hydroxo)- Fe^{III} -(Carboxylato) Configuration as an Active Site Model for Lipoxygenases	217
IX-C Aqueous Organometallic Chemistry	217
IX-C-1 pH-Dependent H_2 -Activation Cycle Coupled to Reduction of Nitrate Ion by Cp^*Ir Complexes	217
IX-C-2 pH-Dependent Cross-Coupling Reactions of Water-Soluble Organic Halides with Organoboron Compounds Catalyzed by an Organometallic Aqua Complex $[(\text{SCS})\text{Pd}^{\text{II}}(\text{H}_2\text{O})]^+$ {SCS = C_6H_3 -2,6-(CH-SBu ^t) ₂ }	217
IX-C-3 pH-Dependent Transfer Hydrogenation of Ketones with HCOONa as a Hydrogen Donor Promoted by $(\eta^6\text{-C}_6\text{Me}_6)\text{Ru}$ Complexes	218
IX-D Single-Molecule Physiology	219
IX-D-1 Myosin V Is a Left-Handed Spiral Motor on the Right-Handed Actin Helix	219
IX-D-2 Pause and Rotation of F_1 -ATPase during Catalysis	219
IX-D-3 F_1 -ATPase Changes its Conformations upon Phosphate Release	219
IX-E Bioinorganic Chemistry of Heme-Based Sensor Proteins	221
IX-E-1 Ligand-Switching Intermediates for the CO-Sensing Transcriptional Activator <i>CooA</i> Measured by Pulse Radiolysis	221
IX-E-2 Conformational Dynamics of the Transcriptional Regulator <i>CooA</i> Protein Studied by Subpicosecond Mid-Infrared Vibrational Spectroscopy	221
IX-E-3 Resonance Raman and Ligand Binding Studies of the Oxygen Sensing Signal Transducer Protein <i>HemAT</i> from <i>Bacillus subtilis</i>	221
IX-F Electronic Structure and Reactivity of Active Sites of Metalloproteins	223
IX-F-1 Trigonal Bipyramidal Ferric Aqua Complex with Sterically Hindered Salen Ligand as a Model for Active Site of Protocatechuate 3,4-Dioxygenase	223
IX-F-2 ^{13}C -NMR Signal Detection of Iron Bound Cyanide Ions in Ferric Cyanide Complexes of Heme Proteins	223
IX-G Molecular Mechanism of Heme Degradation and Oxygen Activation by Heme Oxygenase	224
IX-G-1 Catalytic Mechanism of Heme Oxygenase through EPR and ENDOR of Cryoreduced Oxy-Heme Oxygenase and Asp 140 Mutants	224
IX-H Biomolecular Science	225
IX-H-1 Stationary and Time-Resolved Resonance Raman Spectra of His77 and Met95 Mutants of the Isolated Heme Domain of a Direct Oxygen Sensor from <i>E. coli</i>	225
IX-H-2 Resonance Raman Studies on Xanthine Oxidase: Observation of the Mo^{VI} -Ligand Vibration	225
IX-H-3 Changes in the Abnormal α -Subunit upon CO-Binding to the Normal β -Subunit of Hb M Boston: Resonance Raman, EPR, and CD Study	226
IX-H-4 Coordination Geometry of Cu-Porphyrin in Cu(II)-Fe(II) Hybrid Hemoglobins Studied by Q-Band EPR and Resonance Raman Spectroscopies	226
IX-H-5 Fine-Tuning of Copper(I)-Dioxygen Reactivity by 2-(2-Pyridyl)ethylamine Bidentate Ligands	226
IX-H-6 Modulation of the Copper-Dioxygen Reactivity by Stereochemical Effect of Tetradentate Tripodal Ligands	227
IX-H-7 Reactivity of Hydroperoxide Bound to a Mononuclear Non-Heme Iron Site	227
IX-H-8 A New Mononuclear Iron(III) Complex Containing a Peroxocarbonate Ligand	227

IX-H-9 Formation, Characterization, and Reactivity of Bis(m-oxo)dinickel(III) Complexes Supported by a Series of Bis[2-(2-pyridyl)ethyl]amine Ligands -----	227
IX-H-10 UV Resonance Raman and NMR Spectroscopic Studies on the pH Dependent Metal Ion Release from Pseudoazurin -----	228
IX-I Fast Dynamics of Photoproducts in Solution Phases -----	228
IX-I-1 Time-Resolved Resonance Raman Study on Ultrafast Structural Relaxation and Vibrational Cooling of Photodissociated Carbonmonoxy Myoglobin -----	228
IX-I-2 Vibrational Energy Relaxation of Metalloporphyrins in a Condensed Phase Probed by Time-Resolved Resonance Raman Spectroscopy -----	229
IX-I-3 Mode Dependence of Vibrational Energy Redistribution in Nickel Tetraphenylporphyrin Probed by Picosecond Time-Resolved Resonance Raman Spectroscopy: Slow IVR to Phenyl Peripherals -----	229
RESEARCH FACILITIES -----	231
Laser Research Center for Molecular Science -----	231
Research Center for Molecular-scale Nanoscience -----	231
Equipment Development Center -----	231
Ultraviolet Synchrotron Orbital Radiation Facility -----	231
Computer Center -----	232
SPECIAL RESEARCH PROJECTS -----	233
(a) Chemical Reaction Dynamics -----	233
Folding Mechanism of Protein Molecules Studied by Generalized-Ensemble Algorithms -----	233
Nonadiabatic Chemical Dynamics -----	233
Imaging of Chemical Dynamics -----	233
Stereodynamics and Active Control of Chemical Reactions by Using Electrostatic Hexapole State-Selector and Polarized Laser Excitation -----	234
Monte Carlo Simulation of Chemical Gel -----	234
Electronic Structure and Decay Mechanism of Inner-Shell Excited Molecules -----	234
Computational Study of Quantum Dynamics of a Solute in Solution -----	235
Photodissociation of 16 Valence Electron Systems, OCS and N ₂ O -----	235
Development of Single-Molecule Physiology -----	235
Ultrafast Protein Dynamics Probed by Time-Resolved Resonance Raman Spectroscopy -----	235
(b) Molecular Photophysics and Science -----	237
Development of Dynamic Spectroscopy Apparatus Having Nanometer Spatial Resolution -----	237
(1) Laser Cooling and Trapping of Metastable Helium Atoms -----	237
(2) Laser Spectroscopic Studies of Atoms and Ions in Liquid Helium -----	237
Structure, Relaxation and Control of Reactive Cluster Studied by Two-Color Laser Spectroscopy -----	237
Dynamics of Molecular Superexcited States Studied by Electron and Fluorescence Spectroscopy -----	237
Decay and Dissociation Dynamics of Core Excited Molecules -----	238
(c) Novel Material Science -----	239
Calculations of Large Molecular Systems -----	239
Response of Protein Conformation to Pressure: Theoretical Study on Partial Molar Volume -----	239
Theory for Equilibrium and Non-Equilibrium Properties of Low-Dimensional Molecular Materials with Strong Electron Correlation -----	239
UHV System for MOKE Measurements -----	240
Pulsed Methods of Electron Spin Resonance Spectroscopy -----	240
Spectroscopic Studies of Organic Conductors -----	240
Broad-Line Solid State NMR Investigation of Electronic States in Molecular-Based Conductors -----	241
Development of New Organic Conductors -----	241
Design and Synthesis of Organic Spin-Ladder Systems -----	241
Construction of BL-7A at UVSOR for STM Observation of SR Irradiation Induced Photochemical Reaction on Si Surfaces -----	242
Catalytic Oxidation of Alcohols in Water under Atmospheric Oxygen by Use of an Amphiphilic Resin-Dispersion of Nano-Palladium Catalyst -----	242
Reductive Activation of Carbon Dioxide and Oxidative Activation of Water Aimed at Energy Conversion -----	242
Coordination Chemistry of New Multidentate Ligands and Activation of Small Molecules -----	243
Developments and Researches of New Laser Materials -----	243
Development and Research of Advanced Tunable Solid State Lasers -----	243
Synthesis of Oligonaphthalenes and Oligoanthracenes and Applications for Organic Field-Effect Transistors -----	243
Field Effect Transistors of BTQBT and Its Derivatives -----	244

Generation of Reactive Species via Electron Transfer on Metal Complexes, as Basis of Chemical Energy Conversion Systems -----	244
Electronic Structures and Reactivities of Organic/Metal Clusters -----	244
Local Distribution of Photoexcited States on a Semiconductor Surface as Observed by Scanning Tunneling Spectroscopy -----	244
Electronic Structures and Surface Molecular Orientation of Organic Thin Films and Interfaces by Various Surface Sensitive Spectroscopies -----	245
Development of "Entropy-Saving" Nano-Materials -----	245
Investigation of Dynamics on Photo-Excited Solids and Surfaces by Using the Combination of Synchrotron Radiation and Laser Light -----	246
Construction and Commissioning of In-Vacuum Undulator -----	246
Optical Investigation on Fermiology of Strongly Correlated Electron Systems -----	246
Preparation of Artificial Metalloenzymes by Insertion of Chromium(III) Schiff Base Complexes into Apo-Myoglobin Mutants -----	246
Molecular Mechanism of Oxygen Activation by Metalloenzymes -----	247
OKAZAKI CONFERENCE -----	249
JOINT STUDIES PROGRAMS -----	251
(1) Special Projects -----	251
(2) Research Symposia -----	258
(3) Cooperative Research -----	259
(4) Use of Facility -----	259
(5) Invited Research -----	259
(6) Use of UVSOR Projects -----	259
(7) Use of Facility Program of the Computer Center -----	259
FOREIGN SCHOLARS -----	261
AWARDS -----	265
LIST OF PUBLICATIONS -----	269
REVIEW ARTICLES AND TEXTBOOKS -----	291
AUTHOR INDEX -----	295

Abbreviations

IMS: Institute for Molecular Science
GUAS: The Graduate University for Advanced Studies

ORGANIZATION AND STAFF

Organization

The Institute for Molecular Science comprises twenty research laboratories — each staffed by a professor, an associate professor, two research associates and several technical associates —, two research laboratories with foreign visiting professors, and five research facilities.

The laboratories are grouped into six departments and one facility for coordination chemistry:

Department of Theoretical Studies	Theoretical Studies I Theoretical Studies II Theoretical Studies III ¹⁾ Theoretical Studies IV
Department of Molecular Structure	Molecular Structure I Molecular Structure II ¹⁾ Molecular Dynamics
Department of Electronic Structure	Excited State Chemistry Excited State Dynamics Electronic Structure ¹⁾ Molecular Energy Conversion ²⁾
Department of Molecular Assemblies	Solid State Chemistry Molecular Dynamics Assemblies Molecular Assemblies ¹⁾
Department of Applied Molecular Science	Applied Molecular Science I Applied Molecular Science II ¹⁾ Molecular Clusters ³⁾ (–March '02)
Department of Vacuum UV Photoscience	Photochemistry Chemical Dynamics Interface Molecular Science ³⁾ (–March '02) Synchrotron Radiation Research ²⁾
Coordination Chemistry Laboratories	Complex Catalysis Functional Coordination Chemistry Coordination Bond ¹⁾

The research facilities are:

- Laser Research Center for Molecular Science Advanced Lasers for Chemical Reaction Studies
Advanced Lasers for Synchrotron Radiation Applications
Advanced UV and IR Tunable Lasers
- Research Center for Molecular Materials
(–March '02) Organic Materials Section
Hybrid Materials Section
Materials Characterization Section
Structure Control Section
- Research Center for Molecular-scale Nanoscience Molecular-scale Electronics
(April '02–) Nanocatalysis and Biomolecular Devices
Nano-scale Photoscience
Interface Molecular Science³⁾
Molecular Clusters³⁾
- Equipment Development Center
- UVSOR (Ultraviolet Synchrotron Orbital Radiation) Facility
- Computer Center

The research facilities of ONRI (related to IMS) are:

- Center for Integrative Bioscience
- Research Center for Computational Science

- 1) Professors and associate professors are visiting professors from other universities.
- 2) Research laboratories with foreign visiting professors.
- 3) Professors, associate professors, and research associates, along with their positions, are transferred from other universities.

Scientific Staff

KAYA, Koji

Professor, Director-General

Emeritus Professors

NAGAKURA, Saburo

President, The Kanagawa Academy of Science and Technology

HIROTA, Eizi

Professor Emeritus, The Graduate University for Advanced Studies

KIMURA, Katsumi

Senior Researcher, Molecular Photonics & Photoelectron Group, Communications Research Laboratory

MOROKUMA, Keiji

Professor, Emory University, U. S. A.

INOKUCHI, Hiroo

Chief Scientist of Space Utilization Research Program, National Space Development Agency of Japan

MARUYAMA, Yusei

Professor, Hosei University

YOSHIHARA, Keitaro

Professor, Japan Advanced Institute of Science and Technology

HANAZAKI, Ichiro

Professor Emeritus, The Graduate University for Advanced Studies

IWAMURA, Hiizu

Professor, University of the Air

SAITO, Shuji

Professor, Fukui University

IWATA, Suehiro

Professor, National Institution for Academic Degree

ITO, Mitsuo

Professor Emeritus, The Graduate University for Advanced Studies, Tohoku University

Department of Theoretical Studies

Theoretical Studies I

NAGASE, Shigeru

Professor

OKAMOTO, Yuko

Associate Professor

KOBAYASHI, Kaoru

Research Associate (January '02–)

SUGITA, Yuji

Research Associate (–March '02)¹⁾

NAGASIMA, Takehiro

Technical Associate (–November '01)²⁾

ISHIMURA, Kazuya

Technical Associate (April '02–)

YODA, Takao

IMS Fellow (–March '02); Research Associate of Research for the Future Program (April '02–)

CHOE, Yoong-Kee

IMS Fellow

ITOH, Masakatsu

Research Associate of Research for the Future Program (–March '02)³⁾

YAMAGUCHI, Tsuyoshi

Research Associate of Research for the Future Program (–March '02)⁴⁾

LU, Jing

Visiting Scientist; JSPS Post-Doctoral Fellow (September '01–)

RE, Suyong

JSPS Post-Doctoral Fellow

TAKAGI, Nozomi

Graduate Student (from Tokyo Metropolitan University)* (–March '02); JSPS Post-Doctoral Fellow (April '02–)

YAMAZAKI, Takeshi

JSPS Post-Doctoral Fellow (April '02–)

NOGUCHI, Hiroshi

JSPS Post-Doctoral Fellow

KAWASHIMA, Yukio

Post-Doctoral Fellow (July '02–)

FUKAMI, Kentaro

Graduate Student (from Tokyo Metropolitan University)* (–March, '02)

KOKUBO, Hironori

Graduate Student

MURATA, Katsumi

Graduate Student

SAKAE, Yoshitake

Graduate Student

KIMURA, Masahiro

Graduate Student (from Tokyo Metropolitan University)* (–March '02)

NAGAYOSHI, Kanade

Graduate Student (from Osaka Prefecture University) *

ITO, Satoru

Graduate Student (April '02–)

Theoretical Studies II

NAKAMURA, Hiroki

Professor

TANIMURA, Yoshitaka

Associate Professor

ZHU, Chaoyuan

Research Associate

TAKAMI, Toshiya	Research Associate
SUZUKI, Yoko	Research Associate
KATO, Tsuyoshi	IMS Fellow
FUJISAKI, Hiroshi	IMS Fellow
LEE, Chun-Woo	Visiting Scientist; MONBUSHO Invited Fellow (from Korea Advanced Institute of Science & Technology, Korea) (December '01–February '02)
LEE, Eok Kyun	Visiting Scientist; MONBUSHO Invited Fellow (from Korea Advanced Institute of Science & Technology, Korea) (December '01–February '02)
BIAN, Wensheng	Visiting Scientist; JSPS Post-Doctoral Fellow (–January '02) ⁵⁾
KONDORSKIY, Alexey	Visiting Scientist; JSPS Post-Doctoral Fellow (November '01–)
MIL' NIKOV, Gennady V.	Research Fellow (from Institute of Structural Macrokineitics, Russia) (–February, '02), (May '02–)
NAGAYA, Kuninobu	Graduate Student (–March '02) ⁶⁾
KAMISAKA, Hideyuki	Graduate Student
HINO, Osamu	Graduate Student (–March '02) ⁷⁾
FUKAMI, Hiroshi	Graduate Student (from Kyoto University)*
<i>Theoretical Studies III</i>	
SAITO, Susumu	Visiting Professor (from Tokyo Institute of Technology) (–March '02)
HIRAO, Kimihiko	Visiting Professor (from University of Tokyo) (April '02–)
SHIMOI, Yukihiko	Visiting Associate Professor (from National Institute of Advanced Industrial Science and Technology (AIST)) (–March '02)
TAKAYANAGI, Toshiyuki	Visiting Associate Professor (from Japan Atomic Energy Research Institute) (April '02–)
KOVALENKO, Andriy F.	Research Associate
<i>Theoretical Studies IV</i>	
HIRATA, Fumio	Professor
YONEMITSU, Kenji	Associate Professor
SATO, Hirofumi	Research Associate (–April '02) ⁸⁾
KISHINE, Jun-ichiro	Research Associate
OTSUKA, Yuichi	IMS Fellow (April '02–)
HOLOVKO, Myroslav	Visiting Scientist; MONBUSHO Invited Fellow (from Institute for Condensed Matter Physics, Ukraine) (December '01–March '02)
LUTY, Tadeusz Michal	Visiting Scientist; MONBUSHO Invited Fellow (from Technical University of Wroclaw, Poland) (May '02–August '02)
SUMI, Tomonari	JSPS Post-Doctoral Fellow (–March '02) ⁹⁾
YAMAZAKI, Takeshi	Graduate Student (–March '02)
MIYASHITA, Naoyuki	Graduate Student
WATANABE, Ayumi	Graduate Student
<i>Department of Molecular Structure</i>	
<i>Molecular Structure I</i>	
OKAMOTO, Hiromi	Professor
MORITA, Norio	Associate Professor
IMURA, Kouhei	Research Associate
NAGAHARA, Tetsuhiko	IMS Fellow (April '02–)
<i>Molecular Structure II</i>	
AKUTSU, Hideo	Visiting Professor (from Osaka University)
SASADA, Hiroyuki	Visiting Associate Professor (from Keio University) (–March '02)
WADA, Akihide	Visiting Associate Professor (from Tokyo Institute of Technology) (April '02–)

Molecular Dynamics

KITAGAWA, Teizo
YOKOYAMA, Toshihiko
DINSE, Klaus Peter

KATO, Tatsuhisa
UCHIDA, Takeshi

NAKAGAWA, Takeshi
FURUKAWA, Ko
NAGATOMO, Shigenori
HAYASHI, Naoki
TOYAMA, Namiki
HUDECEK, Jiri

PAL, Biswajit
MATSUOKA, Hideto
HARUTA, Nami
OKUNO, Daichi
SATO, Akira
OKUBO, Shingo

Professor (Center for Integrative Bioscience)
Professor (April '02–)
Visiting Professor (from Technische Universitat Darmstadt, Germany) (August '02–)
Associate Professor
IMS Fellow (April '98–March '99), JSPS Post-Doctoral Fellow (April '99–October '01), Research Associate (November '01–)
Research Associate (April '02–)
Research Associate
Technical Associate
Technical Associate
IMS Fellow
Visiting Scientist; JSPS Invited Fellow (July '00–August '00), Visiting Scientist; JSPS Invited Fellow (from Charles University, Czech Republic) (–March '02)
Visiting Scientist; JSPS Invited Fellow (November '01–)
JSPS Post-Doctoral Fellow (April '02–)
Graduate Student (–March '02)¹⁰⁾
Graduate Student
Graduate Student
Graduate Student

*Department of Electronic Structure**Excited State Chemistry*

NISHI, Nobuyuki
TSUKUDA, Tatsuya
NAKABAYASHI, Takakazu
NEGISHI, Yuichi
AKITA, Motoko

IMAI, Hiroyuki
PROKOP, Petra V
KOSUGI, Kentaroh
OHSHIMO, Keijiro
IKEDA, Shingo
DELI, Geer
MORI, Michiyasu
IWASE, Hiroki
HINO, Kazuyuki

Professor
Associate Professor (–March '02)
Research Associate (–May '02)¹¹⁾
Research Associate
Research Associate of Research for the Future Program (–March '02)¹²⁾
Research Associate of Research for the Future Program
Research Associate of Research for the Future Program
Research Associate of Research for the Future Program
JSPS Post-Doctoral Fellow
Post-Doctoral Fellow (September '01–)
Post-Doctoral Fellow (September '01–February '02)
Post-Doctoral Fellow (April '02–)
Post-Doctoral Fellow (May '02–)
Graduate Student (from Kyushu University)*

Excited State Dynamics

FUJII, Masaaki
SUZUKI, Toshinori
KOHGUCHI, Hiroshi
SAKAI, Makoto
KATAYANAGI, Hideki
SAEKI, Morihisa

MATSUMOTO, Yoshiteru

KIM, Sang-Kyu

WATANABE, Takeshi
NISHIDE, Tatsuhiro
TSUBOUCHI, Masaaki

Professor
Associate Professor
Research Associate
Research Associate
Technical Associate
IMS Fellow (–March '02), Post-Doctoral Fellow (April '02)¹³⁾
Research Fellow (–October '01), IMS Fellow (November '01–March '02), JSPS Post-Doctoral Fellow (April '02–)
Visiting Scientist; MONBUSHO Invited Fellow (from Inha University, Korea) (July–August '02)
JSPS Post-Doctoral Fellow
Post-Doctoral Fellow
Graduate Student

Electronic Structure

YAMASE, Toshihiro

IJIMA, Sumio
OHSHIMA, Yasuhiro

Visiting Professor (from Tokyo Institute of Technology) (–March '02)
Visiting Professor (from Meijo University) (April '02–)
Visiting Associate Professor (from Kyoto University) (–March '02)

MISAWA, Kazuhiko

Visiting Associate Professor (from Tokyo University of Agriculture and Technology) (April '02–)
Research Associate

INOKUCHI, Yoshiya

Molecular Energy Conversion

SWIETLIK, Roman

Visiting Professor (from Institute of Molecular Physics, Poland) (–February '02)

CARRAVETTA, Vincenzo

Visiting Professor (from Institute of Quantum Chemistry and Molecular Energetics, Italy) (February –August '02)

DU, Si-de

Visiting Associate Professor (from Fudan University, China) (–March '02)

BARANOV, Nikolai Viktorovich

Visiting Associate Professor (from Ural State University, Russia) (April–June '02)

KOZLOWSKI, Pawel M.

Visiting Associate Professor (from University of Louisville, USA) (July '02–)

Department of Molecular Assemblies*Solid State Chemistry*

YAKUSHI, Kyuya

Professor

NAKAMURA, Toshikazu

Associate Professor

YAMAMOTO, Kaoru

Research Associate

FUJIYAMA, Shigeki

Research Associate

YAMAMOTO, Takashi

IMS Fellow

WOJCIECHOWSKI, Roman

Visiting Scientist; JSPS Post-Doctoral Fellow (September '01–September '02)

NAKANO, Chikako

Research Fellow

DROZDOVA, Olga

Research Fellow

SUZUKI, Kenji

Graduate Student

Molecular Assemblies Dynamics

KOBAYASHI, Hayao

Professor

FUJIWARA, Hideki

Research Associate

YAMADA, Ryo

Research Associate

WANG, Zhe-Ming

Visiting Scientist; MONBUSHO Invited Fellow (July '02–)

ZHANG, Bin

Visiting Scientist; MONBUSHO Invited Fellow (–May '02), Research Fellow (June '02–)

LEE, Ha-Jin

Visiting Scientist; JSPS Post-Doctoral Fellow (June '02–)

OTSUKA, Takeo

JSPS Post-Doctoral Fellow

TAKADA, Masaki

Graduate Student

Molecular Assemblies

KATO, Reizo

Visiting Professor (from RIKEN)

OGAWA, Takuji

Visiting Professor (from Ehime University)

Department of Applied Molecular Science*Applied Molecular Science I*

WATANABE, Yoshihito

Professor (Center for Integrative Bioscience) (–March '02)

KINOSITA, Kazuhiko, Jr.

Professor (Center for Integrative Bioscience)

AONO, Shigetoshi

Professor (Center for Integrative Bioscience) (May '02–)

INOUE, Katsuya

Associate Professor

HOSOKOSHI, Yuko

Research Associate

KUMAGAI, Hitoshi

JSPS Post-Doctoral Fellow (–March '02)¹⁴⁾

SUZUKI, Kentaro

Graduate Student

KATOH, Keiichi

Graduate Student

OKA, Yoshimi

Graduate Student

Applied Molecular Science II

MASUDA, Hideki

Visiting Professor (from Nagoya Institute of Technology) (–March '02)

AWAZU, Koichi

Visiting Professor (from National Institute of Advanced Science and Technology) (April '02–)

IWATA, Koichi

Visiting Associate Professor (from the University of Tokyo) (–March '02)

KIKUCHI, Koichi

Visiting Associate Professor (from Tokyo Metropolitan University) (April '02–)

OGO, Seiji

Research Associate (–September '01)¹⁵⁾*Molecular Clusters*

KASAI, Toshio

Professor (from Osaka University) (–March '02)

TAKASU, Masako

Associate Professor (from Kanazawa University) (–March '02)

KUBO, Atsushi

Research Associate (from Kyoto University) (–March '02)

CHE, Dock-Chil

Research Associate (from Osaka University) (–March '02)

SHIMIZU, Yuichiro

IMS Fellow (from Tohoku University) (–March '02)

NOGUCHI, Hiroshi

JSPS Post-Doctoral Fellow (–March '02)

NISHIYAMA, Yusuke

Visiting Scientist (from Kyoto University) (–March '02)

HASHINOKUCHI, Michihiro

Graduate Student (from Osaka University)* (–March '02)

NOSAKA, Makoto

Graduate Student (from Kanazawa University)* (–March '02)

FUKUYAMA, Tetsuya

Graduate Student (from Himeji Institute of Technology)* (–March '02)

*Department of Vacuum UV Photochemistry**Photochemistry*

KOSUGI, Nobuhiro

Professor

TAHARA, Tahei

Associate Professor (–April '02)

TAKEUCHI, Satoshi

Research Associate (–April '02)

HATSUI, Takaki

Research Associate

MIZUNO, Misao

Technical Associate (–April '02)

OJI, Hiroshi

IMS Fellow

NAGASONO, Mitsuru

JSPS Post-Doctoral Fellow, IMS Fellow (–July '02)¹⁶⁾

ARZHANTSEV, Sergei Yur'evich

IMS Fellow (–April '02)¹⁷⁾

MANDAL, Debabrata

JSPS Post-Doctoral Fellow (–April '02)¹⁷⁾

FUJINO, Tatsuya

JSPS Post-Doctoral Fellow (–April '02)¹⁷⁾

FUJIYOSHI, Satoru

Graduate Student (–April '02)¹⁷⁾

MASUDA, Suomi

Graduate Student (April '02–)

Chemical Dynamics

URISU, Tsuneo

Professor

MITSUKE, Koichiro

Associate Professor

MIZUTANI, Masakazu

Research Associate

NONOGAKI, Youichi

Research Associate

ONO, Masaki

IMS Fellow (–September '01)

KOU, Junkei

IMS Fellow (April '02–)

MOREÉ, Sam D.

IMS Fellow

MORI, Takanori

Research Fellow (April '02)

WANG, Changshun

Visiting Scientist (April '02–)

WANG, Zhihong

Graduate Student

YAMAMURA, Shusaku

Graduate Student

TAKIZAWA, Morio

Graduate Student

FUJIKI, Satoshi

Graduate Student

RAHMAN, Mashiur

Graduate Student (April '02–)

TAKABAYASHI, Yasuhiro

Graduate Student (from Okayama University)*

KANBARA, Takayoshi

Graduate Student (–March '02)¹⁸⁾

YOKOYAMA, Takahiro

Graduate Student (–March '02)¹⁹⁾*Synchrotron Radiation Research*

SKODJE, Rex T.

Visiting Professor (–December '01)²⁰⁾

WANG, Changshun

Visiting Associate Professor (–March '02)²¹⁾

GU, Ning

Visiting Associate Professor (–June '02)²²⁾

DINSE, Klaus Peter

Visiting Professor (August '02–)²³⁾

BERG, Bernd

Visiting Associate Professor (April '02–)²⁴⁾

GANGAVARAPU, Ranga Rao

Visiting Associate Professor (August '02–)²⁵⁾*Coordination Chemistry Laboratories*

TANAKA, Koji

Director

Complex Catalysis

UOZUMI, Yasuhiro	Professor
YAMASHITA, Masahiro	Visiting Professor (from Tokyo Metropolitan University) (April '02–)
TANIGUCHI, Isao	Visiting Professor (from Kumamoto University) (–March '02)
CHATANI, Naoto	Visiting Associate Professor (from Osaka University) (April '02–)
TANAKA, Yasutaka	Visiting Associate Professor (from Shizuoka University) (–March '02)
YAMANOI, Yoshinori	Research Associate
TAKENAKA, Kazuhiro	IMS Fellow (April '02–)
RHEE, Hak-June	Visiting Associate Professor; MONBUKAGAKUSHO Invited Fellow (from Hanyang University, Korea) (April '02–July '02)
HOCKE, Heiko	Visiting Scientist; JSPS Post-Doctoral Fellow
KIKUCHI, Makoto	Post-Doctoral Fellow (June '02–)
SHIBATOMI, Kazutaka	Post-Doctoral Fellow (–June '02) ²⁶⁾
KOBAYASHI, Yukinari	Visiting Scientist (from Daiichi Pharmaceutical Co. Ltd.)
NAKAO, Ryu	Visiting Scientist (from Zeria Pharmaceutical Co. Ltd.) (–January '02)
NAKAI, Yasushi	Graduate Student
KIMURA, Masahiro	Graduate Student (April '02–)
TAMAKI, Hirotaka	Graduate Student (April '02–)
NAKAZONO, Maki	Graduate Student (from Nagoya City University)* (–March '02)
TANAKA, Hirotaka	Graduate Student (from Nagoya City University)* (–March '02)
KIMURA, Tsutomu	Graduate Student (from Gifu University) (July–August '02)

Functional Coordination Chemistry

TANAKA, Koji	Professor
KAWAGUCHI, Hiroyuki	Associate Professor
WADA, Tohru	Research Associate
MATSUO, Tsukasa	Research Associate
MIZUKAWA, Tetsunori	Technical Associate
YUKI, Masahiro	IMS Fellow (April '02–), Post-Doctoral Fellow (March '02)
SHIREN, Kazushi	Post-Doctoral Fellow
KOIZUMI, Takeaki	Post-Doctoral Fellow
FUJIHARA, Tetsuaki	Post-Doctoral Fellow
OHTSU, Hideki	Post-Doctoral Fellow
AIHARA, Hidenori	Post-Doctoral Fellow (February '02–)
YASUE, Takahiro	Post-Doctoral Fellow (March '02–)
OKAMURA, Rei	Post-Doctoral Fellow (April '02–)
TSUTSUI, Kanako	Research Fellow
KOBAYASHI, Katsuaki	Research Fellow (April '02–)
TOMON, Takashi	Research Fellow (April '02–)
KOMURO, Takashi	Graduate Student (from Nagoya University)*
HINO, Takami	Graduate Student (April '02–)

Coordination Bond

TOKITOH, Norihiro	Visiting Professor (from Kyoto University)
ONITSUKA, Kiyotaka	Visiting Associate Professor (from Osaka University)

Research Facilities***Laser Research Center for Molecular Science***

FUJII, Masaaki	Director
----------------	----------

*Advanced Lasers for Chemical Reaction Studies**Advanced Lasers for Synchrotron Radiation Applications*

SARUKURA, Nobuhiko	Associate Professor
OHTAKE, Hideyuki	Research Associate (–August '02)

MURAKAMI, Hidetoshi
 ONO, Shingo
 SUZUKI, Yuji
 TAKAHASHI, Hiroshi

IMS Fellow
 Graduate Student (from Tokyo University of Science)
 Graduate Student
 Graduate Student

Advanced UV and IR Tunable Lasers

TAIRA, Takunori
 SHOJI, Ichiro
 PAVEL, Nicolaie

Associate Professor
 IMS Fellow (–March '02), Research Associate (April '02–)
 JSPS Invitation Fellowship Program (Long-term) (April '02–)
 Graduate Student
 Graduate Student

SAIKAWA, Jiro
 SATO, Yoichi

Research Center for Molecular-scale Nanoscience

UOZUMI, Yasuhiro

Director (Research Center for Molecular Materials)
 (–March '02)
 Director (April '02–)
 Research Associate (–March '02)²⁷⁾

KAYA, Koji
 KUWAHARA, Daisuke

Molecular-scale Electronics

SUZUKI, Toshiyasu
 TADA, Hirokazu
 TANAKA, Shoji
 SAKAMOTO, Youichi
 TOMURA, Masaaki
 SHIRASAWA, Nobuhiko
 GRAAF, Harald
 FUJIWARA, Eiichi
 KOMATSU, Shingo
 ITO, Kaname
 ARA, Masato
 TAKADA, Masaki

Associate Professor
 Associate Professor
 Research Associate
 Research Associate
 Technical Associate
 IMS Fellow
 IMS Fellow (–September '01)²⁸⁾
 IMS Fellow (April '02–)
 Graduate Student (from Kyushu University)* (–March '02)
 Graduate Student
 Graduate Student
 Graduate Student

Nanocatalysis and Biomolecular Devices

FUJII, Hiroshi
 NAGATA, Toshi
 ITO, Hajime
 KURAHASHI, Takuya
 HOSOKAWA, Yoichi
 KIKUZAWA, Yoshihiro

Associate Professor (Center for Integrative Bioscience)
 Associate Professor
 Research Associate (–March '02)²⁹⁾
 Research Associate (June '02–)
 IMS Fellow (April '02–)
 Graduate Student

Nano-scale Photoscience

TSUKUDA, Tatsuya
 MURAYAMA, Haruno

Associate Professor
 IMS Fellow (April '02–)

Interface Molecular Science

KOMIYAMA, Masaharu
 OKUDAIRA, Koji
 TAKASHIMA, Yoshifumi
 KUBOZONO, Yoshihiro
 MATSUMOTO, Taki
 YOSHIMURA, Daisuke
 LI, Yan Jun
 KANBARA, Takayoshi

 TAKABAYASHI, Yasuhiro
 YAMANE, Hiroyuki
 YOKOYAMA, Takahiro
 KIYOHARA, Kohei

Professor
 Associate Professor
 Research Associate
 Research Associate
 IMS Fellow
 Research Fellow
 Research Fellow
 Graduate Student (from Okayama University)* (–March '02)
 Graduate Student (from Okayama University)*
 Graduate Student (from Chiba University)*
 Graduate Student (from Nagoya University)*
 Graduate Student (from Shimane University)* (April '02–)

Molecular Clusters

TANIMOTO, Yoshifumi
 ISHIDA, Toshimasa
 FUJIWARA, Masao

Professor (April '02–)
 Associate Professor (April '02–)
 Research Associate (April '02–)

OBA, Toru
UECHI, Ichiro

HANASAKI, Mitsuru

FUJIWARA, Umihito

Research Associate (April '02–)

Graduate Student (from Hiroshima University)* (April '02–)

Graduate Student (from Utsunomiya University)* (April '02–)

Graduate Student (from Utsunomiya University)* (April '02–)

Equipment Development Center

YAKUSHI, Kyuya
WATANABE, Michio

Director

Associate Professor

Ultraviolet Synchrotron Orbital Radiation Facility

KOSUGI, Nobuhiro

KAMADA, Masao

KATOH, Masahiro

SHIGEMASA, Eiji

KIMURA, Shin-ichi

HORI, Yo-ichiro

Director

Associate Professor (–September '01)³⁰⁾

Associate Professor

Associate Professor

Associate Professor (April '02–)

Visiting Associate Professor (from Institute of Materials Structure Science)

Research Associate

Research Associate

Research Associate

Research Associate

JSPS Post-Doctoral Fellow

Graduate Student

Graduate Student (from Kobe University)* (April '02–)

HOSAKA, Masahito

GEJO, Tatsuo

TAKAHASHI, Kazutoshi

MOCHIHASHI, Akira

AZUMA, Junpei

TANAKA, Senku

NISHI, Tatsuhiko

Computer Center

HIRATA, Fumio

OKAZAKI, Susumu

AOYAGI, Mutsumi

NANBU, Shinkoh

OONO, Hitoshi

MIURA, Shin-ichi

MINAMINO, Satoshi

MAKI, Jun

IWAHASHI, Kensuke

OKADA, Kazutoshi

KINOSHITA, Tomoko

MIKAMI, Taiji

SATO, Masahiro

KOMATSU, Takahiro

TANAKA, Junji

NAGATA, Takeshi

Director

Professor (October '01–)

Associate Professor (–March '02), Professor (from Kyushu University) (April '02–)

Research Associate

Research Associate

Research Associate (July '02–)

Technical Associate

IMS Fellow

IMS Fellow (Jun '02–)

Post-Doctoral Fellow (–November '01)

Graduate Student

Graduate Student (from Tokyo Institute of Technology)* (October '01–)

Graduate Student (from Tokyo Institute of Technology)* (October '01–)

Graduate Student (from Tokyo Institute of Technology)* (April '02–)

Graduate Student (from Tokyo Institute of Technology)* (April '02–)

Graduate Student (from Hiroshima Univ.)* (April '02–)

Research Facility of Okazaki National Research Institutes

Center for Integrative Bioscience

Department of Strategic Methodology

KINOSITA, Kazuhiko, Jr.

AONO, Shigetoshi

WATANABE, Yoshihito

FUJII, Hiroshi

YOSHIOKA, Shiro

ALI, Md. Yusuf

MAKI, Yasushi

SHIMO, Rieko

ADACHI, Kengo

NAKAI, Hidetaka

Professor

Professor (May '02–)

Professor (–March '02)³¹⁾

Associate Professor

IMS Fellow (–March '02)³²⁾

JSPS Post-Doctoral Fellow

Post-Doctoral Fellow

Post-Doctoral Fellow

Post-Doctoral Fellow

Research Fellow (–March '02)³³⁾

YOGO, Katsunori
KAWASHIMA, Keisuke
SAKAKI, Naoyoshi
ONOUE, Yasuhiro

Graduate Student (from Waseda University)
Graduate Student (from Keio University) (–March '02)³⁴⁾
Graduate Student (from Keio University)
Graduate Student (from Keio University) (April '02–)

Department of Bio-environmental Science

KITAGAWA, Teizo
YAMATO, Takehisa

UCHIDA, Takeshi
UENO, Takafumi
NAGATOMO, Shigenori
HIRAMATSU, Hirotsugu
HARUTA, Nami
OHTA, Takehiro
NAGANO, Yasutomo
GOSSE, Charlie
OKUNO, Daichi
SATO, Akira

Professor
Visiting Associate professor (from Nagoya University)
(April '02–)
Research Associate (November '01–)
Research Associate (–March '02)³¹⁾
Technical Associate
IMS Fellow (April '02–)
IMS Fellow (–March '02)
JSPS Post-Doctoral Fellow (April '02–)
JSPS Post-Doctoral Fellow (April '02–)
JSPS Post-Doctoral Fellow
Graduate Student
Graduate Student

* Carries out graduate research of IMS on Cooperative Education Program of IMS with other graduate schools.

Technical Staff

SAKAI, Kusuo	Technical Division Head
MATSUDO, Osamu	Technical Section Chief
KATO, Kiyonori	Technical Section Chief
NISHIMOTO, Fumio	Technical Section Chief (–June '02)
YAMANAKA, Takaya	Technical Section Chief
NAKAMURA, Eiken	Electronic Structure (Unit Chief)
YOSHIDA, Hisashi	Molecular Assemblies (Unit Chief)
YAMAZAKI, Jun-ichiro	Laser Research Center for Molecular Science (Unit Chief)
UEDA, Tadashi	Laser Research Center for Molecular Science
NAGATA, Masaaki	Research Center for Molecular-scale Nanoscience (Unit Chief)
TAKAYAMA, Takashi	Research Center for Molecular-scale Nanoscience (Unit Chief)
SAKAI, Masahiro	Research Center for Molecular-scale Nanoscience
MAKITA, Seiji	Research Center for Molecular-scale Nanoscience
MIZUTANI, Nobuo	Equipment Development Center (Unit Chief)
SUZUI, Mitsukazu	Equipment Development Center (Unit Chief)
UCHIYAMA, Kouichi	Equipment Development Center
TOYODA, Tomonori	Equipment Development Center
YANO, Takayuki	Equipment Development Center
MATSUSHITA, Koji	Equipment Development Center
HASUMOTO, Masami	UVSOR facility (Unit Chief)
KONDOU, Naonori	UVSOR facility
HAYASHI, Kenji	UVSOR facility
MIZUTANI, Fumiyasu	Computer Center (Unit Chief)
TESHIMA, Fumitsuna	Computer Center
NAITOU, Shigeki	Computer Center

List of Present Addresses

- 1) Laboratory of Supermolecular structure, Department of Structural Biology, Institute of Molecular and Cellular Biosciences, The University of Tokyo, 1-1-1 Yayoi, Bunkyo-ku, Tokyo 113-0032
- 2) Laboratory of Gene-product Informatics, National Institute of Genetics, Yata 1111, Mishima, Shizuoka 411-8540
- 3) National Institute of Advanced Industrial Science and Technology (AIST), AIST Tsukuba Central 1, Tsukuba, Ibaraki 305-8561
- 4) Department of Molecular Design and Engineering, Graduate School of Engineering, Nagoya University, Chikusa, Nagoya 464-8603
- 5) Department of Chemistry and Biochemistry, Texas Tech University, Box 41061, Lubbock, TX 79409-1061, USA
- 6) Laboratoire de Chimie Theorique, Faculte des Sciences, Universite de Sherbrooke, Sherbrooke, Quebec J1K 2R1, Canada
- 7) University of Florida, 2332 New Physics Building, PO Box 118435, Gainesville, FL 32611-8435, USA
- 8) Quantum Molecular Science and Technology, Department of Molecular Engineering, Graduate School of Engineering, Kyoto University, Yoshidahon-machi, Sakyo, Kyoto 606-8501
- 9) Department of Knowledge-based Information Engineering, Faculty of Engineering, Toyohashi University of Technology, 1-1, Hibarigaoka, Tenpaku, Toyohashi 441-8580
- 10) Dept. of Biochemistry, Univ. of Wisconsin-Madison, 433 Babcock Drive, Madison, Wisconsin 53706, USA
- 11) Laboratory of Electronic Structure, Research Institute for Electronic Science, Hokkaido University, Kita, Kita-ku, Sapporo 060-0812
- 12) Division of Organic Synthesis, Institute for Fundamental Research of Organic Chemistry, Kyushu University, 6-10-1 Hakozaki, Higashi-ku, Fukuoka 812-8581
- 13) Material Engineering Laboratory, National Institute for Material Science, 1-2-1 Sengen, Tsukuba 305-0047
- 14) Department of Chemistry, Faculty of Science, Kyushu University, 6-10-1, Hakosaki, Higashi-ku, Fukuoka 812-8581
- 15) Material and Life Science, Graduate School of Engineering, Osaka University, 2-1, Yamadaoka, Suita, Osaka 565-0871
- 16) Kyoto University
- 17) RIKEN
- 18) Graduate Student of Okayama University, Okayama 700-8530
- 19) Interface Molecular Science, IMS

- 20) Department of Chemistry and Biochemistry Campus Box 215 University of Colorado Boulder, CO 80309 USA
- 21) Department of physics, Henan University 85 Ming Lun Street, Kaifeng, Henan, 475001, P.R. China
- 22) Department of Biological Science and Medical Engineering Southeast University Nanjing 210096, P.R. China
- 23) Phys. Chem. III Darmstadt University of Technology Petersenstr.20 D-64287 Darmstadt, Germany
- 24) Department of Physics The Florida State University Tallahassee, FL 32306 USA
- 25) D20-26, Adayar Avenue, IIT Campus, Chennai 600 036, India
- 26) Department of Chemistry, University of Chicago, 5735 S. Ellis Ave, Chicago, Illinois 60637 USA
- 27) Center for Instrumental Analysis, the University of Electro-Communications, 1-5-1 Chofugaoka, Chofu 182-8585
- 28) Department of Electrical Engineering, Princeton University, Princeton, NJ 08544, USA
- 29) Department of Chemistry, Faculty of Science, Hokkaido University, Nishi 8-chome, Kita 10-jo, Kita-ku, Sapporo 060-0810
- 30) Synchrotron Light Application Center, Saga University, 1 Honjyo-cho, Saga 840-8502
- 31) Department of Chemistry, Nagoya University, Nagoya 464-8602
- 32) Center in Molecular Toxicology, Vanderbilt University, Nashville, TN 37232-0146, USA
- 33) Department of Chemistry & Biochemistry, University of California, San Diego, La Jolla, CA 92093-0358, USA
- 34) FUJI PHOTO FILM Co., Ltd.

COUNCIL

KAYA, Koji

Director-General

Councillors

Chairperson	HOSOYA, Haruo	Professor Emeritus, Ochanomizu University
Vice-Chairperson	HIROTA, Noboru	Professor Emeritus, Kyoto University
	ARIKAWA, Yoshiko	Professor, Japan Women's University
	IYOSHI, Atsuo	President, Chubu University
	ISHITANI, Akira	Executive Director, Kanagawa Academy of Science and Technology
	OHTSUKA, Eiko	Fellow, National Institute of Advanced Industrial Science & Technology
	OGINO, Hiroshi	Director, Miyagi Study Center of the University of the Air
	KAIFU, Norio	Director General, National Astronomical Observatory of Japan
	KIMURA, Yoshitaka	Director, Institute of Materials Structure Science, High Energy Accelerator Research Organization
	KYOGOKU, Yoshimasa	Director, Biological Information Research Center, National Institute of Advanced Industrial Science and Technology
	GOTO, Keishi	Former President, Toyohashi University of Technology
	KONDOW, Tamotsu	Visiting Professor, Toyota Technological Institute, Cluster Research Laboratory
	SAHARA, Makoto	Director-General, National Museum of Japanese History
	TAKAHASHI, Riichi	President and Chief Operating Officer, Toyota Central Research & Development Laboratories, Inc.
	TSUCHIYA, Soji	Visiting Professor, Advanced Research Institute for Science and Engineering, Waseda University
	FUKUYAMA, Hidetoshi	Director, The Institute for Solid State Physics, University of Tokyo
	YAMAZAKI, Toshimitsu	Contract Resercher, RI Beam Science Laboratory, RIKEN
	YAMAMURA, Shosuke	Professor Emeritus, Keio University
	BRADSHAW, Alexander M.	Scientific Director, Max-Planck Institute for Plasma Physics
	LINEBERGER, William C.	Professor, University of Colorado

The Council is the advisory board for the Director-General.

* Two of the councillors are selected among distinguished foreign scientists.

Distinguished Research Consultants

NAGAKURA, Saburo	President, The Kanagawa Academy of Science and Technology
INOKUCHI, Hiroo	Chief Scientist of Space Utilization Research Program, National Space Development Agency of Japan
TSUCHIYA, Soji	Visiting Professor, Waseda University
ITO, Mitsuo	Professor Emeritus, Institute for Molecular Science, The Graduate University for Advanced Studies, Tohoku University
HIROTA, Noboru	Professor Emeritus, Kyoto University
KONDOW, Tamotsu	Visiting Professor, Toyota Technological Institute

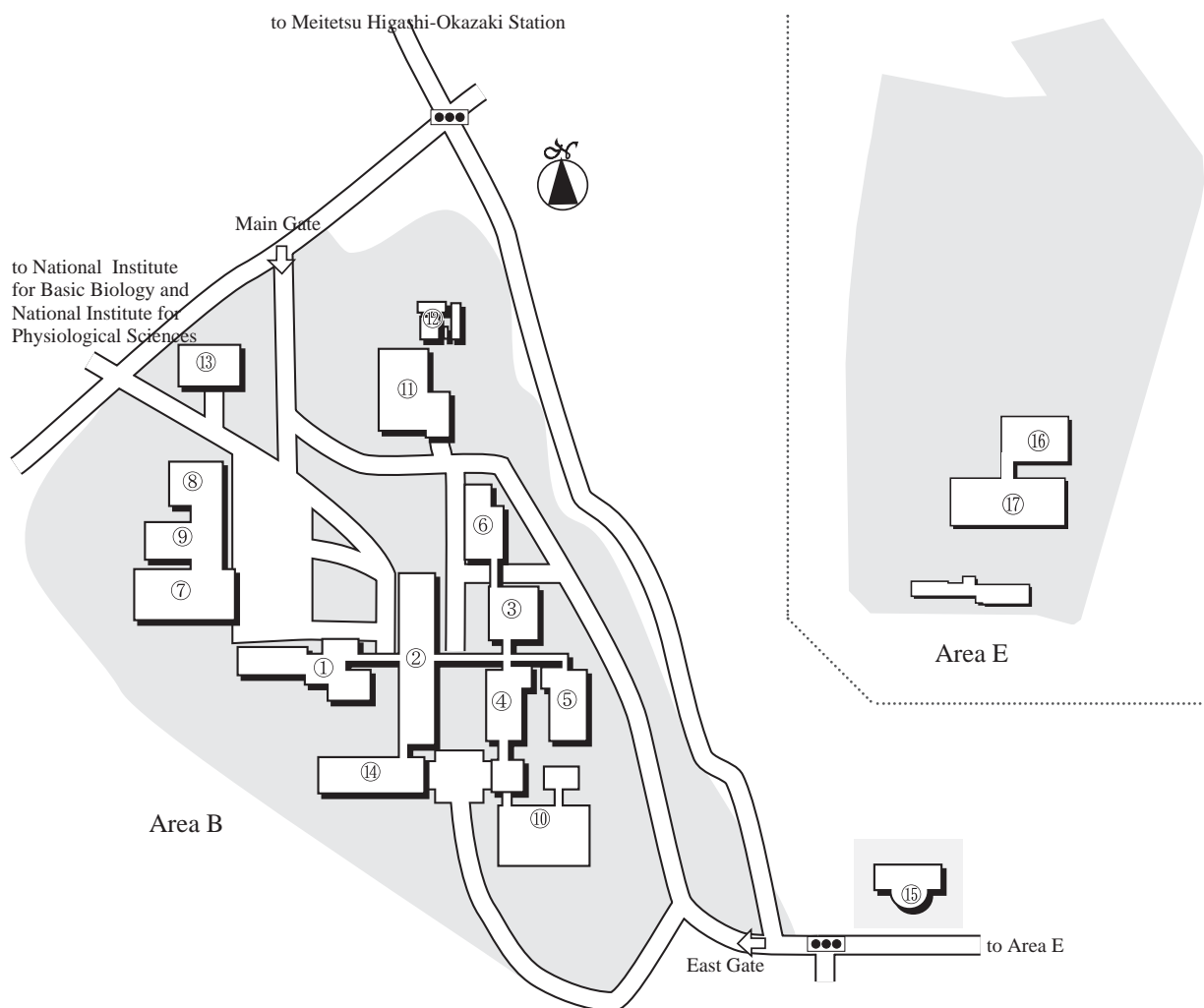
Administration Bureau

KAMADA, Tohru	Director-General, Administration Bureau (–March '02)
MORISHIGE, Kazuko	Director-General, Administration Bureau (April '02–)
SUNADA, Hitoshi	Director, General Affairs Department
YUUKI, Yoshihisa	Director, Finance and Facilities Department
OYAMA, Takuya	Head, General Affairs Division (–June '02)
FURUKAWA, Masato	Head, General Affairs Division (April '02–)
UCHIDA, Yoshio	Head, Personnel Division
HAYASHI, Masanori	Head, Research Cooperation Division (–June '02)
NAGINO, Tomoe	Head, Research Cooperation Division (August '02–)
KITAGAWA, Hiroshi	Head, International Affairs Division
HIRAI, Tokio	Head, Budget Division
YUUKI, Masanori	Head, Accounts Division (–December '01)
KUBOKAWA, Tomoyuki	Head, Accounts Division (January '02–)
KATOH, Masayoshi	Head, Construction Division
SATO, Hisashi	Head, Equipment Division (–March '02)
FUJIMOTO, Shigeo	Head, Equipment Division (April '02–)

BUILDINGS AND CAMPUS

The IMS campus covering 62,343 m² is located on a low hill in the middle of Okazaki city. The inequality in the surface of the hill and growing trees are preserved as much as possible, and low-storied buildings are adopted for conservation of the environment. The buildings of IMS are separated according to their functions as shown in the map. The Research Office Building and all Research Facilities except for the Computer Center are linked organically to the Main Laboratory Buildings by corridors. Computer Center, Library and Administration Buildings are situated between IMS and neighboring National Institute for Basic Biology and National Institute for Physiological Sciences, because the latter two facilities are common to these three institutes.

The lodging facility of IMS called Yamate Lodge, located within ten minutes' walk, has sleeping accommodations for 15 guests and two families. Mishima Lodge, located within four minutes' walk east of IMS can accommodate 74 guests and 20 families. Scientists who visit IMS as well as the two other institutes can make use of these facilities. Foreign visiting scientists can also live at these lodgings with their families during their stays. The Okazaki Conference Center, which has four conference rooms capable of between 50 and 250 attendance, was built in April, 1997 in Mishima area. Two buildings for Center for Integrative Bioscience, Research Center for Computational Science, and research facilities of ONRI were built in February, 2002 in Area E.



- | | |
|--|--|
| 1. Research Office Building | 10. UVSOR Facility |
| 2. Main Laboratory Building | 11. Power Station |
| 3. Equipment Development Center | 12. Waste-Water Disposition Facilities |
| 4. Laser Research Center for Molecular Science | 13. Faculty Club |
| 5. Research Center for Molecular-scale Nanoscience | 14. South Laboratory Building |
| 6. Low-Temperature Facilities Building | 15. Okazaki Conference Center |
| 7. Computer Center | 16. Center for Integrative Bioscience and Research
Center for Computational Science |
| 8. Library | 17. Research Facilities of ONRI |
| 9. Central Administration | |



Okazaki (population 347,000) is 260 km west of Tokyo, and can be reached by train in about 3 hours from Tokyo via Shinkansen and Meitetsu Line.
The nearest large city is Nagoya, about 40 km northwest of Okazaki.



RESEARCH ACTIVITIES I

Department of Theoretical Studies

I-A Theoretical Study and Design of New Bonding, Structures, and Reactions

It is an important subject to develop molecules with novel bonding and structures. Thus, multiple bonds between heavier atoms are investigated which are the focus of interest as new building block for molecular design. In addition, large cage-like molecules and clusters are investigated to characterize guest-host interactions, which serve as molecular containers and recognition. To develop new reactions, the catalytic reactions of enzymes are investigated. A theoretical method to predict molecular crystal structures is in progress.

I-A-1 A Silicon-Silicon Triple Bond Surrounded by Bulky Terphenyl Groups

TAKAGI, Nozomi; NAGASE, Shigeru

[*Chem. Lett.* 966 (2001)]

Since the first synthesis in 1981, a number of stable silicon-silicon doubly bonded compounds have been synthesized and isolated. However, stable silicon-silicon triply bonded compounds, disilynes ($RSi\equiv SiR$), are still unknown, which are the focus of interest in silicon chemistry. In search of an isolable disilyne, effects of bulky terphenyl groups on silicon-silicon triple bonding are investigated. It is predicted that $Ar^*Si\equiv SiAr^*$ ($Ar^* = 2,6$ -bis(2,4,6-triisopropylphenyl)phenyl) is an interesting synthetic target.

I-A-2 The Quest of Stable Silanones: Substituent Effects

KIMURA, Masahiro; NAGASE, Shigeru

[*Chem. Lett.* 1098 (2001)]

Recent remarkable progress in the heavier analogues of ketones is marked by the isolation of silanethione ($R_2Si=S$) and silaneselone ($R_2Si=Se$). As the member of this family, however, isolable silanones ($R_2Si=O$) are still missing except for the transient intermediates and spectroscopic detection, because of the high reactivities due to the polarized $Si^{\delta+}=O^{\delta-}$ bond. DFT and ONIOM calculations are systematically carried out to suppress the high reactivities. Several isolable silanones are predicted, which are worthy of experimental testing.

I-A-3 Substituent Effects on Germanium-Germanium and Tin-Tin Triple Bonds

TAKAGI, Nozomi; NAGASE, Shigeru

[*Organometallics* 20, 5498 (2001)]

Triple bonds between heavier main group elements are of widespread interest. We have suggested that disilynes ($RSi\equiv SiR$) are a viable synthetic target when they bear proper bulky substituents [*Organometallics*

20, 234 (2001)]. It is an important question whether the still heavier analogues are also synthetically accessible and isolable as stable molecules. Effects of bulky aryl groups such as $C_6H_2-2,4,6-\{CH(SiMe_3)_2\}_3$ and $C_6H_3-2,6-(C_6H_2-2,4,6-i-Pr_3)_2$ on germanium-germanium and tin-tin triple bonds are theoretically investigated in search of isolable digermynes ($RGe\equiv GeR$) and distannynes ($RSn\equiv SnR$).

I-A-4 Theoretical Study of an Isolable Compound with a Short Silicon-Silicon Triple Bond; $(tBu_3Si)_2MeSiSi\equiv SiSiMe(Si^tBu_3)_2$

TAKAGI, Nozomi; NAGASE, Shigeru

[*Eur. J. Inorg. Chem.* 2775 (2002)]

According to our theoretical investigations [*J. Organomet. Chem.* 611, 264 (2000)], electropositive silyl groups are electronically more effective than aryl groups in realizing a less trans-bent disilyne with a short silicon-silicon triple bond. However, it has been found that silyl groups such as Si^tBu_3 and $SiDep_3$ ($Dep = 2,6$ -diethylphenyl) are not sufficiently bulky to make disilynes isolable under normal conditions. Therefore, the effects of a very bulky silyl group, $R^{**} = SiMe(Si^tBu_3)_2$, on silicon-silicon triple bonding are investigated using density functional theory. It is found that $R^{**}Si\equiv SiR^{**}$ is stable enough to be isolable and has a silicon-silicon triple bond that is as short as 2.072 Å.

I-A-5 Interesting Compounds Featuring Double Bonding between Heavier Group 15 Elements

SASAMORI, Takahiro¹; TAKEDA, Nobuhiro¹; TOKITOH, Norihiro¹; OKAZAKI, Renji³; KIMURA, Masahiro; NAGASE, Shigeru
(¹Kyoto Univ.; ²Japan Women's Univ.)

[*Angew. Chem. Int. Ed.* 41, 139 (2002)]

[*Bull. Chem. Soc. Jpn.* 75, 661 (2002)]

Distibene ($RSb=SbR$), dibismuthene ($RBi=BiR$), and phosphabismutene ($RP=BiR$) have been synthesized by taking advantage of steric protection using an efficient steric protection group, $C_6H_2-2,4,6-\{CH(SiMe_3)_2\}_3$, as the first examples of double bonds to fifth-row and six-

row elements in group 15. The structural features are investigated using density functional theory by changing the substituent groups.

I-A-6 The First Halogen-Substituted Cyclotrimerenes: A Unique Halogen Walk over the Three-Membered Skeleton and Facial Stereoselectivity in the Diels-Alder Reaction

SEKIGUCHI, Akira¹; ISHIDA, Yutaka¹; FUKAYA, Norihisa¹; ICHINOHE, Masaki¹; TAKAGI, Nozomi; NAGASE, Shigeru
(¹Univ. Tsukuba)

[*J. Am. Chem. Soc.* **124**, 1158 (2002)]

Unsaturated three-membered ring compounds consisting of heavier group 14 elements, cyclotrimetallenes, have attracted considerable attention because of their unique structures; the chemistry has developed very rapidly. However, the heteroatom-substituted cyclotrimetallenes are unknown because of the synthetic difficulty and instability. By introducing electronegative halogen atoms, the first hetero-substituted cyclotrimerenes are synthesized and the structural features are theoretically investigated. The interaction between the low-lying σ^* (Ge-halogen) and high-lying endocyclic π (Ge=Ge) orbitals play an important role.

I-A-7 Effects of the σ^* Orbital of C-Apical O-Equatorial Spirophosphoranes on the Structure, Stereomutation, and Reactivity

AKIBA, Kin-ya¹; MATSUKAWA, Shiro²; ADACHI, Takahiro²; YAMAMOTO, Yohsuke²; RE, Suyong; NAGASE, Shigeru
(¹Waseda Univ.; ²Hiroshima Univ.)

[*Phosphorus, Sulfur Silicon Relat. Elem.* **177**, 1671 (2002)]

[*J. Am. Chem. Soc.* **124**, 13154 (2002)]

Interesting effects of the σ^* orbital of C-apical O-equatorial (O-*cis*) spirophosphoranes are investigated from theoretical and experimental points of view. It is experimentally found that O-*cis* phosphoranes are much more electrophilic on the phosphorus atom than the O-*trans* isomers. It is calculated that the $\sigma^*_{\text{P-O}}$ orbital level of O-*cis* phosphoranes is 19 kcal/mol lower than the $\sigma^*_{\text{P-C}}$ orbital level of O-*trans* phosphoranes. The low-lying σ^* orbital plays an important role in enhancing the electrophilicity of spirophosphoranes.

I-A-8 Theoretical Calculations of Vibrational Modes in Endohedral Metallofullerenes: La@C₈₂ and Sc₂@C₈₄

KOBAYASHI, Kaoru; NAGASE, Shigeru

[*Mol. Phys.* in press]

The electronic properties and reactivities of endohedral metallofullerenes have been extensively investigated both theoretically and experimentally. The metal

motion and cage structure are currently of considerable interest in the far-infrared and Raman spectroscopic study. Thus, theoretical calculations are performed for the representative metallofullerenes, La@C₈₂ and Sc₂@C₈₄, to provide insight into the metal-cage vibrational modes as well as cage structures. The La-based vibrational modes and wave numbers calculated for La@C₈₂ are in good agreement with those assigned experimentally. An interesting finding is that the vibrational frequencies are little changed upon reduction or oxidation. The Sc-based vibrations calculated for Sc₂@C₈₄ are also compared with the available experimental data. In addition, the structures of the Sc₂@C₈₄ isomers are discussed.

I-A-9 A Stable Unconventional Structure of Sc₂@C₆₆ Found by Density Functional Calculations

KOBAYASHI, Kaoru; NAGASE, Shigeru

[*Chem. Phys. Lett.* **362**, 373 (2002)]

In 1997 we predicted that the isolated pentagon rule (IPR) established in fullerene chemistry could be violated by metal-mediated interactions [*J. Am. Chem. Soc.* **119**, 12693 (1997)]. In this context, the recent isolation of Sc₂@C₆₆ and Sc₃N@C₆₈ is noteworthy because there is no IPR-satisfying isomer between C₆₀ and C₇₀. The cage structure and metal position of Sc₂@C₆₆ are theoretically determined. Interestingly, the endohedral C_{2v} structure determined by MEM/Rietveld analysis of the X-ray powder data [*Nature* **408**, 426 (2000)] does not correspond to an energy minimum but collapses with no barrier. Instead, a much more stable C_{2v} structure with two pairs of three-fold fused pentagons is found, which satisfies the observed ¹³C NMR spectrum. Two Sc atoms are highly stabilized in the non-classical C₆₆ cage by electrostatic interactions induced by electron transfer from Sc to C₆₆.

I-A-10 Theoretical Study of the Cations and Anions of La₂@C₈₀ and Sc₃N@C₈₀

MAYER, Bodo¹; KOBAYASHI, Kaoru; NAGASE, Shigeru
(¹IMS and TU-Darmstadt)

Theoretical calculations are performed for the neutral, anionic, and cationic states of La₂@C₈₀ and Sc₃N@C₈₀. It is found that added electrons are localized on the encapsulated metal atoms while electron removal takes place from the carbon cage. As the number of added electrons increases, the spherical carbon cage transforms to an ellipsoid structure and the metal positions is changed. The electron density difference maps reveal the important changes in electronic structures upon reduction and oxidation.

I-A-11 Theoretical Identification of the Structures of C₂₀: Prevalence of the Monocyclic Isomer and Existences of the Smallest Fullerene and Bowl Isomers

LU, Jing¹; RE, Suyong; CHOE, Yoong-Kee; NAGASE, Shigeru; ZHOU, Yunsong²; HAN, Rushan²; PENG, Lianmao²; ZHANG, Xinwei²; ZHAO, Xiangeng²
(¹IMS and Peking Univ.; ²Peking Univ.)

[*Phys. Rev. B* submitted]

Free energies, electron affinities and vibrational modes of C₂₀ isomers are theoretically investigated. The major C₂₀ isomer generated by vaporizing graphite has a monocyclic ring, followed by a tadpole (a short chain attached to a monocyclic ring), chain, and a bicyclic ring. On the other hand, the two C₂₀ isomers synthesized recently [*Nature* **407**, 60 (2000)] have fullerene and bowl structures.

I-A-12 The Size of Silicon Clusters Suitable for Endohedral Metal-Doping

LU, Jing¹; NAGASE, Shigeru
(¹IMS and Peking Univ.)

Structures and electronic properties of metal-doped silicon clusters MSi_n (M = W, Zr, Os, Pt, and Co; n = 8–20) are theoretically investigated. In contrast to a recent experiment [*Phys. Rev. Lett.* **86**, 1733 (2001)] suggesting that a metal atom is encapsulated inside the Si_n cluster, formation of endohedral structures depends strongly on the size of silicon clusters. In addition, several novel stable endohedral structures are found. The size of stable endohedral forms is predicted to be in the range 10 ≤ n ≤ 16.

I-A-13 What is the Smallest Metal-Encapsulated Germanium Clusters?

LU, Jing¹; NAGASE, Shigeru
(¹IMS and Peking Univ.)

Metal-doped germanium clusters MGe_n (M = Hf, W, Os, Ni, and Zn) are investigated using density functional calculations. The smallest metal-encapsulated germanium cluster contain 13 germanium atoms and takes a distorted hexagonal prism structure (W@Ge₁₂ and Os@Ge₁₂). These size and shape differ from those of the smallest metal-encapsulated silicon cluster that contains 11 silicon atoms and has a basketlike structure. The stable ZnGe₁₂ structure is exohedral, although an endohedral icosahedral structure is suggested in a recent theoretical study [*Appl. Phys. Lett.* **80**, 859 (2002)].

I-A-14 Host-Guest Interaction in Molecular Capsule Formation

RE, Suyong; NAGASE, Shigeru

It is of current synthetic interest to develop functional molecular capsules. Carceplex is a complex in which guest molecules are entrapped by a container host molecule. Although it is known that guest molecules act as a template, the encapsulation mechanism is not fully understood. Small changes in the size and shape of guest molecules lead to remarkable changes in the yield

of carceplex. Since the efficient synthesis of carceplex depends strongly on the type of guest molecules, host-guest interactions are systematically investigated by theoretical calculations to reveal the details of formation mechanism.

I-A-15 Does the Axial Ligand of Iron (IV)-Oxo-Porphyrin Affect the Reactivity of Cytochrome P450?

CHOE, Yoong-Kee; NAGASE, Shigeru

Hemoenzymes play versatile roles in living organisms. However, the origin of their various functions has not been fully understood. Among these, alkane hydroxylation by cytochrome P450 has been a subject of intense studies because the reaction intermediates have not been captured experimentally. It has been considered that the coordination of cysteine to heme is responsible for the catalytic action of cytochrome P450. However, there has been much debate on the role of the axial cysteine ligand. Therefore, density functional calculations have been carried out to investigate the roles of the axial cysteine ligand of the iron (IV)-oxo-porphyrin intermediate (compound I) that is generated in the alkane hydroxylation catalyzed by cytochrome P450. The ligand effects are compared with those in enzymes such as tyrosine and histidine.

I-A-16 A Nonspectroscopic Method to Determine the Photolytic Decomposition Pathways of 3-Chloro-3-Alkyldiazirine; Carbene, Diazo and Rearrangement in Excited State

WAKAHARA, Takatsugu¹; NIINO, Yasuyuki²; KATO, Takashi²; MAEDA, Yutaka¹; AKASAKA, Takeshi¹; LIU, Michael T. H.³; KOBAYASHI, Kaoru; NAGASE, Shigeru
(¹Univ. Tsukuba; ²Niigata Univ.; ³Univ. Prince Edward Island)

[*J. Am. Chem. Soc.* **124**, 9465 (2002)]

The C₆₀ fullerene acts as a mechanistic probe for the formation of carbene, diazo compound, and for the rearranged product via the excited state in the photolysis of 3-chloro-3-isopropyl-diazirine and 3-chloro-3-chloromethyldiazirine. The carbene adds to C₆₀ to form methanofullerene, whereas the diazo compound adds to C₆₀ to form fulleroid. The olefin product arises as a result of the rearrangement in the excited state

I-A-17 Prediction of Molecular Crystal Structures by an Ab Initio Pair Potential Method

NAGAYOSHI, Kanade¹; KITAURA, Kazuo²; NAGASE, Shigeru
(¹IMS and Osaka Prefecture Univ.; ²AIST)

It is an important subject to predict the structures of molecular crystals from the component molecules. Therefore, several methods have been suggested to predict crystal structures using empirical atom-atom

potentials. However, these empirical methods are not sufficiently reliable to be widely applicable. Instead, we developed an efficient method to predict lattice constants using ab initio pair potentials. It is the advantage that lattice constants can be calculated without empirical parameters, even if crystals contain any atoms. To realize high-speed calculations, a parallel computing program is developed on PC clusters.

I-B Prediction of Protein Tertiary Structures from the First Principles

Prediction of the three-dimensional structures of protein molecules by computer simulations is a very challenging problem in theoretical molecular science. The difficulty of the problem lies in two facts: (1) the inclusion of accurate solvent effects is non-trivial and time-consuming (2) there exist a huge number of local minima in the energy function, forcing conventional simulations to get trapped in states of energy local minima. We have been exploring the strategies that allow us to overcome these difficulties.

I-B-1 Replica-Exchange Monte Carlo Simulation of a Small Peptide in Aqueous Solution Based on the RISM Theory

mitsutake, Ayori¹; KINOSHITA, Masahiro²; OKAMOTO, Yuko; HIRATA, Fumio
(¹Keio Univ.; ²Kyoto Univ.)

We performed a replica-exchange Monte Carlo simulation of a penta peptide, Met-enkephalin, in aqueous solution that is based on the reference interaction site model (RISM) theory. The RISM theory has been developed from the statistical mechanics of molecular liquids and can calculate the solvation free energy of solute molecules, which depends on temperature. When the total energy depends on temperature, we need to modify the transition probability of replica-exchange process in replica-exchange Monte Carlo simulation. In this paper, we give the formula for the modification of this transition probability and present the results of this simulation.

I-B-2 Comparison of AMBER, CHARMM, OPLS, and GROMOS Force Fields by Generalized-Ensemble Simulations

YODA, Takao; SUGITA, Yuji¹; OKAMOTO, Yuko
(¹Univ. Tokyo)

In order to succeed in the prediction of protein tertiary structures from the first principles, it is essential that we have an accurate potential energy function, or force field, for the protein system. Commonly used force fields are AMBER, CHARMM, OPLS-AA, and GROMOS. In the present work we try to compare these force fields. Our criterion for good force fields is whether or not molecular simulations of short peptide systems in explicit water can reproduce experimental implications of secondary structure formations such as α -helix and β -hairpin, starting from completely random initial conformations. For this purpose it is very important that we use a powerful simulation algorithm that can avoid getting trapped in states of energy local minima. Generalized-ensemble algorithms are such powerful algorithms. In particular, we use our new generalized-ensemble algorithms, replica-exchange multicanonical algorithm and multicanonical replica-exchange method. Indeed we found very different results depending on the force fields; some contradict with the experiments.

I-C Development of Simulation Algorithms for Complex Systems

Developing a powerful simulation algorithm that can alleviate the multiple-minima problem is important in many complex systems. We have been advocating the uses of the so-called generalized-ensemble algorithms such as multicanonical algorithm and replica-exchange method.

I-C-1 An Application of the Multicanonical Monte Carlo Method to the Bulk Water System

MUGURUMA, Chizuru¹; OKAMOTO, Yuko; MIKAMI, Masuhiro²
(¹Chukyo Univ.; ²AIST)

[submitted for publication]

The multicanonical algorithm is based on a non-Boltzmann weight factor and produces flat probability distribution of potential energy artificially. The method allows the system to rove through the complex potential

energy surface without getting trapped in a local minimum state, and has been proven to be efficient for studying first-order phase transitions of complex systems such as spin glasses and proteins. One of the features of the method is that the expectation values of thermodynamic properties can be calculated as a function of temperature by applying the histogram-reweighting techniques to the results of one production run. In the present study, we determined the multicanonical weight factor that can produce flat probability distribution of potential energy corresponding to the temperature range from 170 to 630 K. From the peak of the heat capacity, we found a phase transition at 190 K.

The lower energy structures and oxygen-oxygen radial distribution functions imply that the structure at lower temperatures is irregular. However, the average number of hydrogen bonds per water molecule is nearly equal to four at low temperatures, which suggests the formation of amorphous ice.

I-D Applications of the Zhu-Nakamura Theory to Electronically Nonadiabatic Chemical Reactions

I-D-1 Significant Improvement of the Trajectory Surface Hopping Method by the Zhu-Nakamura Theory

ZHU, Chaoyuan; KAMISAKA, Hideyuki¹;
NAKAMURA, Hiroki
(¹GUAS)

[*J. Chem. Phys.* **115**, 11036 (2001)]

By taking the three-dimensional $D^+ + H_2$ reaction system, the trajectory surface hopping method based on the Zhu-Nakamura theory is demonstrated to work much better than the old one and to be very promising to treat high-dimensional electronically nonadiabatic processes. The difference between the new and old survives even at high initial vibrational states and high energies.

I-D-2 New Implementation of the Trajectory Surface Hopping Method with Use of the Zhu-Nakamura Theory. II. Application to the Charge Transfer Processes in the 3D DH_2^+ System

ZHU, Chaoyuan; KAMISAKA, Hideyuki¹;
NAKAMURA, Hiroki
(¹GUAS)

[*J. Chem. Phys.* **116**, 3234 (2002)]

The newly implemented trajectory surface hopping (TSH) method for the collinear system with use of the Zhu-Nakamura semiclassical theory of nonadiabatic transition [C. Zhu, K. Nobusada, and H. Nakamura, *J. Chem. Phys.* **115**, 3031 (2001)] is extended to treat 3D nonadiabatic reactions. Since the avoided crossing seam becomes a two-dimensional surface in the 3D system, the nonadiabatic transition region and the possibility of classically forbidden hops are enlarged very much in

comparison with those in the collinear case. As a result, the contribution of the classically forbidden hops is quite a bit enhanced in the 3D system. Conservation of total angular momentum J is taken into account by slightly rotating the direction of momentum during the hop in the classically forbidden case. The method is tested by applying to the charge transfer processes in the 3D DH_2^+ system for $J = 0$. Numerical results clearly demonstrate that the new TSH method works very well at all energies and for all initial vibrational states considered compared to the old TSH method based on the Landau-Zener formula. The significant discrepancy between the two TSH methods survives even at high collision energy and high vibrational states in contrast to the collinear case, indicating the importance of the classically forbidden hops in 3D systems. The new TSH method is considered to be a very promising method to deal with high dimensional nonadiabatic dynamics. It should also be noted that the new TSH method does not require any knowledge of nonadiabatic coupling and is based only on adiabatic potentials.

I-D-3 Elucidations of Nonadiabatic Tunneling Type and Conical Intersection Type Reactions with Use of the Zhu-Nakamura Theory

ZHU, Chaoyuan; MIL'NIKOV, G. V.¹;
NAKAMURA, Hiroki
(¹IMS and Inst. Struct. Macrokinetics, Russia)

Based on the model 3D potential energy surfaces, electronically nonadiabatic chemical reaction dynamics are investigated with use of the Zhu-Nakamura theory. The trajectory surface hopping method and the IVR type semiclassical propagation method are employed. The dynamics are compared with the exact quantum computations and also with the usage of the Landau-Zener formula. It is aimed to develop a practically useful methodology applicable to multi-dimensional dynamics.

I-E Theory of Nonadiabatic Transitions

I-E-1 Nonadiabatic Transition: Concepts, Basic Theories and Applications

NAKAMURA, Hiroki

[*Nonadiabatic Transition: Concepts, Basic Theories and Applications* World Scientific / Imperial College Press; Singapore (2002)]

- Chapter 1 Introduction: What is "Nonadiabatic Transition" ?
- Chapter 2 Multi-Disciplinarity
- Chapter 3 Historical Survey of Theoretical Studies

- Chapter 4 Background Mathematics
- Chapter 5 Basic Two-State Theory for Time-Independent Processes
- Chapter 6 Basic Two-State Theory for Time-Dependent Processes
- Chapter 7 Two-State Problems
- Chapter 8 Effects of Dissipation and Fluctuation
- Chapter 9 Multi-Channel Problems
- Chapter 10 Multi-Dimensional Problems
- Chapter 11 Complete Reflection and Bound States in the Continuum
- Chapter 12 New Mechanism of Molecular Switching
- Chapter 13 Control of Nonadiabatic Processes by an

External Field

Chapter 14 Conclusions: Future Perspectives

Appendix A Final Recommended Formulas for General Time-Independent Two-Channel Problem

Appendix B Time-Dependent Version of the Zhu-Nakamura Theory

I-E-2 Semiclassical Theory of Nonadiabatic Transition and Tunneling**ZHU, Chaoyuan; MIL'NIKOV, G. V.¹; NAKAMURA, Hiroki***(¹IMS and Inst. Struct. Macrokinetics, Russia)**[Modern Trends in Chemical Reaction Dynamics K. Liu and X. Yang, Eds., Advanced Series in Physical Chemistry, World Scientific (2003)]*

1. Introduction
2. Zhu-Nakamura Theory
 - 2.1 Summary of the theory
 - 2.2 Landau-Zener type
 - 2.3 Nonadiabatic tunneling type
 - 2.4 Time-dependent version
 - 2.5 Other types of nonadiabatic transitions
3. Applications to Multi-Channel Problems
 - 3.1 Various problems and numerical applications

3.2 Control of molecular processes by external fields

4. Electronically Adiabatic Chemical Reactions

5. Electronically Nonadiabatic Chemical Reactions

5.1 New implementation of the TSH method by the Zhu-Nakamura theory

5.2 Charge transfer processes in the DH_2^+ system

6. Multi-Dimensional Tunneling

6.1 Three types of problems and effects of multi-dimensionality

6.2 Powerful theory for multi-dimensional tunneling

7. Future Perspectives

I-E-3 Analytical Solutions to Wave Packet Dynamics in a Laser Field**NAKAMURA, Hiroki**

Analytical solutions are obtained for the non-adiabatic transition between two linear potentials in coordinate space coupled by a time-dependent laser field within the framework of the dressed-state (or Floquet) representation. This can provide a basis for the analysis of wave packet dynamics in a chirped laser field.

I-F Quantum Dynamics of Chemical Reactions**I-F-1 Accurate Quantum Dynamics of Electronically Nonadiabatic Chemical Reaction in the DH_2^+ System****KAMISAKA, Hideyuki¹; BIAN, Wensheng; NOBUSADA, Katsuyuki²; NAKAMURA, Hiroki**
*(¹GUAS; ²Hokkaido Univ.)**[J. Chem. Phys. **116**, 654 (2002)]*

Three-dimensional accurate quantum dynamics calculations are carried out for the DH_2^+ system for $J = 0$ (J , total angular momentum quantum number) by the hyperspherical coordinate approach with use of the new potential energy surfaces constructed based on the recent *ab initio* quantum chemical calculations. Not only electronically nonadiabatic reactions, *i.e.*, reactive charge transfer processes, but also electronically adiabatic reactions and electronically nonadiabatic non-reactive processes are investigated. Because of the deep well on the electronically adiabatic ground surface, there appear a large number of resonances and the electronically adiabatic reactions are mostly statistical. Non-adiabatic transitions along the potential crossing seam cause deviations from the statistical behavior and some interesting dynamical features are found.

I-F-2 Chemical Reactions in the $\text{O}(^1D) + \text{HCl}$ System I. *Ab Initio* Global Potential Energy Surfaces for the $1^1A'$, $2^1A'$, and $1^1A''$ States**NANBU, Shinkoh; KAMISAKA, Hideyuki¹; BIAN, Wensheng; AOYAGI, Mutsumi²; TANAKA, Kiyoshi³; NAKAMURA, Hiroki**
*(¹GUAS; ²IMS and Kyushu Univ.; ³Hokkaido Univ.)**[J. Theor. Comp. Chem. in press]*

New global *ab initio* potential energy surfaces (PES) are presented for the low-lying $1^1A'$, $1^1A''$ and $2^1A'$ electronic states which are correlated to $\text{O}(^1D) + \text{HCl}$. These potential energy surfaces are computed by using the multi-reference configuration interaction method with the Davidson correction (MRCI+Q). The reference functions are constructed by the complete active space self-consistent field (CASSCF) calculations using the quadruple zeta + polarization basis set augmented with diffuse functions. The computations are carried out at about 5000 molecular conformations on each three-dimensional potential energy surface. The high accuracy of the computations is confirmed by a comparison with the available most accurate data for the ground state $1^1A'$; thus the present work is the first report of the accurate potential energy surfaces for the two excited states. Three low-lying transition states on the excited surfaces, two (TS2 and TS4) on $1^1A''$ and one (TS3) on $2^1A'$, are found. Since TS2 and TS3 are as low as 0.07 eV and 0.28 eV, respectively, and correlate to the $\text{OH}(^2\Pi) + \text{Cl}(^2P)$ product, these excited surfaces are expected to play quite important roles in the reaction dynamics. Possible effects of nonadiabatic couplings

among the three PESs are also briefly discussed, although the nonadiabatic couplings have not yet been estimated. The quantum reaction dynamics on these three PESs are discussed in the second accompanying paper.

I-F-3 Chemical Reactions in the O(1D) + HCl System II. Dynamics on the Ground $1^1A'$ State and Contributions of the Excited ($1^1A''$ and $2^1A'$) States

KAMISAKA, Hideyuki; NANBU, Shinkoh; BIAN, Wensheng; AOYAGI, Mutsumi¹; TANAKA, Kiyoshi²; NAKAMURA, Hiroki
(¹IMS and Kyushu Univ.; ²Hokkaido Univ.)

[*J. Theor. Comp. Chem.* in press]

Using the accurate global potential energy surfaces for the $1^1A'$, $1^1A''$, and $2^1A'$ states reported in the previous sister paper I, detailed quantum dynamics calculations are performed for these three adiabatic surfaces separately for $J = 0$ (J : total angular momentum quantum number). Overall reaction probabilities for $O + HCl \rightarrow OH + Cl$ and $H + ClO$, the branching ratio between the two reactions, effects of the initial rovibrational excitation, and product rovibrational distributions are evaluated in the total energy region $E_{tot} \leq 0.9$ eV. Significant contributions to the overall reaction dynamics are found from the two excited $1^1A''$ and $2^1A'$ potential energy surfaces, clearly indicating the insufficiency of the dynamics only on the found $1^1A'$ surface. The detailed dynamics on the excited surfaces are reported in the third paper of this series.

I-F-4 Chemical Reactions in the O(1D) + HCl System III. Quantum Dynamics on the Excited ($1^1A''$ and $2^1A'$) Potential Energy Surfaces

KAMISAKA, Hideyuki; NANBU, Shinkoh; BIAN, Wensheng; AOYAGI, Mutsumi¹; TANAKA, Kiyoshi²; NAKAMURA, Hiroki
(¹IMS and Kyushu Univ.; ²Hokkaido Univ.)

[*J. Theor. Comp. Chem.* in press]

Using the accurate global potential energy surfaces for the $1^1A''$ and $2^1A'$ states reported in the previous sister paper I, detailed quantum dynamics calculations are performed for these adiabatic surfaces separately for $J = 0$ (J : total angular momentum quantum number). In addition to the significant overall contributions of these states to the title reactions reported in the second paper II of these series, quantum dynamics on these excited potential energy surfaces (PES) are clarified in terms of the PES topographies, which are quite different from that of the ground PES. The reaction mechanisms are found to be strongly selective and nicely explained as vibrationally nonadiabatic transitions in the vicinity of potential ridge.

I-F-5 Use of Diabatic Basis in the Adiabatic-by-Sector R-Matrix Propagation Method in Time-Independent Reactive Scattering Calculations

MIL'NIKOV, G. V.¹; NAKAMURA, Hiroki
(¹IMS and Inst. Struct. Macrokinetics, Russia)

[*Comput. Phys. Commun.* **140**, 381 (2001)]

We propose a new recipe for the R -matrix propagation which combines the ideas of the adiabatic-by-sector (ABS) method and the sequential diagonalization/truncation technique. The R -matrix is determined in the adiabatic representation but the method does not require calculations of adiabatic channel functions at radial points inside the sector of propagation. This is a modification of the previously proposed ABS approach and can significantly reduce the computational time and memory in the energy independent part of scattering calculations. The code is checked by a test calculation of the reaction $O(^3P) + HCl \rightarrow OH + Cl$ using a LEPS potential energy surface (PES). The applicability of the method is further demonstrated by accurate quantum calculations of the endoergic reaction $H(^2S) + O_2(^3\Sigma_g^-) \rightarrow OH(^2\Pi) + O(^3P)$.

I-G Laser Control of Molecular Processes

I-G-1 Control of Photodissociation Branching Using the Complete Reflection Phenomenon: Application to HI Molecule

FUJISAKI, Hiroshi; TERANISHI, Yoshiaki¹; NAKAMURA, Hiroki
(¹IMS and JAERI)

[*J. Theor. Comp. Chem.* in press]

The laser control of photodissociation branching in a diatomic molecule is demonstrated to be effectively achieved with use of the complete reflection phenomenon. The phenomenon and the control condition can be

nicely formulated by the semiclassical (Zhu-Nakamura) theory. The method is applied to the branching between $I(^2P_{3/2})$ ($HI \rightarrow H + I$) and $I(^2P_{1/2})$ ($HI \rightarrow H + I^*$) formation, and nearly complete control is shown to be possible by appropriately choosing an initial vibrational state and laser frequency in spite of the fact that there are three electronically excited states involved. Numerical calculations of the corresponding wavepacket dynamics confirm the results.

I-G-2 Control of Molecular Processes by a Sequence of Linearly Chirped Pulses

NAGAYA, Kuninobu¹; TERANISHI, Yoshiaki²;

NAKAMURA, Hiroki*(¹IMS and Univ. Sherbrooke; ²IMS and JAERI)*

A new scheme of controlling molecular processes by a sequence of linearly chirped pulses is proposed and is applied to selective excitation of an energy level among closely lying ones and to complete electronic excitation of a diatomic molecule. The basic idea is quite different from the conventional ones utilizing chirped pulses in the sense that the present one does not rely on the idea of adiabatic rapid passage at all, but tries to control basic nonadiabatic transitions explicitly. Control of molecular processes can be achieved by controlling nonadiabatic transitions among Floquet (or dressed) states with use of the interference effects. The scheme can be formulated with use of the analytical theories of nonadiabatic transitions, and the proper control parameters can be estimated theoretically. Numerical demonstrations are provided to confirm the robustness of the method in comparison with the other conventional ones. Namely, the present scheme is shown to be stable against the variation of pulse area, complete and selective in population transfer, and fast to accomplish the transition. It is expected that the method can be applied to general multi-level systems and various types of wave packet dynamics. Its experimental realizability can also be expected, since linear chirping can now be relatively easily realized and manipulated.

I-G-3 Selective Excitation among Closely Lying Multi-Levels**NAGAYA, Kuninobu¹; TERANISHI, Yoshiaki²; NAKAMURA, Hiroki***(¹IMS and Univ. Sherbrooke; ²IMS and JAERI)*

[*Laser Control and Manipulation of Molecules A.* Bandrauk, R. J. Gordon and Y. Fujimura, Eds., ACS Symposium Series 821, American Chemical Society (2002)]

A new idea is proposed to accomplish selective and

complete excitation to any specified state among closely lying multi-levels. The basic idea is to control non-adiabatic transitions among dressed states by sweeping the laser frequency periodically. Both three- and four-level models are treated by the semiclassical theory of nonadiabatic transition and conditions of complete excitation are formulated. Numerical demonstrations are presented in comparison with the π -pulse and adiabatic rapid passage.

I-G-4 Photodissociation of H₂⁺ and HD⁺ in an Intense Laser Field**KONDORSKIY, Alexey¹; NAKAMURA, Hiroki***(¹IMS and Lebedev Phys. Inst., Russia)*

The photodissociation of H₂⁺ and HD⁺ by an intense laser pulse is investigated by solving the close-coupling equations without discretization. For the case of H₂⁺ the photodissociation spectra are calculated under the condition mimicking the experimental one and a fairly good agreement with the experiment is obtained. The uncertainty in the relative phases of initial states is found to lead to somewhat of smoothing of the spectra, depending on the pulse length. It is also found that Raman type transitions via intermediate dissociation continuum play an important role in determining the photodissociation spectra. This leads to a population increase of lower vibrational states and deforms the spectral profile. Dissociation from the lower vibrational states due to the bond softening is not strong enough.

Photodissociation spectra and angular distribution are calculated also for HD⁺ under the same conditions as in the H₂⁺ case. The dipole transitions lead to additional structures in the energy spectra and angular distribution. There is a noticeable difference in the peak positions of dissociation spectrum for particles dissociated by the direct electronic dipole transition and by the transitions via intermediate bound states.

The photodissociation dynamics is further clarified by using the three-dimensional plots of the spectra as a function of the field intensity and frequency.

I-H Theory of Multi-Dimensional Tunneling**I-H-1 Practical Implementation of the Instanton Theory for the Ground-State Tunneling Splitting****MIL'NIKOV, G. V.¹; NAKAMURA, Hiroki***(¹IMS and Inst. Struct. Macrokinetics, Russia)*

[*J. Chem. Phys.* **115**, 6881 (2001)]

The instanton theory is reformulated with use of the path integral approach and the Wentzel-Kramers-Brillouin approximation to the Schrödinger equation. Both approaches are shown to provide the same results. A new practically useful semiclassical formula is derived for the tunneling splitting of the ground state,

which can be implemented for high-dimensional systems. The theory is applicable to systems of arbitrary Riemannian metric and is also supplemented by a practical numerical recipe to evaluate the instanton trajectory, *i.e.*, periodic orbit, in multidimensional space. Numerical examples are presented for three-dimensional (3D) and 2D systems of HO₂ and malonaldehyde, respectively.

I-H-2 Instanton Theory for Multi-Dimension Decay through Tunneling**MIL'NIKOV, G. V.¹; NAKAMURA, Hiroki***(¹IMS and Inst. Struct. Macrokinetics, Russia)*

In our recent publication, we have formulated a practically efficient theory for the tunneling splitting of the ground state. The final result is applicable to large dimensional systems with an arbitrary metric system. The idea can be generalized to be applied to decay of a

metastable state through tunneling. An efficient method to find an instanton path and a canonically invariant expression of the decay rate can be formulated. The final result can be applied virtually to any high dimensional systems.

I-I New Methods for Scattering Calculations

I-I-1 Regularization of Scattering Calculations at *R*-Matrix Poles

MIL'NIKOV, G. V.¹; NAKAMURA, Hiroki
(¹IMS and Inst. Struct. Macrokinetics, Russia)

[*J. Phys. B: At., Mol. Opt. Phys.* **34**, 791 (2001)]

Physical quantities of scattering expressed in terms of the *R*-matrix are not well defined *R*-matrix poles. It is shown that these unphysical singularities can be removed and the regularized expressions are obtained. The method is straightforwardly applicable to various scattering theory quantities such as the reactance matrix, the Green function, the cumulative reaction probability

and the density of resonance states.

I-I-2 Calculation of Resonances via the *R*-Matrix Method

MIL'NIKOV, G. V.¹; NAKAMURA, Hiroki
(¹IMS and Inst. Struct. Macrokinetics, Russia)

Using the new spectral representation of Green's function previously proposed by us [*Comput. Phys. Commun.* **135**, 278 (2001)], we calculate the density of states and extract parameters of resonances in scattering system. The method is implemented for the resonances in *d* μ molecule below $\mu(n = 2)$ threshold.

I-J Theoretical Studies of Dissociative Attachment and Dissociative Recombination

I-J-1 Study of Dissociative Electron Attachment to HI Molecule by Using *R*-Matrix Representation for Green's Function

KOLORENC, P.¹; ČÍŽEK, M.¹; HORÁČEK, J.¹;
MIL'NIKOV, G. V.²; NAKAMURA, Hiroki
(¹Charles Univ., Czech Republic; ²IMS and Inst. Struct. Macrokinetics, Russia)

[*Physica Scripta.* **65**, 328 (2002)]

The new method of calculation of scattering Green's function recently proposed by the authors (G. V. Mil'nikov, H. Nakamura and J. Horáček, *Comput. Phys. Commun.* **135**, 278 (2001)) is applied to the process of dissociative attachment of low-energy electrons to HI molecule previously considered by Horáček, Domcke and Nakamura (*Z. Phys. D* **42**, 181(1997)). The calculation is extended to vibrationally and rotationally excited targets gas molecules. The temperature dependence of the dissociative attachment cross section is determined.

I-J-2 Analytical Treatment of the *K*-Matrix Integral Equation in the Dynamics of Superexcited Molecules

PICHL, Lukas¹; HIYAMA, Miyabi²; NAKAMURA, Hiroki

(¹Aizu Univ.; ²Univ. Tokyo)

Superexcited states (SES) constitute one peculiar class of electronically highly excited states of molecules whose internal energies exceed the corresponding lowest ionization potentials. They play important roles in various fields of chemistry and physics as intermediate states of dynamic processes. It is crucial to understand the characteristics of the central SES in order to systematically comprehend the various dynamic processes. Dissociative recombination represents one of good typical examples. According to the difference in the autoionization mechanisms the SESs are classified into the following two kinds: (i) multiply or inner-shell excited state, which is called "SES of the first kind," and (ii) rovibrationally excited Rydberg state, which is called "SES of the second kind." The dynamics of SES are governed by the two basic interactions: the electronic coupling $V(R, \epsilon)$ between the first kind of SES and the electronic continuum, and the quantum defect function $\mu(R)$, where R is the internuclear distance and ϵ is the electron energy. If these two quantities are available together with the potential curves $E_d(R)$ of the first kind of SES, then the MQDT (multi-channel quantum defect theory) presents a very powerful tool to investigate the various dynamics. These quantities should be basically evaluated by quantum chemical electronic structure theory, but it is not easy generally to obtain accurate

absolute values, unfortunately, especially in the case of $V(R, \epsilon)$. It is crucial to use spectroscopic experiments to improve the information. In this sense the interplay among quantum chemistry, dynamics theory, and experiment is very important. There is still one theoretical obstacle in this procedure. That is the solution of the K -matrix singular integral equation. The first order perturbation theory or the grid method is usually employed; but they are not accurate enough or not efficient enough. Here we present a new method which enables us to deal with the equation even analytically. Finally, when non-adiabatic transitions at potential curve crossings are to be analyzed, for instance in order to find out the final state branching in dissociative recombination, the compact and accurate Zhu-Nakamura theory can be used instead of the Landau-Zener formula.

I-K Theoretical Studies of Ultrafast Nonlinear Optical Spectroscopy of Molecules in Condensed Phases

Nonlinear optical interactions of laser fields with matter provide powerful spectroscopic tools for the understanding of microscopic interactions and dynamic processes. We attempt to provide theoretical basis for a wide class of nonlinear spectroscopic techniques, focusing on the underlying physical processes in the condensed phases.

I-K-1 Probing a Colored-Noise Induced Peak of a Strongly Damped Brownian System by One- and Two-Dimensional Spectroscopy

SUZUKI, Yoko; TANIMURA, Yoshitaka

[*Chem. Phys. Lett.* **358**, 51 (2002)]

When dynamics of a system strongly coupled to a white-noise environment is overdamped, in linear spectroscopy, the spectrum is observed as one peak near zero vibrational frequency. We found, however, that if the noise induced by the environment is colored and its correlation time is long, there is an additional peak at a frequency different from the system. We study the multi-dimensional spectrum, to observe the interplay between the overdamped motion and the weakly damped motion induced by the colored noise. Finally, we discuss the connection between the peak due to the colored noise and the Boson peak found in glass materials and supercooled liquids.

I-K-2 Vibrational Spectroscopy of a Harmonic Oscillator System Nonlinearly Coupled to a Heat Bath

KATO, Tsuyoshi; TANIMURA, Yoshitaka

[*J. Chem. Phys.* **117**, 6221 (2002)]

Vibrational relaxation of a harmonic oscillator nonlinearly coupled to a heat bath is investigated by the Gaussian-Markovian quantum Fokker-Planck equation approach. The system-bath interaction is assumed to be linear in the bath coordinate but linear plus square in the system coordinate modeling the elastic and inelastic relaxation mechanisms. Interplay of the two relaxation processes induced by the linear-linear and square-linear interactions in Raman or infrared spectra is discussed for various system-bath couplings, temperatures and correlation times for the bath fluctuations. The one-quantum coherence state created through the interaction with the pump laser pulse relaxes through different pathways in accordance with the mechanisms of the system-bath interactions. Relations between the present theory, Redfield theory and stochastic theory are also discussed.

I-K-3 Two-Dimensional Raman and Infrared Vibrational Spectroscopy for a Harmonic Oscillator System Nonlinearly Coupled with a Colored Noise Bath

KATO, Tsuyoshi; TANIMURA, Yoshitaka

[*J. Chem. Phys.* submitted]

Higher-order vibrational response functions of a harmonic oscillator are reconsidered by assuming a nonlinear coupling with a heat-bath from a quantum Fokker-Planck equation approach. In addition to a conventional linear-linear (LL) system-bath interaction, we consider a square-linear (SL) interaction in a Brownian oscillator model. The LL interaction yields vibrational energy relaxation, while the SL interaction mainly yields phase relaxation. The dynamics of a harmonic system are investigated by numerically integrating the Gaussian-Markovian Fokker-Planck equation under the condition of a colored and strong system-bath fluctuation, where the conventional perturbative approach cannot be applied. The response functions for the fifth-order nonresonant Raman and the third-order infrared (or equivalently the second-order infrared and the seventh-order nonresonant Raman) processes are calculated under the various combination of the LL and SL coupling strength. Results of two-dimensional response demonstrate that this spectroscopic technique is very sensitive to the mechanism of system-bath coupling and the correlation time of bath fluctuation; the signals exhibit echolike peak both in the fifth-order Raman and the third-order IR case, if the SL coupling is strong and the bath fluctuation is slow. We discuss the primary optical transition pathways involved in two-dimensional spectroscopy to study the echolike behavior. The optical pathways of the fifth-order Raman response from an "anisotropic" medium are newly found which were predicted by neither the weak system-bath coupling theory nor the conventional Brownian harmonic oscillator model.

I-K-4 Two-Time Correlation Function of a Two-Dimensional Quantal Rotator in a Colored Noise

SUZUKI, Yoko; TANIMURA, Yoshitaka

[*J. Phys. Soc. Jpn.* **71**, 2414 (2002)]

We study an absorption spectrum of a two-dimensional rotator coupled to a colored harmonic-oscillator bath. The absorption spectrum is analytically calculated from the generating functional of a reduced density matrix element for the rotator degrees of freedom. In the previous letter,¹⁾ the analysis of spectrum is limited to a white noise case. In this paper, we extend our theory to a colored noise case. We present the spectra for different temperatures, damping strength, and the correlation time of the noise. For a weakly damped rotator, at low temperatures, the spectra are sensitive to the system

dynamics that is determined by the quantization of the rotational motion. Such a quantized rotational motion depends on the noise effects. Hence we observe the peak shifts by the noise correlation time. For a strongly damped rotator, we find the bimodal spectrum in the slow modulation case. One of the peaks is caused by the effect of the colored noise, which does not appear in the case of the white noise. This peak is related to a librational motion induced by the coupling between the system and the bath oscillators with the near zero frequencies.

Reference

- 1) Y. Suzuki and Y. Tanimura, *J. Phys. Soc. Jpn.* **70**, 1167 (2001).

I-K-5 Energy-Level Diagrams and Their Contribution to Two-Dimensional Spectroscopic Signal: Distinction between Relaxation Mechanisms by Two-Dimensional Spectroscopy

OKUMURA, Ko¹; TANIMURA, Yoshitaka
(¹*Ochanomizu Univ.*)

We develop explicit Feynman rule for energy-level diagram or the corresponding physical processes in the Liouville space. Thereby we completely identify such diagrams and processes contributing to the two-dimensional response function in the Brownian oscillator model. We classify such diagrams or processes in quartet and numerically present signal separately from each quartet of diagrams or Liouville-space processes. We find that signal from each quartet is distinctly different from the others; we can identify each peaks in frequency domain with a certain quartet. This offers the basis for analyzing and assigning actual two-dimensional peaks and suggests the possibility of Liouville-space-path selective spectroscopy. As an application and also as a demonstration we present an example in which two familiar homogeneous mechanisms of relaxation are distinguished by existence or non-existence of certain peaks on the two-dimensional map; appearance or disappearance of certain peak is sensitive to the coupling mechanism. We also comment on some controversy on the result of a response function in the bilinear Brownian oscillator model.

I-K-6 Two-Dimensional Spectroscopy for a Two-Dimensional Rotator Coupled to a Gaussian-Markoffian Noise Bath

SUZUKI, Yoko; TANIMURA, Yoshitaka

The dynamics of a system in the condensed phase

are more clearly characterized by the multi-time correlation functions of physical observables than two-time ones. We investigate a two-dimensional motion of a rigid rotator coupled to a Gaussian-Markovian harmonic oscillator bath. The analytical expression of a four-time correlation function of a dipole that is the observable of the two-dimensional microwave or infrared spectroscopy is obtained from a generating functional approach. The spectra in the absence of damping are discrete and reveal transitions between eigenstates of the angular momentum quantized due to the cyclic boundary condition. For the weakly damped case, the result predicts an echo-like signal that can be explained by the Liouville space path ways. The two-dimensional spectra are more sensitive to the noise effects than the one-dimensional (linear-absorption) spectra, which mean two-time correlation functions of dipole. It is because the effects of the initial thermal distribution are cancelled through the higher-order optical transition process in the two-dimensional spectroscopy, while such thermal effects determine the profile of the line shape in the one-dimensional spectroscopy. The two-dimensional spectrum reveals three peaks corresponding to transition processes between the rotational energy levels even in the damped case, which cannot be observed in the one-dimensional spectroscopy. For the strongly damped case, the two-dimensional spectra reveal peaks that arise from the strongly damped motion and librational motion caused by the strong coupling between the system and the heat bath oscillators with narrow band spectral distribution. Whereas the effects of these motions are shown in the bimodal line of the one-dimensional spectroscopy, the profile of the two-dimensional spectrum clearly implies the origin of these two peaks.

I-K-7 Absorption Spectra for Two-Dimensional Rotator with Nonlinear System-Bath Coupling

SUZUKI, Yoko; TANIMURA, Yoshitaka

We investigate the relaxation process in a two-dimensional rotator system nonlinearly coupled to a harmonic heat bath with the use of the perturbation theory. In the previous works, we restricted our study to the linear-linear coupling between the system and the bath and obtained the continuous spectra. However, in the many realistic problems, the absorption spectra show discrete lines. To take into account experiments, we assume the system-bath interaction to be linear in the bath coordinate but the periodic function in the system coordinate. Using this coupling, we derive the absorption spectra of the rotator system which relates to a two-time correlation function of the dipole moment.

I-L The Condensed Phase Quantum Dynamics of Molecules and Atoms

We investigate quantum dynamics of molecules or atom in condensed phases by means of various statistical physics approaches involving Monte Carlo method for a reduced density matrix. Effects of dissipation on a spin system, proton tunneling and electron transfer processes are investigated and compared with the classical dynamics.

I-L-1 The Energy Landscape for Solvent Dynamics in Electron Transfer Reactions: A Minimalist Model

TANIMURA, Yoshitaka; LEITE, Vitor B. P.¹; ONUCHIC, Jose' Nelson²

(¹Univ. Estadual Paulista; ²Univ. California, San Diego)

[*J. Chem. Phys.* **117**, 2172 (2002)]

Energy fluctuations of a solute molecule embedded in a polar solvent are investigated to depict the energy landscape for solvation dynamics. The system is modeled by a charged molecule surrounded by two layers of solvent dipolar molecules with simple rotational dynamics. Individual solvent molecules are treated as simple dipoles that can point toward or away from the central charge Ising spins. Single-spin-flip Monte Carlo kinetics simulations are carried out in a two-dimensional lattice for different central charges, radii of outer shell, and temperatures. By analyzing the density of states as a function of energy and temperatures, we have determined the existence of multiple freezing transitions. Each of them can be associated with the freezing of a different layer of the solvent.

I-L-2 A Quantum Master Equation with a Langevin Force; a Realization of a Real-Time Quantum Monte-Carlo Simulation in a Dissipative Environment

TANIMURA, Yoshitaka

A reduced description of a two-level system for a spin-Boson system in a functional integral form is considered. The thermal activation term in the Feynman-Vernon influence functional is expressed as a contribution from a Langevin force with use of an auxiliary function with Gaussian probability distribution. A quantum master equation with the Langevin force, which is valid at any bath temperature without using a rotating wave approximation, is deduced by constructing the finite difference expression of the density matrix elements. The equation amenable to carry out a real-time Monte Carlo simulation, since in addition to a damping term, it contains an external random force. The temperature effects are taken into account through the correlation function of the random force, which is related with the damping term through the fluctuation-dissipation theorem. Trajectories of a quantum random walk numerically generated by solving the equation are presented and discussed.

I-M Theoretical Studies of Correlated Electron Systems

We study biorthogonal formulation of correlated electron system represented in the second quantized form. We illustrate the transcorrelated Hamiltonian approach and discuss the self-consistent field theory using biorthogonal orbitals.

I-M-1 Biorthogonal Approach for Explicitly Correlated Calculations Using the Transcorrelated Hamiltonian

HINO, Osamu¹; TANIMURA, Yoshitaka; TEN-NO, Seiichiro²

(¹Univ. Florida; ²Nagoya Univ.)

[*J. Chem. Phys.* **115**, 7865 (2001)]

A biorthogonal formulation is applied to the non-Hermite transcorrelated Hamiltonian, which treats a large amount of the dynamic correlation effects implicitly. We introduce biorthogonal canonical orbitals diagonalizing the non-Hermitian Fock operator. We also formulate many-body perturbation theory for the trans-

correlated Hamiltonian. The biorthogonal self-consistent field followed by the second order perturbation theory are applied to some pilot calculations including small atoms and molecules.

I-M-2 Application of the Transcorrelated Hamiltonian to the Linearized Coupled Cluster Singles and Doubles Model

HINO, Osamu¹; TANIMURA, Yoshitaka; TEN-NO, Seiichiro²

(¹Univ. Florida; ²Nagoya Univ.)

[*Chem. Phys. Lett.* **353**, 317 (2002)]

Explicitly correlated calculations using the trans-

correlated Hamiltonian are performed at the level of linearized coupled cluster (LCC) theory. Two different reference functions are employed in the calculations and the results are compared with those of the conventional LCC. The application to the water molecule shows a markedly better convergence of the correlation energies when the transcorrelated Hamiltonian is used than in the conventional approach. We also present results for some other ten-electron systems, Ne, HF, NH₃, and CH₄.

I-N Electronic Properties of Nanostructured Materials

I-N-1 Carbon Foam: Spanning the Phase Space between Graphite and Diamond

UMEMOTO, Koichiro¹; SAITO, Susumu^{1,2};
BERBER, Savas³; TOMÁNEK, David^{1,3}
(¹Tokyo Inst. Tech.; ²IMS and Tokyo Inst. Tech.;
³Mishigan State Univ.)

[*Phys. Rev. B* **64**, 193409 (2001)]

We study an unusual class of carbon structures, based on rigidly interconnected segments of graphite. The resulting foamlike systems cover the structural phase space extending from hexagonal diamond to graphite. Related to the most stable phases of carbon, these hybrid systems show an unusually high structural stability at low mass densities. Our density-functional calculations indicate that carbon foam is metallic, stable, and structurally rigid.

I-N-2 Electronic Structure of Ba₄C₆₀ and Cs₄C₆₀

UMEMOTO, Koichiro¹; SAITO, Susumu^{1,2}
(¹Tokyo Inst. Tech.; ²IMS and Tokyo Inst. Tech.)

[*Am. Inst. Phys. Conference Proc.* **590**, 305 (2001)]

We study the electronic structure of body-centered-orthorhombic Ba₄C₆₀ superconductor and Cs₄C₆₀. In both fullerenes, it is found that the band structure is metallic and that the low symmetry of the lattice gives rise to the lifting of the threefold degeneracy of t_{1u} and t_{1g} bands even at the Γ point. We study also the electronic structure of Cs₄C₆₀ under pressure and find it to be a promising candidate of a superconducting Cs fulleride.

I-N-3 Geometric and Electronic Structure of New Carbon-Network Materials: Nanotube Array on Graphite Sheet

MATSUMOTO, Takanori¹; SAITO, Susumu^{1,2}
(¹Tokyo Inst. Tech.; ²IMS and Tokyo Inst. Tech.)

[*J. Phys. Soc. Jpn.* **71**, 2765 (2002)]

We design a new class of carbon network materials with a periodically modified graphite sheet. The modified part corresponds to (6,6) carbon nanotube geometry. Their tube parts form triangular lattice on graphite sheet. On these systems each tube has six heptagons at the bottom, giving rise to a seamless sp^2 -C network with a negative curvature. We consider these nanotube arrays on graphite sheet with three kinds of tube-end geometries and various sizes for both graphite and tube parts. We report their electronic structure obtained by using a realistic tight-binding model, and for selected systems the density-functional theory. Interestingly, results show that most of them are semiconductors although both (6,6) tube and graphite are metallic. The difference in their tube-end geometries

and the sizes of graphite and tube parts affect their electronic structures. Some have nearly flat band states around the Fermi level, showing a possibility of ferromagnetic behavior if hole or electron is doped. Some are direct-gap semiconductors whose interband transition is optically allowed. Their typical gap energies are about 1 eV. Therefore they should emit infrared light.

I-N-4 First Principles Study of H₂ and CH₄ Physisorption on Carbon Nanotubes

AKAI, Yoshio¹; SAITO, Susumu^{1,2}
(¹Tokyo Inst. Tech.; ²IMS and Tokyo Inst. Tech.)

[*Jpn. J. Appl. Phys.* in press]

We study the energetics of physisorption of H₂ and CH₄ molecules on the single-walled carbon nanotube (SWNT) using the local density approximation in the framework of the density-functional theory. The radius of the studied nanotube is 4.69 Å, around the average size of the mass-produced SWNTs. Both inside and outside-wall physisorption processes with various molecular directions and adsorption sites are studied, and compared to those on a flat graphite sheet. It is found that H₂ and CH₄ molecules are generally stably adsorbed on the inside wall as well as on the outside wall. The energy gain upon physisorption of the H₂ on the inside wall of a carbon nanotube is about 0.10 eV, while that of CH₄ is about 0.17 eV. For the CH₄ adsorption, the energy gain depends considerably on a molecular direction. H₂ molecule is also stably adsorbed on the interstitial channel (IC) of the nanotube bundle, and the energy gain is about 0.19 eV. The Adsorption-site dependence is strong in the case of the H₂ adsorption on the outside wall of a nanotube and on the IC of nanotube bundles.

I-O Simulation and Dynamics of Chemical Systems

I-O-1 Quasi-Degenerate Perturbation Theory with General Multiconfiguration Self-Consistent Field Reference Functions

(¹Univ. Tokyo; ²IMS and Univ. Tokyo)

[*J. Chem. Phys.* **116**, 8270 (2002)]

NAKANO, Haruyuki¹; UCHIYAMA, Ryoma¹;
HIRAO, Kimihiko²

(¹Univ. Tokyo; ²IMS and Univ. Tokyo)

[*J. Comput. Chem.* **23**, 1166 (2002)]

The quasi-degenerate perturbation theory (QDPT) with complete active space (CAS) self-consistent field (SCF) reference functions is extended to the general multiconfiguration (MC) SCF references functions case. A computational scheme that utilizes both diagrammatic and sum-over-states approaches is presented. The second-order effective Hamiltonian is computed for the external intermediate configurations (including virtual or/and core orbitals) by the diagrammatic approach and for internal intermediate configurations (including only active orbitals) by the configuration interaction matrix-based sum-over-states approach. The method is tested on the calculations of excitation energies of H₂O, potential energy curves of LiF, and valence excitation energies of H₂CO. The results show that the present method yields very close results to the corresponding CAS-SCF reference QDPT results and the available experimental values. The deviations from CAS-SCF reference QDPT values are less than 0.1 eV on the average for the excitation energies of H₂O and less than 1 kcal/mol for the potential energy curves of LiF. In the calculation of the valence excited energies of H₂CO, the maximum deviation from available experimental values is 0.28 eV.

I-O-2 A Highly Efficient Algorithm for Electron Repulsion Integrals over Relativistic Four-Component Gaussian-Type Spinors

YANAI, Takeshi¹; NAKAJIMA, Takahito¹;
ISHIKAWA, Yasuyuki¹; HIRAO, Kimihiko²

(¹Univ. Tokyo; ²IMS and Univ. Tokyo)

[*J. Chem. Phys.* **116**, 10122 (2002)]

A highly efficient computational scheme has been proposed for the Dirac-Hartree-Fock and the Dirac-Kohn-Sham solutions using the generally contracted kinetically balanced Gaussian-type spinors. Nevertheless, the calculations based on the full Dirac Hamiltonian are limited to small systems if they contain heavy elements. The bottleneck is the calculation of the two-electron repulsions over the four-component GTs. The present study presents an improved algorithm for evaluation of the four-component relativistic integrals.

I-O-3 Accurate Relativistic Gaussian Basis Sets Determined by the Third-Order Douglas-Kroll Approximation with a Finite-Nucleus Model

NAKAJIMA, Takahito¹; HIRAO, Kimihiko²

Highly accurate Gaussian basis sets with a finite-nucleus model are developed for the 103 elements from H to Lr. The present GTO sets augment the relativistic basis sets with a point-charge model proposed in the previous paper of this series. The relativistic third-order Douglas-Kroll approach is adopted in optimizing the orbital exponents of a basis set by minimizing the atom self-consistent field energy. The basis sets are designed to have equal quality and to be appropriate for the incorporation of relativistic effects.

I-O-4 A Density Functional Study of van der Waals Interactions

KAMIYA, Muneaki¹; TSUNEDA, Takao¹; HIRAO, Kimihiko²

(¹Univ. Tokyo; ²IMS and Univ. Tokyo)

[*J. Chem. Phys.* **117**, 6010 (2002)]

The applicability of density functional theory (DFT) to van der Waals (vdW) calculations are investigated by using the long-range exchange correction scheme and the Andersson-Langreth-Lundqvist vdW functional. By calculating bond energy potentials of rare-gas dimers, it was found that the present scheme gives much more accurate potentials for all dimers than conventional sophisticated DFT methods do. We therefore confirmed that vdW bonds are constructed under the balance of long-range exchange and vdW correlation interactions, although neither of these interactions are usually contained in pure exchange-correlation functionals. It was also found that calculated vdW potentials are obviously affected by functional forms for rapidly varying densities. Especially in vdW calculations, we must employ a correlation functional that satisfies the fundamental condition for rapidly varying density.

I-P Theoretical Studies of Quantum Effects in Chemical Reactions

Although the study of quantum mechanical effects in chemical reactions has its long standing history, quantitative understandings of the importance of quantum effects in reactions have not been achieved. We investigate quantum effects, tunneling, resonances, interference, and electronically nonadiabatic transitions, in simple reaction systems by means of various theoretical approaches, including quantum reactive scattering methods, semiclassical dynamics methods, and classical trajectory methods.

I-P-1 Quantum Scattering Calculations of the $O(^1D) + N_2(X^1\Sigma_g^+) \rightarrow O(^3P) + N_2(X^1\Sigma_g^+)$ Spin-Forbidden Electronic Quenching Collision

TAKAYANAGI, Toshiyuki
(JAERI and IMS)

[*J. Phys. Chem. A* **106**, 4914 (2002)]

Three-dimensional quantum scattering calculations have been carried out for the $O(^1D) + N_2 \rightarrow O(^3P) + N_2$ spin-forbidden electronic quenching process using a simplified collision model, in which only the lowest singlet surface and one triplet surface are taken into account. The standard close-coupling technique has been used to obtain nonadiabatic transition probabilities and the coupled-state approximation was applied to calculate the total quenching cross section. The results of the close-coupling calculations have been compared to the results of quasiclassical trajectory surface hopping method. It has been found that the trajectory surface hopping method give too large quenching probabilities compare to the quantum results, in which the quenching dynamics is exclusively resonance-dominated. Detailed analyses of the quantum results show that a curve crossing picture cannot be employed to describe the present nonadiabatic collision. The calculated quenching cross sections have been also compared to experimental data as well as previous theoretical results.

I-P-2 Translational Energy Dependence of NO + NO / $N_2 + O_2$ Product Branching in the $O(^1D) + N_2O$ Reaction: a Classical Trajectory Study on a New Global Potential Energy Surface for the Lowest $^1A'$ State

TAKAYANAGI, Toshiyuki¹; AKAGI, Hiroshi²
(¹IMS and JAERI; ²JAERI)

[*Chem. Phys. Lett.* **363**, 298 (2002)]

An analytical potential energy surface of the lowest singlet $^1A'$ state for the $O(^1D) + N_2O \rightarrow NO + NO / N_2 + O_2$ reaction has been developed on the basis of extensive ab initio electronic structure calculations at the CASPT2/cc-pVDZ level of theory within C_s constraint. A many-body expansion type function was employed to fit the calculated ab initio points. Classical trajectory calculations have been carried out using the newly developed potential energy surface. We found that the initial orientation angle significantly affect the NO +

NO / $N_2 + O_2$ product branching and the branching ratio decreases as the relative translational energy increases.

I-P-3 A CASPT2 Study of the Doublet Potential Energy Surface for the $CH(X^2\Pi) + N_2(X^1\Sigma_g^+)$ Reaction

TAKAYANAGI, Toshiyuki
(JAERI and IMS)

The $HCN_2 \rightarrow H + NCN(^3\Sigma_g^-)$ reaction, which is a key process in the $CH(^2\Pi) + N_2$ reaction mechanisms, has been studied using the ab initio electronic structure method at the CASPT2 level theory. First, we calculated two-dimensional potential energy surfaces as a function of two appropriate coordinates in order to understand overall mechanisms. Then, full-dimensional stationary point searches have been carried out using locally interpolated potential energy surfaces. Our calculations strongly support the recent proposal of Lin and co-workers that the $CH(^2\Pi) + N_2$ reaction does not yield spin-forbidden $N(^4S) + HCN$ products but yield spin-allowed $H(^2\Sigma) + NCN(^3\Sigma_g^-)$ products.

I-Q Electronic Structure of a Molecule in Solution

Chemical reaction is undoubtedly the most important issue in the theoretical chemistry, and the electronic structure is a key to solve the problem. As long as molecules in the gas phase are concerned, the theory for the electronic structure has been enjoying its great success. However, when it comes to molecules in solution, the stage of theory is still an infant. We have recently proposed a new method referred to as RISM-SCF based on the integral equation theory of molecular liquids (RISM) and the ab initio electronic structure theory (SCF).¹⁾ The integral equation approach replaces the reaction field in the continuum models by a microscopic expression in terms of the site-site radial distribution functions between solute and solvent.

$$V_{\lambda} = \sum_j \int 4\pi r^2 \frac{q_j}{r} g_{j\lambda}(r) dr$$

where j and λ specify solvent and solute sites, respectively, and r denotes the solvent density. The site-site radial distribution functions $g_{j\lambda}(r)$ can be calculated from the extended RISM equation. Using V_{λ} the solvated Fock operator is defined as,

$$F^s = F^g - \sum_{\lambda} V_{\lambda} b_{\lambda}$$

where b_{λ} is a population operator of solute atoms. The statistical solvent distribution around solute is determined by the electronic structure or the partial charges of solute, while the electronic structure of solute is influenced by the solvent distribution. Therefore, the Hartree-Fock equation and the RISM equation should be solved in a self-consistent manner. It is this self-consistent determination of the solute electronic structure and the solvent distribution around the solute that features the RISM-SCF procedure.

The same Fock operator can be derived from a variation principle.²⁾ Defining the Helmholtz free energy A as following;

$$A = E_{\text{solute}} + \Delta\mu$$

where E_{solute} is the energy of solute under solvent influence, and $\Delta\mu$ is the solvation free energy represented in terms of the Singer-Chandler formula. The Fock operator for a solute molecule in solvent as well as the RISM-HNC equations can be obtained as the first order variations with respect to the wave functions and the pair correlation functions under the constraint of the orthonormality to the molecular orbitals. The latest development along this line are reported below.

References

- 1) S. Ten-no, F. Hirata and S. Kato, *Chem. Phys. Lett.* **214**, 391 (1993); *J. Chem. Phys.* **100**, 7443 (1994).
- 2) H. Sato, F. Hirata and S. Kato, *J. Chem. Phys.* **105**, 1546 (1996).

I-Q-1 Equilibrium and Nonequilibrium Solvation Structure of Hexaamineruthenium (II,III) in Aqueous Solution: Ab Initio RISM-SCF Study

SATO, Hirofumi; HIRATA, Fumio

[*J. Phys. Chem. A* **106**, 2300 (2001)]

The electronic and solvation structures of the metal

complexes in aqueous solutions, $[\text{Ru}(\text{CH}_3)_6]^{2+}$ and $[\text{Ru}(\text{CH}_3)_6]^{3+}$, which are key species in electron transfer reactions, are studied by using RISM-SCF method. We have found that the effective charge on the ruthenium ion does not change so much on the process of oxydation, and the electron is lost mainly from the ligand groups.

The electrical potential fluctuations around these complexes are nicely described within a linear-response regime, though some nonlinear effect is observed.

I-R Solvation Thermodynamics of Protein and Related Molecules

Concerning biomolecules such as protein, it is a final goal for the biochemistry and biophysics to explore the relation between conformations and biological functions. The first important step toward the goal would be to explain the conformational stability of biomolecules in terms of the microscopic structure of the molecules in

solvent. It is an extremely difficult problem by any means due to the overwhelmingly large degrees of freedom to be handled, including protein and solvent. As long as the small and/or short-time fluctuations of protein around the native structure is concerned, a variety of molecular simulation techniques provides a quite powerful tool to explore the microscopic structure of protein and solvent. However, the techniques are not so effective to characterize stability of the macromolecules in solution, to which the thermodynamic limit ($V \rightarrow \infty, N \rightarrow \infty$, with $V/N = \text{const.}$) is concerned. In such a case, methods based on the statistical mechanics of liquids should be natural choice for sampling configurations of solvent interacting biomolecules. The extended RISM theory is the most promising candidate of such methods, which provides not only solvation thermodynamics but also microscopic description at the level of the pair correlation functions.¹⁾ Obvious technical difficulties which one may face in applying the theory to such a large system are not only the computation time but also the stability of the numerical solution.²⁾

Here, we present our recent effort to tackle the problem using the two theoretical tools based on the statistical mechanics of liquids: the extended RISM and the scaled particle theories (SPT).³⁾ The studies for the solvation thermodynamics of small molecules such as ions are also included because it is regarded as elementary processes for the solvation of biomolecules, and because it is prerequisite for studying the more complicated molecules.

References

- 1) M. Kinoshita, Y. Okamoto and F. Hirata, *J. Am. Chem. Soc.* **120**, 1855 (1998).
- 2) A. Kitao, F. Hirata and N. Go, *J. Phys. Chem.* **97**, 10231 (1993).
- 3) M. Irisa, K. Nagayama and F. Hirata, *Chem. Phys. Lett.* **207**, 430 (1993).

I-R-1 Partial Molar Volumes and Compressibilities of Alkali-Halide Ions in Aqueous Solution: Hydration Shell Analysis with an Integral Equation Theory of Molecular Liquids

IMAI, Takashi¹; NOMURA, Hiroyasu²;
KINOSHITA, Masahiro³; HIRATA, Fumio
(¹Ritsumeikan Univ.; ²Tokyo Denki Univ.; ³Kyoto Univ.)

[*J. Phys. Chem.* **106**, 7308 (2002)]

The partial molar volume and partial molar compressibility of alkali-halide ions in aqueous solution at infinite dilution are calculated based on the RISM-Kirkwood-Buff theory. The theoretical results are in qualitative agreement with the corresponding experimental data. The volume and compressibility values are decomposed into the volume-exclusion and electrostriction contributions. The volume exclusion effect

qualitatively determines the dependence of the partial molar volume on the ion size, while the electrostriction effect dominates in the size dependence of the partial molar compressibility. The partial molar volume and compressibility are further analyzed by using the hydration shell model which enables us to distinguish a contribution from each hydration shell. For the primary hydration shell, we can make contact with the classical models of ion hydration proposed by Frank-Wen and Samoilov. Water molecules in the immediate vicinity of an ion always give a negative contribution to its partial molar volume. The first hydration shell makes a negative contribution to the partial molar compressibility for the ions classified with the "positive hydration" in terms of Samoilov's model, and does the opposite contribution for those with the "negative hydration." The reason why the water structure around a negatively hydrated ion is more compressible is explained in terms of density fluctuations around the ions from a viewpoint of the Landau fluctuation formula for the thermodynamic response functions.

I-S Collective Density Fluctuations in Polar Liquids and Their Response to Ion Dynamics

As to the model for molecular diffusion in polar liquids, there are two quite different points of view. One is the conventional rot-translation model, and the other the interaction-site description which sees the diffusion of a molecule as a correlated motion of each atom (site).¹⁾ It is clearly advantageous to use the interaction-site description compared to the rot-translation model to account for chemical characteristics of solvent as well as solute dynamics. However, the interaction-site description has its own disadvantage in interpreting physical meaning of the results, since it does not give an explicit picture for the rotational relaxation of molecules, which can be directly probed by many experimental means including the dielectric and NMR relaxation. We have solved the problem by extracting collective modes of the density fluctuation from the site-site density correlation functions. In our recent study for dynamics of molecular liquids based on the interaction-site model, we have succeeded to abstract the collective excitations in liquids, which can be identified as optical and acoustic modes, by diagonalizing the collective frequency matrix appearing in the generalized Langevin equation. The two modes arise essentially from the rotational and translational motions of molecules.²⁾ We applied the method to the ion dynamics in a dipolar liquid, and could have explained successfully the peculiar size dependence of friction of alkali and halide ions in

terms of response of the collective excitations in solvent to the solute displacement.³⁾

In the past year, we have elaborated the memory kernel in our generalized Langevin equation base on the mode coupling theory. We have also extended our treatment to dynamics of water and hydrated ions. Those studies as well as other related topics are reviewed below.

References

- 1) F. Hirata, *J. Chem. Phys.* **96**, 4619 (1992).
- 2) S. Chong and F. Hirata, *Phys. Rev. E* **57**, 1691 (1998).
- 3) S. Chong and F. Hirata, *J. Chem. Phys.* **108**, 7339 (1998).

I-S-1 Translational Diffusion and Reorientational Relaxation of Water Analyzed by Site-Site Generalized Langevin Theory

YAMAGUCHI, Tsuyoshi; CHONG, Song-Ho¹; HIRATA, Fumio

(¹*Tech. Univ. München*)

[*J. Chem. Phys.* **116**, 2502 (2002)]

The translational and rotational diffusion coefficients and the dielectric spectrum of water at the ambient condition are calculated using the exponential memory model previously proposed by us. The translational diffusion coefficient is in good agreement with experiments and computersimulations. However, the rotational diffusion and dielectric relaxation of the present theory are about ten times as fast as those of experiments. In order to clarify the origin of the disagreement, the memory kernel is directly obtained from the molecular-dynamics simulation and compared with the exponential model. It is found that the long-time part of the memory kernel, which is not considered in the exponential model, is dominant in the rotational diffusion and the dielectric relaxation of water.

I-S-2 Interaction-Site Model Description of the Reorientational Relaxation of Molecular Liquids: Incorporation of the Interaxial Coupling into the Site-Site Generalized Langevin/Mode-Coupling Theory

YAMAGUCHI, Tsuyoshi; HIRATA, Fumio

[*J. Chem. Phys.* **117**, 2216 (2002)]

The reorientational relaxation of nonlinear molecules in liquids is treated using the site-site generalized

Langevin/mode-coupling theory. We found an inconsistency between the rank-1 reorientational correlation functions of different vectors on a molecule when the molecule is nearly planer. We show that it is because the coupling between the torque and the acceleration of different rotational modes is missing in the theory.

A modification of the theory is proposed to incorporate this coupling, and the inconsistency between the reorientational correlation functions is remedied by the modification. We also apply the modified theory to the reorientational motion of water. The rotational part of the memory function becomes greater compared with the conventional theory, and it approaches to that from the molecular dynamics simulation. The charge-current spectrum of water is also shown to be improved by the modification.

I-S-3 Collective Density Fluctuations and Dynamics of Ions in Water Studied by the Interaction-Site Model of Liquids

HIRATA, Fumio; CHONG, Song-Ho¹

(¹*Tech. Univ. München*)

[*Condens. Mat. Phys.* **4**, 261 (2001)]

The collective excitations in water are studied based on the interaction-site model of liquids. Three collective modes, extracted from a generalized Langevin equation combined with the RISM theory of liquids, are identified as an acoustic mode and two optical modes. The drag force exerted on ions in water is described in terms of the response of these solvent collective excitations to the perturbation of ions. The ion-size dependence of the drag force, which has been a central issue in physical chemistry for long time, is studied in molecular detail based on the novel approach.

I-T Developing Theories of Liquids and Liquid Mixtures

In the past few years, we have been concentrating our effort on building theories for chemical processes in solution. Our main concern in such study was to develop new theories which can describe "solvation" or "solvent effect" on chemical processes of interest by means of the statistical mechanics of liquids. A key to such development is the "RISM theory," and many intriguing chemistry as well as physics have been investigated in our group using the theory at least in qualitative level. On the hand, we are also experiencing serious break down of the theory sometime as we try to explore new problems such as the gas-liquid phase transition, protein solution, and liquid-liquid mixtures.

In what follows, we describe our challenges to explore new problems related to liquids and liquid mixtures. The

challenge inevitably includes methodological development in the statistical mechanics of liquids.

I-T-1 Buthanol-Water Mixture, Structure of *tert*-Butyl Alcohol-Water Mixtures Studied by the RISM Theory

**YOSHIDA, Koji¹; KOVALENKO, Andriy;
YAMAGUCHI, Toshio¹; HIRATA, Fumio**
(¹Fukuoka Univ.)

[*J. Phys. Chem. B* **106**, 5042 (2002)]

We calculated the site-site radial distribution functions for binary mixtures of *tert*-butyl alcohol (TBA) and water over the whole range of TBA molar fraction. The description uses the reference interaction site model (RISM) integral equation theory in the dielectrically consistent approach of Perkyns and Pettitt (DRISM), and the closure approximation of Kovalenko and Hirata (KH) providing appropriate description for association of polar molecular species of density ranging from gas to liquid. We employed the extended simple point charge (SPC/E) model for water, and the optimized potential for liquid simulations (OPLS) force field for TBA. The partial radial distribution functions obtained for the TBA-water mixture are in qualitative agreement with those available from neutron diffraction experiments and molecular dynamics simulations. It is found that hydrogen bonds between all species are enhanced with rise of the TBA concentration. The tetrahedral-like network of hydrogen bonding in dilute TBA aqueous solution gradually turns into the zigzag-like structure for a high TBA concentration. In dilute aqueous solution, TBA molecules cluster by the hydrophobic methyl groups, whereas their hydroxyl groups are incorporated into the water hydrogen-bonding cage surrounding the TBA aggregate. In concentrated TBA, water as well as TBA molecules associate into the zigzag-like hydrogen-bonding chains. The present work shows that the RISM/KH theory is able to qualitatively predict the association structure of alcohol-water liquid mixtures.

I-T-2 Improvement of the Reference Interaction Site Model Theory for Calculating the Partial Molar Volume of Amino Acids and Polypeptides

**KINOSHITA, Masahiro¹; IMAI, Takashi²;
KOVALENKO, Andriy; HIRATA, Fumio**
(¹Kyoto Univ.; ²Ritsumeikan Univ.)

[*Chem. Phys. Lett.* **348**, 337 (2001)]

We propose a simple, efficient bridge correction of the one-dimensional reference interaction site model (RISM) theory. By combining the modified RISM method with the Kirkwood-Buff theory, the partial molar volume is calculated for the 20 amino acids and for oligopeptides of glutamic acids in extended and α -helix conformations. The bridge correction drastically improves agreement between the calculated values and the experimental data.

I-T-3 Description of a Polar Molecular Liquid in a Disordered Microporous Material with Activating Chemical Groups by a Replica RISM Theory

KOVALENKO, Andriy; HIRATA, Fumio

[*Condns. Mat. Phys.* **4**, 643 (2001)]

We develop a replica generalization of the reference interaction site model (replica RISM) integral equation theory to describe the structure and thermodynamics of a polar molecular liquid sorbed in a quenched disordered porous matrix including polar chemical groups. It provides a successful approach to realistic models of molecular liquids, and properly allows for the effect of a quenched disordered medium on the sorbed liquid. The description can be readily extended to a mobile liquid comprising a mixture of ionic and polar molecular species. The replica RISM integral equations are complemented by the HNC closure and its partial linearization, the KH closure. These approximations are adequate to ionic and polar molecular liquids. Closed expressions for the excess chemical potentials of the quenched-annealed system are derived. We extend the description to the case of soft core interaction potentials between all species of the quenched-annealed system, in which the liquid and matrix equilibrium distributions are characterized in general by two different temperatures. The replica RISM/KH-HNC theory is applied to water sorbed in a quenched matrix roughly modeling porous carbonaceous material activated with carboxylic (–COOH) groups. The results are in qualitative agreement with experiment for water confined in disordered materials.

I-T-4 Toward a Molecular Theory for the van der Waals-Maxwell Description of Fluid Phase Transitions

KOVALENKO, Andriy; HIRATA, Fumio

[*J. Theor. Comp. Chem.* in press]

We briefly review developments of theories for phase transitions of molecular fluids and mixtures, from semi-phenomenological approaches providing equations of state with adjustable parameters to first-principles microscopic methods qualitatively correct for a variety of molecular models with realistic interaction potentials. We further present the generalization of the van der Waals-Maxwell description of fluid phase diagrams to account for chemical specificities of polar molecular fluids, such as hydrogen bonding. Our theory uses the reference interaction site model (RISM) integral equation approach complemented with the new closure we have proposed (KH approximation), successful over a wide range of density from gas to liquid. The RISM/KH theory is applied to the known three-site models of water, methanol, and hydrogen fluoride, and qualitatively reproduces their vapor-liquid phase diagrams and the

structure in the gas as well as liquid phases, including hydrogen bonding.

Furthermore, phase transitions of water and methanol sorbed in nanoporous carbon aerogel are described by means of the replica generalization of the RISM approach we have developed. The changes as compared to the bulk fluids are in agreement with simulations and experiment. The RISM/KH theory is promising for description of phase transitions in various associating fluids, in particular, electrolyte as well as non-electrolyte solutions and ionic liquids.

I-U Neutral-Ionic, Dimerization and Photoinduced Phase Transitions and Their Dynamics in Mixed-Stack Organic Charge-Transfer Complexes

Mixed-stack organic charge-transfer complexes have columns of alternating donor and acceptor molecules. Neutral-ionic and dimerization phase transitions are observed in them. Since the dimerization was observed in some neutral compounds, importance of the long-range Coulomb interaction has been pointed out. In such compounds, transfer-modulating electron-lattice coupling is known to be strong. Then, the finite-temperature density-matrix renormalization-group method is used to show that such electron-lattice coupling also brings about dimerization in the neutral phase and that the transition becomes continuous then. The tetrathiafulvalene-*p*-chloranil (TTF-CA) complex, on the other hand, shows the discontinuous and simultaneous, neutral-ionic and dimerization phase transitions. It shows the photoinduced phase transition as well. We have solved the time-dependent Schrödinger equation to reproduce peculiarities found in time-resolved spectroscopy, such as a) the threshold intensity above which the transition takes place, b) the macroscopic coherent oscillations of neutral-ionic phase boundaries, and c) the quick loss of the second-harmonic-generation signal.

I-U-1 Finite-Temperature Phase Diagram of Mixed-Stack Charge-Transfer Complexes

YONEMITSU, Kenji

[*J. Phys. Chem. Solids* **63**, 1495 (2002)]

The mixed-stack organic charge-transfer complex, (BEDO-TTF)(Cl₂TCNQ), has shown a phase transition accompanied with a sharp drop in the magnetic susceptibility and with an increase in the intermolecular overlap, as the temperature is lowered. Here we theoretically consider the possibility for a phase transition from the ionic phase to a neutral phase, which is driven by charge-transfer fluctuations. Using finite-temperature density-matrix renormalization-group calculations for the one-dimensional extended Hubbard model with alternating potentials, we show that, with increasing transfer integral t , a transition from the neutral phase to the ionic phase is induced by spin fluctuations for small t , while another transition from the ionic phase to the neutral phase is induced by charge-transfer fluctuations for large t . Near the phase boundary, the free energy is easily lowered by dimerization of transfer integrals or by staggered magnetic field. Thus, a further transition is also possible to a dimerized nonmagnetic phase or to an antiferromagnetic phase at a lower temperature. In two dimensions, we expect that the effect of charge-transfer fluctuations is larger and that the transition to the dimerized nonmagnetic phase is suppressed.

I-U-2 Lattice and Magnetic Instabilities near the Neutral-Ionic Phase Transition of the One-Dimensional Extended Hubbard Model with Alternating Potentials in the Thermodynamic Limit

YONEMITSU, Kenji

[*Phys. Rev. B* **65**, 205105 (2002)]

The effects of dimerization causing the alternation of transfer integrals on the neutral-ionic phase transition are studied in the one-dimensional extended Hubbard

model with alternating potentials at half filling. The finite-temperature density-matrix renormalization-group method is used to treat the thermodynamic limit. In the ionic phase, the free-energy gain is proportional to $\delta^{4/3}$ with δ being the degree of dimerization even near the phase boundary at low temperatures. In the neutral phase, the free-energy gain is quadratic for small transfer integral far from the phase boundary, but it is nonlinearly enhanced near the boundary. Large transfer integrals make the gain faster than δ^2 , so that they facilitate dimerization. The dimerization in the neutral phase increases the ionicity and lowers the spin excitation energies. These lattice effects are in contrast to the effects of a staggered magnetic field. Relevance is discussed to recently observed dimerization in the neutral phase of ClMePD-DMeDCNQI.

I-U-3 Variation of Excitation Spectra in Mixed-Stack Charge-Transfer Complexes

YONEMITSU, Kenji

[*Phase Transitions* in press]

Local excitation spectra in different spin and charge channels are calculated in the one-dimensional extended Hubbard model with alternating energy levels at half filling for mixed-stack charge-transfer complexes. Near the boundary between the neutral and ionic phases, the electronic system is easily distorted by an additional term that reduces the symmetry and opens a gap. Alternating transfer integrals produce a nonmagnetic spin-Peierls phase; while staggered magnetic fields produce an antiferromagnetic phase. Both of them enhance the ionicity when they are introduced into the neutral phase near the boundary. Accordingly, these additional terms enhance low-energy spin excitations, although these excitations are suppressed when compared with those in the regular ionic phase. The regular ionic phase has a larger spectral weight in the local current channel than the neutral phase. This would imply that, in one dimension and if the lattice effect is negligible, the ionic phase has smaller activation energy in the electric conductivity near the boundary than the

neutral phase.

I-U-4 Dynamic Spin Correlations near Neutral-Ionic Phase Transitions

YONEMITSU, Kenji

[*Physica B* submitted]

Near the neutral-ionic phase transition in the one-dimensional extended Hubbard model with alternating potentials at half filling, the effects of alternating transfer integrals and a staggered magnetic field on the local spin excitation spectrum are studied by using the finite-temperature density-matrix renormalization-group method. In the neutral phase, the alternation increases the ionicity and lowers the spin excitation energies toward the ionic phase, while the staggered magnetic field does not modify the spectrum up to a critical field above which the system becomes ionic.

I-U-5 Thermodynamics of Neutral-Ionic and Ferroelectric Phase Transitions in the Two-Chain System

KISHINE, Jun-ichiro; LUTY, Tadeusz¹;
YONEMITSU, Kenji
(¹Tech. Univ. Wroclaw)

It remains an open issue to clarify the microscopic mechanism of the neutral-ionic phase transition and the photo-induced ferroelectric phase transition in the mixed-stack organic charge-transfer complex, TTF-CA. Of particular importance is to grasp the microscopic origin that distinguishes the neutral-ionic phase transition from the ferroelectric phase transition. The order parameter of the former transition is the charge concentration on the electron donor and acceptor sites, while that of the latter transition is the electric dipole moment that may be related to the microscopic electric current accompanied with the time-reversal symmetry breaking. Starting with a phenomenological argument, we first study thermodynamics of these phase transitions and consider how the interplay of electron correlation, lattice degrees of freedom and dimensionality effects enter the problem. We apply the transfer integral method to a two-chain system with a thermodynamic potential with triple minima. Mapping the problem onto a tunneling Hamiltonian and diagonalizing it, we study the phase transitions upon changing temperature and other controllable parameters. Finally, we discuss the neutral-ionic and ferroelectric phase transitions.

I-U-6 Domain-Wall Dynamics after Photoexcitations near Neutral-Ionic Phase Transitions

MIYASHITA, Naoyuki¹; KUWABARA, Makoto²;
YONEMITSU, Kenji
(¹GUAS; ²Kobe Univ.)

[*Phase Transitions* in press]

Real-time dynamics of domain walls between the

neutral and ionic phases just after photoexcitations is studied by fully solving the time-dependent Schrödinger equation for a one-dimensional extended Peierls-Hubbard model, not by relying on the adiabatic approximation. The unrestricted Hartree-Fock approximation is used for electrons, and the lattice displacements are treated classically. Three characteristic time scales are observed: rapid oscillation of ionicity owing to the local charge transfer; slow oscillation of lattice displacements; and even slower and collective motion of domain walls. Steady growth of a metastable domains is achieved after complicated competition of micro domains. The relevance to recently measured, time-resolved photoreflectance spectra in TTF-CA is discussed.

I-U-7 Variation Mechanisms of Ground-State and Optical-Excitation Properties in Quasi-One-Dimensional Two-Band Electron Systems

YONEMITSU, Kenji; KUWABARA, Makoto¹;
MIYASHITA, Naoyuki²
(¹Kobe Univ.; ²GUAS)

[*Mol. Cryst. Liq. Cryst.* **379**, 467 (2002)]

We study i) the ground-state and optical-excitation properties of halogen-bridged binuclear metal complexes, which are known as MMX chain compounds, by the strong-coupling expansion for a one-dimensional two-orbital extended Peierls-Hubbard model, and ii) the dynamics of domain walls between the neutral and ionic phases in mixed-stack charge-transfer complexes, by solving the time-dependent Schrödinger equation for a one-dimensional extended Peierls-Hubbard model with alternating energy levels. We find in i) that competition between electron-electron and electron-lattice interactions and competition between short- and long-range interactions are both important for the electronic phase variation, and in ii) that charge and lattice dynamics immediately after photoexcitations is complex and not explained simply within the domino picture.

I-U-8 Photoinduced Dynamics of Ionicity near the Neutral-Ionic Phase Boundary in a One-Dimensional Extended Peierls-Hubbard Model

MIYASHITA, Naoyuki¹; KUWABARA, Makoto²;
YONEMITSU, Kenji
(¹GUAS; ²Kobe Univ.)

[*Synth. Met.* submitted]

Dynamics of the ionicity after photoexcitations in mixed-stack charge-transfer complexes is numerically studied by using a one-dimensional extended Peierls-Hubbard model with alternating potentials at half filling. The time-dependent Schrödinger equation and the Newton equation are solved for the electronic and lattice parts, respectively. Fourier analysis is performed for the ionicity. During the photoinduced phase transition, slow components are dominant and very broad reflecting complex motion of domain walls and lattice displacements. After the transition, fast and slow oscillations are

clearly seen, which correspond to the electronic and lattice motion, respectively.

I-V Self-Doping, Nonlinear Excitations and Photoinduced Transitions between Charge and Lattice Ordered Phases of Metal Complexes

Halogen-bridged binuclear platinum complexes show a variety of electronic phases owing to competing kinetic energy, Coulomb repulsion, and electron-lattice coupling. When the ligand is pop, electrons are so localized that the perturbation theory from the strong-coupling limit works very well for the ground and optically excited states. When the halogen is iodine in addition, as the distance between the neighboring MM units increases by changing counter ions or by reducing pressure, a discontinuous transition takes place from the charge-density-wave phase to the charge-polarization phase. This has been explained theoretically. In those materials which show the pressure-induced transition, a photo-induced transition is observed in the hysteresis loop. The transition is, however, only from the charge-density-wave to charge-polarization phases. We have clarified its mechanism. a) The lowest-energy photoexcitation brings about inter-unit charge transfer only in the former phase. b) The high-energy photoexcitation in the latter phase transfers charge so locally that the former phase never proliferates.

I-V-1 Self-Doping Effect on the Mott Transition Accompanied with Three-Fold Charge Ordering in (DCNQI)₂Cu

KUWABARA, Makoto¹; YONEMITSU, Kenji;
OHTA, Hiroshi¹
(¹Kobe Univ.)

[*Synth. Met.* in press]

The commensurate state with three-fold lattice distortion in the insulating phase of (DCNQI)₂Cu is studied based on a two-band Peierls-Hubbard model by using the density-matrix renormalization-group method. With strong electron correlation among the *d* electrons, self-consistent lattice modulation strongly blocks the charge transfer between the π and *d* orbitals in order to keep the commensurability condition even when the π -*d* level difference is widely varied. A transition to an incommensurate phase requires a large deviation of the π -*d* level difference from the optimal case.

I-V-2 Spin Solitons in the Alternate Charge Polarization Background of MMX Chains

KUWABARA, Makoto¹; YONEMITSU, Kenji;
OHTA, Hiroshi¹
(¹Kobe Univ.)

[*APES'01 proc.* in press]

We study spin solitons in the alternate charge polarization background of the MMX chains, using the unrestricted Hartree-Fock approximation to a one-dimensional Peierls-Hubbard model. The effects of the electron-lattice coupling and the electron-electron interaction on the shape of the soliton are discussed.

I-V-3 Photoexcited States and Photoinduced Dynamics in Electronic Phases of MMX-Chain Systems

YONEMITSU, Kenji; MIYASHITA, Naoyuki¹;
KUWABARA, Makoto²
(¹GUAS; ²Kobe Univ.)

[*Synth. Met.* submitted]

In the one-dimensional two-band three-quarter-filled Peierls-Hubbard model for halogen-bridged binuclear metal complexes $R_4[\text{Pt}_2(\text{pop})_4\text{I}]_n\text{H}_2\text{O}$ with counter ion *R* and pop = P₂O₅H₂²⁻, a transition from the charge-density-wave phase to the charge-polarization phase is photoinduced, but the opposite process is not. Its origin is explained by considering differences in low-energy photoexcitations in the two phases and coherence of respective order parameters. The different dynamics is demonstrated by solving the time-dependent Schrödinger equation.

I-V-4 Electromodulation Spectra of Optical Absorption in One-Dimensional Strongly Correlated Systems

KUWABARA, Makoto¹; YONEMITSU, Kenji;
OHTA, Hiroshi¹
(¹Kobe Univ.)

[*Synth. Met.* submitted]

Electromodulation spectra of optical absorption in one-dimensional strongly correlated electron systems are theoretically investigated by numerically solving the time-dependent Hartree-Fock equation for the extended-Hubbard model coupled to a classical external vector potential. The calculated spectra are qualitatively in good agreement with experimental results for one-dimensional Mott insulators.

I-W Dimensional Crossovers in Electronic Phases and Their Excitation Spectra of Quasi-One-Dimensional Organic Conductors

In quasi-one-dimensional segregated-stack organic charge-transfer complexes with a quarter-filled band, (TMTTF)₂X and (TMTSF)₂X, variation of physical properties under physical or chemical pressure can be viewed as a dimensional crossover. At this particular band filling, the umklapp process is essential to the confinement of fermions and to the antiferromagnetic long-range order. The dimensional crossover is demonstrated also in charge-transfer excitation spectra by the finite-temperature density-matrix renormalization-group method. Electron correlation is so strong in the most conducting direction that electron motion is confined in this direction at low energies. The perpendicular motion takes place only incoherently. This explains the observed behavior that is reminiscent of the doped Mott insulators.

I-W-1 Dimensional Crossovers and Phase Transitions in Strongly Correlated Low-Dimensional Electron Systems: Renormalization-Group Study

KISHINE, Jun-ichiro; YONEMITSU, Kenji

[*Int. J. Mod. Phys. B* **16**, 711 (2002)]

In this review article, we have described our recent achievement on dimensional crossovers and phase transitions from incoherent metallic phases, based on the two-loop level perturbative renormalization-group approach. As a canonical example, we first take up spin-density-wave phase transitions in the quasi-one-dimensional organic conductors (TMTTF)₂X and (TMTSF)₂X, and elucidate the nature of the transitions in terms of the dimerized quarter-filled Hubbard chains. Secondly, we discuss the novel superconductivity in the doped ladder system Sr_{14-x}Ca_xCu₂₄O₄₁ under high pressure, and analyze the superconducting transition from the incoherent metallic phase (spin gap metal phase) in terms of the weakly-coupled Hubbard ladders. Thirdly, motivated by the experimental findings of the crossover from an antiferromagnetic phase, Anderson localization phase, and a normal Fermi liquid phase upon Cu doping in a organic compound (DI-DCNQI)₂Ag_{1-x}Cu_x, we discuss interplay of randomness, electron correlation, and dimensionality effects in weakly-coupled half-filled Hubbard chains

with weak quenched random potentials. Finally we discuss some two-dimensional electron systems where the two-loop renormalization-group procedure is well defined and works.

I-W-2 Correlation-Induced Dimensional Crossovers of Charge-Transfer Excitations in Quasi-One-Dimensional Organic Conductors

YONEMITSU, Kenji

[*Synth. Met.* in press]

Applying the finite-temperature density-matrix renormalization-group method to the spinless fermion model on a two-leg ladder, we have calculated the dynamical structure factors for the local charge transfer processes along the chains and across the chains. The intra-chain excitation spectra are sensitive to the inter-chain transfer integral and the chemical potential, while the inter-chain excitation spectra are sensitive to the intra-chain electron correlation. These dynamical properties are due to the collective motions of fermions along the chains and the energy-dependent confinement of fermions in the chains. At low but finite energies, the effects of the increasing inter-chain transfer integral on the local charge-transfer spectra are similar to those of the chemical potential deviating from zero.

I-X Underlying Gauge Structure and Competing Orders in Underdoped Cuprate Superconductors

The key issue in theoretical understanding of the high-temperature cuprate superconductors is how to describe the low-density carriers coupled with competing infrared collective degrees of freedom originating from strong correlation inherent in the doped Mott insulators. Although realization of the *d*-wave superconducting ground state upon doping has been established both experimentally and theoretically, it still remains as a highly challenging problem to describe the low-energy contenders such as the flux phase, the antiferromagnetic phase, the stripe phase, and so on. Here, we take account of the contenders as much as possible. First, based on an SU(2) formulation of the *t*-*J* model, we consider a superconducting vortex, where the flux state is stabilized in its core, and propose its physical consequences. Then, as a next step, both flux and antiferromagnetic degrees of freedom are included.

I-X-1 Signature of the Staggered Flux State around a Superconducting Vortex in Underdoped Cuprates

KISHINE, Jun-ichiro; LEE, Patrick A.¹; WEN, Xiao-Gang¹
(¹MIT)

[*Phys. Rev. B* **65**, 064526 (2002)]

Based on the SU(2) lattice gauge theory formulation of the t - J model, we discuss possible signature of the unit cell doubling associated with the staggered flux (SF) state in the lightly doped spin liquid. Although the SF state appears only dynamically in a uniform d -wave superconducting state, a topological defect [SU(2) vortex] freezes the SF state inside the vortex core. Consequently, the unit cell doubling shows up in the hopping and pairing order parameters of physical electrons. We find that whereas the center of the vortex core is a SF state, as one moves away from the core center, a correlated staggered modulation of the hopping and pairing becomes predominant. We predict that over the region outside the core and inside the internal gauge field penetration depth around a vortex center, the local density of states exhibits staggered peak-dip (SPD) structure inside the V-shaped profile when measured on the bonds. The SPD structure has its direct origin in the unit cell doubling associated with the SF core and the robust topological texture, which has little to do with the symmetry of the d -wave order parameter. Therefore the structure may survive the tunneling matrix element effects and easily be detected by STM experiment.

I-X-2 Underlying SU(2) Gauge Structure and Hidden Staggered Flux State in the Lightly Doped Spin Liquid

KISHINE, Jun-ichiro

[*J. Phys. Chem. Solids* **63**, 1559 (2002)]

The staggered flux state, that enters the low-energy spectrum of the d -wave superconducting state in the lightly doped spin liquid systems is discussed, based on an SU(2) lattice gauge theory formulation of the t - J model. An appropriate gauge transformation to describe physical quantities such as staggered orbital currents is proposed. Using this gauge (physical gauge), the staggered orbital current correlation is computed and consistency with a Gutzwiller-projected Monte Carlo analysis is argued.

I-X-3 Coexistence of Staggered Flux and Antiferromagnetic States in Superconducting Vortices in the Lightly Doped Mott Insulator

MORITA, Yoshifumi¹; KISHINE, Jun-ichiro; LEE, Patrick A.²
(¹Univ. Tokyo; ²MIT)

Based on an SU(2) lattice gauge theory formulation of the t - J model, we numerically studied electronic states inside superconducting vortices in the lightly

doped Mott insulator. Applying the Bogoliubov-de Gennes type formulation to the vortices in the system, we found that an antiferromagnetic state coexists with the staggered flux state for doping smaller than some critical concentration. This is the first finding of the coexistence of the resonating-valence-bond type on-bond singlets and the on-site spin degrees of freedom. Relevance of this finding to the recent NMR experiments on the vortex core states is argued.

RESEARCH ACTIVITIES II

Department of Molecular Structure

II-A Development of Near-Field Dynamic Spectroscopy and Application to Mesophase Systems

Recent developments in ultrashort pulsed lasers have made ultrafast spectroscopy a mature technique for analyzing dynamic behavior of molecular systems. As for spatial resolution, near-field optical microscopy, which enables spatial resolution beyond the diffraction limit of light, shows remarkable progress in technology in these days. Combination of these advanced optical technologies may offer a direct probe of molecular dynamical processes in mesoscopic systems. It may bring essential and basic knowledge for analyzing origins of characteristic features and functionalities of mesophase systems. We are constructing an apparatus for near-field dynamic spectroscopy with femtosecond temporal resolution and nanometer spatial resolution. Preliminary experimental results are presented here.

II-A-1 Development of an Ultrafast Near-Field Spectroscopy and Observation of Dynamic Processes in GaAs Crystal

IMURA, Kohei; OKAMOTO, Hiromi

We have developed an instrument, where a fs pump-probe technique is combined with a scanning near-field optical microscope having a 100-nm spatial resolution, for the purpose of obtaining information on spatially resolved molecular dynamics. We have examined the performance of our instrument and feasibility of applications to the studies of molecular dynamics by using a GaAs crystal.

Experimental set-up consists of an excitation light source, a near-field microscope, and detection systems. The output from a mode-locked Ti:sapphire laser ($\lambda = 780$ nm, ~ 100 fs pulse duration) is split into two beams. The beams are collinearly combined again into one beam after one beam passes through a motorized optical delay line. Positive group velocity dispersion arising from a long optical fiber (for a near-field probe) is pre-compensated by a grating-prism pulse stretcher before the optical beam is coupled to the cleaved end of the fiber. The other end of the fiber has been fabricated as a near-field probe. The near-field probe (commercial) is tapered and Au metal coated, and has an aperture (~ 100 nm) at the tip. The aperture probe is used to illuminate the sample, and also to collect photoluminescence (PL) from the sample. The PL is detected either by a CCD after dispersed by a monochromator or by a photomultiplier tube after passing through optical filters. To obtain PL images, the sample is raster-scanned beneath the tip, and a sample-tip distance is regulated at ~ 10 nm by the shear force feedback mechanism. This feedback signal also gives topographic image of the sample.

We have measured the excitation laser power (P) dependence of the PL intensity (I) from the GaAs crystal around 870 nm, and have found a relationship as $I \propto P^{1.5}$. This finding indicates two-photon process involved in the PL. We have performed time-correlated measurements for the two-photon PL from GaAs crystal at ~ 870 nm. In Figure 1, the PL intensity is plotted against the delay time between the two optical beams.

Except for the region around the origin of the delay time, where it shows an interferometric pattern (not shown in Figure 1), a relatively slow decrease of the intensity with delay time is observed. This plot gives information essentially equivalent to that obtained by the time-resolved absorption correlation method (*i.e.*, dynamics in the one-photon excited state). A relaxation time constant 52 ps is obtained by assuming a single exponential decay. The background PL with no delay time dependence is due to the two-photon PL arising from each optical pulse, as well as a single photon inter-band transition.

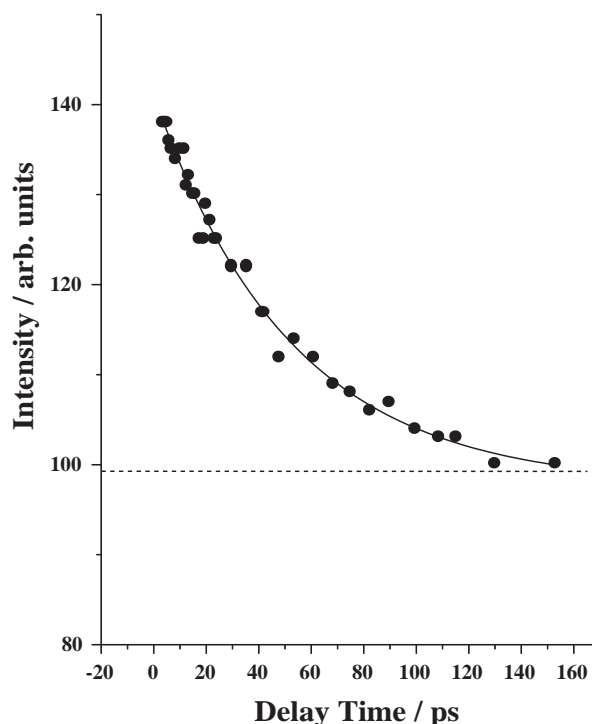


Figure 1. Near-field time-correlated PL signal of GaAs crystal.

II-A-2 Near-Field Autocorrelation Measurements of Femtosecond Light Pulses at a Tip of a 100-nm Apertured Probe by Two-Photon-Induced Photoconductivity

NAGAHARA, Tetsuhiko; IMURA, Kohei; OKAMOTO, Hiromi

In ultrafast pump-probe experiments, it is essential to characterize temporal profiles of the pump and probe light pulses. The technique most commonly used for that purpose is based on a Michelson-type autocorrelator combined with phase-matched second harmonic generation (SHG) in nonlinear crystals. For ultrafast experiments under scanning near-field optical microscopes (SNOM), however, such a conventional autocorrelation technique with the SHG crystal is not practical because of unsatisfied phase-matching condition and low radiation energy emerging from the apertured fiber probe. By the use of two-photon-induced photoconductivity in semiconductors, autocorrelation measurements under SNOM are possible. Autocorrelation trace of 470 fs full width at half maximum (FWHM) was reported in SNOM geometry.¹⁾ Utilizing this technique, time resolution of our newly developed femtosecond SNOM apparatus has been measured.

The photocurrent output of a GaAsP diffusion type photodiode was detected by a lock-in amplifier. The signal has been confirmed to be of quadratic response (Figure 1A). Femtosecond light pulses were obtained from a mode-locked Ti:sapphire laser (pulse duration <100 fs). Normal group velocity dispersion arising from the optical fiber for the apertured probe was pre-compensated by a grating pair. Figure 1B shows the autocorrelation trace of the Ti:sapphire laser pulses at a tip of a 100-nm apertured fiber probe. The FWHM obtained is ~100 fs, which indicates that dispersion by the fiber is successfully pre-compensated in our apparatus. The spatial uniformity of the detector sensitivity was also examined (Figure 1C), by scanning the probe with the distance between the detector surface and the probe tip kept constant. There was no detectable correlation between the topographic structure and the photocurrent image. The dark spots found in Figure 1C may be ascribed to defect sites of the semiconductor.

Reference

1) W. Schade, J. Preusser, D. L. Osborn, Y. Y. Lee, J. deGouw and S. R. Leone, *Opt. Commun.* **162**, 200 (1999).

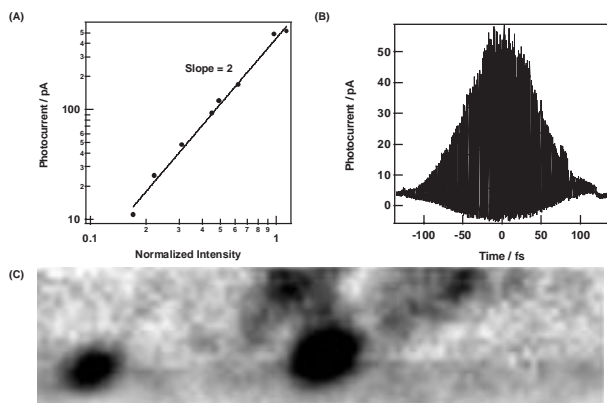


Figure 1. (A) Peak diode current as a function of normalized incident pulse energy. Solid line shows a quadratic fit to the data. (B) Autocorrelation signal obtained at the tip of the 100-nm apertured probe. (C) Spatial image (area size: 5 $\mu\text{m} \times 1.25 \mu\text{m}$) of photocurrent.

II-A-3 Structure and Photophysics of PIC J-Aggregates Studied by Scanning Near-Field Optical Microscopy

IMURA, Kohei; NAGAHARA, Tetsuhiko; OKAMOTO, Hiromi

Molecular assemblies such as J-aggregates have received much attention over the past decades because of their characteristic optical properties. The J-aggregates are characterized by a strong and sharp optical absorption band, called J-band, which is red-shifted with respect to the monomer absorption. It has been interpreted that the strong absorption arises from the interactions between the monomeric molecular transition dipoles. Intermolecular interaction between dipoles causes the coherent delocalization of excitons over an aggregate. Pseudoisocyanine (PIC) dye is known as a typical molecule which forms a J-aggregate. Barbara and co-workers^{1,2)} have studied PIC J-aggregates by scanning near-field optical microscopy. We have also observed structures and photophysics of PIC J-aggregates to examine performance of the scanning near-field microscope we have constructed recently.

PIC J-aggregate was prepared in PIC-PVS (polyvinylsulfate) hot solution and spin coated onto a substrate (cover glass). Spin-coated J-aggregate was excited by the second harmonic (527 nm) output of Nd:YLF laser through a sub-wavelength-sized (100 nm) aperture probe. J-band fluorescence from the aggregate (~575 nm) was collected by a high NA objective lens and detected by a photomultiplier tube. In order to investigate structures of the J-aggregate, the sample is scanned beneath the probe by keeping the sample-probe distance constant. Fluorescence and simultaneously obtained topographic images proved that produced J-aggregates have fibrous structures. The aggregates are longer than 10 μm in length, 10–150 nm in width, and 1–50 nm thick, depending on the sample preparation condition. We have also investigated the polarization characteristics of the near-field fluorescence for the fibrous J-aggregates. It has been found that the fluorescence from the J-aggregate depends little on the polarization of the excitation light. On the other hand, polarization of the fluorescence is strongly correlated to the fiber direction as seen in Figures 1(c) and (d). The latter observation indicates that the direction of transition dipole for the J-band fluorescence lies along the long axis of the J-aggregate as reported before.²⁾ Time-resolved spectroscopic studies of the aggregates are under progress.

References

- 1) D. A. Higgins and P. F. Barbara, *J. Phys. Chem.* **99**, 3 (1995).
- 2) D. A. Higgins, P. J. Reid and P. F. Barbara, *J. Phys. Chem.* **100**, 1174 (1996).

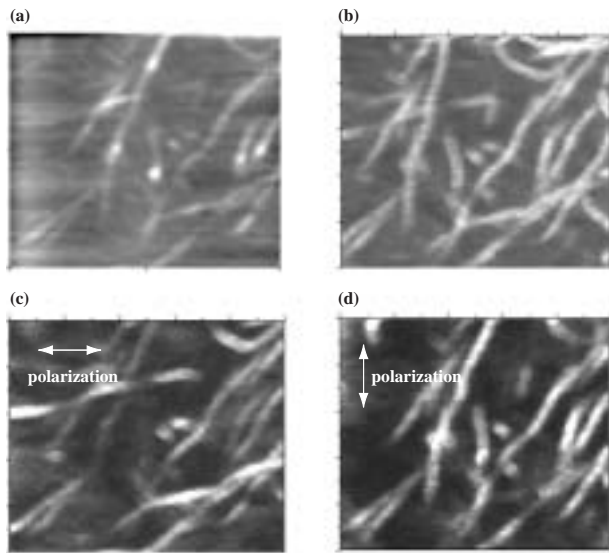


Figure 1. Observed images of J-aggregates (scan range $5\ \mu\text{m} \times 5\ \mu\text{m}$). (a) Shear-force topography. (b) Unpolarized fluorescence image. (c) Horizontally and (d) vertically polarized fluorescence images.

II-B Laser Cooling and Trapping of Metastable Helium Atoms

In the past two decades, extensive developments have occurred in the laser cooling and trapping of neutral atoms, with many workers reporting the application of these techniques to such diverse atomic species as alkali atoms, alkali earth atoms, and rare gas atoms. Among these, the helium atom is unique on account of its small mass, simple energy level structure, and easy availability in two isotopic forms (^3He and ^4He) of differing quantum statistics. For this reason, we have been studying the laser cooling and trapping of helium atoms.

II-B-1 New Design for Efficient Magneto-Optical Trapping of Metastable Helium Atoms

MORITA, Norio

The first step for Bose-Einstein condensation of metastable helium atoms is to realize an efficient magneto-optical trap (MOT). For this purpose, it is especially important to increase the intensity of a metastable atomic beam for loading the atoms into a MOT. To obtain an intense metastable beam, it is necessary to collimate the beam as tightly as possible. In our new apparatus, the metastable beam is collimated using a chain of corner cube prisms and laser beams with two detuned frequencies; the length of the collimation region along the atomic beam is 300 mm. The far detuned laser light can collimate more diverging atoms and the less detuned one collimates less diverging atoms. From our simulation, it is confirmed that this system can collimate an initial divergent beam with a spread of ± 70

mrad at a velocity of 850 m/s into an almost collinear beam.

After deceleration through the Zeeman cooling process, the collimated metastable beam at a velocity of 150 m/s is deflected by an angle of 30 degrees using laser beams with curved wavefront, which are produced by a pair of cylindrical mirrors. The metastable beam is then introduced to a small glass cell, in which the atoms are trapped and further cooled for the Bose-Einstein condensation. Due to this deflection of the metastable beam, the trapping region is prevented from the attack of the intense ground state helium beam, and we can expect the longer lifetime of the trap.

While these atomic loading system is designed for a metastable beam source cooled with liquid nitrogen, we are preparing another system for liquid-helium-cooled metastable beam source in order to obtain a further intense metastable beam. Experiments with these systems are now in progress.

II-C Spectroscopic Studies on Atoms and Ions in Liquid Helium

Atoms and ions in liquid helium are known to reside in bubble-like cavities due to the Pauli repulsive force between electrons. Physical properties of these exotic surroundings are determined by the potential energy of the impurity- He_n system, the surface tension energy of the liquid helium, and the pressure-volume work. Spectroscopic studies of such impurity atoms and ions in liquid helium are expected not only to give information on the structure and dynamics of the bubbles but also to contribute to the study on the property of superfluid liquid helium.

II-C-1 Laser Spectroscopy of Eu Atoms in Liquid ^3He and ^4He

MORIWAKI, Yoshiki¹; MORITA, Norio
(¹Toyama Univ.)

Spectra of impurity atoms in liquid helium often explicitly reflect physical properties of the liquid. In this meaning, it may especially be interesting to investigate the spectral difference between impurity atoms in liquid ^3He and ^4He , because each liquid has much different physical properties at a temperature below the lambda point (2.1 K); for example, the fluidity is super and normal for ^4He and ^3He , respectively, the dispersion relation is well determined for ^4He but not well for ^3He , and the number density and surface tension are much different between ^3He and ^4He .

In this study we have experimentally obtained some

spectra of Eu atoms in liquid ^4He and ^3He . Excitation spectra of the $4f^6(^7F)5d6s^2\ ^8F_{7/2} \leftarrow 4f^76s^2\ ^8S_{7/2}$ transition at several temperatures are shown in Figure 1. With decreasing the temperature, very sharp spectra appear and their intensities both in liquid ^4He and ^3He are increased. It is reasonable to interpret these sharp spectra as zero phonon lines, because the interaction between He atoms and the inner-shell electron excited in Eu atom is quite weak during the transition. Side bands are also seen, but they are only in the upper energy side for both liquid ^4He and ^3He . The shift of the zero phonon line and the spectral width of the side band are both smaller for liquid ^3He than for ^4He . This fact can be understood by the difference in the number density and surface tension between ^4He and ^3He : smaller number density and surface tension of ^3He result in the smaller spectral shift and width. An especially interesting spectral feature is that, only for liquid

^4He , some peaks other than the phonon side bands are also seen at a temperature of 1.1 K, but they are not seen for ^3He . It is quite possible that these are roton or maxon spectra of liquid ^4He . Further investigation is now in progress.

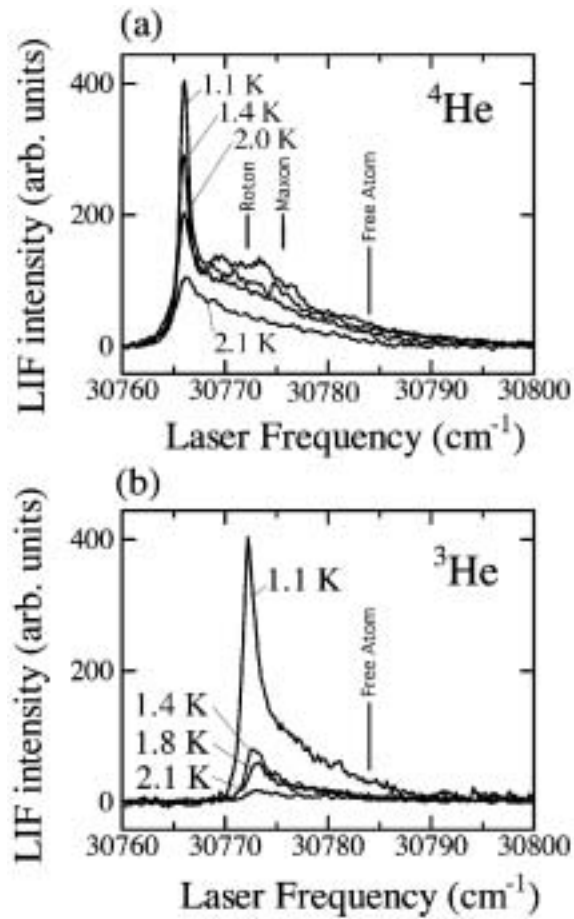


Figure 1. Excitation spectra of the $4f^6(^7F)5d6s^2\ ^8F_{7/2} \leftarrow 4f^76s^2\ ^8S_{7/2}$ transition of Eu atoms in (a) liquid ^4He and (b) liquid ^3He at several temperatures.

II-D Electron Transfer Regulation in Tetraheme Cytochromes *c*

Tetraheme cytochromes *c* are involved in the anaerobic energy metabolism. Cytochrome *c*₃ (cyt *c*₃) is an electron transport protein working in strictly anaerobic sulfate-reducing bacteria. This is a small (M. W. ≈ 14,000) soluble protein and shows very low redox potentials (typically, -240 ~ -357 mV vs. NHE). Small tetraheme cytochrome *c* (ST cyt *c*) is found in facultative anaerobes of *Shewanella* species and is the smallest tetraheme cytochrome (M. W. ≈ 12,000). The four hemes in ST cyt *c* is arranged in a chain-like manner in contrast to the cyclic heme architecture in cyt *c*₃. The major aims of this project is to elucidate the mechanism of the regulation of the electron transfer in tetraheme cytochromes *c* on the basis of tertiary structure and heme architecture. For this purpose, we are characterizing two different cytochromes mentioned above by NMR and electrochemistry. Since porphyrin is one of important elemental materials in nano-science, elucidation of the function of particular heme architectures would also contribute to this field.

II-D-1 Redox-Coupled Conformational Alternations in Cytochrome *c*₃ from *D. vulgaris* Miyazaki F on the Basis of its Reduced Solution Structure

HARADA, Erisa^{1,2}; FUKUOKA, Yuki²; OHMURA, Tomoaki³; FUKUNISHI, Arima²; KAWAI, Gota⁴; FUJIWARA, Toshimichi¹; AKUTSU, Hideo¹
(¹Osaka Univ.; ²Yokohama Natl. Univ.; ³Mitsubishi Heavy Ind.; ⁴Chiba Inst. Tech.)

[*J. Mol. Biol.* **319**, 767 (2002)]

Heteronuclear NMR spectroscopy was performed to determine the solution structure of ¹⁵N-labeled ferrocyanochrome *c*₃ from *Desulfovibrio vulgaris* Miyazaki F (*Dv*MF). Although the folding of the reduced cytochrome *c*₃ in solution was similar to that of the oxidized one in the crystal structure, the region involving hemes 1 and 2 was different. The redox-coupled conformational change is consistent with the reported solution structure of *Desulfovibrio vulgaris* Hildenborough ferrocyanochrome *c*₃, but is different from those of other cytochromes *c*₃. The former is homologous with *Dv*MF cytochrome *c*₃ in amino acid sequence. Small displacements of hemes 1 and 2 relative to hemes 3 and 4 were observed. This observation is consistent with the unusual behavior of the ²CH₃ signal of heme 3 reported previously. As shown by the ¹⁵N relaxation parameters of the backbone, a region between hemes 1 and 2 has more flexibility than the other regions. The results of this work strongly suggest that the cooperative reduction of hemes 1 and 2 is based on the conformational changes of the C-13 propionate of heme 1 and the aromatic ring of Tyr43, and the interaction between His34 and His35 through covalent and coordination bonds. Furthermore, it turned out that the unusual conformational distortion is involved in the attachment of heme 2. This will be associated with the unique structural properties of heme 2 in cytochromes *c*₃.

II-D-2 A Role of the Aromatic Ring of Tyr43 in Tetraheme Cytochrome *c*₃ from *Desulfovibrio vulgaris* Miyazaki F

OZAWA, Kiyoshi³; YASUKAWA, Fumiko³; TAKAYAMA, Yuki²; KUMAGAI, Jiro³;

OHMURA, Tomoaki⁴; CUSANOVICH, Michael A.⁵; TOMIMOTO, Yusuke⁶; OGATA, Hideaki⁶; HIGUCHI, Yoshiki⁶; AKUTSU, Hideo¹
(¹IMS and Osaka Univ.; ²Osaka Univ.; ³Yokohama Natl. Univ.; ⁴Mitsubishi Heavy Ind.; ⁵Unv. Arizona; ⁶Kyoto Univ.)

A novel *c*-type multiheme cytochrome overproduction system has been used to prepare large quantities of *Desulfovibrio vulgaris* Miyazaki F cytochrome *c*₃ and two mutations of the highly conserved aromatic residue, Tyr43. Tyrosine 43 is positioned parallel to the fifth heme axial ligand, His34, of heme 1 in the tetraheme cytochrome *c*₃. The macroscopic and microscopic formal redox potentials of Y43L and Y43F cytochromes *c*₃ were determined by differential pulse polarography and ¹H-NMR. Although the replacement of tyrosine with leucine increased all the redox potentials, the phenylalanine mutation generally decreased them. This strongly suggests that the aromatic ring at this position is important for maintenance of the extremely low redox potentials of cytochrome *c*₃. The effect of the leucine and phenylalanine mutations on the interacting potential between heme 1 and heme 2 shows that the aromatic ring is also involved in the cooperative reduction of these hemes. Furthermore, temperature dependent line-width broadening in partially reduced samples established that the aromatic ring at position 43 participates in the control of the kinetics of intramolecular electron exchange. The rate of reduction of Y43L cytochrome *c*₃ by 5-deazariboflavin semiquinone under partially reduced conditions was significantly different from that of the wild-type in the last stage of the reduction, supporting the involvement of Tyr43 in regulation of reduction kinetics.

II-D-3 A Directional Redox-Regulator Based on the Heme-Chain Architecture in the Small Tetraheme Cytochrome *c* from *Shewanella oneidensis*

HARADA, Erisa²; KUMAGAI, Jiro³; OZAWA, Kiyoshi³; IMABAYASHI, Shinichiro³; TSAPIN, Alexandre S.⁴; NEALSON, Kenneth H.⁴; MEYER, Terrance E.⁵; CUSANOVICH, Michael A.⁵; AKUTSU, Hideo¹
(¹IMS and Osaka Univ.; ²Osaka Univ.; ³Yokohama

Natl. Univ.; ⁴Cal. Inst. Tech.; ⁵Univ. Arizona)

[*FEBS Lett.* in press]

The macroscopic and microscopic redox potentials of the four hemes of the small tetraheme cytochrome *c* (STC) from *Shewanella oneidensis* were analyzed. The macroscopic potentials range from -248 to -138 mV, which are higher than those of *D. vulgaris* cytochrome *c*₃. The microscopic redox potentials show that the order of reduction is from hemes in the C-terminal domain (hemes 3 and 4) to the N-terminal domain (heme 1), showing the polarization of the tetraheme chain during the reduction. This makes heme 4 the most efficient electron delivery site. The redox characteristics of this heme architecture fit to multistep reduction of other redox centers through either heme 3 or heme 4. This mechanism could successfully elucidate the reduction mechanism of the flavin in fumarate reductase (flavo-cytochrome *c*). The characteristics of STC are completely different from those of a cyclic heme arrangement in cytochrome *c*₃. For the first time, the important role of the heme arrangement in a multiheme protein was brought to light.

II-E Studies on Higher-Order Gaussian Light Beams

II-E-1 Simple Generation of Higher-Order Gaussian Beams and the Application to Spectroscopy

SASADA, Hiroyuki
(IMS and Keio Univ.)

Recently optical vortices have attracted considerable attentions because of the phase singularity and the characteristic intensity distribution. In particular, the dark region is very useful to trap and guide cold atoms provided by laser cooling.¹⁾ Several methods of generating the optical vortices have been reported so far, but their efficiencies are rather low.

Last year we demonstrated a simple and efficient generation of optical vortices using glass plates and an astigmatic mode converter. However, the phase jump introduced by the glass edge is so sharp that the generated beam consists of many higher-order Gaussian modes, and hence has too many vortices.

To overcome these difficulties, we have demonstrated a novel method using an interferometer. A Gaussian beam is first split into two beams by a polarizing beam splitter. Each beam is reflected once by a mirror, then overlapped again with a small misalignment at a beam splitter. A $\lambda/2$ -wave plate is located in an arm to allow the two beams to interfere. The phase difference between two arms is adjusted so that the two beams have an opposite phase against each other at an output port. The resultant beam is very close to the HG₁₀ mode (HG: Hermite-Gaussian). It is further converted into the LG₀₁ mode (LG: Laguerre-Gaussian) with an optical vortex by an astigmatic mode converter. This method is also extended to generate the HG₁₁, HG₂₁, LG₁₀, and LG₁₁ beams.

Reference

- 1) T. Kuga, Y. Torii, N. Shiokawa, T. Hirano, Y. Shimizu and H. Sasada, *Phys. Rev. Lett.* **78**, 4713 (1997).

II-F Ultrafast Dynamics of Surface Adsorbed Species

Understanding of reaction dynamics at surfaces using ultra-short laser techniques is an important issue to clarify the mechanism of the reactions. Real-time observation of temporal change of surface species induced by UV, visible, and (Near-) infrared pump pulses is carried out using mid-IR pump-probe vibrational spectroscopy and Sum-frequency generation (SFG) spectroscopy which is one of the non-linear spectroscopies using ultra-short laser has high sensitivity for detection of molecular vibrations of adsorbed species on surface in the first layer. The aim of this study is the identification of molecular structures of the intermediates generated by electronic, vibrational, or thermal excitation and understanding of the reaction kinetics including potential energies, activation barriers, and entropies. Typical systems of our recent studies are formate (DCOO) adsorbed on Ni(111) surface, CO on Ni(111) surface, and D₂O on OD groups in alumina.

II-F-1 Time-Resolved Study of Formate on Ni(111) by Picosecond SFG Spectroscopy

KUSAFUKA, Koji¹; ONDA, Ken¹; NOGUCHI, Hidenori¹; KUBOTA, Jun¹; DOMEN, Kazunari¹; HIROSE, Chiaki¹; WADA, Akihide²
(¹Tokyo Inst. Tech.; ²IMS and Tokyo Inst. Tech.)

[*Surf. Sci.* **502/503**, 313 (2002)]

Time-resolved vibrational measurements were carried out on formate (HCOO) adsorbed on Ni(111) surface by combining the sum-frequency generation (SFG) method and picosecond laser system (time-resolution of 6 ps). Rapid intensity decrease (within the time-resolution) followed by intensity recovery (time-constant of several 10s ps) of CH stretching signal was observed when picosecond 800 nm pulse was irradiated on the sample surface. From the results of temperature and pump fluence dependences of temporal behaviour of signal intensity, we concluded that the observed intensity change was induced by non-thermal process. Mechanism of the temporal intensity change was discussed.

II-F-2 SFG Spectroscopy of CO/Ni(111): UV Pumping and Transient Hot Band Transition of Adsorbed CO

BANDARA, Athula¹; KANO, Satoru S.²; ONDA, Ken¹; KATANO, Satoshi¹; KUBOTA, Jun¹; DOMEN, Kazunari¹; HIROSE, Chiaki¹; WADA, Akihide³
(¹Tokyo Inst. Tech.; ²Hosei Univ.; ³IMS and Tokyo Inst. Tech.)

[*Bull. Chem. Soc. Jpn.* **75**, 1125 (2002)]

A UV excitation by a picosecond pulse at 266 nm induced an unusual shoulder to the $\nu_{\text{CO}} = 1 \leftarrow 0$ resonance peak of CO/Ni(111) monitored by sum-frequency generation (SFG) of visible and IR pulses. The observed line shape was reproduced by the use of a dipole-dipole interaction model with the coherent potential approximation (CPA) where the hot band transition with a population ratio of 0.3 to 0.7 ($\nu = 1$ to $\nu = 0$) was assumed. Neither the transition to the two-phonon bound state nor the coupling with the low-frequency phonon modes explained the observed changes. The shoulder appeared only during the UV excitation, which indicat-

ed that the electronically driven excitation, presumably by the hot electrons generated by the irradiation, dominated the process. As possible mechanisms, the involvement of intermediate negative ion resonance state and/or the non-adiabatic coupling of electronic states with C–O stretching mode were considered.

II-F-3 Surface Hydroxyl Group and Adsorbed Water on γ -Al₂O₃ Studied by Picosecond Infrared Pump-Probe Experiment

ONDA, Ken¹; TANABE, Kinuka¹; NOGUCHI, Hidenori¹; WADA, Akihide³; SHIDO, Takahumi²; YAMAGUCHI, Aritomo²; IWASAWA, Yasuhiro²
(¹Tokyo Inst. Tech.; ²Univ. Tokyo; ³IMS and Tokyo Inst. Tech.)

[*J. Phys. Chem. B* **105**, 11456 (2001)]

Picosecond infrared-infrared pump-probe experiments in the OD stretching region were carried out on dehydrated and multilayer water-adsorbed γ -Al₂O₃. For the dehydrated γ -Al₂O₃, transient bands assigned to the bleaching and hot bands of the OD stretching mode of isolated surface hydroxyl groups were observed, and the population lifetime (T_1) of the vibrational excited state ($\nu = 1$) of the mode was 200 ± 10 ps at 293 K. The characteristic temperature dependence of T_1 is indicative of a seven-phonon process. For the water-adsorbed γ -Al₂O₃, the transient bleaching and transient hot bands with a lifetime of 10–12 ps were observed by excitation of the absorption peak at 2630 cm^{-1} . In addition to these bands, weak transient bands were observed in the low frequency region. These results are considered evidence of the existence of isolated water molecules on the γ -Al₂O₃ surface. Pure dephasing is also discussed based on the bandwidth of the observed transient bands.

II-G Spin Reorientation Transitions of Ultrathin Magnetic Films Induced by Chemisorption

Magnetic anisotropy of ultrathin metal films is one of the most attractive subjects in magnetism. When one considers magnetic anisotropy of thin films within the framework of the classical electromagnetic theory, one finds that in-plane magnetization is always more stable than perpendicular magnetization. Perpendicular magnetic anisotropy (PMA) is, however, sometimes observed in real systems and the understanding of the origin of PMA is important from the viewpoints of both fundamental physics and technological applications to new-generation high-density recording media. We have been investigating the microscopic mechanism of PMA that is stabilized by gaseous adsorption on magnetic film surfaces by means of the synchrotron radiation x-ray magnetic circular dichroism (XMCD) technique. A goal of these works is spin engineering by which the magnetization of ultrathin metal films can be controlled artificially.

II-G-1 Perpendicular Magnetic Anisotropy in Co/Pd(111) Stabilized by Chemisorption of CO and NO

YOKOYAMA, Toshihiko; MATSUMURA, Daiju¹; AMEMIYA, Kenta¹; KITAGAWA, Soichiro¹; SUZUKI, Norihiro¹; OHTA, Toshiaki¹
(¹Univ. Tokyo)

[*J. Phys.: Condens. Matter* in press]
[*Phys. Rev. B* **66**, 024402 (2002)]

Spin reorientation transitions of ultrathin Co/Pd(111) films induced by adsorption of atoms and molecules have been investigated by means of Co $L_{III,II}$ -edge x-ray magnetic circular dichroism (XMCD). We have examined CO, NO, O and H as chemisorbed species. Figures 1(a) and 1(b) show the Co $L_{III,II}$ -edge XMCD spectra on clean and CO-adsorbed 4.5 ML Co/Pd(111) at 200 K, respectively. In clean Co/Pd(111) [Figure 1(a)] the XMCD signal appears only in the grazing-incidence ($\theta = 30^\circ$) spectrum, while in CO-adsorbed Co/Pd(111) the normal-incidence ($\theta = 90^\circ$) spectrum gives a two-times more intense XMCD signal than the $\theta = 30^\circ$ spectrum. These observation directly implies that the magnetization direction varies from in-plane to perpendicular upon CO adsorption. We observed a similar adsorbate-induced spin reorientation transition in the NO case as well, while in O or H adsorption no transitions took place. We have investigated detailed Co-thickness dependence in the case of CO. Figures 1(c) and 1(d) show the Co spin magnetic moments of clean and CO-adsorbed Co/Pd(111), respectively. The critical thickness of the spin reorientation transition in CO-adsorbed Co is found to be ~ 6.5 ML, which is by ~ 3 ML greater than that of clean Co (~ 3.5 ML), implying the stabilization of PMA by CO adsorption.

The most important information from XMCD is the orbital magnetic moments, which determine the magnetic easy axis in spite of very small contribution to the total magnetic moments. Figure 1(e) shows the orbital magnetic moments of Co on clean and CO-adsorbed Co/Pd(111). Below ~ 3.5 ML the *surface normal* orbital moment is found to be left *unchanged*, while above ~ 6.5 ML the *surface parallel* orbital moment is *reduced* significantly after CO adsorption. We conclude that the observed stabilization of perpendicular magnetic anisotropy due to adsorption is ascribed to *quenching* of the

surface parallel orbital magnetic moment.

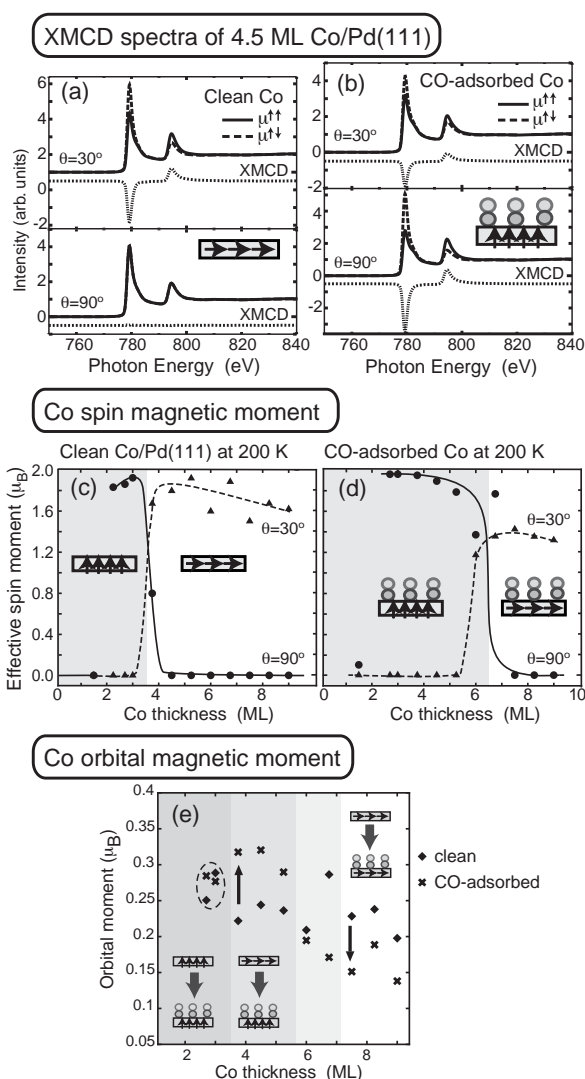


Figure 1. (a), (b): Co $L_{III,II}$ -edge circularly polarized (solid and dashed lines) and XMCD (dotted line) spectra of 4.5 ML Co/Pd(111) at 200 K before (a) and after (b) CO adsorption. θ is the angle between surface normal and the x-ray electric field ($\theta = 30^\circ$ and $\theta = 90^\circ$ correspond to grazing and normal x-ray incidence, respectively). It is found that the magnetic easy axis rotates from in-plane in (a) to perpendicular in (b).

(c), (d): Co thickness dependence of the Co spin magnetic moments at 200 K. Hatched areas indicate the PMA regions. The critical thickness for the spin reorientation transition is ~ 3.5 ML for clean Co (c) and ~ 6.5 ML for CO-adsorbed Co (d), this indicating that the perpendicular magnetic anisotropy is stabilized upon CO adsorption.

(e): Co thickness dependence of the Co orbital magnetic moments at 200 K. After CO adsorption, the perpendicular orbital moment does not vary so much (see the data below ~ 3.5 ML), while the in-plane orbital moment reduces significantly (see the ones above ~ 7 ML).

II-H Local Structures in Photoinduced States of Molecular-Based Magnetic Materials

Molecular-based magnets provide noble properties such as photoinduced magnetism. Photoinduced phase transition is closely related to bistability of the ground state in the material. Light irradiation stimulates the macroscopic phase transition between the ground state and the metastable state, although thermal fluctuation triggers the thermal phase transition. Although it has been believed that the photoinduced phase is the same state as the thermally induced phase, recent investigations have reported some differences in structure from the high-temperature phase. We have been studying local structures and electronic properties of photoinduced phases of Prussian-blue analogues and other metal-complex magnets by means of x-ray absorption fine structure (XAFS) spectroscopy. XAFS is one of the most suitable methods for these purposes since the technique does not require long-range order in the sample and provide element-specific information about each metal atom.

II-H-1 Photoinduced Phase Transition of $\text{RbMnFe}(\text{CN})_6$ Studied by X-Ray-Absorption Fine Structure Spectroscopy

YOKOYAMA, Toshihiko; TOKORO, Hiroko¹; OHKOSHI, Shin-ichi¹; HASHIMOTO, Kazuhito¹; OKAMOTO, Kaoru¹; OHTA, Toshiaki¹
(¹Univ. Tokyo)

[Phys. Rev. B **66**, 184111 (2002)]

A Prussian-blue analogue of $\text{RbMnFe}(\text{CN})_6$ shows a thermally induced first-order phase transition ($T_{c\downarrow} = 231$ K and $T_{c\uparrow} = 304$ K) and also turns to a ferromagnetic phase below 12 K. Upon visible-light irradiation, the ferromagnetism is quenched and the phase is transformed to the metastable nonmagnetic state. In this work, we have investigated the photoinduced magnetic phase transition of $\text{RbMnFe}(\text{CN})_6$ by means of XAFS spectroscopy.

Mn and Fe *K*-edge x-ray-absorption near-edge structure spectra have clarified that upon the phase transition, a Fe 3*d* electron is transferred to the Mn 3*d* level; the electronic state of Mn changes from trivalent (d^4 , spin momentum $S = 2$) to divalent (d^5 , $S = 5/2$), while the Fe state correspondingly varies from divalent (d^6 , $S = 0$) to trivalent (d^5 , $S = 1/2$). Such a tautomeric scheme in the photoinduced phase transition is exactly the same as in the thermally induced transition.

Local structures have been investigated by the extended x-ray-absorption fine-structure analysis for the photoinduced phase as well as for the low- and high-temperature phases. The low-temperature phase shows a significant Jahn-Teller distortion in the Mn(III) octahedron, where the Mn–N distances for four shorter and two longer bonds are 1.964 ± 0.008 Å and 2.21 ± 0.01 Å, respectively. The high-temperature phase gives a longer Mn–N distance of 2.211 ± 0.006 Å, although

some minor contribution from a shorter distance still remains. It is also revealed that the atomic configuration of the –Fe–C–N–Mn– chain is essentially collinear and that the Rb ions locate at the center of the cubic lattice. The photoinduced phase was found to be structurally and electronically identical to the high-temperature phase. Summary of the present investigation is given in Figure 1.

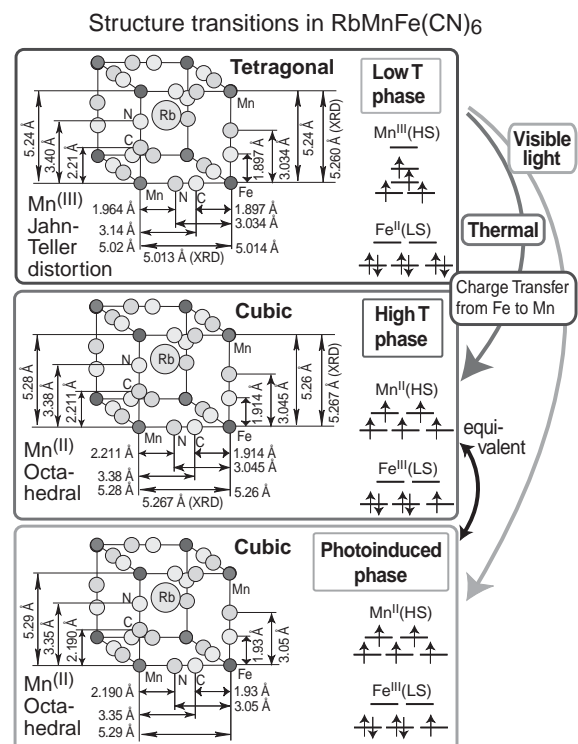


Figure 1. Summary of the present investigation for the phase transitions in $\text{RbMnFe}(\text{CN})_6$.

II-I Molecular and Electronic Structures of Metallofullerenes

The continued interest in radical ions of fullerenes and metallofullerenes has resulted from the discovery of superconductivity in the CT complexes of alkali metals with fullerenes. Spectroscopic information concerning the electronic and spin states of the metallofullerenes has been obtained by ESR measurements.

II-I-1 Spin Dynamics of Lanthanum Metallofullerenes

OKUBO, Shingo; KATO, Tatsuhisa

Full separation of topological isomers of each $\text{La}@C_n$ component ($n = 76$ to 90) was attempted by 2-stage HPLC separation with chlorobenzene eluent, and all species of $\text{La}@C_n$ with even number n from 76 to 90 were detected. Their Electron Spin Resonance (ESR) spectra were recorded at various temperatures. The line width of the ESR spectrum in CS_2 solution was analyzed by the theory on the basis of hydrodynamics. Enormous variety of ESR spectra of $\text{La}@C_n$ s was obtained in terms of g factor, hyperfine coupling constant, and line width. The feature of the temperature dependence of the line width was almost interpreted by the hydrodynamics, and the electronic structure of $\text{La}@C_n$ was deduced from the ESR parameters. However in the cases of the isomer I of $\text{La}@C_{80}$ and isomer II of $\text{La}@C_{84}$ abnormally large line width was measured, as shown in Figure. The topological cage structure of $\text{La}@C_{80}$ and $\text{La}@C_{84}$ reflected on the specific spin dynamics.

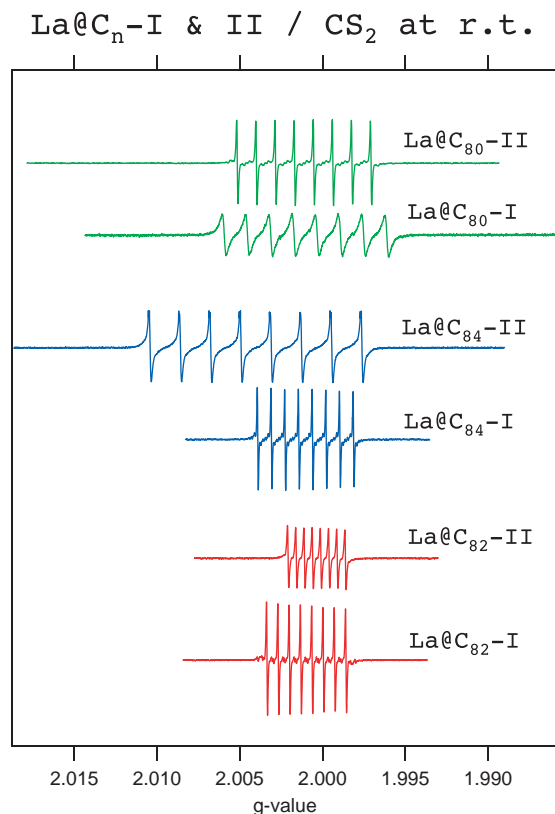


Figure 1. X-band ESR spectra of both isomers I and II of $\text{La}@C_{80}$, $\text{La}@C_{82}$, and $\text{La}@C_{84}$ in CS_2 solution.

II-I-2 Electronic State of Scandium Trimer Encapsulated in C₈₂ Cage

KATO, Tatsuhisa; OKUBO, Shingo; SHINOHARA, Hisanori¹
(¹Nagoya Univ.)

The ESR spectrum of $\text{Sc}_3@\text{C}_{82}$ in toluene and CS_2 solutions exhibits the symmetric hyperfine splitting of the 22 lines with a line width of 0.5 gauss at room temperature, which was consistent with the structure of $\text{Sc}_3@\text{C}_{82}$ having the C_{3v} symmetry. The line widths of the 22 lines were much broader than that for $\text{Sc}@C_{82}$. The broader line width of the scandium trimer in C_{82} could reflect the intra-molecular dynamics that averaged among three Sc metals' environments in the Jahn-Teller distorted structure of the whole molecule. The intra-molecular dynamics is the inherent nature of the Sc trimer encapsulated in the C_{82} cage with the symmetry of C_{3v} . The intra-molecular charge transfer from the central metal to the fullerene cage would give the stable electronic structure of an endo-metallofullerene. The X-ray diffraction study reported that there was no bonding electron between the cage and the trimer, and that the charge state of the Sc_3 was $3+$ leading to the electronic structure of $(\text{Sc}_3)^{3+}@\text{C}_{82}^{3-}$. Electron spin resonance (ESR) spectrum of the scandium trimer encapsulated in the C_{82} cage ($\text{Sc}_3@\text{C}_{82}$) was measured at the low temperature. The spectrum exhibited the specific pattern due to the strongly an-isotropic hyperfine tensor of the scandium trimer. The electronic state of the $\text{Sc}_3@\text{C}_{82}$ was given from the analysis of the hyperfine tensor, as shown in Figure 1.

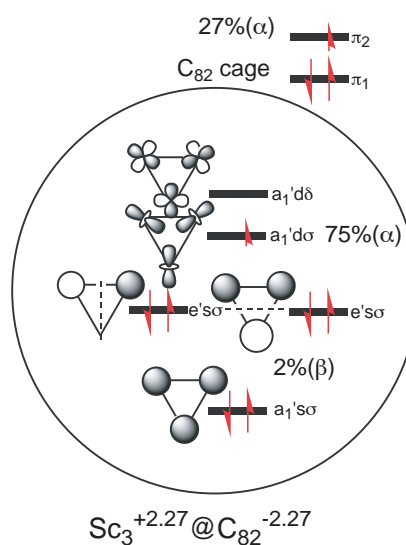


Figure 1. The Electronic structure of $\text{Sc}_3@\text{C}_{82}$ molecule deduced from the analysis of the hyperfine tensor of Sc metal.

II-I-3 Efficient Reduction of Metallofullerenes by Solvation of Pyridine and Dimethylformamide

OKUBO, Shingo; KATO, Tatsuhisa; MAEDA, Yutaka¹; AKASAKA, Takeshi¹
(¹Univ. Tsukuba)

Various solvents have been used in the extraction of endohedral metallofullerenes from the raw soot produced by the arc-discharge method. Toluene, CS₂, and chlorinated benzenes have been used generally as solvent. On the other hand, pyridine and dimethylformamide (DMF) are known to give effective enrichment of metallofullerenes in the extraction, and aniline is especially effective for endohedral metallo-C₆₀. The specific affinity of these solvents with metallofullerenes would be attributed to the electronic interaction of the lone pair electron on nitrogen of the solvent with the π orbital of the metallofullerene's cage. However the exact nature of the interaction has not been clarified as yet. We recently presented the evidence that anions of La@C₈₂-I and Gd@C₈₂-I are easily produced with almost 100% yield by the solvation of pyridine and DMF. The formation of the La@C₈₂-I anion was confirmed by Vis-NIR and ¹³C-NMR measurements, which gave identical spectra with those of the La@C₈₂-I anion reported before. The ¹³⁹La-NMR and ¹³C-NMR spectra of La@C₈₂-I anion are respectively shown in Figure. The chemical shift of the ¹³⁹La-NMR line corresponded with that reported before. For assignment the anion generated in DMF, ¹³C-NMR spectrum was measured under same condition of electrochemically method in literature. After addition of electrolyte (TBAP) and removed DMF, the anion of La@C₈₂ generated in DMF

was dissolved in a mixture of CS₂ and acetone (1:1). The spectrum is in good agreement with that prepared by electrochemical method. The electron spin resonance (ESR) and Vis-NIR spectra of Gd@C₈₂-I dissolved in pyridine and DMF also give good agreements with those of the anion produced by electrochemical reduction. It could be generally concluded that the solvation of pyridine, and DMF, and aniline leads to the efficient reduction of endohedral metallofullerenes.

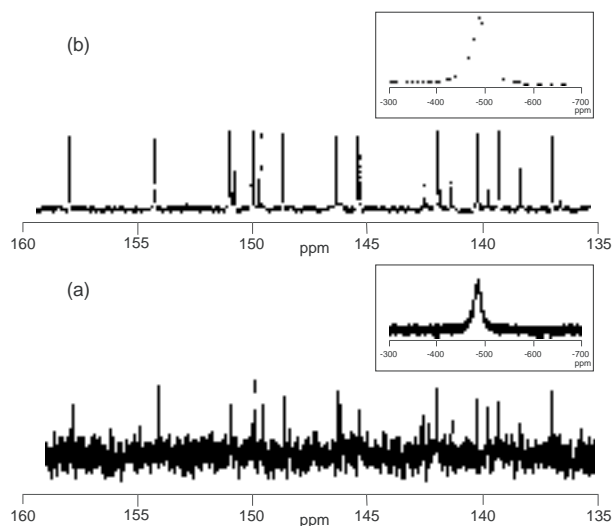


Figure 1. ¹³⁹La-NMR spectrum of La@C₈₂-I recorded in the DMF-d7 solution (a) and that of the La@C₈₂-I anion produced by electrochemistry (b), as shown in the inset of Figure. ¹³C-NMR spectrum of La@C₈₂-I in DMF (a) was measured under same condition of electrochemically method (b) in literature.

II-J High Field and Pulsed Electron Spin Resonance Spectroscopy

Electron spin resonance (ESR) spectroscopy has been a powerful technique for the characterization of radical species. The modern development of EPR spectroscopy enables us to investigate the heterogeneous and disordered system in detail. Especially the high frequency and pulsed EPR methods achieve the substantial resolution enhancement of spectrum. The advanced EPR spectroscopy is applied to study on the reaction mechanism in the heterogeneous system and the detection of the multi-cation species.

II-J-1 High-Field/High-Frequency ESR Study of Gadolinium Metallofullerenes

FURUKAWA, Ko; TOYAMA, Namiki; OKUBO, Shingo; KATO, Tatsuhisa

A high-field/high-frequency ESR spectrometer is a powerful means to determine the complicated spin state of metallofullerenes. The analysis of the spin states of Gd@C₈₂-I and related species are reported here. The electronic structure of a gadolinium metallofullerene is stabilized by the intra-molecular charge transfer, and is described by the electronic configuration of Gd(4f⁷)-

@C₈₂(π^1), as shown in the Figure 1. The complicated electron spin state would be expected because of the combination of the octet spin site of gadolinium with the π spin of the fullerene cage. If the exchange interaction of J between the π spin and the octet spin is negative, these spins couple in anti-ferromagnetic manner and the resultant spin quantum number S will be 3. If the π spin on the cage is cancelled by adding an extra spin on the π orbital, S will be 7/2. This cancellation would be attained in the case of Gd@C₈₂ anion, or in the case of the dimerization of two Gd@C₈₂s. The π spin on the cage has the key function for the determination of the total spin state, and we confirmed the spin

state of Gd@C₈₂-I in its monomer form, dimer form, and anion form by the high-field/high-frequency ESR measurement as shown in Figure 1.

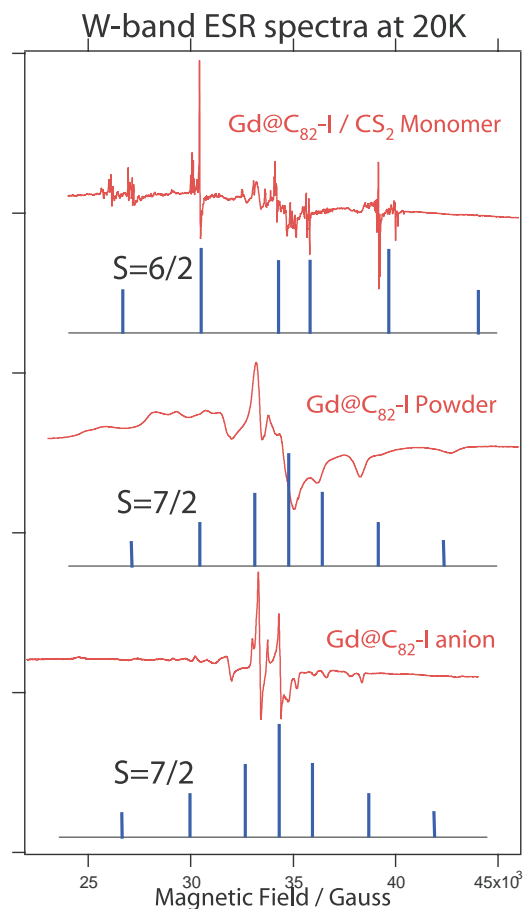


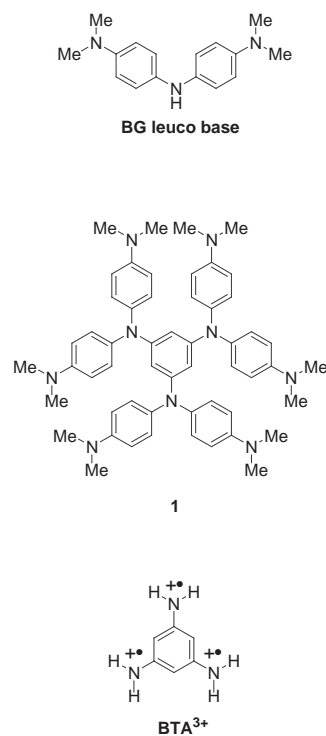
Figure 1. The high-field/high-frequency ESR (95 GHz) spectra of Gd@C₈₂-I in its monomer form, dimer form, and anion form produced by the electrochemical method.

II-J-2 A Bindschedler's Green-Based Arylamine: Its Polycations with High-Spin Multiplicity

KANEMOTO, Katsuichi; KATO, Tatsuhisa; ITO, Akihiro¹; INO, Haruhiro¹; MATSUI, Yuki¹; TANAKA, Kazuyoshi¹
(¹Kyoto Univ.)

Intramolecular high-spin correlation in a series of the successively generated polycationic species of Bindschedler's green-based arylamine, *N,N,N',N',N'',N''*-hexakis[4-(dimethylamino)phenyl]-1,3,5-benzenetriamine (**1**) have been investigated by continuous and pulsed EPR spectroscopy. Cyclic voltammetry shows multi-redox behavior of **1** that can be reversibly oxidized from monocation to hexacation. Depending on quantity of the added oxidant, the characteristic EPR spectra are observed for polycations of **1** in frozen solution. Unequivocal determination of the spin state at each oxidation stage of **1** is given by a pulse EPR technique, that is, electron spin transient nutation spectroscopy as shown in Figure 1. Observation of the unusual spin state after annealing of the highly charged poly-

cations of **1** is also reported.



Scheme 1. (1): Molecular structures of *N,N,N',N',N'',N''*-hexakis[4-(dimethylamino)phenyl]-1,3,5-benzenetriamine.

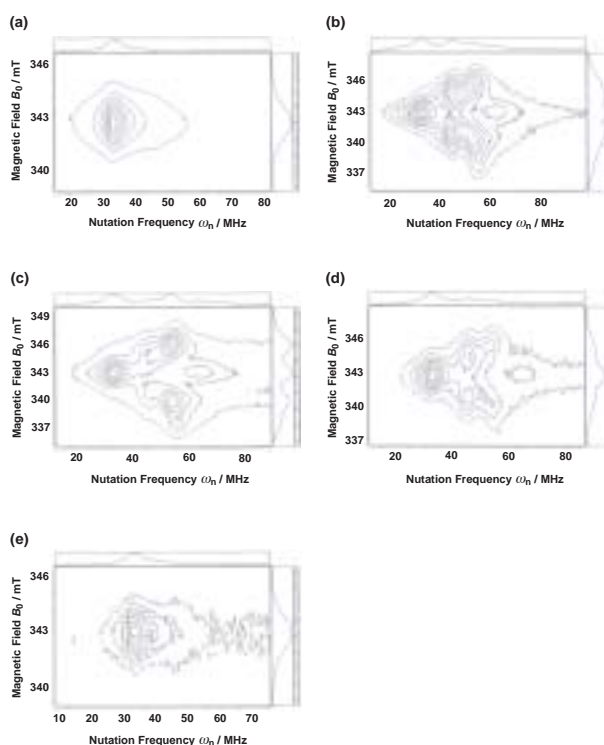


Figure 1. Field-swept electron spin transient nutation spectra of **1** oxidized by (a) 1 molar equiv, (b) 2 molar equiv, (c) 3 molar equiv, (d) 4 molar equiv, and (e) 5 molar equiv of TBA·SbCl₆ in *n*butyronitrile at 5 K. ω_1 corresponds to about 30 MHz.

II-K State Correlated Raman Spectroscopy

The vibrational Raman polarizability tensor responds to molecular reorientational relaxation process, and the structural environment in condensed media. The measurement of Raman scattering is a powerful technique for the study of molecular motion and of the mechanism of phase transition. We've built up the system of multichannel type detection of Raman scattering combined with the temperature controlled cell.

II-K-1 Molecular Ordering Deformation Induced by Externally Applied Electric Field in an Antiferroelectric Liquid Crystal

HAYASHI, Naoki; KATO, Tatsuhisa; ANDO, Tomohiro¹; FUKUDA, Atsuo¹
(¹Shinshu Univ.)

[*Jpn. J. Appl. Phys.* **41**, 5292 (2002)]

Molecular orientational ordering in an antiferroelectric liquid crystal was studied by observing polarized Raman scattering in a homogeneously aligned thin sample exposed to static electric field. The apparent orientational order parameters gradually increased with the applied electric field strength even in the pretransitional regime from antiferro- to ferroelectric phase although the averaged molecular orientation was hardly changed. (See Figure 1) This change in the order parameters indicates the deformation of the *c*-director and is represented by the similar equation describing the nematic director deformation induced by an external electric field, in which the electric coherence length was inversely proportional to the applied electric field strength.

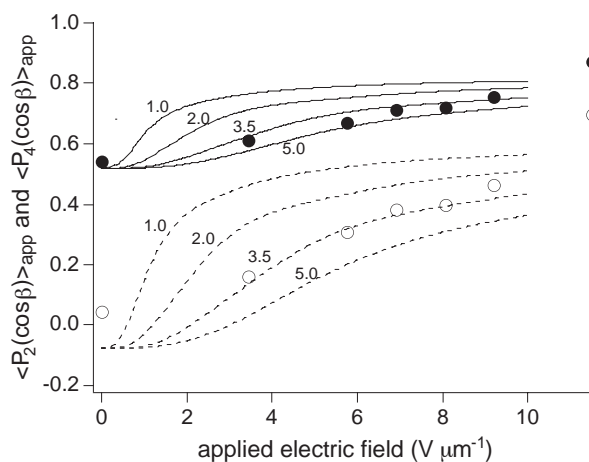


Figure 1. Apparent orientational order parameters under static electric field, solid circle: $\langle P_2(\cos\beta) \rangle_{\text{app}}$; open circle: $\langle P_4(\cos\beta) \rangle_{\text{app}}$. The solid and dotted lines are $\langle P_2(\cos\beta) \rangle_{\text{app}}$ and $\langle P_4(\cos\beta) \rangle_{\text{app}}$ given by the model calculation. The numbers beside the lines show the values of $\xi_b E$; 1.0, 2.0, 3.5 and 5.0 V. Here, ξ_b is the electric coherence length and E is the applied electric field strength.

RESEARCH ACTIVITIES III Department of Electronic Structure

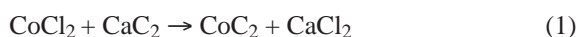
III-A Synthesis and Characterization of Exotic Molecule-Based Nano-Clusters with Transition Metals : Behavior as Single Domain Magnets

Molecule-based nanoclusters with transition metals are highly important in introducing electronic and magnetic functionalities in nanoelectronic devices. In view of electronic structure of metal- π conjugate systems, $M-C_2$ molecules, where $M = Fe, Co, Ni$ etc., are expected to generate $d-\pi^*$ interaction networks on cluster $(M-C_2)_n$ formation or on solidification. The ground state of $Co-C_2$ molecule is predicted to be 4B_1 with a symmetric triangular configuration where the $4s$ and d -orbital occupation numbers are far from integer, and the energy range of the upper sextets is only 5–6 kcal/mol (A.V. Arbuzniz and M. Hendriks, *Chem Phys. Lett.* **320**, 575 (2000)). Thus this high spin molecule should be very much suitable for making molecule-based nanocluster magnets. Here we report how we have generated molecule-based $(Co-C_2)_n$ magnets. The nano-size clusters isolated in amorphous carbon matrices are demonstrated to work as room-temperature single domain magnets.

III-A-1 Magnetic Behavior of Crude CoC_2 Solid Synthesized in Acetonitrile Solution

HINO, Kazuyuki¹; KOSUGI, Kentaroh; SEKIYA, Hiroshi¹; NISHI, Nobuyuki
(¹Kyushu Univ.)

CoC_2 molecules are synthesized from $CoCl_2$ and CaC_2 in acetonitrile or benzonitrile solution. The reaction scheme is expected as follows:



This reaction occurs on the surface of the CaC_2 particles in the solutions. Thus the structure of the solid products is not homogeneous. The infrared spectrum of the raw materials indicated that the commercial CaC_2 was heavily contaminated with $Ca(OH)_2$ and H_2O . The product solid was washed with water to convert CaC_2 to $Ca(OH)_2$ and C_2H_2 and the residual $CoCl_2$, $CaCl_2$ and $Ca(OH)_2$ were also removed by water. The color of the final product was greenish black. The infrared spectrum of the product exhibited the doublet band at 1375 and 1475 cm^{-1} that corresponds to the doublet band of CaC_2 at 1420 and 1500 cm^{-1} . The energy dispersed X-ray emission analysis indicated that the cobalt to carbon ratio changes from particle to particle in the range of 1.5 to 2.0. The particles containing higher oxygen concentration (due to water or OH contamination) exhibited lower ratios. The evolution of $(CoC_2)_n$ clusters in these particles is thought to be blocked by the inclusion of the hydroxide or water molecules. Figure 1 shows the temperature dependence of the magnetic susceptibility of the solid CoC_2 synthesized in acetonitrile. The CoC_2 solid produced in benzonitrile solution showed much larger susceptibility and the reason is ascribed to less water contamination in benzonitrile. The inserted graph in Figure 1 shows the magnetic hysteresis curve of the product in acetonitrile. The cohesive force of the CoC_2 solid produced in benzonitrile solution was 500 Oe at 1.8 K. Thus the $Co^{++}C_2^{-}$ salt compound becomes cluster

magnets at the temperatures lower than 4.5 K. The removal of the interstitial impurity species from the solid is expected to produce crystalline magnets that works at higher temperatures.

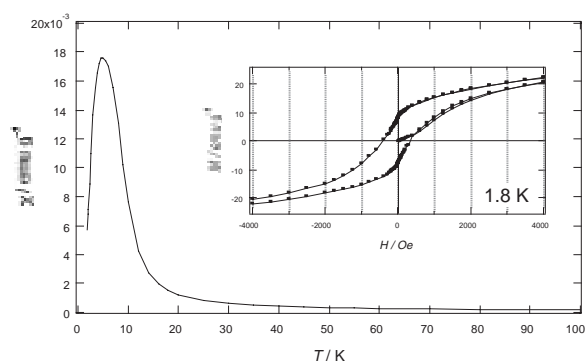


Figure 1. Temperature change of the magnetic susceptibility of CoC_2 solids synthesized from $CoCl_2$ and CaC_2 in acetonitrile solution.

III-A-2 Electron Microscope and EXAFS Study of Matrix Embedded $(Co-C_2)_n$ Nano-Cluster Magnets

NISHI, Nobuyuki; KOSUGI, Kentaroh; HINO, Kazuyuki¹; YOKOYAMA, Toshihiko; OKUNISHI, Eiji²
(¹Kyushu Univ.; ²JEOL Co. Ltd.)

$(Co-C_2)_n$ nanoparticles are synthesized from CH_2Cl_2 solution of $Co_4(CO)_{12}$ by heating up to 210 °C in a closed vessel. The cluster particles are embedded in amorphous carbon. Transmission electron microscope (TEM) observation of the particles provides a size distribution with an average size of 12 nm. Figure 1-a shows a TEM image of a relatively large nanocluster embedded in the matrix. Although most of the nanoparticles exhibited the single array of the lattice stripes (just like a single nanocrystals) as seen in the expanded image c, the upper part of this particle shows disor-

dered, thereby, three dimensional “step” structure around the border region between the upper and the middle parts (expanded image b). The image of the step area reminds us a structure similar to NaCl type crystals. The image of the matrix in the expanded view c shows an amorphous structure in contrast to the ordered structure of the particle. Figure 1-b displays the electron energy loss spectra of the nanoparticles (a) and the matrix (b) observed with an electron beam size of 2.5 nm. The bottom frame shows that the Co-L bands at 781 and 796 eV are seen for the nanoparticle but the matrix does not show any signals of Co component. The shape of the matrix C-K band is characteristic of amorphous carbon, while the spectral feature of the nanoparticle exhibits the enhanced π^* resonance at 285 eV and the low energy shift of the σ^* resonance, characteristic of unsaturated (sp or sp^2) carbon bonds. The intensity ratio of the C-K bands provides a ratio of cobalt to carbon to be 1 : 2. The ratio and the presence of the π^* resonance band indicates that the cluster is $(\text{Co}^{2+}\text{C}_2^{2-})_n$. The observed salt type structure image similar to that of a $\text{Ca}^{2+}\text{C}_2^{2-}$ crystal is in accord with this assignment. The radial structure function (RSF) obtained by Fourier transformation of extended X-ray absorption fine structure (EXAFS) provided the strongest Co–C peak at 2.08 Å and the two Co–Co peaks at 3.18 Å and 3.9(\pm 0.2) Å. These structural parameters are also in good agreement with the salt type structure for the $(\text{Co}^{2+}\text{C}_2^{2-})_n$ clusters, although the every Co and C_2 in the cluster is bonded with $d-\pi^*$ valence bond networks.

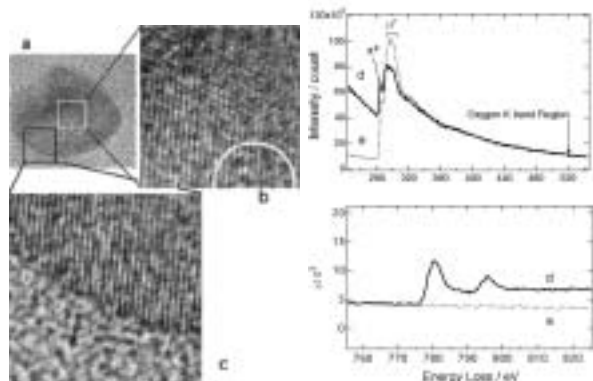


Figure 1. left: A TEM image of a relatively large particle in the matrix. The upper part was scraped off by the slicing knife of the microtome cutting machine exhibiting the disordered steps (image b). ($5 \times 5 \text{ nm}^2$) Image c shows the structural contrast of the nanoparticle with that of the amorphous carbon matrix. ($6 \times 6 \text{ nm}^2$)

Right: Electron energy loss spectra of the nanoparticle (of which image is shown on the left, spectrum d) and the matrix (spectrum e).

III-A-3 Magnetic Behavior of Matrix Embedded $(\text{Co}-\text{C}_2)_n$ Nano-Clusters as Single Domain Room-Temperature Magnets

KOSUGI, Kentaroh; HINO, Kazuyuki¹;
YOKOYAMA, Toshihiko; NISHI, Nobuyuki
(¹Kyushu Univ.)

Magnetic properties of the $(\text{Co}-\text{C}_2)_n$ nanoparticles embedded in the amorphous carbon matrix were mea-

sured with a SQUID magnetometer (Quantum Design MPMS-7S). Figure 1 shows the temperature change of the magnetic susceptibility under the zero-field cooling (ZFC) condition and the field cooling (FC) at 10 Oe external field. The susceptibility decreases with decreasing temperature from 300 K to 20 K at zero field suggesting that the particles are interacting and prone to align antiparallel to each other, while under the field cooling condition it increases with decreasing temperature. This means that the 10 Oe external field aligns the magnetic moments of the particles along the field direction. The two curves behaves just oppositely, and the average values are nearly temperature independent. The hysteresis shows that the saturation magnetization and the residual magnetization increases at lower temperatures while the cohesive force decreases at lower temperature. This behavior is in accord with the theoretical expectation for single domain magnets which exhibit cohesive force in inverse proportional to the saturation magnetization (S. Chikazumi, *Physics of ferromagnetism*, Shokabo, Vol II, 269 (1984)).

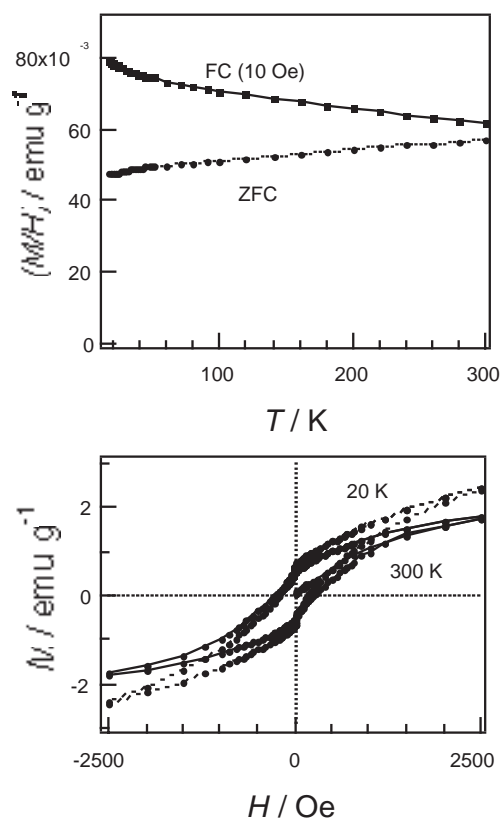


Figure 1. top: Temperature change of magnetic susceptibility of the matrix embedded $(\text{Co}-\text{C}_2)_n$ nano-clusters measured under the zero-field cooling condition (ZFC) and the field cooling (FC) condition. bottom: magnetic hysteresis curves at 300 K (solid curve) and 20 K (dotted curve).

III-A-4 Construction of Vacuum Apparatus for Mass-Resolved Spectroscopies of Non-Volatile Solid Samples

INOKUCHI, Yoshiya; HINO, Kazuyuki¹; NISHI, Nobuyuki
(¹Kyushu Univ.)

In order to apply mass-resolved spectroscopic methods to non-volatile samples, we need to vaporize them in a vacuum apparatus. In particular, for the samples prone to be damaged by water or oxygen, it is necessary to introduce them into the vacuum apparatus without being exposed by the air. Recently, we have constructed a new apparatus for mass-resolved spectroscopies of non-volatile (and non-metallic) solid samples. Figure 1 shows a schematic diagram of the apparatus. It consists of a liquid beam source, a titanium rotating drum, and a time-of-flight mass spectrometer. Non-volatile samples are dissolved in some volatile solvents. The solutions are injected through a modified injector needle into the vacuum chamber as a liquid beam. The surface of the rotating titanium drum is located at 5 mm away from the exit of the needle. The solvent is vaporized, and only the solute species are fixed on the drum. The solid sample on the drum is laser-desorped by the third harmonics of a Nd:YAG laser (355 nm) introduced through a hole between a sample chamber and a main chamber. The gaseous sample is ionized by three types of ionization technique: matrix-assisted laser desorption-ionization (MALDI), electron impact (EI), and resonance-enhanced multiphoton ionization (REMPI). The produced ions are mass-analyzed by the time-of-flight mass spectrometer. Since the non-volatile samples are directly introduced into the spectrometer as solutions and fixed on

the drum, the samples does not contact with the air. We can obtain excitation spectra of the samples by scanning the wavelength of the ionization laser. Photodissociation spectra of the sample ions can be measured by the introduction of a dissociation laser into the drift region of the spectrometer.

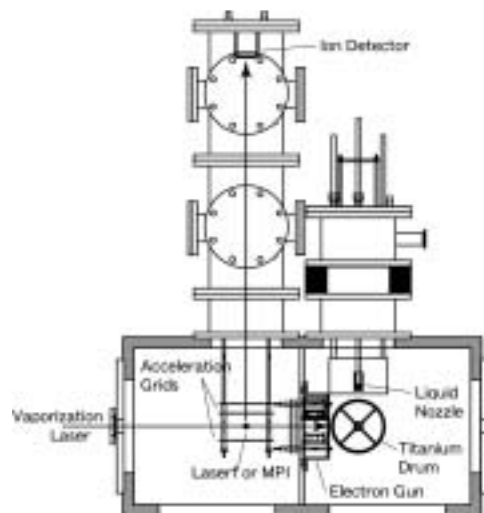


Figure 1. Schematic diagram of a time-of-flight mass spectrometer for solid samples.

III-B States of Neutral and Ionic Molecular Associates in Solutions

States of molecular associates particularly in aqueous solutions are of great importance in understanding the role of molecules in living organisms. We found that any ideally mixed state cannot be seen in protic-protic mixtures such as water-alcohol, water-acetic acid, and alcohol-acetic acid systems on the molecular level at solute molar fractions (χ_A) higher than 0.001. In such a system, solute-solute association is highly favored resulting in microscopic phase separation. Here we demonstrate that aprotic solvent such as acetonitrile can produce ideally mixed state(s) for acetic acid.

III-B-1 States of Molecular Associates in Binary Mixtures of Acetic Acid with Protic and Aprotic Polar Solvents: A Raman Spectroscopic Study

NAKABAYASHI, Takakazu; NISHI, Nobuyuki

[*J. Phys. Chem. A* **106**, 3491 (2002)]

The local structure of acetic acid in protic and aprotic polar solvents have been studied by Raman spectroscopy and ab initio calculations with the self-consistent reaction field (SCRf) method. As acetic acid is diluted in water, the C=O stretching Raman band of acetic acid becomes broader and shows a higher wavenumber shift from 1666 to 1710 cm^{-1} , which arise from the generation of acetic acid microphases. In the region of $0.001 \leq \chi_A$ (acetic acid mole fraction) ≤ 0.2 , both the peak position and the bandwidth of the C=O band are hardly changed, indicating that the acetic acid microphases exist even in the diluted solution at $\chi_A = 0.001$.

In alcohols (methanol, 1-butanol, and 1-hexanol), the spectral changes in the C=O stretching band with the dilution are almost the same as those observed in water, suggesting that the same acetic acid microphases are formed in the alcohol solutions at $\chi_A \geq 0.001$. In acetonitrile, however, the spectral changes are apparently different from those in the protic solvents: two higher wavenumber C=O bands at 1725 and 1754 cm^{-1} appear in the region of $0.001 \leq \chi_A \leq 0.3$. From the ab initio SCRf calculations, we assign the 1725 and 1754 cm^{-1} bands to the cyclic dimer consisting of acetic acid and acetonitrile monomers and to the noncomplexed acetic acid monomer, respectively. Such two bands are also observed in other nitriles and ethers, suggesting that the monomeric molecules are preferentially formed in aprotic polar solvents. From these results, it is concluded that binary solution of acetic acid and the protic solvent do not get homogeneously mixed even in the low acid concentration region of $\chi_A \geq 0.001$, while homogeneously mixed states at molecular levels occur

in the binary solutions of acetic acid and the aprotic polar solvents when the acetic acid mole fraction is small.

III-C Ultrafast Dynamics and Scanning Tunneling Microscopy

We have constructed a low temperature scanning tunneling microscope system combined with an ultrafast light sources in addition to the femtosecond time-resolved ionization detected spectrometer.

III-C-1 Construction of an Apparatus for Direct Observation of Reactions Induced by Ultrafast Laser Pulses Using a Low Temperature STM

OHSHIMO, Kejiro; NAKABAYASHI, Takakazu; WATANABE, Kazuo¹; NAGATA, Takashi¹; NISHI, Nobuyuki
(¹Univ. Tokyo)

Recent advances in laser technology have led to the development of ultrafast spectroscopic techniques that enable us to examine the dynamics of chemical reactions in the femto to picosecond time range. The next stage is to perform the real-space and high-resolution imaging of ultrafast chemical reactions. The ability to view molecular structural changes on an atomic scale in real time promises great progress in many fields of chemistry and physics. In the present study, we have constructed an apparatus for the visualization of photochemical reactions at surfaces by using a low-temperature UHV STM and a picosecond pulse laser system. Experimental arrangement is schematically depicted in Figure 1. The constructed system has two helium cooled STM cryostats, one of which operates to 8 K and has two optical windows for irradiation of laser beams. The angle of incidence is 45° with respect to the STM-tip axis. Optical illumination is provided by two independently tunable picosecond OPA systems. By using frequency mixings, we have obtained the tuning of light between 189 and 11200 nm with microjoule pulse energy and 4 ps pulse duration. Picosecond pump-probe experiments can be carried out with an optical delay stage. The other STM is constructed for low temperature STS studies. A sample in this cryostat can be controlled at any temperature between 4 K and 50 K and kept at 4 K for at least 24 hours without refilling He liquid. A sputtering and annealing system in a preparation chamber obtains a clean flat surface of a substrate. A molecular beam doser is equipped for the adsorption of target molecules onto a substrate. A pulse injection system with a high-speed solenoid valve is also installed for the deposition of nanoparticles and biomolecules. Both the STM cryostats have been confirmed to perform atomic resolution on topograph images of Si(111) surfaces at liquid helium temperatures. By using the former STM cryostat, we have observed Pd clusters with ≈ 6 nm diameters on Au(111) surfaces.

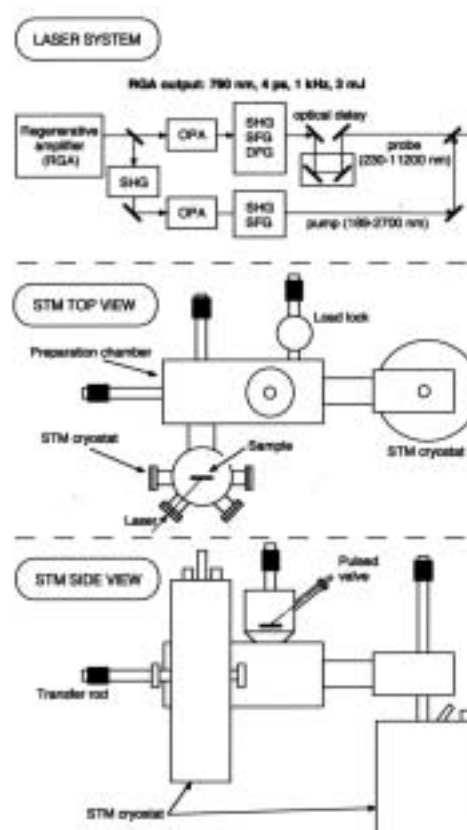


Figure 1. Schematic drawing of the experimental setup.

III-C-2 Construction of a Femtosecond Time-Resolved Ionization Detected Spectrometer

OKABE, Chie¹; NAKABAYASHI, Takakazu; INOKUCHI, Yoshiya; SEKIYA, Hiroshi¹; NISHI, Nobuyuki
(¹Kyushu Univ.)

A time-of-flight mass spectrometer combined with a supersonic molecular beam and a femtosecond laser system has been constructed to observe the ultrafast reaction dynamics of molecules and clusters in the gas phase. The femtosecond laser system consists of a mode-locked Ti:sapphire oscillator with a tunable wavelength from 720 to 850 nm, a regenerative amplifier pumped by a frequency-doubled Nd:YLF laser at 1 kHz, and an optical parametric amplifier (OPA) system. The output from the OPA is tuned between 300 and 10000 nm by mixing techniques and is used for pumping sample molecules to the photoexcited states. A portion

of the output from the regenerative amplifier is frequency doubled (or tripled) and used as a probe beam for ionizing transient molecules generated by the pump beam. After passing through fixed (for the pump beam) and variable (for the probe beam) optical delay lines, the pump and probe beams are superimposed by a dichroic mirror, and focused into a vacuum chamber with an $f = 350$ mm focal lens. Gas mixture of sample molecules and helium is expanded into the vacuum chamber through a pulsed nozzle with a 0.80 mm orifice diameter and a 300 microsec pulse duration. The laser beams merge with the molecular beam and ionize the sample molecules in the acceleration region. The product ions are mass analyzed in the time-of-flight mass spectrometer and are detected using a microsphere plate detector. The ion signals are collected at a 10 Hz repetition rate synchronized with the opening of the pulsed nozzle and are fed into a digital storage oscilloscope. The oscilloscope and the optical delay stage are controlled by a microcomputer through a GPIB interface. The instrumental response function is determined by the pump-probe ionization experiments on pyrazine and benzene that are known to exhibit an instrument-limited rise. It is estimated to be a Gaussian function with a full width at half maximum of 230 fs. Time-resolved multiphoton ionization intensities of N-salicylideneaniline and diarylethene derivatives have been observed by using this spectrometer.

III-C-3 Picosecond Time-Resolved Raman Studies on the Photochromic Reactions of Diarylethenes

OKABE, Chie¹; NAKABAYASHI, Takakazu;
NISHI, Nobuyuki; FUKAMINATO, Tuyoshi¹;
KAWAI, Tsuyoshi¹; IRIE, Masahiro¹; SEKIYA,
Hiroshi¹
(¹Kyushu Univ.)

Diarylethenes are promising photochromic compounds for optoelectronic applications because of their fatigue-resistant and thermally irreversible properties. The open forms of diarylethenes are mostly colorless and turn to the closed forms by UV irradiation. The generated closed forms are thermally stable and exhibit absorption spectra in the visible region. Upon irradiation of visible light, the closed forms revert back to the original open forms. In the present study, we have first measured picosecond time-resolved Stokes and anti-Stokes Raman spectra of diarylethenes in solutions, in order to obtain the rates and mechanisms of these photochromic reactions. We have used 1,2-bis(2,5-dimethyl-

3-thienyl)perfluorocyclopentene for the ring-closure reaction, and 1,2-bis(3,4-dimethyl-5-phenyl-2-thienyl)perfluorocyclopentene for the ring-opening reaction. Two common features of the ring-closure and ring-opening reactions are found: the photochromic reactions proceed in the time scale less than 4 ps and the vibrationally excited molecules in the ground electronic (S_0) state are generated as the intermediate state. Figure 1 shows the time-resolved anti-Stokes Raman spectra of 1,2-bis(3,4-dimethyl-5-phenyl-2-thienyl)perfluorocyclopentene. The observed two anti-Stokes Raman bands at 1545 and 1599 cm^{-1} are assignable to the C=C stretching modes of the thiophene and cyclopentene moiety of the generated S_0 open forms, respectively. The intensity of the cyclopentene moiety relative to that of the thiophene moiety becomes smaller with the delay time, indicating part of the excess energy generated via the ring-opening reaction is localized on the C=C stretching mode of the cyclopentene moiety. This means that the C=C stretching mode of the cyclopentene moiety is one of the promoting or the accepting modes in the ring-opening reaction.

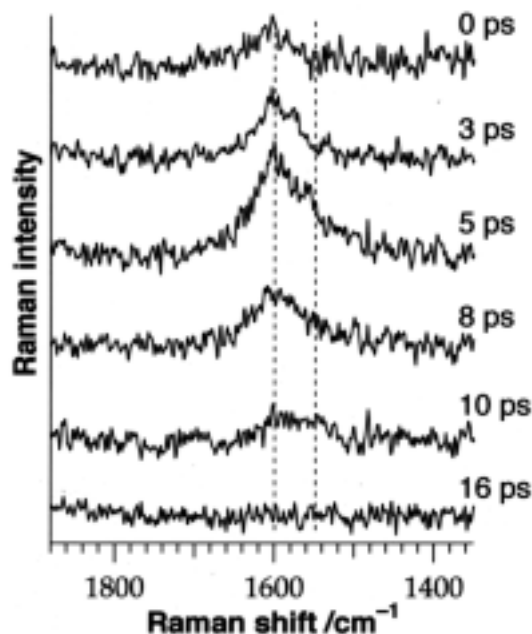


Figure 1. Picosecond time-resolved anti-Stokes Raman spectra of 1,2-bis(3,4-dimethyl-5-phenyl-2-thienyl)perfluorocyclopentene in acetonitrile. Pump, 480 nm; probe, 395 nm. The delay time is given on the right side of each spectrum.

III-D Spectroscopic and Dynamical Studies of Molecular Cluster Ions

Electron deficiency of molecular cluster cations can attract electron rich groups or atoms exhibiting charge transfer or charge resonance interaction in the clusters. This causes dynamical structural change such as proton transfer or ion-core switching in hot cluster ions or clusters in solution.

III-D-1 Intermolecular Interactions in Aniline/Benzene Hetero-Trimer and Aniline Homo-Trimer Ions

OHASHI, Kazuhiko¹; INOKUCHI, Yoshiya; NISHI, Nobuyuki; SEKIYA, Hiroshi¹
(¹Kyushu Univ.)

[*Chem. Phys. Lett.* **357**, 223 (2002)]

The charge distribution and binding features of aniline/benzene hetero-trimer and aniline homo-trimer ions are investigated by vibrational spectroscopy and by near-infrared photodissociation and spontaneous unimolecular dissociation of mass-selected cluster ions. The absence of the charge resonance absorption indicates the charge localization in the trimer ions. Substantial red-shifts and enhanced intensities of the NH-stretching transitions suggest large intermolecular perturbations. The trimer ions are stabilized by the hydrogen-bonding interaction through the NH₂ group of the charged aniline with the neutral molecules rather than the charge-delocalization interaction among the component molecules.

III-D-2 Infrared Photodissociation Spectroscopy of Protonated Formic Acid-Water Binary Clusters, H⁺·(HCOOH)_n·H₂O (*n* = 1–5). Spectroscopic Study of Ion Core Switch Model and Magic Number

INOKUCHI, Yoshiya; NISHI, Nobuyuki

[*J. Phys. Chem. A* **106**, 4529 (2002)]

Infrared spectra of protonated formic acid-water binary clusters, H⁺·(HCOOH)_n·H₂O (*n* = 1–5), are investigated by infrared photodissociation spectroscopy and ab initio molecular orbital calculations. The asymmetric OH stretching vibration of water is observed in the infrared photodissociation spectra of the clusters with *n* = 1–3; it disappears in the spectra of the *n* = 4 and 5 clusters. On detailed comparison of the observed infrared spectra with calculated ones, the most stable geometric structures are obtained for the *n* = 1–5 clusters. These results suggest that the clusters switch the ion cores from HCOOH₂⁺ for *n* = 1–3 to H₃O⁺ for *n* = 4 and 5. The *n* = 5 cluster has a cyclic-type structure; the H₃O⁺ ion core is fully surrounded and stabilized by five formic acid molecules. This characteristic nature produces a magic number of the *n* = 5 cluster.

III-D-3 Infrared Photodissociation Spectroscopy of Aniline⁺–(Water)_{1,2} and Aniline⁺–(Methanol)_{1,2}

HONKAWA, Yoshiki¹; INOKUCHI, Yoshiya; OHASHI, Kazuhiko¹; NISHI, Nobuyuki; SEKIYA, Hiroshi¹
(¹Kyushu Univ.)

[*Chem. Phys. Lett.* **358**, 419 (2002)]

Infrared photodissociation spectra of the aniline ion

solvated by water and methanol molecules are measured in the 2600–3800 cm⁻¹ region. Substantially red-shifted and broadened transition is distinctly observed at 3105 and 2915 cm⁻¹ for aniline⁺–(H₂O)₁ and aniline⁺–(CH₃OH)₁, respectively, and assigned to the stretching vibration of the hydrogen-bonded NH oscillator of the aniline⁺ moiety. The spectra of aniline⁺–(H₂O)₂ and aniline⁺–(CH₃OH)₂ demonstrate a large perturbation to both of the NH oscillators, indicating that each NH bond is bound to a solvent molecule in the most stable structure.

III-D-4 Intracluster Proton Transfer in Aniline–Amine Complex Ions

INOKUCHI, Yoshiya; OHASHI, Kazuhiko¹; HONKAWA, Yoshiki¹; SEKIYA, Hiroshi¹; NISHI, Nobuyuki
(¹Kyushu Univ.)

[*Chem. Phys. Lett.* **359**, 283 (2002)]

The intracluster proton transfer in aniline–amine complex ions is investigated by infrared photodissociation spectroscopy and density functional theory calculations. The proton acceptors include ammonia, methylamine, dimethylamine and trimethylamine in ascending order of proton affinity. The spectra of (aniline–ammonia)⁺ and (aniline–methylamine)⁺ demonstrate the persistence of the aniline ion unit in the complexes. For (aniline–dimethylamine)⁺ and (aniline–trimethylamine)⁺, the spectra imply the transformation to the anilino radical (C₆H₅NH) unit, suggesting the occurrence of the proton transfer.

III-D-5 LIF and IR Dip Spectra of Jet-Cooled *p*-Aminophenol–*M* (*M* = CO, N₂): Hydrogen-Bonded or van der Waals-Bonded Structure?

MORI, Hirotoshi¹; KUGISAKI, Hitomi¹; INOKUCHI, Yoshiya; NISHI, Nobuyuki; MIYOSHI, Eisaku¹; SAKOTA, Kenji¹; OHASHI, Kazuhiko¹; SEKIYA, Hiroshi¹
(¹Kyushu Univ.)

[*J. Phys. Chem. A* **106**, 4886 (2002)]

Intermolecular interaction and stable structures of the *p*-aminophenol–*M* (*M* = CO, N₂) 1:1 complexes have been studied by measuring the S₁–S₀ fluorescence excitation spectra and the IR dip spectra in the OH and NH stretch region. We also have performed ab initio calculations to obtain stable structures and calculated infrared spectra of the complexes. The S₁–S₀ electronic origin of the CO complex is 141 cm⁻¹ red shifted from that of the monomer. This shift is smaller than that of the N₂ complex (153 cm⁻¹), although the molecular polarizability of CO is larger than that of N₂. The IR dip spectrum of the CO complex shows that the OH stretching frequency is 26 cm⁻¹ lower than that of the monomer. On the other hand, the N₂ complex displays no shift. We conclude that the CO molecule is bonded to the OH group *via* a hydrogen bond in *p*-aminophenol–CO, whereas the N₂ molecule is van der Waals-

bonded to the π cloud of the aromatic ring in *p*-aminophenol–N₂.

III-D-6 Structure and Intermolecular Hydrogen Bond of Jet-Cooled *p*-Aminophenol–(H₂O)₁ Studied by Electronic and IR-Dip Spectroscopy and Density Functional Theory Calculations

MORI, Hirotoshi¹; KUGISAKI, Hitomi¹;
INOKUCHI, Yoshiya; NISHI, Nobuyuki;
MIYOSHI, Eisaku¹; SAKOTA, Kenji¹; OHASHI,
Kazuhiko¹; SEKIYA, Hiroshi¹
(¹Kyushu Univ.)

[*Chem. Phys.* **277**, 105 (2002)]

The structure and hydrogen bonding interaction in jet-cooled *p*-aminophenol–H₂O 1:1 complex have been studied by measuring the fluorescence excitation, dispersed fluorescence, and IR-dip spectra. In the electronic spectrum we identified only one isomer, where the oxygen atom of water is bonded to the hydroxy proton of *p*-aminophenol. Four stable isomers are obtained by ab initio calculations at the MP2/6-31G(d) level, while density functional theory calculations provide four or three isomers depending on the basis sets. It has been shown that theoretical IR spectra with small basis sets are not in agreement with the experimental IR spectrum. The experimental IR spectrum has been well reproduced by the B3LYP/6-311+G(d,p) calculations, showing that diffuse functions are necessary to describe the intermolecular hydrogen bond in *p*-aminophenol–H₂O. The vibronic levels in the *S*₁ state of *p*-aminophenol–H₂O have been assigned with the aid of the dispersed fluorescence spectra. The formation of the intermolecular hydrogen bond substantially reduces the frequency of the amino inversion mode in the *S*₁ state due to nonlocal character of this mode.

III-D-7 Positive Charge Distribution in (Benzene)₁(toluene)₂⁺ and (Benzene)₂(toluene)₁⁺ Studied by Photodissociation Spectroscopy

INOKUCHI, Yoshiya; OHASHI, Kazuhiko¹;
SEKIYA, Hiroshi¹; NISHI, Nobuyuki
(¹Kyushu Univ.)

[*J. Chem. Phys.* in press]

The positive charge distribution in benzene–toluene hetero-trimer ions is investigated by photodissociation spectroscopy in the near-infrared (6000–14000 cm⁻¹) and infrared (2800–3150 cm⁻¹) regions. The electronic spectra of (benzene)₁(toluene)₂⁺ and (benzene)₂(toluene)₁⁺ in the near-infrared region display a strong band at 9430 and 8330 cm⁻¹, respectively. These bands are ascribed to the charge resonance band; the positive charge is not localized on a single molecule. The vibrational spectrum of (benzene)₁(toluene-*d*₈)₂⁺ shows three distinct bands at 3054, 3084, and 3108 cm⁻¹; these bands are assigned to the CH stretching vibrations of the benzene moiety. The similarity of the spectral features to those of the neutral benzene monomer suggests that

the benzene molecule in the (benzene)₁(toluene)₂⁺ ion has a neutral character. The positive charge is localized on the toluene dimer unit with a structure written as (toluene)₂⁺⋯(benzene)₁. The vibrational spectrum of (benzene)₂(toluene)₁⁺ bears a resemblance to that of (benzene)₂⁺. The vibrational spectrum of (benzene-*d*₆)₂(toluene)₁⁺ shows dissimilar features to the spectrum of the neutral toluene monomer, suggesting that a certain amount of the positive charge is carried by the toluene moiety. These results are explained by the charge resonance interaction between (benzene)₂ and (toluene)₁. A simple perturbation theory is applied for determining the positive charge distribution in (benzene)₂(toluene)₁⁺. The probability of finding the charge on the (benzene)₂ and (toluene)₁ moieties is analyzed to be 58 and 42 %, respectively.

III-D-8 Infrared Photodissociation Spectroscopy of [Aniline–(Water)_{*n*}]⁺ (*n* = 1–8)

INOKUCHI, Yoshiya; HONKAWA, Yoshiki¹;
OHASHI, Kazuhiko¹; SEKIYA, Hiroshi¹; NISHI,
Nobuyuki
(¹Kyushu Univ.)

Infrared photodissociation spectra of [aniline–(H₂O)_{*n*}]⁺ (*n* = 1–8) are measured in the 2700–3800 cm⁻¹ region. The spectra are interpreted with the aid of density functional calculations. A substantially red-shifted and broadened transition is distinctly observed at 3105 cm⁻¹ for the *n* = 1 ion, and assigned to the stretching vibration of the hydrogen-bonded NH oscillator of the aniline⁺ moiety. The spectrum of the *n* = 2 ion demonstrates a large perturbation to both of the NH oscillators, indicating that each NH bond is bound to a water molecule in the most stable structure. For the *n* = 3 ion, three broad bands exist at 3070, 3230, and 3420 cm⁻¹, and there are two maxima and a weak hump at 3637, 3723, and 3696 cm⁻¹. The calculated spectrum of the 2-1 branch structure resembles the observed one very well. For the *n* = 4 ion, there exist three strong bands at 2960, 3100, and 3430 cm⁻¹, and a very weak one at 3550 cm⁻¹. The observed spectrum in the 3600–3800 cm⁻¹ region is decomposed into four bands at 3640, 3698, 3710, and 3734 cm⁻¹. These bands are originated from the 2-2 branch isomer except for the 3550 and 3710 cm⁻¹ bands. These two bands are due to the other isomer that has the five-membered ring. A characteristic transition in the observed spectrum of the *n* = 5 ion is the 3684 cm⁻¹ band, which hardly emerges in the spectra of *n* = 1–4. This band is assigned to the free OH stretching vibration of the three-coordinated (double-acceptor–single-donor) H₂O, indicating the ring structure. The *n* = 5 ion has the five-membered ring structure with the fifth water molecule bound to the terminal (double-acceptor) H₂O. The observed spectra of the *n* = 6–8 ions show features quite different from those of *n* = 1–5; a very strong and broad band emerges around 3400 cm⁻¹. It is suggested that the *n* = 6–8 ions have the proton transfer form with some ring structure.

III-E Spectroscopy and Dynamics of Vibrationally Excited Molecules and Clusters

This research group is studying structure and dynamics of molecules and clusters by two-color double resonance spectroscopy. New spectroscopic methods will also be developed to observe the higher vibrational state under collision-free condition.

A molecular cluster is a microscopic system of solution and/or crystal, and is thought to provide detailed information on relaxation and reaction dynamics in condensed phase. However the previous studies are concentrated to stable clusters which has no reaction pathway after photo-excitation. Consequently, spectroscopic information which concerns the reaction mechanism has not been obtained sufficiently. In this research project started from 2000, we will apply various laser spectroscopies to the reactive clusters to reveal detailed mechanism of intracuster reaction.

For the study of the ground state, the structure of the cluster can be determined by the combination of the IR dip spectroscopy and *ab initio* MO calculations.¹⁾ The IR dip spectroscopy is a kind of IR-UV double resonance spectroscopy which provides the spectrum which corresponds to the infrared absorption spectrum of the cluster (see Figure 1). A tunable IR laser is introduced to the clusters and is scanned its frequency over the fundamental vibrational region (typically 2400 ~ 4000 cm^{-1}). Then a tunable UV laser, of which the frequency is fixed to the S_1 origin of a specific cluster, is introduced and resonant enhanced multiphoton ionization signal *via* S_1 is monitored. When the IR laser is resonant to a vibrational level of the cluster, the ion signal decreases much because of loss of the population in the vibrational ground state. Thus, the IR absorption spectrum of the cluster can be measured by this depletion spectroscopy. The same spectrum can be obtained when the fluorescence intensity from S_1 is monitored instead of the ion current.

The IR spectrum in the excited state S_1 can also be measured by the depletion spectroscopy, when the UV laser is introduced before the IR laser (the UV-IR fluorescence dip spectroscopy; see Figure 2). The molecule is excited to S_1 by the UV laser, and the fluorescence intensity is monitored as well as the IR dip spectroscopy for S_0 . Then the S_1 molecules are further excited to the vibrationally excited level in S_1 by the IR laser. In general, the fluorescence quantum yield decreases in the higher vibronic level. Thus, the total fluorescence intensity decreases when the IR laser frequency is resonant to the vibrational level in S_1 .

Similarly, the IR spectrum of the ionic cluster can be measured by the depletion spectroscopy (mass-selected ion dip spectroscopy; see Figure 3). The ionic cluster can be prepared by the multiphoton ionization *via* S_1 , and the ion current due to the cation cluster of the specific size can be measured through a mass-filter. When the ionic cluster is vibrationally excited by the IR laser, the cluster is dissociated by the vibrational predissociation. Therefore, the IR transition can be measured by the decrease of the parent cluster. The same spectrum can be obtained by monitoring the enhancement of fragments (mass-selected multiphoton dissociation spectroscopy). In addition to these "dip" spectroscopies, the nonresonant ionization detected IR spectroscopy²⁾ and the PFI-ZEKE photoelectron spectroscopy³⁾ are also important tool to obtain the spectral information in the cation and the overtone states. Based on these spectroscopic techniques, we have measured the IR spectra of solvated clusters,⁴⁾ such as phenol/ammonia,⁵⁾ naphthol/alcohol,⁶⁾ carbazole/water⁷⁾ and 7-azaindole dimers,⁸⁾ and have discussed the relation among geometrical structure, electronic state and intracuster reactions.

From 2001, we have been developing the new ultrafast time-resolved IR spectroscopy for the reactive clusters. The pico second time-resolved vibrational spectroscopy is one of the ideal way to reveal the reaction mechanism directly. Here, we will demonstrate its usefulness by applying the hydrogen transfer reaction in photoexcited PhOH-

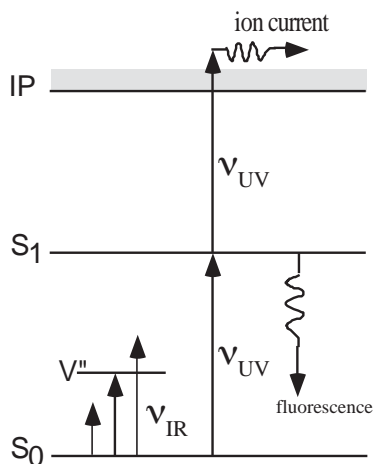


Figure 1. Principle of the IR Dip Spectroscopy. The IR transition in the ground state cluster can be measured.

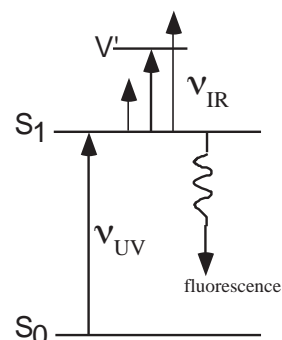


Figure 2. Principle of the UV-IR Fluorescence Dip Spectroscopy. The IR transition of the cluster in the S_1 state can be obtained.

(NH_3) $_n$ cluster.⁹⁾ Figure 4 shows the principle of the picosecond time-resolved UV-IR-UV ion dip spectroscopy. The reactive cluster ($\text{PhOH}-(\text{NH}_3)_n$ in present case) is excited to S_1 by a picosecond UV laser ν_{UV} and the photochemical reaction (hydrogen transfer) is triggered. The final reaction product, *i. e.* (NH_3) $_{n-1}\text{NH}_4$, is ionized by a nanosecond UV laser ν_{ION} which is irradiated after 100 ns from ν_{UV} and the population of the reaction product is monitored as a mass peak of (NH_3) $_{n-1}\text{NH}_4^+$. A picosecond tunable IR laser ν_{IR} is irradiated after t ps from ν_{UV} and is scanned over vibrational region. If ν_{IR} is resonant to vibrational levels of the transient species, the population of the final reaction product decreases due to the vibrational predissociation of the transient species. Therefore, the vibrational transitions of the transient species at t ps can be observed as decrease of ion current of the final reaction product.

Time resolved UV-IR-UV ion dip spectra of phenol-(NH_3) $_3$ are shown in Figure 5. The numbers in the left hand sides of each spectrum indicate the delay time from ν_{UV} to ν_{IR} . Here the spectrum at -20 ns corresponds to the IR spectrum of $\text{PhOH}-(\text{NH}_3)_3$ in S_0 , in which the sharp bands at 3400 cm^{-1} , the broad bands at $\sim 3200\text{ cm}^{-1}$ and the very broad background are assigned to the degenerated antisymmetric stretch vibration ν_3 in NH_3 , the totally symmetric stretch vibration ν_1 in NH_3 and the OH stretch vibration ν_{OH} in phenol, respectively. The spectrum at $+180$ ns shows the vibrational transitions of the final reaction product *via* S_1 , *i. e.* (NH_3) $_2\text{NH}_4$, and 1) two intense bands at 3180 cm^{-1} and 3250 cm^{-1} and 2) a broad band at $2700 \sim 3100\text{ cm}^{-1}$ which have been assigned to

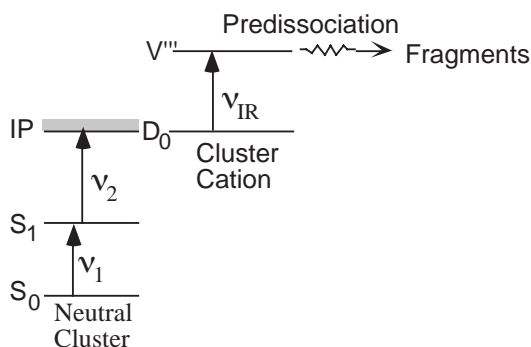


Figure 3. Principle of the mass-selected IR Ion Dip Spectroscopy. The IR transition of the cluster cation can be measured by the depletion of the parent cluster cation. The same spectrum can be measured by monitoring the enhancement of the fragments produced by the IR predissociation.

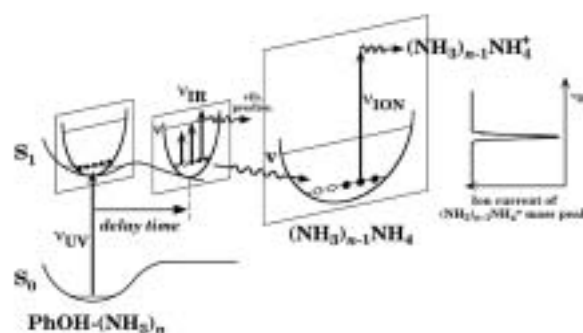
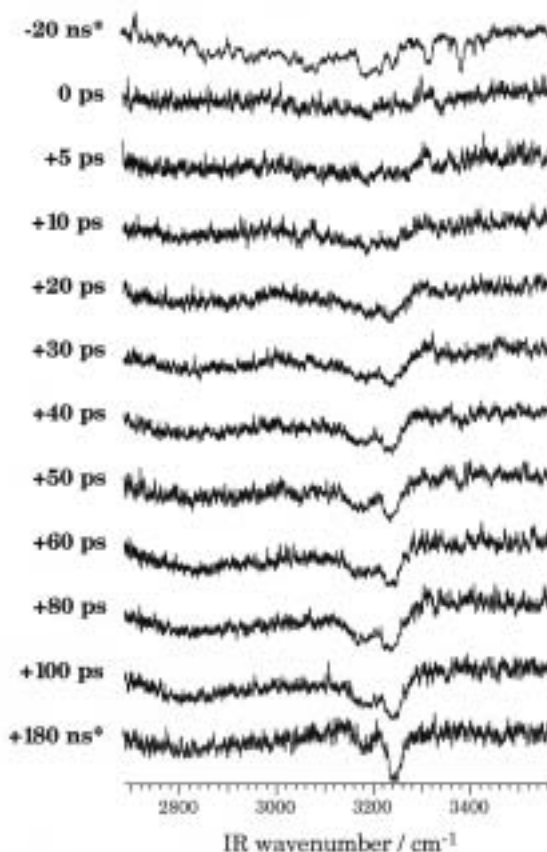


Figure 4. Principle of picosecond time-resolved UV-IR-UV ion dip spectroscopy. Potential curves of S_0 and S_1 are schematically drawn along O-H stretch coordinate. Potential curves in different sections on the S_1 O-H stretch coordinate are drawn along arbitrary N-H stretch coordinates.

Figure 5. Picosecond time-resolved UV-IR-UV ion dip spectra of the transient species from the electronically excited $\text{PhOH}-(\text{NH}_3)_3$ which was observed by fixing ν_{UV} to the low vibronic band in the S_1 state of $\text{PhOH}-(\text{NH}_3)_3$ (281.49 nm) and monitoring (NH_3) $_2\text{NH}_4^+$ due to ν_{ION} (355 nm). Times indicated at the left side of each spectrum mean the delay times between ν_{UV} and ν_{IR} . The spectra whose delay times are -20 ns and $+180\text{ ns}$ (indicated by *) are obtained by nanosecond laser system, which have been reported in the previous paper.⁵⁾



vibrational transitions concerned with NH_4 .

One can see that the vibrational bands rise with increasing delay time. The spectral feature at +100 ps is already similar to that of the final reaction product (+180 ns). Here, the intense band at 3250 cm^{-1} rises slower than the band at 3180 cm^{-1} . The relative intensities of the two bands become comparable at 40 ps, thereafter, the higher band at 3250 cm^{-1} clearly grows further. Thus, the rising time constant of the band at 3250 cm^{-1} is apparently different from that of the 3180 cm^{-1} -band. This remarkable difference between the two intense bands suggests that each vibrational transition is derived from different species. The existence of two transient species are naturally interpreted by considering the isomers of $(\text{NH}_3)_2\text{NH}_4$; the most stable $\text{NH}_3\text{-NH}_4\text{-NH}_3$ and the meta-stable $\text{NH}_4\text{-NH}_3\text{-NH}_3$. The co-existence of isomers is strongly supported by *ab initio* calculations.

As described above, we have successfully measured the picosecond time resolved IR spectra of the transient species for the ESHT of $\text{PhOH-(NH}_3)_3$ for the first time. It proves that the picosecond UV-IR-UV ion dip spectroscopy is a powerful tool to explore the dynamics of the intracluster reaction.

References

- 1) R. Yoshino *et al.*, *J. Phys. Chem. A* **102**, 6227 (1998).
- 2) T. Omi *et al.*, *Chem. Phys. Lett.* **252**, 287 (1996); S. Ishiuchi *et al.*, *Chem. Phys. Lett.* **283**, 243 (1998).
- 3) K. Takazawa *et al.*, *Chem. Phys. Lett.* **189**, 592 (1992); K. Müller-Dethlefs *et al.*, *Z. Naturforsch. Teil A* **39**, 1089 (1984); K. Müller-Dethlefs and M. C. R. Cockett, "Zero Kinetic Energy (ZEKE) Photoelectron Spectroscopy," Chapter 7, "Nonlinear Spectroscopy for Molecular Structure Determination," R. W. Field *et al.*, Eds., (Blackwell Science, Oxford, 1998), and references therein.; E. W. Schlag, "ZEKE Spectroscopy" (Cambridge University Press, Cambridge, 1998), and references therein.
- 4) K. Suzuki, Y. Emura, S. Ishiuchi and M. Fujii, *J. Electron Spectrosc.* **108**, 13 (2000), K. Suzuki, S. Ishiuchi and M. Fujii, *Faraday Discuss.* **115**, 229 (2000), K. Sakota, N. Yamamoto, K. Ohashi, H. Sekiya, M. Saeki, S. Ishiuchi, M. Sakai and M. Fujii, *Chem. Phys. Lett.* **341**, 70 (2001).
- 5) S. Ishiuchi, M. Saeki, M. Sakai and M. Fujii, *Chem. Phys. Lett.* **322**, 27 (2000).
- 6) M. Saeki, S. Ishiuchi, M. Sakai and M. Fujii, *J. Phys. Chem. A* **105**, 10045 (2001).
- 7) M. Sakai, K. Daigoku, S. Ishiuchi, M. Saeki, K. Hashimoto and M. Fujii, *J. Phys. Chem. A* **105**, 8651 (2001).
- 8) H. Yokoyama, H. Watanabe, T. Omi, S. Ishiuchi and M. Fujii, *J. Phys. Chem. A* **105**, 9366 (2001).
- 9) S. Ishiuchi, M. Sakai, K. Daigoku, T. Ueda, T. Yamanaka, K. Hashimoto and M. Fujii, *Chem. Phys. Lett.* **347**, 87 (2001).

III-E-1 Hydrogen Transfer in Photo-Excited Phenol/Ammonia Clusters by UV-IR-UV Ion Dip Spectroscopy and Ab Initio MO Calculations I: Electronic Transitions

(¹Tokyo Metropolitan Univ./ACT-JST)

[*J. Chem. Phys.* in press]

ISHIUCHI, Shun-ichi; DAIGOKU, Kota¹; SAEKI, Morihisa; SAKAI, Makoto; HASHIMOTO, Kenro¹; FUJII, Masaaki

(¹Tokyo Metropolitan Univ./ACT-JST)

[*J. Chem. Phys.* in press]

The electronic spectra of reaction products via photo-excited phenol / ammonia clusters (1:2~5) have been measured by UV-near-IR-UV ion dip spectroscopy. Compared with the electronic spectra of hydrogenated ammonia cluster radicals the reaction products have been proven to be $(\text{NH}_3)_{n-1}\text{NH}_4$ ($n = 2 \sim 5$), which are generated by excited-state hydrogen transfer in $\text{PhOH-(NH}_3)_n$. By comparing the experimental results with *ab initio* molecular orbital calculations at multi-reference single and double excitation CI level, it has been found that the reaction products, $(\text{NH}_3)_{n-1}\text{NH}_4$ (for $n = 3$ and 4), contain some isomers.

III-E-2 Hydrogen Transfer in Photo-Excited Phenol/Ammonia Clusters by UV-IR-UV Ion Dip Spectroscopy and Ab Initio MO Calculations II: Vibrational Transitions

ISHIUCHI, Shun-ichi; DAIGOKU, Kota¹; SAEKI, Morihisa; SAKAI, Makoto; HASHIMOTO, Kenro¹; FUJII, Masaaki

The vibrational spectra of phenol/ammonia clusters (1:2 ~ 5) in S_0 and those of their photo chemical reaction products, $(\text{NH}_3)_{n-1}\text{NH}_4$ ($n = 2 \sim 5$), which are generated by excited-state hydrogen transfer, have been measured by UV-IR-UV ion dip spectroscopy. The geometries, IR spectra and normal modes of phenol- $(\text{NH}_3)_n$ ($n = 1 \sim 5$) have been examined by *ab initio* molecular orbital calculations, at the second-order Møller-Plesset perturbation theory level with large basis sets. For the $n = 2$ and 3 reaction products, similar vibrational analyses have been carried out. From the geometrical information of reactants and products, it has been suggested that the reaction products have memories of the reactant's structure, which we call "memory effect."

III-E-3 Picosecond Time-Resolved Infrared Spectra of Photo-Excited Phenol-(NH₃)₃ Cluster

ISHIUCHI, Shun-ichi; SAKAI, Makoto; DAIGOKU, Kota¹; UEDA, Tadashi; YAMANAKA, Takaya; HASHIMOTO, Kenro¹; FUJII, Masaaki

(¹Tokyo Metropolitan Univ./ACT-JST)

[*Chem. Phys. Lett.* **347**, 87 (2001)]

Picosecond time-resolved IR spectra of phenol- $(\text{NH}_3)_3$ have been measured by UV-IR-UV ion dip spectroscopy for the first time. It was found that the

time-evolution of two vibrational bands at 3180 cm^{-1} and 3250 cm^{-1} is different from each other. The results show that two transient species are generated from the photo-excited phenol-(NH_3)₃ cluster. From *ab initio* calculation, the transient species are assigned to two isomers of (NH_3)₂NH₄.

III-E-4 Picosecond Time-Resolved Nonresonant Ionization Detected IR Spectroscopy on 7-Azaindole Dimer

SAKAI, Makoto; ISHIUCHI, Shun-ichi; FUJII, Masaaki

[*Eur. Phys. J. D* in press]

The picosecond time-resolved IR spectrum of the 7-azaindole dimer has been measured by picosecond time-resolved nonresonant ionization detected IR spectroscopy. This new time-resolved technique was developed by combining nonresonant ionization detected IR (NID-IR) spectroscopy with tunable picosecond IR and UV lasers. The time-resolved NID-IR spectrum from 2600 cm^{-1} to 3800 cm^{-1} shows a drastic change from 1.5 ps to 11 ps time evolution. A mode-specific vibrational redistribution has been suggested.

III-E-5 Structure of Hydrogen-Bonded Clusters of 7-Azaindole Studied by IR Dip Spectroscopy and Ab Initio Molecular Orbital Calculation

YOKOYAMA, Hiroshi¹; WATANABE, Hidekazu²; OMI, Takuichiro¹; ISHIUCHI, Shun-ichi; FUJII, Masaaki
(¹Waseda Univ./PRESTO; ²AIST)

[*J. Phys. Chem. A* **105**, 9366 (2001)]

The IR spectrum of 7-azaindole monomer, 7-azaindole reactive and nonreactive dimers, and 7-azaindole (H_2O)_{*n*} (*n* = 1–3) clusters in a supersonic jet from 2600 cm^{-1} to 3800 cm^{-1} have been measured using IR dip spectroscopy. The vibrational transitions in the ground state were clearly observed and were assigned to the CH and NH stretching vibrations of 7-azaindole and the OH stretching vibrations of water molecules in the clusters. The observed IR spectra of 7-azaindole monomer and 7-azaindole(H_2O)_{*n*} (*n* = 1–3) clusters were compared to theoretical ones obtained by *ab initio* MO calculations. From a comparison, it is concluded that 7-azaindole-(H_2O)_{*n*} (*n* = 1–3) clusters have a ring structure due to a cyclic hydrogen-bond network. This conclusion is consistent with an analysis based on high-resolution spectroscopy. Similarly, the IR dip spectrum suggests that the 7-Azaindole reactive dimer has a cyclic hydrogen-bond network, forming a symmetric planer structure. It is strongly suggested from the IR spectrum and the *ab initio* calculations that the nonreactive dimer contains a water molecule between 7-azaindole molecules.

III-E-6 Structures of Carbazole-(H_2O)_{*n*} (*n* = 1–3) Clusters Studied by IR Dip Spectroscopy and a Quantum Chemical Calculation

SAKAI, Makoto; DAIGOKU, Kota¹; ISHIUCHI, Shun-Ichi; SAEKI, Morihisa; HASHIMOTO, Kenro¹; FUJII, Masaaki
(¹Tokyo Metropolitan Univ./ACT-JST)

[*J. Phys. Chem. A* **105**, 8651 (2001)]

The IR spectra of carbazole and carbazole-(H_2O)_{*n*} (*n* = 1–3) clusters in a supersonic jet have been measured by IR dip spectroscopy. The spectra show clear vibrational structures of both the monomer and the clusters in the 2900–3800 cm^{-1} frequency region. The observed vibrational bands are assigned to the NH stretch of carbazole and the OH stretches of H_2O molecules in the clusters. The geometries and IR spectra of carbazole-(H_2O)_{*n*} clusters were calculated at the HF/6-31G and B3LYP/6-31++G(d,p) levels. From a comparison of the observed and calculated IR spectra, the structures of the cluster have been determined.

III-E-7 Structure of 1-Naphthol/Alcohol Clusters Studied by IR Dip Spectroscopy and Ab Initio Molecular Orbital Calculations

SAEKI, Morihisa; ISHIUCHI, Shun-Ichi; SAKAI, Makoto; FUJII, Masaaki

[*J. Phys. Chem. A* **105**, 10045 (2001)]

The structures of 1-naphthol/alcohol clusters, 1-NpOH(ROH)_{*n*} (*n* = 1–3; ROH = MeOH, EtOH, and *t*-BuOH), have been investigated by resonant two-photon ionization (R2PI) spectroscopy and ion-detected IR dip spectroscopy. Based on the calculated spectra obtained by *ab initio* MO calculations, the spectra of 1-NpOH-(MeOH)_{*n*} was analyzed. The analysis elucidated that 1-NpOH(MeOH)_{2,3} was a ring structure. From a similarity of the spectral pattern, the structures of 1-NpOH(EtOH)_{*n*} and 1-NpOH(*t*-BuOH)_{*n*} were also determined to be a ring conformation. From a frequency shift of the hydrogen-bonded OH stretching vibration, the hydrogen bonding is weakened by a steric hindrance due to an alkyl group of ROH. The difference in the solvation mechanism between 1-NpOH(MeOH)_{*n*} and 1-NpOH-(H_2O)_{*n*} is discussed.

III-E-8 Pulsed Field Ionization Zero Kinetic Energy Photoelectron Study on Methylanisole Molecules in a Supersonic Jet

KINOSHITA, Shin-ichi¹; KOJIMA, Hiroshi¹; SUZUKI, Tadashi¹; ICHIMURA, Tejiro¹; YOSHIDA, Keigo; SAKAI, Makoto; FUJII, Masaaki
(¹Tokyo Inst. Tech.)

[*Phys. Chem. Chem. Phys.* **3**, 4889 (2001)]

Pulsed-field ionization zero kinetic energy (PFI-ZEKE) photoelectron spectra were measured for jet-cooled *o*-, *m*-, and *p*-methylanisoles for the first time. The low-frequency bands observed at around the origin band in the spectra were assigned to the methyl internal rotational bands of the cations. The potential curves and the Franck-Condon factors for the methyl internal rota-

tional motion were calculated by the one-dimensional free-rotor approximation. The potential barrier height was found to change drastically on ionization, suggesting that the electronic structure should mainly affect the potential barrier of the methyl internal rotation.

tion. The spectroscopic and theoretical results are in agreement with a relatively weak intramolecular hydrogen bond.

III-E-9 The PFI-ZEKE Photoelectron Spectrum of *m*-Fluorophenol and its Aqueous Complexes: Comparing Intermolecular Vibrations in Rotational Isomers

YOSHIDA, Keigo; SUZUKI, Kazunari; ISHIUCHI, Shun-ichi; SAKAI, Makoto; FUJII, Masaaki; DESSENT, Caroline E. H.¹; MÜLLER-DETHLEFS, Klaus¹

(¹Univ. York, UK)

[*Phys. Chem. Chem. Phys.* **4**, 2534 (2002)]

Pulsed Field Ionization–Zero Kinetic Energy (PFI-ZEKE) Photoelectron spectroscopy has been applied to study the cationic ground states of the rotational isomers of *m*-fluorophenol and its hydrogen-bonded clusters with H₂O and D₂O. The *cis*- and *trans*- monomer isomers are assigned by comparing the observed ionization potentials with values obtained from *ab initio* calculations (HF/6-31G*). Both monomers display very similar vibrational frequencies, indicating that the geometric structures of the two cations are similar. In contrast, the *cis*- and *trans*-aqueous clusters display distinctive intermolecular vibrational frequencies (*e.g.* the intermolecular stretching vibrations appear at 239 and 228 cm⁻¹ in the *cis*- and *trans*-isomers respectively). The origin of the different intermolecular interactions in the isomeric clusters is discussed with reference to the *ab initio* calculations.

III-E-10 OH- and CH-Stretching Overtone Spectra of Catechol

KJAERGAARD, Henrik G.¹; HOWARD, Daryl L.¹; SCHOFIELD, Daniel P.¹; ROBINSON, Timothy W.¹; ISHIUCHI, Shun-ichi; FUJII, Masaaki

(¹Univ. Otago, New Zealand)

[*J. Phys. Chem. A* **106**, 258 (2002)]

We have recorded the CH-, OH-, and OD-stretching fundamental and overtone spectra of catechol (1,2-dihydroxybenzene, pyrocatechol) and selectively deuterated catechol. Conventional and intracavity photoacoustic spectroscopy were used to record room temperature spectra of catechol in solution and in the vapor phase, whereas nonresonant ionization detected spectroscopy was used to study catechol in a supersonic jet. The spectra can be explained in terms of a local mode model with one oscillator for each of the non-equivalent CH, OH, or OD bonds. Intensities of the CH-, OH-, and OD-stretching transitions were calculated with an anharmonic oscillator local mode model and *ab initio* determined dipole moment functions. Our simple calculations are in good agreement with the observed intensities. Line widths in the jet-cooled spectra are discussed in terms of intramolecular vibrational redistri-

III-F Ultrafast Molecular Dynamics Studied by Time-Resolved Photoelectron Imaging

Femtosecond pump-probe time-resolved photoelectron imaging is a novel experimental approach to probe electronic and nuclear dynamics in real time. Since photoionization can occur from any part of the potential energy surfaces with any multiplicity, the method provides a versatile means to follow dephasing and reaction processes.

III-F-1 Ionization Dynamics of NO A ($2\Sigma^+$) State Studied by Time-Resolved Photoelectron Imaging

TSUBOUCHI, Masaaki¹; SUZUKI, Toshinori
(¹GUAS)

Photoionization dynamics of NO from the $A^2\Sigma^+$ ($3s\sigma$ Rydberg) state is studied by femtosecond photoelectron imaging method. The photoelectron angular distribution (PAD) observed in the laboratory frame (LF) is convolution of the PAD in the molecular frame (MF) with the molecular axis distribution in space. Our method utilizes a rotational wavepacket created by coherent excitation of the molecular ensemble to control the axis distribution, and the LF-PAD is measured as a function of this distribution. Then, the LF-PAD is deconvoluted with the axis distribution to obtain the MF-PAD. The PADs in (1+1') REMPI *via* the A state are well expressed by expansion with the Legendre polynomials,

$$I(\theta; t) \propto 1 + \beta_2(t)P_2(\cos\theta) + \beta_4(t)P_4(\cos\theta).$$

Figure 1 shows the time dependence of the expansion coefficients, β_L , observed for several probe wavelengths. All profiles exhibit modulation with 8.4 ps time period in agreement with the rotational constant of NO in the A state, $B = 1.997\text{ cm}^{-1}$. The phase of the modulation varies with the probe wavelength, clearly indicating that the ionization dynamics of NO from the A state is energy-dependent. The ionization dynamical parameters are extracted from the β_L parameters.

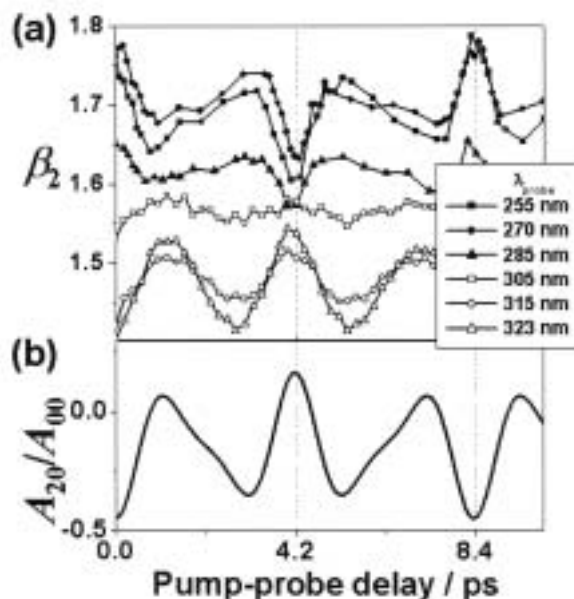


Figure 1. (a) Temporal profiles of the β_2 anisotropy parameter of LF-PADs observed by [1+1'] femtosecond photoelectron imaging with several probe wavelengths. (b) Calculated time evolution of the alignment parameter, A_{20}/A_{00} , for the molecular axis distribution,

$$P(\theta, \phi) = A_{00}Y_{00}(\theta, \phi) + A_{20}Y_{20}(\theta, \phi),$$

on the optically excited NO A state.

III-F-2 Theoretical Analysis of Rotational Revivals in Intersystem Crossing in Pyrazine

TSUBOUCHI, Masaaki¹; WHITAKER, Benjamin J.²; SUZUKI, Toshinori
(¹GUAS; ²Leeds Univ.)

In our previous work, we have visualized the decay of the S_1 and the buildup of the T_1 state in the $S_1(n, \pi^*) \rightarrow T_1(n, \pi^*)$ intersystem crossing (ISC) of pyrazine using the (1+2') femtosecond photoelectron imaging.^{1,2} A rotational wavepacket motion created by coherent excitation of multiple rovibrational states in the S_1 state was clearly observed in the temporal behavior of photoelectron intensities. The signature of the rotational wavepacket motion is also seen in the T_1 state, however, this amplitude was much smaller than the one observed for the S_1 state. We attempted theoretical analysis of this phenomenon. A model Hamiltonian matrix for a singlet state and multiple triplet states is diagonalized to form molecular eigenstates, and coherent excitation of these ensemble states is considered. The spin-orbit coupling strength and the density of triplet states are assumed to reproduce the observed dephasing time. The time-dependent alignment in the S_1 and T_1 states are calculated. Figure 1 shows the experimental and calculated time evolutions of the alignment parameter, A_{20}/A_{00} , for the molecular axis distribution,

$$P(\theta, \phi) = A_{00}Y_{00}(\theta, \phi) + A_{20}Y_{20}(\theta, \phi).$$

The rotational quantum beats in the singlet and triplet signals are reproduced well, where the model correctly predicts weaker alignment for the triplet states.

References

- 1) T. Suzuki *et al.*, *J. Chem. Phys.* **111**, 4859 (1999).
- 2) Tsubouchi *et al.*, *Phys. Rev. Lett.* **115**, 8810 (2001).

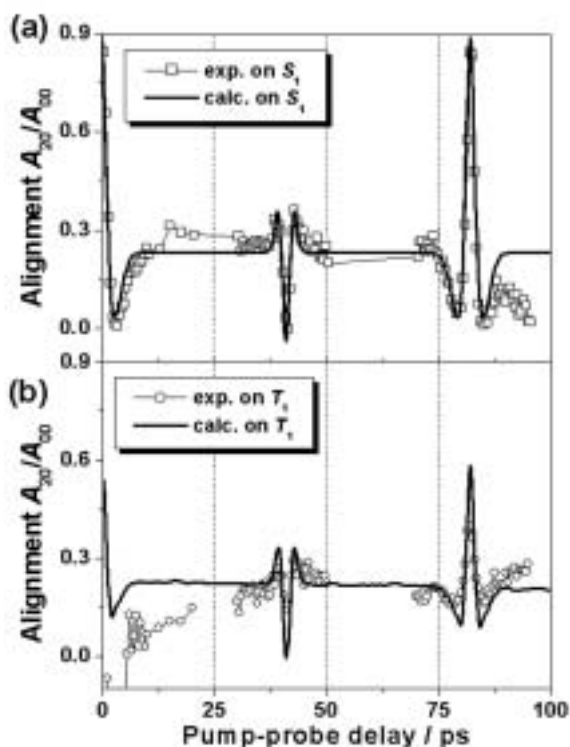


Figure 1. Time evolutions of the alignment parameter, A_{20}/A_{00} , for the molecular axis distribution,

$$P(\theta, \phi) = A_{00}Y_{00}(\theta, \phi) + A_{20}Y_{20}(\theta, \phi),$$

on (a) the S_1 and (b) the T_1 state. Square (\square) and circle (\circ) represent the experimentally determined alignment parameter which derived from the time profiles of the photoionization partial cross section from the S_1 and the T_1 state, respectively. Solid lines are simulation profiles taking into account the rotational wavepacket motion.

III-F-3 Femtosecond Photoelectron Imaging on Pyridazine: S_1 Decay Rate and $3s$ and $3p$ Rydberg State Energetics

**KIM, Sang Kyu¹; MATSUMOTO, Yoshiteru;
SUZUKI, Toshinori**
(¹Inha Univ., Korea)

Diazabenzenes have received extensive experimental and theoretical studies as the benchmark systems for investigation of electronic dephasing processes. In particular, pyrazine is the best-studied molecule of an intermediate case and it is well accepted now that the optically prepared S_1 pyrazine dephases into the T_1 manifold with a lifetime of 110 ps. Our previous study on pyrazine by time-resolved photoelectron imaging has firmly established this dynamics by visualizing both the decay of the S_1 and the buildup of T_1 characters in real time.¹⁾⁻³⁾ Comparing with pyrazine and pyrimidine, pyridazine is the least-studied member of diazabenzene. There seem to be still debates on various fundamental properties of excited state such as the S_1 lifetime, spectral assignment of S_1 origin, and energetics of low-lying Rydberg states. Another interesting issue is that although pyrazine dephases mainly to the triplet manifold, it has been suggested that pyridazine dephases down to the ground electronic state. We have performed the first time-resolved study on the excited states of pyridazine by femtosecond photoelectron imaging. The lifetime of the S_1 state is 340 ps at the origin and decreases at higher vibrational energies, and no clear signature of the triplet states was observed. The $3s$ (n^{-1}) and $3p$ (n^{-1}) Rydberg states of pyridazine are identified in angle- and energy-resolved photoelectron images obtained by the $(1+2')$ excitation where these Rydberg states act as intermediate resonant states in photoionization process, providing respective term values of 5.67 and 6.27 eV.

References

- 1) T. Suzuki *et al.*, *J. Chem. Phys.* **111**, 4859 (1999).
- 2) Tsubouchi *et al.*, *Phys. Rev. Lett.* **115**, 8810 (2001).
- 3) Song *et al.*, *J. Chem. Phys.* **86**, 4500 (2001).

III-G Non-Adiabatic Photodissociation Dynamics of Fundamental Molecules

Detailed investigation on photodissociation dynamics of fundamental molecules is extremely important not only for elucidating chemical reaction mechanisms but also for accurate modeling of atmospheric chemistry. Hyperthermal kinetic energy distribution of reaction products, hot band contribution in photoabsorption, and non-adiabatic dynamics are important for understanding isotope fractionation, branching ratios in bimolecular reactions *etc.* in the atmosphere.

III-G-1 Non-Adiabatic Bending Dissociation of OCS: The Effect of Bending Excitation on the Transition Probability

KATAYANAGI, Hideki; SUZUKI, Toshinori

[*Chem. Phys. Lett.* **360**, 104 (2002)]

In our previous work, an interesting non-adiabatic

dissociation mechanism of OCS induced by fast bending motion in the electronically excited state has been discovered.¹⁾ In the present work, UV photodissociation dynamics of OCS starting from the bending excited (010) state was compared to that from the ground vibrational state (000). The rotational distribution of $\text{CO}(X^1\Sigma^+)$ was measured by (2+1) resonance enhanced multiphoton ionization, in which dissociations from the two different initial states were discriminated from the

translational energies of the CO fragments. Quantitative analysis revealed that the non-adiabatic transition probability in dissociation starting from (010) was 0.21 that is similar to but slightly smaller than the value, 0.34, from (000).

Reference

1) Suzuki *et al.*, *J. Chem. Phys.* **109**, 5778 (1998).

III-G-2 Velocity Map Fragment Imaging on 205 nm Photodissociation of Nitrous Oxide

KATAYANAGI, Hideki; NISHIDE, Tatsuhiro;
SUZUKI, Toshinori

Photodissociation of N₂O at 205 nm is reexamined by the velocity map ion imaging of N₂ and O(¹D₂) fragments. The kinetic energy distribution of the O atoms measured by using (2+1) REMPI via the ¹P₁ state is in excellent agreement with the one reported previously by

a conventional imaging method without two-dimensional space focusing.¹⁾ The angular distribution of the O atoms is expressed by expansion with up to the 6-th order Legendre polynomial, indicating the orbital alignment as reported previously.¹⁾ A bell-shaped rotational distribution of N₂ is observed, where its width is somewhat narrower than previous observations. From the rotational distribution of N₂ due to photoexcitation from the (000) and (010) states of N₂O and the ion image of state-selected N₂, the magnitude of the transition strengths from the (000) and (010) levels were estimated. The angular anisotropy of N₂ fragments is in excellent agreement with the results by Neyer *et al.*²⁾ Rather low angular anisotropy, $\beta < 1.0$, indicates that photo-absorption to the A''(¹Σ⁻) state is not negligible at 205 nm.

References

1) Suzuki *et al.*, *Chem. Phys. Lett.* **256**, 90 (1996).

2) Neyer *et al.*, *J. Phys. Chem. A* **103**, 10388 (1999).

III-H Development of New Devices for Molecular Dynamics Experiments

III-H-1 Three Dimensional Photofragment Imaging Using a Fast Response Imager

SUZUKI, Toshinori; KATAYANAGI, Hideki

An inverse Abel transform is often used for reconstructing a 3D object from its 2D projection, when the original distribution is cylindrically symmetric. In pump and probe experiments, this condition is fulfilled only when the polarization directions of the two beams are aligned parallel to each other. For investigating vector correlation in photodissociation, it is useful to use cross polarization of two laser beams, which inevitably destroys the cylindrical symmetry required for an inverse Abel transform. For obtaining the 3D scattering distribution for cross polarization, time and position sensitive detection methods must be employed. Currently, a delay line anode imaging device is widely used for the time and position sensitive detection of particles. However, this method is able to receive particles only less than 10 in a given response time, about 10 ns, and it is not ideal for the experiments with low repetition lasers, where tens of particles are detected within 10 ns. We use a dual microchannel plate backed by a plastic scintillator with an emission life time of about 3 ns and capture a transient image on this screen with a gated camera with a time-resolution of 3 ns. Several designs for the acceleration electrodes were carefully tested.

III-H-2 High Repetition Rate Two Dimensional Imaging Using C-MOS Imager

SUZUKI, Toshinori; TSUBOUCHI, Masaaki

The imaging experiment suffers from non-uniform

sensitivity of an imaging system over the area. This originates from an unavoidable pulse height (brightness) distribution of an MCP with a phosphor screen, and the most effective method to correct it is to perform real-time image processing on each image due to a single laser shot. Previously, we have performed real-time thresholding and centroiding calculations for measurements with 25 Hz system rate, while it is no longer applicable to experiments run at 1 kHz since it is by far higher rate of a regular video rate, 25 Hz. In collaboration with HAMAMATSU Co. Ltd., a 1 kHz C-MOS camera system with a real-time image processing was constructed and tested by performing 2D real-time electron counting with a 1 kHz Ti:sapphire femtosecond laser.

III-H-3 Construction of a Rotating-Source Crossed Beam Apparatus

KOYGUCHI, Hiroshi; SUZUKI, Toshinori

A new crossed beam apparatus with a rotating source has been designed for reactive scattering experiments on the O(¹D₂) reactions. The crossing angle can be varied from 30 to 180 degrees for continuously changing the collision energies. The O(¹D₂) atoms are generated by photolysis of O₂ molecules at 157 nm produced by a F₂ laser.

III-I Structure and Properties of Polyoxometalates with a Magnetic, Electronic, or Biological Significance

Polyoxometalates constitute model systems for the study of the electron and energy transfer in the infinite metal-oxide lattice and their simplicity allows to treat at the molecular scale the coupling of electronic and nuclear movements, which is an inherent problem for the mixed-valence systems. As is clear from such a variety of both structure and reactivity of polyoxometalates, our current works on polyoxometalates are 1) structure/reactivity relationships with particular regard to the mechanism of electron transfer reactions, 2) magnetic interaction and molecular magnetic device, 3) energy-transfer mechanism and luminescence device (including nonlinear optical device), 4) encapsulation of templates in the photo-induced self-assembly process, 5) template-exchange reaction and topology, and 6) antibacterial effects on methicillin-resistant *Staphylococcus aureus* (MRSA) and human gastric pathogen of *Helicobacter pylori*.

III-I-1 Synthesis and Crystal Structure of a Novel Vanadium-Containing Tungstobismutate(III)K₁₂[(VO)₃(BiW₉O₃₃)₂]-30H₂O

BOTAR, Bogdan¹; YAMASE, Toshihiro²;
ISHIKAWA, Eri¹
(¹Tokyo Inst. Tech.; ²IMS and Tokyo Inst. Tech.)

[*Inorg. Chem. Commun.* **4**, 551 (2001)]

The tris(vanadyl)-substituted tungstobismutate(III) [(VO)₃(BiW₉O₃₃)₂]¹²⁻ anion has been synthesized by reaction of α -B[BiW₉O₃₃]⁹⁻ with VOSO₄ in aqueous solution. The anion is made of two α -B[BiW₉O₃₃]⁹⁻ unit linked by a belt of three exterior VO²⁺ groups into an assembly of virtual D_{3h} symmetry. The three vanadium centers are well separated by V...V distance of 5.375(4)–5.474(4) Å.

III-I-2 Crystallization and Structural Characterization of Two Europium Molybdates, Eu₄Mo₇O₂₇ and Eu₆Mo₁₀O₃₉

NARUKE, Haruo¹; YAMASE, Toshihiro²
(¹Tokyo Inst. Tech.; ²IMS and Tokyo Inst. Tech.)

[*J. Solid State Chem.* **161**, 85 (2000)]

Crystals of two new europium molybdates, Eu₄Mo₇O₂₇ and Eu₆Mo₁₀O₃₉, were grown in a melt of Eu₂O₃·6.1–6.5MoO₃ obtained by thermal decomposition of [Eu₂(H₂O)₁₂Mo₈O₂₇]-6H₂O or firing of the Eu₂O₃ + 8MoO₃ mixture at 800 °C for 2 h in air. Repeated uses of reaction containers are effective in the crystallization. Eu₄Mo₇O₂₇ crystallized in monoclinic, C2/c (No. 15), $a = 23.031(1)$, $b = 14.720(1)$, $c = 14.4097(7)$ Å, $\beta = 105.174(2)^\circ$, $V = 4714.8(4)$ Å³, $Z = 8$, $R_1 = 0.035$, and $wR_2 = 0.064$. Eu₄Mo₇O₂₇ is a layer compound consisting of {MoO₄}- and {Mo₃O₁₁}-containing layers parallel to the bc plane and interstitial Eu atoms. Eu₆Mo₁₀O₃₉ crystallized in monoclinic, C2/c (No. 15), $a = 12.3008(5)$, $b = 19.6596(9)$, $c = 13.7691(47)$ Å, $\beta = 100.8934(9)^\circ$, $V = 3269.8(2)$ Å³, $Z = 4$, $R_1 = 0.036$, and $wR_2 = 0.101$. The structure of Eu₆Mo₁₀O₃₉ is constructed of three-dimensionally arranged {MoO₄} and {Mo₂O₇} groups and Eu atoms, being closely related to the structure of Ce₆Mo₁₀O₃₉. In both compounds, Eu

atoms achieve seven- or eight-fold coordination by O atoms (< 2.7 Å), and two EuO_{*n*} polyhedra share their edges or faces with a short Eu...Eu separation ranging from 3.6297(8) to 3.7168(6) Å.

III-I-3 Nanocluster Crystals of Lacunary Polyoxometalates as Structure-Design-Flexible, Inorganic Nonlinear Materials

MURAKAMI, Hidetoshi; KOZEKI, Toshimasa;
SUZUKI, Yuji; ONO, Shingo; OHTAKE, Hideyuki;
SARUKURA, Nobuhiko; ISHIKAWA, Eri¹;
YAMASE, Toshihiro²
(¹Tokyo Inst. Tech.; ²IMS and Tokyo Inst. Tech.)

[*Appl. Phys. Lett.* **79**, 3564 (2001)]

Lacunary polyoxometalates, large inorganic, structure-design-flexible, nanocluster crystals are found to have optical nonlinearity than KH₂PO₄ by the powder second-harmonic-generation method. Moreover, the capability of generating ultraviolet radiation down to around 300 nm is found. The basic criteria to design the high nonlinearity are also discovered by the reduction of the molecular symmetry.

III-I-4 A Three-Dimensional Inorganic/Organic Hybrid Vanadium Oxide Complex with Pentacoordinate Co^{II}, [CoV₂O₆(4,4'-bipy)]

YANG, Lan¹; NARUKE, Haruo¹; YAMASE, Toshihiro²
(¹Tokyo Inst. Tech.; ²IMS and Tokyo Inst. Tech.)

[*Acta Crystallogr., Sect C: Cryst. Struct. Commun.* **57**, 1378 (2001)]

The title compound, poly{[cobalt(II)- μ -(hexaaxodivandium- $O:O'$)]- μ -bipyridine-N:N'}, [CoV₂O₆(C₁₀H₈N₂)], has been prepared hydrothermally and characterized by elemental analyses, IR spectroscopy and single-crystal X-ray diffraction. The structure consists of bimetallic oxide layers, [Co₂V₄O₁₂], linked through 4,4'-bipyridine ligands into a three-dimensional network.

III-I-5 Tb₂Mo₄O₁₅

NARUKE, Haruo¹; YAMASE, Toshihiro²
(¹Tokyo Inst. Tech.; ²IMS and Tokyo Inst. Tech.)

[*Acta Crystallogr., Sect E* **57**, 1106 (2001)]

The title compound, tetramolybdenum(VI) diterbate (III), was prepared by pyrolysis of Tb₂(H₂O)₁₂Mo₈O₂₇·6H₂O at 1023 K for 2 h in air. The structure consists of trigonal bipyramidal MoO₅, tetrahedral MoO₄, and monocapped trigonal prismatic TbO₇ units. The two MoO₅ and two MoO₄ units are corner-shared, to form a Mo₄O₁₅ group.

III-I-6 H₂O₂-Based Epoxidation of Bridged Cyclic Alkenes with [P{Ti(O₂)₂W₁₀O₃₈}]⁷⁻ in Monophasic Systems: Active Site and Kinetics

GAO, Feixue¹; YAMASE, Toshihiro²; SUZUKI, Hideo¹
(¹Tokyo Inst. Tech.; ²IMS and Tokyo Inst. Tech.)

[*J. Mol. Catal. A* **180**, 97 (2002)]

The H₂O₂-based epoxidation of bridged cyclic alkenes in a monophasic system containing low concentrations (< 2 mM) of [Buⁿ₄N]₄[Pr₂NH₃]₂H[P{Ti(O₂)₂W₁₀O₃₈}]₂·H₂O (**1**) (with two η²-peroxotitanium sites in the anion) has been studied in search of the catalytically active species involved. ³¹P-NMR spectra of **1**, measured under a variety of conditions, revealed that the active species was not hydroperoxotitanium complex [P{Ti(OOH)}₂W₁₀O₃₈]⁷⁻ or [P{Ti(OOH)}Ti(O₂)W₁₀O₃₈]⁷⁻. The reaction pathways for the alkene epoxidation are discussed to understand the kinetics (especially the initial [H₂O₂] dependence). It was concluded that the net catalytic reaction for the epoxidation occurred through the two-electron oxidation at the hydroperoxotitanium site in the catalyst.

III-I-7 Photochemical Formation of a Lacunary Tire-Shaped Anion, [Mo₁₄₂O₄₃₂H₂₆(H₂O)₅₈]¹⁴⁻, through Degradative Self-Assembly of [Mo₃₆O₁₁₂(H₂O)₁₆]⁸⁻: Topology of Ring-Structural Molybdenum Blues

YAMASE, Toshihiro¹; PROKOP, Petra²
(¹IMS and Tokyo Inst. Tech.; ²Tokyo Inst. Tech.)

[*Angew. Chem. Int. Ed. Engl.* **41**, 466 (2002)]

A diamagnetic blue 28-electron reduced species [Mo^V₂₈Mo^{VI}₁₁₄O₄₃₂H₂₆(H₂O)₅₈]¹²⁻ ({Mo₁₄₂}) was produced photochemically through the degradative self-assembly of [Mo₃₆O₁₁₂(H₂O)₁₆]⁸⁻ ({Mo₃₆}). The molybdenum blue photochemistry favors not only the mechanistic investigation of the degradation self-assembly processes but also provides a basis for the molecular design of nano-sized ring clusters.

III-I-8 Size-dependent Population of Trivalent Rare Earth Cations (RE³⁺) in [(RE)₂(H₂O)₂(SbW₉O₃₃)(W₅O₁₈)₂]¹⁵⁻, and Structural Characterization of a Lutetium-Polyoxotungstate Complex [Lu₃(H₂O)₄(SbW₉O₃₃)₂(W₅O₁₈)₂]²¹⁻

NARUKE, Haruo¹; YAMASE, Toshihiro²
(¹Tokyo Inst. Tech.; ²IMS and Tokyo Inst. Tech.)

[*Bull. Chem. Soc. Jpn.* **75**, 12756 (2002)]

The effect of ionic radius of trivalent rare earth cations (RE³⁺) on the population at two square-antiprismatic sites (*Site I* and *Site II*) in [(RE)₂(H₂O)₂(SbW₉O₃₃)(W₅O₁₈)₂]¹⁵⁻ was studied by luminescence spectroscopic and X-ray crystallographic measurements in the Eu/Y- and Eu/Lu-mixed systems. The results indicated that a small RE³⁺ cation favorably occupies *Site II* where RE³⁺ is coordinated by four bridging O atoms of [SbW₉O₃₃]⁹⁻ and four terminal O atoms of [W₅O₁₈]⁶⁻. With the help of a structural characterization of pure [(RE)₂(H₂O)₂(SbW₉O₃₃)(W₅O₁₈)₂]¹⁵⁻ (RE = Er, Y, Dy, Eu, Sm), the large occupancy of small RE³⁺ at *Site II* was explained by a favorable coordination of [SbW₉O₃₃]⁹⁻ for small RE³⁺. A trial of the isostructural Lu complex unexpectedly showed formation of a novel [Lu₃(H₂O)₄(SbW₉O₃₃)₂(W₅O₁₈)₂]²¹⁻ complex which consists of two [Lu(SbW₉O₃₃)(W₅O₁₈)]¹²⁻ groups linked by [Lu(H₂O)₄]³⁺ with C₂ configuration.

III-I-9 Gd₄Mo₇O₂₇, a Novel Phase in the Gd₂O₃-MoO₃ System

NARUKE, Haruo¹; YAMASE, Toshihiro²
(¹Tokyo Inst. Tech.; ²IMS and Tokyo Inst. Tech.)

[*Acta Crystallogr., Sect E* **57**, i62 (2002)]

The title compound, heptamolybdenum(VI) tetragadolinate(III), a novel phase in the Gd₂O₃-MoO₃ system, has been prepared by pyrolysis of [Gd₂(H₂O)₁₂·Mo₈O₂₇]₂·6H₂O at 1023 K for 2 h in air. The compound can be described as a layer structure consisting of [MoO₄]-, [Mo₃O₁₁]-, and [Gds]-containing layers, which are stacked along the *a* direction. The coordination polyhedra of square-antiprismatic GdO₈ and monocapped trigonal prismatic GdO₇ are dimerized to give [Gd₂O_{*n*}] (*n* = 12 and 13) groups which possess short Gd···Gd separation [3.6345(4)–3.6404(4) Å].

III-I-10 Time-Resolved ESR-Spectroscopic Investigation of Polyoxometalate Photochemistry

YAMASE, Toshihiro
(IMS and Tokyo Inst. Tech.)

[*Catal. Catal.* **44**, 340 (2002)]

The time-resolved ESR spectroscopy is based on the detection of electron spin polarization (ESP) which let us enable to investigate the dynamics of the photochemically produced radicals. After a brief qualitative

and conceptual review of time-resolved ESR spectroscopy, exemplar photoredox reactions of polyoxometalates are discussed based on the observable chemically-induced-dynamic-electron -polarization (CIDEP) spectra which can be explained by the triplet mechanism.

III-J Electronic Spectroscopy and Excited-State Dynamics of Aromatics Clusters

Clusters are model systems for elucidating intermolecular interactions that control macroscopic properties of the molecules in condensed phases, such as liquids and crystals. We are investigating geometry and bonding topology of clusters containing aromatic molecules as well as their dynamical behavior after photoexcitation. This year we focus on detailed reexamination of electronic spectra of (benzene)_n clusters. Because benzene is a fundamental aromatic molecule with high symmetry, their aggregates have been subjected to vast numbers of experimental and theoretical studies for more than a quarter of a century. Still, there remain not a few issues under debate especially concerning to their electronic spectra. We succeeded in solving some of them by the present reexamination.

III-J-1 S₁–S₀ Vibronic Spectrum of the Benzene Tetramer

IIMORI, Toshifumi^{1,2}; OHSIMA, Yasuhiro³
(¹Kyoto Univ.; ²Nagoya Univ.; ³IMS and Kyoto Univ.)

[*J. Chem. Phys.* **117**, 3656 (2002)]

We reinvestigated the S₁–S₀ electronic transitions of (benzene)_n clusters by two-color mass-selective resonantly enhanced two-photon ionization (R2PI) and UV–UV hole burning spectroscopies. In this study, we explored the band system that has been assigned to the trimer for two decades. Hole burning measurements by monitoring the trimer ion isotopomer channels in the expansion of a mixture of C₆H₆ and C₆D₆ have shown the contribution of six spectral carriers in the R2PI spectra, two of which are isotopically pure clusters. The other hetero isotopic species containing at least one C₆H₆ moiety appear in two adjacent isotopomer channels. It is argued that the band system should be re-assigned to the neutral tetramer having four equivalent sites, which are detected in daughter ion mass channels due to efficient fragmentation after ionization even with two-color excitation. The experimental results are consistent with a distorted tetrahedral structure with S₄ symmetry predicted as the global minimum by several model calculations. This conclusion is further supported by an analysis of exciton splittings in the C₆H₆-localized origin band, and this analysis provides coupling constants for the excitation exchange in the S₁ state. Other experimental results reported so far pertaining to this species are reconsidered on the basis of the new assignment.

III-J-2 S₁–S₀ Vibronic Spectrum of the Benzene Trimer

IIMORI, Toshifumi^{1,2}; AOKI, Yasuhiro¹;
OHSIMA, Yasuhiro³
(¹Kyoto Univ.; ²Nagoya Univ.; ³IMS and Kyoto Univ.)

[*J. Chem. Phys.* **117**, 3675 (2002)]

We further reexamined the S₁–S₀ transition of the (benzene)_n cluster that appears only in the dimer ion channel and thus has been assigned to an isomer of the neutral dimer other than the extensively studied T-shaped form. Mass-selective resonantly enhanced two-photon ionization (R2PI) excitation and UV–UV hole burning spectra are measured in the 0₀⁰ and 6₀⁰ vibronic regions. It is established from the observed spectra monitoring three isotopomer channels, (C₆H₆)₂⁺, [(C₆H₆)(C₆D₆)]⁺, and (C₆D₆)₂⁺, that efficient fragmentation following ionization prohibits one to observe the two-color R2PI spectra in the parent ion channels, similar to the case for the benzene tetramer as presented in III-J-1. Three neutral isotopomers containing at least one C₆H₆ moiety are identified, and this result argues the reassignment of the band system to the neutral benzene trimer with a cyclic form, where the three benzene sites are equivalent. The spectra of the homo isotopomers [(C₆H₆)₃ and (C₆D₆)₃] in the two vibronic regions exhibit small splittings due to the excitation exchange interactions, and this observation is discussed on the symmetry of the cluster geometry. Energetics pertaining to neutral and ionic benzene clusters are also discussed with previous experimental studies to assess a reason of the efficient fragmentation in the ionic states after R2PI for the trimer and larger clusters but not for the dimer.

III-K Electronic Spectroscopy of Molecules in Pendular States

When a molecule is subjected to a strong external electric field, pendular states are realized, where the electrostatic interaction by the field exceeds the molecular rotational energy and free rotation of the molecule changes to libration confined in the interaction potential. Thus, spectroscopic studies of pendular states will provide fundamental information toward establishing artificial manipulation of molecular orientation. We recently started investigation of electronic spectra of aromatic molecules in a strong DC electric field.

III-K-1 Construction of an Apparatus for Measurements of Fluorescence Excitation Spectra in a Strong DC Electric Field

KANYA, Reika¹; OHSHIMA, Yasuhiro²
(¹Kyoto Univ.; ²IMS and Kyoto Univ.)

We have recently constructed an experimental apparatus that enables measurements of fluorescence excitation spectra of molecules in a strong DC electric field. The apparatus is consisted of two differentially pumped vacuum chambers, as shown in Figure 1. A sample vapor diluted in He carrier gas is expanded through a heated pulsed nozzle, collimated by a conical skimmer, and passed through the center of two parallel electrodes in the second chamber. A linearly polarized light from a pulsed dye laser goes across the molecular beam in right angles, and the resultant fluorescence propagating to the downstream of the molecular beam is filtered and imaged onto a photomultiplier tube (PMT). The output of PMT is pre-amplified and fed into a boxcar. A combination of a Glan-laser polarizer and a variable wave plate is used to obtain highly polarized laser light with arbitrary orientation of linear polarization. The electrodes are so-called of Rogowski-type, which are designed to minimize the field inhomogeneity at their edges. By applying positive and negative high voltages to each of the electrodes, a uniform DC electric field up to 200 kV/cm can be achieved.

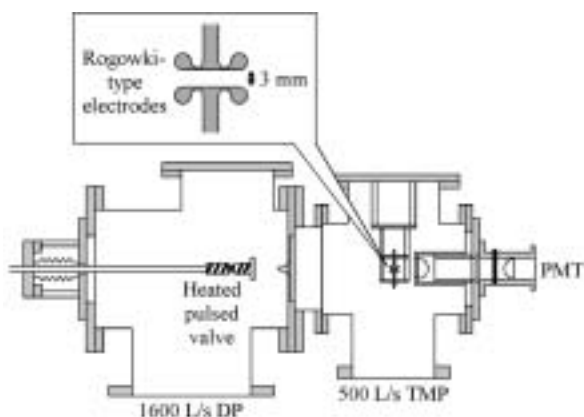


Figure 1. Schematic diagram of the experimental apparatus for measurements of fluorescence excitation spectra in a strong DC electric field. Close up of the Rogowski-type electrodes is shown as an inset.

III-K-2 Laser-Induced Fluorescence Spectra of Pendular-State Aromatics in a Strong DC Electric Field

KANYA, Reika¹; OHSHIMA, Yasuhiro²
(¹Kyoto Univ.; ²IMS and Kyoto Univ.)

With the experimental setup described in III-K-1, electronic transitions of several aromatic molecules like 9-cyanoanthracene (CNA) and *p*-aminobenzonitrile were observed under various DC electric field strengths. Figure 1 shows the S_1 - S_0 origin of CNA in the external electric field. The band contour changes drastically as the increase of the external field. In addition, altering polarization of the laser against the field provides an

entirely different shape in the spectra.

Because it is highly demanding computation to derive oscillator strength in a strong electric field for large asymmetric-top molecules like aromatics, some approximate method is indispensable. Considering that the interaction between the field and the molecular permanent dipole is dominant, we adopt a molecule-fixed axis system that is appropriate for the interaction. Then, the Hamiltonian is separated into zero-order terms that manifest pendular states for a symmetric top and remaining off-diagonal terms. Perturbation-theory treatments of the latter terms afford acceptably accurate calculations with greatly reduced computational time. Besides, we derived analytically, for the first time, energy levels and wavefunctions of a symmetric top in the pendular limit with corresponding quantum numbers.

Gross features of asymmetric-top pendular spectra are described in terms of the zero-order energy levels and selection rules. Indeed, the observed dependences for CNA on the electric field and the laser polarization are explained consistently, and its electric dipole moment is found to be increased by ~ 1.3 D after the $S_1 \leftarrow S_0$ excitation.

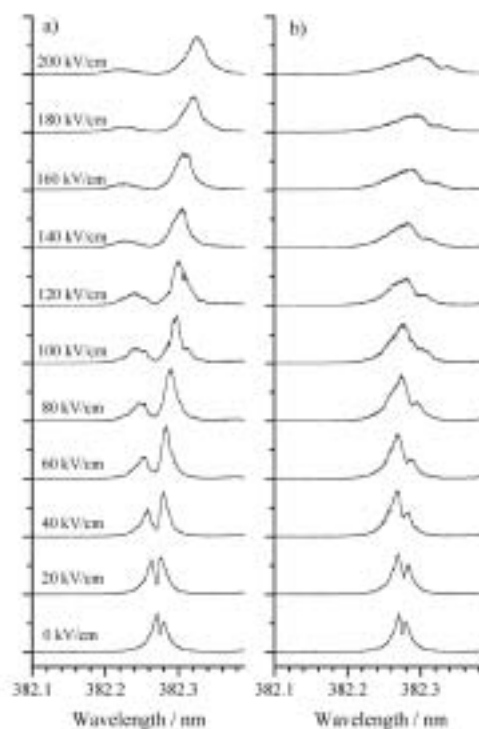


Figure 1. Electric field effects in LIF spectra of the S_1 - S_0 origin band of CNA. An angle between the laser polarization and the field is a) parallel, and b) perpendicular.

III-L Wave Packet Engineering Using a Phase-Programmable Femtosecond Optical Source

We proposed “wave packet engineering” which realizes mutual conversion between phase information of photonic and quantum wave packets by means of light-matter interaction. A phase-programmable femtosecond optical source is indispensable for such interactive control of photonic and quantum wave packets. We demonstrate control of quantum wave packets in organic molecules and semiconductors using phase-programmed pulses.

III-L-1 Single Molecular Phase-to-Amplitude Converter

MISAWA, Kazuhiko; MATSUDA, Isao¹; LANG, Roy¹

(¹ Tokyo Univ. Agric. Tech., CREST(JST))

Control of quantum wave packets has been recently studied in various systems such as atoms, molecules, and semiconductors using chirp-controlled and phase-locked double pulses.¹⁾ In the present study, we observed wave-packet shaping by means of the phase-programmed femtosecond pulses in a cyanine dye molecule. The intra-pulse phase pattern of the pulses was converted to the amplitude of luminescence from the cyanine molecules.

The phase-programmable femtosecond optical source is composed of a femtosecond pulse oscillator, phase modulator and phase analyzer as shown in Figure 1. A femtosecond pulse with a spectral band width as broad as 160 nm is converted onto the Fourier plane. After a phase shift is provided to each spectral component with a spatial light modulator on the Fourier plane, the pulse is reconstructed. The output from the phase modulator is characterized by frequency resolved optical gating (FROG). The temporal profile and phase information of the femtosecond pulses can be obtained from the FROG measurement. A desired phase pattern can be realized through the iterative adjustment of the phase mask by analyzing the phase information. The center wavelength, pulse energy, duration, and phase-shift division of the source output were 802 nm, 0.64 nJ, 14 fs, and $6\pi/700$ radian, respectively. Figure 2 shows the spectra and phase dispersions for positively-chirped ($\Phi'' = 500$ fs²), transform-limited (0 fs²) and negatively-chirped pulses (-500 fs²).

Ethanol solution of a cyanine dye (IR-140) at a concentration of 4×10^{-4} M is circulated in a 0.5-mm thick quartz cell. The luminescence spectra of spontaneous emission are measured to evaluate the remaining excited-state population. Figure 3 shows the difference luminescence spectra of the positively-chirped (PC) and negatively-chirped (NC) excitations from the transform-limited excitation. The luminescence intensity is increased and decreased in case of PC and NC excitations, respectively. This chirp-dependent luminescence can be explained in terms of intra-pulse pump-dump process.²⁾ NC pulse induces narrow spatial distribution of the excited wave packet, while it is easily broadened and quickly escapes from the Franck-Condon window in PC case. The overlap integral between the excited- and ground-state wave packets determines the population, and as a result, the luminescence intensity.

In conclusion, we observed the remarkable dependence of luminescence intensity and the excited-state population in IR-140 molecules on the chirped pulse from the phase-programmable femtosecond optical source. The observed shaping of quantum wave packet opens a new possibility to process the intra-pulse phase information.

References

- 1) *Quantum Control of Molecular Reaction Dynamics*, R. J. Gordon and Y. Fujimura, Eds. (World Scientific, 2001).
- 2) K. Misawa and T. Kobayashi, *J. Chem. Phys.* **113**, 7546 (2000).

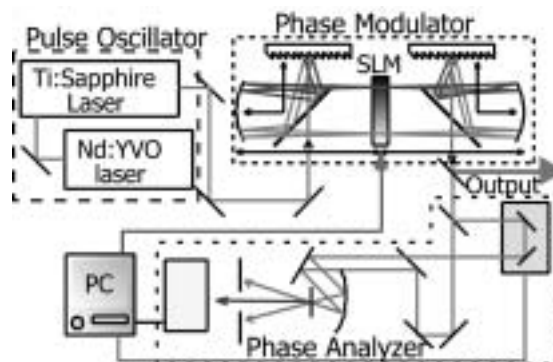


Figure 1. Schematic diagram of the phase-programmable femtosecond optical source.

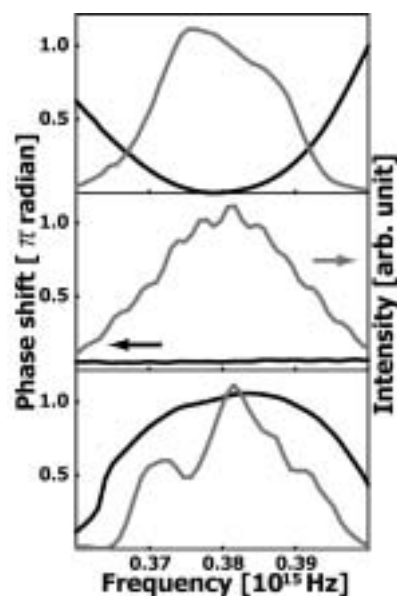


Figure 2. Spectra and phase dispersions of positively-chirped (top), transform-limited (middle) and negatively-chirped pulses (bottom).

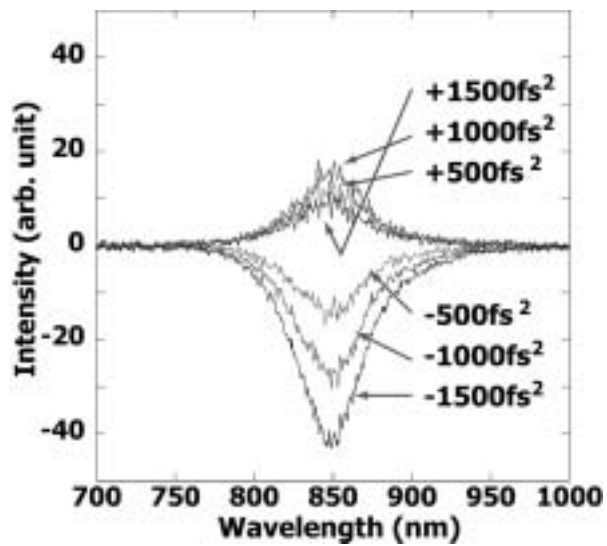


Figure 3. Difference luminescence spectra from IR-140 dye by the positively and negatively-chirped excitations with respect to the transform limited pulse.

RESEARCH ACTIVITIES IV

Department of Molecular Assemblies

IV-A Spectroscopic Study of Charge Carriers in Organic Conductors

The low-frequency reflectivity of an organic conductor provides us with a wealth of information on the nature of charge carriers. For instance, the anisotropy of a band structure, bandwidth, effect of electron-electron correlation, and electron-molecular vibration (EMV) coupling parameters can be extracted from the analysis of the reflectivity or optical conductivity curve. We are investigating the polarized reflection spectra of various organic conductors in the spectral region of 50–33000 cm^{-1} and in the temperature range of 6–300 K. Usually the molecular vibrations (local phonons) are screened by strong electronic transition by charge carriers. Therefore, very few molecular vibrations are detected in the reflection spectrum. In this sense, the Raman spectroscopy is a complementary method to reflection spectroscopy for understanding molecular vibrations in a metallic state. Since some molecules have charge-sensitive vibrational modes, the Raman spectroscopic method is a powerful tool to detect the site-charge distribution (oxidation state of molecule). We are investigating the charge ordering (CO) phenomena in organic conductors using the technique of infrared and Raman spectroscopy. In the organic charge-transfer salts, CO is originated from the localization of the charge carriers. Since the charge carriers in organic crystal is located at the boundary between localized and extended (delocalized) states, CO will be widely found through the phase transition. The charge ordering was first found in inorganic narrow-band systems such as copper, manganese, and vanadium oxides. Recently, CO has been found in several organic conductors, and the electronic phase diagrams of typical organic conductors are re-examined taking CO into account. The CO state is drawing attention, since CO is theoretically considered as being related to the unconventional superconducting mechanism. The Raman and infrared spectra change dramatically at the CO phase-transition temperature, since CO is accompanied by a charge disproportionation, forming an inhomogeneous charge distribution. Our goal is the complete understanding of the CO phase transition through the interpretation of the vibrational spectra, and the drawing of a P - T phase diagram.

IV-A-1 Raman Study of the Charge Ordering in α -(BEDT-TTF) $_2$ I $_3$ at High Pressure

WOJCIECHOWSKI, Roman; YAMAMOTO, Kaoru; YAKUSHI, Kyuya; KAWAMOTO, Atsushi¹
(¹Hokkaido Univ.)

We have carried out Raman experiments on α -(BEDT-TTF) $_2$ I $_3$ to investigate the site-charge distribution among BEDT-TTFs in the paramagnetic semi-metal-like (PM) and diamagnetic insulating (DI) phases at ambient and quasi-hydrostatic pressures. We focused on the charge-sensitive ν_2 and ν_3 modes of BEDT-TTF, which are related to the ring and central C=C stretching modes with A_g symmetry. We found a distinctive spectral change associated with metal-insulator phase transition up to 1.5 GPa (above this pressure the DI phase was suppressed).

In the DI phase, ν_2 splits into four bands labeled by \mathbf{c}_{1a} , \mathbf{c}_{1b} , \mathbf{c}_2 , and \mathbf{c}_3 , which are confirmed by the isotope shift of the central ^{13}C - ^{13}C band). The presence of the four bands of ν_2 indicates the presence of the four crystallographically non-equivalent BEDT-TTFs. This observation means that the inversion symmetry characteristic of the PM phase disappears in the DI phase. The magnitude of the observed splitting and the symmetry breaking indicate that charges are disproportionate in so-called horizontal stripes (perpendicular to stacks). Quasi-hydrostatic pressures induce a progressive downshift of \mathbf{c}_{1a} and \mathbf{c}_{1b} accompanied with an upshift of \mathbf{c}_2 and \mathbf{c}_3 , indicating the continuous change of the charge disproportionation (CD) ratio, while the band position is

temperature independent under a constant pressure. Assuming the linear dependence of the ν_2 frequency on the ionicity of BEDT-TTF, the CD ratio between the charge-rich and charge-poor sites is evaluated as *ca.* $0.2e : 0.8e$ at low pressures, which gradually decreases to *ca.* $0.3e : 0.7e$ near 1.5 GPa. The CD ratio decreases and eventually CD is discontinuously suppressed above 1.5 GPa. This is because the transfer integrals (t) increase faster than the inter-site (V) Coulomb repulsions (on-site (U) is pressure independent) as expected. In the PM phase the ν_2 mode is split into two \mathbf{a}_1 and \mathbf{a}_2 bands (for ^{13}C substituted sample three bands were observed) indicating not uniform charge distribution among BEDT-TTFs. The charge difference evaluated from the splitting between the \mathbf{a}_1 and \mathbf{a}_2 bands is small, say $0.4e : 0.6e$, which is weakly dependent upon the pressure.

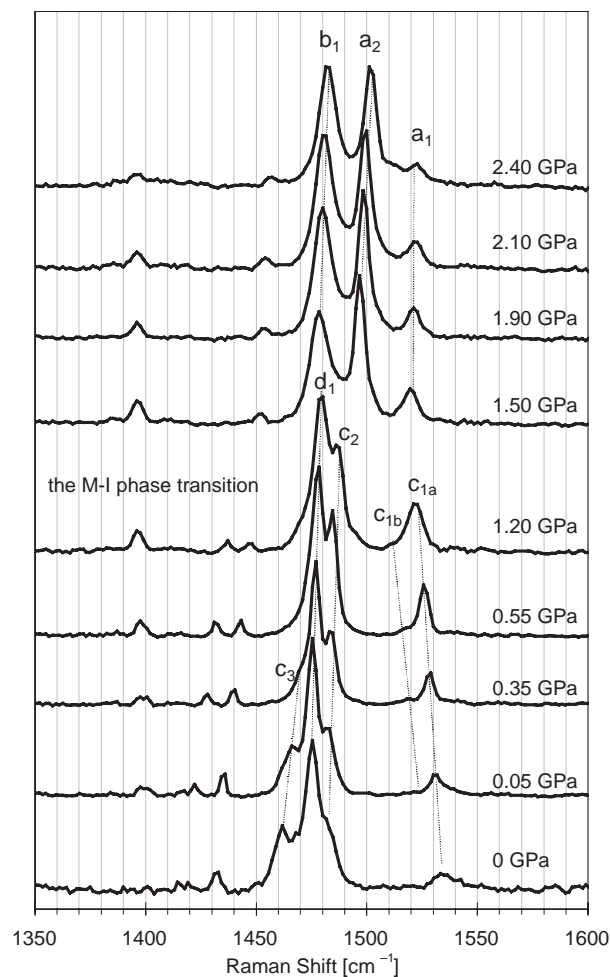


Figure 1. The pressure dependence of the α -(BEDT-TTF) $_2$ I $_3$ Raman spectra taken at 20 K with 514 nm laser line polarized along b -axis *i.e.* perpendicular to the stacks.

IV-A-2 Raman Study of the Charge Ordering in α' -(BEDT-TTF) $_2$ IBr $_2$ at High Pressure

WOJCIECHOWSKI, Roman; YAMAMOTO, Kaoru; NAKANO, Chikako; YAKUSHI, Kyuya; INOKUCHI, Makoto¹
(¹SUT Yamaguchi)

Raman spectroscopy experiments have been carried out for α' -(BEDT-TTF) $_2$ IBr $_2$ at ambient and under several quasi-hydrostatic pressures up to 2.3 GPa. We have focused on the charge-sensitive ν_2 and ν_3 modes of BEDT-TTF', which are related to the rings and central C=C stretching modes with A_g symmetry. We have examined these modes from room temperature to 20 K in order to detect the change in charge-distribution resulting from the structureless phase transition at 250 K at ambient pressure. We first confirmed from the splitting of ν_2 (a_1 , a_2) and ν_3 (b_1 , b_2) [See the spectrum at ambient pressure in Figure 1] that this phase transition is characterized as the charge-ordering (CO) phase transition. On increasing pressure, the phase-transition temperature (T_{CO}) decreases monotonously. Eventually above 1 GPa, the Raman spectra characteristic of the CO phase, which consist of two ν_2 (a_1 , a_2) and two ν_3 (b_1 , b_2), are suppressed in the entire temperature range.

This suggests that inter-stack transfer integrals between BEDT-TTFs increases faster than the inter-site Coulomb repulsion when the unit cell volume is reduced by pressure. In the semiconducting phase of α' -(BEDT-TTF) $_2$ IBr $_2$, the Raman spectra consist of a rather broad band in contrast to the spectrum of metallic β -(BEDT-TTF) $_2$ IBr $_2$ or θ -(BEDT-TTF) $_2$ I $_3$ salts, in which ν_2 and ν_3 are well separated. We have found that the pressure over 1.8 GPa is required for this compound to reach the uniform charge distribution like metallic salts [See the spectra above 1.8 GPa in Figure 1].

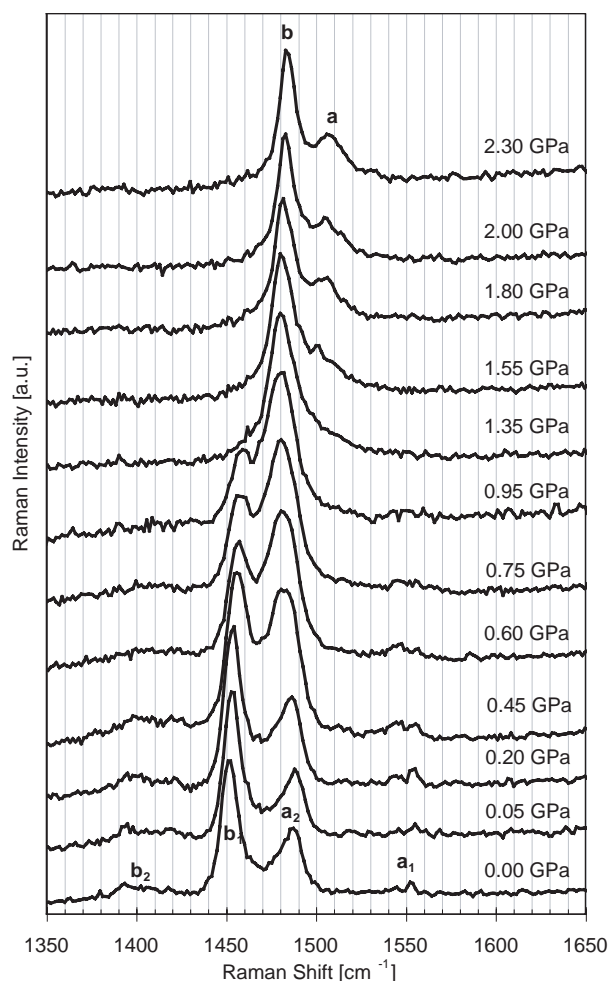


Figure 1. Raman spectra recorded at 100 K under several pressures up to 2.3 GPa, from the (001) crystal face with 514 nm laser line polarized parallel to $[1\bar{1}0]$ *i.e.* perpendicular to BEDT-TTF stacks.

IV-A-3 Charge Ordering in θ -(BEDT-TTF) $_2$ TM(SCN) $_4$ ($M = Co$ and Zn) Studied by Vibrational Spectroscopy

SUZUKI, Kenji¹; YAMAMOTO, Kaoru; YAKUSHI, Kyuya
(¹IMS and GUAS)

[Synth. Met. to be published]

Mori *et al.* systematically synthesized the series of θ -(BEDT-TTF) $_2$ MM'(SCN) $_4$, [$M = Cs, Rb, Tl; M' = Co, Zn$], (abbreviated as θ -MM'), and proposed the phase

diagram which demonstrated the relation between the metal-insulator transition temperature and the dihedral angle between BEDT-TTF molecules in adjacent stacks.¹⁾ Recent experimental and theoretical studies including our research group have manifested that the MI transition of θ -RbM' is caused by the charge ordering (CO). θ -TIM' [M' = Co, Zn] have the largest dihedral angle among the θ -MM' family, which means that these compounds have the most narrow bandwidth. We examined the Raman and infrared spectra of these two compounds in the temperature range of 50–300 K. Vibrational spectra of θ -TlCo at low temperature suggest the charge ordering with a horizontal stripe accompanying a doubling of the unit cell. θ -TlZn, which has larger dihedral angle, also underwent a charge-ordering phase transition at $T_{CO} = 165$ K. Different from θ -RbZn and θ -TlCo, however, the fluctuation of CO appeared at 240 K, which is much higher than T_{CO} . Furthermore, the pattern of ν_3 modes is quite different from θ -RbZn, which reflects the structure-sensitive nature of ν_3 modes, which was claimed in our preceding paper.²⁾

References

- 1) H. Mori, S. Tanaka and T. Mori, *Phys.Rev.B* **57**, 12023 (1998).
- 2) K. Yamamoto, K. Yakushi, K. Miyagawa and K. Kanoda, *Phys.Rev.B* **65**, 085110 (2002).

IV-A-4 High-Pressure Raman Study on a 1/3-Filled System (BEDT-TTF)₃CuBr₄

YAMAMOTO, Kaoru; YAKUSHI, Kyuya;
YAMAURA, Jun-ichi¹; ENOKI Toshiaki²
(¹Univ. Tokyo; ²Tokyo Inst. Tech.)

While most CT salts showing charge ordering (CO) belong to 1/4-filled system, the semiconducting phase of the 1/3-filled system (BEDT-TTF)₃CuBr₄ is identified as the CO state by the X-ray diffraction and Raman measurements. In the present study, we investigated the critical behavior of the charge distribution across the phase boundary between the CO and pressure-induced metallic phases. Figure 1 shows the pressure dependence of the Raman spectrum measured at 150 K. The spectrum showed four bands **a**₁, **a**₂, **b**₁, and **b**₂ (**a**₂ and **b**₁ are almost degenerated at ambient pressure). Based on the polarization dependence, we have assigned **a**₁ and **a**₂ to ring C=C based stretching-mode ν_2 (a_g). Note that the peak separation of **a**₁ and **a**₂ is gradually reduced as the pressure is increased. Then, the two bands are almost merged into one band close to 1 GPa around which the DC conductivity changes into metallic behavior. Since the frequency of ν_2 shifts roughly in proportional to the molecular charge, the approaching of the two bands manifests that the charge disproportionation is continuously suppressed under the application of pressures. It should be important to distinguish whether the pressured-induced phase transformation is a phase transition or crossover phenomena.

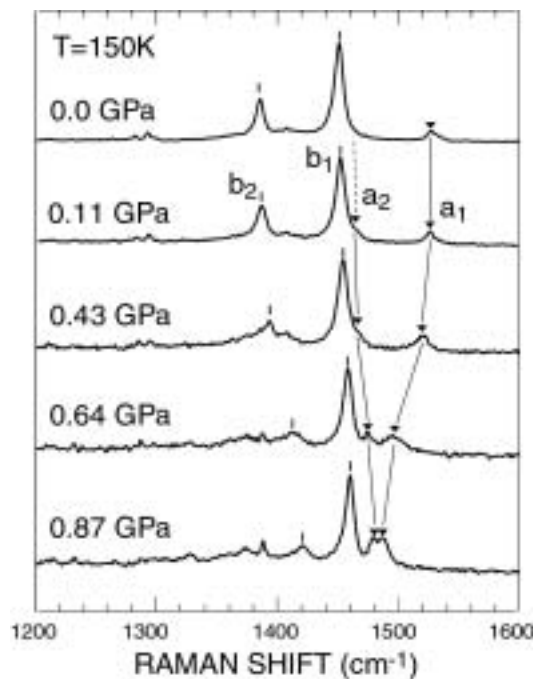


Figure 1. Pressure dependence of the Raman spectrum of (ET)₃CuBr₄. The exciting ($\lambda_{ex} = 780$ nm) and scattered lights are polarized along the a^* and c axes.

IV-A-5 Infrared and Raman Studies of the Charge Ordering in the Organic Semiconductor κ -[(Et)₄N](ET)₄Co(CN)₆·3H₂O

SWIETLIK, Roman¹; OUAHAB, Laurence²;
GUILLEVIC, J.²; YAKUSHI, Kyuya
(¹IMS and Inst. Mol. Phys., Poland; ²Univ. Rennes, France)

[Macromolecular Symposia to be published]

Polarized infrared reflectance and Raman spectra of the charge transfer salt κ -[(Et)₄N](ET)₄Co(CN)₆·3H₂O were measured as a function of temperature. The salt undergoes a phase transition at $T = 150$ K which is related to a charge ordering inside the conducting ET layers. The charge ordering has a considerable influence on vibrational as well as electronic spectra. New vibrational bands related to ET⁺ cations are seen below 150 K. Moreover, formation of a new energy gap (charge gap) in electronic excitation spectrum is observed.

IV-A-6 Charge-Ordering and Magnetic Phase Transitions in θ -(BDT-TTP)₂Cu(NCS)₂

YAKUSHI, Kyuya; YAMAMOTO, Kaoru;
SIMONYAN, Mkhital; OUYANG, Jianyon;
NAKANO, Chikako; MISAKI, Yohji¹; TANAKA, Kazuyoshi¹
(¹Kyoto Univ.)

[Phys. Rev. B to be published]

The charge ordering (CO) in organic charge-transfer (CT) salts draws much attention, since the theoretical studies suggest the relation between the charge fluctua-

tion and the pairing mechanism in superconductivity (SC). The experimental study on charge ordering of organic CT salts has been conducted most intensively in θ -type ET salts. The θ -ET salt is a quarter-filled quasi-two-dimensional (Q2D) system without a dimerized ET unit. In non-dimerized θ -ET salts, the charge localization is accompanied by charge disproportionation (CD) and generates charge-rich and charge-poor sites such as $(0.5+\delta, 0.5-\delta)$. We have discovered such CO phase transition at $T_{CO} \sim 250$ K in non-dimerized Q2D system, θ -(BDT-TTP)₂Cu(NCS)₂.¹⁾ The CO pattern in a variety of ET-based CT salts was theoretically considered. In the framework of mean-field theory, Seo examined the three types of CO patterns, the horizontal, diagonal, and vertical stripes. In this context, the magnetic property gives some information about the CO pattern. The magnetic susceptibility of $30 \text{ K} < T < 300$ K follows the Curie-Weiss law with Curie constant of 0.154 emuK/mol and Weiss temperature of -29 K. We roughly estimate the exchange interaction between the localized charges as $|J| = 8$ K. The single-crystal ESR experiment shows a magnetic phase transition to a spin-singlet state at 5 K. We examined the selection rule of the polarized Raman spectrum. Both the Raman spectra and magnetic properties suggest the vertical stripe along the b -axis. In addition to the pattern of CO, we discussed the following three subjects. (1) Through the analysis of the ν_2 modes, we presented the parameter CD ratio δ as 0.4. (2) The linewidth of ν_2 suggested the charge fluctuation above T_{CO} . (3) The structural fluctuation for the doubling of the unit cell was found at 200 K.

Reference

- 1) J. Ouyang, K. Yakushi, Y. Misaki and K. Tanaka, *Phys. Rev. B* **63**, 054301 (2001).

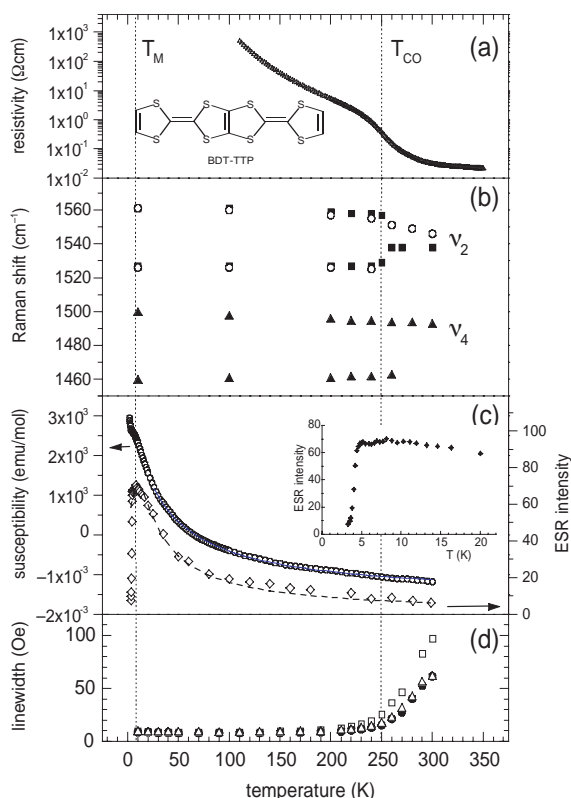


Figure 1. (a) Temperature dependence of resistivity. (b) Temperature dependence of the frequency of ν_2 (solid square) in the $(c,c+b)$ spectrum, ν_2 (open circle) in $(a,a+b)$, and ν_4 (solid triangle) in $(a,a+b)$. (c) Magnetic susceptibility and ESR intensity. The solid and broken lines are respectively the best-fit curves of the Curie-Weiss model and the Bonner-Fisher model with $J = -7.9$ K. The low-temperature region of ESR intensity is expanded in the inset. (d) ESR linewidth. Open squares, open triangles, and solid circles respectively correspond to the signals of $H||a^*$, $H||c$, and $H||b$. T_{CO} and T_M represent the charge-ordering and magnetic phase transition temperatures, respectively.

IV-A-7 Spectroscopic Studies of Charge-Ordering System in Organic Conductors

YAKUSHI, Kyuya; YAMAMOTO, Kaoru, SWIETLIK, Roman¹; WOJCIECHOWSKI, Roman²; SUZUKI, Kenji³; KAWAMOTO, Tadashi⁴; MORI, Takehiko⁴; MISAKI, Yohji⁵; TANAKA, Kazuyoshi⁵

(¹IMS and Inst. Mol. Phys., Poland; ²IMS and Tech. Univ. Lodz, Poland; ³GUAS; ⁴Tokyo Inst. Tech.; ⁵Kyoto Univ.)

[Macromolecular Symposia to be published]

We reviewed our infrared and Raman studies of charge-ordering phase transitions in organic charge-transfer salts. In molecular conductors, the molecular orbital barely overlaps with those of neighbor molecules. Therefore, the transfer integral (t), which contributes to the delocalization of charge, is usually smaller than the on-site (U) and off-site (V) Coulomb interactions that contribute to the localization of the charges. Strong correlation effect originates from the comparative magnitude among t , U , and V , and thus many molecular conductors are located at the boundary between a metal (delocalized state) and insulator (localized state). When the charge is localized, the charge often induces a charge disproportionation (CD) and eventually generates an inhomogeneous charge distribution. This localized state is called as a charge-ordered (CO) state, since the localized charges often form a new periodic structure. It is well known that the frequency of some C=C stretching modes, for example, in BEDT-TTF show downshift depending upon the degree of oxidation of the molecule. Using the C=C stretching mode as a probe of the oxidation state, we investigate the CO phase transition. We first introduce θ -(BEDT-TTF)₂ MM' (SCN)₄ ($M = \text{Rb, Cs, Tl}$; $M' = \text{Zn, Co}$) as typical examples of a charge-ordering system. We apply the same spectroscopic technique to α' -(BEDT-TTF)₂IBr₂, θ -(BDT-TTF)₂Cu(NCS)₂, and (TTM-TTF)I₃, which show the phase transitions from low-resistivity state to high-resistivity state.

IV-A-8 Charge and Molecular Arrangement in (DI-DCNQI)₂Ag Studied by Vibrational Spectra

YAMAMOTO, Kaoru; YAKUSHI, Kyuya; HIRAKI, Koichi¹; TAKAHASHI, Toshihiro¹; KANODA, Kazushi²; MENEGHETTI, Moreno³

(¹Gakushuin Univ.; ²Univ. Tokyo; ³Univ. Padua, Italy)

The quasi-one-dimensional (Q1D) radical anion salt (DI-DCNQI)₂Ag (DI-Ag) (Figure 1a) shows anti-ferromagnetic (AF) ordering below 5.5 K, in contrast to the ordinary Q1D systems that fall down to a spin-singlet state. NMR study proposed that the charge localization (CL) in DI-Ag is the first example of the Wigner crystallization in organic charge-transfer salts. While this proposal has stimulated much interest in the charge-ordering (CO) phenomenon in various strongly correlated systems, no direct evidence has been reported so far for the emergence of CO in the present material. We have suggested *via* infrared reflectance study that the molecular arrangement is dimerized (short-range order) from room temperature, although the proposed model is based on a uniform molecular stacking. To investigate the charge distribution as well as the molecular arrangement, we measured the temperature dependence of the Raman spectrum.

Figure 1b shows the temperature dependence of the Raman spectrum. Two lines **a**₁ and **b**₁ found at room temperature are attributed to *a_g* type of C=C and C=N stretching modes, respectively. On lowering temperature, the spectrum exhibited additional bands **a**₂ and **b**₂ attributable to the vibronic bands of **a**₁ and **b**₁. We confirmed that the infrared signals of the C=C and C=N modes appeared at different frequencies from these Raman bands. The present result indicates that the dimerized molecular stack ($4k_F$ bond-order wave (BOW)) transforms into a tetramerized one ($2k_F$ BOW) with an effective inversion center at low temperatures. Hence, the present result suggests that the AF-CL phase should be the $2k_F$ BOW state, rather than the $4k_F$ CDW state (Wigner crystal).

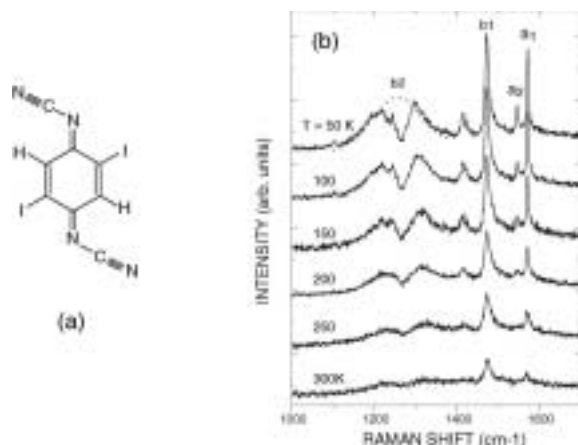


Figure 1. (a) Molecular structure of DI-DCNQI. (b) Temperature dependence of the Raman spectrum measured at ambient pressure. ($\lambda_{\text{ex}} = 633$ nm) Dotted line shows guide for eyes.

IV-A-9 Charge Distribution and Molecular Arrangement in the Pressure-Induced Metallic Phase of (DI-DCNQI)₂Ag

YAMAMOTO, Kaoru; YAKUSHI, Kyuya;
HIRAKI, Koichi¹; TAKAHASHI, Toshihiro¹;
KANODA, Kazushi²; MENEGHETTI, Moreno³
(¹Gakushuin Univ.; ²Univ. Tokyo; ³Univ. Padua, Italy)

[Synth. Met. submitted]

In contrast to the NMR study which suggests the Wigner-crystal-like charge-ordered state (CO), our previous infrared and Raman study has suggested the important role of lattice modulation rather than the Coulomb interaction for the charge localization (CL) in DI-Ag. It has been confirmed in this compound that the localized charge is released to be metallic at moderate pressures (*ca.* 10 kbar). So the high-pressure experiment will provide crucial data to elucidate the localized state. In the present study, we measured high-pressure Raman spectrum using a sapphire-anvil cell to investigate the pressure dependence of the charge-sensitive C=C and C=N stretching modes.

Figure 1 shows the Raman spectrum observed at 100 K under various pressures. The split phonon bands, (**a**₁, **a**₂) and (**b**₁, **b**₂), are respectively assigned to the stretching modes of C=C and C=N. Under the application of pressure, **a**₂ and **b**₂ were readily suppressed and almost completely disappeared at *ca.* 1 GPa. Note that **a**₂ and **b**₂ do not merge with their parent peaks **a**₁ and **b**₁ when they are suppressed. This result indicates that no detectable change occurs in the charge distributions between the localized and metallic states. This result supports our previous conclusion: The localized state of DI-Ag is not regarded as the Wigner crystal but the $2k_F$ BOW state coexisting with SDW.

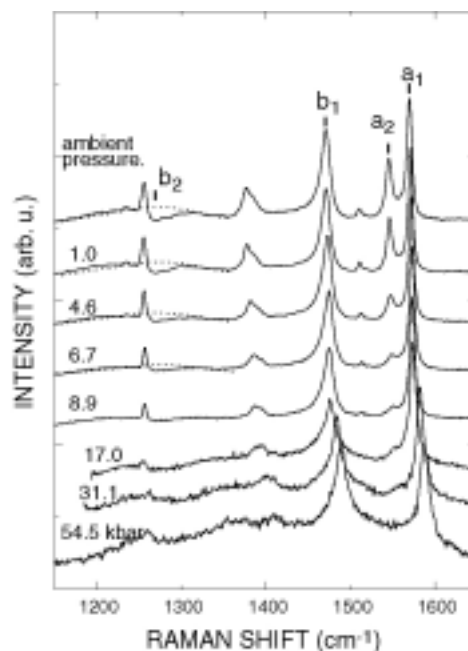


Figure 1. Pressure dependence of the Raman spectrum of DI-Ag measured at 100 K. ($\lambda_{\text{ex}} = 780$ nm)

IV-A-10 Study of the Phase Transitions of (DI-DCNQI)₂M (*M* = Ag, Li, Cu) through the Analysis of the Temperature Dependent Vibronic and Vibrational Infrared Absorptions

MENEGHETTI, Moreno¹; PECILE, C.¹;
YAKUSHI, Kyuya; YAMAMOTO, Kaoru;
KANODA, Kazushi²; HIRAKI, Koichi³
(¹Univ. Padova, Italy; ²Univ. Tokyo; ³Gakushuin Univ.)

[J. Solid State Chem. in press]

The temperature dependent phase transitions of 2,5-DI-DCNQI (diiodo-dicyanoquinon-diimine) title compounds are analyzed by looking at the BOW (bond order wave) and at the CDW (charge density wave) which characterizes the transitions. The analysis is done by studying temperature dependent powder infrared spectra which allow one to have a separate evaluation of both types of contribution to the phase transition of these molecular metals. A model for the spectroscopic infrared features related to the transitions is reported and used for the analysis. It is found that all the title compounds develop a BOW structure at low temperature with characteristics which recall an instability toward a tetramerized $2k_F$ periodicity particularly for the Ag and Li compounds. An appreciable CDW amplitude contribution to the transitions is not found in the spectra.

IV-A-11 Development of a High-Pressure Cell for Raman Measurement Using Sapphire Anvil

YAMAMOTO, Kaoru; YAKUSHI, Kyuya

[*J. Spectrosc. Soc. Jpn.* **51**, 72 (2002)]

Diamond is most widely used as anvils for a high-pressure cell. However, the strong Raman band at 1332 cm^{-1} of diamond disturbs our Raman study of charge ordering in organic conductors. We can avoid this serious problem by using sapphire anvils, which has been often adopted for the anvil of high-pressure cell. Because sapphire is more brittle than diamond, sapphire anvils are sometimes broken before the pressure is elevated to several GPa. Although a soft gasket can relieve the strain on the anvil surface, the aperture in such gaskets is easily distorted. To prevent the distortion of aperture and the strain on sapphire surface at the same time, we have prepared the following coated gasket. The body of the gasket was made of stainless steel (Inconel 600) plate. The hard plate was covered with copper by means of electroplating. We performed high-pressure Raman measurement using the copper coated Inconel gasket (0.3 mm thick, ϕ 0.5 mm aperture) with sapphire anvils (1.5 mm height, ϕ 1.2 mm culet). Figure 1 of IV-A-9 shows the resultant Raman spectrum measured from the charge-transfer salts DI-Ag. It demonstrates that the coated gasket enables us to generate pressures over *ca.* 5 GPa without any special modifications for the pressure cell that is designed originally for diamond anvils.

IV-A-12 Optical Study of Two-Dimensional Organic Metal (EO-TTP)₂AsF₆ (EO-TTP=2-(4,5-ethylenedioxy-1,3-dithiol-2-ylidene)-5-(1,3-dithiol-2-ylidene)-1,3,4,6-tetrathiapentalene)

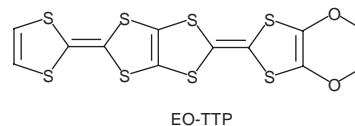
DROZDOVA, Olga¹; YAKUSHI, Kyuya; MISAKI, Yohji²; TANAKA, Koji²

(¹IMS and Yoffe Inst. Phys.; ²Kyoto Univ.)

[*J. Solid State Chem.* in press]

The charge-transfer salts of organic electron donor molecules involving TTP skeleton provide an enormous number of stable metals down to low temperature. EO-

TTP belongs to the metallic BDT-TTP family with an asymmetric structure, in which ethylenedioxy group is substituted at one of the five member rings. Polarized reflectance spectra were measured on the conductive (010) plane of metallic (EO-TTP)₂AsF₆ single crystal. At room temperature, well-defined plasma edges ap-



peared in both directions parallel ($E||a$) and perpendicular ($E\perp a$) to the molecular stack. It was found from the Drude analysis that the effective mass ratio of (EO-TTP)₂AsF₆ was 4 times larger than that of (TMTSF)₂PF₆ and half of β -(BEDT-TTF)₂I₃ which has a closed Fermi surface. The intra- and inter-stack transfer integrals were estimated from the plasma frequencies in the framework of tight-binding model. Based on these transfer integrals, we suggested that the Fermi surface was open in the k_c direction. Using a generalized Drude model, we obtained the frequency dependence of relaxation rate, which conformed to $\gamma(\omega) = \gamma_0 + b\omega^2$ in the frequency range of $1800\text{--}5500\text{ cm}^{-1}$. This result suggests the view that (EO-TTP)₂AsF₆ has exceptionally weak electron-electron and electron-phonon interaction among organic conductors.

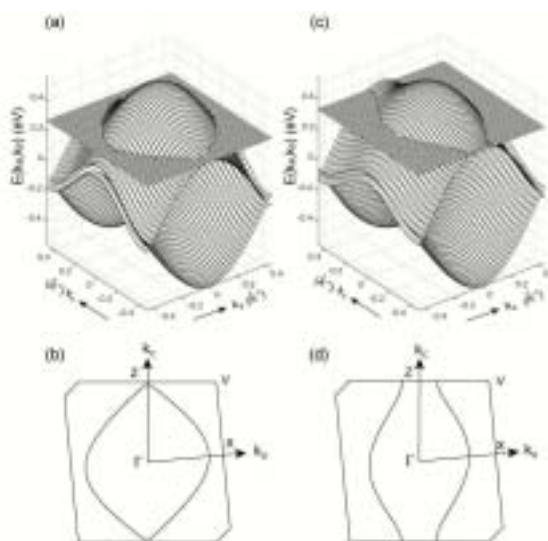


Figure 1. Energy dispersion $E(k_a, k_c)$ in a reciprocal cell and Fermi surface in a Wigner-Seitz cell: (a) $E(k_a, k_c)$ and (b) Fermi surface calculated using the theoretically calculated transfer integrals; (c) $E(k_a, k_c)$ and (d) Fermi surface calculated using the experimentally obtained transfer integrals.

IV-B Microscopic Investigation of Molecular-Based Conductors

The aim of this research is to clarify the electronic states (charge and spin states) of molecular based compounds with curious electronic phases by microscopic point of view. Although the fundamental properties of molecular based conductors have been very well clarified, it is true that there still remain several unsolved questions in the molecular based conductors.

Microscopic investigations are advantageous for understanding the detailed electronic structures of molecular based compounds. To clarify the low temperature electronic states, we performed the NMR, and ESR measurements for molecular based conductors.

IV-B-1 EPR Investigation of the Electronic States in β' -type $[\text{Pd}(\text{dmit})_2]_2$ Compounds (where dmit is the 1,3-dithia-2-thione-4,5-dithiolato)

NAKAMURA, Toshikazu; TAKAHASHI, Toshihiro¹; AONUMA, Shuji²; KATO, Reizo^{2,3}
(¹Gakushuin Univ.; ²Univ. Tokyo; ³IMS and Inst. Phys. Chem. Res.)

[*J. Mater. Chem.* **11**, 2159 (2001)]

Magnetic investigations of organic conductors, β' -type $[\text{Pd}(\text{dmit})_2]_2$, have been performed by Electron Paramagnetic Resonance (EPR) measurements. We found that most of them except one compound underwent antiferromagnetic transitions. Although they are isostructural with little differences in lattice parameters, their spin-spin correlations and antiferromagnetic transition temperatures show strong counter ion dependence. The EPR g -values of $\text{Pd}(\text{dmit})_2$ cannot be explained within the framework of isolated radical description which is a good approximation for conventional organic conductors. The electronic structures of a series of molecular conductors based on $\text{Pd}(\text{dmit})_2$ at ambient pressure are discussed from microscopic points of view.

IV-B-2 NMR Study of Charge Localized States of $(\text{TMTTF})_2\text{Br}$

FUJIYAMA, Shigeki; NAKAMURA, Toshikazu

[*J. Phys. Chem. Solids* **63**, 1259 (2002)]

¹³C NMR study was performed for a quasi-one-dimensional organic conductor $(\text{TMTTF})_2\text{Br}$ using a single crystal in which two central carbon sites of TMTTF molecules were labeled with ¹³C. To investigate the relation between the charge localization around 100 K and its magnetic ground state from the microscopic point of view, we measured the NMR spectra and nuclear relaxation. We found slight broadening of the spectra above the magnetic phase transition temperature ($T_N \sim 15$ K). We discuss this anomaly with the newly measured data of uniform susceptibility and ESR.

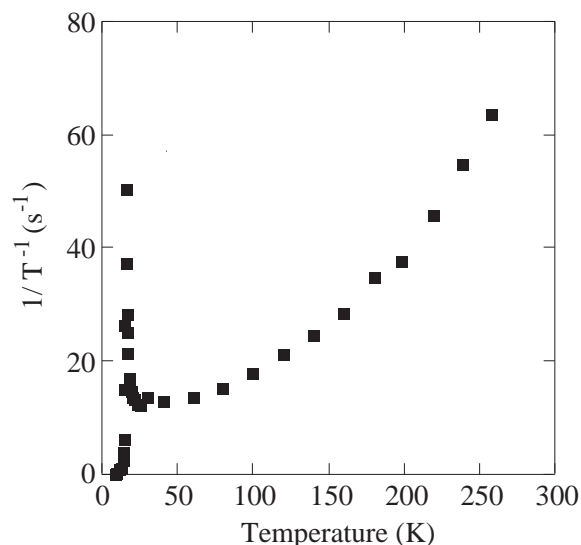


Figure 1. Temperature dependence of spin lattice relaxation rate $1/T_1$ of ¹³C NMR. The values are deduced by fitting the experimental recovery data with a single exponential.

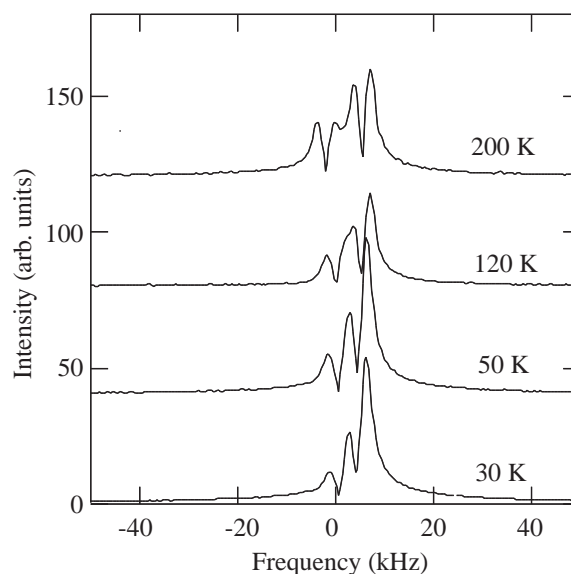


Figure 2. Temperature dependence of ¹³C NMR spectra of $(\text{TMTTF})_2\text{Br}$ above 30 K. The horizontal axis indicates the deviation from 87.25 MHz.

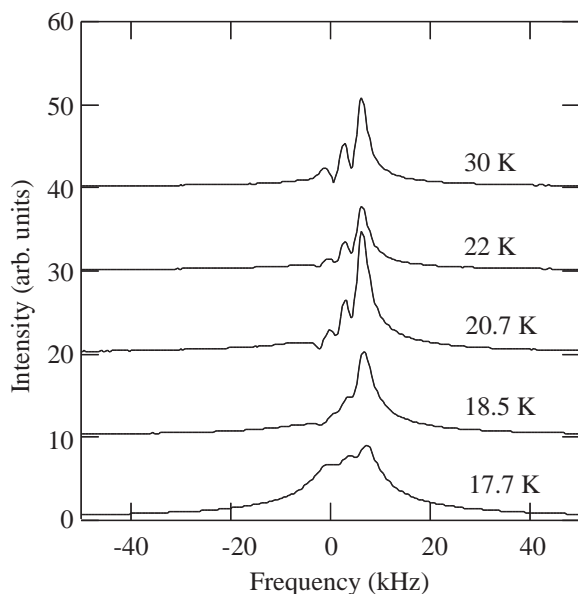


Figure 3. Temperature dependence of the ^{13}C NMR absorption lines between 17 K and 30 K.

IV-B-3 Magnetic Investigation of Possible Quasi-One-Dimensional Two-Leg Ladder Systems, $(\text{BDTFP})_2\text{X}(\text{PhCl})_{0.5}$ ($\text{X} = \text{PF}_6, \text{AsF}_6$)

NAKAMURA, Toshikazu; TAKAHASHI, Kazuko¹;
ISE, Toshihiro¹; SHIRAHATA, Takashi¹;
URUICHI, Mikio; YAKUSHI, Kyuya; MORI,
Takehiko²
(¹Tohoku Univ.; ²IMS and Tokyo Inst. Tech.)

[*J. Phys. Soc. Jpn.* **71**, 2022 (2002)]

ESR and ^1H -NMR investigations of the quasi-one-dimensional organic conductors, $(\text{BDTFP})_2\text{X}(\text{PhCl})_{0.5}$ ($\text{X} = \text{PF}_6, \text{AsF}_6$), were carried out. The low-temperature physical properties of the title compounds are quite different from each other, although those at R.T. are very similar. The PF_6 salt undergoes a spin-singlet transition around 170 K. On the other hand, the AsF_6 salt shows a discontinuous transition of first order around 230 K, in association with an abrupt jump in the spin susceptibility. The AsF_6 salt shows spin-gap behavior below 50 K, but it undergoes an antiferromagnetic transition at 14 K. The low-temperature electronic states of the title compounds are discussed by microscopic point of view.

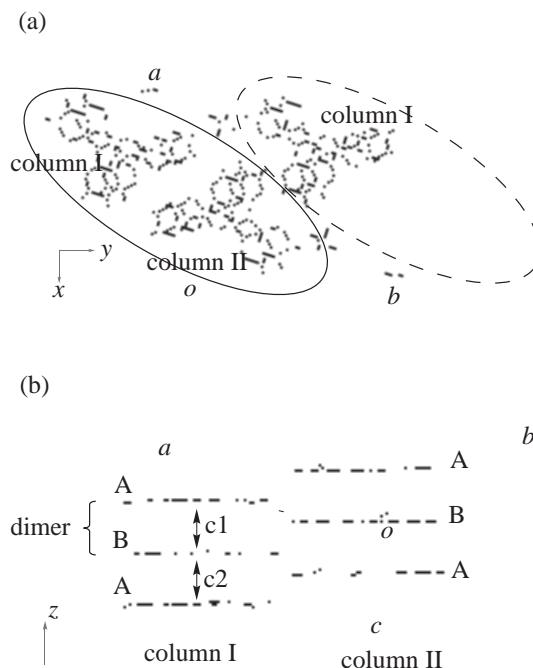


Figure 1. Crystal structure of $(\text{BDTFP})_2\text{X}(\text{PhCl})_{0.5}$: (a) possible two-leg ladder structures, (b) dimerization along the stacking axes.

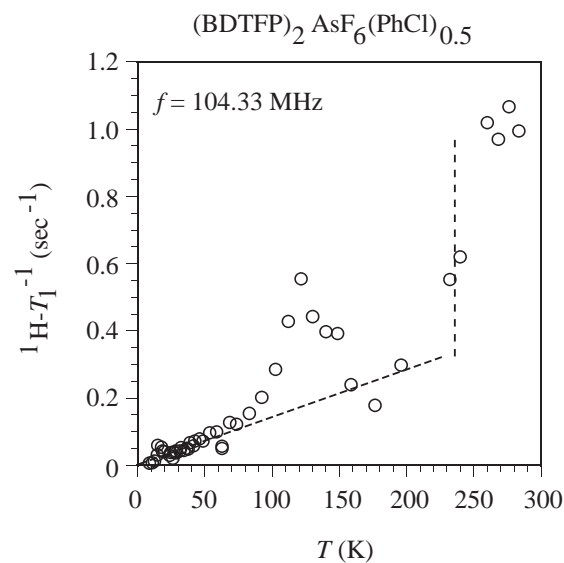


Figure 2. Temperature dependence of the ^1H -NMR spin-lattice relaxation rate, $^1\text{H}-T_1^{-1}$, of $(\text{BDTFP})_2\text{AsF}_6(\text{PhCl})_{0.5}$ for a single crystal.

IV-B-4 Microscopic Investigation of a New Two-Component Organic Conductor with Itinerant and Localized Spins: $(\text{CHTM-TTP})_2\text{TCNQ}$

NAKAMURA, Toshikazu; TANIGUCHI,
Masateru¹; MISAKI, Yohji¹; TANAKA,
Kazuyoshi¹; NOGAMI, Yoshio²
(¹Kyoto Univ.; ²Okayama Univ.)

[*J. Phys. Soc. Jpn.* in press]

Low-temperature electronic phases in a new two-

component organic conductor, a segregated-stack charge-transfer salt called $(\text{CHTM-TTP})_2\text{TCNQ}$, are investigated. The ESR g tensor analyses indicate that there exist itinerant CHTM-TTP spins and localized TCNQ spins at R.T. The temperature dependence of the physical parameters reveals that this salt undergoes two drastic, successive phase transitions at low temperatures. The effective moment of the localized TCNQ spins decreases at the 245 K transition and completely disappears at the transition around 195 K. These curious physical properties are explained by the drastic changes in the electronic states of the two different types of spins. The spin susceptibility was decomposed into the contribution of each of the two spin species by using ESR, $^1\text{H-NMR}$, and static susceptibility analyses. We present a microscopic investigation of the two-spin system with itinerant and localized moments.

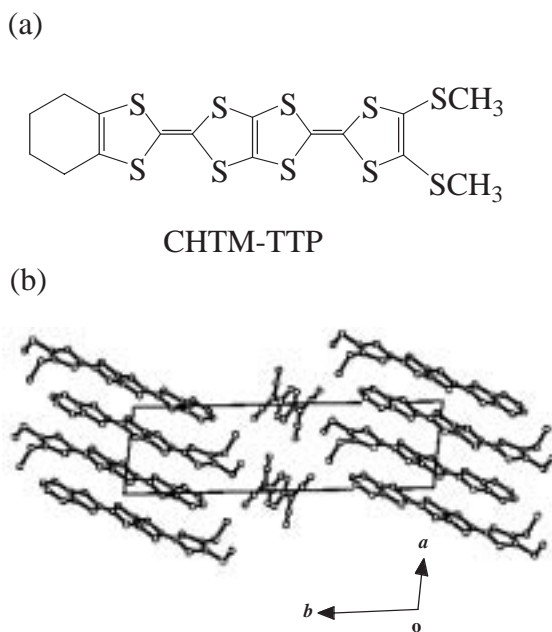


Figure 1. (a) Molecular structure of CHTM-TTP. (b) Crystal structure of $(\text{CHTM-TTP})_2\text{TCNQ}$ at R.T.

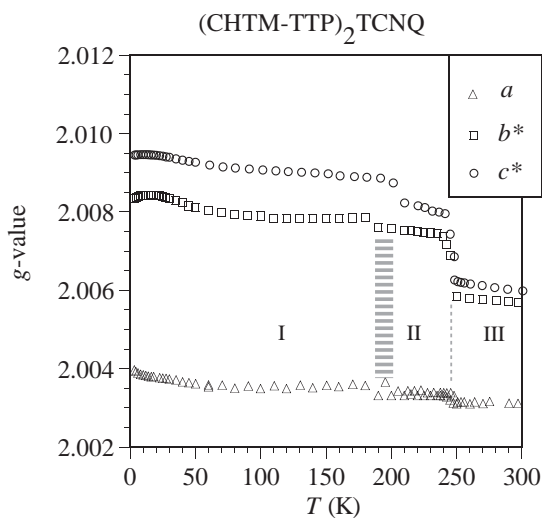


Figure 2. Temperature dependence of the g values of $(\text{CHTM-TTP})_2\text{TCNQ}$ applying the external static field along the a (triangle), b^* (square), and c^* (circle) crystal axes.

IV-B-5 ESR Study of the Charge Ordering States in $(\text{TMTTF})_2\text{X}$

NAKAMURA, Toshikazu

ESR investigations were performed for a series of organic conductors, $(\text{TMTTF})_2\text{X}$ ($\text{X} = \text{SbF}_6, \text{AsF}_6, \text{PF}_6, \text{ReO}_4, \text{ClO}_4, \text{SCN}, \text{Br}$). The ESR linewidth shows abrupt jumps or humps in the paramagnetic insulating region. The $(\text{TMTTF})_2\text{X}$ compounds are roughly divided into three groups in the aspect of the anisotropy of the ESR linewidth at low-temperatures. We discuss the low-temperature charge distributed pattern from the microscopic point of view.

Figure 1 show the temperature dependence of the peak-to-peak ESR linewidth, ΔH_{pp} , of $(\text{TMTTF})_2\text{ReO}_4$. The angular dependence of the ΔH_{pp} for the c^*a plane at 300 K, 170 K and 110 K is shown in the inset of Figure 1. While the ΔH_{pp} reveals the standard anisotropic behavior in the metallic region, that at 110 K follows the formula for dipole-dipole interacted spins. This fact indicates that the electronic dipoles contribute to the ESR linewidth in the low temperature region. Considering the anisotropy of the ESR linewidth, we can estimate the charge distribution patterns in the low temperature phase. According to the experimental result, $\Delta H_a \gg \Delta H_{b'} \sim \Delta H_{c^*}$, the possible charge ordering pattern is $-\text{O}-\text{O}-\text{o}-\text{o}-$ along the stacking axes (O and o indicate the charge rich and poor sites, respectively) with the wave-number, $Q = (1/2, 0, 1/2)$.

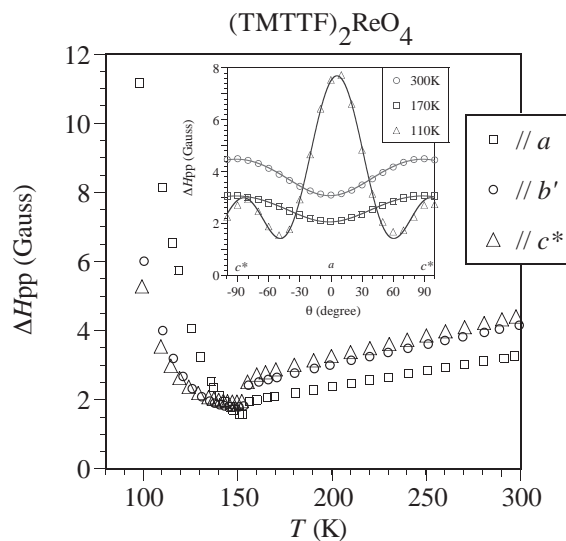


Figure 1. Temperature dependence of the peak-to-peak ESR linewidth, ΔH_{pp} , of $(\text{TMTTF})_2\text{ReO}_4$ for a single crystal. The inset shows the angular dependence of the ΔH_{pp} at 300 K, 170 K and 110 K. The static magnetic field applied in the c^*a -plane.

IV-C Magnetic Organic Superconductors and Related Systems

Molecular materials are expected to play an important role in the future development of electronic devices. For the realization of molecular electronic devices, it is essential to develop a “dual-action system” whose conducting properties can be sharply controlled by external forces. One of the prospective dual-action molecular system is a composite system consisting of organic layers responsible for electron conduction and inorganic layers with localized magnetic moments, whose conductivity can be controlled by tuning magnetic state of the inorganic layers. We have recently discovered the first example of dual-functional magnetic organic conductor whose superconducting state can be sharply switched on or off by controlling the metamagnetic transition of the magnetic anion layers. In addition to the dual functionality of molecular conductors, the field-induced superconductivity of the organic conductors reported by us in 2001 has attracted an increasing interest. In organic systems, there are two well-known conductors showing field-induced superconducting transition: Chevrel type compound $\text{Eu}_{0.75}\text{Sn}_{0.25}\text{Mo}_6\text{S}_{7.2}\text{Se}_{0.8}$ and heavy Fermion system CePb_3 . Unlike these inorganic conductors, $\lambda\text{-(BETS)}_2\text{FeCl}_4$ has an antiferromagnetic insulating ground state. That is, $\lambda\text{-(BETS)}_2\text{FeCl}_4$ is the first conductor exhibiting the insulator \rightarrow metal \rightarrow superconductor transitions with increasing magnetic field. We have recently discovered that the first antiferromagnetic organic superconductor, $\kappa\text{-(BETS)}_2\text{FeBr}_4$ undergoes a field-induced superconducting transition. The field-induced superconductivity seems to be a common feature of the organic superconductor with localized magnetic moments in the anion layers.

IV-C-1 An Indication of Magnetic-Field-Induced Superconductivity in a Bi-Functional Layered Organic Conductor, $\kappa\text{-(BETS)}_2\text{FeBr}_4$

FUJIWARA, Hideki; KOBAYASHI, Hayao;
FUJIWARA, Emiko¹; KOBAYASHI, Akiko¹
(¹Univ. Tokyo)

[*J. Am. Chem. Soc.* **124**, 6816 (2002)]

We have investigated BETS conductors, $\lambda\text{-}$ and $\kappa\text{-}$ $(\text{BETS})_2\text{FeX}_4$ ($X = \text{Cl}$ and Br), and reported several interesting properties, such as the novel magnetic-field-induced superconductivity under very high magnetic field ($18 \text{ T} < H < 41 \text{ T}$) in $\lambda\text{-(BETS)}_2\text{FeCl}_4$. Here we report the magnetoresistance of the antiferromagnetic organic superconductor, $\kappa\text{-(BETS)}_2\text{FeBr}_4$ up to 15 T and the observation of the onsets of the magnetic-field-induced superconductivity as the cooperative phenomena between the superconductivity and magnetism. As shown in the upper inset of Figure 1, with an increase of the applied magnetic field at 0.58 K, the resistivity suddenly increased at about 1.6 T for the magnetic field applied parallel to the a axis ($H//a$), and the system recovered its metallic state. These results suggest that the internal field originated from the AF coupling between the π electrons and the ferromagnetically aligned Fe^{3+} spins, which was sharply induced at 1.6 T, destroyed abruptly the superconducting state. In addition, a conspicuous resistivity decrease was observed just below the abrupt resistivity increase at 1.6 T. This decrease around 1.6 T suggests the compensation of the external field by the internal field created by Fe^{3+} spins and the stabilization of the superconducting state. Further anomalies were observed at 10–15 T below 0.75 K both for $H//a$ and $H//c$ as shown in Figure 1. The resistivity changes between 1.19 K (the normal state) and the lowest measured temperatures strongly suggest the onset of the magnetic-field-induced superconductivity around 12.5 T. Because of the existence of the metamagnetic transition which makes this system a

dual functional material and gives rise to the field-induced resistivity decreases suggesting the stabilization of the superconducting state at two characteristic magnetic fields of 1.6 T and 12.5 T.

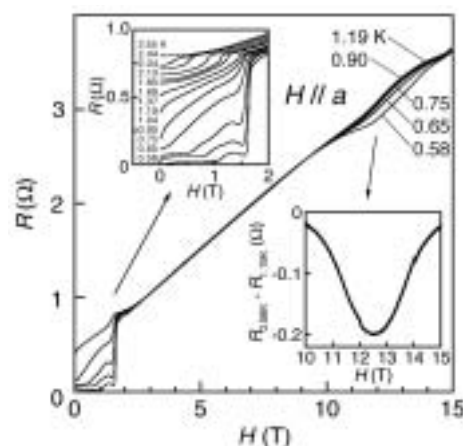


Figure 1. Magnetic field dependence of the magnetoresistance up to 15 T at the indicated temperatures in the figures with an application of the magnetic field in parallel with the a axis. The upper inset is the data measured between 0 T and 2 T. The lower insets are the resistivity differences between the data at 1.19 K and one at the lowest measured temperature (0.58 K).

IV-C-2 Dual-Action Molecular Superconductors with Magnetic Anions

ZHANG, Bin; TANAKA, Hisashi; FUJIWARA, Hideki; KOBAYASHI, Hayao; FUJIWARA, Emiko¹; KOBAYASHI, Akiko¹
(¹Univ. Tokyo)

[*J. Am. Chem. Soc.* **124**, 9982 (2002)]

Recently, the reports on the marvelous field-effect switching between insulating and superconducting states, which is the widest possible variation of electri-

cal properties of materials, have attracted an extremely large attention though it has not been reconfirmed yet. We have found that similar switching phenomena can take place in bulk organic superconductors with magnetic anions. It is easily imagined that the superconducting state will be broken if the magnetic moments in the anion layers are forced to orient ferromagnetically. We found that the unprecedented combination of metamagnetism and organic superconductivity is realized in the first antiferromagnetic organic superconductor, κ -(BETS)₂FeBr₄ (BETS = bis(ethylenedithio) tetraselenafulvalene) and observed the superconducting state to be sharply switched on or off by controlling the magnetic state of the anion layers by external field (the critical magnetic field of metamagnetic transition is 1.6 T). More novel switching phenomena was also found in the other modification of BETS salts. As reported before, the diluted magnetic anion system, λ -(BETS)₂Fe_xGa_{1-x}Cl₄ ($0.35 < x < 0.5$) undergoes metal \rightarrow superconductor \rightarrow insulator transitions with lowering temperature ($T_c \approx 4$ K, $T_{SC \rightarrow Ins} \approx 3.4$ K). We measured the magnetoresistance up to 15 T at $T < 3.4$ K. When magnetic field was applied to the direction perpendicular to the ac conduction plane, the insulator \rightarrow superconductor \rightarrow metal transitions were observed with increasing magnetic field. While for the field perpendicular to the ac conduction plane, the insulator \rightarrow superconductor \rightarrow metal \rightarrow superconductor transitions and insulator \rightarrow superconductor transition took place at $2.5 < T < 3.4$ K and $T < 2$ K, respectively. T - H phase diagram indicates that the field induced superconducting phase appear around 14 T. Owing to the unique phase diagram with narrow superconducting region neighboring both insulating and metallic phases, the sharp insulator \rightleftharpoons superconductor \rightleftharpoons metal switching can be realized by modulating the external magnetic field.

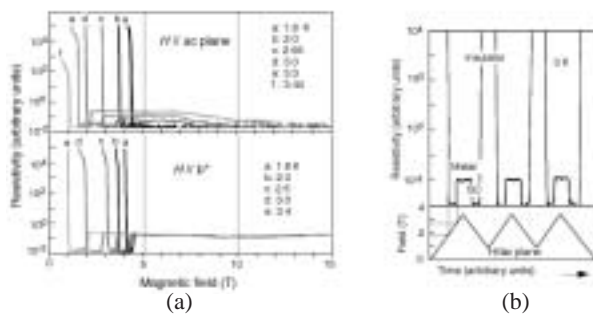


Figure 1. (a) The magnetoresistance of λ -(BETS)₂Fe_{0.4}Ga_{0.6}Cl₄ up to 15 T at 1.6–3.4 K for the magnetic fields parallel and perpendicular to the conduction plane. (b) An example of the insulator-superconductor-metal triple step switching behavior of λ -(BETS)₂Fe_{0.4}Ga_{0.6}Cl₄ coupled with the periodic modulation of magnetic field around 2.5 T ($H//ac$ plane) at 3 K.

IV-C-3 A Series of Organic Conductors κ -(BETS)₂FeBr_xCl_{4-x} ($0 \leq x \leq 4$) Exhibiting Successive Antiferromagnetic and Superconducting Transitions

FUJIWARA, Emiko; FUJIWARA, Hideki;
KOBAYASHI, Hayao; OTSUKA, Takeo¹;
KOBAYASHI, Akiko¹
(¹Univ. Tokyo)

[Adv. Mater. 14, 1376 (2002)]

In contrast to λ -type salt, where the crystals of λ -(BETS)₂FeBr_xCl_{4-x} are obtained only for small x -range ($x < 1.0$), Br and Cl atoms are exchanged freely in κ -type salts κ -(BETS)₂FeBr_xCl_{4-x} ($0 \leq x \leq 4$). Therefore, the magnetic and superconducting properties of κ -type salt can be changed continuously in the wide range. In this paper, we have examined the x -dependence of the electromagnetic properties of a series of the antiferromagnetic organic superconductors, κ -(BETS)₂FeBr_xCl_{4-x} ($0 \leq x \leq 4$). By collecting the experimental results of the electrical resistivities and magnetic susceptibilities, the temperature vs. x -value phase diagram of κ -(BETS)₂FeBr_xCl_{4-x} ($0 \leq x \leq 4$) was obtained. Both superconducting and antiferromagnetic transition temperatures are lowered with decreasing x . It is interesting that the lattice constants a and c in the conduction plane exhibit small x -dependences, in spite of the strong x -dependence of resistivity behavior. In addition, despite of the shortening of the lattice constant along the direction perpendicular to the conduction plane ($//b$), the magnetic interaction tends to be decreased with increasing the Cl content, suggesting the importance of the intermolecular magnetic interaction through the Br atom.

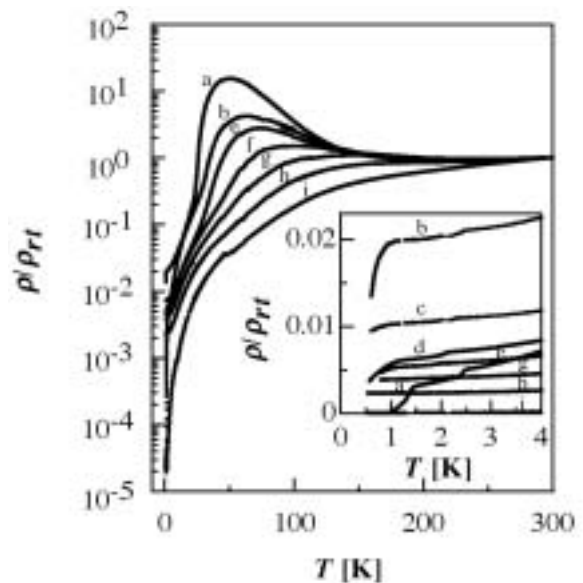


Figure 1. Temperature dependences of electrical resistivities of κ -(BETS)₂FeBr_xCl_{4-x}. a: $x = 4$, b: $x = 3.86$, c: $x = 3.54$, d: $x = 3.43$, e: $x = 2.96$, f: $x = 2.82$, g: $x = 1.69$, h: $x = 1.04$ and i: $x = 0$. The inset shows the resistivity behavior at low temperature region.

IV-C-4 Magnetic Molecular Conductors Based on BETS Molecules and Divalent Magnetic Anions [BETS = Bis(ethylenedithio)-tetraselenafulvalene]

FUJIWARA, Emiko; GRITSENKO, Victor;
FUJIWARA, Hideki; TAMURA, Itaru;
KOBAYASHI, Hayao; TOKUMOTO, Madoka¹;
KOBAYASHI, Akiko²

(¹IMS and Electrotec. Lab. (AIST); ²Univ. Tokyo)

[*Inorg. Chem.* **41**, 3230 (2002)]

Several conducting salts based on BETS molecules and divalent magnetic anions such as the $(\text{CoCl}_4)^{2-}$, $(\text{CoBr}_4)^{2-}$ and $(\text{MnBr}_4)^{2-}$ were prepared. Electrocrystallization by using the $(\text{CoCl}_4)^{2-}$ anion gave two kinds of crystals. Block-shaped crystals were cleared to be $(\text{BETS})_2\text{CoCl}_4$, which is an insulator with the high-spin state of cobalt $3d$ spin. On the other hand, the X-ray crystal structure analysis of a plate-shaped crystal of the $(\text{CoCl}_4)^{2-}$ salt revealed the system to be κ - $(\text{BETS})_4\text{CoCl}_4(\text{EtOH})$, which is metallic down to 0.7 K. The electronic band structure calculation gave a typical two-dimensional cylindrical Fermi surface. However, there is only very weak antiferromagnetic interaction between the $s = 3/2$ cobalt $3d$ spins due to its anion-solvent-intermingled layer structure. On the other hand, the electrocrystallization by using the $(\text{MnBr}_4)^{2-}$ anion yielded the plate-shaped black crystals of the $(\text{MnBr}_4)^{2-}$ salt. Crystal structure analysis of the $(\text{MnBr}_4)^{2-}$ salt showed that the salt is θ - $(\text{BETS})_4\text{MnBr}_4(\text{EtOH})_2$ with alternating the donor and anion/solvent mixed layers. The stacking direction in one donor layer is perpendicular to those of the neighboring layers. The electrical and magnetic properties of the θ - $(\text{BETS})_4\text{MnBr}_4(\text{EtOH})_2$ salt showed the metallic behavior down to *ca.* 30 K and the paramagnetism of the high-spin manganese $3d$ spins. Band structure calculation of this salt gave an elliptical cylindrical Fermi surface. Since the Fermi surfaces of the adjacent donor layers are rotated to each other by 90° , the θ - $(\text{BETS})_2\text{MnBr}_4(\text{EtOH})_2$ salt becomes a two-dimensionally isotropic metal.

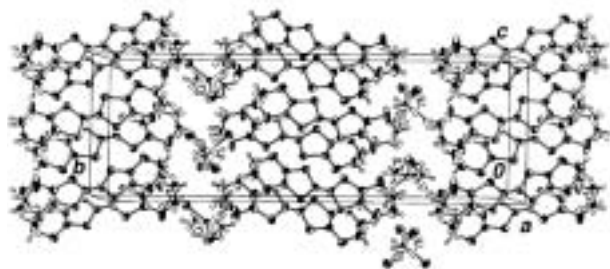


Figure 1. Crystal structure of κ - $(\text{BETS})_4\text{CoCl}_4(\text{EtOH})$.

IV-C-5 Crystal Structure of BETS^{2+} Dication Salt $(\text{BETS})\text{TlCl}_5$ and Formal Charge Dependence of Bond Lengths of BETS^{+Q} ($Q = 0-2$)

ZHANG, Bin; TANAKA, Hisashi; FUJIWARA, Emiko; FUJIWARA, Hideki; KOBAYASHI, Hayao; KOBAYASHI, Akiko¹; ZHU, Daoben²
(¹Univ. Tokyo; ²Inst. Chem., China)

It is necessary to find out the BETS salt with higher oxidation state of BETS for getting the relation between bond lengths and formal charge (Q) of BETS (BETS^{+Q}). But the molecular structure of BETS with oxidation state greater than +1 has not been reported so far. Thin, black plate $(\text{BETS})\text{TlCl}_5$ crystal was got from electrocrystallization method. The composition was determined by EDS (Energy Dispersive X-ray Spectrometer). The crystal has a triclinic unit cell and the cell param-

eters are: $a = 9.052(3) \text{ \AA}$, $b = 10.542(3) \text{ \AA}$, $c = 6.210(1) \text{ \AA}$, $\alpha = 103.56(2)^\circ$, $\beta = 100.76(2)^\circ$, $\gamma = 67.07(2)^\circ$, $V = 527.6(2) \text{ \AA}^3$. Donors are packed with side-by-side mode to form segregated column along b axis. The linear $[\text{TlCl}_5]^{2-}$ unit with octahedral $[\text{TlCl}_6]$ unit shared an apex along a axis in the crystal. The Tl-Cl bond lengths are in the range $2.416(3)$ – $2.692(3) \text{ \AA}$ which are consistent with the length of $\text{Tl}^{3+}\text{-Cl}$. There are short contacts between $\text{S}\cdots\text{S}$ and $\text{S}\cdots\text{Se}$ atoms in the BETS columns and donor-anion contacts between $\text{Cl}\cdots\text{Se}$, $\text{Cl}\cdots\text{S}$ atoms. The $\text{C-H}\cdots\text{Cl}$ hydrogen bonds also exist as shown in Figure 1. The crystal is an insulator and shows paramagnetic behavior from 300 K to 1.9 K. Combining the data of the bond lengths of various charge-transfer salts of BETS with different oxidation states (BETS^{+Q}), we can get a relation of $Q = 10.76 - 9.58\delta$, and $\delta = (b + c) - (a + d)$, where a, b, c, d are the bond lengths of TTF core.

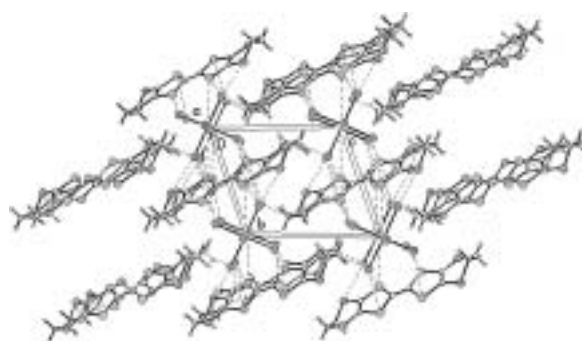


Figure 1. Packing diagram of $(\text{BETS})\text{TlCl}_5$ viewed along c axis

IV-C-6 Charge-Transfer Salt of $[\text{C}_{12}\text{H}_8\text{S}_4\text{Se}_4\text{Cl}_2]\text{FeCl}_4\cdot\text{C}_6\text{H}_5\text{Cl}$

ZHANG, Bin; KOBAYASHI, Hayao; WANG, Zheming¹; ZHU, Daoben²
(¹Peking Univ., China; ²Inst. Chem., China)

Crystals of the title salt were obtained electrochemically. The donor $\text{C}_{12}\text{H}_8\text{Cl}_2\text{S}_4\text{Se}_4$: 2,2'-(1,2-dichloroethanediyl)-dene)bis(4,5-dithiolene-1,3-diselena) was formed from BETS under high voltage. The cell parameter is: $a = 8.669(4)$, $b = 30.571(1)$, $c = 10.388(4) \text{ \AA}$, $\beta = 102.13(4)^\circ$, $V = 2691.5(6) \text{ \AA}^3$, $P2_1/n$, $Z = 4$. Except ethylene groups, all the atoms of the donor are coplanar with the maximum derivation of 0.09 \AA . The donor molecules form dimers. FeCl_4^- anions and $\text{C}_6\text{H}_5\text{Cl}$ molecules are in the interstitial positions between the dimers. $\text{C}_6\text{H}_5\text{Cl}$ plane is perpendicular to that of dimer. The crystal is a semiconductor and shows paramagnetic behavior.

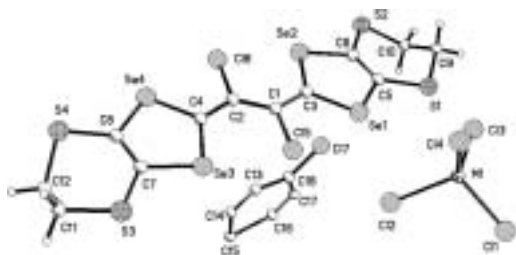


Figure 1. Molecular configuration.

IV-C-7 A New Charge-Transfer Salt of $(\text{BETS})_4\text{Fe}_2(\text{C}_2\text{O}_4)_5$

ZHANG, Bin; KOBAYASHI, Hayao; WANG, Zheming¹; ZHU, Daoben²
(¹Peking Univ., China; ²Inst. Chem., China)

The preparation, crystal structure and physical properties of charge-transfer salt based on BETS molecules and metal oxalate counter ions $(\text{BETS})_4\text{Fe}_2(\text{C}_2\text{O}_4)_5$ were examined. There are two phases. One is monoclinic $P2_1/n$ and the cell parameters are $a = 17.078(4)$, $b = 11.180(2)$, $c = 19.975(5)$ Å, $\beta = 102.026(5)^\circ$, $V = 3730.3(15)$ Å³. The other takes $C2/m$ space group and the lattice constants are $a = 23.3982(7)$, $b = 11.1365(4)$, $c = 16.9771(7)$, $\beta = 123.798(1)^\circ$, $V = 3676.2(2)$ Å³. In these two phases, $\text{Fe}_2(\text{C}_2\text{O}_4)_5$ groups

and BETS molecules are arranged in “checker board” mode. In the $P2_1/n$ phase, BETS molecules are packed with the longest directions parallel to [101] direction. The formal charge of BETS is +1. The crystal showed a semiconductor-to-insulator transition around 80 K. There are antiferromagnetic interaction between Fe(III) ions. The χ vs. T curve gave $g = 2.0$ and $J = -6.1$ cm⁻¹.

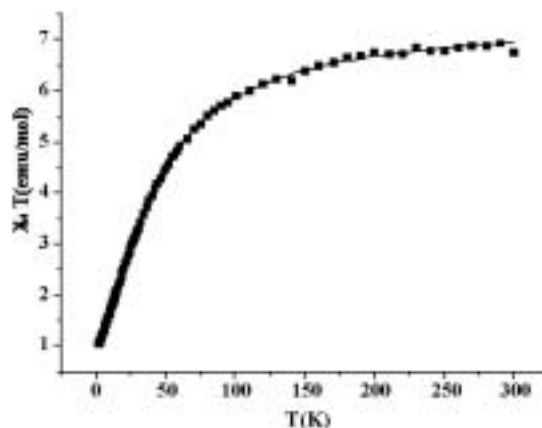


Figure 1. The $\chi_M T$ vs T curve of $(\text{BETS})_4\text{Fe}_2(\text{C}_2\text{O}_4)_5$ (magnetic field = 1000 Oe). The solid line represents the best fit using the Heisenberg isotropic exchange model for a linear dimer $\text{Fe}^{\text{III}}-\text{Fe}^{\text{III}}$.

IV-D Development of New Conducting Molecular Materials

Molecule can be regarded as the smallest nano-system where various functions can be assembled. Although physics and chemistry of the bulk systems with typical electronic functions such as molecular superconductors and molecule-based magnets have been developed greatly in the last two decades, the development of the basic science of the “nano-molecular systems” seems to be insufficient. It seems that many fascinating ideas on the electronically functional molecular systems such as molecular circuit remain to be realized for a long time. Although present our starting point seems to be rather trivial, we hope to contribute in future to make a bridge between the well-established field of bulk molecular functions and that of molecular nano-systems for the steady progress in the studies of electronic molecular functions. Presently we are trying to develop new types of molecular systems with novel electroic functions. The “dual-functional” magnetic conductors exhibiting superconducting switching mentioned before is one example. Other main targets are: (1) magnetic conductors and superconductors composed of single-component molecules and (2) pure organic magnetic metals.

IV-D-1 Development of Conducting Crystals Based on Single-Component Transition Metal Complex Molecules with Extended-TTF Ligands

KOBAYASHI, Akiko¹; FUJIWARA, Emiko¹;
SUZUKI, Wakako¹; TANAKA, Hisashi; OKANO, Yoshinori; KOBAYASHI, Hayao
(¹Univ. Tokyo)

Until quite recently, it was believed that molecular conductors consist of more than two chemical species. Charge transfer between molecules comprising conduction bands and another chemical species has been considered indispensable to generate charge carriers. However, we have prepared the crystal of a neutral complex, $[\text{Ni}(\text{tmdt})_2]^{0+}$ (tmdt = trimethylenetetra-

fulvalenedithiolate), and found that it is highly conducting (400 Scm^{-1} at room temperature) and metallic behavior down to 0.6 K. Besides $\text{Ni}(\text{tmdt})_2$, various molecular conductors composed of neutral transition metal complex molecules with extended TTF-like ligands such as ptdt, dmdt and tmdt were developed ($M = \text{Ni, Pd, Pt, Cu, Co, Au}$; ptdt = propylenedithiotetrafulvalenedithiolate, dmdt = dimethyltetrafulvalenedithiolate, tmdt = trimethylenetetrafulvalenedithiolate). The synthetic works were made under strictly inert atmosphere because these metal complexes were very sensitive to oxygen. By electrochemical oxidation, black microcrystals of the neutral complexes were obtained. Since only very small single or powder crystals were obtained, the resistivity measurements were made on the compressed powder

samples. However, as shown in Table 1, many crystals with very high conductivities were discovered: for example, $[\text{Ni}(\text{dmdt})_2]$, 250 Scm^{-1} ; $[\text{Ni}(\text{dmdt})_2]$, 200 Scm^{-1} ; $[\text{Pd}(\text{dmdt})_2]$, 150 Scm^{-1} .

Table 1. Single-component molecular conductors based on metal complexes with extended-TTF ligands

complex	starting material	$\sigma(300 \text{ K})$ (compaction pellet sample)	
$[\text{Ni}(\text{dmdt})_2]$	$(\text{Me}_2\text{N})_2[\text{Ni}(\text{dmdt})_2]$	200 Scm^{-1}	Metallic down to 230 K
$[\text{Pd}(\text{dmdt})_2]$	$(\text{Me}_2\text{N})_2[\text{Pd}(\text{dmdt})_2]$	150 Scm^{-1}	Semiconductor
$[\text{Ni}(\text{tmdt})_2]$	$(\text{Me}_2\text{N})_2[\text{Ni}(\text{tmdt})_2]$	250 Scm^{-1}	Metallic down to 70 K
$[\text{Co}(\text{dmdt})_2]$	$(\text{Me}_2\text{N})_2[\text{Co}(\text{dmdt})_2]$	0.05 Scm^{-1}	Semiconductor $E_g=85 \text{ meV}$
$[\text{Co}(\text{tmdt})_2]$	$(\text{Me}_2\text{N})_2[\text{Co}(\text{tmdt})_2]$	1.5 Scm^{-1}	Semiconductor $E_g=24 \text{ meV}$
$[\text{Cu}(\text{dmdt})_2]$	$(\text{Me}_2\text{N})_2[\text{Cu}(\text{dmdt})_2]$	1.2 Scm^{-1}	Semiconductor $E_g=60 \text{ meV}$
$[\text{Cu}(\text{tmdt})_2]$	$(\text{Me}_2\text{N})_2[\text{Cu}(\text{tmdt})_2]$	5.1 Scm^{-1}	Semiconductor $E_g=60 \text{ meV}$
$[\text{Au}(\text{dmdt})_2]$	$(\text{Me}_2\text{N})_2[\text{Au}(\text{dmdt})_2]$	4 Scm^{-1}	Semiconductor $E_g=21 \text{ meV}$
$[\text{Au}(\text{tmdt})_2]$	$(\text{Me}_2\text{N})_2[\text{Au}(\text{tmdt})_2]$	14 Scm^{-1}	(Metallic)
$[\text{Ni}(\text{tdt})_2]$	$(\text{Me}_2\text{N})_2[\text{Ni}(\text{tdt})_2]$	16 Scm^{-1}	Semiconductor $E_g=35 \text{ meV}$
$[\text{Pd}(\text{tdt})_2]$	$(\text{Me}_2\text{N})_2[\text{Pd}(\text{tdt})_2]$	0.3 Scm^{-1}	Semiconductor $E_g=94 \text{ meV}$
$[\text{Ni}(\text{tmdt})_2]$	$(\text{Bu}_2\text{N})_2[\text{Ni}(\text{tmdt})_2]$	8 Scm^{-1}	Metallic down to 120 K
$[\text{Co}(\text{tdt})_2]$	$(\text{Me}_2\text{N})_2[\text{Co}(\text{tdt})_2]$	196 Scm^{-1}	(Metallic)

IV-D-2 A Conducting Crystal Based on a Single-Component Paramagnetic Molecule $[\text{Cu}(\text{dmdt})_2]$ (dmdt = dimethyltetrafulvalene dithiolate)

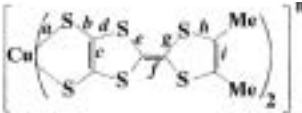
TANAKA, Hisashi; KOBAYASHI, Hayao;
KOBAYASHI, Akiko¹
(¹Univ. Tokyo)

[*J. Am. Chem. Soc.* **124**, 10002 (2002)]

By the realization of single-component molecular metals, the possibility of the development of the new types of molecular conductors has been extended. For example, it will be possible to develop metallic molecular magnets based on single-component molecules containing magnetic ions such as Cu^{2+} and Co^{2+} , where the intermolecular magnetic interactions are mediated by π conduction electrons. We have examined the crystal structure, electrical resistivity and magnetic properties of crystal of $[\text{Cu}(\text{dmdt})_2]^{0+}$ (dmdt = dimethyltetrafulvalenedithiolate), to contribute to clarify the possibility of single-component magnetic molecular conductors. The resistivity measurements on the compaction pellet sample showed fairly high conductivity though the quality of the crystals was poor (about 3 Scm^{-1} at room temperature) and the activation energy was very small ($\approx 40 \text{ meV}$). The temperature dependence of the susceptibility was completely fitted by a Curie-Weiss plot ($\chi_{\text{rt}} = 1.09 \times 10^{-3} \text{ emu}\cdot\text{mol}^{-1}$, $C = 0.33 \text{ emu}\cdot\text{K}\cdot\text{mol}^{-1}$, $\theta = -4.2 \text{ K}$). The Curie constant suggests the existence of 84% of $S = 1/2$ spin moments (estimated on the basis of a g -value (2.035) obtained by EPR experiments). These results suggest the possibility of the development of the single-component magnetic conductor. The comparison of the bond lengths of $[\text{Cu}(\text{dmdt})_2]^{0+}$ and $[\text{Cu}(\text{dmdt})_2]^{2-}$ showed that by the oxidation from (2-) to (0+), all the C=C bonds become longer, indicating that the LUMO has bonding character on each C=C bond (see Table 1). On the other hand, except the bond h showing very small positive change,

S-C bonds tend to be shortened, suggesting antibonding character of LUMO on C-S bonds. Large changes in the bonds b and c indicate the large amplitude of LUMO on the S and C atoms in the central five-membered ring. These features are in good agreement with the general features of the calculated molecular orbitals reported previously.

Table 1. The average bond lengths (\AA) of $[\text{Cu}(\text{dmdt})_2]^n$ ($n = 2-, 0+$)



	$n=2-$	$n=0+$	Δ
a	2.287(1)	2.282(1)	-5
b	1.738(3)	1.683(1)	-55
c	1.341(4)	1.414(9)	73
d	1.766(3)	1.743(4)	-23
e	1.756(3)	1.738(4)	-18
f	1.342(5)	1.361(1)	19
g	1.758(3)	1.737(4)	-21
h	1.748(3)	1.762(4)	14
i	1.330(5)	1.353(9)	23

IV-D-3 Novel π -Electron Donors for Magnetic Conductors Containing a PROXYL Radical

FUJIWARA, Hideki; FUJIWARA, Emiko¹;
KOBAYASHI, Hayao
(¹Univ. Tokyo)

[*Chem. Lett.* 1048 (2002)]

Development of magnetic conductors bearing both conductivity and magnetism has recently played a quite important role in the research of the multifunctionality of organic molecular materials. Recently, we synthesized several new donors containing a TEMPO radical and reported the structures and physical properties of their cation radical salts. Among them, we synthesized the donors **1** and **2** consisting of a TTF moiety and a PROXYL (2,2,5,5-tetramethylpyrrolidin-1-yloxy) radical part because the PROXYL radical is quite stable to air and heat and the corresponding donor molecules will have a relatively small steric hindrance due to the symmetrical structure and smaller size of the PROXYL radical than that of the TEMPO radical. An X-ray crystal structure analysis revealed the structure of **1**. We also clarified the magnetic and electrochemical properties of novel TTF donors **1** and **2** containing a PROXYL radical. Furthermore we prepared the iodine complex of the ethylenedithio derivative **1** and cleared that the salt has 1:1 ratio (donor: I_3^-) and showed insulating conducting behavior and disappearance of the cation radical moments probably due to the strong singlet formation although the PROXYL radical part showed independent behavior with a weak antiferromagnetic interaction.

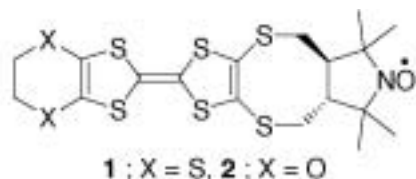


Figure 1. Structure of 1, 2.

IV-D-4 Novel TTP Donors Containing a PROXYL Radical for Magnetic Molecular Conductors

FUJIWARA, Hideki; FUJIWARA, Emiko¹;
KOBAYASHI, Hayao

(¹Univ. Tokyo)

The development of new electron donors involving a magnetic centre are of quite interest to investigate the interplay between the π conducting electrons generated by an oxidation and the localized radical spins, and several donors containing a stable radical have been synthesized to try for novel bifunctional materials. We synthesized novel electron donors **1** and **2** consisting of the TTP framework and a stable PROXYL (2,2,5,5-tetramethyl-pyrrolidin-1-yloxy) radical part as racemic mixtures, where TTP framework was developed by Y. Misaki *et al.* and regarded as a series of promising donors for the realization of stable metallic states. We cleared the structures of the TTP derivatives containing a PROXYL radical **1** and **2** and investigated the magnetic and electrochemical properties of these donors. Furthermore, we prepared the cation radical salts of these donors and studied their electrical and magnetic properties. Among them, the FeCl_4^- salts of **1** showed the highest conductivity (1 Scm^{-1}) in the cation radical salts based on the donors containing a localized radical spin. The χT values of this salt around room temperature correspond to the sum of the contributions from one PROXYL radical, high spin Fe^{3+} and small amount of conducting electrons from the cation radical moments, suggesting the coexistence of these three different magnetic moments.

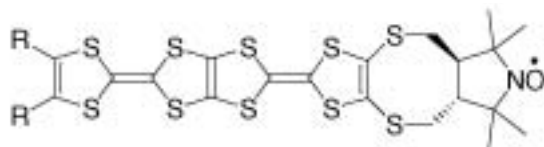


Figure 1. Structure of 1 and 2.

IV-D-5 Synthesis and Physical Properties of New Molecular Conductors Based on Lanthanoid Nitrate Complex Anions

CUI, HengBo¹; OTSUKA, Takeo¹; KOBAYASHI, Akiko¹; MISAKI, Yohji²; KOBAYASHI, Hayao

(¹Univ. Tokyo; ²Kyoto Univ.)

Molecular conducting salts based on BDT-TTP [2,5-bis(1,3-dithiol-2-ylidene)-1,3,4,6-tetrathiapentalene] donor molecules and lanthanide nitrate complex anions $[\text{Ln}(\text{NO}_3)_5]^{-2}$ ($\text{Ln} = \text{Tb}, \text{Dy}, \text{Ho}, \text{Er}, \text{Tm}, \text{Yb}$ and Lu) were synthesized as plate-shaped crystals whose compo-

sitions are $(\text{BDT-TTP})_5[\text{Ln}(\text{NO}_3)_5]$ and they are all isostructural. All these crystals were metallic down to 2K. The electronic band structure calculation gave a two-dimensional Fermi surface that explained their stable metallic states. Magnetic susceptibility measurements of the seven salts $[\text{Ln}(\text{NO}_3)_5]^{-2}$ ($\text{Ln} = \text{Tb}, \text{Dy}, \text{Ho}, \text{Er}, \text{Tm}, \text{Yb}$ and Lu) showed paramagnetic moments on rare-earth ions which were superimposed on the Pauli paramagnetism of metallic π electrons. Especially, the magnetic susceptibilities of the $(\text{BDT-TTP})_5[\text{Ho}(\text{NO}_3)_5]$ and $(\text{BDT-TTP})_5[\text{Tm}(\text{NO}_3)_5]$ salts showed that there seem to be some antiferromagnetic interactions. On the other hand, the Weiss temperatures for $(\text{BDT-TTP})_5[\text{Ln}(\text{NO}_3)_5]$ ($\text{Ln} = \text{Tb}, \text{Dy}, \text{Er}$ and Yb) salts are rather small.

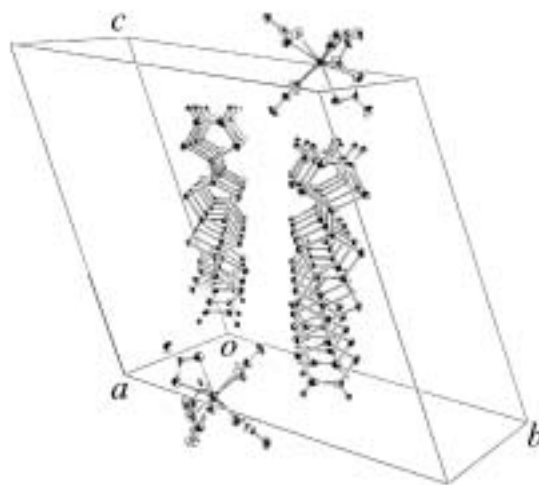


Figure 1. Crystal structure of $(\text{BDT-TTP})_5[\text{M}(\text{NO}_3)_5]$.

IV-E Control of Intermolecular Interactions with Chemical and Physical Methods

The electronic state of the molecular conductor is quite sensitive to molecular arrangement and orientation that are governed by the inter-molecular interaction. Design of the inter-molecular interaction is indispensable in the rational development of molecular conductors to still higher forms. An introduction of supramolecular chemistry is a possible solution to this problem. This means that we change our viewpoint from the molecule to the *supramolecular synthon*. Tellurium has a strong tendency to form secondary bonds in crystalline compounds. We have used the tellurium-based secondary bond as a supramolecular synthon in anion radical salts.

On the other hand, the electronic state of molecular conductors can be quite sensitive to the pressure application if they are situated near the phase boundary and are soft enough to allow appreciable changes of molecular arrangement and orientation. The application of hydrostatic pressure has played significant roles in changing electronic states of low-dimensional molecular conductors. Furthermore, recent development of the uniaxial stress and strain methods have enabled selective or anisotropic regulation of the intermolecular interaction and provided a powerful means to search for novel electronic states. We have examined the uniaxial strain effect in the two-dimensional strongly correlated system based on the metal dithiolene complex.

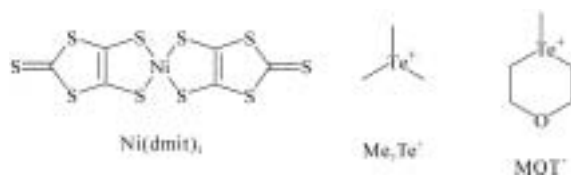
IV-E-1 Unique Structural and Physical Properties of Ni(dmit)₂ Anion Radical Salts Characterized by Short Te...S Contacts, where dmit = 1,3-dithiole-2-thione-4,5-dithiolate

FUJIWARA, Masahiro¹; KATO, Reizo
(¹Univ. Tokyo)

[*J. Chem. Soc., Dalton Trans.* in press]

Five new Ni(dmit)₂ anion radical salts, [Me₃Te]-[Ni(dmit)₂]₂ **1**, [Me₃Te][Ni(dmit)₂]₃-acetone **2**, α-[MOT][Ni(dmit)₂]₂ **3**, β-[MOT][Ni(dmit)₂]₂ **4** and γ-[MOT][Ni(dmit)₂]₂ **5** (MOT = 1-oxa-4-methyl-4-telluracyclohexane), have been prepared by the galvanostatic electrolysis (Scheme). X-ray crystal structure analyses show that all the salts are characterized by short Te...S contacts (3.41 ~ 3.85 Å) between the anions and cations. Each salt shows unique molecular packing of the Ni(dmit)₂ units. Electronic structures deeply depend on these unique molecular arrangements. Among them, **1** and **3** show metallic behavior (down to 60 and 160 K, respectively) and the resistivity of **4** is almost independent from the room temperature and increases moderately below 40 K.

This work has revealed that the Te(IV)-based cations have an ability to induce novel arrangements of the Ni(dmit)₂ units through the intermolecular Te...S contacts. Our results would open a way to the feasible control of the arrangement of the Ni(dmit)₂ anion radical by tuning cations with various shapes.



Scheme 1. Molecular structures of Ni(dmit)₂, Me₃Te⁺, and MOT⁺.

IV-E-2 Uniaxial Strain Effect in the Two-Dimensional Strongly Correlated System, β⁻-(CH₃)₄As[Pd(dmit)₂]₂ (dmit = 1,3-dithiole-2-thione-4,5-dithiolate)

KATO, Reizo; TAJIMA, Naoya¹; TAMURA, Masafumi¹; YAMAURA, Jun-ichi²
(¹RIKEN; ²Univ. Tokyo)

[*Phys. Rev. B* in press]

The molecular conductor β⁻-(CH₃)₄As[Pd(dmit)₂]₂ is a two-dimensional strongly correlated system based on the dimer structure (Figure 1). At low temperature, this system is a Mott insulator under ambient and hydrostatic pressure conditions. The electrical resistivities of this system have been measured under uniaxial strain along all three crystallographic axes. When the strain is applied parallel to the *b* axis within the *a-b* conducting layer, the non-metallic behavior is readily suppressed and superconductivity appears at 4 K under 7 kbar (Figure 2). On the other hand, small strain around 2 kbar along both the *a*- and *c*-axis directions effectively enhances the non-metallic behavior. With further increase of the strain, the non-metallic behavior is suppressed, but cannot be removed even at 15 kbar. These unusual results suggest the crucial role of intra- and inter-dimer interactions that affect the band width and the effective on-site Coulomb interaction.

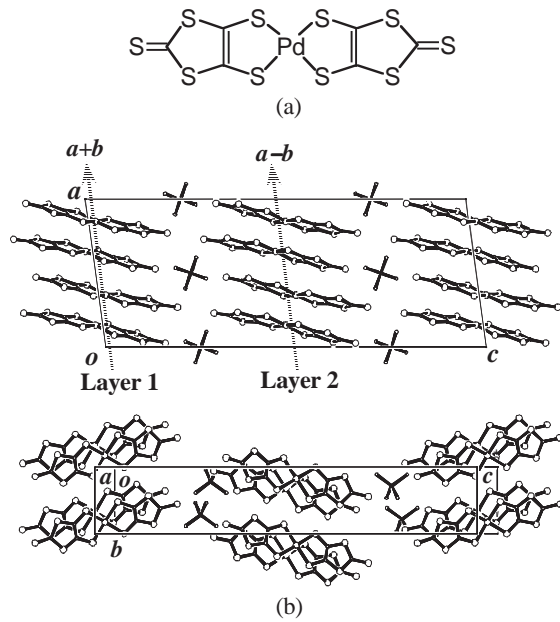


Figure 1. (a) Molecular structure of $\text{Pd}(\text{dmit})_2$. (b) Crystal structure of $\beta'-(\text{CH}_3)_4\text{As}[\text{Pd}(\text{dmit})_2]_2$.

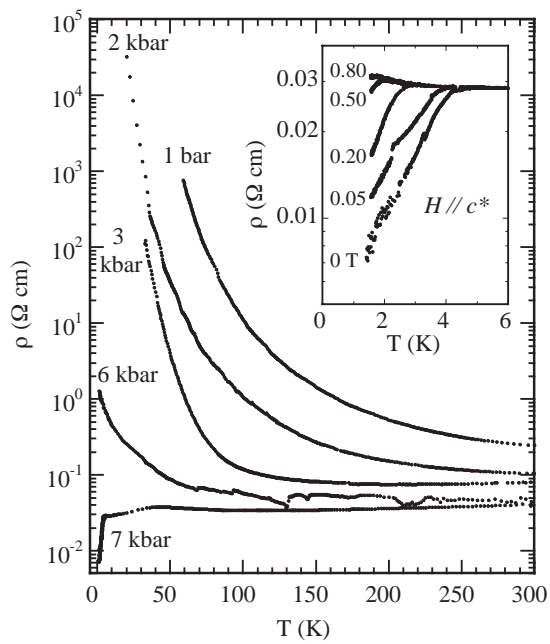


Figure 2. Temperature-dependence of the resistivity (ρ) under the uniaxial strain along the b axis. The inset shows the resistivity under the magnetic field parallel to the c^* direction at 7 kbar.

IV-F Synthetic Approach Toward Single Molecular Transistors

Organic molecules are promising candidates for nano size transistor in two categories of the electronic devices. One is single electron transistor, in which the molecules are used as discrete charge pools. The merit of using organic molecules in this style of devices is that molecules have precise size with determinate electronic states providing stable electronic properties. The other is single molecular field effect transistor, molecules working as the electronic conductor. In this case, resonant tunneling mechanism is expected to work, and the molecular orbital engineering can be utilized in designing complex electronic circuits. In order to realize these appealing devices, we have been constructing optimized nano electrodes and optimized molecules.

IV-F-1 Synthesis of Novel Ruthenium Complexes Optimized for Molecular Single Electron Transistor

OGAWA, Takuji¹; ENDO, Hiroaki²
(¹IMS, JST and Ehime Univ.; ²Ehime Univ.)

[to be published]

Single electron transistors utilize the Coulomb blockade phenomena with nano size particles as the charge pool. The blockade energy is definitely determined only by the size of the particles, and in order to possess enough energy to work at room temperature the size should be not more than 1 nm. It is still difficult to make this size of nano particles with perfectly same radius. We hope that by using metal complex molecules as the charge pool bearing definite redox states, the blockade energies are controlled by the redox potentials, which are determined by the molecular structure.

The molecule prepared have ruthenium complex moiety in the center, which is protected by a dendrimer layer. The protecting layer provides the tunneling barrier to prevent direct contact between each molecule and of the molecule with the electrodes. The carboxylic group at the surface of the molecule will work as the anchor to the doped silicon electrodes.

IV-F-2 Preparation of Porphyrin Wires Optimized for Molecular Field Effect Transistors

OGAWA, Takuji¹; OZAWA, Hiroaki²
(¹IMS, JST and Ehime Univ.; ²Ehime Univ.)

[to be published]

Although several reports of “single molecular electronic devices” have already published, no one has succeeded the electronic measurement with observing the molecules between the electrodes. We aimed molecular wires that are visible with atomic force microscopy (AFM) even on the rough surface of the nano gap electrodes.

The molecules prepared are porphyrin derivatives that have two meso aryl groups with dendrimers at three and five positions and two ethynyl groups at the remaining meso positions. Molecular mechanics calculations showed that the diameter of the wire is about 5–6 nm that will be easily observed on the rough surface of the

nano gap electrodes.

IV-F-3 Synthesis of Octopus Shaped Self Standing Molecular Jacks

OGAWA, Takuji¹; BABA, Miyuki²
(¹IMS, JST and Ehime Univ.; ²Ehime Univ.)

[to be published]

Thiol (-SH) / gold electrodes are the most often used combination for “single molecular electronics” to connect the molecule to the electrodes. The limitations of this combination are (1) electronic contact of this bond is not ideal and significant electronic barrier exist between the molecule and the electrode, (2) the space per molecule is small and a large number of molecules can be connected even to the nano scale electrodes, which disturb the measurements of single molecule.

We have prepared porphyrin derivatives with four meso aryl groups, whose three and five positions are substituted with long alkyl chains with disulfide groups at the ends. The disulfide groups will work as the anchor of the molecule to fix them to gold electrodes. The diameter of the molecule is about 10 nm. So, if the surface area of the nano electrodes is 30 × 30 nm, only nine molecules can be adsorbed on the surface at the maximum. By introducing rhodium metal in the center of the porphyrin molecule, axial ligands can be connected to the metal that will be the molecular wire standing perpendicularly to the electrode surface.

RESEARCH ACTIVITIES V

Department of Applied Molecular Science

V-A Synthesis of Chiral Molecule-Based Magnets

Construction of molecule-based magnetic materials, which have additional properties such as conductivity or photo reactivity, is now becoming a challenging target. Specific goals aimed for these molecule-based magnets include: i) the ability to design the molecular building blocks and to organize them in the solid for desired dimensionality, ii) the optical transparency. The physical characteristic of current interest involves optical properties, particularly with respect to natural optical activity. When a magnet has optical transparency and chiral structure, the magnetic structure of crystal expects to be a chiral spin structure. These magnets will show an asymmetric magnetic anisotropy and magneto-chiral dichroism⁴. This category materials don't only have scientific interest but also have the possibility for use in new devices. When we construct chiral molecule-based magnets, chirality must be controlled not only in the molecular structure, but in the entire crystal structure. As a consequence of this difficulty, only few examples of this type of magnet exist. Up to the present reported chiral magnets have low dimensional magnetic structures, the magnetic ordering temperatures are below 10 K. To afford a high- T_C magnet, dimensionality of magnetic structure must be extended in two or three dimension. When we introduce magnetic bricks, which have more than three connections for the construction of magnets, we can expect to make two or three-dimensional magnets. To make high dimensionality molecule-based magnets, we recently discovered using cyano bridged complex with chiral organic ligands.

V-A-1 Structure and Magnetic Properties of a Chiral Two-dimensional Ferrimagnet with T_C of 38 K

INOUE, Katsuya; KIKUCHI, Koichi¹
(¹IMS and Tokyo Metropolitan Univ.)

Synthesis, magnetic properties and structure of new chiral, transparent, high $T_C = 38$ K molecule-based two-dimensional ferrimagnet, $[\text{Cr}(\text{CN})_6][\text{Mn}(\text{S})\text{-pnH}(\text{H}_2\text{O})](\text{H}_2\text{O})$; ((S)-pn = (S)-1,2-diaminopropane) are described. The complex was obtained as green needle crystal by the reaction of $\text{K}_3[\text{Cr}(\text{CN})_6]$, $\text{Mn}(\text{ClO}_4)_2$, and (S)-1,2-diaminopropane dihydrochloride ((S)-pn·2HCl) in 1:1:1 molar ratio in methanol/ H_2O (1:1) solution under argon atmosphere (adjusted pH 6–7 by KOH). X-ray structural analysis revealed a crystallized chiral space group of Orthorhombic, $P2_12_12_1$; moreover, the complex demonstrated a two-dimensional magnetic network. The magnetic measurements of the complex show Mn^{II} and Cr^{III} ions interact ferrimagnetically and magnetic transition occurs at 38 K.



Figure 1. A single crystal of a chiral molecular ferrimagnet, $[\text{Cr}(\text{CN})_6][\text{Mn}(\text{S})\text{-pnH}(\text{H}_2\text{O})](\text{H}_2\text{O})$.

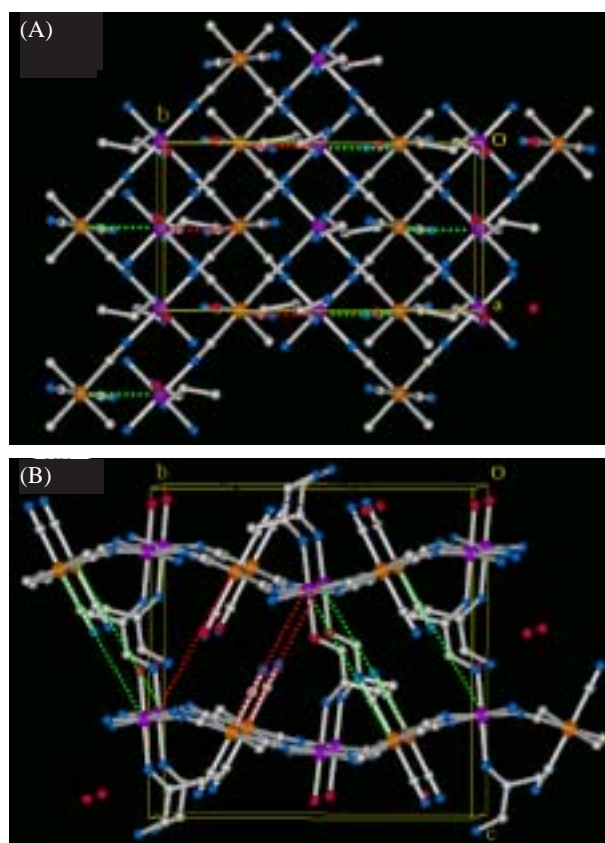


Figure 2. Crystal structure of $[\text{Cr}(\text{CN})_6][\text{Mn}(\text{S})\text{-pnH}(\text{H}_2\text{O})](\text{H}_2\text{O})$. (A) Projection onto the ab plane. (B) Projection onto the bc plane.

V-B Hydrothermal Synthesis of Molecule-Based Magnets

Coordination polymers are attracting much interest due to the strength and rigidity of the extended lattices for gas absorption and intercalation and for the connectivity between magnetic ions in designing molecule-based magnets. They belong to a subset of organic-inorganic hybrid materials, and usually employ a central metal ion and a multitopic organic ligands or a coordination complex having ambidentate ligands, such as cyanide and oxalate. In some cases, other organic ligands are used to control the dimensionality or structure. The choice of the metals and of the ligands depends on the desired properties. On the one hand, there is strong interest by scientists studying catalysis and the absorption of gases originating from the possibility of creating structures with cavities, channels or pores and, consequently, large surface areas. On the other hand, there is increasing interest from magneto-chemists due principally to the realization of organizing the magnetic orbitals of the moment carriers to favor a particular magnetic ground state. The field of coordination polymers based on organic radicals is a very active area, indeed. Several ground states have been established and a clear molecular-orbital picture to explain the observations is emerging. For the realizing strong magnetic interaction, it is better to use simple and small organic ligands, such as cyanide or carboxylate ions. The metal complexes with such ligands are usually less solvability. The thermal synthesis is powerful method to make large single crystals for such complexes.

V-B-1 Self-Organized Metallo-Helicates and –Ladder with 2,2'-Biphenyldicarboxylate ($C_{14}H_8O_4$)²⁻: Synthesis, Crystal Structures, and Magnetic Properties

KUMAGAI, Hitoshi¹; INOUE, Katsuya; KURMOO, Mohamedally¹

(¹IMS and Inst. Phys. Chem. Materials Strasbourg, France)

We report on the hydrothermal synthesis, single-crystal structures and magnetic properties of three one-dimensional coordination polymers employing the 2,2'-biphenylcarboxylate dianion, ($C_{14}H_8O_4$)²⁻, as the

bridging component. [$M^II(H_2O)_4(C_{14}H_8O_4)$], where $M = Co$ and Ni , consist of helical chains of square-planer $M^II(H_2O)_4$ bridged by $C_{14}H_8O_4$ with each carboxylate group acting as a mono-dendate ligand. The magnetic properties are those of paramagnets with an antiferromagnetic exchange for Co complex and a ferromagnetic exchange for Ni complex. $Cu(C_{14}H_8O_4)(H_2O)_2$ is composed of tetracarboxylato-dimeric units bridged into ladders by biphenyl units. The ladders are packed parallel to each other, and narrow channels are present due to insufficient space filling of the biphenyl rings. Its magnetic behavior follows that of a Bleaney-Bowers singlet-triplet model with a gap of 470 K.

V-C Synthesis and Characterization of Quantum-Spin Systems

There has been considerable current interest in the study of a low-dimensional quantum-spin system with an energy gap. For such study, organic radicals will provide good examples of ideal Heisenberg spin systems, since they consist only of light elements. By the appropriate design of molecules, we can obtain a variety of spin systems. In these years, we focus on the spin-ladder system, which is interesting in terms of Haldane state and the high T_C superconductivity. For the $S = 1/2$ Heisenberg spin ladder with antiferromagnetic legs and rungs, the ground state of the resonating valence bond (RVB) state or the dimerized state is theoretically expected. Experimentally, the singlet ground state was observed in some ladder systems formed by Cu-based compounds. The study of spin ladder systems has been mainly devoted to that of $S = 1/2$, but that of $S = 1$ is also interesting. We have succeeded in synthesis of the first example of a spin ladder system of $S = 1$ by BIP-TENO. Peculiar properties are observed and theoretical study is also activated.

V-C-1 Magnetic Properties of Organic Two-Leg Spin Ladder Systems with $S = 1/2$ and $S = 1$

KATOH, Keiichi¹; HOSOKOSHI, Yuko; INOUE, Katsuya; BARTASHEVICH, M. I.²; NAKANO, Hiroki³; GOTO, Tsuneaki²

(¹GUAS; ²Univ. Tokyo; ³Himeji Inst. Tech.)

Magnetic properties of spin systems on the two-leg ladder made of organic radicals are studied. The magnetization measurements below 4.2 K in pulsed magnet fields up to about 50 T were done for BIP-BNO as an $S = 1/2$ ladder and for BIP-TENO as an $S = 1$ ladder. An energy gap above the singlet ground state is observed in each compound. Experimental results of magnetizations and susceptibilities are understood from the analysis using the results of the numerical diagonalizations.

[*J. Phys. Chem. Solids* **63**, 1277 (2002)]

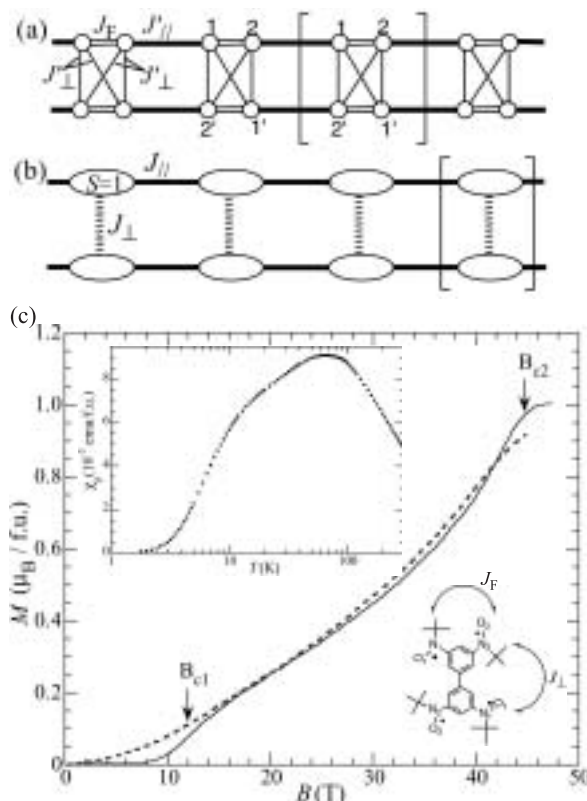


Figure 1. Magnetic exchange coupling scheme in BIP-TENO crystals. A circle and a bond represent an $S = 1/2$ and the exchange coupling, respectively: J_F and J_{\perp} correspond to intramolecular exchange couplings and J_{\parallel} is intermolecular one. (b) Extreme limit of the model (a) when $J_F \rightarrow \infty$. (c) Magnetization curves of BIP-TENO in pulsed high magnetic fields. Solid and dotted curves are the results for 1.7 and 4.2 K, respectively. Inset: Temperature dependence of the paramagnetic susceptibility of BIP-TENO.

V-C-2 Low Dimensionality Observed by ESR Measurements in $S = 1$ Spin Ladder Substance BIP-TENO

OHTA, Hitoshi¹; KIRITA, Keizo¹; KUNIMOTO, Takashi¹; OKUBO, Suzumu¹; HOSOKOSHI, Yuko; KATO, Keiichi²; INOUE, Katsuya; OGASAWARA, Akira³; MIYASHITA, Seiji³
(¹Kobe Univ.; ²GUAS; ³Univ. Tokyo)

[*J. Phys. Soc. Jpn.* **71**, 2640 (2002)]

X-band ESR measurements of BIP-TENO single crystal, which is an $S = 1$ spin ladder model substance, have been performed in the temperature region from 3.5 to 300 K. At room temperature, the angular dependences of g -value and line width were observed. The line shape and the angular dependence of the line width showed the typical behavior of the low dimensional antiferromagnet. The temperature dependence measurements showed the minimum of the line width and the dynamical g -shift, which were also the typical behavior of the low dimensional antiferromagnet. However, the direction of the dynamical g -shift does not coincide with the well known Nagata's theory, and the comparison with the recent direct ESR calculation by Miyashita *et al.* is discussed.

V-D Organic Ferrimagnetism

In the last decades, the magnetism of molecule-based material has drawn much interest. After the discovery of the organic ferromagnet in 1991, search for an organic ferrimagnet attracts great interest and is considered as one of today's challenging targets in material science. Although a number of ferrimagnets are realized in inorganic-organic hybrid systems, a genuine organic ferrimagnet has not yet been realized. In 1980's, ferrimagnetism is proposed as an effective strategy to give organic materials spontaneous magnetizations by the alternant arrangement of two kinds of organic radicals having different spin-multiplicities. All the reported ferrimagnets include at least two magnetic components: bimetallic compounds or metal complexes with organic radicals. In order to achieve this challenging subject of an organic ferrimagnet from a different viewpoint, we propose here a single-component strategy: utilizing a triradical including an $S = 1$ and an $S = 1/2$ units within a molecule and connecting the $S = 1$ and $S = 1/2$ units by intra- and intermolecular antiferromagnetic interactions. Our new strategy to use a single component has the advantages of the easiness of controlling the crystal structure and the good crystallinity for quality and size.

V-D-1 Magnetic Properties on an Organic Ferrimagnetic Compound and Related Materials

HOSOKOSHI, Yuko; KATO, Keiichi¹; INOUE, Katsuya
(¹GUAS)

[*Synth. Met.* in press]

Search for an organic ferrimagnet has been one of the challenging targets in the field of material science. Recently, we have reported the successful results for the crystals of a novel organic triradical of PNNBNO, 2-[3',5'-bis(*N*-*tert*-butylaminoxy)phenyl]-4,4,5,5-

tetramethyl-4,5-dihydro-1*H*-imidazol-1-oxyl 3-oxide. This is the first example of a genuine organic ferrimagnetic material having well-defined chemical and crystal structure with $T_C = 0.28$ K. The properties of PNNBNO are described and the magnetic interactions of this system are discussed in comparison with the related oligoaminoxyl.

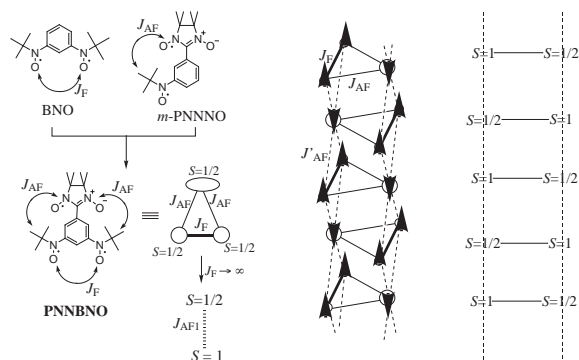


Figure 1. Scheme of the single component strategy for organic ferrimagnetism.

V-E Pressure Effects on Molecular Magnetism

'Pressure' is a powerful tool to control the molecular packings and physical properties. The molecule-based materials with small densities are 'soft' and can be expected to show large pressure effects. For the magnetic measurements with high-accuracy, we have developed a small high-pressure clamp cell made of non-magnetic Cu-Ti alloy which can be equipped to a Quantum Design SQUID magnetometer for the *dc* and *ac* magnetic measurements. The inner pressure of the clamp cell has been calibrated by the superconducting transition temperature of Pb. We have already discovered that some kind of structural change can be suppressed by pressurization. We are now studying the pressure effects on the molecule-based magnetic materials in wider range. In molecular materials, the spin density are delocalized and distributed in a molecule and the spin-density-distribution plays an important role in the exchange interactions. It is attractive to control the sign of the exchange coupling by pressurization. The pressure effects on the related compounds with similar crystal structures are studied.

V-E-1 Pressure Effects on Molecular Magnets of Mn Complexes with Bisaminoxylbenzene Derivatives

SUZUKI, Kentaro¹; HOSOKOSHI, Yuko; INOUE, Katsuya
(¹GUAS)

[*Mol. Cryst. Liq. Cryst.* **379**, 247 (2002)]

Pressure effects on the magnetic properties of a series of quasi-one-dimensional molecular magnets have been studied. The complexes of $Mn(hfac)_2$ ($hfac = \text{hexafluoroacetylacetonate}$) with 1,3-bis(*N*-*tert*-butylaminoxyl)benzene and its 5-halo- derivatives, abbreviated as $\mathbf{1}_X$ ($X = H, F, Cl$ and Br), have almost the same ferrimagnetic chain structure. The difference is seen in the interchain molecular arrangement. The complexes of $\mathbf{1}_H$ and $\mathbf{1}_F$ are metamagnets with weak interchain antiferromagnetic interactions, whereas $\mathbf{1}_{Cl}$ and $\mathbf{1}_{Br}$ are ferrimagnets with weak interchain ferromagnetic interactions. In two metamagnets ($\mathbf{1}_H$, $\mathbf{1}_F$), the pressurization simply results in the enhancement of the interchain antiferromagnetic interactions, which is reflected by the higher transition temperature and spin-flipping field. On the other hand, in the ferrimagnet ($\mathbf{1}_{Cl}$), the metamagnetic behavior is observed under pressure. It is suggested that the subtle change of the relative arrangement of chain structures affects the interchain ferromagnetic interactions.

V-E-2 Pressure-Induced Metamagnetic Behavior in a Quasi-One-Dimensional Molecule-Based Ferrimagnet

SUZUKI, Kentaro¹; HOSOKOSHI, Yuko; INOUE, Katsuya
(¹GUAS)

[*Chem. Lett.* 316 (2002)]

Pressure effects on a molecule-based ferrimagnet of $[Mn(hfac)_2] \cdot (Br-BNO)$ ($\mathbf{1}_{Br}$) were studied, where $hfac = \text{hexafluoroacetylacetonate}$ and $Br-BNO = 5\text{-bromo-1,3-bis}(N\text{-tert-butylaminoxyl)benzene}$. At ambient pressure, $\mathbf{1}_{Br}$ is a ferrimagnet with $T_C = 5.4$ K. We observed the metamagnetic behavior of $\mathbf{1}_{Br}$ under pressure.

V-F Bioinorganic Studies on Structures and Functions of Non-Heme Metalloenzymes Using Model Complexes

Metal-containing enzymes have been widely distributed in both plants and animals and have been related to metabolic processes such as hydroxylation, oxygen transport, oxidative catalysis, electron transfer, and so on. In this project, their structural/functional models have been originally constructed and studied using physico-chemical methods.

V-F-1 Novel Phosphate Bond Formation in a Cobalt(III) Complex System

FUNAHASHI, Yasuhiro¹; YONEDA, Atsuro¹;
TAKI, Chiyo¹; OZAWA, Tomohiro¹;
JITSUKAWA, Koichiro¹; MASUDA, Hideki²
(¹Nagoya Inst. Tech.; ²IMS and Nagoya Inst. Tech.)

[*Inorg. Chem.* submitted]

Reaction of an aqueous solution (pH 3) of [Co^{III}(tpa)(CO₃)]Cl (**1**) (tpa = tris(2-pyridylmethyl)amine) with 2 equiv. of an active phosphate ester, disodium 4-nitrophenylphosphate (NPP), in the presence of a catalytic amount of active charcoal at 60 °C gave [Co^{III}(tpa)(PO₄)] (**2**) (7.8% yield) and [Co^{III}(tpa)₂(μ-P₂O₇)]Cl₂ (**3**) (50.7% yield). The structures of **2** and **3** were determined by X-ray crystallography. Complex **3** has a novel molecular structure with ligation of the two Co(III) centers *via* an NPP-derived bridging-diphosphate. The phosphate bond formation does not occur without active charcoal or under conditions of neutral pH. A proposed reaction mechanism involves initiation by hydrolysis of NPP to give **2** with the phosphate bond formed as an intermediate dimer structure.

V-F-2 Syntheses and Structures of Tetrakis(1-methyluracilato)palladium Complexes Capturing Alkali Metal Ions. A New Type of Metallo-Podand

MIZUTANI, Mamoru¹; MIWA, Satoshi^{1,2};
FUKUSHIMA, Nobuhiro^{2,3}; FUNAHASHI,
Yasuhiro¹; OZAWA, Tomohiro¹; JITSUKAWA,
Koichiro¹; MASUDA, Hideki⁴
(¹Nagoya Inst. Tech.; ²SIGI Japan; ³Collaboration Lab.;
⁴IMS and Nagoya Inst. Tech.)

[*Inorg. Chim. Acta* in press]

Four tetrakis(1-methyluracilato)palladium complexes containing alkali metal ions, [Li₂Pd(1-MeU⁻)₄] (**1**), [Na₂Pd(1-MeU⁻)₄] (**2**), [K₂Pd(1-MeU⁻)₄] (**3**), and [Cs₂Pd(1-MeU⁻)₄] (**4**), have been prepared from M₂PdCl₄ (M = Li⁺, Na⁺, K⁺, and Cs⁺) and four equivalents of 1-methyluracil (1-MeUH). The X-ray crystal structure analyses of complexes **2**, **3** and **4** have revealed that each palladium atom is coordinated in a square-planar geometry with four 1-MeUH-derived N3-deprotonated imidato groups, upright-oriented with angles of 60 ~ 70° from the basal coordination plane. Interestingly, the carbonyl groups of the four imidato rings form two cavities above and below the Pd(II) atom, and two alkali

metal ions are incorporated with Pd–M distances of 3.007(4) and 3.137(3) Å for **2**, 3.432(3) and 3.594(3) Å for **3**, and 3.746(1) and 3.999(1) Å for **4**, respectively. The cavity sizes of the three complexes are tunable according to the ionic radii of the alkali metal ions. ¹H-NMR spectra of complexes **1–4** indicate that all proton signals of the 1-MeU⁻ moiety shifted upfield relative to those of free 1-MeU⁻. The magnitude of the up-field shifts, **1** < **2** < **3** < **4**, corresponds well to the order of the ionic potentials of alkali metal ions. These up-field shifts are reduced by coordination of 5-fluoro-1-methyluracil in place of 1-MeUH, indicating that the electron-donating character of 1-MeU⁻ to Pd(II) is decreased by substitution with an electron-withdrawing fluoro group. These observations suggest that the up-field shifts may be rationalized in terms of π-back donation from Pd(II) dπ-orbital to imidato π*-orbital and the ionic potentials of alkali metals, which have also been investigated on the basis of the DFT calculation. On the basis of these characteristic features, the [M₂Pd(1-MeU)₄] complexes may be classified as a new type of metallo-podand that captures alkali metal ions.

V-F-3 Investigations of the Effects of Intramolecular Hydrogen Bonding Networks on Tripodal Trihydroxamate-Type Artificial Siderophores

MATSUMOTO, Kenji¹; OZAWA, Tomohiro¹;
JITSUKAWA, Koichiro¹; MASUDA, Hideki²
(¹Nagoya Inst. Tech.; ²IMS and Nagoya Inst. Tech.)

[*Inorg. Chem.* submitted]

The solution behavior of the iron(III) complex with tris[2-{(N-acetyl-N-hydroxy)glycylamino}ethyl]amine (TAGE) has been investigated using ¹H NMR, UV-vis, and FAB mass spectroscopies and cyclic voltammetry in efforts to characterize the hydrogen bonding networks between the amide hydrogens and coordinating aminohydroxy oxygens of the complex. Temperature dependencies of ¹H-NMR spectra for Al(III) and Ga(III) complexes of TAGE indicate that hydrogen bonding networks are maintained even in polar solvents such as DMSO-d₆ and D₂O. The UV-vis spectra of the Fe(III)-TAGE complex in various pH conditions show that TAGE forms a tris(hydroxamato)iron(III) complex in an aqueous solution from pH 4–8. On the other hand, tris[2-{(N-acetyl-N-hydroxy)propylamido}ethyl]amine (TAPE; a TAGE analogue that does not form hydrogen bonds), does not form the tris(hydroxamato)iron(III) complex in the same pH range. Both the stability constant (logβ_{FeTAGE} = 28.6; β_{FeTAGE} = [Fe^{III}TAGE]/-

($[\text{Fe}^{3+}][\text{TAGE}^{3-}]$) and pM ($-\log[\text{Fe}^{3+}]$) value for Fe^{III} -TAGE (pM 25) are comparable to those of ferrichrome, a natural siderophore ($\log\beta = 29.1$ and pM 25.2). The rate of the ligand exchange reaction between Fe^{III} -TAGE and EDTA is $6.7 \times 10^{-4} \text{ s}^{-1}$, a rate similar to those of the ferrichromes. The redox potential of Fe^{III} -TAGE in aqueous solution is -227 mV (vs. NHE) at pH 7, about 200 mV higher than those of Fe^{III} -TAPE and ferric natural trihydroxamates. The high redox potential of Fe^{III} -TAGE is interpreted in terms of the intramolecular hydrogen bonding networks wherein both iron(III) and iron(II) complexes are tightly fixed and stabilized by the TAGE ligand. In a biological activity experiment, TAGE promotes the growth of the siderophore-auxotroph gram-positive bacterium *Microbacterium flavescens*, and thus mimics the activity of ferrichrome. These results indicate that the artificial siderophore TAGE is a good structural and functional model for ferrichrome and that the intramolecular hydrogen bonding networks provide stability for the complex and allow the redox potential to increase even in an aqueous solution.

V-F-4 The Role of the Zn(II) Site in Cu,Zn SOD (1). Synthesis and Characterization of Novel Hydroperoxo-Zinc(II) Intermediates

WADA, Akira¹; JITSUKAWA, Koichiro¹; MASUDA, Hideki²

(¹Nagoya Inst. Tech.; ²IMS and Nagoya Inst. Tech.)

[*J. Amer. Chem. Soc.* Submitted]

A novel Zn–OOH species has been prepared using an original ligand bis(6-neopentylamino-2-pyridylmethyl)(2-pyridylmethyl)amine (H_2BNPA), whose synthesis was determined by ¹H-NMR and ESI-mass spectroscopic methods. The formation of $[\text{Zn}(\text{H}_2\text{BNPA})(\text{OOH})]^+$ has been confirmed from the ESI-mass spectral measurements of the reactions of $[\text{Zn}(\text{H}_2\text{BNPA})(\text{OH})]^+$ with H_2O_2 and subsequent addition of CO_2 as well as the X-ray structure of the product crystal obtained from the reaction solution kept at 0 °C under CO_2 , $[\{\text{Zn}(\text{H}_2\text{BNPA})\}_2(\text{CO}_4^{2-})]^{2+}$. Comparisons of the reactivities of Zn(II)–OOH and Cu(II)–OOH species toward CO_2 have suggested that the hydroperoxide bound to Zn(II) ion exhibits a higher nucleophilicity/basicity than that of hydroperoxide bound to Cu(II). This implies that in the 2nd half of the reaction cycle of Cu,Zn SOD, the transformation of hydroperoxide to hydrogen peroxide tends to proceed within the coordination sphere of Zn(II) site instead of within the coordination sphere of Cu(II).

V-F-5 Epoxidation Activities of Mononuclear Ruthenium-oxo Complexes with a Square Planar 6,6'-Bis(benzoylamino)-2,2'-bipyridine and Axial Ligands

JITSUKAWA, Koichiro¹; SHIOZAKI, Hiroyoshi¹; MASUDA, Hideki²

(¹Nagoya Inst. Tech.; ²IMS and Nagoya Inst. Tech.)

[*Tetrahedron Lett.* **43**, 1491 (2002)]

Some ruthenium complexes with a square planar ligand, H_2BABP , ($[\text{Ru}^{\text{II}}(\text{babp}^{2-})(\text{dmsO})_2]$ (**1**), $[\text{Ru}^{\text{II}}(\text{babp}^{2-})(\text{dmsO})(\text{im})]$ (**2**), $[\text{Ru}^{\text{II}}(\text{babp}^{2-})(\text{dmsO})(\text{py})]$ (**3**), and $[\text{Ru}^{\text{II}}(\text{babp}^{2-})(\text{dmsO})(\text{Phpy})]$ (**4**)) have been prepared as a catalyst of oxygen transfer reaction. Catalytic activity of the metal-oxo species derived by the reaction of **1** ~ **4** with PhIO has been affected by the axial ligands of the complexes, whose oxidation active species has been interpreted in terms of contribution of both characters of Ru(V)=O and Ru(IV)–O·.

V-F-6 Reactivity of Hydroperoxide Bound to a Mononuclear Non-Heme Iron Site

WADA, Akira¹; OGO, Seiji; NAGATOMO, Shigenori; KITAGAWA, Teizo; WATANABE, Yoshihito; JITSUKAWA, Koichiro²; MASUDA, Hideki¹

(¹IMS and Nagoya Inst. Tech.; ²Nagoya Inst. Tech.)

[*Inorg. Chem.* **41**, 616 (2002)]

The first isolation and spectroscopic characterization of the mononuclear hydroperoxo-iron(III) complex, $[\text{Fe}(\text{bppa})(\text{OOH})]^{2+}$ (**2**), and the stoichiometric oxidation of substrates by the mononuclear iron-oxo intermediate generated by its decomposition have been described. The purple species **2** obtained from reaction of $[\text{Fe}(\text{bppa})(\text{HCOO})](\text{ClO}_4)_2$ with H_2O_2 in acetone solution at $-50 \text{ }^\circ\text{C}$ gave characteristic UV-vis ($\lambda_{\text{max}} = 568 \text{ nm}$, $\epsilon = 1200 \text{ M}^{-1} \text{ cm}^{-1}$), ESR ($g = 7.54, 5.78$ and 4.25 , $S = 5/2$), and ESI mass spectra ($m/z = 288.5$ corresponding to the ion, $[\text{Fe}(\text{bppa})(\text{OOH})]^{2+}$), which revealed that the complex **2** is a high-spin mononuclear iron(III) complex with a hydroperoxide in an end-on fashion. The resonance Raman spectrum of **2** in d_6 -acetone revealed two intense bands at 621 and 830 cm^{-1} , in which the former band shifted to 599 cm^{-1} when reacted with ¹⁸O-labeled H_2O_2 and the latter band showed a small isotope shift to 813 and 826 cm^{-1} upon reaction with $\text{H}_2^{18}\text{O}_2$ and D_2O_2 , respectively. Reactions of the isolated (bppa)Fe^{III}–OOH (**2**) with various substrates (single turnover oxidations) exhibited that the iron-oxo intermediate generated by decomposition of complex **2** is a nucleophilic species formulated as $[(\text{bppa})\text{Fe}^{\text{III}}\text{–O}\cdot]$.

V-F-7 Reactivity Control for Epoxidation of Olefins and Dehydrogenation of Alcohols Catalyzed by Ruthenium-oxo Complexes

JITSUKAWA, Koichiro¹; MORISHIMA, Yuji¹; SHIOZAKI, Hiroyoshi¹; OKA, Yoshiyuki¹; MASUDA, Hideki²

(¹Nagoya Inst. Tech.; ²IMS and Nagoya Inst. Tech.)

[*Shokubai* **43**, 440 (2001)]

Several ruthenium complexes with tripodal polypyridine or diamidobipyridine ligands were prepared for investigation of catalytic activity on the oxygen transfer reactions. Ruthenium(V)-oxo species generated through the reaction of low-valent ruthenium complex and PhIO was observed in the ESI-mass spectroscopy. Their catalytic activities for epoxidation of olefins, hydroxy-la-

tion of alkanes and dehydrogenation of alcohols were affected by the coordination environment and redox property of the starting ruthenium complexes. These findings are explained by the hypothesis as follows: Ruthenium-oxo species generated on the complexes with non-porphine ligands show both characters of Ru(V)=O and Ru(IV)-O·. The former intermediate favors epoxidation pathway and the latter radical one.

V-F-8 Crystal Structure and Solution Behavior of the Iron(III) Complex of the Artificial Trihydroxamate Siderophore with Tris(3-aminopropyl)amine Backbone

MATSUMOTO, Kenji¹; SUZUKI, Naomi¹;
OZAWA, Tomohiro¹; JITSUKAWA, Koichiro¹;
MASUDA, Hideki²
(¹Nagoya Inst. Tech.; ²IMS and Nagoya Inst. Tech.)

[*Eur. J. Inorg. Chem.* **10**, 2481 (2001)]

Microorganisms produce low molecular weight compounds called siderophores for an uptake of iron. A large number of siderophores have hydroxamates or catecholates as the iron binding site that exhibits very high affinity for iron(III) ion, and their siderophores form very stable iron(III) complexes. The high stability of Fe(III)-siderophore complexes is attributed to not only such chelating effect but also hydrogen bonding and van der Waals interactions and predisposition of ligands. Thus, the ligand backbones are quite important for the stabilization of iron(III) complexes. Many tripodal artificial siderophores were synthesized as ferrichrome and enterobactin analogues; the synthetic siderophores adopt various tripodal backbones as follows, *e.g.*, tris(2-aminoethyl)amine (TREN), triaminomethylbenzene, 1,5,9-triazacyclododecane, nitrilotriacetic acid, 1,1,1-tris{(2-carboxyethoxy)methyl}propane. Among such tripodal backbones, TREN has been frequently used. Recently, we also have reported the synthesis of tris[2-{(N-acetyl-N-hydroxy)glycylamino}ethyl]amine (TAGE) as the artificial siderophore with TREN anchor, whose iron(III) complex showed extremely high stability ($\log\beta = 28.7$). From the crystal structure of the iron(III) complex, this higher stability was revealed to be attributed to the intramolecular hydrogen bonding networks. However, the tripodal anchors such as TREN have been reported to make reduce the stability of iron(III) complexes than the natural siderophore-iron (III) complexes, which are presumed to be due to the small size of the anchor for an iron(III) chelation. On the other hand, tris(3-aminopropyl)amine (TRPN), whose alkyl chains are one methylene longer than TREN, has not been much used, and the details are little described, despite the similarity in these structures. At this stage, we newly synthesized tris[{3-(N-acetyl-N-hydroxy)-glycylamino}propyl]amine (TAGP, Figure 1) as a trihydroxamate artificial siderophore with TRPN anchor in order to examine the efficiency of the size. Tris[{3-(N-acetyl-N-hydroxy)-glycylamino}propyl]amine (TAGP) forms the 1 : 1 tris(hydroxamato)-iron(III) complex even at a low pH (~2), which promotes the growth of the siderophore-auxotrophic mutant *Microbacterium flavescens*. Here,

we described the crystal structure and solution behavior of its iron(III) complex.

V-F-9 Reverse Reactivity in Hydroxylation of Adamantane and Epoxidation of Cyclohexene Catalyzed by the Mononuclear Ruthenium-oxo Complexes with 6-Substituted Tripodal Polypyridine Ligands

JITSUKAWA, Koichiro¹; OKA, Yoshiyuki¹;
EINAGA, Hisahiko¹; MASUDA, Hideki²
(¹Nagoya Inst. Tech.; ²IMS and Nagoya Inst. Tech.)

[*Tetrahedron Lett.* **42**, 3467 (2001)]

The electronic character of the ruthenium complexes with tripodal polypyridine ligands, which is controlled by the substituted groups at pyridine 6-position, gives rise to differences in the reactivity for the ruthenium catalyzed hydroxylation of adamantane and epoxidation of cyclohexene with PhIO as an oxidant; Ru complexes containing electron-withdrawing groups promote the epoxidation, while those containing electron-donating groups promote the hydroxylation.

V-F-10 Characterization of an NH- π Interaction in Co(III) Ternary Complexes with Aromatic Amino Acids

KUMITA, Hideyuki¹; KATO, Takashi¹;
JITSUKAWA, Koichiro¹; EINAGA, Hisahiko¹;
MASUDA, Hideki²
(¹Nagoya Inst. Tech.; ²IMS and Nagoya Inst. Tech.)

[*Inorg. Chem.* **40**, 3936 (2001)]

The NH- π interaction has been detected in the crystal structures of Co(III) ternary complexes with N,N-bis(carboxymethyl)-(S)-phenylalanine (BCMPA) and aromatic amino acids including: (S)-phenylalanine ((S)-Phe), (R)-phenylalanine ((R)-Phe), and (S)-tryptophan ((S)-Trp)). Additionally, this interaction has been studied in solution for Co(III) ternary complexes with BCMPA or NTA (NTA = nitrilotriacetic acid) and several amino acids (AA) by means of electronic absorption, circular dichroism (CD), and ¹H NMR spectroscopies. The CD intensities of the Co(III) complexes with aromatic amino acids measured in the *d-d* region ($\sim 20.5 \times 10^3 \text{ cm}^{-1}$) are significantly decreased in ethanol solutions relative to water. Analogous complexes with aliphatic amino acids do not exhibit this solvent effect. The ¹H NMR spectra of the Co(III) complexes with aromatic amino acids measured in DMSO-d₆ and D₂O exhibit up-field shifts of the N-H peaks compared with those with aliphatic amino acids for both cases, which suggest a shielding effect due to the aromaticity. The up-shift values coincide with those experimentally evaluated from the crystal structures. The magnitude of the upfield shifts observed in DMSO-d₆ agrees well with Hammett's rule and similar tendency is slightly characterized also in D₂O, indicating that the increase of π -electron densities on the aromatic rings exerts a larger shielding effect for the NH protons and it is reduced in aqueous solution. In ligand-substitution reactions of the

carbonatocobalt(III) complexes with amino acids, the yields of those with aromatic amino acids are higher than the yields obtained for complexes with aliphatic amino acids. This observation is discussed in connection with the important contribution of the NH- π interaction as one of the promotion factors in the reaction.

V-F-11 The Role of the Zn(II) Site in Cu,Zn SOD. (2) Evidence of Superoxide Disproportionation Catalyzed by Sterically- and Electrostatically-Controlled Zinc(II) Complexes

WADA, Akira¹; JITSUKAWA, Koichiro¹; MASUDA, Hideki²

(¹Nagoya Inst. Tech.; ²IMS and Nagoya Inst. Tech.)

[J. Amer. Chem. Soc. submitted]

The role of the Zn(II) site in the disproportionation reaction of superoxide catalyzed by Cu,Zn superoxide dismutase (Cu,Zn SOD) has been systematically examined using sterically- and electrostatically-controlled Zn(II) complexes in an aprotic solvent (MeCN/DMSO (9:1)) by cyclic voltammetry, ESI-mass spectroscopy and ESR spectroscopy. Interestingly, higher SOD activity was observed in the Zn(II) complexes with lower Lewis acidity and in Zn(II) complexes without a superoxide-accessible site. These findings clearly indicate that the efficient catalytic SOD reaction is due to efficient access of superoxide to the Zn(II) ion. Here we offer a new proposal for the role of Zn(II) site in Cu, Zn SOD and propose an alternate mechanism for the 2nd step of SOD reaction.

V-F-12 SOD Activities of the Copper Complexes with Tripodal Polypyridylamine Ligands Having a Hydrogen Bonding Site

JITSUKAWA, Koichiro¹; HARATA, Manabu¹; ARII, Hidekazu¹; SAKURAI, Hiromu²; EINAGA, Hisahiko¹; MASUDA, Hideki³

(¹Nagoya Inst. Tech.; ²Kyoto Pharmaceutical Univ.; ³IMS and Nagoya Inst. Tech.)

[Inorg. Chim. Acta **324**, 108 (2001)]

For investigation of the correlation with the coordination structures of the copper complexes and their superoxide dismutation activities, four mononuclear copper complexes with tris(2-pyridylmethyl)-amine derivatives containing pivalamido or neopentyl-amino groups at pyridine 6-position, [Cu(tnpa)(OH)]ClO₄ (**1**), [Cu(tapa)Cl]ClO₄ (**2**), [Cu(tapa)(OH)]ClO₄ (**3**), and [Cu(bppa)](ClO₄)₂ (**4**), and two dinuclear copper complexes, [Cu₂(tppen)(H₂O)₂](ClO₄)₂ (**5**) and [Cu₂(tppen)Cl₄] (**6**), were prepared as single crystals suitable for X-ray analysis except the complex **3**. Such hydrogen bonding moiety at pyridine 6-position of these ligands is regarded as a Arg 141 residue around copper site in native bovine superoxide dismutase (SOD). Coordination geometry around copper ion in **1** ~ **3**, **5**, and **6** was determined to have 5-coordinate trigonal bipyramidal or square pyramidal structure both in crystal and solution phases on the basis of their X-ray

analyses or spectroscopic results. However, that in **4** was 4-coordinate square planar structure. The redox potentials of the mononuclear complexes, **1** ~ **4**, (Cu(II)/Cu(I) couple) were within the range between -330 mV (vs. NHE at pH 7. O₂/O₂^{•-}) and + 890 mV (vs. NHE. O₂^{•-}/H₂O₂), which were in good range for superoxide dismutation, so that these complexes were used for investigating their catalytic activity. Moderate dismutation activities were demonstrated in the cases of **1** ~ **3** in comparison with other mononuclear copper complexes previously reported, although **4** showed the lowest activity of all. The distorted structure around copper center, such as 5-coordinate trigonal bipyramidal or square pyramidal structure, is important for demonstrating SOD activity. In addition, the activities caused by the dinuclear complex, **5** and **6**, were higher than those by the mononuclear ones. 6-Neopentylamino or 6-amino group of the tripodal polypyridine ligands, which is designed as a hydrogen bonding moiety, plays an important role for acceleration of activity in the SOD mimics through stabilization of superoxide species binding to the metal center.

V-F-13 Site-Selective Recognition of Amino Acids by Co(III) Complexes Containing a (N)(O)₃-Type Tripodal Tetradentate Ligand

KUMITA, Hideyuki¹; MORIOKA, Taiju¹; OZAWA, Tomohiro¹; JITSUKAWA, Koichiro¹; EINAGA, Hisahiko¹; MASUDA, Hideki²

(¹Nagoya Inst. Tech.; ²IMS and Nagoya Inst. Tech.)

[Bull. Chem. Soc. Jpn. **74**, 1035 (2001)]

The bis-*N,N*-carboxymethyl-(*S*)-phenylalaninato carbonato cobalt(III) complex, [Co(bcmpa)(CO₃)]²⁻, has been prepared as a simple model that enables the recognition of an amino acid (Haa) whose coordination behaviours in solution have been characterized by electronic absorption (AB), circular dichroism (CD) and ¹H-NMR spectroscopies. The reaction of the K₂[Co-(bcmpa)(CO₃)] complex with amino acids (Haa) has predominantly afforded the [Co(bcmpa)(aa)] complex in the *trans(N)*-configuration mode, rather than in the *cis(N)*-form. By using amino acid derivatives with bulky substituents at their amino or carboxylate sites under a neutral condition, the reactions have been demonstrated to be initiated by coordination of the amino nitrogen site. Interestingly, the *cis(N)*-complex, which is isolated as a minor product, isomerizes to the *trans(N)*-form in the presence of active charcoal under pH 7 in an aqueous solution. The site-selective coordination of Haa to the [Co(bcmpa)(CO₃)]²⁻ complex and the stereoselective isomerization of the [Co(bcmpa)(aa)]⁻ complex have been explained to be regulated by weak non-covalent interactions within the ligands, whose origin has been discussed based on a detailed examination of the crystal structures of the *trans(N)*- and *cis(N)*-K[Co(bcmpa)(aa)] complexes.

V-G Probing Time-Dependent Processes in Solution with Time-Resolved Spectroscopic Methods

A solute molecule surrounded by solvent molecules is exposed to dynamic environments of rapidly changing energy, polarity, or relative distance and orientation with adjacent molecules. The effects of these fluctuations, which are caused by the room temperature solvent molecules, are clearly demonstrated when the solute molecule experiences a chemical reaction. Intermolecular energy transfer and rotational or translational diffusion determine the fate of the chemical reaction.

Time-resolved spectroscopy is quite effective for studying time-dependent events occurring in solution. We use various types of time-resolved spectroscopy for observing dynamical processes. In this Annual Review, we report on five research projects, in which we use femtosecond time-resolved fluorescence spectroscopy with single channel detection, picosecond time-resolved fluorescence spectroscopy with multi-channel detection, picosecond time-resolved Raman spectroscopy, and nanosecond time-resolved infrared spectroscopy. We discuss (i) fast internal conversion of biphenyl, (ii) disagreement between Stokes- and anti-Stokes scattering frequencies observed under strong pump or probe light field, (iii) photoinduced Cl transfer reaction between biphenyl and carbon tetrachloride that results in the generation of the trichloromethyl (CCl_3) radical, (iv) solvent- and temperature-dependent Raman spectral changes of S_1 *trans*-stilbene and the mechanism of the *trans* to *cis* isomerization, and (v) picosecond dynamics of stepwise double proton-transfer reaction in the excited state of the 2-aminopyridine/acetic acid system.

V-G-1 Femtosecond Time-Resolved Anisotropy Measurement of Biphenyl Fluorescence

IWATA, Koichi¹; TAKEUCHI, Satoshi; TAHARA, Tahei²

(¹IMS and Univ. Tokyo; ²IMS and RIKEN)

The fluorescence intensity and its anisotropy decay of biphenyl were observed in the hexane solution. Biphenyl in hexane was photoexcited with a linearly polarized femtosecond light pulse at 260 nm. Time dependence of the fluorescence intensity as well as its anisotropy was measured with the up-conversion method. The observed fluorescence decay curve showed a fast decay component of 0.4 ps, in addition to a slow component that corresponds to the reported fluorescence decay time of 16 ns. The fluorescence anisotropy was approximately 0.4 at time 0, indicating that the direction of the fluorescence transition dipole at time 0 is same as the S_2 - S_0 absorption transition at 270 nm. The observed decay curve of the anisotropy was well fitted by a superposition of two exponential decay functions, with the time constants of 0.3 ps and 9 ps. The S_2 - S_1 internal conversion rate of biphenyl is thus estimated to be 0.3 ps.

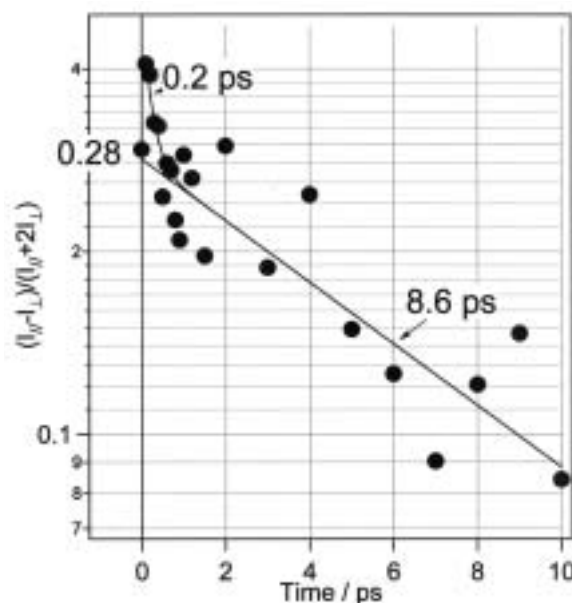


Figure 1. Observed curve of fluorescence anisotropy decay of biphenyl in hexane.

V-G-2 Effect of Pump and Probe Light Field on Picosecond Time-Resolved Resonance Raman Spectra of S_1 *trans*-Stilbene. Disagreement between Stokes- and Anti-Stokes Scattering Frequencies

IWATA, Koichi

(IMS and Univ. Tokyo)

[Bull. Chem. Soc. Jpn. 75, 1075 (2002)]

Picosecond time-resolved spontaneous resonance Raman spectra of the first excited singlet (S_1) state of *trans*-stilbene were measured with various power densities of pump or probe light, for both the Stokes and anti-Stokes scattering regions. Careful calibration of the peak positions of the 285 cm^{-1} Raman bands reveals that the Stokes scattering band and the anti-Stokes

scattering band shift to the same direction in absolute wavenumber, or to the opposite directions in Raman shift, when the pump or probe power density is increased. The direction of the wavenumber shift caused by the pump light field is opposite to that caused by the probe. Because of these apparent peak shifts, the Stokes Raman band and the anti-Stokes Raman band are recorded at different Raman shifts. The intrinsic change of the vibrational level spacing and the apparent peak shift caused by the pump or probe light field can be clearly separated by calculating the "symmetric" and "anti-symmetric" components from the Stokes and anti-Stokes peak positions. The experimental results are not explained by the optical Stark effect in its simplest form. Possible mechanisms to account for the results are discussed.

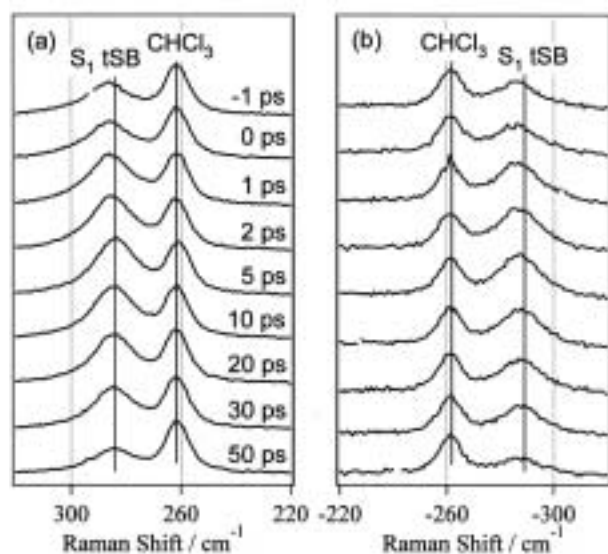


Figure 1. Time-resolved Raman spectra of S_1 *trans*-stilbene in chloroform. Stokes scattering bands (a) and Anti-Stokes scattering bands (b). Raman bands from S_1 *trans*-stilbene and solvent chloroform as well as time delay for each spectrum is indicated in the figure.

V-G-3 Photoinduced Cl Transfer Reaction between Biphenyl and Carbon Tetrachloride Studied by Nanosecond Time-Resolved Infrared Spectroscopy and Picosecond Time-Resolved Fluorescence Spectroscopy

IWATA, Koichi¹; TAKAHASHI, Hiroaki²
(¹IMS and Univ. Tokyo; ²Waseda Univ.)

[*J. Mol. Struct.* **598**, 97 (2001)]

Photochemical reaction between biphenyl and carbon tetrachloride is studied with nanosecond time-resolved infrared spectroscopy and picosecond time-resolved fluorescence spectroscopy. Fluorescence lifetime of biphenyl in carbon tetrachloride solutions is measured with a picosecond time-resolved fluorescence spectrometer. The recorded lifetime is 3.8 ps, shorter than fluorescence lifetime in cyclohexane by a factor of four thousands. After the photoexcitation of biphenyl in carbon tetrachloride, the trichloromethyl (CCl_3) radical is formed as a reaction intermediate, which is confirmed

by the detection of the radical's 896 cm^{-1} infrared band with nanosecond time-resolved infrared spectroscopy. One of the Cl atoms in solvent carbon tetrachloride is transferred to biphenyl to form the CCl_3 radical and a biphenyl-Cl adduct. Together with the already reported spectroscopic detection of the CCl_3 radical as an intermediate in photochemical reactions of *trans*-stilbene or anthracene with carbon tetrachloride, it is likely that this series of reactions are common for aromatic molecules.

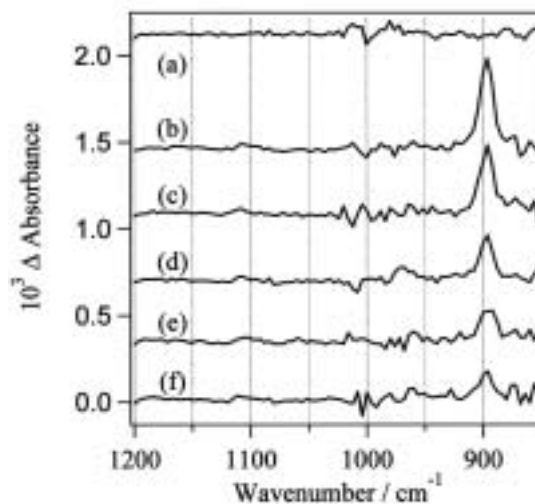


Figure 1. Time-resolved infrared difference spectra of biphenyl after photoexcitation in a carbon tetrachloride solution. Averaged spectrum for (a) -5 to $0\ \mu\text{s}$, (b) 0 to $5\ \mu\text{s}$, (c) 10 to $15\ \mu\text{s}$, (d) 20 to $25\ \mu\text{s}$, (e) 30 to $35\ \mu\text{s}$, and (f) 40 to $45\ \mu\text{s}$. Transient absorption band from the trichloromethyl (CCl_3) radical is observed at 896 cm^{-1} .

V-G-4 Analysis of the Solvent- and Temperature-Dependent Raman Spectral Changes of S_1 *trans*-Stilbene and the Mechanism of the *Trans* to *Cis* Isomerization: Dynamic Polarization Model of Vibrational Dephasing and the C=C Double-Bond Rotation

IWATA, Koichi¹; OZAWA, Ryosuke²;
HAMAGUCHI, Hiro-o²
(¹IMS and Univ. Tokyo; ²Univ. Tokyo)

[*J. Phys. Chem. A* **106**, 3614 (2002)]

Solvent- and temperature-dependent band shape changes of the olefinic C=C stretch Raman band of S_1 *trans*-stilbene have been analyzed on the basis of the dynamic polarization model. The analysis has shown that the solvent-induced dynamic polarization gives rise to the dephasing of the C=C stretch vibration and, concomitantly, triggers and facilitates the rotation around the C=C bond leading to the *trans* to *perpendicular* (and eventually to *cis*) isomerization. Picosecond time-resolved Raman spectra have been measured in three alkane solvents, hexane, octane, and decane at a number of different temperatures ranging from 268 K to 338 K and a total of 40 peak positions and the bandwidths have been determined for the C=C stretch band. The correlation plot of the bandwidth against peak position shows a clear linear relationship that is predicted by the dynamic polarization model.

Picosecond time-resolved fluorescence measurements have been performed in the same three alkane solvents at five different temperatures from 283 K to 313 K and 15 rates of the *trans* to *perpendicular* isomerization have been determined. The plot of the peak position against the rate of isomerization indicates another linear relationship between these two quantities which have no obvious reason to be correlated with each other. The dynamic polarization model accounts very well for this linear relationship and yields a new formula that relates the rate of isomerization to the frequency of the solvent-induced dynamic polarization. This formula seems to possess certain generality because it shows an excellent numerical agreement with the Arrhenius formula. The new formula derived from the dynamic polarization model gives the molecular-level details of the reaction process as to how the reaction is triggered and in what time scale the reaction actually proceeds. A new view of the photoisomerization of *trans*-stilbene has thus been obtained.

V-G-5 Picosecond Dynamics of Stepwise Double Proton-Transfer Reaction in the Excited State of the 2-Aminopyridine/Acetic Acid System

**ISHIKAWA, Hironori²; IWATA, Koichi¹;
HAMAGUCHI, Hiro-o²**
(¹IMS and Univ. Tokyo; ²Univ. Tokyo)

[*J. Phys. Chem. A* **106**, 2305 (2002)]

The dynamics of the amino-imino double proton-transfer tautomerism reaction of the 2-aminopyridine (2AP)/acetic acid system in hexane have been investigated with steady-state absorption, steady-state fluorescence, and picosecond time-resolved fluorescence spectroscopies. It has been confirmed that the double proton transfer reaction takes place in the excited state of the double hydrogen-bonded complex of 2AP with acetic acid. The imino tautomer fluorescence shows a rise behavior with a 5 ps time constant at 480 nm, while a decay with a 5 ps time constant has been observed at 360 nm. The rate of this kinetics is reduced to 7 ps with deuterium substitution. From the comparison with the steady-state fluorescence spectra of proton-transferred model compounds, the 5 ps decaying species has been identified as the intermediate in which one proton is transferred from acetic acid to 2AP. It is thus concluded that the 5 ps time constant represents the second proton-transfer process which follows the first proton transfer that is too fast to be detected in the present experiment. The photoexcited double hydrogen-bonded complex of 2AP and acetic acid undergoes a stepwise double proton-transfer reaction within 5 ps in the excited state.

V-H Structures and Properties of Lanthanoid-Metallofullerenes

Lanthanoid-containing metallofullerenes with C_{82} cages, $M@C_{82}$ (M is a lanthanoid metal atom), are the most widely investigated metallofullerenes. Accordingly to the oxidation state of the metal atom inside, they are classified into two groups; in one the metal atom takes the divalent state, and in the other it takes the trivalent state. Whether the two types of metallofullerenes have a common cage have been one of questions of lanthanoid-metallofullerenes. Recently we revealed that two types of metallofullerenes have a common cage and investigated the correlation between the absorption spectra and the cage structures on lanthanoid-metallofullerenes.

V-H-1 Spectroscopic Studies of Endohedral Metallofullerenes

KODAMA, Takeshi¹; KUSUDA, Masaya¹; OZAWA, Norio¹; FUJII, Ryosuke¹; SAKAGUCHI, Koichi¹; NISHIKAWA, Hiroyuki¹; IKEMOTO, Isao¹; KIKUCHI, Koichi²; MIYAKE, Yoko¹; ACHIBA, Yohji¹

(¹Tokyo Metropolitan Univ.; ²IMS and Tokyo Metropolitan Univ.)

[*New diamond and Frontier Carbon Technology* **11**, 367 (2001)]

We have measured the absorption spectra of the cations of $La@C_{82}$ and $Ce@C_{82}$, which are trivalent-type metallofullerenes. The obtained spectra resemble not only each other but also those of the neutral species of $Ca@C_{82}(IV)$ and $Tm@C_{82}(III)$, which are divalent-type metallofullerenes. Moreover we found that four metallofullerenes have an identical cage. To assign the absorption spectra, we performed a semi-empirical calculation at the level of single configuration interaction for $Ca@C_{82}(IV)$. It was revealed that any charge

transfer transitions from the C_{82} cage to the encapsulated metal atom cannot have large oscillator strength.

V-H-2 Structural Study of Three Isomers of $Tm@C_{82}$ by ¹³C NMR Spectroscopy

KODAMA, Takeshi¹; OZAWA, Norio¹; MIYAKE, Yoko¹; SAKAGUCHI, Koichi¹; NISHIKAWA, Hiroyuki¹; IKEMOTO, Isao¹; KIKUCHI, Koichi²; ACHIBA, Yohji¹

(¹Tokyo Metropolitan Univ.; ²IMS and Tokyo Metropolitan Univ.)

[*J. Am. Chem. Soc.* **124**, 1452 (2002)]

The ¹³C NMR spectra were measured for three isomers of $Tm@C_{82}$, which is one of the divalent metallofullerenes. The molecular symmetries were determined for each isomer: isomer I has C_s symmetry, isomer II has C_2 symmetry, and isomer III has C_{2v} symmetry. Moreover the cage structure of $Tm@C_{82}(III)$ was found to be $C_{82}(9)$. As a result, it was revealed that $Tm@C_{82}(III)$ has a cage identical to that of $La@C_{82}$, which is one of the trivalent metallofullerenes.

V-I Development of Organic Superconductors

Since the discovery of superconductivity in a series of salts of TMTSF, TCF (tetrachalcogenafulvalene) derivatives have served as π -electron donors for the development of new organic superconductors. Although considerable research effort in this field has focused on the construction of TCF-type donors with extended π -conjugation, these donors, except for the DTEDT donor, failed to yield any organic superconductors. Besides TCF derivatives, our reported BDA-TTP donor gives three superconducting salts, but its π -electron system is the as that of TCF derivatives. Then it is possible that donor molecules with a less extended π -system that that of TCF derivatives produce superconductor? We attempted to find an answer to this question in the DHTTF donor system. We have also investigated the properties other salts of BDA-TTP.

V-I-1 New Organic Superconductors Consisting of an Unprecedented π -Electron Donor

NISHIKAWA, Hiroyuki¹; MORIMOTO, Takanobu¹; KODAMA, Takeshi¹; IKEMOTO, Isao¹; KIKUCHI, Koichi²; YAMADA, Jun-ichi³; YOSHINO, Harukazu⁴; MURATA, Keizo⁴

(¹Tokyo Metropolitan Univ.; ²IMS and Tokyo Metropolitan Univ.; ³Himeji Inst. Tech.; ⁴Osaka City

Univ.)

[*J. Am. Chem. Soc.* **124**, 730 (2002)]

We designed and synthesized the DODHT donor with a reduced π -system as well as a bulky cis-fused dioxane ring. This donor forms crystalline salts with AsF_6 and PF_6 that display a variety of the pressure-induced resistive behavior and become superconducting at 3.3 and 3.1 K under 16.5 kbar pressure. X-ray analy-

sis show the donor molecules stacked head-to-tail to form the β'' -type arrangement with weak intermolecular interactions in both salts.

V-I-2 Tetrachloroferrate (III) Salts of BDH-TTP and BDA-TTP: Crystal Structures and Physical Properties

KIKUCHI, Koichi¹; NISHIKAWA, Hiroyuki²; IKEMOTO, Isao²; TOITA, Takashi³; AKUTSU, Hiroki³; NAKATSUJI, Shin-ichi³; YAMADA, Jun-ichi³

(¹IMS and Tokyo Metropolitan Univ.; ²Tokyo Metropolitan Univ.; ³Himeji Inst. Tech.)

[*J. Solid State Chem.* in press]

Three FeCl_4 salts based on non-TTF donors, BDH-TTP and BDA-TTP, have been prepared and characterized as κ -(BDH-TTP) $_2\text{FeCl}_4$, β -(BDA-TTP) $_2\text{FeCl}_4$, and (BDA-TTP) $_3\text{FeCl}_4\cdot\text{PhCl}$. The κ -(BDH-TTP) $_2\text{FeCl}_4$ salt, with a room-temperature conductivity (σ_{rt}) of 39 Scm^{-1} , is metallic down to 1.5 K, and its magnetic susceptibility obeys the Curie-Weiss law with a Curie constant (C) of $4.25 \text{ emuKmol}^{-1}$ and a Weiss constant (θ) of 0.041 K. β -(BDA-TTP) $_2\text{FeCl}_4$ exhibits metallic behavior ($\sigma_{\text{rt}} = 9.4 \text{ Scm}^{-1}$) with a sharp metal-to-insulator (MI) transition ($T_{\text{MI}} = 113 \text{ K}$) and antiferromagnetic ordering with the Néel temperature of near 8.5 K, whereas the solvated (BDA-TTP) $_3\text{FeCl}_4\cdot\text{PhCl}$ salt is a semiconductor with a thermal activation energy of 0.11 eV ($\sigma_{\text{rt}} = 2.0 \times 10^{-2} \text{ Scm}^{-1}$) and exhibits Curie-Weiss behavior ($C = 4.42 \text{ emuK mol}^{-1}$, $\theta = -0.35 \text{ K}$).

V-J Stereodynamics of Crossed Beam Reactions

Reactions of metastable noble gas atoms with small molecules have provided a long-standing interest because of the diversity of reaction channels. Penning ionization consists of a spontaneous ionization of intermediate collisional complex, therefore it is a process of fundamental interest behind its importance in plasma and astrochemistry. It has been demonstrated that Penning ionization probes the electron density distribution of the orbital from where the electron is removed, and the collision energy dependence of the ionization cross section has been suggested to be a good measure to clarify anisotropy of intermolecular forces. The reactivity depends not only on the anisotropy of the coupling matrix but also on stereo-anisotropic intermolecular forces. Therefore we study how such steric effect depends on collision energy, as well as on mutual orientation of reactants.

V-J-1 Stereo-Selectivity in the Penning Ionization Reaction of CH_3X ($\text{X} = \text{Cl}, \text{Br}, \text{I}$) + $\text{Ar}({}^3\text{P}) \rightarrow \text{CH}_3\text{X}^+ + \text{Ar} + \text{e}^-$

OKADA, Seiki¹; OHOYAMA, Hiroshi¹; KASAI, Toshio²
(¹Osaka Univ.; ²IMS and Osaka Univ.)

[*Chem. Phys. Lett.* **355**, 77 (2002)]

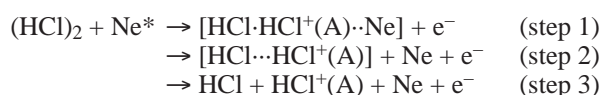
Recently, we have performed the direct observation of steric effect in CH_3Cl Penning ionization with the metastable argon atom using the hexapole state-selector, and we verified a good correlation between stereo-selectivity in the Penning ionization cross section and the spatial distribution of the electron density of HOMO orbital of the CH_3Cl molecule. In order to substantiate the above-mentioned relationship, we extended the study by replacing halogen atom of the molecule. In the present study, we determined the steric opacity functions for the two similar Penning ionization reactions of CH_3X ($\text{X} = \text{Br}, \text{I}$) + $\text{Ar}({}^3\text{P}) \rightarrow \text{CH}_3\text{X}^+ + \text{Ar} + \text{e}^-$ at an average collision energy of 0.1 eV. We find that the most reactive site shifts from the collinear X-end toward sideways as the mass number of X increases (i.e. from Br to I). Taking into account the previously obtained result for the CH_3Cl reaction, a good correlation can be seen again between the steric opacity function and the electron density distributions of the lone-pair HOMO orbital of CH_3X molecule.

V-J-2 Evidence for the $\text{HCl}^+(\text{A})$ Formation in the Reaction of $\text{Ne}({}^3\text{P})$ with the Size-Selected HCl Dimer Using an Electrostatic Hexapole Field

IMURA, Kohei; OHOYAMA, Hiroshi²; KASAI, Toshio¹
(¹IMS and Osaka Univ.; ²Osaka Univ.)

[*Chem. Lett.* 1136 (2001)]

There has been no evidence so far that reaction of $\text{Ne}({}^3\text{P})$, with the HCl dimer produces $\text{HCl}^+(\text{A})$, though the corresponding HCl monomer reaction produces $\text{HCl}^+(\text{A})$ in the vibrational states $\nu' = 0, 1$, and 2. Naaman and co-workers pointed out that chemical reactivity of monomers and clusters strongly depends on species of the reactant atom. For the $\text{Ne}^*(\text{HCl})_2$ reaction, there are many exit channels open such as electronic excitation, ionization, and dissociation from energetic point of view. In this work, Penning ionization of $\text{Ne}({}^3\text{P})$ metastable atom with size-selected HCl dimer was studied by using an electrostatic hexapole state-selector and chemiluminescence detection. We find that the HCl dimer can also produce $\text{HCl}^+(\text{A})$ ions in the reaction with $\text{Ne}({}^3\text{P})$ just like its corresponding monomer reaction. The internal energy distribution of $\text{HCl}^+(\text{A})$ in the dimer reaction is found to be cooler than that in the monomer reaction, reflecting the third-body effect in the dimer. The suggested reaction scheme is shown as follows.



V-K Photodissociation Dynamics

Photo-initiated reaction of weakly hydrogen bonded halide dimer, $(\text{HX})_2$, has a basic potentiality to produce $[\text{XHX}]$ transient specie by means of the hydrogen atom elimination from $(\text{HX})_2$ dimer. By measuring translational energy distribution of the eliminated hydrogen atom, one can extract information about van der Waals interaction of reactants in the $\text{X} + \text{HX}$ reaction system. We study the 243-nm photo-dissociation of the DCI clusters by using a Doppler-selected TOF (DS-TOF) technique in order to detect $[\text{CIDCI}]$ transient species. We employed the hexapole method to select only the DCI dimer in cluster beam and to exclude any ambiguity about precursor cluster size.

V-K-1 Photodissociation of DCI Dimer Selected by an Electrostatic Hexapole Field Combined with Doppler-Selected TOF Technique: Observation of [CIDCI] Transient Species

CHE, Dock-Chil; HASHINOKUCHI, Mitihiro¹; SHIMIZU, Yuichiro; KASAI, Toshio¹
(¹IMS and Osaka Univ.)

[*Phys. Chem. Chem. Phys.* **3**, 4979 (2001)]

The photodissociation of DCI dimer, which is preferentially selected from the cluster beam using a hexapole electrostatic field prior to the photolysis, has been studied by a Doppler-selected time-of-flight (DS-TOF) technique at 243 nm. We observed the [CIDCI] transient species through the hydrogen atom elimination from (DCI)₂. By measuring the dependence of the enhancement for the photodissociated D-atom signal upon the hexapole voltage, we find that the DS-TOF spectrum exhibits two kinds of velocity components; one is fast velocity component which originates from only dimer photodissociation, and the other is slow velocity component which originates from not only dimer but also higher sizes of the DCI clusters. For the fast velocity component, the observed spectrum shows an oscillating structure, which could reflect a footprint of nascent internal states (mainly vibration) of the [CIDCI] transient species. The spacing of the observed peaks is about 1000 cm⁻¹, which is much smaller than

that of the normal stretching frequency (2091 cm⁻¹) of the DCI monomer. This result suggests that the observed spectrum reflects the strong perturbation from the Cl atom in [CIDCI].

V-K-2 A New Channel of Hydrogen Elimination in the 121.6-nm Photodissociation of Formic Acid Detected by a Doppler-Selected TOF Mass Spectrometry

HASHINOKUCHI, Mitihiro¹; KOUMURA, Ryouji²; CHE, Dock-Chil; KASAI, Toshio¹
(¹IMS and Osaka Univ.; ²Osaka Univ.)

[*J. Mass Spectrom. Soc. Jpn.* **50**, 7 (2002)]

The 121.6-nm photodissociation of formic acid was investigated by a Doppler-Selected TOF mass spectrometry (DS-TOF-MS) that enables us to map out 3D velocity distributions of photodissociated products through REMPI for the H atoms. The main channel is found to be the HCOO* formation. A new channel of H + CO + OH(X) hydrogen elimination reaction is observed. We estimate that the branching ratio to [H + HCOO*] with respect to [H + CO + OH(X)] is ~ 5 and those to HCOO(X), HOCO(X) and [2H + CO₂] formation channels are very small. These results show that the DS-TOF-MS method is useful to determine branching ratios and internal energy distributions of photodissociated products in both excited and ground states.

V-L Non-Destructive Structure Determination of Neural Clusters

Van der Waals clusters give a great interest as interfaces on chemical and physical properties between the gas phase and the condensed phase. Especially, the relationship between structure and dynamics is often called stereodynamics. From this sense, it is important to determine structure of cluster and to select special size and/or geometric isomers of cluster. In general, relative population of geometric isomers has been discussed in terms of stability of the isomers at equilibrium structure, but such a common sense is not necessarily appropriate in the case if dynamics of the cooling process induces special selectivity on isomer formation. It is plausible that different conditions for cluster beam preparation produced different clusters. Along this context, we investigate cooling process of geometric isomers during cluster formation.

V-L-1 Focusing and Selecting the Linear Type HBr-N₂O by Using a 2 m Long Electrostatic Hexapole Field

OKANO, Akihiko¹; OHYAMA, Hiroshi¹; KASAI, Toshio²
(¹Osaka Univ.; ²IMS and Osaka Univ.)

[*J. Chem. Phys.* **116**, 1325 (2002)]

Although N₂O-HCl and N₂O-HBr are expected to have similar two types of geometric isomers from the analogs of ONN-HF, it has been reported that extensive searches revealed only bent N₂O-HCl and N₂O-HBr and that there was no trace of linear ONN-HCl or

ONN-HBr. We performed focusing and selecting the HBr-N₂O cluster beam by using a 2m-long electrostatic hexapole field. The observed focusing curve shows a clear evidence that the linear type HBr-N₂O isomer which has symmetry of symmetric top molecule was preferentially produced in the cluster beam nevertheless our previous *ab initio* calculation predicts the bent type isomer. The best fit simulation for the experimental focusing curve was achieved only if we assume vibrational excitation in the van der Waals mode of the linear type HBr-N₂O. The permanent dipole moment is determined to be 0.70 ± 0.05 D. The potential energy of the O-end bent type is more stable than the N-end linear type. From the potential energy surface made by transferring HBr-N₂O geometry, the formation of the

two isomers is selected at a fairly long bond length between HBr and N₂O.

V-M Reaction Dynamics at Surfaces

The interaction of hydrogen with surfaces has been a subject of intense interest in surface science because it is the simplest paradigm relevant to single valence electron. The reaction of hydrogen on a surface can be an ideal candidate for testing validity of various concepts in surface chemical reaction. Also, it is known that adsorbed hydrogen can provide a significant effect on kinematical and electronic properties in the surface region of materials, inducing embrittlement and fracture. To understand how hydrogen interacts with surface atoms and reacts with other atoms on the surface and its possible diffusion into and from the bulk is important in various fields; heterogeneous catalysis, material science, metallurgy, hydrogen storage, etc. These phenomena embodied in hydrogen interaction with metal surfaces encompass most of basic physical and chemical concepts in material science.

V-M-1 Hydrogen-Exchange Reactions *via* Hot Hydrogen Atoms Produced in the Dissociation Process of Molecular Hydrogen on Ir{100}

MORITANI, Kousuke¹; OKADA, Michio¹;
NAKAMURA, Mamiko¹; KASAI, Toshio²;
MURATA, Yoshitada³

(¹Osaka Univ.; ²IMS and Osaka Univ.; ³Univ. Electro-Commun.)

[*J. Chem. Phys.* **115**, 9947 (2001)]

Adsorption of hydrogen(deuterium) on Ir{100} surface has been studied with temperature-programmed desorption and direct measurements of describing molecules using quadrupole mass spectrometry at ~ 100 K. H₂ exposure of the D-pre-covered Ir{100} surface was found to induce the desorption of HD and D₂ molecules. This result can not to be explained by conventional simple adsorption/desorption kinetics and it suggests that energetic H atoms (hot H atoms) produced in the dissociation process of incident H₂ molecules react with pre-adsorbed D atoms and then desorb as HD molecules or produces secondary energetic D atoms via energy transfer. Secondary energetic D atoms also induce associative reactions with pre-adsorbed D atoms and desorb as D₂ molecules. We propose the hot-H-atom-mediated reaction based on both empirical and steady-state approximation models for interpreting the present experimental results.

V-N Simulation of Molecular Clusters

Monte Carlo simulation is a powerful method for studying soft matter such as polymer, gel and biological molecules. We performed the structure analysis of chemical gel and characterized gel with cross-linkers. For vesicles, we studied self-assembly, fusion, adhesion and structural changes due to mechanical forces. In both systems, we obtained qualitatively good agreement with experimental results, and gave some insights to the mechanism of order formation of soft matter.

V-N-1 Characterization of Gel Using Modeled Radical Polymerization with Cross Linkers Performed by Monte Carlo Method

NOSAKA, Makoto¹; TAKASU, Masako¹; KATOH, Kouichi²

(¹IMS and Kanazawa Univ.; ²Kanazawa Univ.)

[*J. Chem. Phys.* **115**, 11333 (2001)]

In this study, some physical quantities for characterization of gel are proposed. Polymer networks (gel) are investigated by Monte Carlo simulation using modeled free-radical cross-linked polymerization in continuous system. The distributions of degree of polymerization for clusters obtained in this simulation show qualitatively good agreement with the experimental results. Linkers are classified to two types according to the roles in networks, and their ratios are discussed. The normal and weighted ratios of gel are defined using percolation theory. These ratios are compared with the changes in distribution.

V-N-2 Analysis of Intra- and Inter-Linkers in Gels by Brownian Dynamics Simulation

NOSAKA, Makoto¹; TAKASU, Masako¹

(¹IMS and Kanazawa Univ.)

The process of gelation was analyzed by Brownian dynamics simulation using modeled radical polymerization with cross-linkers. Particle densities were set near the gelation threshold determined experimentally (monomer density $d = 200$ mM 400 mM and 600 mM). We performed simulations under two conditions that did (Rule D) and did not (Rule A) prohibit the formation of intra-linkers. With Rule D, we observed gelation at $d = 600$ mM, and clustering at $d = 400$ mM. On the other hand, with Rule A, we did not observe gelation with any of the densities tested. We only observed clustering at $d = 600$ mM. Some quantities were investigated by comparing the results under the two conditions.

V-N-3 Self-Assembly of Amphiphiles into Vesicles: a Brownian Dynamics Simulation

NOGUCHI, Hiroshi; TAKASU, Masako¹

(¹IMS and Kanazawa Univ.)

[*Phys. Rev. E* **64**, 041913 (2001)]

We studied the vesicles of amphiphilic molecules using a Brownian dynamics simulation. An amphiphilic molecule is modeled as the rigid rod, and the hydro-

phobic interaction is mimicked by the local density potential of the hydrophobic particles. The amphiphilic molecules self-assemble into vesicles with bilayer structure. The vesicles are in fluid phase, and we calculated the lateral diffusion constant and the rate of the flip-flop motion of molecules in vesicles. The self-assembly kinetics into vesicles was also investigated.

V-N-4 Fusion Pathways of Vesicles, a Brownian Dynamics Simulation

NOGUCHI, Hiroshi; TAKASU, Masako¹

(¹IMS and Kanazawa Univ.)

[*J. Chem. Phys.* **115**, 9547 (2001)]

We studied the fusion dynamics of vesicles using a Brownian dynamics simulation. Amphiphilic molecules spontaneously form vesicles with a bilayer structure. Two vesicles come into contact and form a stalk intermediate, in which a necklike structure only connects the outer monolayers, as predicted by the stalk hypothesis. We have found a new pathway of pore opening from stalks at high temperature: the elliptic stalk bends and contact between the ends of the arc-shaped stalk leads to pore opening. On the other hand, we have clarified that the pore-opening process at low temperature agrees with the modified stalk model: a pore is induced by contact between the inner monolayers inside the stalk.

V-N-5 Adhesion of Nanoparticles to Vesicles: a Brownian Dynamics Simulation

NOGUCHI, Hiroshi; TAKASU, Masako¹

(¹IMS and Kanazawa Univ.)

[*Biophys. J.* **83**, 299 (2002)]

We studied the interaction of bilayer vesicles and adhesive nanoparticles using a Brownian dynamics simulation. The nanoparticles are simple models of proteins or colloids. The adhering nanoparticle induces the morphological change of the vesicle: budding, formation of two vesicles in which only outer monolayers are connected, and fission. We also show that the nanoparticle promotes the fusion process: fusion-pore opening from a stalk intermediate, a neck-like structure that only connects outer monolayers of two vesicles. The nanoparticle bends the stalk, and induces the pore opening.

V-N-6 Structural Changes of Pulled Vesicles: a Brownian Dynamics Simulation

NOGUCHI, Hiroshi; TAKASU, Masako¹
(¹IMS and Kanazawa Univ.)

[*Phys. Rev. E* **65**, 051907 (2002)]

We studied the structural changes of bilayer vesicles induced by mechanical forces using a Brownian dynamics simulation. Two nanoparticles, which interact repulsively with amphiphilic molecules, are put inside a vesicle. The position of one nanoparticle is fixed, and the other is moved by a constant force as in optical-trapping experiments. First, the pulled vesicle stretches into a pear or tube shape. Then the inner monolayer in the tube-shaped region is deformed, and a cylindrical structure is formed between two vesicles. After stretching the cylindrical region, fission occurs near the moved vesicle. Soon after this the cylindrical region shrinks. The trapping force ~ 100 pN is needed to induce the formation of the cylindrical structure and fission.

V-O Development of Broadband Solid-State NMR Spectroscopy

There are two different fields of solid-state NMR. One is biological, chemical and polymer NMR and the other is magnetic or metallic NMR. The former NMR employs resonant-type NMR probes, which can be tuned only over bandwidth of a few 100 kHz. Nuclear spins are controlled very precisely by sculpted RF pulse sequences. The unambiguous assignments of the lines are possible by using chemical shifts and spin-spin or dipolar couplings. One big outcome is that NMR teaches us not only a local information of an observed nucleus, but also correlations between different nuclei. The NMR parameters offered challenging problems for quantum chemical calculations and are now well predictable. The commercialization promoted rapid developments of sophisticated instruments with high resolution and sensitivity and the developments seems to be almost completed. However, in magnetic or metallic samples, most NMR works have been focused on only local information, like Knight shifts, hyperfine couplings, and relaxation times. Two-dimensional correlation NMR seems to be unpopular for these samples.

In magnetic and metallic samples, usually resonance lines are much broader than the diamagnetic samples. Ordinary resonant type NMR probes have a narrow tuning range and are inconvenient. It is possible to observe the spectra by a magnetic field sweep and with a fixed carrier frequency. However, sometimes the magnetic properties depend on the strength of static magnetic field. For example, the chemical shift of conducting samples can be field dependent due to the de Haas-van Alphen Effect (more generally Aharonov-Bohm effect).^{1),2)} We may also need a broadband NMR probe for frequency sweep experiments for studying such a subject. For ferromagnetic samples, the sensitivity of NMR is enhanced because motions of nuclear spins are coupled with motions of a macroscopic magnetization or domain walls. Detuned coils have been often used in a frequency sweep spectrometer. However, if the sensitivity is optimized, it may be possible to observe small patterned films, where various domain structures were theoretically investigated.

Here we reexamined a transmission line NMR probe, which was proposed by Lowe and coworkers in 70s.^{3),4)} The probe is expected to work in a wide frequency range below a certain cut-off frequency. The circuit resembles to that of a low-pass filter, which consists of π sections with a coil and two capacitors. The characteristic impedance must be adjusted to cable impedance by choosing an appropriate capacitance value. Some numerical results have been described in a previous report. We extended the numerical works from flat transmission coils to cylindrical transmission coils, since the latter form was easier to produce by using tip capacitors.

When we have a broadband NMR probe, we also need a broadband RF generator. Adiabatic pulses may be very effective for this purpose. Other types of selective RF pulses may be also useful, when we excite only a part of a spectral region. Conventional rectangular pulses are inconvenient, since its excitation envelope extends over a wide frequency range. Pulse shaping is commonly employed in a solution state spectrometer. However, for solid samples, the modulation must be much faster than the solution. Even in many high-resolution solid state NMR works, a phase transient due to a fast RF switching have been ignored. Using a fast RF modulator can solve these problems and fast modulated RF pulses. It would be also an attractive subject how various forbidden transitions can be controlled by shaped RF pulses.

References

- 1) R.G. Goodrich, S. A. Khan and J.M. Reynolds, *Phys. Rev. B* **3**, 2379 (1971).
- 2) A. Kubo, "Field dependent chemical shift of mesoscopic samples," Bunshikoukou-zou-toronnkai, Kobe, 3P091 (2002).
- 3) I. J. Lowe and M. Engelsberg, *Rev. Sci. Instrum.* **45**, 631 (1974).
- 4) I. J. Lowe and D. W. Whitson, *Rev. Sci. Instrum.* **48**, 268 (1977).

V-O-1 Numerical Simulations and Experiments on the Transmission Line Probe

KUBO, Atsushi¹; ICHIKAWA, Shinji²
(¹IMS and Kyoto Univ.; ²Toyama Science Museum)

Previously, we have reported the numerical simulations of flat transmission line coils. We extended the simulation to cylindrical transmission line coils and constructed NMR probes by using the cylindrical coils. Lowe and co-workers mentioned that flat coils have advantages of the construction and the RF field homogeneity. However, our numerical result showed the homogeneity of a cylindrical coil was comparable to that of a flat coil. The homogeneity was mainly caused by the reflections of RF at the both ends of the coil, where the characteristic impedance was different from

the value at the coil center. The RF field strength decreases as the carrier frequency increases, because there is a phase delay between neighboring coil sections. The

$$\nu_d^{\text{cylinder}} = (Z_0 / \pi^2 \mu_0 a) (p/a)^2$$

characteristic decay frequency is given by where Z_0 , p , and a are a characteristic impedance, a pitch, and a diameter of the coil. The resonance frequency of the observed nuclei must be smaller than ν_d^{cylinder} . This condition restricts the size of the coil. We wound coils with the size $a = 2.3$ mm and $p = 1.2$ mm. At first, we made probes with $Z_0 = 50 \Omega$. The RF field strength at 400 MHz (¹H) was determined to be 60 kHz in experiments and was calculated to be 40 kHz for an input RF power of 100 W. However, the RF field strength of the ²³Na experiments at 106 MHz was found

much weaker (11 kHz) both in the experiments and in the calculation. The RF field strength was improved by twice when Z_0 was decreased to 12.5Ω and $\lambda/4$ cable impedance transformers were inserted at both the input and the output ports. The bandwidth was reduced to 30 MHz if $\lambda/4$ cable transformers were used. It is still much larger than the bandwidth of the ordinary resonant probe.

There are still some rooms for a further implementation. Noise of NMR signals is determined by resistive components in a probe circuit. In a transmission line probe, one port of the probe is terminated by a load or a transmitter (or a receiver). RF switches connect and disconnect them. The noise may be mainly generated at the load. If the load is cooled or resistance at load is reduced by appropriate impedance transformations, the signal to noise ratio might be improved. An ideal load must generate no thermal noise and absorb the signal completely. It may be also attractive to use a superconductor for the NMR probe circuit. One big problem of superconducting NMR probes (mainly used MRI) is that the probe Q becomes too high. The bandwidth of the probe is typically about 40 kHz, which allows only the observation of solution-state ^1H signals. The transmission line probe has a fast recovery time as a coaxial cable if the impedance is properly matched with the feeding and the receiving cables. More flexible design of superconducting probes may be possible by using transmission lines.

tion technologies. If there are several users who are interested in our fast digital RF modulator, it may be possible to order a company, who has a soldering machine, to make the printed circuit boards.

V-O-2 Developments of Fast Digital RF Frequency Modulator

YOSHIDA, Hisashi; KUBO, Atsushi¹
(¹IMS and Kyoto Univ.)

We used a quadrature digital upconverter AD9857 (Analog Devices). This IC generates the carrier signals and mixes them with the modulation signals digitally, so that the modulated RF output ($f_0 + f_m$) is expected to be free from the leakage of the carrier frequency signals (f_0) and the counter-quadrature signals ($f_0 - f_m$), which are unavoidable in analog modulators. We added a memory module for supplying digital amplitude data to AD9857. The memory module contains a large SRAM (256k words) and small SRAMs (2k words) for storing series of shaped pulses, starting addresses, and numbers of data in a shaped pulse, respectively. The memory module is controlled by three external TTL signals. It can be used in either a single pulse mode or a CW mode. In the latter mode, a shaped pulse is repeated until the external TTL signal is turned to high. The other TTL signals are employed to initialize the start address and to trigger pulsing. For the details of the design, please contact with Mr. Yoshida in Equipment Development Center. Some fast ICs were only available in a TSSOP package (lead pitch 0.65 mm). Mr. Yoshida did quite elaborate soldering works. Although commercial fast function generators are available, it is quite expensive and is not so convenient for magnetic resonance experiments. It may also have some pedagogical merit to know the actual design of the modulator, since the RF modulation is commonly used in communication technologies, and is a prototype of optical communica-

RESEARCH ACTIVITIES VI

Department of Vacuum UV Photochemistry

VI-A Electronic Structure and Decay Mechanism of Inner-Shell Excited Molecules

This project is being carried out at the Beamline 4B of the UVSOR facility. We have three subprojects: (A) spin-orbit, exchange, and molecular field splittings in S $2p$ and P $2p$ excited states, (B) molecules and radicals in condensed phase and in rare gas matrix, and (C) ionic fragmentations following the inner-shell resonance excitation. In (A), we have found some spin-forbidden ionized and excited states in non-radiative (photoelectron emission) and radiative (photon emission) deexcitation spectra in collaboration with the Uppsala University. In (C), we are concentrating on theoretical interpretation of our experimental data measured for last several years.

VI-A-1 Spin-Forbidden Shake-Up States in the Valence Ionization of CS₂

HATSUI, Takaki; NAGASONO, Mitsuru¹;
SHIGEMASA, Eiji; KOSUGI, Nobuhiro
(¹Kyoto Univ.)

Photoelectron spectroscopy (PES) is widely used to investigate the one-electron energy level in various systems. All lines which have been observed so far in PES are doublet ionized state in the case of molecules with singlet ground state. The shake-up satellites can be enhanced by exciting at resonances. In this report we for the first time demonstrate that invisible (dark) spin-forbidden states in non-resonant PES can be observed by PES at sulfur $2p$ resonances with strong singlet-triplet mixing *via* spin-orbit coupling of the sulfur $2p$ core electrons. Figure 1 shows an example of our PES of CS₂, recorded on the S $2p_{3/2} \rightarrow 3\pi_u^*$ resonance and below the resonance. Within the (LS) coupling scheme, the excited states are described as strongly mixed states with singlet and triplet components, where the intensity comes from dipole-allowed singlet components. Intermediate states in the resonant PES have triplet components as well, which open up transitions to quartet ionized states in addition to doublet states. Satellite 0 is not observed in the non-resonant spectrum at all. Satellite 1 is assigned to the lowest doublet shake-up state with the $^2\Pi_u$ symmetry [1] allowed in the non-resonant PES spectra. The satellite 0 is assigned to a transition to the quartet counterpart ($^4\Pi_u$) of the doublet state based on *ab initio* configuration interaction calculations.

Reference

1) P. Baltzer *et al.*, *Chem. Phys.* **202**, 185 (1996).

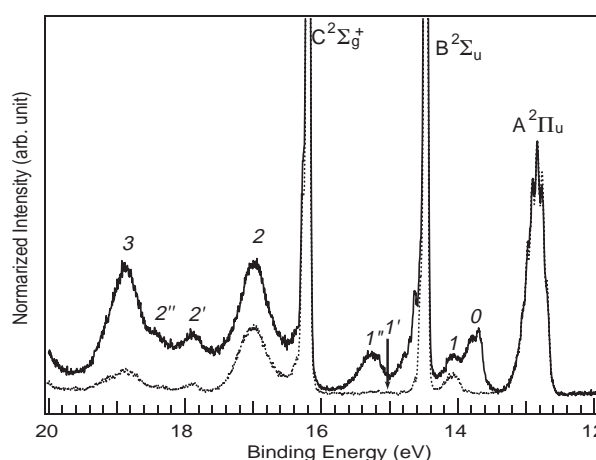


Figure 1. PES spectrum of CS₂ recorded at the $2p_{3/2} \rightarrow 3\pi_u^*$ resonance (163.22 eV) and non-resonant spectrum recorded below the sulfur $2p$ excitation region (151.2 eV).

VI-A-2 Spin- and Symmetry Forbidden Ionized States of OCS Molecule

MASUDA, Suomi¹; HATSUI, Takaki;
SHIGEMASA, Eiji; KOSUGI, Nobuhiro
(¹GUAS)

Some satellite structures in the photoelectron spectrum (PES) are enhanced by exciting at the resonances. In this work, we have measured resonant PESs of OCS molecule and successfully found the spin- and symmetry forbidden shake-up states ($^4\Pi$ and $^2\Phi$) as well as the lowest double shake-up state ($^2\Pi$).

Photoabsorption spectrum of OCS shows transitions to $4\pi^*$, $10\sigma^*$ and Rydberg states below the sulfur $2p$ ionization threshold. Due to the spin-orbit interaction, each transition is split into the $2p_{3/2}$ and $2p_{1/2}$ manifolds. Figure 1 shows resonant PES of OCS at the $2p_{3/2} \rightarrow 4\pi^*$ resonance (solid line) as well as an off-resonance one (dotted line). In the non-resonant PES, a very weak band 1 is clearly observed, which is assigned to the lowest $^2\Pi$ shake-up satellite, of which the intensity is borrowed from the A state ($^2\Pi(2\pi^{-1})$). In the resonant case, additional strong satellite bands 0 and 2 are found. These satellites are not observed in the non-resonant PES. Based on *ab initio* MRCI calculations, the bands 0

and 1 are assigned to the quartet and doublet Π satellites with the $(3\pi_x^{-1} 3\pi_y^{-1} 4\pi^{+1})$ electron configuration. The Band 2 is assigned to be the lowest symmetry-forbidden ${}^2\Phi$ states.

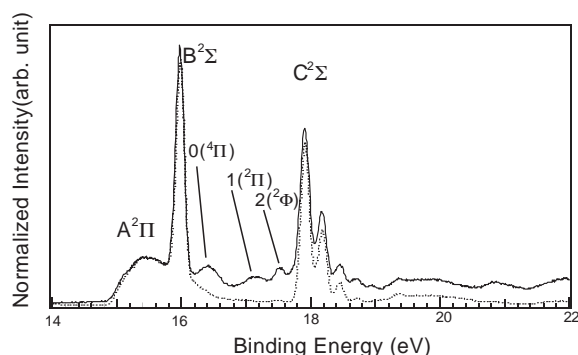


Figure 1. Photoelectron spectra of OCS molecule excited at the $2p_{3/2} \rightarrow 4\pi^*$ resonance (164.4 eV) (solid line) and at off-resonance 10 eV below the $2p_{3/2} \rightarrow 4\pi^*$ resonance (dotted line).

VI-A-3 Measurements of Sulfur 2p Photoelectron and Sulfur L-emission of SF₆ at Sulfur 2p Resonances

KOSUGI, Nobuhiro; HATSUI, Takaki; GUO, Jinghua¹; NORDGREN, Joseph²
(¹Lawrence Livermore Natl. Lab.; ²Uppsala Univ.)

The sulfur 2p photoabsorption spectrum of SF₆ molecule shows strong valence excitations and shape resonances as well as very weak Rydberg series (inset in Figure 1), which are characteristic of systems surrounded by electronegative atoms. In this study, sulfur 2p photoelectron spectra and sulfur L-emission spectra have been measured at these resonances. At the resonances below the threshold, triplet valence excited states are found in the soft x-ray emission spectra through singlet-triplet mixed 2p excitations due to the spin-orbit interaction. Above the ionization threshold, dependence upon the excitation energy is generally small in most cases because non-resonant contribution is dominant. In the case of SF₆, the branching ratio between $2p_{3/2}$ and $2p_{1/2}$ photoelectron peaks, however, shows distinct variation upon the excitation energy in photoelectron spectra (Figure 1) and emission spectra. This behaviour has been attributed to the strong exchange interaction between core hole and excited electron at the resonances.

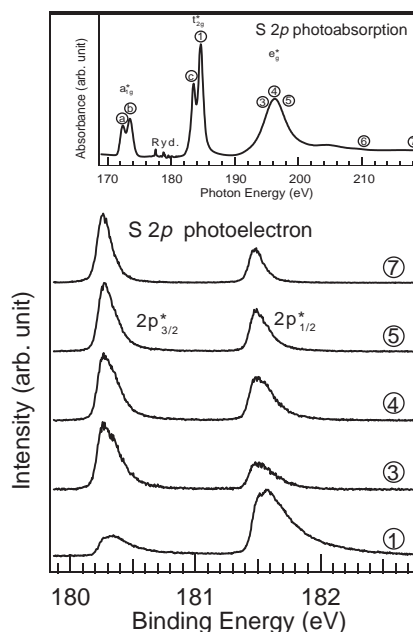


Figure 1. Photoelectron spectra of SF₆ recorded at the sulfur 2p resonances (shown in inset).

VI-A-4 N 1s Photoabsorption of N₂ Trapped in Rare Gas Matrices

NAGASONO, Mitsuru¹; OJI, Hiroshi; HATSUI, Takaki; SHIGEMASA, Eiji; KOSUGI, Nobuhiro
(¹Kyoto Univ.)

The gaseous N₂ spectrum shows complex structures in the N 1s threshold region, resulting from resonances by transitions into π^* , σ^* , Rydberg and multiple-electron excited states. Some of them have diffuse character and should have environmental effects around the molecule. In the present work, we have measured N 1s excitation spectra of N₂ trapped in rare gas matrices.

On a new beamline BL4B at UVSOR, N 1s photoabsorption spectra were measured with an electron yield method for rare-gas matrix isolated and condensed N₂, and with a transmission method for gaseous N₂. Samples were prepared by mixing gaseous N₂ with rare gas, Ne, Ar, Kr or Xe, in a vacuum vessel and evaporated on an Au coated Cu plate. The temperature of the plate was below 6.5 K by a cryostat. The ratios N₂ to rare gas were 1/10 and 1/1.

Figure 1 shows that 3s and 3p Rydberg-like excited states exhibit blue shifts in photon energy in the matrix phase. The shift of the Rydberg excitation energy is determined by competition between the shifts of the ionization potential and the term value. The ionization potential becomes smaller as the distance between the N₂ and the neighbors, or the cage size, smaller. On the other hand, the term value is related to the antibonding character in the Rydberg state, and the antibonding character depends on the overlap of the Rydberg orbital with the valence orbital of the neighbor species; that is, the term value becomes smaller as the cage size smaller. Thus, the observed matrix effect indicates that the variation of the term value for the 3s and 3p Rydberg is larger than that of the ionization potential.

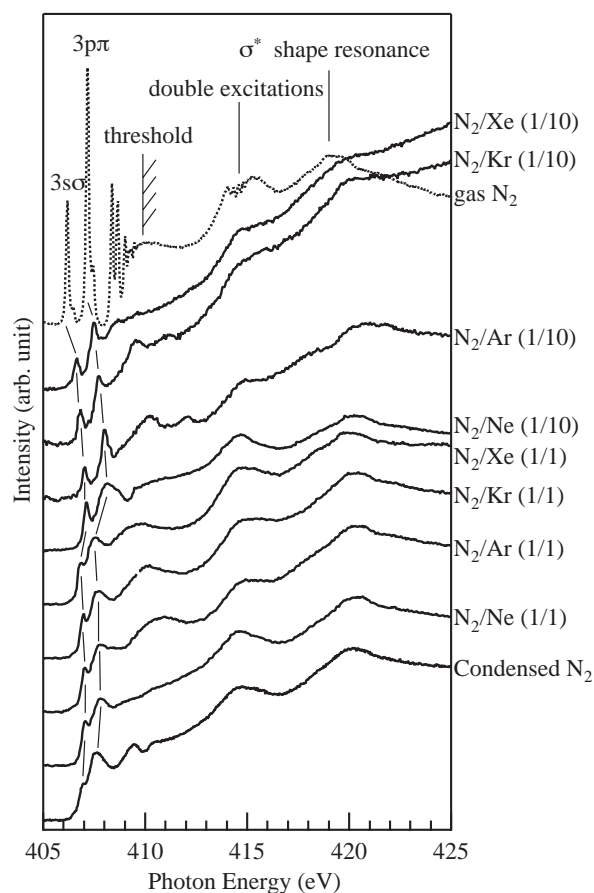


Figure 1. The N $1s$ photoabsorption spectra near the N $1s$ ionization threshold region for the N₂ in gaseous phase, rare gas matrix phases and condensed phase.

VI-A-5 Ab Initio CI Calculation for O $1s \rightarrow \sigma^*$ Core-Excited States of Ozone: Difference in Direction between Transition Dipole Moment and Photodissociation

OJI, Hiroshi; KOSUGI, Nobuhiro

The transition dipole moment (μ) for the O $1s \rightarrow \sigma^*(7a_1)$ excitation of O₃ were calculated by *ab initio* configuration interaction (CI) method. Accurate evaluation of μ is necessary to investigate detailed dynamics of photodissociation of polyatomic molecules following the core-excitation, since the direction of μ with respect to the bond axis acts as an essential factor in determining the anisotropy parameter for fragment species. We have examined molecular structure dependence of μ by changing the length of one bond in O₃.

The molecular structure of O₃ with the definitions of bond-length R , R' , ϕ and the axes of coordinates are illustrated in Figure 1(a). The MO patterns for ground and core-excited states at the equilibrium structure ($R = R' = 0.127$ nm, $\phi = 118^\circ$) obtained by one electron approximation are shown in Figure 1(b). In the ground state, the shape of MO reflects its C_{2v} symmetry and there is some deviation between the direction of μ and that of O_a–O_c bond axis. In the core excited state, the shape is strongly distorted by core excitonic effect, but μ is not still parallel with the bond. The results of CI calculation was $\theta = 8.34^\circ$, as seen in Table 1. If the

length of R is shortened, θ becomes larger. On the other hand, when R is lengthened, θ gradually decreases, but does not become almost 0 until $R = 0.25$ nm. The present results indicate that the direction of the $1s \rightarrow \sigma^*$ transition dipole μ is not always parallel to the σ bond and more or less affected by the neighboring atoms that are not directly connected with the core-excited atom.

Table 1. Results of the CI calculation for the components of μ (μ_x , μ_z) and the angle between the directions of μ and O_a–O_c bond (θ) as functions of R , when the terminal O (O_a) core is excited.

R / nm	μ_x / a.u.	μ_z / a.u.	θ / deg
0.120	0.013663	-0.038903	19.35
0.125	0.019042	-0.050656	12.19
0.127	0.007505	-0.051173	8.34
0.140	0.004682	-0.054426	4.92
0.170	0.003143	-0.054332	3.31
0.200	0.002290	-0.055824	2.35
0.250	0.000128	-0.057585	0.13

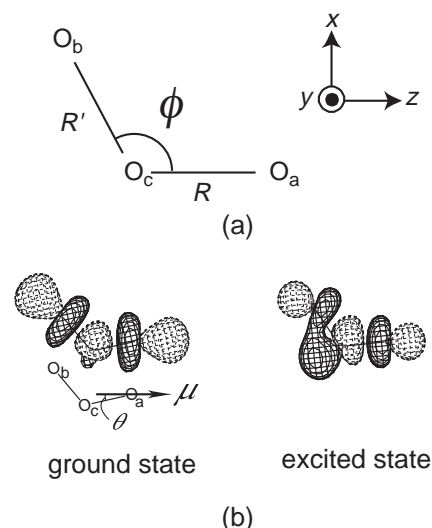


Figure 1. (a) The structure of O₃. The axis of coordinate used in the calculation is also illustrated. (b) MO patterns of $\sigma^*(7a_1)$ of O₃ in the ground and excited states when the terminal oxygen (O_a) core is excited. The definition of the angle θ is illustrated.

VI-B Soft X-Ray Photoelectron-Photoabsorption Spectroscopy and Electronic Structure of Transition Metal Compounds

In this project, we were using the crystal monochromator Beamline 1A of the UVSOR facility, which restrict the photon energy to the range higher than the Ni 2p edge (> 800 eV), but now are using Beamline 4B, covering the lower photon energy (< 800 eV). We can excite the first row elements to their 1s resonance states. We are interested in linear polarization dependence of inner-shell resonant excitations for planar complex molecules/ions in the single crystal, and in resonantly-emitted photoelectron by tuning the photon energy to inner-shell resonances. Dr. Hiroshi Oji has been working as a postdoctoral IMS fellow since April 2000, and Dr. Takaki Hatsui as a research associate since August 2000.

VI-B-1 B 1s- and La 4d-Edge Photoabsorption and Resonant Photoelectron Spectroscopy of Rare-Earth Borocarbide LaB₂C₂

OJI, Hiroshi; HASEGAWA, Shinji; SUZUKI, Kazuya¹; KOSUGI, Nobuhiro
(¹Yokohama Natl. Univ.)

Last year we reported the La 3d-edge X-ray absorption spectroscopic (XAS) and valence-band resonant photoelectron spectroscopic (RPES) studies of lanthanum borocarbide (LaB₂C₂) at UVSOR-BL1A, where we could obtain the information about the degree of charge transfer between La atoms and BC sheets. In the present work, B 1s-edge (~ 200 eV) and La 4d-edge (~ 100 eV) XAS and valence-band RPES were measured at the BL4B soft X-ray beamline of the UVSOR facility to obtain further information about the electronic structure of LaB₂C₂.

La 4d-edge XAS spectrum of LaB₂C₂ is shown in Figure 1. The assignments of the peaks are indicated in the figure.¹⁾ The valence- and inner-valence RPES spectra of LaB₂C₂ at various photon energies (indicated by numbers) are shown in Figure 2. Abscissa corresponds to the binding energy relative to the Fermi level (E_F). La 5p bands (~ 20 eV) are significantly enhanced in the on-resonant (La 4d) spectrum. Especially, an anomalous change of the photoemission branching ratio between 5p_{3/2} and 5p_{1/2} intensity can be seen. Actually, this anomaly is also observed in other La compounds. Ogasawara *et al.* attributed this to the multiplet dependence of the Auger transition probabilities.¹⁾ The intensity of the all valence- and inner-valence band begins to decrease from the photon energy of "5," and almost no structure can be observed at "10." Such a phenomenon was not observed in the RPES spectra at B K-edge (not shown here).

Reference

1)H. Ogasawara *et al.*, *Solid State Commun.* **81**, 645 (1992).

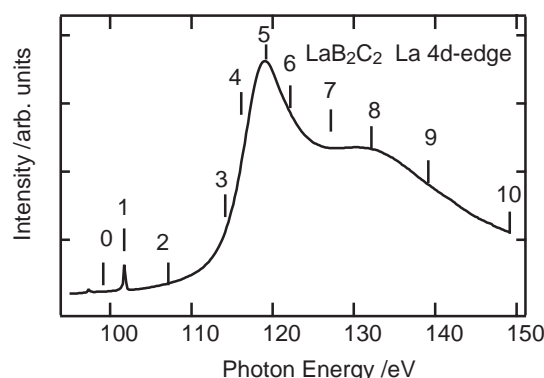


Figure 1. La 3d-edge XAS spectrum of LaB₂C₂.

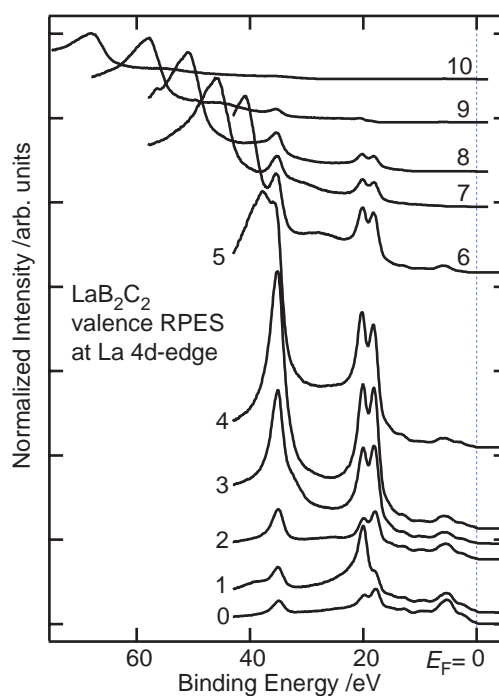


Figure 2. The valence and inner-valence RPES spectra of LaB₂C₂ of various photon energies.

VI-C Observation of Vibrational Coherence (Wavepacket Motion) in Solution-Phase Molecules Using Ultrashort Pulses

With recent remarkable improvements of ultrashort-pulse lasers, we are now able to generate an optical pulse shorter than a few tens of femtoseconds. Owing to its ultrashort duration and broad frequency bandwidth, the ultrashort pulse can excite a molecule ‘impulsively’ to generate a coherent superposition of vibrational eigen states either in the excited state or in the ground state. This vibrationally coherent state evolves in time, which is called wavepacket motion. The observation and control of the wavepacket motion is one of the most interesting topics in modern spectroscopy. In this project, we study vibrational coherence in the condensed-phase molecules by using ultrashort optical pulses having a duration of ten ~ a few tens of femtoseconds.

VI-C-1 Excited-State Vibrational Coherence of Solution-Phase Molecules Observed in the Third-Order Optical Process Using Extremely Short Pulses

TAKEUCHI, Satoshi; FUJIYOSHI, Satoru¹;
TAHARA, Tahei²
(¹GUAS; ²IMS and RIKEN)

[RIKEN REVIEW in press]

Excited-state vibrational coherence of solution-phase polyatomic molecules was studied by two different time-domain spectroscopic methods. Raman-active low-frequency vibrations in the excited state of *trans*-stilbene were observed through transient impulsive stimulated Raman scattering. In transient absorption spectroscopy with a 40-fs resolution, a different vibrational mode of the same excited state was observed as a “beat” in the pump-induced absorption signal. We discussed the selection of the vibrational modes by noting the difference in the third-order optical processes relevant to the two spectroscopies. The vibrational coherence of a “reacting” excited state was also observed for ultrafast photodissociation of diphenylcyclopropenone.

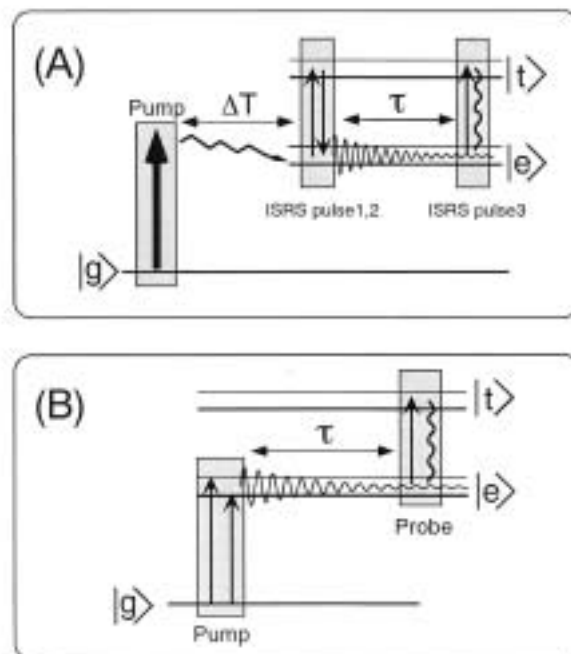


Figure 1. The third-order optical processes utilized to observe the excited-state vibrational coherence. (A) transient ISRS, (B) transient absorption.

VI-D Studies of Primary Photochemical/Physical Processes Using Femtosecond Electronic Spectroscopy

Ultrafast spectroscopy is playing an essential role in elucidation of photochemical reactions. Thanks to the recent advance in laser technology, we are now able to examine the dynamics of chemical reactions that take place in the femtosecond time region. In this project, we study primary photochemical/physical processes of the condensed-phase molecules using time-resolved fluorescence and absorption spectroscopy whose time-resolution is a few hundreds femtoseconds. Time-resolved fluorescence and absorption spectroscopy are complimentary to each other. The advantage of fluorescence spectroscopy lies in the fact that fluorescence originates from the transition between the “well-known” ground state and the excited state in question. Thus time-resolved fluorescence spectroscopy can afford unique information not only about the dynamics but also other properties of the excited singlet states such as their energies and oscillator strengths. On the other hand, however, time-resolved absorption spectroscopy is considered to be more versatile because it can detect not only fluorescent excited singlet states but also other “dark” transients.

VI-D-1 Femtosecond/Picosecond Time-Resolved Spectroscopy of *Trans*-Azobenzene: Isomerization Mechanism Following $S_2(\pi\pi^*) \leftarrow S_0$ Photoexcitation

FUJINO, Tatsuya; ARZHANTSEV, Sergei, Yu.;
TAHARA, Tahei¹
(¹IMS and RIKEN)

[*Bull. Chem. Soc. Jpn.* **75**, 1031 (2002)]

Photoisomerization dynamics and the electronic relaxation process of *trans*-azobenzene after the $S_2(\pi\pi^*) \leftarrow S_0$ photoexcitation were investigated in solution by femtosecond and picosecond time-resolved spectroscopy (UV-visible absorption, Raman, and fluorescence). Femtosecond time-resolved absorption spectroscopy was performed to observe the transient absorption of the S_2 and S_1 states. Immediately after photoexcitation, a very broad transient absorption peaked at 475 and 600 nm was observed. This transient absorption decayed rapidly within 0.5 ps, and this ultrafast component was attributed to the $S_n \leftarrow S_2(\pi\pi^*)$ absorption. After the decay of the S_2 state, a transient absorption showing peaks at 410 nm and 500 nm was observed, which was ascribable to the S_1 state. This transient absorption is similar to the $S_n \leftarrow S_1$ absorption that is observed after $S_1 \leftarrow S_0$ photoexcitation. Picosecond time-resolved Raman measurements were carried out to obtain information about the molecular structure of azobenzene in the S_1 state. The NN stretching frequency in the S_1 spectrum was determined with use of ¹⁵N-substituted azobenzene, and it was found that the NN stretching frequency in the S_1 state is very close to that in the S_0 state (1428 cm⁻¹ in the S_1 and 1440 cm⁻¹ in the S_0). This fact indicated that the NN bond retains a double bond character in the S_1 state. A good similarity was also found between the S_1 and S_0 Raman spectrum. The double bond nature of the NN bond as well as a good similarity between the S_1 and S_0 Raman spectra indicates that the observed S_1 state has a planar structure around the NN bond. The Raman data indicate that the observed S_1 state is not a twisted excited state that appears during the rotational isomerization, but the excited state that is populated during the $S_2 \rightarrow S_1 \rightarrow S_0$ relaxation process retaining a planar molecular structure. Anti-Stokes Raman measurements were performed to obtain information about the vibrational relaxation process. The anti-Stokes Raman spectra showed that the S_1 state was highly vibrationally excited. It was also observed that the hot bands due to the S_0 state appear after the decay of the S_1 state and that the S_0 hot bands disappear with a time constant of ~ 16 ps in hexane. Femtosecond time-resolved and steady-state fluorescence spectroscopy was performed and it revealed that the $S_2 \rightarrow$ 'planar' S_1 relaxation process is the major relaxation pathway following S_2 photoexcitation. The quantum yield of the $S_2 \rightarrow$ 'planar' S_1 electric relaxation was evaluated by comparing the intensity of the S_2 and S_1 fluorescence, and it was found to be almost unity. A series of time-resolved spectroscopy demonstrated that the S_2 rotational isomerization pathway, which had been believed so far, does not exist. It has been clarified that the isomerization occurs in the S_1 state after $S_2 \rightarrow S_1$

relaxation. Consequently, it is concluded that the isomerization of azobenzene takes place in the S_1 state by inversion in both cases of S_2 and S_1 photoexcitation.

VI-D-2 Ultrafast Fluorescence of the Chromophore of the Green Fluorescent Protein in Alcohol Solutions

MANDAL, Debabrata; TAHARA, Tahei¹;
WEBBER, N. M.²; MEECH, S. R.²
(¹IMS and RIKEN; ²Univ. East Anglia)

[*Chem. Phys. Lett.* **358**, 495 (2002)]

The ultrafast fluorescence dynamics of solutions of the chromophore responsible for emission from the Green Fluorescent Protein are measured by fluorescence up-conversion. Decays are non-exponential but well fit by a sum of two-exponentials. All decays have a prompt rise time. The two decay times are approximately independent of wavelength, but their weights are wavelength dependent, in a manner consistent with a spectral narrowing with time. The longer decay time has a weak dependence on medium viscosity.

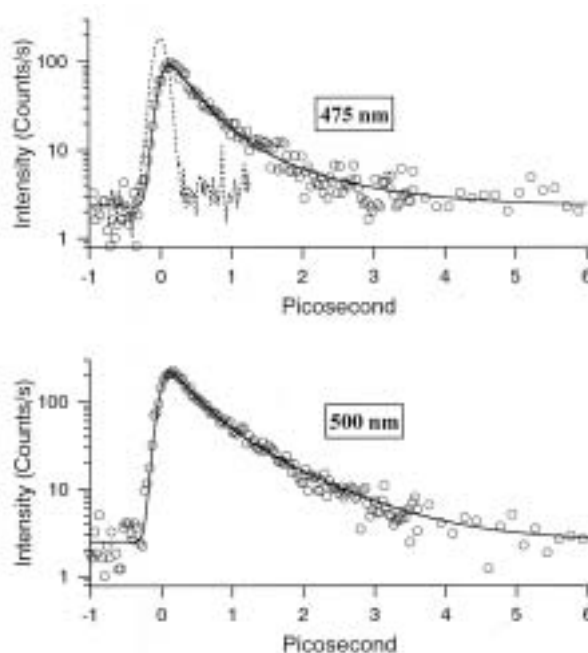


Figure 1. Fluorescence decay data for the anion of **I** in basic methanol, measured as a function of the emission wavelength. The data are fit to a sum of two exponential terms (solid line). Also shown in the 475 nm data is the instrument response function to illustrate time resolution.

VI-D-3 Femtosecond Study of Solvation Dynamics of DCM in Micelles

MANDAL, Debabrata; SOBHAN, Sen¹; TAHARA, Tahei²; BHATTACHARYYA, Kankan¹
(¹Indian Association Cultivation Sci.; ²IMS and RIKEN)

[*Chem. Phys. Lett.* **359**, 77 (2002)]

Solvation dynamics of 4-(dicyanomethylene)-2-methyl-6-(*p*-dimethylamino-styryl) 4H-pyran (DCM) has been studied in neutral (triton X-100, TX) and cationic (cetyl trimethyl ammonium bromide, CTAB) micelles using femtosecond upconversion. Since DCM is insoluble in bulk water the observed solvation dynam-

ics reports the relaxation dynamics exclusively at the micellar interface. It is observed that the solvation dynamics in TX is slower than that in CTAB. The solvation dynamics is described by components of 2.1, 165 and 2050 ps for TX and 0.23, 6.5 (average 1.75 ps) and 350 ps for CTAB.

VI-E Studies of Photochemical Reactions Using Picosecond Time-Resolved Vibrational Spectroscopy

Time-resolved vibrational spectroscopy is a very powerful tool for the study of short-lived transient species. It often affords detailed information about the molecular structure of transients, which is not obtainable with time-resolved electronic spectroscopy. However, for molecules in the condensed phase, we need energy resolution as high as 10 cm^{-1} in order to obtain well-resolved vibrational spectra. This energy resolution is compatible only with time-resolution slower than one picosecond because of the limitation of the uncertainty principle. In this sense, picosecond measurements are the best compromise between energy resolution and time resolution for time-resolved frequency-domain vibrational spectroscopy. In this project, we study photochemical processes and/or short-lived transient species by using picosecond time-resolved Raman spectroscopy.

VI-E-1 Picosecond Time-Resolved Raman Study of the Solvated Electron in Water

MIZUNO, Misao; TAHARA, Tahei¹
(¹IMS and RIKEN)

[*J. Phys. Chem. A* submitted]

Picosecond time-resolved Raman spectra of water were measured under the resonance condition with the electronic transition of the solvated electron. Transient Raman bands were observed in the OH bend and OH stretch regions in accordance with the generation of the solvated electron. The lifetime of the transient Raman bands were shortened by the addition of the electron scavenger, in exactly the same manner as the solvated electron absorption. It was concluded that the observed transient Raman bands are attributed to the water molecules that directly interact with the electron in the first solvation shell. The resonance enhancement factors were estimated as high as $\sim 10^5$ (the OH bend) and $\sim 10^3$ (the OH stretch) when the probe wavelength was tuned to the absorption maximum of the $s \rightarrow p$ transition of the solvated electron. This very high resonance enhancement indicated that the vibrational state of the solvating water molecules are strongly coupled with the electronic state of the electron, and that it is necessary to consider them together when we consider the vibronic state of the local solvation structure. The probe wavelength dependence of the transient Raman intensity was examined in a wide range from 410 nm to 800 nm. The obtained excitation profiles suggested that the $s \rightarrow p$ conduction transition does not significantly contribute the resonance Raman enhancement. The polarized Raman measurement was also undertaken for the OH bend band. The non-zero depolarization ratio was observed, which implied that the nondegeneracy of the three sublevels in the excited p state can be observed in a time scale of the Raman

process. The OH bending and OH stretching frequencies of the solvating water molecule are red-shifted compared with the frequencies of the bulk water, indicating a structural change is induced by the strong interaction with the electron.

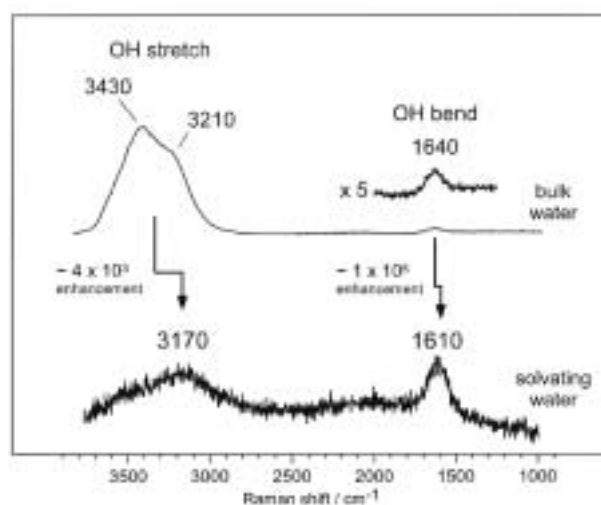


Figure 1. The non-resonance Raman spectrum of bulk water (top; 600 nm excitation) and the resonance Raman spectrum of the water molecules that solvate the electron (bottom; 620 nm excitation).

VI-E-2 Observation of Resonance Hyper-Raman Scattering from all-trans-Retinal

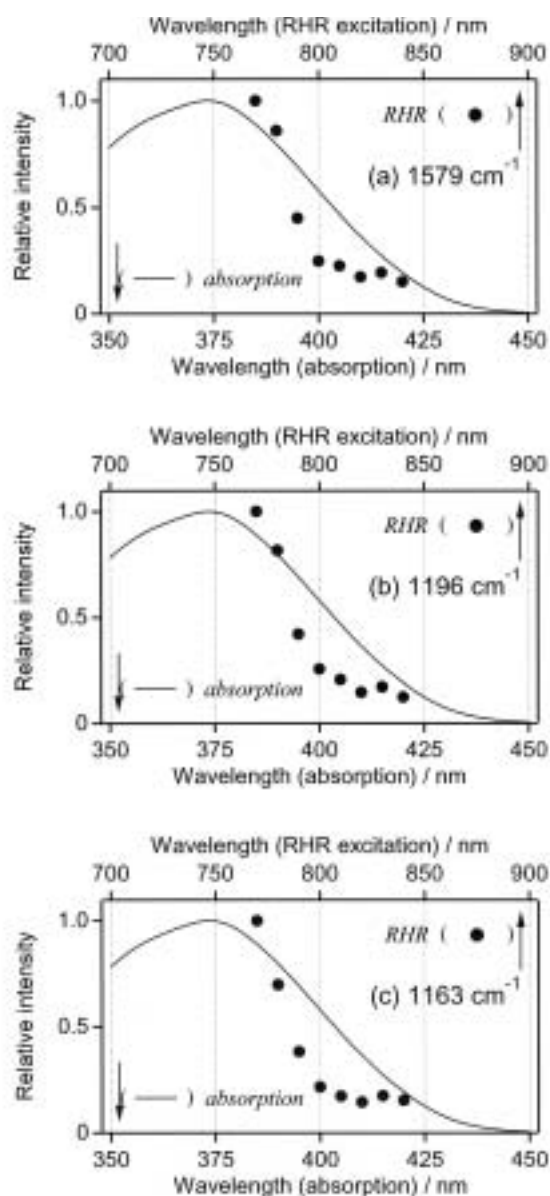
MIZUNO, Misao; HAMAGUCHI, Hiro-o¹;
TAHARA, Tahei²
(¹Univ. Tokyo; ²IMS and RIKEN)

[*J. Phys. Chem. A* **106**, 3599 (2002)]

Hyper-Raman scattering of *all-trans*-retinal was measured for the first time in solution at room tempera-

ture. Under the two-photon resonance condition, the intensity of hyper-Raman scattering was so strong that it could be measured from a diluted solution at concentration as low as $1 \times 10^{-3} \text{ mol dm}^{-3}$. Hyper-Raman excitation profiles were examined in the excitation wavelength range from 770 nm to 840 nm ($\lambda_{\text{ex}}/2$: 385–420 nm). In this excitation range, the intensity of all the hyper-Raman bands monotonously increased with shortening excitation wavelength, and the hyper-Raman spectral feature was very similar to that of resonance Raman spectra excited with double the excitation energy ($\lambda_{\text{ex}}/2$). The resonance mechanism of hyper-Raman scattering was discussed and it was concluded that hyper-Raman scattering gains intensity enhancement from a two-photon resonance with the “ $^1\text{B}_u$ ” state, not with the “ $^1\text{A}_g$ ” state, through the Frank-Condon (the A term) mechanism.

Figure 1. The hyper-Raman excitation profiles of (a) 1579 cm^{-1} (the C=C stretch), (b) 1196 cm^{-1} (the C–C stretch), and (c) 1163 cm^{-1} (the C–C stretch). Black circles and solid lines indicate the intensity of resonance hyper-Raman (RHR) bands and one-photon absorption spectrum, respectively. The excitation profiles of each hyper-Raman band have been normalized by the hyper-Raman intensity measured at 770 nm.



VI-F Synchrotron Radiation Stimulated Surface Reaction and Nanoscience

Synchrotron radiation (SR) stimulated process (etching, CVD) has excellent characteristics of unique material selectivity, low damage, low contamination, high spatial resolution, and high precision *etc.* In this project, nanolevel controlled structures are created by using synchrotron radiation stimulated process, and the reaction mechanisms are investigated by using STM and AFM. Concerning the SR etching, we are considering to apply this technique to the microfabrication of integrated protein transistor circuits.

VI-F-1 Patterning SiO₂ Thin Films Using Synchrotron Radiation Stimulated Etching with a Co Contact Mask

WANG, Changshun¹; WANG, Zhihong; MORÉ, Sam D. ; YAMAMURA, Shusaku; NONOGAKI, Youichi; URISU, Tsuneo
(¹Henan Univ.)

[*J. Vac. Sci. Technol., B* submitted]

Patterning SiO₂ thin films on Si(100) surface was successfully demonstrated using the synchrotron radiation (SR) stimulated etching with the SF₆ + O₂ as the reaction gas and a Co contact mask, as shown in Figure 1. The etching completely stopped at the SiO₂/Si(100) interface. The morphology of the Si surface after the etching, evaluated by the atomic force microscopy (AFM), was almost atomically flat ($R_a \sim 0.33$ nm), and an well-ordered self-assembled monolayer (SAM) of dodecene was deposited on the SR etched region area-selectively, as shown in Figure 2. Co was found to show sufficient resistivity against the SR etching as a mask material and to be easily removed by a dilute acid, without damaging the SAM. The SR etching of the SiO₂ thin films on the Si surface with the Co contact mask is a suitable patterning technique for the area-selective deposition of alkyl SAMs.

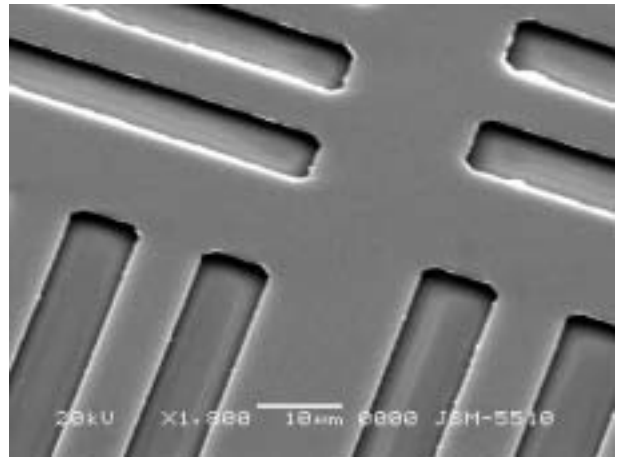


Figure 1. The SEM image of the pattern obtained by the SR etching SiO₂.

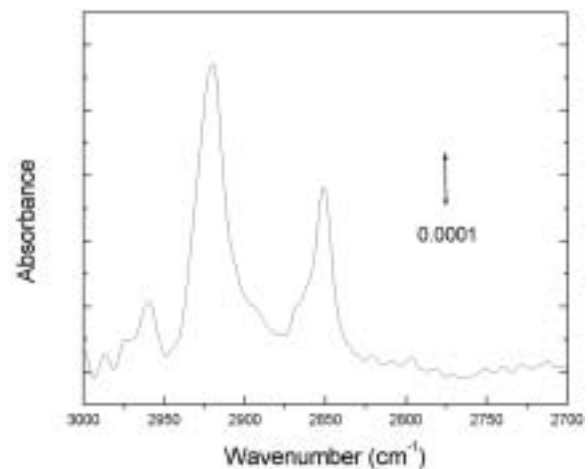


Figure 2. An IRTS of the dodecene SAM deposited on the SR etched surface.

VI-G Noble Semiconductor Surface Vibration Spectroscopy

As a new high sensitive and high resolution surface vibration spectroscopy technique, we are developing an infrared reflection absorption spectroscopy using buried metal layer substrate (BML-IRRAS), which have unique characteristics of high resolution and high sensitivity at finger print regions. Several Si surface chemical reactions are investigated using this BML-IRRAS. As a new fabrication technique of BML substrate, we have almost succeeded in developing the wafer bonding technique. It is considered that BML-IRRAS is also extremely useful in the research of bio-material integration on Si substrates.

VI-G-1 Infrared Reflection Absorption Spectroscopy Using CoSi₂ Buried Metal Layer Substrate Made by Wafer-Bonding

YAMAMURA, Shusaku; YAMAUCHI, Shouichi¹; WATANABE, Satoru²; TABE, Michiharu³; KASAI, Toshio⁴; NONOGAKI, Youichi; URISU, Tsuneo (¹DENSO Res. Lab.; ²Fujitsu Lab.; ³Shizuoka Univ. ; ⁴Saitama Univ.)

[*Jpn. J. Appl. Phys.* submitted]

The conventional infrared reflection absorption spectroscopy (IRRAS) covers wide energy regions including so-called finger print region with sub-monolayer sensitivity. However, it is applicable only for the metal. Therefore we have developed the IRRAS using buried metal layer (BML) substrate. BML wafers have been made so far by ion implantation method. This method, however, has several problems. A large ion current required for the ion implantation often cause the breakdown of the ion implanter. It is difficult to remove the surface roughness due to the ion implantation damage even after epitaxial growth. Wafer-bonding technique have a possibility to solve these. We have fabricated BML substrates with atom-level flat surfaces by a wafer-bonding technique with a Co deposited Si (100) wafer and SIMOX or SOI wafer (Figure 1). Using the BML substrate fabricated by this method, we successfully observed the stretching and bending vibration bands of self-assembled alkyl monolayers of octadecyltrichlorosilane (OTS) and octenyltrichlorosilane (OTTS) on the Si (100) surface.

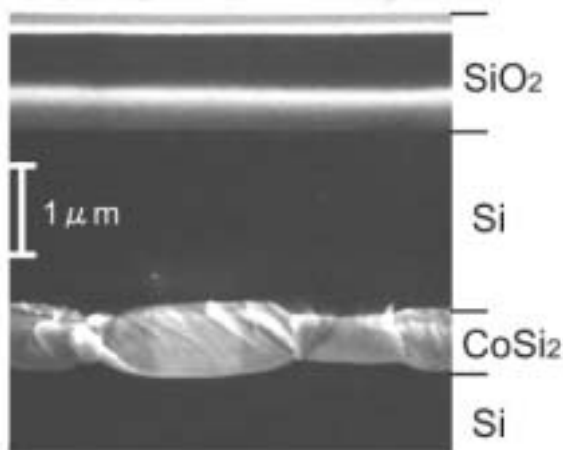


Figure 1. Cross-sectional SEM image of Si(100)/CoSi₂/Si(100) BML substrate made from the SOI wafer.

VI-G-2 Hydrogen Diffusion and Chemical Reactivity with Water on Nearly Ideally H-Terminated Si(100) Surface

WANG, Zhihong; NODA, Hideyuki¹; NONOGAKI, Youichi; YABUMOTO, Norikuni²; URISU, Tsuneo (¹Hitachi Ltd.; ²NTT Adv. Tech. Corp.)

[*Jpn. J. Appl. Phys.* **41**, 4275 (2002)]

A nearly ideally H-terminated condition for a

Si(100) 2×1 surface is determined from the dependence of the peak intensity and the linewidth of the coupled monohydride symmetric stretching vibration on the hydrogen exposure and exposure temperature, which has been investigated with infrared reflection absorption spectroscopy (IRRAS) using CoSi₂ buried metal layer substrate. Even for nearly ideally H-terminated surfaces, the linewidth significantly changes depending on the hydrogen exposure and the exposure temperature. The concentration of deuterium atoms incorporated in the Si bulk is measured by temperature programmed desorption, and it is concluded that hydrogen diffusion into the subsurface of Si has a significant influence on the linewidth broadening. The chemical reactivity with water on the H-terminated Si surface is also investigated.

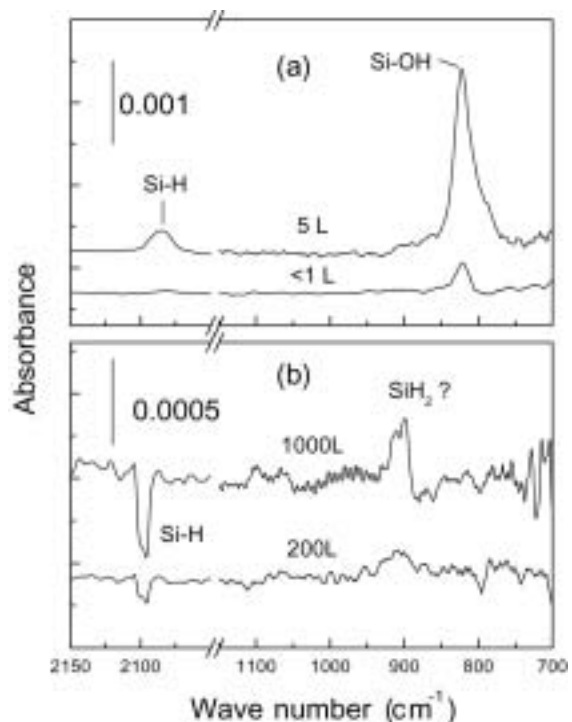


Figure 1. Observed BML-IRRAS spectra (circles) of atomic H-exposed H₂O: Si(100)-(2×1) surfaces at $T_m = 373$ K for $D = 1000$ L (top) and $D = 50$ L (bottom). The results of curve-resolutions assuming a Lorentzian form are compared (solid and dotted lines).

VI-G-3 Atomic Hydrogen-Induced Oxidation on Water-Adsorbed Si(100)-(2×1) Surfaces

WANG, Zhihong; URISU, Tsuneo; NANBU, Shinkoh; MAKI, Jun; AOYAGI, Mutsumi; WATANABE, Hidekazu¹; OOI, Kenta¹ (¹Natl. Inst. Adv. Ind. Sci. Tech.)

[*Phys. Rev. B* submitted]

Infrared reflection absorption spectroscopy using buried metal layer substrates (BML-IRRAS) and density functional cluster calculations are used to analyze the atomic hydrogen-induced oxidation on water-adsorbed Si(100)-(2×1) surfaces. In addition to the oxygen inserted coupled monohydrides previously reported, zero, one and two oxygen inserted dihydride species have been

clearly observed for the first time due to the high sensitivity of BML-IRRAS for the perpendicular dynamic dipole moment in the finger print region. It is also found that double oxygen insertion is clearly favored over single oxygen insertions. A new oxidation mechanism, $\text{H-Si-Si-OH} + 2\text{H} \rightarrow \text{SiH}_2 + \text{Si(O)H}_2$ is proposed. In high exposure regions, $\text{H-Si-O-Si-H} + 2\text{H} \rightarrow \text{SiH}_2 + \text{Si(O)H}_2$ reaction is also observed.

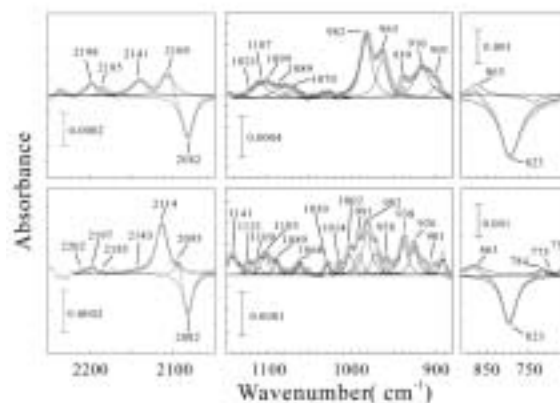


Figure 1. Change of the BML-IRRAS spectra by exposing to water at 373 K, (a) in the case of clean Si(100)(2×1) surface, and (b) nearly ideally H-terminated Si(100)(2×1) surface.

VI-H Integration of Bio-Functional Materials on Silicon

Integration of bio-functional materials such as lipids and proteins are expected to find important applications in biosensors, development of new medicines, and diagnosis of intractable diseases *etc.* In this project, we are investigating the area selective modification of Si surfaces by depositing the self assembled alkyl monolayers, and the integration of lipid bilayers supporting channel proteins keeping their bio-activities. Our special interests are developing “protein transistors” and co-integrating them together with the Si MOS FETs on the same Si chip.

VI-H-1 Hydrophobic/Hydrophilic Interactions of Cytochrome *c* with Functionalized Self-Assembled Monolayers on Silicon

MORÉ, Sam D. ; HUDECECK, Jiri¹; URISU, Tsuneo
(¹Charles Univ.)

[*Surf. Sci.* in press]

Cytochrome *c* (horse heart) has been adsorbed onto self-assembled monolayers (SAM) on silicon single crystal substrates. Layer thickness was determined using ellipsometry and atomic force microscopy (AFM) in the DFM tapping mode in air. Both hydrophilic (COOH containing SAM) and hydrophobic self-assembled monolayers were used. The protein layers were found to consist of adsorbed 2-dimensional islands.

Concentration, exposure time and the defect-density of the self-assembled monolayer substrates determined the wetting properties of the resulting layer, indicating that the surface orientation of the protein is driven by the interaction with the substrate. On well ordered self-assembled monolayers, the protein layer thicknesses were 1.76 nm for charged surfaces and 2.3 nm for hydrophobic surfaces. Self-assembled monolayers of a lower density resulted in a prevalence of cytochrome *c* islands of 3.2 nm thickness for both cases.

Defects in the SAM facilitate protein adsorption, a denser monolayer of a third orientation type, which leads to the largest adsorbed protein density. At the protein-film air interface 2-dimensional protein islands form, which can be manipulated with an AFM tip in the

case of CH₃-terminated SAMs, but not in the case of COO⁻ containing layers.

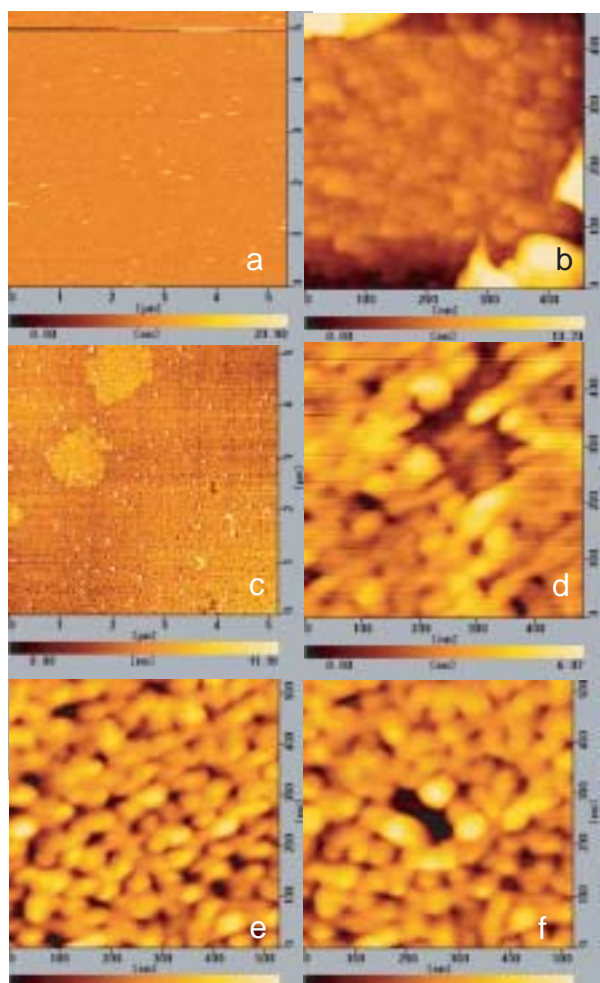


Figure 1. (a) and (b) eicocene terminated SAM prior protein adsorption, (c) and (d) after protein adsorption on a SAM with large defect density. (e) and (f) after selective movement of protein islands into the second layer.

VI-H-2 Influence of Substrate Roughness on the Formation of Self-Assembled Monolayers (SAM) on Silicon(100)

MORÉ, Sam D. ; GRAAF, Harald; BAUNE, Micheal¹; WANG, Changshun; URISU, Tsuneo (¹Bremen Univ.)

[*Jpn. J. Appl. Phys.* **41**, 4390 (2002)]

The peak shifts of the CH₂-vibration are an indicator of the amount of gauche-conformational disorder present in aliphatic self-assembled monolayers (SAM). The property of the SAM layer was characterized by measuring the -CH₃ and -CH₂ stretching vibration modes using FTIR transmission spectroscopy, investigating the relationship between the surface roughness and the peak position as a function of temperature and alkyl chain-length. With increasing substrate surface roughness both the symmetric CH₂-peak as well as the asymmetric CH₂-peak shift to higher wave numbers. The magnitude of the shift is about 6 cm⁻¹ at 150 °C and is due to a change from a condensed, almost *all-trans* conformational phase to liquid like layers.

For polished substrates although increased temperatures lead to a slightly more ordered SAM, the layers were in almost an “*all-trans*”-conformational phase independent on the coverage. From these results an “island growth and annealing effect”-model is proposed, which explains relation between the disorder increase and the surface roughness.

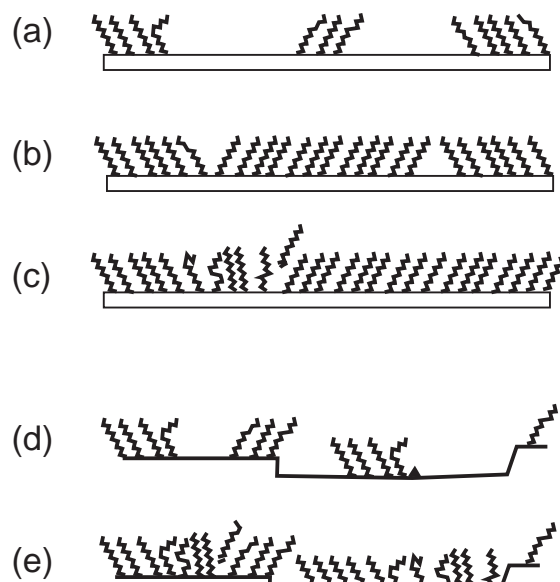


Figure 1. Model for SAM layer growth on flat and rough surfaces explaining the increase of disorder on rough surfaces. (a) Self assembled monolayer starts to form at several sites on the flat Si-surface (b) Domain formation due to different nucleation sites. Monolayer orders itself due to van der Waals forces (c) Domains anneal and gaps are filled with additional molecules, if the temperature is high enough and the reaction time is sufficient. (d) Self-assembled monolayer starts to form at many sites on the rough surface (e) Self-assembled monolayer starts to anneal, but steps and defects inhibit the process, as the overlap between the chains at the steps is too small. The relative but not the absolute surface coverage is smaller and the disorder, due to gauche defects, larger.

VI-I Photoionization and Photodissociation Dynamics Studied by Electron and Fluorescence Spectroscopy

Molecular photoionization is a major phenomenon in vacuum UV excitation and provides a large amount of information on fundamental electron-core interactions in molecules. Especially, neutral resonance states become of main interest, since they often dominate photoabsorption cross sections and lead to various vibronic states which are inaccessible in direct ionization. We have developed a versatile machine for photoelectron spectroscopy in order to elucidate dynamical aspects of superexcited states such as autoionization, resonance Auger decay, predissociation, vibronic couplings, and internal conversion. Two-dimensional photoelectron spectroscopy, allows us to investigate superexcited states in the valence excitation region of acetylene, nitric oxide, carbonyl sulfide, sulfur dioxide and so on. In this method, the photoelectron yield is measured as a function of both photon energy and electron kinetic energy (binding energy). The spectrum, usually represented as a contour plot, contains rich information on photoionization dynamics.

Photofragmentation into ionic and/or neutral species is also one of the most important phenomena in the vacuum UV excitation. In some cases, the fragments possess sufficient internal energy to de-excite radiatively by emitting UV or visible fluorescence. It is widely accepted that fluorescence spectroscopy is an important tool to determine the fragments and to clarify the mechanisms governing the dissociation processes of diatomic and polyatomic molecules. This year we have carried out fluorescence spectroscopy of H₂O in the photon energy region of 15–30 eV.

VI-I-1 Formation and Autoionization of a Dipole-Forbidden Superexcited State of CS₂

HIKOSAKA, Yasumasa¹; MITSUKE, Koichiro
(¹*Inst. Mater. Struct. Sci.*)

[*J. Phys. Chem. A* **105**, 8130 (2001)]

Two-dimensional photoelectron spectroscopy has been performed in the photon energy region of 14.60–15.35 eV, to investigate forbidden superexcited states of CS₂. The two-dimensional photoelectron spectra for the CS₂⁺($\tilde{X}^2\Pi_g$) and CS₂⁺($\tilde{B}^2\Sigma_u^+$) bands show remarkable formation of vibrational levels excited with one quantum of the antisymmetric stretch vibrational mode at $E_{hv} \sim 14.88$ eV. This vibrational excitation is attributable to autoionization from a dipole-forbidden superexcited state which is formed through vibronic interaction with the $5p\sigma_u$ Rydberg state converging to CS₂⁺($\tilde{C}^2\Sigma_g^+$). The forbidden superexcited state is assigned as the $v = 1$ vibrational state in the ν_3 mode of the $3d\sigma_g$ Rydberg member converging to CS₂⁺($\tilde{C}^2\Sigma_g^+$). Preference in the autoionization of the forbidden superexcited state was discussed.

VI-I-2 Autoionization and Neutral Dissociation of Superexcited HI Studied by Two-Dimensional Photoelectron Spectroscopy

HIKOSAKA, Yasumasa¹; MITSUKE, Koichiro
(¹*Inst. Mater. Struct. Sci.*)

Two-dimensional photoelectron spectroscopy of hydrogen iodide has been performed in the photon energy region of 11.10–14.85 eV, in order to investigate dynamical properties on autoionization and neutral dissociation of Rydberg states HI*(R_A) converging to HI⁺($\tilde{A}^2\Sigma^+_{1/2}$). A two-dimensional photoelectron spectrum in Figure 1 exhibits strong vibrational excitation of HI⁺($\tilde{X}^2\Pi_{3/2}$) over a photon energy region from ~ 12 to 13.7 eV, which is attributable to autoion-

izing feature of the $5d\pi$ HI*(R_A) state. Noticeable features around the photon energy region of 13.5–14.5 eV are assigned as resulting from autoionizing transitions from I* [converging to I⁺(3P_0 or 1)] into I⁺(3P_2). The formation mechanism of I* is due to the predissociation of HI*(R_A) by the repulsive HI* state of Rydberg type converging to HI⁺($^4\Pi_{1/2}$).

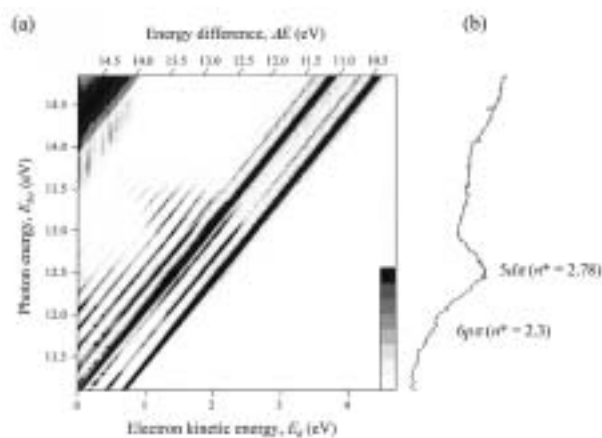


Figure 1. (a) Two-dimensional photoelectron spectrum of HI in the photon energy range of 11.10–14.85 eV. The electron yield, measured as a function of both photon energy E_{hv} and electron kinetic energy E_k , is presented by the plots with eight tones from light to dark on a linear scale. The intense structures are truncated. Diagonal lines attached on the top of this figure denote the energy difference defined by $\Delta E = E_{hv} - E_k$. (b) The curve obtained by summing electron counts over the whole range of E_k as a function of E_{hv} .

VI-I-3 Development of the Apparatus for High-Resolution Dispersed Spectroscopy and Fluorescence Excitation Spectroscopy at BL3A2

MITSUKE, Koichiro

The fluorescence was collected by an optical detec-

tion device in Figure 1 made up of spheroidal and spherical mirrors facing each other across the photoexcitation region (*PR*), *i.e.* the source of the fluorescence.¹⁾ One focal point of the spheroidal mirror fell at *PR*, while the other focal point was at the surface of an optical-fiber bundle. The fluorescence light was reflected back to *PR* by the spherical mirror and was then focused onto the surface of the fiber bundle by the spheroidal mirror. This detection system can collect light from about 62% of the full-sphere solid angle. The fluorescence passed through the optical-fiber bundle (transmission ~ 55% at 400 nm).

In dispersed fluorescence spectroscopy we utilized a 300 mm focal-length imaging spectrograph equipped with a liquid-nitrogen cooled CCD array detector. The overall detection efficiency, including the two mirrors, fiber bundle, and imaging spectrograph, was estimated to be $(1-5) \times 10^{-3}$ with the slit width of the spectrograph being 250 μm . When we fulfilled fluorescence excitation spectroscopy by scanning the wavelength of synchrotron radiation, we replaced the CCD array detector by a photomultiplier tube. In this case, the overall detection efficiency was estimated to be $(1.4 \pm 0.3) \times 10^{-3}$ at the slit widths of the monochromator of 2 mm. All spectra were corrected by the wavelength dependence of the relative detection efficiency.

Reference

- 1) K. Mitsuke and M. Mizutani, *Bull. Chem. Soc. Jpn.* **74**, 1193 (2001).

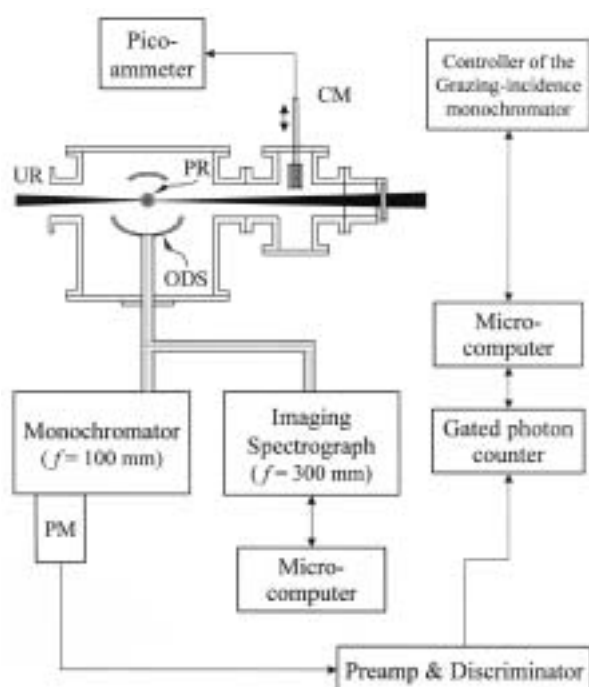


Figure 1. Schematic diagram of the apparatus for dispersed fluorescence spectroscopy and fluorescence excitation spectroscopy. UR, monochromatized undulator radiation; PR, photoexcitation region (not to scale); ODS, optical detection system composed of two mirrors and an optical-fiber bundle; CM, gold-mesh current monitor; PM, photomultiplier.

VI-I-4 UV and Visible Dispersed Spectroscopy for the Photofragments Produced from H₂O in the Extreme Ultraviolet

MITSUKE, Koichiro

[*J. Chem. Phys.* **117**, 8334 (2002)]

The photofragmentation of H₂O has been studied by fluorescence spectroscopy in the photon energy region between $E_{h\nu} = 16.9-54.5$ eV at the beam line 3A2 of UVSOR. The fluorescence in the wavelength range of 280–720 nm was dispersed with an imaging spectrograph. The dispersed spectra in Figure 1 exhibit the hydrogen Balmer lines of $\text{H}^*[n^2L', J' \rightarrow 2^2L'', J'']$ ($n = 3-9$) and the emission band systems of $\text{H}_2\text{O}^+ [\tilde{A}^2A_1(0, v', 2, 0) \rightarrow \tilde{X}^2B_1(0, 0, 0)]$, $[\text{OH}^+(\tilde{A}^3\Pi_Q, v' \rightarrow \tilde{X}^3\Sigma^-, v'')]$, and $[\text{OH}^+(\tilde{A}^2\Sigma^+, v' \rightarrow \tilde{X}^2\Pi_Q, v'')]$. The fluorescence cross sections for these transitions have characteristic dependences on $E_{h\nu}$ and vibrational quantum numbers. The cross section summed over the Balmer lines takes a minimum value at $E_{h\nu} = 21.7$ eV and is very small even at 24.9 eV beyond which it steadily increases with increasing $E_{h\nu}$. This behavior is understood as that the superexcited states correlating with $\text{H}^*(n \geq 3) + \text{OH}(\tilde{A}^2\Sigma^+)$ are too repulsive to be accessible below $E_{h\nu} \sim 30$ eV by the Franck-Condon transitions from $\text{H}_2\text{O}(\tilde{X}^1A_1)$ and as that the Balmer emission below 30 eV is mainly due to the $\text{H}^*(n \geq 3) + \text{H}(n = 1) + \text{O}(^3P_g)$ channel. The appearance energy 25.5 ± 0.3 eV of the $\text{OH}^+(\tilde{A}^3\Pi_Q, v' \rightarrow \tilde{X}^3\Sigma^-, v'')$ transitions is much higher than the dissociation limit of 21.5 eV for the $\text{OH}^+(\tilde{A}^3\Pi_Q) + \text{H}(n = 1)$ channel, but is consistent with the vertical ionization energy to $\text{H}_2\text{O}^+[(1b_1)^{-2}(4a_1)^1 2A_1]$ that has been assumed to correlate with the above dissociation limit. The vibrational distribution of $\text{OH}^+(\tilde{A}^3\Pi_Q)$ evaluated from the $\text{OH}^+(\tilde{A}^3\Pi_Q, v' \rightarrow \tilde{X}^3\Sigma^-, v'')$ band intensities is similar to the prior distribution in the rigid-rotor harmonic-oscillator approximation.

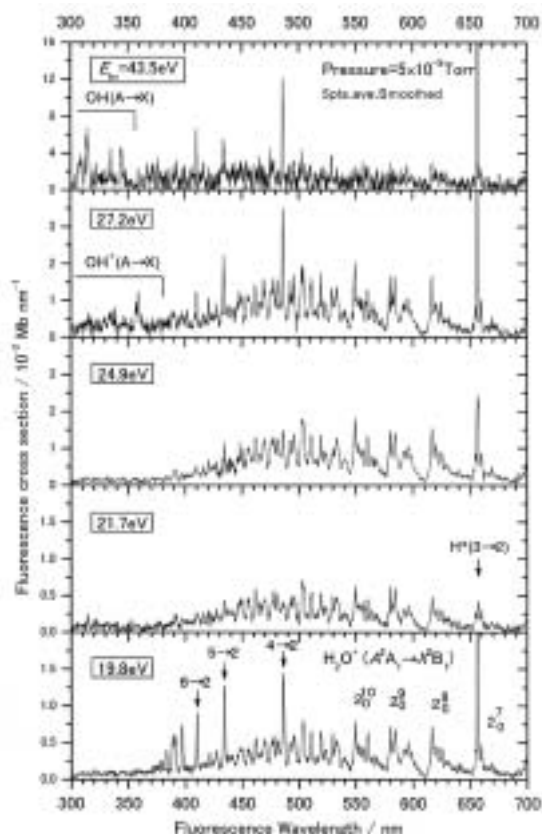


Figure 1. Dispersed fluorescence spectra of H_2O encompassing the wavelength region 300–700 nm at six photon energies between $E_{h\nu} = 19.8$ and 43.5 eV. The $2_0^{v_2}$ symbols in the panel of $E_{h\nu} = 21.7$ eV designate the vibrational progression in the bending mode v_2 of the $\text{H}_2\text{O}^+[\tilde{A}^2A_1(0, v_2, 0) \rightarrow \tilde{X}^2B_1(0, 0, 0)]$ transition. The hydrogen Balmer lines $\text{H}^*[n^2L'J' \rightarrow 2^2L''J'']$ ($n = 3-9$) are indicated by the $(n \rightarrow 2)$ marks.

VI-J Vacuum UV Spectroscopy Making Use of a Combination of Synchrotron Radiation and a Mode-Locked or Pulsed UV Laser

An ultraviolet laser system has been developed which synchronizes precisely with the synchrotron radiation (SR) from the storage ring of the UVSOR facility. A mode-locked Ti:sapphire laser is made to oscillate at the frequency of the ring in a multibunch operation mode. The delay timing between SR and laser pulses can be changed from 0 to 11 ns. The following combination studies have been performed: (1) two-photon ionization of helium atoms studied as the prototype of the time-resolved experiment, (2) laser induced fluorescence (LIF) excitation spectroscopy of $\text{N}_2^+(X^2\Sigma_g^+)$ ions produced by synchrotron radiation photoionization of N_2 or N_2O , and (3) LIF excitation spectroscopy of $\text{CN}(X^2\Sigma^+)$ radicals produced by synchrotron radiation photodissociation of CH_3CN .

VI-J-1 Partial Photoionization Cross Sections for $\text{N}_2^+(X^2\Sigma_g^+, v_X = 0, 1)$ Measured by a Laser Synchrotron Radiation Combination Technique

MITSUKE, Koichiro; MATSUMURA, Hisashi¹
(¹Chiba Univ.)

[*J. Electron Spectrosc. Relat. Phenom.* submitted]

Molecular superexcited states undergo autoionization into various vibrational levels of a low-lying ionic state with branching ratios BR considerably different from those for the direct ionization. The BR values are determined chiefly by the molecular constants on the potential energy surfaces involved and transition pro-

babilities for autoionization. In this study, N_2 is subjected to photoionization with the monochromatized undulator radiation into $\text{N}_2^+(X^2\Sigma_g^+, v_X = 0 \text{ or } 1)$ which is then probed by LIF excitation spectroscopy in the laser wavelength of the $(B^2\Sigma_u^+, v_B = 0 \text{ or } 1) \leftarrow (X^2\Sigma_g^+, v_X = 0 \text{ or } 1)$ transition, respectively. Partial cross sections for production of $\text{N}_2^+(X^2\Sigma_g^+, v_X = 0 \text{ and } 1)$ are measured as a function of the undulator photon energy. The cross section curves show peaks originating from transitions to Rydberg states converging to $\text{N}_2^+(A^2\Pi_u, v_A = 0-4)$. Relative peak intensities differ from the $v_X = 0$ to 1 curves. Vibrational BR s resulting from autoionization of $\text{N}_2^+(A^2\Pi_u)$ were studied by a Franck-Condon Analysis.

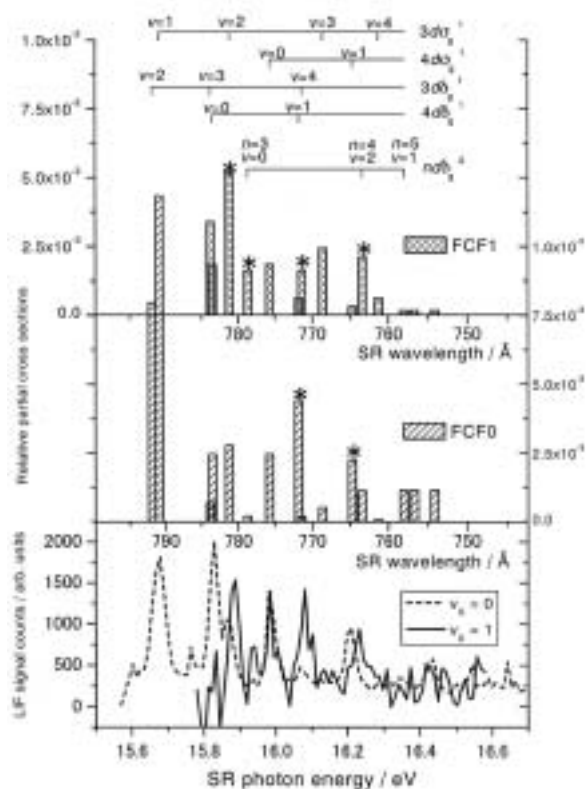


Figure 1. (Lowest Panel) Yield curves of N_2^+ ($X^2\Sigma_g^+$, $v_X = 0$ or 1) from N_2 obtained from the LIF count rate of the (B , $v_B = 0$ and 1) \rightarrow (X , $v_X = 1$ or 2) transitions, respectively. (Upper two panels) Partial cross sections for production of $N_2^+(X^2\Sigma_g^+$, $v_X = 0$ and 1) calculated by Franck-Condon Analysis.

VI-K Extreme UV Photoionization Studies by Employing a Dragon-Type Grazing-Incidence Monochromator

On the beam line BL2B2 in UVSOR a grazing incidence monochromator has been constructed which supplies photons in the energy region from 20 to 200 eV [M. Ono, H. Yoshida, H. Hattori and K. Mitsuke, *Nucl. Instrum. Methods Phys. Res., Sect. A* **467-468**, 577 (2001)]. This monochromator has bridged the energy gap between the beam lines BL3A2 and BL8B1, thus providing for an accelerating demand for the high-resolution and high-flux photon beam from the research fields of photoexcitation of inner-valence electrons, L -shell electrons in the third-row atom, and $4d$ electrons of the lanthanides.

Since 2001 we have tried taking photoion yield curves of fullerenes at BL2B2. Geometrical structures and electronic properties of fullerenes have attracted widespread attention because of their novel structures, novel reactivity, and novel catalytic behaviors as typical nanometer-size materials. Moreover, it has been emphasized that the potential for the development of fullerenes to superconductors ($T_c \sim 50$ K) and strong ferromagnetic substances is extremely high. In spite of such important species spectroscopic information is very limited in the extreme UV region, which has been probably due to difficulties in obtaining enough amount of sample. The situation has been rapidly changed in these few years, since the techniques of syntheses, isolation, and purification have been advanced so rapidly that appreciable amount of fullerenes is obtainable from several distributors in Japan.

VI-K-1 Anisotropy of Fragment Ions from SF_6 by Photoexcitation of a Valence- or Sulfur $2p$ -Electron between 23 and 210 eV

ONO, Masaki¹; MITSUKE, Koichiro
(¹Louisiana State Univ.)

[*Chem. Phys. Lett.* in press]

The anisotropy of the fragment ions produced by photoexcitation of SF_6 has been measured using synchrotron radiation in the energy range of 23–210 eV. In

spite of the highly symmetrical molecule the strong anisotropy is observed at lower photon energies. Anisotropy gradually decreases with increasing photon energy. The behavior of the curve of the asymmetry parameter has been interpreted qualitatively by means of simulation using partial oscillator strengths for the formation of fragment ions in the region of valence electron excitation (16–63 eV). Only SF_5^+ ions are assumed to have an anisotropic angular distribution, which can be explained in terms of transitions into neutral excited states of valence type. With increasing photon energy the branching ratio for the SF_5^+ ion

decreases, while the contribution of direct photoionization may increase. As a result the asymmetry parameter involving all the fragment ions declines steadily with the photon energy. Moreover, inner valence-electron excitation between 35 and 50 eV is found to open new decay channels which produce photoions isotropically. The asymmetry parameter remains constant at 0.01–0.02 below the sulfur $2p_{3/2,1/2}$ edges (< 180 eV), whether the photon energy is chosen at on- or off-resonance. Above the edges it decreases down to almost zero, in accord with the opening of the LVV Auger decay channels.

VI-K-2 Construction of the Photoionization Spectrometer for Fullerenes and Metallofullerenes

MITSUKE, Koichiro; ONO, Masaki¹; KOU, Junkei; MORI, Takanori; HARUYAMA, Yusuke²; KUBOZONO, Yoshihiro
(¹Louisiana State Univ.; ²Okayama Univ.)

Figure 1 shows the photograph of the apparatus designed to carry out extreme UV photoionization of fullerenes. A copper sample holder is mounted inside a radiation shield made of stainless steel. The vapor of the fullerene discharged from a small orifice is subjected to irradiation of the synchrotron radiation supplied from the Dragon-type monochromator. A drift tube was equipped between parallel plate electrodes placed above the oven unit and the housing of a microchannel plate electron multiplier detector. Insertion of the drift tube allows us to drastically reduce bothering background counts due to stray electrons and impurities and then realize a stable operation of the oven.

In the case of C_{60} the sample of 99.98% purity was purchased and further purified by eliminating organic solvent such as benzene or toluene through heating the sample one day in vacuum at 300 °C. In order to prepare the number density of fullerenes high enough at the interaction volume we increased the temperature of an oven up to 500 °C. The sublimation rate measured by using a quartz-oscillator thickness monitor was around 100–150 ng/s. We were able to find the optimum experimental conditions that keep a steady flow of the C_{60} vapor at the interaction volume.

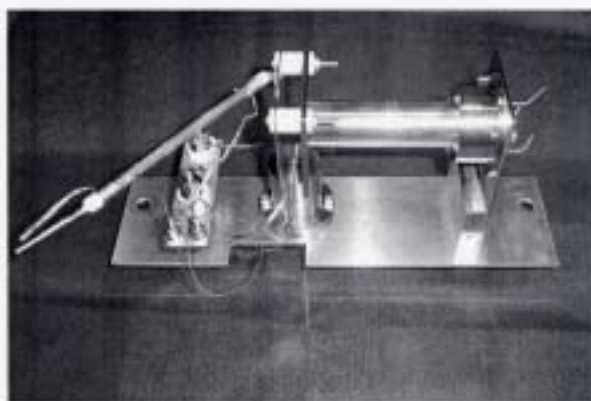


Figure 1. Photograph of the photoionization spectrometer developed for fullerenes.

VI-K-3 Photoion Yield Spectra of C_{60} in the Region of 23–210 eV

MITSUKE, Koichiro; ONO, Masaki¹; KOU, Junkei; MORI, Takanori; HARUYAMA, Yusuke²; KUBOZONO, Yoshihiro
(¹Louisiana State Univ.; ²Okayama Univ.)

In 1992 Hertel and coworkers have reported the photoionization efficiency curve for C_{60}^+ and revealed an intense broad peak at the photon energy of ~ 20 eV.¹ They assigned it as resulting from excitation of surface plasmon in C_{60} : Collective longitudinal motion of multiple valence electrons is excited when C_{60} absorbs a transverse-wave light. So far much knowledge has been accumulated in the lower energy side of this plasmon peak, whereas there has been no experimental data between the high energy side and region containing the carbon $1s$ edge (~ 290 eV). This situation motivates us to take the efficiency curve encompassing the range from 23 to 210 eV.

Figure 1 shows a photoion yield curve of C_{60} plotted as a function of the photon energy. Above the three shoulders at 26, 33, and 47 eV the ion yield goes down monotonically with increasing photon energy. Figure 1 also shows representative data points from the literature.^{1,2} Our data depend on the photon energy most weakly and behave similarly to those of Ref. 2) at ≤ 32 eV. The Hertel's spectrum completely differs from the other curves. The three shoulders, appearing only in our spectrum, are attributed to the shape resonance, *i.e.* promotion of an electron up to a vacant valence virtual orbital which is characterized by a high orbital angular momentum.

References

- 1) I.V. Hertel *et al.*, *Phys. Rev. Lett.* **68**, 784 (1992).
- 2) Yoo *et al.*, *J. Chem. Phys.* **96**, 911 (1992).

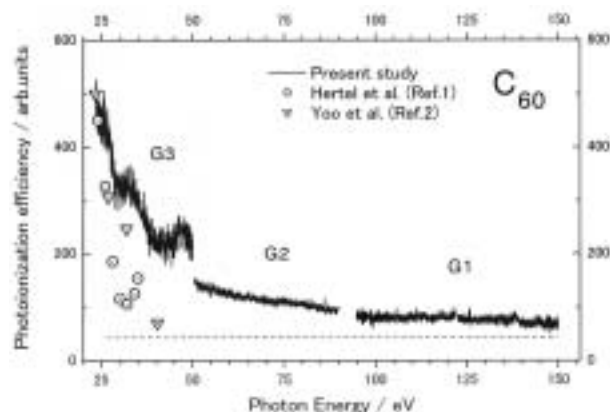


Figure 1. Photoionization efficiency curves of C_{60} .

RESEARCH ACTIVITIES VII

Coordination Chemistry Laboratories

Prof. Masahito Yamashita, Prof. Naoto Chatani took the position of Laboratory of Synthetic Coordination Chemistry from April 2002. Prof. Isao Taniguchi (Kumamoto University) and Assoc. Prof. Yasutaka Tanaka (Shizuoka University) finished their term as Adjunct Prof. of the Synthetic Coordination Chemistry in March 2002. Their effort during their term is gratefully appreciated. Prof. Nobuhiro Tokito (Kyoto University) and Assoc. Prof. Kiyotaka Onizuka (Osaka University) continue the position of the Coordination Bond.

VII-A Development of Novel Transition Metal Complex Catalysts Having MOP Ligands

Transition metal-mediated organic transformations have emerged as a powerful tool in the domain of synthetic organic chemistry. Catalytic asymmetric reactions have attracted significant interest for their synthetic utility. One of the most exciting and challenging subjects in research on the catalytic asymmetric synthesis is development of the novel chiral ligands. Recently, we have designed and prepared a series of homochiral monophosphine ligands bearing axially chiral binaphthyl backbone, so-called MOP, which were identified as effective chiral ligands in various asymmetric catalysis, in particular hydrosilylation of olefins.

VII-A-1 Asymmetric Hydrosilylation of Styrenes Catalyzed by Palladium-MOP Complexes: Ligand Modification and Mechanistic Studies

HAYASHI, Tamio; HIRATE, Seiji; KITAYAMA, Kenji; TSUJI, Hayato; TORII, Akira; UOZUMI, Yasuhiro

[*J. Org. Chem.* **66**, 1441 (2001)]

In the palladium-catalyzed asymmetric hydrosilylation of styrene with trichlorosilane, several chiral monophosphine ligands, (*R*)-2-diarylphosphino-1,1'-binaphthyls, were examined for their enantioselectivity. The highest enantioselectivity was observed in the reaction with (*R*)-2-bis[3,5-bis(trifluoromethyl)phenyl]phosphino-1,1'-binaphthyl, which gave (*S*)-1-phenylethanol of 98% ee after oxidation of the hydrosilylation product, 1-phenyl-1-(trichlorosilyl)ethane. The palladium complex of (*R*)-2-bis[3,5-bis(trifluoromethyl)phenyl]phosphino-1,1'-binaphthyl also efficiently catalyzed the asymmetric hydrosilylation of substituted styrenes on the phenyl ring or at the β position to give the corresponding chiral benzylic alcohols of over 96% ee. Deuterium-labeling studies on the hydrosilylation of regiospecifically deuterated styrene revealed that β -hydrogen elimination from 1-phenylethyl(silyl)-palladium intermediate is very fast compared with reductive elimination giving hydrosilylation product when (*R*)-2-bis[3,5-bis(trifluoromethyl)phenyl]phosphino-1,1'-binaphthyl is used. The reaction of *o*-allylstyrene with trichlorosilane gave (1*S*,2*R*)-1-methyl-2-(trichlorosilylmethyl)indan (91% ee) and (*S*)-1-(2-(propenyl)phenyl)-1-trichlorosilylethanes (95% ee). Based on their opposite configurations at the benzylic position, a rationale for the high enantioselectivity of (*R*)-2-bis[3,5-bis(trifluoromethyl)phenyl]phosphino-1,1'-binaphthyl is proposed.

VII-A-2 Modification of Chiral Monodentate Phosphine Ligands (MOP) for Palladium-Catalyzed Asymmetric Hydrosilylation of Cyclic 1,3-Dienes

HAYASHI, Tamio; HAN, Jin Wook; TAKEDA, Akira; TANG, Jun; NOHMI, Kenji; MUKAIDE, Kotaro; TSUJI, Hayato; TORII, Akira; UOZUMI, Yasuhiro

[*Adv. Synth. Catal.* **343**, 279 (2001)]

Several MOP ligands containing aryl groups at 2' position of (*R*)-2-(diphenylphosphino)-1,1'-binaphthyl skeleton were prepared and used for palladium-catalyzed asymmetric hydrosilylation of cyclic 1,3-dienes with trichlorosilane. Highest enantioselectivity was observed in the reaction of 1,3-cyclopentadiene catalyzed by a palladium complex (0.25 mol%) coordinated with (*R*)-2-(diphenylphosphino)-2'-(3,5-dimethyl-4-methoxyphenyl)-1,1'-binaphthyl, which gave (*S*)-3-(trichlorosilyl)cyclopentene of 90% ee.

VII-A-3 (*R*)-2-Diphenylphosphino-2'-methoxy-1,1'-binaphthyl

UOZUMI, Yasuhiro; KAWATSURA, Motoi; HAYASHI, Tamio

[*Org. Syn.* **78**, 1 (2002)]

There exist transition metal-catalyzed reactions where the bisphosphine-metal complexes can not be used because of their low catalytic activity and/or low selectivity towards a desired reaction pathway and therefore chiral monodentate phosphine ligands are required for the realization of new types of catalytic asymmetric reactions. Unfortunately, there have been reported only a limited number of monodentate chiral

phosphine ligands, which are not so useful as bisphosphine ligands with few exceptions. Recently, the monodentate optically active phosphine ligand, 2-diphenylphosphino-2'-methoxy-1,1'-binaphthyl (MeO-MOP) and its analogs have been demonstrated to provide high enantioselectivity in palladium-catalyzed hydrosilyla-

tion of olefins and palladium-catalyzed reduction of allylic esters by formic acid. The procedures described here allow the convenient preparation of MOP and has advantages over previously published sequences. MeO-MOP can be prepared through 5 steps from binaphthol without racemization and the over all yield is 90%.

VII-B Green and Risk-Free Catalysis

Catalytic organic transformations under mild, safe, and green conditions is an important goal in synthetic organic chemistry. We recently reported that several palladium-catalyzed reactions, including π -allylic substitution, carbonylation, the Heck reaction, and Suzuki-Miyaura cross-coupling, took place in water by use of palladium-phosphine complexes bound to an amphiphilic polystyrene-poly(ethylene glycol) graft copolymer (PS-PEG) resin. PS-PEG resin-supported rhodium complexes was designed and prepared with a view toward using them in water. Rhodium-catalyzed hydroformylation, cyclotrimerization of alkynes, and Michael-type addition of arylboronic acids were found to proceed smoothly in water. Palladium-Catalyzed doublecarbonylation under very mild and safe conditions using Pd/PPh₃/DABCO/THF system was also investigated.

VII-B-1 Amphiphilic Resin-Supported Rhodium-Phosphine Catalysts for C-C Bond Forming Reactions in Water

UOZUMI, Yasuhiro; NAKAZONO, Maki

[*Adv. Synth. Catal.* **344**, 274 (2002)]

Amphiphilic resin-supported rhodium-phosphine complexes were prepared on polystyrene-poly(ethylene glycol) graft co-polymer (1% DVB cross-linked) beads. The immobilized rhodium complexes exhibited high catalytic activity in water to promote hydroformylation of 1-alkenes, [2+2+2] cyclotrimerization of internal alkynes forming benzene rings, and 1,4-addition of arylboronic acids.

VII-B-2 Double Carbonylation of Aryl Iodides with Primary Amines under Atmospheric Pressure Conditions Using Pd/PPh₃/DABCO/THF System

UOZUMI, Yasuhiro; ARII, Taro; WATANABE, Toshihiro

[*J. Org. Chem.* **66**, 5272 (2001)]

Double carbonylation of iodobenzene, *p*-iodoanisole, *p*-iodotoluene, and *m*-iodotoluene with primary alkylamines was catalyzed by a Pd-PPh₃ complex in THF in the presence of DABCO as base at 25 °C under atmospheric pressure of carbon monoxide to give phenyl, anisyl, *p*-tolyl, and *m*-tolyl glyoxamides, respectively, with selectivity greater than 90%.

VII-C Electrochemical Analysis of Biological Functions of Metalloproteins and their Mutated Molecules and its Applications to Coordination Chemistry for Catalysis

Using surface-functionalized electrodes, biological functions and bioelectrochemical properties of metalloproteins and their mutated and redox-center modified molecules have been analyzed electrochemically to develop new bioelectrocatalytic systems and bioelectro-functional devices.

Surface structures and properties of functional modified electrodes have also been examined at molecular level using STM, electrochemical and other spectroscopic techniques.

VII-C-1 Effects of Alkyl Chain as a Spacer on Electrochemical Reaction and SEIRA Spectra for Self-Assembled Monolayer Having Anthraquinone Redox Center

NISHIYAMA, Katsuhiko¹; KUBO, Atsushi¹;
TANIGUCHI, Isao²; YAMADA, Mami³;
NISHIHARA, Hiroshi³

(¹Kumamoto Univ.; ²IMS and Kumamoto Univ.; ³Univ. Tokyo)

[*Electrochemistry* **69**, 980 (2001)]

Self-assembled monolayers (SAMs) of 1-mercapto-anthraquinone (AQSC0), bis(3-(1-anthraquinonylthio)-propyl)disulfide (AQSC3) and bis(6-(1-anthraquinonylthio)hexyl)disulfide (AQSC6), on a gold electrode were investigated by cyclic voltammetry and surface enhanced infrared absorption spectroscopy (SEIRAS). A redox wave was observed for all the anthraquinone (AQ) derivatives and the redox potential shifted *ca.* -60 mV/pH in the pH region from 1 to 7. The peak separation of the voltammograms depended on the spacer length of the AQ derivatives, and the heterogeneous electron transfer rates of AQSC0, AQSC3 and AQSC6 at pH 1 were 7.5, 2.3×10^{-1} , and $3.1 \times 10^{-3} \text{ s}^{-1}$, respectively. For the SEIRA spectra of AQSC0 and AQSC3, the C=O stretching and C-C stretching bands of AQ ring were clearly observed, suggesting that the AQ ring plane is perpendicular or tilted to the electrode surface. The SEIRA signal of the AQ derivatives decreased with an increase in the alkyl chain length, indicating that the AQSC3 and AQSC6 molecules were adsorbed on the electrode not by the sulfide S atoms but by the thiolate S atoms.

VII-C-2 Analysis of Biological Functions of Metalloproteins Using Biocompatible Modified Electrodes

TANIGUCHI, Isao

(IMS and Kumamoto Univ.)

[*Anal. Sci.* **17**, 1355 (2001)]

Recent developments on bioelectroanalytical chemistry of metalloproteins have been discussed for the following subjects. 1) Surface structures for the rapid electron transfer of metalloproteins (in particular for cytochrome *c*) have been discussed and 3-mercapto-

pyridine has been shown as a new surface modifier for cytochrome *c* electrochemistry. 2) Biological functions and electron transfer kinetics of myoglobin have been analyzed by comparing electrochemical properties of native molecule with those of artificially designed molecules. For electron transfer kinetics, the re-organization energy due to the structural change at the redox center during electron transfer reaction has been shown to play an important role. 3) Use of ferredoxin as an electron-donating mediator, bioelectrocatalytic reactions have been demonstrated. These results suggest that electrochemical techniques using functional electrodes are useful for analysis and use of biological functions of metalloproteins.

VII-C-3 Interfacial Structures of Self-Assembled Monolayers of 2-Pyridinethiol on Au(111) Studied by In Situ Tunneling Microscopy

SAWAGUCHI, Takahiro¹; MIZUTANI, Fumio¹;
TANIGUCHI, Isao²

(¹Natl. Inst. Biosci. Human Tech.; ²IMS and Kumamoto Univ.)

[*Anal. Sci.* **17**, 1383 (2001)]

In situ Scanning Tunneling Microscope (STM) operating under electrochemical condition was used to study self-assembled monolayers of 2-pyridinethiol (2-PySH) on Au(111) in perchloric acid solution. Each molecule appeared as two spots, presumably originated from adsorption through S and N atoms of 2-pyridinethiolate with a vertical orientation on the Au(111) surface. The ordered 2-pyridinethiolate monolayers exhibited a *p* ($4 \times \sqrt{7R-40.9^\circ}$) structure, which was constructed by alternative arrangements of two types of molecular rows with differently rotated molecules. In situ STM also revealed that the monolayer consisted of molecularly ordered domains with the *p* ($4 \times \sqrt{7R-40.9^\circ}$) structure, its mirror structure defined as *p* ($4 \times \sqrt{7R-19.1^\circ}$), and their rotational structures. Detailed interfacial structures and molecularly ordered domains of 2-pyridinethiolate monolayer have been elucidated by in situ STM imaging in aqueous solution.

VII-C-4 NADP⁺ Sensor on *Chrorella* Ferredoxin/Ferredoxin-NADP⁺-Reductase Modified Indium Oxides

**NISHIYAMA, Katsuhiko¹; IKEBE, Hisami¹;
HOSHIDE, Yasuhiro¹; NAGAI, Hidenori¹;
TANIGUCHI, Isao²**
(¹Kumamoto Univ.; ²IMS and Kumamoto Univ.)

[*Chem. Sens.* **17**, 92 (2001)]

Chlorella ferredoxin (ChFd) was immobilized electrostatically with the aid of cationic polypeptides such as poly-L-lysine (PLL) or poly-L-ornithine onto indium oxide electrodes. Clear redox waves of the immobilized ChFd was observed. In the presence of ferredoxin-NADP⁺-reductase (FNR) and NADP⁺, NADP⁺ was reduced to NADPH electrocatalytically at the modified electrode. Also, both ChFd and FNR were immobilized on the electrode, and the prepared ChFd/FNR modified electrode was applied to the NADP⁺ sensor.

VII-C-5 Surface pKa of Amine-Terminated Self-Assembled Monolayers Evaluated by Direct Observation of Counter Anion by FT-Surface Enhanced Raman Spectroscopy

NISHIYAMA, Katsuhiko¹; KUBO, Atsushi¹; UEDA, Akihiro¹; TANIGUCHI, Isao²
(¹Kumamoto Univ.; ²IMS and Kumamoto Univ.)

[*Chem. Lett.* **80** (2002)]

The acid-base reaction of aminothanethol (2-AT) and 6-amino-1hexanethiol (6AT) self-assembled monolayers (SAMs) on a gold electrode was monitored by fourier-transform surface enhanced Raman spectroscopy (FT-SERS). A band attributed to counter anion, such as ClO₄⁻ or NO₃⁻ for NH₃⁺, was clearly observed during protonation of the amino group of 2AT or 6AT. The nband intensity decreased with increasing solution pH. The surface pKa's of 2AT and 6AT SAMs on a gold electrode at 0 V vs. Ag/AgCl (saturated KCl) were 5.0 ± 0.2 and 3.8 ± 0.3, as evaluated from the intensity-pH curve.

VII-C-6 Ion Selectivity for Electrode Reactions on Functionalized Monolayer Modified Electrode

**TANIGUCHI, Isao¹; HARA, Kazunori²;
ISHIMOTO, Hitoshi²; IWAI, Mitsuru²;
RANGARAJAN, Srinivasan²**
(¹IMS and Kumamoto Univ.; ²Kumamoto Univ.)

[*Chem. Sens.* **18**, 133 (2002)]

Electrode reactions of various ionic species on pyridine-, pyrimidine-, benzene- and related thiolate modified Au(111) and Au(100) single crystal surfaces were carried out. Clear selectivity of the electrode reaction for a given ionic species depending on the modified surface was seen. Charge of the ionic species was not so important. In particular, on the benzenethiolate modified electrode surface, the electrode reaction of ferri-/ferro- redox couple in acidic solution was clearly inhibited, but no inhibition was observed for the electrode reaction of ferri-/ferro-cyanide redox couple. On

the other hand, by increasing the number of -SH group in the benzene ring (1,4-dithiol < 1,3,5 trithiol < 1,2,4,5 tetrathiol), ferri-/ferro redox couple showed an increased enhancement of the electrochemical responses, but ferri-/ferro-cyanide redox couple showed an inhibition on the electrode reaction. On the bases of the properties of the modified electrode surfaces obtained by STM image, impedance analysis, contact angle and other data, the surface hydrophilicity (or hydration/dehydration of the ionic species) of the modified electrodes was concluded to play an important role on the electrode reaction of ferri-/ferro- redox couple.

VII-C-7 In-Situ STM Observation of Coronene Epitaxial Adlayers on Au(111) Surfaces Prepared by the Transfer of Langmuir Films

**UEMURA, Shinobu¹; SAKATA, Masayo¹;
TANIGUCHI, Isao²; HIRAYAMA, Chuichi¹;
KUNITAKE, Masashi¹**
(¹Kumamoto Univ.; ²IMS and Kumamoto Univ.)

[*Thin Solid Films* **409**, 206 (2002)]

A highly ordered epitaxial adlayer of coronene on an Au(111) surface was prepared by a wet process technique, which consisted of the simple transfer of Langmuir films. The structure and dependence on potential of the adlayer were then investigated by in situ scanning tunneling microscopy (STM). The adlayer processed a (4×4)-Au(111) superlattice structure, and each coronene molecule was visualized as an individual hexagon on high-resolution STM images. The multilayer portion was present without any potential control, probably due to the excess generated by the transfer. The adsorption behavior of coronene, including the formation of the multilayers, showed dependence on the potential. A flawless adlayer without the presence of any multilayers was achieved by the application of negative potential, in which the multilayer-substrate interaction was adequately weakened.

VII-C-8 New Route to Protoporphyrins III and XIII from Common Starting Pyrroles

HAREAU, G. P. -J¹; NEYA, Saburo²; FUNASAKI, Noriaki²; TANIGUCHI, Isao³
(¹Kumamoto Univ.; ²Kyoto Pharmaceutical Univ.; ³IMS and Kumamoto Univ.)

[*Tetrahedron Lett.* **43**, 3109 (2002)]

A new approach to protoporphyrins III (2') and XIII (3') has been developed based on a single set of starting materials, namely, 2,4-dimethyl-3-(2-chloroethyl)-carbethoxypyrrole (4) and 3,3'-di(2-methoxycarbonyl-ethyl)-4,4'-dimethyldipyrromethane-5,5' dicarboxylic acid (5) for both targets. The biladiene route was adopted for the preparation of 2' (five steps, 18% overall yield) while the coupling of two pyrromethenes was used to synthesize 3' (four steps, 11% overall yield).

VII-D Nano-Sciences of Advanced Metal Complexes

Recently, nano-sciences or nano-technologies have been attracting much attention because they show very interesting physical properties based on the non-linearity and quantum effect. There are two methods to obtain the nano-size materials, that is, "top-down" and "bottom-up." The top-down method such as laser abrasion has a limitation to make particles with less than 100 nm. On the other hand, the bottom-up method is promising to control the nano-size since the chemical reactions are available. However, the researches based on the bottom-up methods are rare and such methods have not been accomplished so far. There are three types of the target materials such as inorganic compounds, organic compounds, and metal complexes. The inorganic compounds easily take three-dimensional bulk structures. The organic compounds easily take 0- and 1-dimensional bulk materials. Therefore, neither inorganic nor organic compounds are suitable for the nano-sciences. On the other hand, the metal complexes easily take nano-size clusters where they are surrounded with the organic ligands. Therefore, the nano-sciences of the advanced metal complexes are most promising. As for the non-linearity, we focus on the gigantic third-order optical non-linearity. As for the quantum effect, we focus on the single-molecule magnets, nano-wire molecule-magnets, and nano-network molecule-magnets.

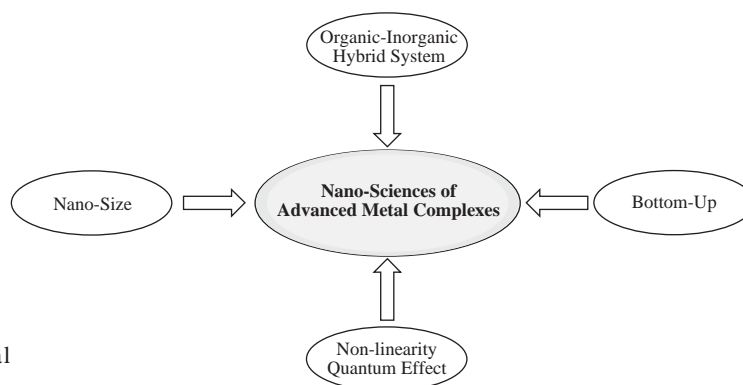


Figure 1. Nano-sciences of advanced metal complexes.

VII-D-1 Tuning of Electronic Structures of Quasi-One-Dimensional Bromo-Bridged Ni(III) Complexes with Strong Electron-Correlation by Doping of Co(III) Ions, $[\text{Ni}_{1-x}\text{Co}_x(\text{chxn})_2\text{Br}]_2\text{Br}_2$

YAMASHITA, Masahiro¹; YOKOYAMA, Kohei²; FURUKAWA, Sachie²; MANABE, Toshio²; ONO, Takashi²; NAKATA, Kazuya²; KACHITERAJIMA, Chihiro²; IWAHORI, Fumiyasu²; ISHII, Tomohiko²; MIYASAKA, Hitoshi²; SUGIURA, Ken-ichi²; MATSUZAKI, Hiroyuki³; KISHIDA, Hideo³; OKAMOTO, Hiroshi³; TANAKA, Hisaaki⁴; MARUMOTO, Kazuhiro⁴; ITO, Hiroshi⁴; KURODA, Shin-ichi⁴

(¹IMS and Tokyo Metropolitan Univ.; ²Tokyo Metropolitan Univ.; ³Univ. Tokyo; ⁴Nagoya Univ.)

[*Inorg. Chem.* **41**, 1998 (2002)]

The Ni(III) complexes doped by Co(III) ions, $[\text{Ni}_{1-x}\text{Co}_x(\text{chxn})_2\text{Br}]_2\text{Br}_2$ have been synthesized by electrochemical oxidation methods. The single crystal reflectance spectrum of $x = 0.118$ shows an intense CT band about 0.5 eV, which is lower than that of $[\text{Ni}(\text{chxn})_2\text{Br}]_2\text{Br}_2$ (1.3 eV). The single-crystal electrical conductivities at room temperature of these compounds increase with increase of the amounts of doping of Co(III) ions. In the ESR spectra, peak-to-peak line widths at room temperature change about 600 G in $[\text{Ni}(\text{chxn})_2\text{Br}]_2\text{Br}_2$ to 200 G in $x = 0.118$. Such a large x dependence of line widths seems to be ascribed to the increasing contribution from the increasing Curie spins which have smaller

line width. Therefore, we have succeeded in tuning the electronic structures of quasi-one-dimensional bromo-bridged Ni(III) complexes with strong electron-correlations by doping Co(III) ions.

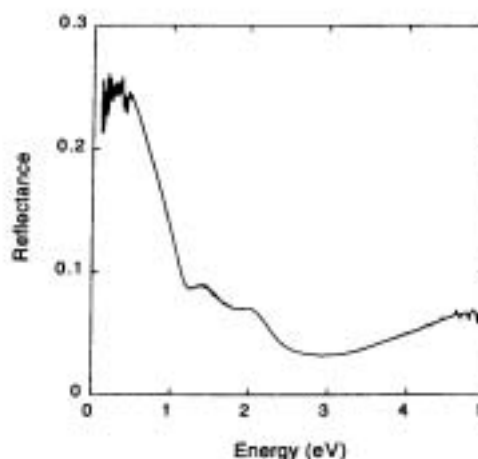


Figure 1. Single-crystal reflectance spectrum of $[\text{Ni}_{0.882}\text{Co}_{0.118}(\text{chxn})_2\text{Br}]_2\text{Br}_2$.

VII-D-2 Angle-Resolved Photoemission Study of the MX-Chain Compound $[\text{Ni}(\text{chxn})_2\text{Br}]_2\text{Br}_2$: Spin-Charge Separation in Hybridized d - p Chains

FUJIMORI, Shin-ichi¹; INO, Akihiro¹; OKANE, Tetsuo¹; FUJIMORI, Atsushi¹; OKADA, Kozo²; MANABE, Toshio³; YAMASHITA, Masahiro⁴;

KISHIDA, Hideo⁵; OKAMOTO, Hiroshi⁵
 (¹Spring-8; ²Okayama Univ.; ³Tokyo Metropolitan Univ.; ⁴IMS and Tokyo Metropolitan Univ.; ⁵Univ. Tokyo)

[*Phys. Rev. Lett.* **88**, 247601-1 (2002)]

Angle-resolved photoemission experiments have been carried out for a quasi-one-dimensional (1D) MX-chain compound $[\text{Ni}(\text{chxn})_2\text{Br}]\text{Br}_2$, which shows a gigantic nonlinear optical effect. A "band" having about 500 meV energy dispersion is found in the first half of the Brillouin zone, but disappears at $kb/\pi \sim 1/2$. These spectral features are well reproduced by the d - p chain model with a small charge-transfer energy Δ compared with that in 1D Cu-O compounds. It is proposed that this smaller Δ is the origin of the absence of clear spin-charge separation in the photoemission spectra and the strong nonlinear optical effect.

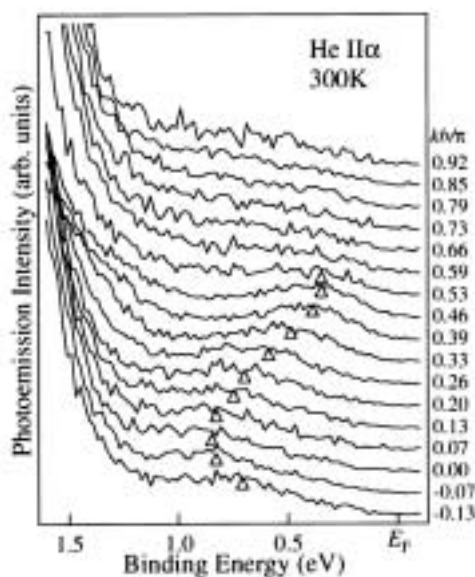


Figure 1. ARPES spectra of $[\text{Ni}(\text{chxn})_2\text{Br}]\text{Br}_2$.

VII-D-3 ESR Detection of Induced Spin Moments in Halogen-Bridged Mixed-Metal Complexes $\text{Ni}_{1-x}\text{Pd}_x(\text{chxn})_2\text{Br}_3$

TANAKA, Hisaaki¹; MARUMOTO, Kazuhiro¹; KURODA, Shin-ichi¹; MANABE, Toshio²; YAMASHITA, Masahiro³
 (¹Nagoya Univ.; ²Tokyo Metropolitan Univ.; ³IMS and Tokyo Metropolitan Univ.)

[*J. Phys. Soc. Jpn.* **71**, 1370 (2002)]

ESR measurements have been performed on single crystals of the quasi-one-dimensional halogen-bridged mixed-metal complexes, $\text{Ni}_{1-x}\text{Pd}_x(\text{chxn})_2\text{Br}_3$, where on-site Coulomb interaction (Ni^{3+} case) and electron-phonon interaction (Pd^{2+} - Pd^{4+} case) are competing with each other. Monotonic decrease of principal g -values from $g(\text{Ni})_{\text{max}} = 2.118$ to $g(\text{Pd})_{\text{max}} = 2.113$ was observed as x increases. This indicates that the magnetic Pd^{3+} ions with smaller g -value than that of Ni^{3+} are induced from non-magnetic Pd^{2+} - Pd^{4+} chain, which is

consistent with the previous observed spin susceptibility enhancement in this system. In addition, monotonic decrease of the ESR linewidth is observed as x increases indicating the contribution of Pd^{3+} ions with longer spin-lattice relaxation time T_{1D} , which is supported by using isomorphous chlorine complexes $\text{Ni}(\text{chxn})_2\text{Cl}_3$ and $\text{Pd}(\text{chxn})_2\text{Cl}_3$.

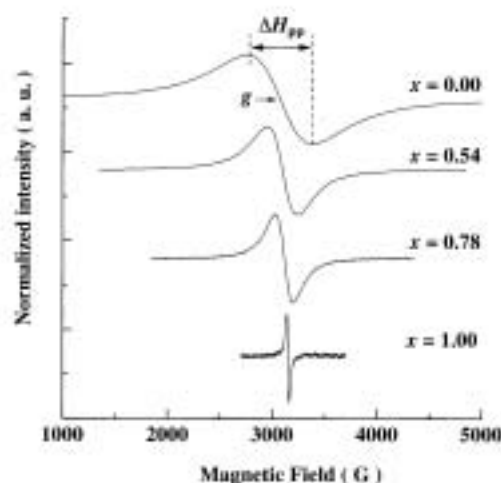


Figure 1. First derivative ESR spectra of single crystalline $\text{Ni}_{1-x}\text{Pd}_x(\text{chxn})_2\text{Br}_3$.

VII-D-4 A Chemical Modification of a Mn_{12} Single-Molecule Magnet by Replacing Carboxylate Anions with Diphenylphosphate Anions

KURODA-SOWA, Takayoshi¹; FUKUDA, Satoshi¹; MAEKAWA, Masahiko¹; MUNAKATA, Megumu¹; MIYASAKA, Hitoshi²; YAMASHITA, Masahiro³
 (¹Kinki Univ.; ²Tokyo Metropolitan Univ.; ³IMS and Tokyo Metropolitan Univ.)

[*Chem. Lett.* 682 (2002)]

Diphenylphosphate anion can replace with benzoate anions of $[\text{Mn}_{12}\text{O}_{12}(\text{O}_2\text{CPh})_{16}(\text{H}_2\text{O})_4]$ to afford a novel Mn_{12} single-molecule magnet (SMM) with mixed bridging ligands.

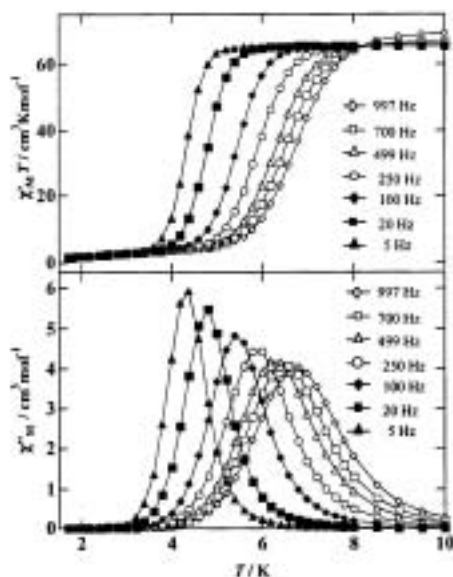


Figure 1. AC magnetic susceptibility data in the form of χ'_{M-T} - T (top) and χ''_{M-T} - T (bottom) plots.

VII-D-5 Construction of a One-Dimensional Chain Composed of Mn_6 Clusters and 4,4'-Bipyridine Linker: The First Step for Creation of "Nano-Dots-Wires"

NAKATA, Kazuya¹; SUGIMOTO, Kunihisa²;
ISHII, Tomohiko¹; SUGIURA, Ken-ichi¹;
YAMASHITA, Masahiro³
(¹Tokyo Metropolitan Univ.; ²Rigaku Co. Ltd.; ³IMS
and Tokyo Metropolitan Univ.)

[Chem. Lett. 658 (2002)]

Treatment of a mixed-valence Mn_6 cluster, $[Mn_6O_2(t-BuCO_2)_{10}(t-BuCO_2H)_4]$ (1), with 4,4'-bipyridine (bpy) in dichloromethane/1,2-dichloroethane solution gave a one-dimensional polymer chain compounds, $[Mn_6O_2(t-BuCO_2)_{10}(t-BuCO_2H)_2(bpy)]$ (2), in which the present cluster core was maintained as a building block.

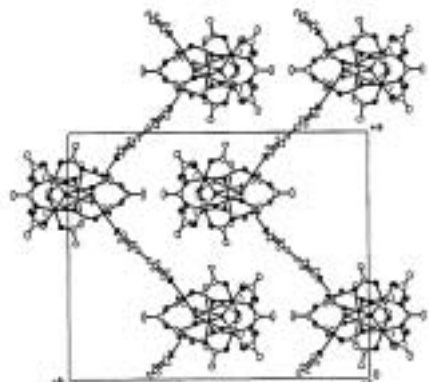


Figure 1. Packing diagram of the 1D chain compound projected along the c axis.

VII-D-6 Framework Engineering by Anions and Porous Functionalities Cu(II)/4,4'-bpy Coordination Polymers

NORO, Shin-ichiro¹; KITAURA, Ryo¹; KONDO, Mituru¹; KITAGAWA, Susumu¹; ISHII, Tomohiko²; MATSUZAKA, Hiroyuki²;
YAMASHITA, Masahiro³
(¹Kyoto Univ.; ²Tokyo Metropolitan Univ.; ³IMS and Tokyo Metropolitan Univ.)

[J. Am. Chem. Soc. 124, 2568 (2002)]

A combination of framework-builder (Cu(II) ion and 4,4'-bipyridine (4,4'-bpy) ligand) and framework regulator (AF_6 type anions; $A = Si, Ge,$ and P) provides a series of novel porous coordination polymers. The highly porous coordination polymers $\{[Cu(AF_6)(4,4'-bpy)_2]_8H_2O\}_n$ ($A = Si$ (1a.8H₂O), Ge (2a.8H₂O)) afford robust 3-dimensional (3-D), microporous networks (3D Regular Grid) by using AF_6^{2-} anions. The channel size of these complexes is *ca.* $8 \times 8 \text{ \AA}^2$ along the c -axis and $6 \times 2 \text{ \AA}^2$ along the a -axis or b -axis. When compounds 1a.8H₂O or 2a.8H₂O were immersed in water, a conversion of 3-D networks (1a.8H₂O or 2a.8H₂O) to interpenetrated network $\{[Cu(4,4'-bpy)_2(H_2O)_2] \cdot AF_6\}_n$ ($A = Si$ (1b) and Ge (2b)) (2D-interpenetration) took place. The 2-D interpenetrated network 1b shows unique dynamic anion-exchange properties, which accompany drastic structural conversions. When a PF_6^- monoanion instead of AF_6^{2-} dianion was used as the framework-regulator with another co-counteranion (coexistent anions), porous coordination polymer with various types of frameworks. Interestingly, these Cu(II) frameworks are rationally controlled by counteranions and selectively converted to other frameworks.

VII-D-7 New Microporous Coordination Polymer Affording Guest-Coordination Sites at Channel Walls

NORO, Shin-ichiro¹; KITAGAWA, Susumu¹;
YAMASHITA, Masahiro²; WADA, Tatsuo³
(¹Kyoto Univ.; ²IMS and Tokyo Metropolitan Univ.; ³RIKEN)

[Chem. Commun. 222 (2002)]

Utilization of a metalloligand, $\{[Cu(2,4-pydc)_2(H_2O)] \cdot 2Et_3NH\}$ (1) (2,4-pydc = pyridine-2,4-dicarboxylate), as a building unit provides a novel porous coordination polymer, $\{[ZnCu(2,4-pydc)_2(H_2O)_3(DMF)] \cdot DMF\}_n$ (2), in which the Zn(II) ion at the node of the network acts as a linker and the Cu(II) ion in the channel wall is available for guest-coordination.

VII-E Large Macrocyclic Formation Assisted by Coordination Bonds

There has been still continuous interest in large macrocyclic molecules due to their cavities formed inside the macrocycle capable of accommodating second molecules as a substrate. The macrocycles often exhibit size and/or shape selectivity, so-called molecular recognition, when binding to the substrate. However, the synthetic complexity of large macrocycles, *e.g.*, the multi-step reactions and the low yield in the ring-closure step, impedes progress in molecular recognition of rather large substrates. Coordination bonds which are slightly weaker than covalent bonds but are easy to form and sensitive to angle seem the most likely candidate for the bond in the ring-closure step. Here we report on a large macrocycle formation from a pair of ligand and metal through coordination bonds. The ligand is bidentate but impossible to be coordinated to a metal simultaneously due to the structure. A 2:2 metal-ligand complex possessing the macrocyclic cavity was thus selectively formed although an infinite ligand-metal array was also possible.

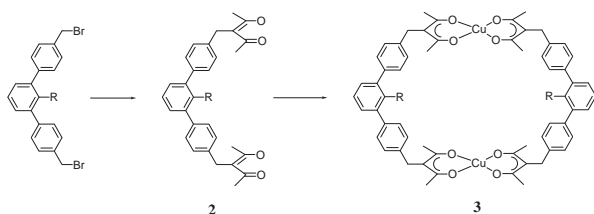
VII-E-1 Solution and Solid-State Characterization of a Dicopper Receptor for Large Substrates

DAVIDSON, Gerg J. E.¹; BAER, Andrew J.¹;
CÔTE, Adrien P.¹; TAYLOR, Nicholas J.¹;
HANAN, Gerry S.¹; TANAKA, Yasutaka³;
WATANABE, Masashi²

(¹Univ. Waterloo; ²Shizuoka Univ.; ³IMS and Shizuoka Univ.)

[*Can. J. Chem.* **80**, 496 (2002)]

Ligand **2** contains two metal-binding domains separated by a rigid spacer and assembles into a dicopper receptor **3** with a large central cavity with no evidence of catenation.



VII-F Development of New Carbonylation Reactions

Carbonylation is recognized as one of useful, reliable, and powerful synthetic methods of carbonyl compounds, such as aldehydes, ketones, esters, lactones, and so on. Our research effort is directed towards the discovery of *novel* type of the catalytic carbonylation reactions; (i) direct carbonylation at C–H bonds and (ii) cycloaddition reaction using carbon monoxide as a one-atom assembling unit (carbonylative cycloaddition reaction).

VII-F-1 Ru₃(CO)₁₂-Catalyzed Coupling Reaction of *sp*³ C–H Bonds Adjacent to a Nitrogen Atom in Alkylamines with Alkenes

CHATANI, Naoto¹; ASAUMI, Taku²; YORIMITSU, Shuhei²; IKEDA, Tsutomu²; KAKIUCHI, Fumitoshi²; MURAI, Shinji²
(¹Osaka Univ. and IMS; ²Osaka Univ.)

[*J. Am. Chem. Soc.* **123**, 10935 (2001)]

Catalytic reactions which involve the cleavage of an *sp*³ C–H bond adjacent to a nitrogen atom in *N*-2-pyridynyl alkylamines are described. The use of Ru₃(CO)₁₂ as the catalyst results in the addition of the *sp*³ C–H bond across alkene bond to give the coupling products. A variety of alkenes, including terminal, internal, and cyclic alkenes, can be used for the coupling reaction. The presence of directing groups, such as pyridine, pyrimidine, and an oxazoline ring, on the nitrogen of the amine is critical for a successful reaction. This result indicates the importance of the coordination of the nitrogen atom to the ruthenium catalyst. In addition, the nature of the substituents on the pyridine ring has a significant effect on the efficiency of the reaction. Thus, the substitution of an electron-withdrawing group on the pyridine ring as well as a substitution adjacent to the *sp*² nitrogen in the pyridine ring dramatically retards the reaction. Cyclic amines are more reactive than acyclic ones. The choice of solvent is

also very important. Of the solvents examined, 2-propanol is the solvent of choice.

VII-F-2 Catalytic Carbonylation Reactions of Benzyne Derivatives

CHATANI, Naoto¹; KAMITANI, Akihito²; OSHITA, Masayuki²; FUKUMOTO, Yoshiya²; MURAI, Shinji²

(¹Osaka Univ. and IMS; ²Osaka Univ.)

[*J. Am. Chem. Soc.* **123**, 12686 (2001)]

Carbonylation reactions of benzyne are described. The treatment of 2-trimethylsilylphenyl trifluoromethanesulfonate (**1**) with CsF and a catalytic amount of Co₄(CO)₁₂ in CH₃CN at 10 atm of CO at 60 °C gives anthraquinone (**2**). The product **2** consists of two molecules of benzyne, which is generated from the reaction of **1** with CsF, and two molecules of CO. The use of substituted benzyne precursors gives a nearly 1:1 mixture of regioisomers, indicating that a benzyne mechanism is operating. The reaction of **1a** with allyl acetate under CO (1 atm) in CH₃CN in the presence of [(π -C₃H₅)PdCl]₂, dppe, and CsF at 80 °C gives 2-methyleneindanone (**3**). The results on the reaction of substituted benzyne precursors clearly support the intervention of a free benzyne or similar species. The present reaction demonstrates the first example of the catalytic carbonylation of benzyne.

VII-G Development of Cycloisomerization Reactions

Cycloisomerization of enynes is useful methods for the construction of various ring systems from structurally simple acyclic starting materials. An issue critical to the synthetic utility of the cycloisomerization is whether complete conversion with formation of only one product can be attained, because difficulty in separation of the unreacted starting material from the product is foreseen. Simple metal halides, such as [RuCl₂(CO)₂]₂, PtCl₂, [IrCl(CO)₃]_n, and AuCl₃ was found to be the effective catalyst for the skeletal reorganization of enynes. The catalysis is initiated by the electrophilic addition of these metal halides to alkynes. This project focuses on the development of new catalytic reaction that consists of the new activation method of C–C triple bonds by metal halides.

VII-G-1 Cycloisomerization of ω -Aryl-1-Alkynes: GaCl₃ as a Highly Electrophilic Catalyst for Alkyne Activation

CHATANI, Naoto¹; INOUE, Hiroki²; MURAI, Shinji²
(¹Osaka Univ. and IMS; ²Osaka Univ.)

[*J. Org. Chem.* **67**, 1414 (2002)]

Cycloisomerization of a variety of ω -aryl-1-alkynes, where ω = 5 or 6, in the presence of a catalytic amount of GaCl₃ provided dihydronaphthalene derivatives or dihydrobenzocycloheptenes, respectively, in high yields. The reactions of the substrates containing electron-withdrawing groups on the aromatic ring were

significantly improved with GaCl₃ catalyst, compared with the previously reported catalytic system.

VII-H Multi-Electron Reduction of Carbon Dioxide through Metal-Carbonyl and Oxidative Activation of Water *via* Metal-Oxo Complexes

An electrophilic attack of CO₂ to coordinatively unsaturated low valent metal complexes affords $M-\eta^1\text{-CO}_2$ complexes, which are smoothly converted to $M\text{-CO}$ ones in protic and aprotic media. Organic synthesis through $M\text{-CO}$ complexes derived from CO₂, therefore, is highly desired in the viewpoint of C1 chemistry. A major problem to make multi-electron reduction of CO₂ is reductive cleavages of $M\text{-CO}$ bonds (CO evolution). This problem may be overcome by the construction of a catalytic system, which can supply electrons to carbonyl group of $M\text{-CO}$ bonds with depressing of an increase in the electron density at the central metal. Such requirements would be fulfilled by the metal complexes with a structurally flexible ligand having an ability to not only open and close a chelate ring for CO₂ binding but also to form a metallacycle including metal and carbon atoms of $M\text{-CO}$ bonds for inhibition of the bond cleavage.

High valent metal-oxo complexes are feasible candidates for oxidation and hydroxylation of non-activated hydrocarbons from the viewpoints of the enzymatic activity of P-450 enzymes. Mechanistic understandings of the reactivity of high-valent metal-oxo complexes have, however, been limited because no reasonable synthetic route for metal-oxo complex from dioxygen has been proposed so far in artificial systems. On the other hand, Ru-OH₂ complexes are smoothly converted to high-valent Ru=O ones by sequential electron and proton loss, and the latter has attracted much attention in the viewpoint of the elucidation of reactivity of metal-oxo frameworks. Taking into account that quinone undergoes stepwise reduction to yield semiquinone and catecholate, introduction of quinone ligands into the Ru-OH₂ framework would assist smooth conversion from aqua to oxo ligands without changing of the oxidation states of the central Ru.

VII-H-1 Syntheses of New Ruthenium Carbonyl Terpyridine *o*-Phenylene Complexes: Strong Interaction between Carbonyl and *o*-Phenylene Ligands

SUGIMOTO, Hideki¹; TANAKA, Koji
(¹Osaka City Univ.)

[*J. Organomet. Chem.* 280 (2001)]

Ruthenium carbonyl *o*-phenylene complexes, Ru(CO)(3,6-Bu₂seq)(trpy)]PF₆ (**1**)]PF₆ and [Ru(CO)(*o*-monothioat)(trpy)] (**2**) were prepared by the reaction of [Ru(CO)C₁₂(trpy)] with the corresponding *o*-phenylenes in 2-methoxyethanol. X-ray crystallographic study of **1**]BF₄ indicated that the ruthenium center is coordinated by carbonyl, three nitrogens of trpy and two oxygens of 3,6-Bu₂seq. ESR of **1**]PF₆ and **2** indicated that the electronic structures of ruthenium-*o*-phenylene unit of the complexes have Ru(II)-3,6-Bu₂seq and Ru(II)-*o*-monothioat forms, respectively. Significant differences in the redox behavior and the spectroscopic properties between **1**]PF₆ and **2** and [RuCl(3,5-Bu₂seq)(trpy)] were ascribed to the strong interaction between *o*-phenylene and carbonyl ligands through Ru(II).

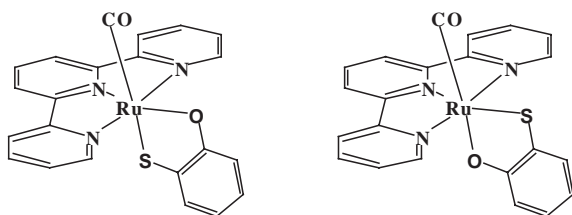


Figure 1. Two isomers of **2**.

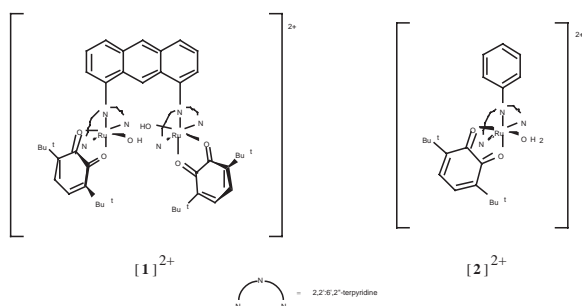
VII-H-2 Synthesis and Redox Properties of Bis(ruthenium-hydroxo)complexes with Quinone and Bipyridine Ligand as a Water-Oxidation Catalysts

WADA, Tohru; TSUGE, Kiyoshi; TANAKA, Koji

[*Inorg. Chem.* 40, 329 (2001)]

The novel bridging ligand 1,8-bis(2,2':6',2''-terpyridyl)anthracene (btpyan) is synthesized by three reactions from 1,8-diformylanthracene to connect two [Ru(L)(OH)]⁺ units ($L = 3,6\text{-di-tert-butyl-1,2-benzoquinone}$ (3,6-*t*Bu₂qui) and 2,2'-bipyridine (bpy)). An addition of *t*BuOK (2.0 equiv) to a methanolic solution of [Ru^{II}₂(OH)₂(3,6-*t*Bu₂qui)₂(btpyan)](SbF₆)₂ (**1**)](SbF₆)₂ results in the generation of [Ru^{II}₂(O)₂(3,6-*t*Bu₂sq)₂(btpyan)]⁰ (3,6-*t*Bu₂sq = 3,6-*di-tert-butyl-1,2-semiquinone*) due to the reduction of quinone coupled with the dissociation of the hydroxo protons. The resultant complex [Ru^{II}₂(O)₂(3,6-*t*Bu₂sq)₂(btpyan)]⁰ undergoes ligand-localized oxidation at $E_{1/2} = +0.40$ V (*vs* Ag/AgCl) to give [Ru^{II}₂(O)₂(3,6-*t*Bu₂qui)₂(btpyan)]²⁺ in MeOH solution. Furthermore, metal-localized oxidation of [Ru^{II}₂(O)₂(3,6-*t*Bu₂qui)₂(btpyan)]²⁺ at $E_p = +1.2$ V in CF₃CH₂OH/ether or water gives [Ru^{III}₂(O)₂(3,6-*t*Bu₂qui)₂(btpyan)]⁴⁺, which catalyzes water oxidation. Controlled-potential electrolysis of **1**)](SbF₆)₂ at +1.70 V in the presence of H₂O in CF₃CH₂OH evolves dioxygen with a current efficiency of 91% (21 turnovers). The turnover number of O₂ evolution increases to 33 500 when the electrolysis is conducted in water (pH 4.0) by using a **1**)](SbF₆)₂-modified ITO electrode. On the other hand, the analogous complex [Ru^{II}₂(OH)₂(bpy)₂(btpyan)](SbF₆)₂ (**2**)](SbF₆)₂ shows neither dissociation of the hydroxo protons, even in the presence of a large excess of *t*Bu-

OK, nor activity for the oxidation of H₂O under similar conditions.

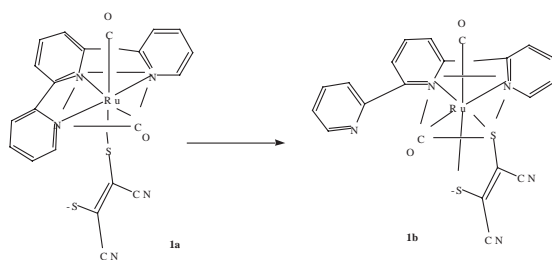


VII-H-3 Ruthenium Terpyridine Complexes with Mono- and Bi-Dentate Dithiolene Ligands

SUGIMOTO, Hideki¹; TSUGE, Kiyoshi; TANAKA, Koji
(¹Osaka City Univ.)

[*J. Chem. Soc., Dalton Trans.* 57 (2001)]

The reaction of [Ru(CO)₂Cl(terpy)]PF₆ (terpy = 2,2':6':2''-terpyridine) with Na₂mnt (mnt = S₂C₂(CN)₂) initially produced [Ru(CO)₂(mnt)(terpy-κ³NN'N'')] **1a**, which rearranged to [Ru(CO)₂(mnt-κ²SS')(terpy-κ²NN')] **1b** in solution. The molecular structures of **1a** and **1b** indicate that the rearrangement proceeds *via* a five-coordinated complex with monodentate mnt and bidentate terpy. The reaction of [Ru(CO)₂Cl(terpy)]PF₆ with 3,4-toluenedithiol (H₂tdt) gave [Ru(CO)₂(tdt-κ²SS')(terpy-κ²NN')] **2b** but [Ru(CO)₂(tdt-κS)(terpy-κ³NN'N'')] **2a** was not identified. Thus, ruthenium complexes with bidentate dithiolene and bidentate terpyridine seem to be more stable than those with monodentate dithiolene and tridentate terpyridine. Neither [Ru(CO)₂(pdt-κS)(terpy-κ³NN'N'')] **3a** nor [Ru(CO)₂(pdt-κ²S)(terpy-κ²NN')] **3b** (pdt = PhC(S)-C(S)Ph) was obtained in the reaction of [Ru(CO)₂Cl(terpy)]PF₆ with the Cs⁺ salt of pdt²⁻ in CH₃OH under N₂. The same reaction conducted under aerobic conditions afforded [Ru(CO)(C(O)OCH₃)(SC(Ph)C(Ph)-SC(O)OMe)(terpy-κ³NN'N'')] **3a** resulting from double addition of CO₂ and CH₃OH to the terminal sulfur of pdt and a carbonyl carbon of **3a**, respectively, followed by esterification of the resultant [Ru(CO)(C(O)OCH₃)(SC(Ph)C(Ph)SC(O)OH)(terpy-κ³NN'N'')] in CH₃OH. The addition of CO₂ to the sulfur of **3a** is ascribed to the strong basicity and weak chelating ability of pdt compared with those of mnt and tdt. A series of [RuX(dithiolene)(terpy)]ⁿ⁺ (X = dmsO, Cl or OSO₂CF₃; n = 0 or 1) were also prepared.

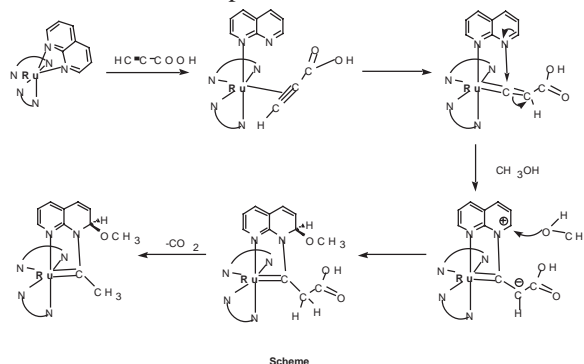


VII-H-4 A Ru-Carbene Complex with a Metallacycle Involving a 1,8-Naphthylidene Framework

TOMON, Takashi; OYAMA, Dai¹; WADA, Tohru; SHIREN, Kazushi; TANAKA, Koji
(¹Fukushima Univ.)

[*Chem. Commun.* 1100 (2001)]

A CH₃OH/H₂O solution containing [1](PF₆)₂ and HCCC(O)OH was refluxed for 2 h, and [2a](PF₆)₂ was obtained from the solution. Recrystallization of the crude product from CH₃CN/CH₃OH gave single crystals of [2a](PF₆)₂·CH₃CN in 64% yield. The similar reaction between [1](SbF₆)₂ and HCCC(O)OH in C₂H₅-OH/H₂O under similar reaction conditions afforded [2b](SbF₆)₂ in 56% yield. The ruthenium atom of **2a**²⁺ has octahedral geometry with four nitrogen atoms of two bpy ligands, one nitrogen from napy and one carbon of the CCH₃ group. The characteristic features of **2a**²⁺ are the C–N bond formation between the CCH₃ group and one nitrogen of napy, and the attachment of the CH₃O group to the 2-position of the napy moiety. The resultant five-membered metallacycle consisting of Ru, N(1), C(11), N(2), and C(2) atoms in an almost planar structure, and the sum of the bond angles around the five-membered ring is almost 360. Despite the attachment of CH₃O to the 2-position of the napy moiety, the resultant ligand still maintains the planar structure in **2a**²⁺. As a result, the napy moiety and the five-membered metallacycle are co-planar. The Ru–N(4) (2.156(9) Å) bond trans to Ru–C(2) is substantially longer than the other Ru–N bonds of **2a**²⁺ (2.03(1)–2.08(1) Å), suggesting a strong trans effect of the carbene ligand. The Ru–C(2) bond distance (1.93(1) Å) is in the expected range of hexa-coordinated ruthenium carbene bonds (1.941–1.98 Å), and the bond length is longer than those expected for penta-coordinated ruthenium carbene complexes (1.810–1.861 Å). The ¹³C NMR spectrum of **2a**²⁺ also showed the carbon signal of the Ru–CCH₃ group at 293 ppm as a singlet, similar to most Ru carbene complexes.



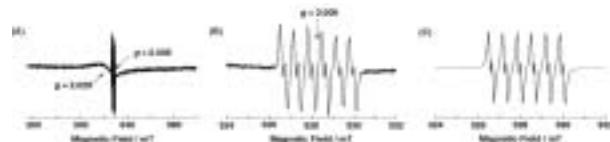
VII-H-5 Ruthenium Oxy Radical Complex Containing o-Quinone Ligand Detected by ESR Measurements of Spin Trapping Technique

KOBAYASHI, Katsuaki; OHTSU, Hideki; WADA, Tohru; TANAKA, Koji

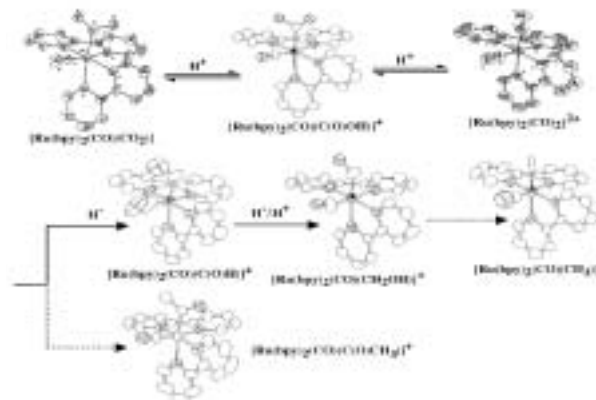
[Chem. Lett. 868 (2002)]

The ESR spectrum obtained upon an addition of a 3 equiv of *t*BuOK and DMPO to a CH₂Cl₂ solution of [Ru(trpy)(3,5-dbQ)(OH₂)]²⁺ at 193 K is depicted in Figure 1A and 1B, which shows an isotropic broad signal without hyperfine structure ($g = 2.029$, $\Delta H_{\text{msl}} = 7.3$ mT) together with 12-line sharp signal centered at $g = 2.006$ (Figure 1B). The pattern of ESR spectrum was not perturbed by a change of modulation amplitude within 0.14 mT. The hyperfine coupling constants values of the characteristic 12-line sharp signal ($g = 2.006$, $a_{\text{N}}^{\alpha} = 1.32$, $a_{\text{H}}^{\beta} = 0.63$ and $a_{\text{H}}^{\gamma} = 0.20$ mT) are determined by the computer simulation. The ESR signal centered at $g = 2.029$ is very close to those of the Ru^{II}-semiquinone complex, [Ru^{II}(trpy)(35*t*Bu₂SQ)AcO⁻] ($g = 2.030$, $\Delta H_{\text{msl}} = 8.0$ mT), thus, the isotropic broad signal ($g = 2.029$) can be assigned to the Ru^{II}-SQ moiety. The signal intensity resulted from the Ru^{II}-SQ moiety linearly increased with increasing amounts of *t*BuOK, when more than 1 eq of *t*BuOK was added to the solution. The other ESR signal centered at $g = 2.006$ can be assigned to the DMPO spin adduct, [Ru^{II}(trpy)-(35*t*Bu₂SQ)(O)(DMPO)]⁰.

Formation of the DMPO spin adduct is further confirmed by ESI mass spectrum which exhibited a signal at m/z 684. The observed mass and isotope patterns corresponded to [Ru^{II}(trpy)(35*t*Bu₂SQ)(¹⁶O)(DMPO)]⁺. The labeling experiment using H₂¹⁸O showed an expected signal at m/z 686 corresponding to [Ru^{II}(trpy)(35*t*Bu₂SQ)(¹⁸O)(DMPO)]⁺ suggesting that an oxyl radical ligand was generated by the deprotonation of an aqua ligand. Thus, oxyl radical is induced by the acid-base equilibrium of the aqua ligand coupled with the reduction of the quinone ligand.



catalyzed by metal complexes and the metal–carbon bond strength of each intermediate. The ruthenium–carbon bond distance of [Ru(bpy)₂(CO)L]^{*n*+} largely depends on the hybrid orbital of the carbon atom bonded to ruthenium and lengthens in the order Ru–C_{sp} < Ru–C_{sp2} < Ru–C_{sp3}. An unusual shift of the $\nu(\text{Ru-L})$ bands to higher wavenumber with decrease of the Ru–L bond distances was discussed in terms of σ - and π -character of the ruthenium–carbon bonds.



VII-H-6 Multi-Electron Reduction of CO₂ via Ru-CO₂-C(O)OH, -CO, -CHO, and -CH₂OH Species

TANAKA, Koji; OYAMA, Dai

A series of [Ru(bpy)₂(CO)L]^{*n*+} ($L = \text{CO}_2, \text{C(O)OH}, \text{CO}, \text{CHO}, \text{CH}_2\text{OH}, \text{CH}_3, \text{and C(O)CH}_3; n = 0, 1, 2$) were prepared and their molecular structures were determined by X-ray analyses. These complexes are reasonable models of reaction intermediates in the multi-electron reduction of CO₂ catalyzed by metal complexes, since reductive cleavage of the Ru–L bonds of the complexes in protic media affords HCOOH, CO, HCHO, CH₃OH, and CH₄ as two-, four-, six- and eight-electron reduction products of CO₂. The free energy required in the reduction of CO₂ progressively decreases with an increase of the number of electrons participating in the reduction of CO₂. The Ru–L bond character of the series of [Ru(bpy)₂(CO)L]^{*n*+} was assessed by the $\nu(\text{Ru-L})$ bands and the Ru–L bond distances from the viewpoint of elucidation of a correlation between free energy changes in the multi-electron reduction of CO₂

VII-I Silanechalcogenolato Complexes

Transition metal–chalcogenido clusters have attracted attention in light of their relevance to various active sites of metalloproteins, desulfurization catalysis, and inorganic functional materials. An important and challenging subject in this chemistry is to develop rational methods to synthesize desirable chalcogenido cluster complexes of high nuclearity, by assembling suitable metal–chalcogenido fragments. Compared with complexes containing alkyl(aryl) chalcogenolato ligands, the coordination chemistry of silanechalcogenolates has yet to be explored. However, the use of silanechalcogenolates has the following two advantages in developing rational synthetic routes to transition metal chalcogenido clusters. First, silicon–chalcogen (sulfur, selenium, and tellurium) bonds are expected to be more labile and more readily cleaved under a mild condition than corresponding carbon–chalcogen bonds. Secondly, the reactivity of silanechalcogenolato ligands can be controlled by steric and electronic properties of substituents in the silyl group. In this project, we are studying the chemistry of transition metal silanechalcogenolato complexes and their use as a precursor for cluster synthesis.

VII-I-1 Palladium Dimethylsilanedithiolato Complex: a Precursor for Ti–Pd and Ti–Pd–Ti Heterometallic Complexes

KOMURO, Takashi¹; MATSUO, Tsukasa;
KAWAGUCHI, Hiroyuki; TATSUMI, Kazuyuki¹
(¹Nagoya Univ.)

[*Chem. Commun.* 988 (2002)]

The bis-silylated sulfides ($R_3Si)_2S$ have been widely used to prepare a variety of metal sulfide clusters, because these reagents exploit the strength of the Si–O and Si–Cl bond to replace a halide, alkoxide, acetate or oxide with a sulfido ligand under very mild and controlled conditions. Therefore, a metal-silanethiolato complex (e.g., $M-SSiR_3$) would be expected to serve as a synthetic precursor of homo- and hetero-metallic sulfido clusters. However, compounds containing the silanethiolato ligand are less common compared with alkylthiolato complexes. The silanedithiolato complex $Pd(S_2SiMe_2)(PEt_3)_2$ (**1**) reacted with $(C_5H_5)TiCl_3$ and $TiCl_4(thf)_2$ to produce the heterometallic clusters $(C_5H_5)TiCl(\mu-S)_2Pd(PEt_3)_2$ (**2**) and $TiCl_2(S)(\mu-S)_2Pd_2(PEt_3)_4$ (**3**) along with silicon–sulfur bond cleavage, respectively.

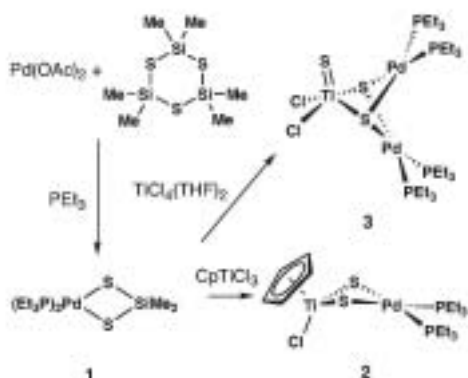


Figure 1.

VII-I-2 Synthesis and Reactions of Triphenylsilanethiolato Complexes of Manganese(II), Iron(II), Cobalt(II), and Nickel(II)

KOMURO, Takashi¹; KAWAGUCHI, Hiroyuki;
TATSUMI, Kazuyuki¹
(¹Nagoya Univ.)

[*Inorg. Chem.* **41**, 5083 (2002)]

Reactions of $Fe[N(SiMe_3)_2]_2$ with 1 and 2 equiv of Ph_3SiSH in hexane afforded dinuclear silanethiolato complexes, $[Fe\{N(SiMe_3)_2\}(\mu-SSiPh_3)]_2$ (**1**) and $[Fe(SSiPh_3)(\mu-SSiPh_3)]_2$ (**2**), respectively. Various Lewis bases were readily added to **2**, generating mononuclear adducts, $Fe(SSiPh_3)_2(L)_2$ [$L = CH_3CN$ (**3a**), $4-tBuC_5H_4N$ (**3b**), PEt_3 (**3c**), $(L)_2 = tmeda$ (**3d**)]. From the analogous reactions of $M[N(SiMe_3)_2]_2$ ($M = Mn, Co$) and $[Ni(NPh_2)_2]_2$ with Ph_3SiSH in the presence of TMEDA, the corresponding silanethiolato complexes, $M(SSiPh_3)_2(tmeda)$ [$M = Mn$ (**4**), Co (**5**), Ni (**6**)], were isolated. Treatment of **3a** with $(PPh_4)_2[MoS_4]$ or $(NEt_4)_2[FeCl_4]$ resulted in formation of a linear trinuclear Fe–Mo–Fe cluster $(PPh_4)_2[MoS_4\{Fe(SSiPh_3)_2\}_2]$ (**7**) or a dinuclear complex $(NEt_4)_2[Fe_2(SSiPh_3)_2Cl_4]$ (**8**). On the other hand, the reaction of **3a** with $[Cu(CH_3CN)_4](PF_6)$ gave a cyclic tetranuclear copper cluster $Cu_4(SSiPh_3)_4$ (**9**), where silanethiolato ligands were transferred from iron to copper. Silicon–sulfur bond cleavage was found to occur when the cobalt complex **5** was treated with $(NBu_4)F$ in THF, and a cobalt-sulfido cluster $Co_6(\mu_3-S)_8(PPh_3)_6$ (**10**) was isolated upon addition of PPh_3 to the reaction system. The silanethiolato complexes reported here are expected to serve as convenient precursors for sulfido cluster synthesis.

VII-J Coordination Chemistry of New Multidentate Ligands and Activation of Small Molecules

This project is focused on the design and synthesis of new ligands that are capable of supporting novel structural features and reactivity. Currently, we are investigating multidentate ligands based on aryloxy, thiolate, and amidinate. Our recent efforts have been directed toward activation of small molecules.

VII-J-1 Binuclear Iron(II) Complex from a Linked-bis(amidinate) Ligand: Synthesis and its Reaction with Carbon Monoxide

KAWAGUCHI, Hiroyuki; MATSUO, Tsukasa

[*Chem. Commun.* 958 (2002)]

We synthesized and fully characterized binuclear iron(II) complexes supported by a linked bis(amidinate) ligand. As part of a program aimed at developing new ancillary ligands to support reactive binuclear metal centers, we chose to employ a *trans*-cyclohexane-linked bis(amidinate) ligand L^{2-} . The use of this linked bis(amidinate) ligand leads to isolation of double-stranded binuclear complexes of iron(II), in which metal centers are coordinatively unsaturated. According to X-ray analyses, the size of a cage created by the L^{2-} ligands is flexible. Furthermore, another interesting aspect of this system is the ligand self-recognition in the assembly process. Although the racemic L^{2-} ligand is used, the reaction of racemic $Li_2(L)$ with $FeCl_2$ exclusively affords two discrete homochiral metal complexes Λ, Λ - $Fe_2(L^{RR})_2$ and Δ, Δ - $Fe_2(L^{SS})_2$. The robustness of this homochiral binuclear frame is examined in the reaction with CO.

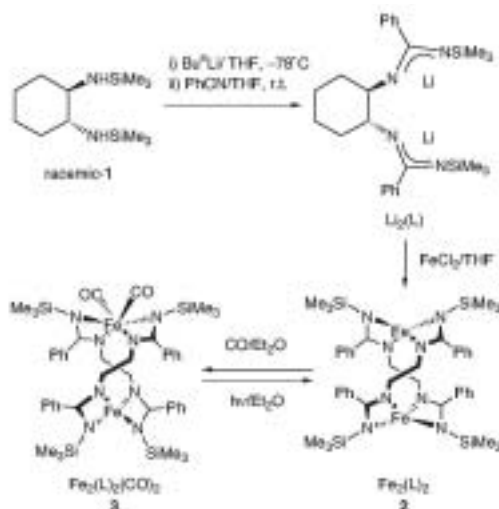


Figure 1.

VII-J-2 Synthesis and Structures of Ti(III) and Ti(IV) Complexes Supported by a Tridentate Aryloxy Ligand

MATSUO, Tsukasa; KAWAGUCHI, Hiroyuki; SAKAI, Masahiro

[*J. Chem. Soc., Dalton Trans.* 2536 (2002)]

Titanium complexes of the tridentate aryloxy $Me-L^{3-}$ [$H_3(Me-L) = 2,6$ -bis(4,6-dimethylsalicyl)-4-*tert*-butylphenol] have been prepared. Reaction of $TiCl_4$ with 1 equiv of $H_3(Me-L)$ gave $[Ti(Me-L)Cl]_2$ **1**. Recrystallization of **1** from THF resulted in formation of the THF adduct $Ti(Me-L)Cl(THF)_2$ **2**. Treatment of **1** with $[NEt_4]Cl$ in THF quantitatively gave $[NEt_4][Ti_2(Me-L)_2Cl_3]$ **3**. Complex **1** was reduced with 2 equiv of potassium to produce the Ti(III) complex $[Ti(Me-L)(DME)]_2$ **4**. Structures of **1**, **2**, **3**, and **4** have been determined by X-ray analyses. For **1**, **2**, and **4**, the $Me-L$ ligand assumes a U-conformation. In the case of **3**, it is coordinated in an S-conformation.

VII-J-3 Dinitrogen-Bond Cleavage in a Niobium Complex Supported by a Tridentate Aryloxy Ligand

KAWAGUCHI, Hiroyuki; MATSUO, Tsukasa

[*Angew. Chem., Int. Ed. Engl.* **41**, 2792 (2002)]

The $N \equiv N$ triple bond cleavage took place in the reaction of $[Nb(tBu-L)Cl_2]_2$ (**1**) with $LiBHET_3$, resulting in the formation of $[Nb(tBu-L)(\mu-N)Li(THF)]_2$ (**3**) [$H_3(tBu-L) = 2,6$ -bis(4,6-methyl-*tert*-butyl-salicyl)-4-*tert*-butylphenol]. On the other hand, the analogous reaction of $[Nb(Me-L)Cl_2]_2$ (**2**) with $LiBHET_3$ yielded $[Nb_2(Me-L)_2(\mu-H)(\mu-Cl)(THF)_2]Li_4(THF)_4Cl_2$ (**4**) [$H_3(Me-L) = 2,6$ -bis(4,6-dimethylsalicyl)-4-*tert*-butylphenol] concomitant with reduction of the metal center from Nb^V to Nb^{III} . Structures of **3** and **4** have been determined by X-ray diffraction analyses. Repeating the experiment under an atmosphere of $^{15}N_2$ affords $[Nb(tBu-L)(\mu-^{15}N)Li(THF)]_2$ (**3-¹⁵N**). The ^{15}N NMR spectrum of **3-¹⁵N** shows a single peak at δ 312, thus unambiguously confirming the origin of the bridging ligands in **3** to be N_2 . This work clearly shows that each $R-L^{3-}$ ligand behaves in a very distinctive manner with respect to dinitrogen activation and metal-metal interaction.

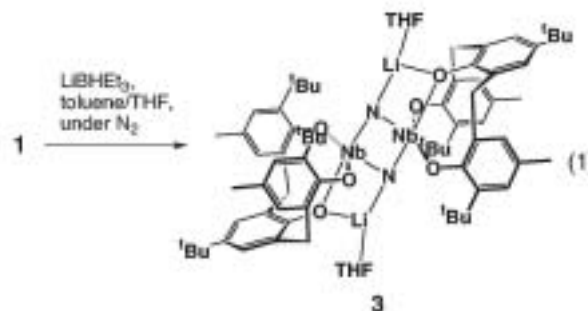


Figure 1.

VII-K Synthesis of Compounds Having a Novel Bonding Containing Heavier Main Group Elements

Double-bond compounds of main group elements of the second row such as olefins, carbonyl compounds, aromatic compounds, and azo compounds play very important roles in organic chemistry. However, the chemistry of their heavier element homologues has been undeveloped most probably due to their high reactivity and instability under ambient conditions. Since the first isolation of stable diphosphene (P=P), silene (Si=C), and disilene (Si=Si) in 1981 by taking advantage of steric protection, various double-bond compounds containing heavier main group elements have been synthesized and characterized.

On the other hand, we have developed an extremely bulky aromatic substituent, 2,4,6-tris[bis(trimethylsilyl)methyl]phenyl (denoted as Tbt hereafter) and 2,6-bis[bis(trimethylsilyl)methyl]-4-tris(trimethylsilyl)methylphenyl (denoted as Bbt hereafter). These substituents were found to be very effective steric protection groups for a variety of reactive species containing a heavier main group element. We have synthesized a variety of unprecedented low-coordinate compounds of heavier main group elements as stable compounds by taking advantage of kinetic stabilization using a new type of steric protection groups, Tbt and Bbt, and elucidated their properties.

VII-K-1 Syntheses and Crystal Structures of the First Disulfur and Diselenium Complexes of Platinum

NAGATA, Kazuto¹; TAKEDA, Nobuhiro¹; TOKITOH, Norihiro²
(¹Kyoto Univ.; ²IMS and Kyoto Univ.)

[*Angew. Chem. Int. Ed. Engl.* **41**, 136 (2002)]

The chemistry of complexes with diatomic chalcogen ligands has attracted much attention due to their unique structure, biological interest, potential for hydrogen-transfer catalysis, and synthetic utility as a precursor of new metal cluster complexes. However, since sulfur and selenium ligands have a strong propensity for bridging metal atoms, it is often difficult to prepare their mononuclear diatomic complexes. To our knowledge, the disulfur and diselenium complexes of platinum remain unknown, although the dioxygen analogues, *e. g.*, [(Ph₃P)₂PtO₂], have been extensively studied.

When platinum dichlorides **1a,b** were reduced by an excess of lithium naphthalenide in THF and the resulting platinum(0) species [(ArMe₂P)₂Pt] (**2a,b**) were successively treated with elemental sulfur (3 equiv. as S) and elemental selenium, the first platinum disulfur and diselenium complexes [(ArMe₂P)₂PtE₂] (**3a,b**: E = S; **4a,b**: E = Se) were obtained, respectively. The structures of **3a,b** and **4a,b** were identified by mass spectrometry, elemental analysis, and multinuclear NMR spectroscopy, and the molecular structures of **3b** and **4b** were finally determined by X-ray crystallographic analysis. The molecular structures of **3a,b** and **4a,b** are very similar, and these complexes have a square-planar geometry and a three-membered PtE₂ (E = S, Se) ring as well as an analogous dioxygen complex [(Ph₃P)₂PtO₂].

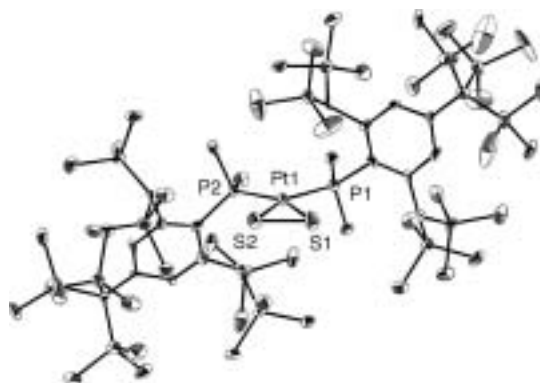
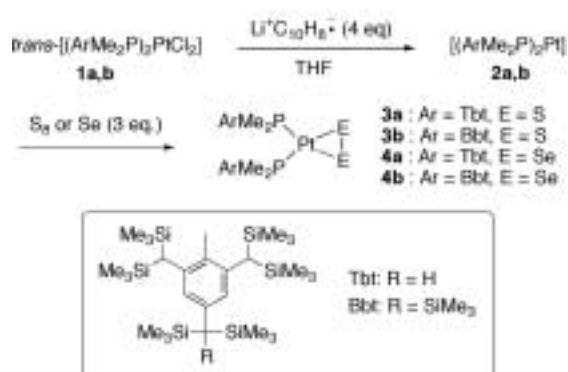


Figure 1. ORTEP drawing of a disulfur complex of platinum **3b**.

VII-K-2 Synthesis and Structure of the First Stable Phosphabismuthene

SASAMORI, Takahiro¹; TAKEDA, Nobuhiro²; FUJIO, Mizue¹; KIMURA, Masahiro³; NAGASE, Shigeru; TOKITOH, Norihiro⁴
(¹Kyushu Univ.; ²Kyoto Univ.; ³Tokyo Metropolitan Univ.; ⁴IMS and Kyoto Univ.)

[*Angew. Chem. Int. Ed. Engl.* **41**, 139 (2002)]

Recently, there has been much interest in doubly bonded compounds between group 15 elements, *i. e.*, heavier congeners of azo-compounds. Homonuclear

doubly bonded systems between heavier group 15 elements are no more imaginary species even in the case of bismuth, and the next target molecules are heteronuclear doubly bonded systems, which may be key compounds of great importance in the systematic elucidation of the intrinsic nature of low-coordinated compounds of heavier main group elements.

The first stable phosphabismuthene **1** was successfully synthesized by the condensation reaction of BbtBiBr_2 with Mes^*PH_2 in the presence of 1,8-diazabicyclo[5.4.0]undec-7-ene (DBU) in hexane at room temperature. It is noteworthy that compound **1** is not only a new member of a novel class of heteronuclear doubly bonded systems between heavier group 15 elements but also the first example of a stable species with a double bond between the third and sixth row main group elements. Phosphabismuthene **1** features a double bond between phosphorus and bismuth atom in the solid state and even in solution, as suggested by the NMR and UV/vis spectra and X-ray crystallographic analysis.

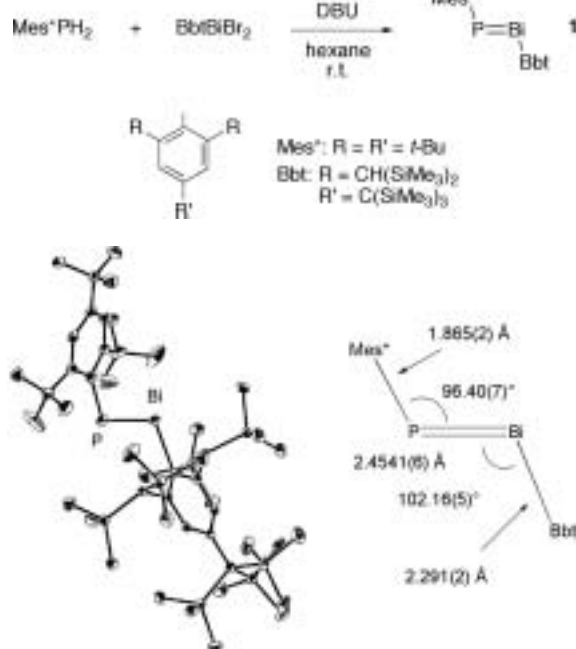


Figure 1. ORTEP drawing of phosphabismuthene **1**.

VII-K-3 Synthesis of Kineically Stabilized Silaneselone and Silanetellone

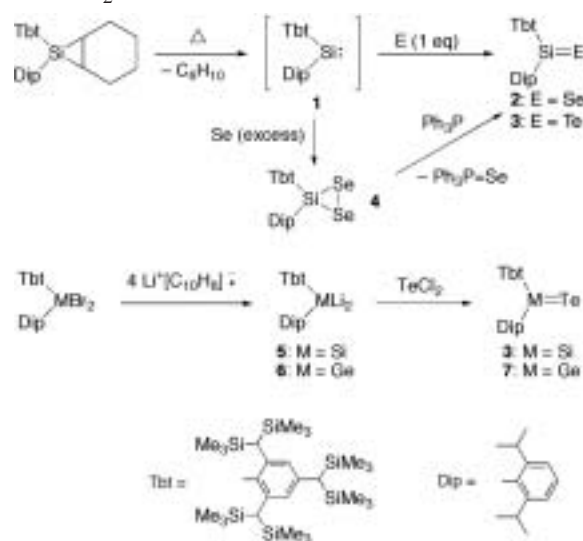
TOKITOH, Norihiro¹; SADAHIRO, Tomoyuki²; HATANO, Ken³; SASAKI, Takayo⁴; TAKEDA, Nobuhiro⁴; OKAZAKI, Renji²
(¹IMS and Kyoto Univ.; ²Univ. Tokyo; ³Kyushu Univ.; ⁴Kyoto Univ.)

[*Chem. Lett.* 34 (2002)]

Since ketones play very important roles in organic chemistry, much interest has been focused on the chemistry of double-bond compounds between heavier group 14 and group 16 elements (we refer to this family of heavier congeners of ketones as “heavy ketones”). As for silicon-containing heavy ketones, only a silanethione

bearing 2,4,6-tris[bis(trimethylsilyl)methyl]phenyl (Tbt) and 2,4,6-triisopropylphenyl (Tip) groups [Tbt(Tip)-Si=S] was isolated as a stable compound. Although some examples are known for silaneselones stabilized by the intramolecular coordination of a nitrogen atom and transient silaneselones as reactive intermediates, no coordination-free examples have been synthesized yet for silaneselones and silanetellones so far.

Kinetically stabilized silaneselone **2** and silanetellone **3** were successfully synthesized by direct chalcogenation of silylene **1** with elemental chalcogen. The formation of **2** and **3** was confirmed by multinuclear NMR spectroscopy and trapping experiments. Deselenation of diselenasilirane **4**, which was generated by the reaction of **1** with an excess of selenium, also gave **2**. In addition, metallanetellones, **3** and **7**, were synthesized by a new synthetic method for heavy ketones, *i. e.*, the reaction of dilithiomethane, **5** and **6**, with TeCl_2 .



VII-K-4 The First Stable 9-Silaanthracene

TAKEDA, Nobuhiro¹; SHINOHARA, Akihiro¹; TOKITOH, Norihiro²
(¹Kyoto Univ.; ²IMS and Kyoto Univ.)

[*Organometallics* 21, 256 (2002)]

Since aromatic compounds play very important roles in organic chemistry, much attention has been also paid to silaaromatics. However, there are few reports on the synthesis and isolation of silaaromatic compounds stable at room temperature because of their high reactivity. Recently, we have succeeded in the synthesis of the first stable 2-silanaphthalene and silabenzene by taking advantage of an efficient steric protection group, 2,4,6-tris[bis(trimethylsilyl)methyl]phenyl (Tbt). In contrast, silaanthracenes have never been isolated as stable compounds, although there are some reports of the chemical trapping of intermediary silaanthracenes and of observation by UV/vis spectroscopy of unstable silaanthracenes in matrices at low temperature.

The first stable 9-silaanthracene **1** was successfully synthesized by the reaction of the corresponding silyl triflate **2** with 1.0 molar amount of lithium diisopropyl-

amide. The aromaticity of **1** is discussed on the basis of the NMR, UV/vis, and Raman spectra, X-ray structural analysis, and theoretical calculations. Although 9-silaanthracene **1** is thermally stable even at 100 °C in solution, treatment of **1** with H₂O at room temperature gave the corresponding silanol (90%) via the 1,4-addition of water to the 9- and 10-positions of 9-silaanthracene ring. Furthermore, 9-silaanthracene **1** reacted with styrene and benzophenone at room temperature to give the corresponding [2 + 4] cycloadduct in good yields.

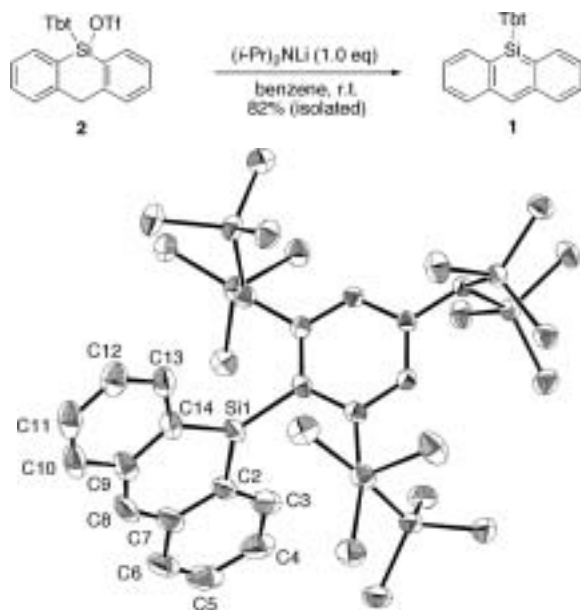


Figure 1. ORTEP drawing of 9-silaanthracene **1**.

VII-K-5 Synthesis and Characterization of an Extremely Hindered Tetraaryl-Substituted Digermene and its Unique Properties in the Solid State and in Solution

TOKITOH, Norihiro¹; KISHIKAWA, Kuniyuki²; OKAZAKI, Renji²; SASAMORI, Takahiro³; NAKATA, Norio³; TAKEDA, Nobuhiro³
(¹IMS and Kyoto Univ.; ²Univ. Tokyo; ³Kyoto Univ.)

[*Polyhedron* **21**, 563 (2002)]

During the last two decades remarkable progress has been made in the chemistry of low-coordinate compounds of heavier group 14 elements, especially in those of dimetallenes and metallylenes because of their unique structures and reactivities. In this paper, we present the synthesis and characterization of an extremely hindered digermene **1** bearing 2,4,6-tris[bis(trimethylsilyl)methyl]phenyl (Tbt) group.

Digermene **1** was synthesized by the reaction of Tbt(Mes)GeCl₂ with lithium naphthalenide, and its crystal structure was determined by X-ray crystallographic analysis. An equilibrium between the digermene **1** and the corresponding germylene **2** was observed by the UV/vis spectra, and the thermodynamic parameters for the dissociation of digermene **1** to germylene **2** were obtained from temperature dependence of the absorption of **1**. Reactions of the digermene with O₂, W(CO)₅-

(THF), *etc.* in solution proceeded via the germylene, while, in the solid state, the digermene reacts with O₂ without the dissociation into the germylene.

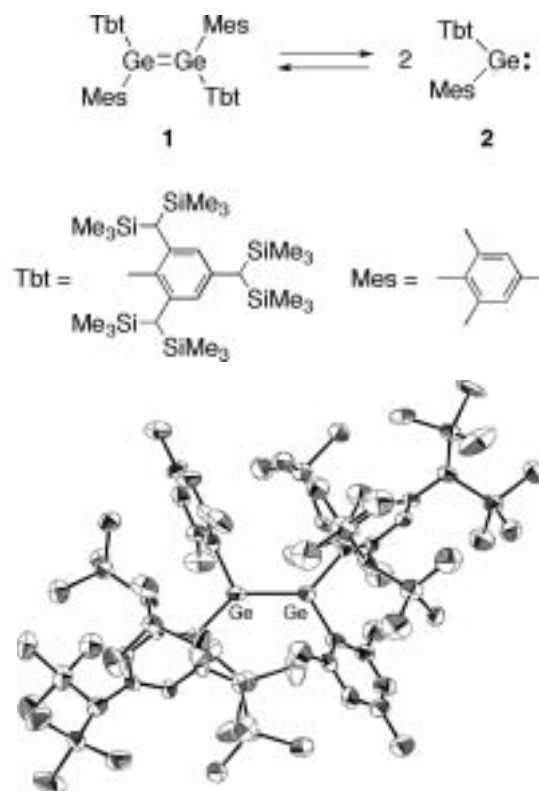


Figure 1. ORTEP drawing of digermene **1**.

VII-K-6 Syntheses, Structures and Properties of Kinetically Stabilized Distibenes and Dibismuthenes, Novel Doubly Bonded Systems between Heavier Group 15 Elements

SASAMORI, Takahiro¹; ARAI, Yoshimitsu²; TAKEDA, Nobuhiro³; OKAZAKI, Renji²; FURUKAWA, Yukio⁴; KIMURA, Masahiro⁵; NAGASE, Shigeru; TOKITOH, Norihiro⁶
(¹Kyushu Univ.; ²Univ. Tokyo; ³Kyoto Univ.; ⁴Waseda Univ.; ⁵Tokyo Metropolitan Univ.; ⁶IMS and Kyoto Univ.)

[*Bull. Chem. Soc. Jpn.* **75**, 661 (2002)]

The syntheses of stable compounds containing multiple bonds between heavier main group elements have been among the frontiers of great interest in chemical research. Nowadays, as for the heavier dipnictene series, numerous examples of kinetically stabilized diphosphenes (RP=PR), diarsenes (RA=AsR), and phospharsenes (RP=AsR) have been isolated and fully characterized, and their various chemical properties have been revealed. However, distibene (RSb=SbR) and dibismuthene (RBi=BiR) had not been reported until our successful syntheses of the first stable distibene and dibismuthene utilizing a very effective and bulky substituent, 2,4,6-tris[bis(trimethylsilyl)methyl]phenyl (Tbt) group.

Stable distibenes and dibismuthenes were successfully synthesized by taking advantage of an efficient

steric protection group, Tbt or 2,6-bis[bis(trimethylsilyl)methyl]-4-[tris(trimethylsilyl)methyl]phenyl (Bbt) group. The crystallographic analysis and spectroscopic studies of these stable dipnictenes led to the systematic comparison of structural parameters and physical properties for all homonuclear doubly bonded systems between heavier group 15 elements. In addition to these experimentally obtained results, theoretical calculations for these doubly bonded systems also revealed the intrinsic character of dipnictenes.

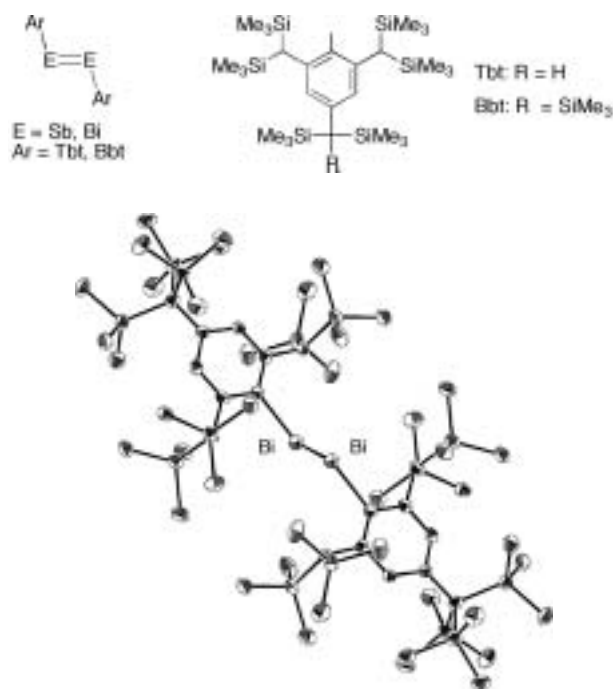


Figure 1. ORTEP drawing of BbtBi=BiBbt.

VII-K-7 Synthesis and Properties of the First Stable Germabenzene

NAKATA, Norio¹; TAKEDA, Nobuhiro¹;
TOKITOH, Norihiro²
(¹Kyoto Univ.; ²IMS and Kyoto Univ.)

[*J. Am. Chem. Soc.* **124**, 6914 (2002)]

Recently, much attention has been focused on the chemistry of $[4n + 2]$ π -electron ring systems containing at least one heavier group 14 element. However, no synthesis and isolation of these compounds as stable molecules had been reported until quite recently due to their extremely high reactivity. We have recently succeeded in the synthesis and characterization of the first stable silabenzene, 2-silanaphthalene, 9-silaanthracene, and 2-germanaphthalene by taking advantage of an efficient steric protection group, 2,4,6-tris[bis(trimethylsilyl)methyl]phenyl (Tbt). These successful results in the sila- and germaaromatic systems naturally prompted us to extend this method to the synthesis of a germabenzene, which is the most fundamental germaaromatic compound having a simple 6 π -electron ring system.

The first stable germabenzene **1** was successfully synthesized by the reaction of the corresponding chloro-

germane **2** with lithium diisopropylamide in THF. The molecular structure and aromaticity of **1** were discussed on the basis of its NMR, UV-vis, and Raman spectra, X-ray crystallographic analysis, and theoretical calculations. Although the structural and spectroscopic data showed that **1** had aromaticity, in the reaction with various reagents, germabenzene **1** underwent 1,2- and/or 1,4-addition to the 1-germabuta-1,3-diene moiety reflecting the extremely high reactivity of the Ge-C double bond.

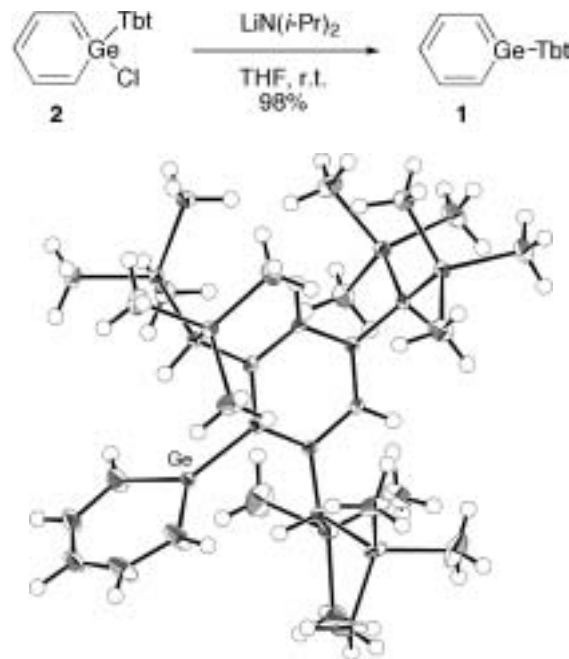


Figure 1. ORTEP drawing of germabenzene **1**.

VII-K-8 Reactions of 2-Germanaphthalene with Elemental Sulfur and Selenium: Synthesis of Novel Cyclic Polychalcogenides Containing a Germanium, Trichalcogenagermolanes

NAKATA, Norio¹; TAKEDA, Nobuhiro¹;
TOKITOH, Norihiro²
(¹Kyoto Univ.; ²IMS and Kyoto Univ.)

[*Chem. Lett.* 818 (2002)]

The chemistry of cyclic polychalcogenides has attracted much interest because of their unique structures, reactivities and biological activities. Among them, however, cyclic polychalcogenides containing a germanium atom have been little known. Herein, we present the synthesis of novel Ge-containing cyclic polychalcogenides by the reactions of the first stable 2-germanaphthalene **1** bearing 2,4,6-tris[bis(trimethylsilyl)methyl]phenyl (Tbt) with elemental sulfur and selenium.

The reactions of a kinetically stabilized 2-germanaphthalene **1** with elemental sulfur and selenium resulted in the formation of novel five-membered cyclic trichalcogenides, **2** and **3**, containing a germanium, and the molecular structure of the triselenide was determined by X-ray crystallographic analysis. Desulfurization of **2** with 3 equivalent of Ph₃P resulted in the

formation of **1** (76%), while deselenation of **3** with 3 equivalent of Ph_3P gave a novel heterocycle, 1-selena-2,5-digermacyclopentane **4** (82%).

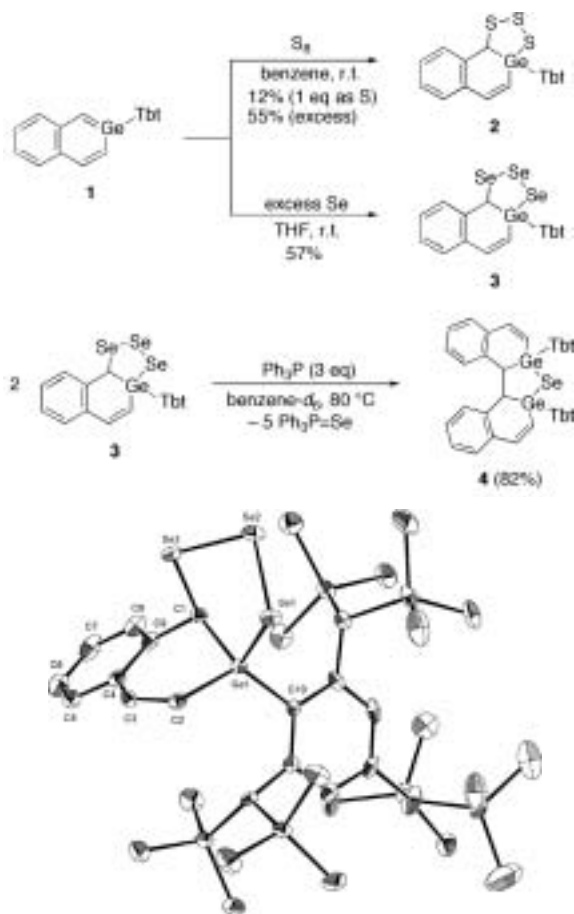


Figure 1. ORTEP drawing of triselenagermolane **3**.

VII-K-9 Synthesis and Properties of the First Stable 1-Silanaphthalene

TAKEDA, Nobuhiro¹; SHINOHARA, Akihiro¹; TOKITO, Norihiro²
(¹Kyoto Univ.; ²IMS and Kyoto Univ.)

[Organometallics in press]

In recent decades, much interest has been paid to the chemistry of silicon analogs of aromatic compounds. However, the properties of sila-aromatic compounds have not been fully revealed yet because of the extreme instability of the low-coordinated silicon compounds. Very recently, we have succeeded in the synthesis of the first stable silabenzene, 2-silanaphthalene, and 9-silanthracene by taking advantage of an extremely bulky substituent, 2,4,6-tris[bis(trimethylsilyl)methyl]phenyl (Tbt). On the other hand, there is no report for the synthesis of 1-silanaphthalene, which is a structural isomer of 2-silanaphthalene, although much attention has been focused on the similarities and differences between 1- and 2-silanaphthalenes.

The first 1-silanaphthalene **1** was successfully synthesized as moisture-sensitive, pale yellow crystals by taking advantage of Tbt group. The structure of **1**

was determined based on its ^1H , ^{13}C , and ^{29}Si NMR, Raman, and UV/vis spectra together with theoretical calculations. These data clearly indicated that **1** has aromaticity comparable with naphthalene as well as Tbt-substituted 2-silanaphthalene. In contrast to the thermal stability of 2-Tbt-2-silanaphthalene, 1-Tbt-1-silanaphthalene (**1**) underwent a ready [2 + 4] dimerization reaction in solution even at room temperature.



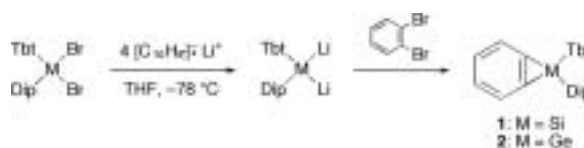
VII-K-10 Synthesis and Isolation of the First Germacyclopropabenzene: A Study to Elucidate the Intrinsic Factor for the Ring Deformation of Cyclopropabenzene Skeletons

TOKITO, Norihiro¹; HATANO, Ken²; SASAKI, Takayo³; SASAMORI, Takahiro³; TAKEDA, Nobuhiro³; TAKAGI, Nozomi; NAGASE, Shigeru
(¹IMS and Kyoto Univ.; ²Kyushu Univ.; ³Kyoto Univ.)

[Organometallics in press]

Since the finding of significant deformation for the fused aromatic rings in the series of benzocycloalkanes, it has been one of the important subjects assigned to organic chemists to solve a riddle for such deformation. Cyclopropabenzene has attracted special attention because of the most severely enforced deformation in this series. Recently, we have synthesized and isolated silacyclopropabenzene **1** as the first example of a stable heteracyclopropabenzene by taking advantage of the characteristic reactivity of the sterically hindered dilithiosilane, $\text{Tbt}(\text{Dip})\text{SiLi}_2$ (Tbt = 2,4,6-tris[bis(trimethylsilyl)methyl]phenyl, Dip = 2,6-diisopropylphenyl), towards 1,2-dibromobenzene. This successful isolation of **1** naturally prompted us to examine the synthesis of germacyclopropabenzene.

The treatment of an overcrowded diaryldilithio-germane, $\text{Tbt}(\text{Dip})\text{GeLi}_2$, generated by exhaustive reduction of $\text{Tbt}(\text{Dip})\text{GeBr}_2$, with 1,2-dibromobenzene resulted in the isolation of the first stable germacyclopropabenzene **2**, which was fully characterized by ^1H and ^{13}C NMR spectra, FAB-MS, and X-ray structural analysis. As well as the case of silacyclopropabenzene **1**, the structural parameters of **2** indicated that the germacyclopropane ring can enjoy annelation with much less perturbation, in contrast to the severe distortion in cyclopropabenzene rings.



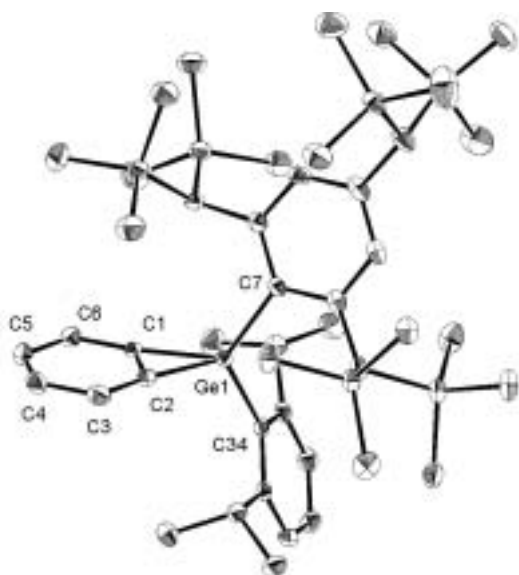


Figure 1. ORTEP drawing of germacyclopropabenzene 1.

VII-L Precise Synthesis of Functional Macromolecules Using Organometallic Complexes

The helix is one of the most important and fundamental secondary structures of macromolecules and is closely related to the unique functionalities of biomacromolecules. This project focuses on the development of precise polymerization catalyzed by organometallic complexes providing novel functional macromolecules, in which not only molecular weight and sequence but also secondary structures are well controlled. We also examined the physical and chemical properties of the resulting helical polymers.

VII-L-1 Helical Poly(aryl isocyanide)s Possessing Chiral Alkoxy-carbonyl Groups

TAKEL, Fumie¹; HAYASHI, Hiroko¹; ONITSUKA, Kiyotaka²; TAKAHASHI, Shigetoshi¹
(¹Osaka Univ.; ²Osaka Univ. and IMS)

[*Polymer J.* **33**, 310 (2001)]

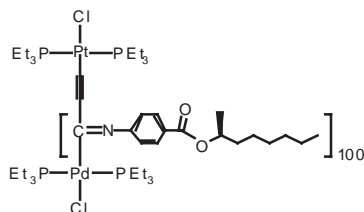
The relation between the structure of chiral monomers and the selectivity of the screw sense of poly(aryl isocyanide)s having several kinds of chiral alkoxy-carbonyl groups was determined. The selectivity of screw sense in the poly(aryl isocyanide)s depends on the some structural factors including the position of chiral substituents on aromatic rings, the position of stereogenic center, and the bulkiness of chiral groups.

VII-L-2 Formation of an Optically Active Helical Polyisocyanide Langmuir-Blodgett Film

FENG, Fei¹; MIYASHITA, Tokuji¹; TAKEL, Fumie²; ONITSUKA, Kiyotaka³; TAKAHASHI, Shigetoshi²
(¹Tohoku Univ.; ²Osaka Univ.; ³Osaka Univ. and IMS)

[*Chem. Lett.* 764 (2001)]

An optically active helical polyisocyanide synthesized with a screw-sense selective living polymerization formed a condensed monolayer on the water surface and was transferred onto a solid support as Y-type LB film with an ordered orientation.

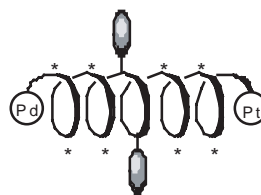
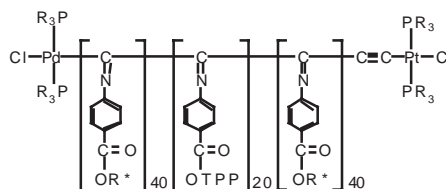


VII-L-3 Helical Chiral Polyisocyanides Possessing Porphyrin Pendants: Determination of Helicity by Exciton Coupled Circular Dichroism

TAKEL, Fumie¹; HAYASHI, Hiroko¹; ONITSUKA, Kiyotaka²; KOBAYASHI, Nagao³; TAKAHASHI, Shigetoshi¹
(¹Osaka Univ.; ²Osaka Univ. and IMS; ³Tohoku Univ.)

[*Angew. Chem., Int. Ed.* **40**, 4092 (2001)]

A novel and practical method for determining the helical sense of poly(aryl isocyanide)s has been developed by using exciton coupled CD of the porphyrin Soret band in triblock copolymers between chiral isocyanide monomers and an achiral tetraphenylporphyrin derivative.



RESEARCH ACTIVITIES VIII

Laser Research Center for Molecular Science

VIII-A Developments and Researches of New Laser Materials

Although development of lasers is remarkable, there are no lasers which lase in ultraviolet and far infrared regions. However, it is expected that these kinds of lasers break out a great revolution in not only the molecular science but also in the industrial world.

In this project we research characters of new materials for ultraviolet and far infrared lasers, and develop new lasers by using these laser materials.

VIII-A-1 Ce³⁺:LiCaAlF₆ Crystal for High-Gain or High-Peak-Power Amplification of Ultraviolet Femtosecond Pulses and New Potential Ultraviolet Gain Medium: Ce³⁺:LiSr_{0.8}Ca_{0.2}AlF₆

LIU, Zhenlin¹; KOZEKI, Toshimasa; SUZUKI, Yuji; SARUKURA, Nobuhiko; SHIMAMURA, Kiyoshi²; FUKUDA, Tsuguo²; HIRANO, Masahiro¹; HOSONO, Hideo^{1,3}

(¹ERATO; ²Tohoku Univ.; ³Tokyo Inst. Tech.)

[*IEEE J. Sel. Top. Quantum Electron.* **7**, 542 (2001)]

To develop high-peak-power ultrashort pulse laser systems in the ultraviolet region, a large Ce³⁺:LiCaAlF₆ (Ce:LiCAF) crystal, a tunable ultraviolet laser medium with large saturation fluence and broad gain spectrum width, was grown successfully with a diameter of more than 70 mm. To demonstrate high small signal gain, a four-pass confocal amplifier with 60 dB gain and 54 mJ output energy was constructed. Chirped pulse amplification (CPA) in the ultraviolet region was demonstrated using Ce:LiCAF for higher energy extraction. A modified bow-tie-style four-pass amplifier pumped by 100-mJ 266-nm 10-Hz pulses from a Q-switched Nd:YAG laser had 370-times gain and delivered 6-mJ 290-nm pulses. After dispersion compensation, the output pulses can be compressed down to 115 fs. This is the first ultraviolet, all-solid-state high-peak-power CPA laser system using ultraviolet gain media, and this demonstration shows further scalability of the Ce:LiCAF CPA system. Additionally, a new gain medium, Ce³⁺:LiSr_{0.8}Ca_{0.2}AlF₆, with longer fluorescence lifetime and sufficient gain spectrum width over 18 nm was grown to upgrade this system as a candidate for a final power amplifier gain module.

VIII-A-2 Optical Fiber for Deep Ultraviolet Light

OTO, Masanori¹; KIKUGAWA, Shinya²; SARUKURA, Nobuhiko; HIRANO, Masahiro³; HOSONO, Hideo^{3,4}

(¹Showa Electric Wire Cable; ²Asahi Glass Co. Ltd.; ³ERATO; ⁴Tokyo Inst. Tech.)

[*IEEE Photonics Technol. Lett.* **13**, 978 (2001)]

Deep ultraviolet optical fibers are fabricated using modified SiO₂ glasses containing 2000-ppm fluorine for

the clad and 200 ppm for the core. The transmission at 193 nm is improved to more than 60%/m by optimizing the fiber drawing condition. The H-2-impregnation into the fiber suppresses the degradation of the transmission by irradiation of ArF excimer laser (50 mJ/cm²/pulse). Further improvement may be expected by reducing oxygen-deficient center (I) defect generation in the drawing process.

VIII-A-3 Crystal Growth of Fluorides for Optical Applications

SHIMAMURA, Kiyoshi¹; SATO, Hiroki¹; BENSALAH, Amina¹; SUDESH, Vikas¹; MACHIDA, Hiroshi²; SARUKURA, Nobuhiko; FUKUDA, Tsuguo¹

(¹Tohoku Univ.; ²Tokin Corp.)

[*Cryst. Res. Technol.* **36**, 801 (2001)]

Ce-doped and undoped LiCaAlF₆, LiSrAlF₆, LiYF₄, LiLuF₄ and KMgF₃ single crystals were grown by the Czochralski technique under CF₄ atmosphere. The effective distribution coefficients of Ce³⁺ in LiCaAlF₆, LiSrAlF₆, LiYF₄ and LiLuF₄ were determined to be 0.031, 0.028, 0.116 and 0.054, respectively. Laser output energy of 60 mJ and 27 mJ were obtained using the grown Ce:LiCaAlF₆ and Ce:LiLuF₄ single crystals, respectively. Undoped LiCaAlF₆ and KMgF₃ single crystals showed a transmission edge at 112 nm and 115 nm, respectively.

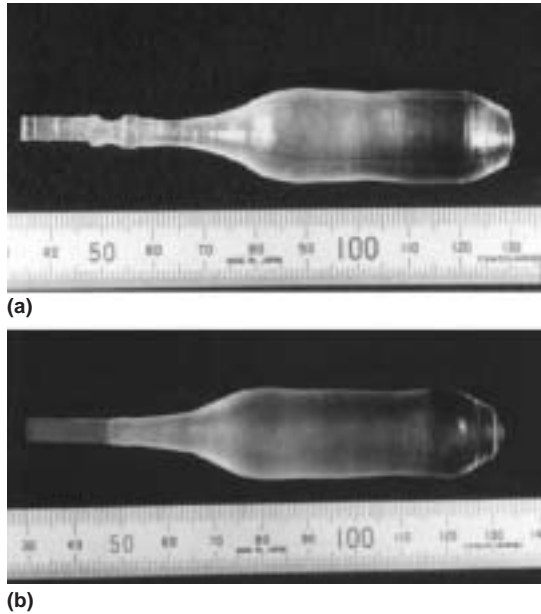


Figure 1. As-grown Ce-doped (a) LiCaAlF_6 and (b) LiSrAlF_6 single crystals 18 mm in diameter pulled along the a -axis.

VIII-A-4 Growth of Ce-Doped Colquiriite- and Scheelite-Type Single Crystals for UV Laser Applications

SHIMAMURA, Kiyoshi¹; SATO, Hiroki¹; BENSALAH, Amina¹; MACHIDA, Hiroshi²; SARUKURA, Nobuhiko; FUKUDA, Tsuguo¹ (¹Tohoku Univ.; ²Tokin Corp.)

[*Opt. Mater.* **19**, 109 (2002)]

Ce-doped Colquiriite- and Scheelite-type fluoride single crystals were grown by the Czochralski technique. The formation of inclusions and cracks accompanying the crystal growth was investigated. The effective distribution co-efficients of Ce^{3+} in LiCaAlF_6 , LiSrAlF_6 , LiYF_4 and LiLuF_4 were determined to be 0.031, 0.028, 0.116 and 0.054, respectively. Ultraviolet pulse generations with an output energy of 60 and 27 mJ were obtained from Ce: LiCaAlF_6 and Ce: LiLuF_4 lasers.

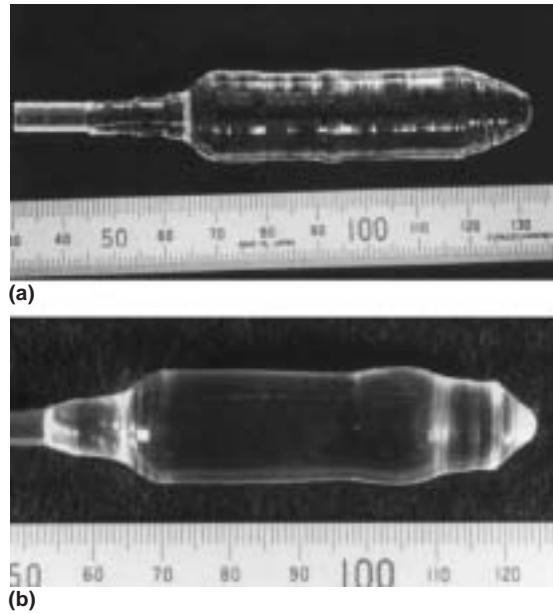


Figure 1. As-grown Ce-doped: (a) LiYF_4 and (b) LiLuF_4 single crystals of 18 mm in diameter pulled along the a -axis.

VIII-A-5 High-Energy Pulse Generation from Solid-State Ultraviolet Lasers Using Large Ce:Fluoride Crystals

LIU, Zhenlin¹; SHIMAMURA, Kiyoshi²; FUKUDA, Tsuguo²; KOZEKI, Toshimasa; SUZUKI, Yuji; SARUKURA, Nobuhiko (¹ERATO; ²Tohoku Univ.)

[*Opt. Mater.* **19**, 123 (2002)]

A large $\text{Ce}^{3+}:\text{LiCaAlF}_6$ (Ce:LiCAF) crystal with 15 mm diameter was grown successfully by the Czochralski method. Owing to its large size, 60 mJ, 289 nm pulses were generated directly from a quasi-coaxially pumped Ce:LiCAF laser. In addition, a new noncollinear Brewster-angle-pumping disk oscillator scheme was demonstrated for further output-energy scaling. An ultraviolet solid-state $\text{Ce}^{3+}:\text{LiLuF}_4$ (Ce:LLF) laser which was pumped transversely by a KrF excimer laser with the repetition rate of 1 Hz produced a 27 mJ, 309 nm pulse using a large Ce:LLF crystal which was grown by the Czochralski method, and the slope efficiency was approximately 17%.

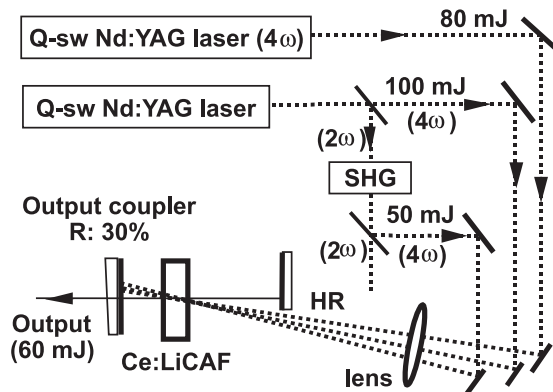


Figure 1. Experimental setup for high-power Ce:LiCAF laser pumped by the fourth harmonics of two Q-switched Nd:YAG lasers.

VIII-A-6 New Adjustment Technique for Time Coincidence of Femtosecond Laser Pulses Using Third Harmonic Generation in Air and its Application to Holograph Encoding System

KAWAMURA, Ken-ichi¹; ITO, Naoko²;
SARUKURA, Nobuhiko; HIRANO, Masahiro¹;
HOSONO, Hideo^{1,3}
(¹ERATO; ²Mater. Struct. Lab.; ³Tokyo Inst. Tech.)

[*Rev. Sci. Instrum.* **73**, 1711 (2002)]

The third harmonic generation of light (266 nm) is enhanced, sensitively depending on the time delay between a pair of pulses split from a single 800 nm femtosecond laser pulse, when they are focused and collided in air. This finding offers a convenient and widely applicable technique to detect temporal and spatial overlapping of two femtosecond pulses. This technique has several advantages over the conventional sum frequency generation method using nonlinear optical crystals, since it obviates the need for expensive crystals, free from phase matching, and elimination of temporal walk off. By applying it to "a holographic encoding system using an interference femtosecond laser pulse," a periodic fringe spacing is minimized to ~ 430 nm by extending the colliding angle between two-pulse beams up to ~ 160 °C.

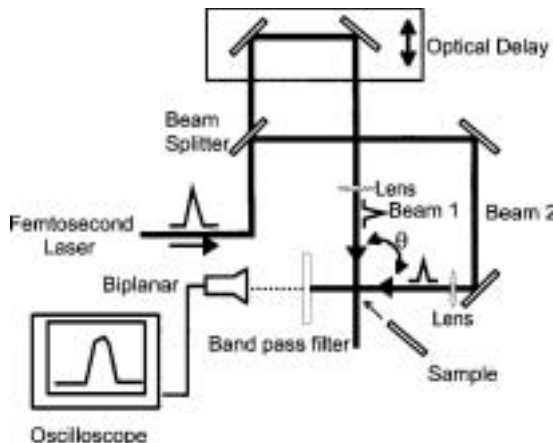


Figure 1. Experimental setup for holographic encoding system.

VIII-A-7 Hybrid Time-Resolved Spectroscopic System for Evaluating Laser Material Using a Table-Top-Sized, Low-Jitter, 3-MeV Picosecond Electron-Beam Source with a Photocathode

SUZUKI, Yuji; KOZEKI, Toshimasa; ONO, Shingo;
MURAKAMI, Hidetoshi; OHTAKE, Hideyuki;
SARUKURA, Nobuhiko; NAKAJYO, Terunobu¹;
SAKAI, Fumio¹; AOKI, Yasushi¹
(¹Sumitomo Heavy Industries, Ltd.)

[*Appl. Phys. Lett.* **80**, 3280 (2002)]

Hybrid time-resolved spectroscopy of laser media comparing electron-beam excitation and optically excited cases is performed using a newly developed, table-top-sized, low-jitter, 3-MeV picosecond electron-beam source with a photocathode. The properties of an electron-beam-pumped Ce³⁺:LiCaAlF₆ (Ce:LiCAF) ultraviolet laser medium significantly differ from those of an optically pumped medium.

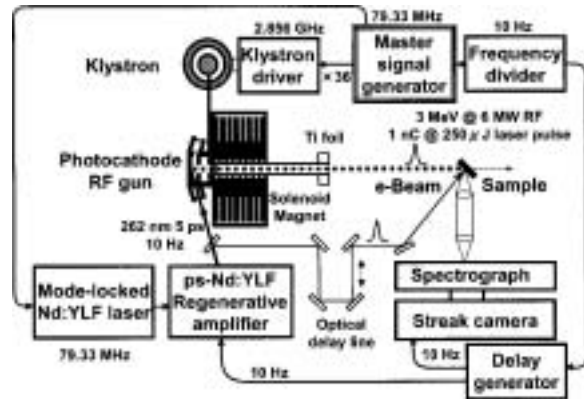


Figure 1. Experimental setup. The photocathode rf gun was irradiated with 262-nm optical pulses from a Nd:YLF regenerative system synchronously operated with a 2.856-GHz, 6-MW klystron to accelerate the extracted 1-nC photoelectron beam. The e-beam was irradiated onto the sample after being passed through titanium foil. A portion of the pumping optical pulse irradiated the same sample to compare the excitation scheme. A streak camera was equipped with a 30-cm spectrograph to measure the fluorescence spectrum and fluorescence lifetime.

VIII-A-8 Simultaneous Measurement of Thickness and Water Content of Thin Black Ink Films for the Printing Using THz Radiation

OHTAKE, Hideyuki; SUZUKI, Yuji; ONO, Shingo;
SARUKURA, Nobuhiko; HIROSUMI, Tomoya¹;
OKADA, Tomoaki²
(¹AISIN SEIKI Co., Ltd.; ²Mitsubishi Heavy Industry Co., Ltd.)

[*Jpn. J. Appl. Phys., Part 2* **41**, L475 (2002)]

Using THz radiation, a simple, noncontact, simultaneous method is applied to measure thickness and water content of black ink films independently from frequency-dependent and frequency-independent absorption characteristics of black ink films.

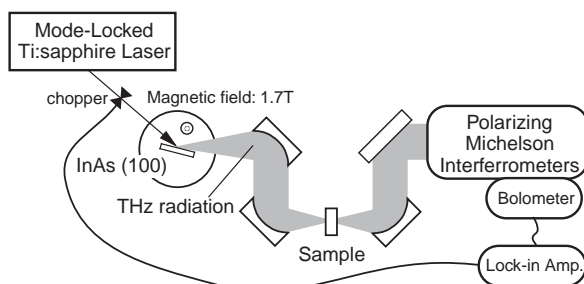


Figure 1. Experimental setup for simultaneously measuring thickness and water content of thin black ink films. The magnetic field direction is from the back to the surface.

VIII-A-9 Far-Infrared Absorption Measurements of Polypeptides and Cytochrome *c* by THz Radiation

YAMAMOTO, Kohji¹; TOMINAGA, Keisuke¹;
SASAKAWA, Hiroaki¹; TAMURA, Atsuo¹;
MURAKAMI, Hidetoshi; OHTAKE, Hideyuki;
SARUKURA, Nobuhiko
(¹Kobe Univ.)

[*Bull. Chem. Soc. Jpn.* **75**, 1083 (2002)]

Pulsed terahertz (THz) radiation and black-body radiation are applied to measure far infrared (FIR) absorption spectra of polypeptides and cytochrome *c* in the wavenumber region from 7 cm^{-1} to 160 cm^{-1} . In the region from 7 cm^{-1} to 55 cm^{-1} , FIR absorption cross sections of polyglycine and poly-*L*-alanine in powder are greater than those of glycine and *L*-alanine in powder. On the other hand, FIR absorption spectra of cytochrome *c* in lyophilized powder show little dependence on protein structures. The structures of biopolymers are investigated by mid-IR absorption (polypeptides and cytochrome *c*) and by resonance Raman scattering (cytochrome *c*). FIR spectral features of biopolymers in the THz frequency region are qualitatively discussed in terms of density of states and homogeneous/inhomogeneous broadening.

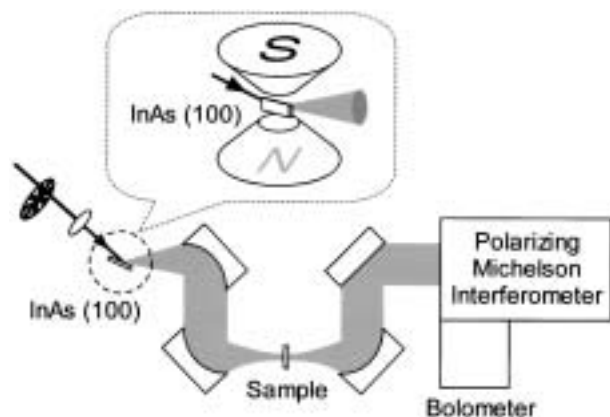


Figure 1. FIR absorption spectrometer using the THz radiation. Pulses at 800 nm with 70-fs width at 80-MHz repetition rate irradiate an InAs wafer, which is placed in a magnetic flux density of 1.7 T generated by an electromagnet. The (100)-InAs surface is parallel to a direction of the magnetic flux density. The THz radiation from the (100)-InAs is collimated by an off-axis parabolic mirror. The THz radiation is focused at a sample position and collimated again by an off-axis mirror. Intensity of the THz radiation is detected by a germanium bolometer which is cooled by helium liquid. Chopping frequency of the pump pulse is 200 Hz. A polarizing Michelson interferometer is vacuumsealed. All the FIR absorption system other than the polarizing Michelson interferometer is open to air. When using the black-body radiation for FIR absorption measurements, the generation part of the THz-radiation is replaced by a black-body.

VIII-A-10 0.43 J, 10 Hz Fourth Harmonic Generation of Nd:YAG Laser Using Large $\text{Li}_2\text{B}_4\text{O}_7$ Crystals

SUZUKI, Yuji; ONO, Shingo; MURAKAMI, Hidetoshi; KOZEKI, Toshimasa; OHTAKE, Hideyuki; SARUKURA, Nobuhiko; MASADA, Genta¹; SHIRAISHI, Hiroyuki¹; SEKINE, Ichiro¹
(¹Mitsubishi Materials Corp.)

[*Jpn. J. Appl. Phys., Part 2* **41**, L823 (2002)]

Using large-sized $\text{Li}_2\text{B}_4\text{O}_7$ crystals, 0.43 J, 266 nm pulses are obtained from a 10 Hz Nd:YAG laser with a total conversion efficiency of 30.5%. Moreover, 4 W operation for over 15 h is demonstrated.

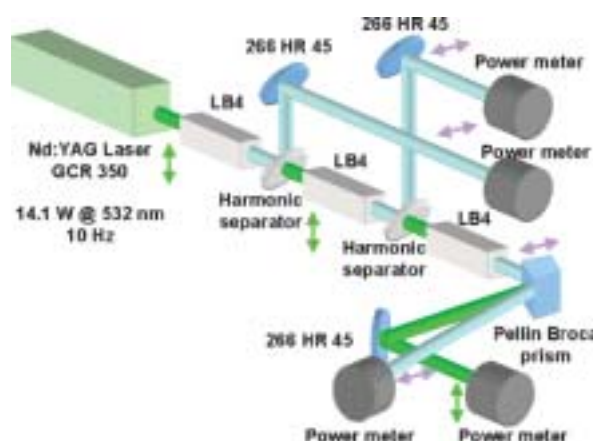


Figure 1. Experimental setup for three-cascade, fourth harmonic generation using LiB_4 crystals.

VIII-A-11 Electron-Beam Excitation of a $\text{Ce}^{3+}:\text{LiCaAlF}_6$ Crystal for Future High-Peak-Power UV Lasers

KOZEKI, Toshimasa; SUZUKI, Yuji; SAKAI, Masahiro; OHTAKE, Hideyuki; SARUKURA, Nobuhiko; SHIMAMURA, Kiyoshi¹; FUKUDA, Tsuguo¹; NAKAJYO, Terunobu²; SAKAI, Fumio²; AOKI, Yasushi²
(¹Tohoku Univ.; ²Sumitomo Heavy Industries Ltd.)

[*Appl. Phys. B* **74**, S185 (2002)]

In this experiment, we performed ultrafast spectroscopy on an electron-beam-excited $\text{Ce}^{3+}:\text{LiCaAlF}_6$ ($\text{Ce}:\text{LiCAF}$) crystal. The time-resolved fluorescence spectrum and lifetime with e-beam pumping differ significantly from those in the optically pumped case. These results suggest a new pumping scheme for an ultrashort pulse amplifier.

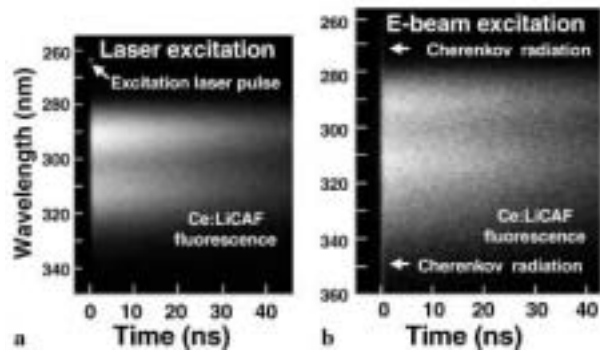


Figure 1. The streak camera images of the fluorescence from Ce:LiCAF, excited **a** by a 262-nm-pulse and **b** by an electron pulse. In the case of electron pulse excitation, a broadband, short-duration Cherenkov radiation is clearly seen.

VIII-B Development and Research of Advanced Tunable Solid State Lasers

Diode-pumped solid-state lasers can provide excellent spatial mode quality and narrow linewidths. The high spectral power brightness of these lasers has allowed high efficiency frequency extension by nonlinear frequency conversion. Moreover, the availability of new and improved nonlinear optical crystals makes these techniques more practical. Additionally, quasi phase matching (QPM) is a new technique instead of conventional birefringent phase matching for compensating phase velocity dispersion in frequency conversion. These kinds of advanced tunable solid-state light sources, so to speak "Chroma Chip Lasers," will assist the research of molecular science.

In this projects we are developing Chroma Chip Lasers based on diode-pumped-microchip-solid-state lasers and advanced nonlinear frequency conversion technique.

VIII-B-1 Thermal-Birefringence-Induced Depolarization in Nd:YAG Ceramics

SHOJI, Ichiro; SATO, Yoichi; KURIMURA, Sunao; LUPEI, Voicu¹; TAIRA, Takunori; IKESUE, Akio²; YOSHIDA, Kunio³
(¹IMS and IAP, Romania; ²JFCC; ³Osaka Inst. Tech.)

[*Opt. Lett.* **27**, 234 (2002)]

Nd:YAG ceramics are promising candidates for high-power and high-efficiency microchip laser materials because highly transparent and highly Nd³⁺-doped samples are available¹⁾ without degradation in thermomechanical properties.²⁾ We have investigated the optical properties of Nd:YAG ceramics and succeeded in microchip laser oscillation.³⁾ In this work we have investigated depolarization effect caused by thermally induced birefringence in Nd:YAG ceramics, which should be an essential issue for controlling polarization under high-power operation.

Thermal birefringence effect was measured with the pump-probe experiment. A Ti:sapphire laser oscillating at 808 nm was used as the pump source, which was focused onto the sample with the radius of 80 μm . The linearly polarized He-Ne laser beam of 1 mm radius was used as the probe. After passing through the sample, only the depolarized component of the probe beam was detected. The measured samples were 1.0, 1.3, 2.0, and 3.4 at.% Nd³⁺-doped YAG ceramics, and 1.0 and 1.3 at.% Nd:YAG single crystals. The thickness of each sample was ~ 1 mm, and (111)-cut samples were used for the single crystals.

Figure 1 shows the depolarization as a function of Nd³⁺ concentration at the absorbed pump power of 1000 mW. We found that the depolarization is nearly same between the ceramic and single-crystal YAG for the same Nd³⁺ concentrations. Because YAG ceramics consist of a lot of YAG single-crystal grains (their sizes are in several tens of microns) with various directions, which means that the birefringence effect in a ceramic sample is average of that in those grains, we suppose our results indicate that the average is close to the birefringence effect for (111)-cut Nd:YAG single crystals.

Moreover, it was also found that the depolarization became larger in samples with higher Nd³⁺ concentrations even if the same pump power was absorbed. We believe that the main reason is the difference of thermal

loading for the samples with different Nd³⁺ concentrations. For a highly Nd³⁺-doped sample, in which the interaction between Nd³⁺ ions is significant, the amount of nonradiative relaxation increases and radiative quantum efficiency gets smaller. Under the condition of no laser extraction, the smaller quantum efficiency causes larger thermal loading, that is, more heat generation in the sample even at the same absorbed power, and this induces larger thermal birefringence. The dotted line in Figure 1 shows the calculated result, in which we used the values of thermal loading obtained by Lupei *et al.*⁴⁾ The agreement between the experiment and rough estimation is satisfactory. When lasing occurs, on the other hand, thermal birefringence is expected to be greatly reduced because the thermal loading is then independent of radiative quantum efficiency. This means that *cw* or high-repetition-rate, high-average-power Q-switched operation is preferable for highly Nd³⁺-doped ceramics.

References

- 1) A. Ikesue, T. Kinoshita, K. Kamata and K. Yoshida, *J. Am. Ceram. Soc.* **78**, 1033 (1995).
- 2) T. Taira, A. Ikesue and K. Yoshida, *OSA Trends in Optics and Photonics* **19**, 430 (1998).
- 3) I. Shoji, S. Kurimura, Y. Sato, T. Taira, A. Ikesue and K. Yoshida, *Appl. Phys. Lett.* **77**, 939 (2000).
- 4) V. Lupei, A. Lupei, N. Pavel, T. Taira, I. Shoji and A. Ikesue, *Appl. Phys. Lett.* **79**, 590 (2001).

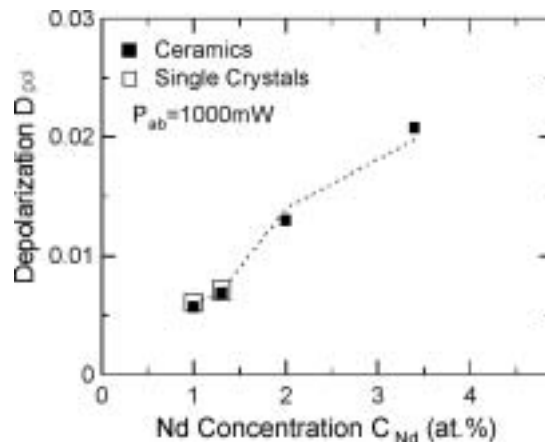


Figure 1. Depolarization as a function of Nd³⁺ concentration for the ceramic and single-crystal samples at the absorbed pump power of 1000 mW. The dotted line is the calculation taking account of increase of thermal loading.

VIII-B-2 Intrinsic Reduction of the Depolarization Loss in Solid-State Lasers by Use of a (110)-Cut $\text{Y}_3\text{Al}_5\text{O}_{12}$ Crystal

SHOJI, Ichiro; TAIRA, Takunori

[*Appl. Phys. Lett.* **80**, 3048 (2002)]

Thermally induced birefringence in solid-state laser materials is a serious problem in developing high-power and high-beam-quality lasers and amplifiers because it causes bifocusing and depolarization of a linearly polarized beam. A number of techniques which use a 90° rotator and a quarter-wave plate, *etc.*, have been suggested to compensate the depolarization. However, these compensations have been applied exclusively for (111)-cut YAG crystals, presumably because the (111) plane has simple, circularly symmetrical birefringence so that using (111)-cut rods is conventional. We report intrinsic reduction of depolarization without any compensation by use of Nd:YAG rods cut other than (111).

Koehler and Rice analyzed thermally induced birefringence in Nd:YAG rods with various directions,^{1,2)} and concluded that the amount of depolarization at the high-power limit is independent of rod directions, as shown in Figure 1. However, there were two mistakes in their theory. Figure 1 also shows the dependence of the depolarization on absorbed pump power based on our calculation when the laser beam radius r_a is equal to the rod radius r_0 . The amount of depolarization depends on the directions of planes and polarizations even at high power, and becomes smallest when the angle between the direction of polarization and the crystal axis, γ , is equal to 45° in the (100) plane, the amount for which is half that for the (111) plane at high power and 1/6 at low power.

Moreover, we have found that the depolarization can be greatly reduced by use of a (110)-cut rod under condition that r_a is smaller than r_0 . When the distance from the center of the rod, r , is as large as r_0 , the eigenvectors are directed nearly to the radial and the tangential directions at all the angles. On the other hand, when r is small, all eigenvectors are nearly aligned in one direction. Because of this nature, if the direction of the polarization is close to the crystal axis, a beam with small radius can propagate through the rod almost undepolarized. Figure 2 shows, as an example, dependence of the depolarization on the absorbed pump power when $r_a = r_0/5$ and $\gamma = 0^\circ$. The depolarization for the (110) plane reduces to about 1/50 of that for the (111) plane. This condition can be realized by use of an aperture to control the beam size in the case of the uniform pumping. A composite material in which the doped YAG is surrounded by the undoped YAG also makes the same condition and realizes better extraction efficiency. For the end pumping, on the other hand, the condition is easily satisfied because the focused pump beam itself plays a role as a gain aperture.

References

- 1) W. Koehler and D. K. Rice, *J. Quantum Electron* **QE-6**, 557 (1970).
- 2) W. Koehler and D. K. Rice, *J. Opt. Soc. Am.* **61**, 758 (1971).

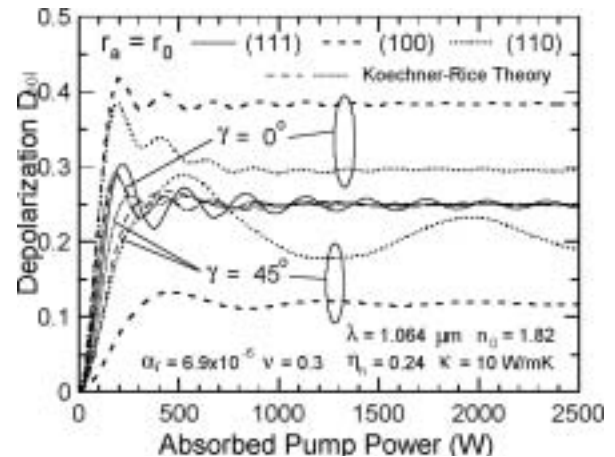


Figure 1. Dependence of the depolarization on the absorbed pump power for the (111), (100), and (110) planes based on Koehler and Rice's theory (thin curves) and our calculation (thick curves).

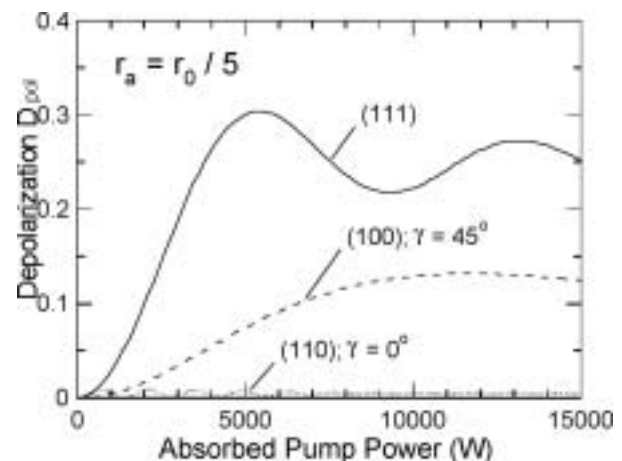


Figure 2. Dependence of the depolarization on the absorbed pump power for the (111), (100), and (110) planes when $r_a = r_0/5$.

VIII-B-3 The Effect of Nd Concentration on the Spectroscopic and Emission Decay Properties of Highly-Doped Nd:YAG Ceramics

LUPEI, Voicu¹; LUPEI, Aurelia¹; GEORGESCU, Serban¹; TAIRA, Takunori; SATO, Yoichi; IKESUE, Akio²

(¹IAP-NILPRP, Romania; ²JFCC)

[*Phys. Rev. B* **64**, 092102 (2001)]

The renewed interest in the use of highly concentrated Nd:YAG laser materials for constructing solid state lasers rises important questions concerning the effect of Nd concentration (C_{Nd}) on the spectroscopic and emission decay characteristics that determine the performances of these lasers. Highly doped Nd:YAG components can be produced by various techniques such as crystal growth by the Thermal Gradient Technique,¹⁾ flux,²⁾ epitaxial thin film deposition³⁾ or ceramic techniques.⁴⁾ Despite of the fact that some of these components have been used in laser experiments, no detailed account of the effect of C_{Nd} on their spectro-

copic and emission decay properties has been reported. This work reports the results of spectroscopic and emission decay investigations of Nd:YAG ceramics with up to 9-at.% Nd.

High optical quality transparent Nd:YAG ceramics have been produced by the technique described in Reference 4). The high-resolution transmission spectra were measured at temperatures between 10 and 300 K by using a high-resolution (better than 0.3 cm^{-1}) one-meter double monochromator. For the emission decay a photon counting technique of 20-ns resolution was used and the excitation was made non-selectively at room temperature with the 2nd harmonic of a Q-switched Nd:YAG laser (10-nsec pulse width). The intensity of excitation was kept low in order to avoid a high population of the emitting level $^4F_{3/2}$ (under $\sim 1\%$) that could favor upconversion by excited state absorption or energy transfer.

The transmission spectra of Nd:YAG ceramic samples of 1-at.% Nd are similar to those of single crystals⁵⁾ of the same C_{Nd} . No obvious line shifts or broadenings have been observed in any spectral range in agreement with previous investigations on 1-at.% Nd:YAG ceramics.⁶⁾ With increasing Nd concentration the positions of the spectral lines remain practically unchanged with very slight shifts for some of the optical transitions and with a selective broadening. The structures of the satellites in the low-temperature high-resolution spectra at 1-at.% Nd do not contain any additional satellites with respect to those reported in single crystals,⁵⁾ showing that no additional defects in the vicinity of the Nd ions occur. The only major satellites in the transmission spectra of the Nd:YAG ceramics are those connected with crystal-field perturbations inside of statistical ensembles of Nd^{3+} ions sitting on near lattice sites. At low Nd concentrations the most important of such ensembles are Nd ion pairs: the satellites corresponding to the first (*n.n.*)- and second (*n.n.n.*)- order pairs are clearly resolved in most of the optical transitions (satellites M_1 , spectral shift up to 5 to 6 cm^{-1} and M_2 , shift up to 2 to 3 cm^{-1} , respectively), as shown in Figure 1 for the transition $^4I_{9/2}(Z_1) \rightarrow ^2P_{1/2}$ at various Nd concentrations. With increasing of C_{Nd} the relative intensities of the pair lines increase, while the ones of the isolated ions decrease. Moreover, at very high concentrations, new satellites T, whose relative intensities increase with C_{Nd} faster than those of the pairs, show up. Most likely these new satellites are connected with triads of Nd^{3+} ions on near lattice sites, the larger spectral shift being consistent with the expected larger mutual crystal-field perturbation inside of these ensembles.

The weakly excited emission decay at room temperature is accelerated and shows departures from exponentials with increasing C_{Nd} (as shown in Figure 2) The decay can be divided into four successive temporal regions: (i) a very sharp drop that terminates practically within the first two microseconds of the decay and whose extent on the intensity scale increases almost proportionally to C_{Nd} ; (ii) a quasi-exponential portion that blurs at high C_{Nd} ; (iii) a non-exponential dependence; (iv) a new quasi-exponential dependence. The border between these regions is not sharp and the transition is gradual. The extent of the regions (ii) and (iii)

reduces with increasing C_{Nd} : the region (iv) is not seen in the decay of the diluted samples during 6–8 e-foldings of low noise decay at the low pump intensities used in this experiment. The emission quantum efficiency η_{qe} in the presence of energy transfer can be then determined. It decreases with increasing C_{Nd} and all the excitation lost non-radiatively by cross-relaxation is transformed into heat. This limits the possibilities of using concentrated Nd:YAG components in laser emission regimes implying the storage of excitation energy (the Q-switched regime). However, these materials show good prospect to be used in continuous-wave regimes, where the effect of the reduction of η_{qe} with increasing C_{Nd} on the threshold can be compensated by an enhanced absorption of the pump radiation.

References

- 1) Y. Zhou, *J. Crystal Growth* **78**, 31 (1986).
- 2) P. Gavrilovic, M. S. O'Neill, J. H. Zarabi, J. E. Williams, W. H. Grodkiewicz and B Bruce, *Appl. Phys. Lett.* **65**, 1820 (1994).
- 3) D Pelenc, B. Chambaz, I Chartier, B. Ferrand and J. C. Vial, *J. Phys. (France) IV* **1**, 311 (1991).
- 4) A. Ikesue, T. Kinoshita, K. Kamata and K. Yoshida, *J. Am. Ceram. Soc.* **78**, 1033 (1995).
- 5) V. Lupei, A. Lupei, C. Tiseanu, S. Georgescu, C. Stoicescu and P. Nanau, *Phys. Rev. B* **51**, 8 (1995).
- 6) M. Sekita, H. Haneda, T. Yanagitani and S. Shirasaki, *J. Appl. Phys.* **67**, 453 (1990).

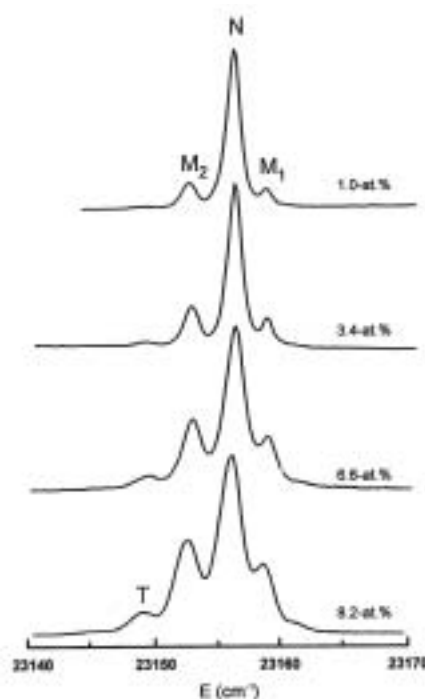


Figure 1. $^4I_{9/2} \rightarrow ^2P_{1/2}$ transmission spectra for different concentrations at low temperature.

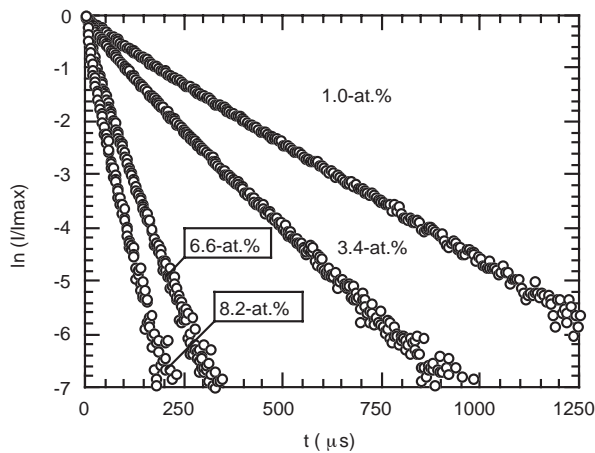


Figure 2. ${}^4F_{3/2}$ emission decays for Nd:YAG ceramics of different concentrations at room temperature.

VIII-B-4 Spectroscopy and Laser Emission under Hot Band Resonant Pumping in Highly Doped Nd:YAG Ceramics

LUPEI, Voicu¹; TAIRA, Takunori; LUPEI, Aurelia¹; PAVEL, Nicolaie; SHOJI, Ichiro; IKESUE, Akio²

(¹IAP-NILPRP, Romania; ²JFCC)

[*Opt. Commun.* **195**, 225 (2001)]

Owing to important thermo-mechanical properties, such as hardness, high thermal conductivity and high stress-fracture limit as well as to its fairly good spectroscopic properties (four-level laser scheme, high emission cross-section, fairly long lifetime), Nd:YAG remains a material of choice for the construction of solid-state lasers. However, the inability of the conventional growth techniques for bulk single-crystals (Czochralski) to incorporate Nd concentrations (C_{Nd}) above 1.2–1.4 at.% without a serious deterioration of the optical and structural properties, together with the sharp and relatively weak absorption lines at these concentrations limit the use of these crystals both in the direction of the high power lasers and of very efficient microchip lasers. This paper investigates the spectroscopic properties and the emission dynamics of Nd^{3+} ions in highly concentrated Nd:YAG ceramics. The implication of these properties on the laser emission is discussed and illustrated with the 1064-nm emission under hot band resonant pump in the emitting level.

The samples under study are Nd:YAG ceramics with Nd concentrations up to 9-at.%, produced as described in Reference 1). The main techniques of investigation are the high spectral resolution optical transmission and the high temporal resolution emission decay. The laser emission was investigated on samples of up to 3.8-at.% Nd under Ti:Sapphire laser end-pumping.

The transmission spectra at room temperature enable the selection of optical transitions suitable for diode laser pumping. A very promising such transition could be the doubly-peaked band centered around 885 nm made up by the hot bands $Z_2 \rightarrow R_1$ and $Z_3 \rightarrow R_2$ of the absorption ${}^4I_{9/2} \rightarrow {}^4F_{3/2}$. Our measurements show that the absorption coefficients of the two peaks of the 885-

nm band are approximately equal at room temperature and become appreciable at high values of C_{Nd} : they increase from $\sim 1.7 \text{ cm}^{-1}$ at 1-at.% Nd to $\sim 6.5 \text{ cm}^{-1}$ at 4-at.% and 13 to 14 cm^{-1} at 9-at.% Nd, while the FWHM increases from $\sim 2.5 \text{ nm}$ at 1-at.% Nd to $\sim 3.2 \text{ nm}$ at 9-at.% Nd, very suitable for diode laser pumping.

The room temperature global emission decay under low intensity non-selective pump of Nd:YAG ceramic samples show C_{Nd} -dependent departures from exponential.²⁾ The quantum efficiency η_{qe} , which was determined as a function of C_{Nd} by using the energy transfer parameters obtained from the emission decay, is shown in Figure 1. This dependence is different from that used traditionally $\eta_{qe} = [1 + C_{Nd}/C_0]^{-1}$, which is based on a C_{Nd}^2 -dependence of the transfer function at all Nd concentrations, but is in a very good agreement with the reported data on quantum efficiency,³⁾ fractional thermal load⁴⁾ and pump-induced birefringence.⁵⁾ These results indicate that the concentrated Nd:YAG ceramics show potential for construction of efficient CW solid state lasers.

The CW 1064-nm laser emission potential of the concentrated Nd:YAG ceramics was investigated under resonant pump in ${}^4F_{3/2}$ level at 885-nm in an end-pump laser configuration. The Nd concentration of the laser active component was 3.8-at.%; the quantum efficiency η_{qe} was ~ 0.32 , leading to a figure of merit $\eta_{qe}C_{Nd}$ of 1.21 and to a calculated product $\eta_{qe}\tau_D$ of $\sim 83 \mu\text{sec}$. The uncoated plane parallel 1.5-mm thick active component was placed in a 25-mm plane-concave resonator with a 50-mm radius output coupler. The end pumping was made with a Ti:sapphire laser focused on the sample in a 160- μm diameter spot. The emission power versus the absorbed power is represented in Figure 2. For a 5% transmission output coupler the threshold of emission in absorbed power was $\sim 65 \text{ mW}$ and the slope efficiency $\sim 40\%$, and at 500-mW absorbed power the laser emitted in excess of 167-mW in a beam with a M^2 factor equal to 1.61.6. Analysis of these data shows that for a given output coupler transmission T , the threshold and the slope efficiency can be consistently described by using the same value of the global loss parameter $(T + L)\eta_B^{-1}$, where η_B is the superposition factor of the laser mode and the pump volumes and L represents all the other losses, including the residual Fresnell loss at the wavelength of emission. This global loss parameter amounts to 0.10.005 for $T = 0.05$ and 0.045 ± 0.002 for $T = 0.01$; these two values are consistent with a superposition factor of ~ 0.73 , in agreement with the measured ratio of the laser emission and the pump beam diameters, and with a loss parameter $L = 0.023$.

In conclusion the laser emission of a 3.8-at.% Nd ceramic laser component under hot band resonant pump at 885-nm with a Ti:sapphire laser is demonstrated. The laser active component used in this experiment is the most concentrated Nd:YAG active component reported to lase at 1064 nm. The performances of this laser could be improved by using coated active components of higher optical quality.

References

- 1) A. Ikesue, T. Kinoshita, K. Kamata and K. Yoshida, *J. Am. Ceram. Soc.* **78**, 1033 (1995).
- 2) V. Lupei, A. Lupei, S. Georgescu, T. Taira, Y. Sato and A.

- Ikesue, *Phys. Rev. B* **64**, 092102 (2001).
 3) K. K. Deb, R. G. Buser and J. Paul, *Appl. Opt.* **20**, 1203 (1981).
 4) T. Y. Fan, *IEEE J. Quantum Electron.* **29**, 1457 (1993).
 5) I. Shoji, Y. Sato, S. Kurimura, T. Taira, A. Ikesue and K. Yoshida, *Advanced Solid State Lasers Conference*, Seattle-USA, Jan. 2001, paper ME14.

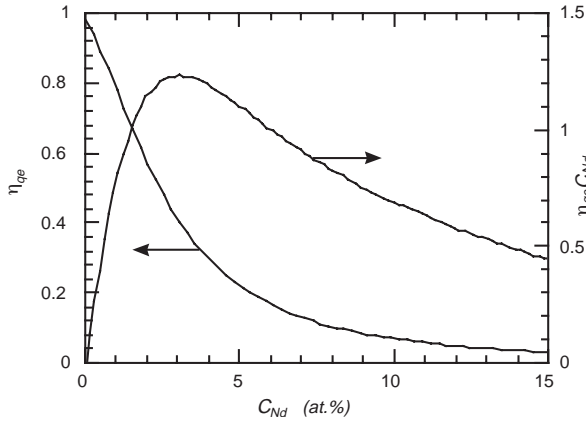


Figure 1. Calculated concentration dependence of emission quantum efficiency η_{qe} and of $\eta_{qe}C_{Nd}$ parameter.

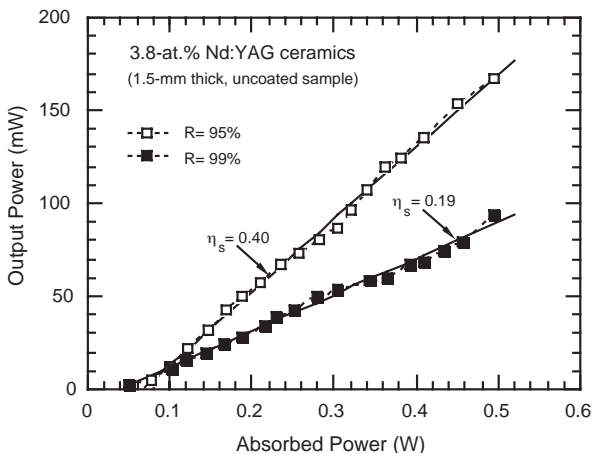


Figure 2. Output power function of absorbed power for an uncoated 3.8-at.% Nd:YAG ceramics sample under 885-nm end pumping by Ti:sapphire laser.

VIII-B-5 Efficient Laser Emission in Concentrated Nd Laser Materials under Pumping into the Emitting Level

LUPEI, Voicu¹; PAVEL, Nicolaie²; TAIRA, Takunori
 (¹IAP-NILPRP, Romania; ²IMS and IAP-NILPRP, Romania)

[*IEEE J. Quantum Electron.* **38**, 240 (2002)]

The enhancement of overall efficiency, low transverse-mode laser emission in miniature lasers, and scaling to high powers are among the most important directions in the development of solid-state lasers. The first of these implies an increase of slope efficiency and a reduction of emission threshold; the second relies on increased absorption of the pump while the third imposes the reduction on heat generation. A suitable

choice of the laser material, with optimised spectroscopic and thermo-mechanical properties, of the optical pumping scheme or of the laser design is then crucial. There is no laser material to fulfill optimally all these requirements and thus the choice is limited within well-defined segments of performance.

The present paper shows that a means to overcome weak pump absorption on transitions directly to the $^4F_{3/2}$ level in the diluted (~ 1 -at.%) Nd laser-materials is to increase the Nd concentration (C_{Nd}). The use of concentrated Nd laser materials requires the examination of several important basic aspects such as the state of Nd ions in YAG samples produced by various techniques, and the effect of C_{Nd} on the spectroscopic and population dynamics properties, in order to select new transitions suitable for pumping and to determine the range of C_{Nd} adequate for laser emission. The Nd:YAG ceramic samples used in this investigation have up to 9-at.% Nd and were supplied by the Japan Fine Ceramics Center, Nagoya, Japan, while the Nd:YAG crystals (2.4 and 3.5-at.%) and Nd:YVO₄ crystals (1, 2, and 3-at.%) were purchased.

The pumping at 885 nm in Nd:YAG reduces the quantum defect with respect to the 808-nm pumping into $^4F_{5/2}$ by about 30% in the case of 1064-nm emission and by $\sim 58\%$ for 940-nm emission, thus contributing to a considerable reduction in the fractional thermal load. Thus, the near degeneracy of the $Z_2 \rightarrow R_1$ and $Z_3 \rightarrow R_2$ absorption lines could be useful for the occurrence of absorption bands suitable for direct diode laser pumping into the $^4F_{3/2}$ state. This near degeneracy takes place in many Nd laser materials and it could help to get more efficient or more powerful emission even from laser active components with good spectroscopic characteristics but poorer thermo-mechanical properties. In the case of Nd:YVO₄, no accidental degeneracy of the thermally-activated transitions occurs. However, for this material the absorption line $Z_1 \rightarrow R_1$ at 879.8 nm has a FWHM similar to the traditional pump transition $Z_1 \rightarrow ^4F_{5/2}(1)$ at 808.6 nm, while the peak absorption coefficient is only 40–50% smaller. This reduction can be easily compensated by an increase in C_{Nd} . Thus in the case of Nd:YVO₄, the transition $Z_1 \rightarrow R_1$ of the $^4I_{9/2} \rightarrow ^4F_{3/2}$ absorption can be used for direct pumping into the emitting level, leading to a reduction of the quantum defect with respect to 808.6-nm pump by 27.4% in the case of 1064-nm $^4F_{3/2} \rightarrow ^4I_{11/2}$ emission and by 65.6% for 915-nm $^4F_{3/2} \rightarrow ^4I_{9/2}$ emission.

For Nd:YVO₄ the effects of the energy transfer on the emission decay are very poorly characterized and an analysis similar to YAG^{1,2)} is not possible at the present time. However, the investigation of emission decay in Nd:GdVO₄ (a crystal similar with YVO₄) gives energy transfer parameters about two times larger than in Nd:YAG.³⁾ Moreover, the investigation of the pump intensity effect on laser emission in Nd:YVO₄ concludes that the up-conversion processes by energy transfer in this crystal are much stronger than in Nd:YAG.⁴⁾ Thus, a stronger decrease of emission quantum efficiency with increased C_{Nd} in Nd:YVO₄ could be expected, although figures of merit $\eta_{qe}C_{Nd}$ larger than for 1-at.% Nd doping could be still obtained for a certain range of higher C_{Nd} .

The 1064-nm laser emission in concentrated

Nd:YAG ceramics and single crystals and in Nd:YVO₄ crystals is investigated using oscillators end pumped by Ti:sapphire laser. Figure 1a shows the laser output power function of the absorbed power for the Nd:YAG ceramic laser components. The most concentrated component to lase under 885-nm pumping was a 0.4-mm thick sample of 6.8-at.% Nd: for the 95% output mirror the slope efficiency (versus the absorbed power) was 20% with the emission threshold of 144 mW. For a 1.5-mm thick 3.8-at.% Nd sample and a 95% output coupler reflectivity the slope efficiency was 42%, the threshold of emission was 58 mW and the output power reaches in excess of 132 mW for 350 mW absorbed pump with a laser beam M² factor of 1.6 × 1.6. The highest slope of 51% was obtained for the output mirror of 90% reflectivity, but with an increased threshold pump power of 115 mW. The laser output power versus the absorbed power for uncoated 2.4-at.% (3.0-mm thick) and 3.5-at.% (1.0-mm thick) Nd:YAG crystals under 885-nm pumping is shown in Figure 1b, in comparison with those of a standard 1-at.% (3.0-mm thick) Nd component. For the 1-at.% Nd:YAG sample the slope efficiency was 0.54 and the threshold absorbed power was 31 mW. A deterioration of these parameters with increasing C_{Nd} was observed: while for the 2.4-at.% Nd:YAG crystal the slope efficiency was 0.50 and the absorbed power at threshold was 45 mW, for the 3.5-at.% Nd:YAG sample the slope efficiency decreased to 0.46 with a threshold absorbed power of 65 mW. Figure 2 presents the laser performances for 0.9-mm thick Nd:YVO₄ components in the configuration E//c-crystal axis and with the 95% reflectivity output coupler. In spite of using uncoated active elements the laser parameters obtained with the 1-at.% Nd sample are substantially improved (slope efficiency of 70% and absorbed pump power at threshold of 21 mW) with respect to those reported in Reference 5) for a thicker sample. For the 2-at.% Nd component the threshold of emission in absorbed power was 44 mW, the slope efficiency reached 67% and for 420-mW absorbed power the laser emitted 265 mW at 1064 nm. A slope efficiency of 58% and a threshold of 58 mW absorbed power were determined for the 3-at.% Nd:YVO₄ sample. The residual losses L were determined as ~0.005, 0.01 and ~0.016 for the 1, 2, and 3-at.% Nd:YAVO₄ crystals, respectively.

In conclusions, the investigation of the effect of Nd concentration on emission decay of Nd:YAG indicates that up to quite high concentrations the reduction of the emission quantum efficiency by self-quenching can be compensated by the increase of pump absorption. Efficient CW laser emission is demonstrated under direct pumping into the ⁴F_{3/2} emitting level of Nd:YAG crystals with up to 3.5-at.% Nd, Nd:YAG ceramics with up to 6.8-at.% Nd, and Nd:YVO₄ crystals with up to 3-at.% Nd. Superior performance as compared to traditional pumping into the ⁴F_{5/2} state were obtained. It is inferred that direct pumping into the emitting level of concentrated Nd materials can improve the efficiency of solid-state lasers in the free-generation or low-storage regimes and opens the possibility of scaling these lasers to high powers.

References

- 1) V. Lupei, A. Lupei, S. Georgescu, T. Taira, Y. Sato and A. Ikesue, *Phys. Rev. B* **64**, 092102 (2001).
- 2) V. Lupei, A. Lupei, N. Pavel, T. Taira, I. Shoji and A. Ikesue, *Appl. Phys. Lett.* **79**, 590 (2001).
- 3) V. Ostroumov, T. Jensen, J. P. Meyn, G. Huber and M.A. Noginov, *J. Opt. Soc. Am. B* **15**, 1052 (1998).
- 4) Y.F. Chen, C.C. Liao, Y.P. Lan and S.C. Wang, *Appl. Phys. B* **70**, 487 (2000).
- 5) R. Lavi, S. Jackel, Y. Tzuk, M. Winik, E. Lebiush, M. Katz and I. Paiss, *Appl. Opt.* **38**, 7382 (1999).

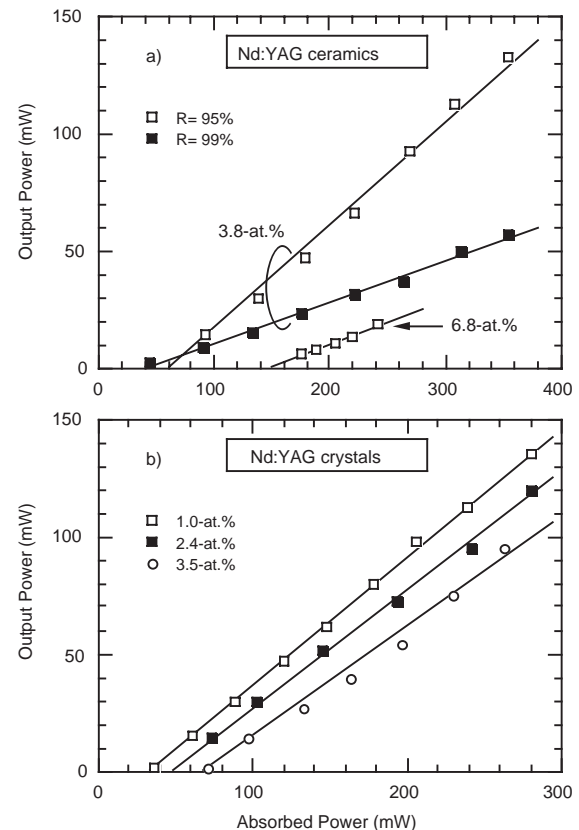


Figure 1. 1064-nm laser emission characteristics for (a) uncoated 3.8 and 6.8-at.% Nd:YAG ceramics and for (b) uncoated Nd:YAG crystals under 885-nm pumping.

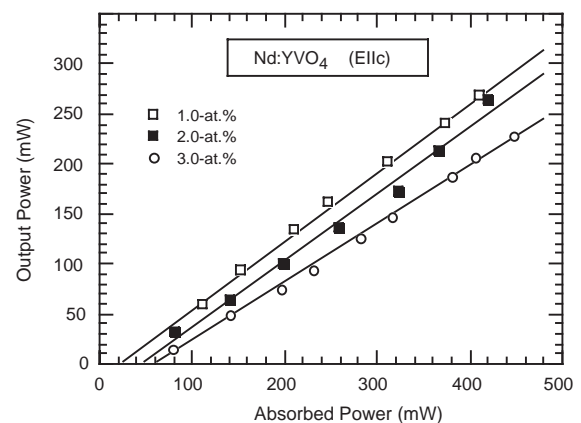


Figure 2. Comparative 1064-nm laser performances for Nd:YVO₄ components under 880-nm pumping (E//c-crystal axis) with a 95% reflectivity output coupler.

VIII-B-6 1064-nm Laser Emission of Highly Doped Nd:Yttrium Aluminium Garnet under 885-nm Diode Laser Pumping

LUPEI, Voicu¹; PAVEL, Nicolaie²; TAIRA, Takunori

(¹IAP-NILPRP, Romania; ²IMS and IAP-NILPRP, Romania)

[*Appl. Phys. Lett.* **80**, 4309 (2002)]

Owing to the high optical-to-electrical efficiency and to the ability to excite resonantly the energy levels of the laser active ions, the diode laser pumping has a major role in increasing the efficiency of the solid-state lasers. The resonant excitation of Nd³⁺ emission was demonstrated at early stages of laser development by exciting Nd:CaWO₄ directly into the emitting level on the transition $^4I_{9/2} (Z_2) \rightarrow ^4F_{3/2} (R_2)$ by the 880-nm recombination radiation of GaAs diodes.¹⁾ The first diode laser pumped Nd:YAG lasers in transverse²⁾ or longitudinal³⁾ pumping configurations used the direct excitation of the emitting level on the 869-nm transition $^4I_{9/2} (Z_1) \rightarrow ^4F_{3/2} (R_2)$. Due to the weak absorption on this transition and to the lack of suitable pump diodes, the 869-nm pumping was soon replaced by the 808-nm pumping into the stronger absorption $^4I_{9/2} (Z_1) \rightarrow ^4F_{5/2} (S_1)$. Unfortunately, this introduces a parasitic upper quantum defect between the pump- and the emitting laser levels that contributes to the reduction of the laser emission parameters and to the generation of heat by non-radiative processes in the pumped laser material.

The pumping into the emitting level of Nd-doped materials has received a renewed attention in the last few years: in case of Nd:YAG successful attempts have been made with diluted (~1-at.% Nd) single crystals under Ti:sapphire or diode laser pumping^{4),5)} and with highly-doped ceramics or single crystals^{6),7)} under Ti:sapphire pump. This paper demonstrates CW laser emission of highly doped Nd:YAG ceramics (up to 3.5-at.% Nd) and single crystals (up to 3.8-at.% Nd) under 885-nm diode laser pumping. The laser emission of a 2.4-at.% Nd:YAG single crystal passively Q-switched with a Cr⁴⁺:YAG saturable absorber under CW diode laser pumping at 885 nm is also reported.

A fiber array packed diode bars FAP-81-16C-800B laser (Coherent Co.) whose output is delivered in a 19-fiber bundle confined within an 800- μ m diameter aperture with NA = 0.15 was used as pumping source. With a collimating achromatic lens of 60-mm focal length and a focusing achromatic lens of 50-mm focal length the end face of the fiber bundle was imaged into the laser active components in a 780- μ m diameter spot. The laser active components were Nd:YAG single crystals of 1-at.% (3-mm thick), 2.4-at.% (3-mm thick) and 3.5-at.% Nd (1.0-mm thick) and Nd:YAG ceramics of 3.8-at.% Nd (1.5 and 2.5-mm thick), AR coated on both sides for 885 and 1064 nm. A plane-concave resonator of 50 mm length with an output mirror of 0.25-m radius of curvature was used. The active component was placed close to the rear mirror, which was coated HR for 1064 nm and HT for the pumping wavelength.

Figure 1a shows the laser performances for the 2.4-at.% Nd:YAG crystal. The maximum slope efficiency of

0.64 was obtained for a 90% reflectivity output mirror, with a corresponding emission threshold 1.51 W. The slope efficiency and the threshold become 0.62 and 0.87 W for 95% reflectivity and 0.26 and 0.25 mW for 99% reflectivity. The output power obtained with 95% reflectivity output mirror for the laser materials used in this experiment is presented in Figure 1b: the best results, i.e. a slope efficiency of 0.67 and 0.71 W absorbed power at threshold, were obtained with the 1.0-at.% Nd:YAG crystal of 3.0-mm thickness. The laser parameters vs. incident power reveal the practical advantages of the concentrated materials: for the region close to the maximum operating point, where the diode wavelength is ~ 885 nm, the measured slope efficiency in input power for the 3-mm thick crystals is 0.26 for 1-at.% Nd and 0.43, i.e. by 65% larger, for 2.4-at.% Nd. At the same time the emission threshold is by ~ 40 % lower for the second crystal and the absorption efficiency is larger by ~ 75%.

The passive Q-switching regime was investigated with Cr⁴⁺:YAG saturable absorber (SA) crystals. A plane-plane resonator with the active medium positioned near the rear mirror and the SA crystal placed closed of the output mirror was investigated. Figure 2 shows the average power vs. the absorbed power for a 70-mm length resonator. With a Cr:YAG SA of 90% initial transmission (T_0) and an output mirror of 95% reflectivity an average output power of 0.95 W resulted for 5.2-W absorbed power. The maximum repetition rate was 7.1 kHz with the pulse width 37.5 ns over the entire range of absorbed power: this corresponds to a maximum pulse energy of 134 μ J and ~ 3.6 kW peak power. With a 90% reflectivity output mirror the average power decreases to 0.84 W; the pulse width reduces to 26.5 ns, corresponding to ~ 161- μ J pulse energy and ~6 kW peak power. With a Cr:YAG SA of $T_0 = 85%$ and a 95% reflectivity output mirror the laser emitted max. 0.56-W average power at 3.2-kHz repetition rate: the pulse had 175 μ J energy and 5.6-kW peak power. In spite of using a non-optimised scheme, improved laser characteristics (lower threshold, higher average power and pulse energy) resulted compared with a 1.1-at.% composite Nd:YAG laser passively Q-switched by Cr:YAG under 808-nm diode pumping.⁸⁾

In conclusion, highly efficient 1064-nm CW laser emission under 885-nm diode pumping in concentrated Nd:YAG crystals (up to 3.5-at.% Nd) and ceramics (up to 3.8-at.% Nd) is reported. First highly doped (2.4-at.%) Nd:YAG laser passively Q-switched by a Cr⁴⁺:YAG saturable absorber is demonstrated.

References

- 1) R. Newman, *J. Appl. Phys.* **34**, 437 (1963).
- 2) M. Ross, *Proc. IEEE* **56**, 196 (1968).
- 3) L. J. Rosenkrantz, *J. Appl. Phys.* **34**, 4603 (1972).
- 4) R. Lavi and S. Jackel, *Appl. Opt.* **39**, 3093 (2000).
- 5) R. Lavi, S. Jackel, A. Tal, E. Lebiush, Y. Tzuk and S. Goldring, *Opt. Commun.* **195**, 427 (2001).
- 6) V. Lupei, A. Lupei, N. Pavel, T. Taira, I. Shoji and A. Ikesue, *Appl. Phys. Lett.* **79**, 590 (2001).
- 7) V. Lupei, N. Pavel and T. Taira, *Opt. Lett.* **26**, 1678 (2001).
- 8) N. Pavel, J. Saikawa, S. Kurimura and T. Taira, *Jpn. J. Appl. Phys.* **40**, 1253 (2001).

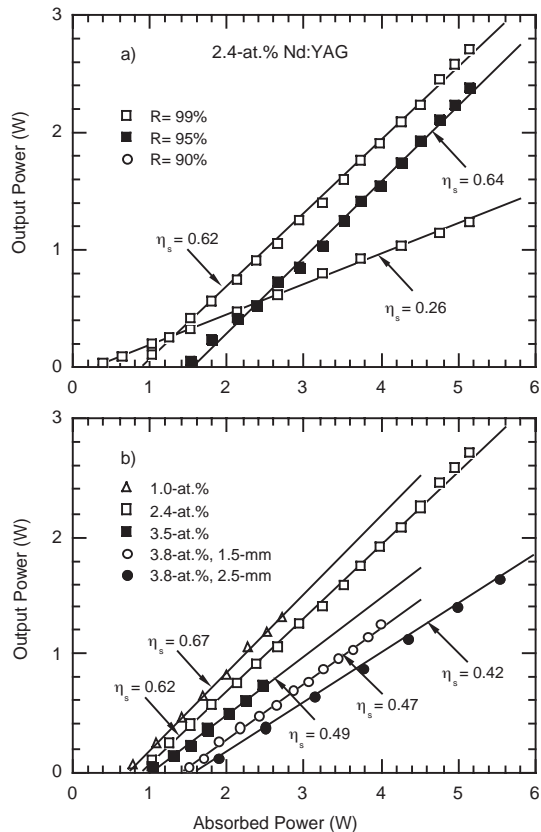


Figure 1. 1064-nm laser emission characteristics for (a) a 2.4-at.% Nd:YAG crystal and for (b) the Nd:YAG laser active components used in experiments and a 95% reflectivity output mirror under 885-nm diode laser pumping.

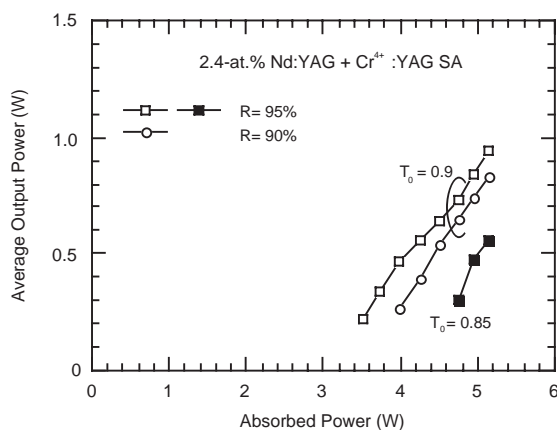


Figure 2. Average output power of a CW diode pumped at 885 nm highly-doped (2.4-at.%) Nd:YAG laser passively Q-switched by Cr^{4+} :YAG saturable absorber.

VIII-B-7 Diode Edge-Pumped Microchip Composite Yb:YAG Laser

DASCALU, Traian; TAIRA, Takunori; PAVEL, Nicolaie

[*Jpn. J. Appl. Phys.* **41**, 606 (2002)]

High power microchip laser based on Yb^{3+} doped materials has been recognized as very useful in the ultrafast-laser field.^{1,2)} Thermal effects in the laser gain

medium generally limit power scaling of diode-pumped solid-state microchip lasers. Yb:YAG is a gain medium that has improved properties relative to Nd^{3+} -doped gain media³⁾ for addressing this issue and efficient room-temperature laser operation (slope efficiency of 65%) has been demonstrated in this material despite the fact that it is a quasi-four-level laser.⁴⁾ Besides of choice of gain medium the configuration that is chosen for pumping, cooling, and extraction plays a critical role in power scaling of microchip laser. Despite of the Yb:YAG low quantum defect, large thermal effects occur at high pumping power. One solution to diminish the thermal lens is to orient the heat flux collinearly with the direction of laser propagation. We propose an edge pumped Yb:YAG microchip scheme. This scheme can be used efficiently only if the pumping power is concentrated into a small region of the microchip consequently a composite material was designed.

The composite material consists in an Yb:YAG core of hexagonal or square shape surrounded by circular shaped undoped YAG. The composite crystal consists of an Yb:YAG doped core surrounded by an undoped YAG region, the core and the undoped crystal being diffusion bonded. The crystal has one side high reflectivity (HR) coated at the laser wavelength and the opposite side anti reflection (AR) coated and it is mounted with its HR coated side on a highly effective micro channel cooling system, Figure 1. Two fiber-coupled diode lasers delivering more than of 100 W at 940 nm are used for pumping. Inside of the microchip the pumping beam propagates by total internal reflection and intersects the Yb:YAG core where it is partially absorbed.

Continuous laser operation was obtained from the 2 at% Yb doped crystal by using an optical resonator of 50-mm length with output coupler of 100-mm radius of curvature and 97% reflectivity output mirror. The slope efficiency for laser operation at more than three times above the threshold is 50% and the laser delivers maximum 1.8 W output power for 5.1 W absorbed power.

In order to evaluate the laser performances under low thermal effects the microchip was operated in quasi-CW mode with a duty factor of 2.5% and 2.4 Hz repetition rate. Figure 2 presents the output vs. input power for the 10-at. % doped sample with 97% reflectivity output mirror. Laser emission with 42% slope efficiency and 41-W output peak power at 220-W input power was demonstrated. The experiments show the potential of the microchip laser to be scaled in the range of tens of watts output power.

References

- 1) C. Honninger, R. Paschotta, M. Graf, F. Morier-Genoud, G. Zhang, M. Moser, S. Biswal, J. Nees, A. Braun, G.A. Mourou, A. Giesen, W. Seeber and U. Keller, *Appl Phys. B* **69**, 3 (1999).
- 2) C. Honninger, I. Johannsen, M. Moser, G. Zhang, A. Giesen and U. Keller, *Appl. Phys. B* **65**, 423 (1997).
- 3) L.D. DeLoach, S.A. Payne, L.L. Chase, L.K. Smith, W.L. Kway and W.F. Krupke, *IEEE J. Quantum Electron.* **29**, 1179 (1993).
- 4) K. Contag, M. Karzewski, C. Stewen, A. Giesen and H. Hugel, *Quantum Electronics* **29**, 697 (1999).

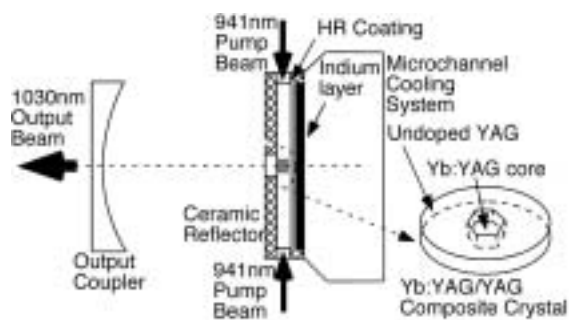


Figure 1. The diode radial-pumped composite Yb:YAG microchip laser.

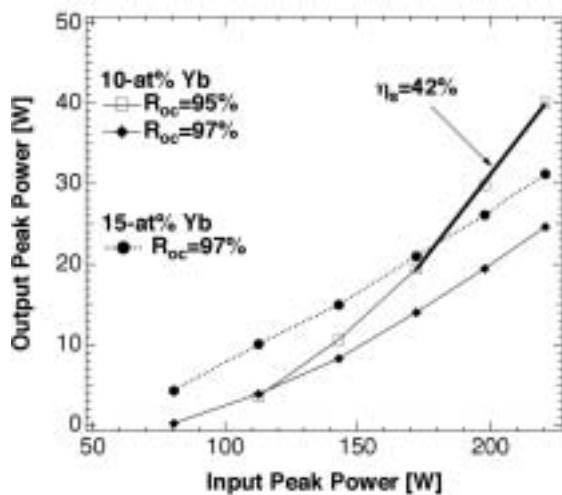


Figure 2. Output power vs. input power for quasi CW laser operation for 10-at. % Yb-doping crystal, $2 \times 2 \text{ mm}^2$ square core dimensions and 15-at. % Yb-doping crystal, $1.2 \times 1.2 \text{ mm}^2$ square core dimensions. Here R represents the output mirror reflectivity.

Research Center for Molecular-Scale Nanoscience

VIII-C Development of Organic Semiconductors for Molecular Thin-Film Devices

Organic light-emitting diodes (OLEDs) and organic field-effect transistors (OFETs) based on π -conjugated oligomers have been extensively studied as molecular thin-film devices. Organic semiconductors with low injection barriers and high mobilities are required for highly efficient OLEDs and OFETs. Radical cations or anions of an organic semiconductor have to be generated easily at the interface with an electrode (or a dielectric), and holes or electrons must move fast in the semiconducting layer. Compared with organic *p*-type semiconductors, organic *n*-type semiconductors for practical use are few and rather difficult to develop. Recently, we found that perfluorinated oligomers are efficient electron-transport materials for OLEDs.

VIII-C-1 Perfluoro-1,3,5-tris(*p*-Oligophenyl)benzenes: Amorphous Electron-Transport Materials with High Glass-Transition Temperature and High Electron Mobility

KOMATSU, Shingo; SAKAMOTO, Youichi;
SUZUKI, Toshiyasu; TOKITO, Shizuo¹
(¹NHK Sci. Tech. Res. Labs.)

[*J. Solid State Chem.* in press]

Perfluoro-1,3,5-tris(*p*-quaterphenyl)benzene (**PF-13Y**) and perfluoro-1,3,5-tris(*p*-quinquephenyl)benzene (**PF-16Y**) have been synthesized and characterized. They showed higher glass transition temperatures compared with perfluoro-1,3,5-tris(*p*-terphenyl)benzene (**PF-10Y**). Organic light-emitting diodes (OLEDs) were fabricated using these materials as the electron-transport layers. **PF-13Y** and **PF-16Y** are better electron-transporters than **PF-10Y**. The electron mobilities of **PF-10Y** and Alq₃ were measured by the time-of-flight technique. **PF-10Y** showed higher electron mobilities (10^{-4} cm²/Vs) and weaker electric field dependence compared with Alq₃.

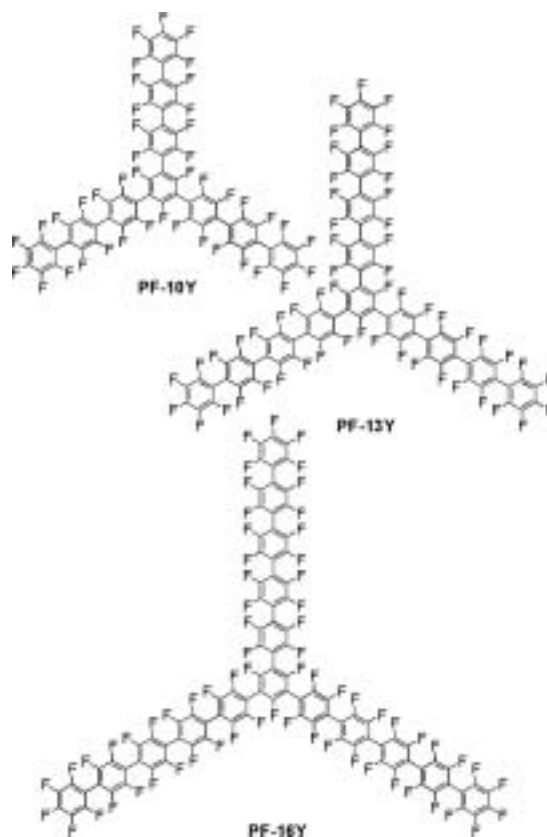


Figure 1. Perfluoro-1,3,5-tris(*p*-oligophenyl)benzenes.

VIII-C-2 Synthesis and Properties of Iridium Complexes Bearing Perfluoroaryl-Substituted 2-Phenylpyridine

SHIRASAWA, Nobuhiko; SAKAMOTO, Youichi;
SUZUKI, Toshiyasu; TSUZUKI, Toshimitsu¹;
TOKITO, Shizuo¹
(¹NHK Sci. Tech. Res. Labs.)

Perfluorophenyl derivatives of 2-phenylpyridine, 2-(*p*-C₆F₅-phenyl)pyridine (**1a**), 5-C₆F₅-2-phenylpyridine (**1b**), and 5-C₆F₅-2-(*p*-C₆F₅-phenyl)pyridine (**1c**), have been prepared. Their iridium(III) acetylacetonato complexes (**2a-c**) were satisfactorily synthesized in a one-pot reaction of a free ligand and an iridium salt in 2-ethoxyethanol at 105 °C, and the subsequent reaction

with acetylacetonate in the presence of a base at 50 °C for 4 h. When the reaction was carried out at 140 °C, the substitution reaction of fluoride with 2-ethoxyethoxide at para position took place. When applied to OLED devices, compounds **2a-c** showed emissions from greenish yellow to yellow at room temperature with the external quantum efficiency up to 14.7%.

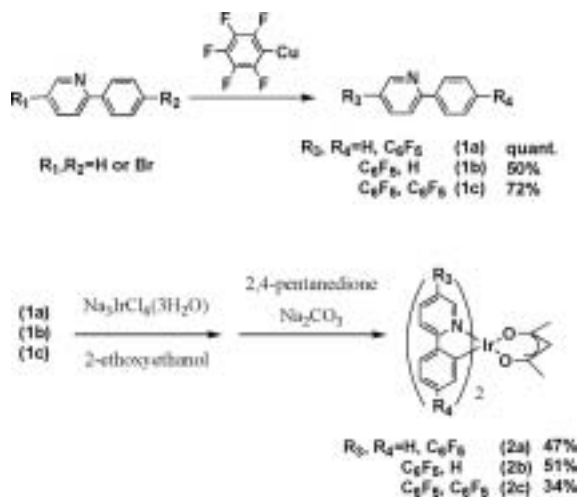


Figure 1. Synthesis of C_6F_5 -substituted ppy and their iridium acac derivatives.

VIII-D Field Effect Transistors with Organic Semiconductors

The mechanism of carrier transport in organic semiconductors and carrier injection from metal electrodes becomes the most important subject to be elucidated for the construction of high performance organic thin film devices. We have studied electrical properties of organic films using field effect transistors.

VIII-D-1 Electrical Characteristics of Phthalocyanine Films Prepared by Electrophoretic Deposition

TAKADA, Masaki¹; YOSHIOKA, Hirokazu²;
TADA, Hirokazu; MATSUSHIGE, Kazumi²
(¹GUAS; ²Kyoto Univ.)

[*Jpn. J. Appl. Phys.* **41**, L73 (2002)]

Electrical properties of phthalocyanine (Pc) films prepared by an electrochemical process were investigated using field effect transistors (FETs). Copper-Pc (CuPc) films were deposited electrophoretically on voltage-applied cathodic electrodes from trifluoroacetic acid/dichloromethane mixed solution containing protonated monomeric CuPc molecules. Optical absorption spectra showed that the CuPc films had α -type polymorphs. The grains grew with reaction time to close a gap between the FET electrodes. FET studies showed that CuPc films after annealing exhibited a *p*-type semiconducting behavior. Carrier mobility, conductivity and carrier density of the films were $1.4 \times 10^{-5} \text{ cm}^2/\text{Vs}$, $7.7 \times 10^{-7} \text{ S/cm}$ and $6.6 \times 10^{16} \text{ cm}^{-3}$, respectively. It is revealed that electrophoretic deposition is applicable for the preparation of active layers in organic electronic devices.

VIII-D-2 BTQBT (bis-(1,2,5-thiadiazolo)-*p*-Quinobis(1,3-dithiole)) Thin Films; A Promising Candidate for High Mobility Organic Transistors

TAKADA, Masaki¹; GRAAF, Harald;
YAMASHITA, Yoshiro²; TADA, Hirokazu
(¹GUAS, ²Tokyo Inst. Tech.)

[*Jpn. J. Appl. Phys.* **41**, L4 (2002)]

BTQBT (bis-(1,2,5-thiadiazolo)-*p*-quinobis(1,3-dithiole)) films have been prepared as active semiconducting layers of organic field effect transistors (FETs). BTQBT films showed a *p*-type semiconducting behavior. The hole mobility and on/off ratio of BTQBT films under ultrahigh vacuum conditions reached to $0.2 \text{ cm}^2/\text{Vs}$ and 10^8 , respectively, by optimization of the growth conditions. These values are in the same order as those of pentacene thin films, which indicates that BTQBT molecules have a great potential for active layers of organic electronic devices.

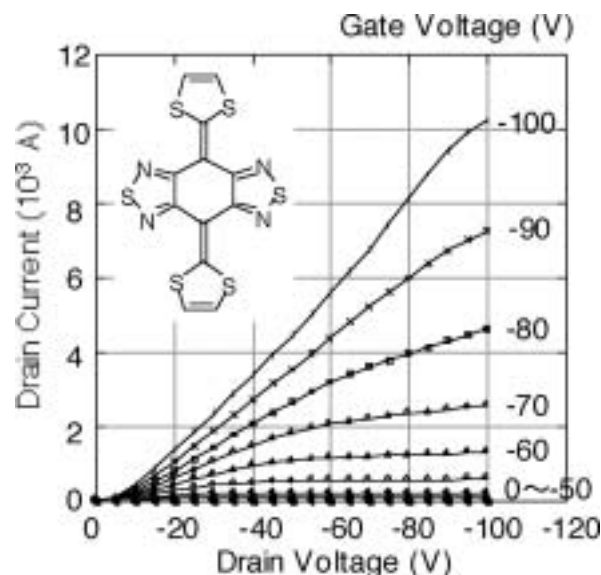


Figure 1. FET characteristics of BTQBT films measured in UHV.

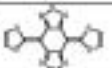
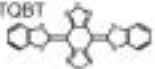
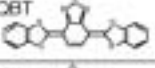
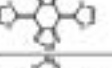
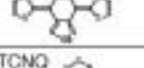
VIII-D-3 Field Effect Transistors of BTQBT and Its Derivatives

TAKADA, Masaki¹; YAMASHITA, Yoshiro²;
TADA, Hirokazu
(¹GUAS; ²Tokyo Inst. Tech.)

[*Proc. MRS 725*, P10.3 (2002)]

We have prepared and characterized thin film field effect transistors (FETs) of bis-(1, 2, 5- thiadiazolo)-*p*-quinobis(1, 3-dithiole) (BTQBT) and its derivatives. Preparation and characterization of the films were carried out under ultrahigh vacuum condition. Most materials examined showed *p*-type semiconducting behaviors. Among *p*-type molecules, BTQBT films deposited at room temperature showed *p*-type semiconducting behaviors with mobility of $0.1 \text{ cm}^2/\text{Vs}$. The on/off drain current ratio was 10^7 . The mobility and on/off ratio reached to $0.2 \text{ cm}^2/\text{Vs}$ and 10^8 , respectively, by optimizing the film growth conditions. These performances are almost comparable to those of pentacene and polythiophene thin films, indicated that BTQBT molecule is a prominent semiconducting material as a high mobility thin film. It was also found that tetracyanoquinodimethane (TCNQ) derivative showed an *n*-type semiconducting behavior with an electron mobility of $8.9 \times 10^{-4} \text{ cm}^2/\text{Vs}$.

Table 1. Field Effect Mobilities of BTQBT and Its Derivatives.

	type	Mobility(cm ² /Vs)	On/off ratio
BTQBT 	p	1.0×10^{-1} (0.2 at 50°C)	10^7
DB-BTQBT 	p	4.6×10^{-4}	10^4
DB-TQBT 	p	1.6×10^{-5}	50
TQBT 	p	1.2×10^{-3}	3
BSQBT 	p	1.3×10^{-6}	10
BTDA-TCNQ 	n	8.9×10^{-4} Al electrodes	10^2

VIII-D-4 Preparation of Nanometer-Gap Electrodes for Field Effect Transistors by Electroplating

YAMADA, Ryo; TAKADA, Masaki¹; OISHI, Osamu; TADA, Hirokazu
(¹GUAS)

A pair of electrodes with a nanometer-scale spacing

was fabricated by electroplating of gold onto micrometer gap electrodes prepared through conventional photolithography. The electrodes were prepared on SiO₂ formed on a heavily doped Si substrate which serves as a gate electrode. Figure 1 shows a SEM micrograph of the electrode fabricated by this method. It was shown that the drain current changed as a function of a gate voltage when Ti-phthalocyanine thin film was deposited onto this electrode. Thus, the electrode made by this method can be used for the study of organic thin film field effect transistors.

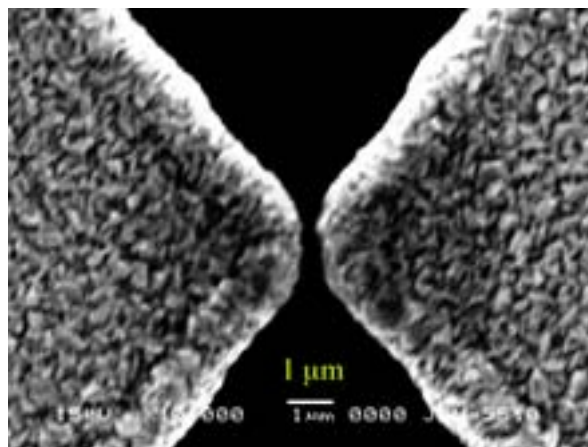


Figure 1. SEM Photograph of Nanometer Gap Electrodes.

VIII-E Preparation and Characterization of Highly Ordered Molecular Films on Silicon Bound with Si-C Covalent Bond

Self-assembled monolayers (SAMs) have received considerable attention because of their potential applications to molecular scale electronic devices. Covalently bond alkane SAMs formed by reaction between alkene and hydrogen terminated silicon are of increasing interest as nano-interface for molecular electronics devices fabricated on silicon microstructures. We have studied the growth manner and electronic structure of Si-C junction using scanning probe microscope such as STM (scanning tunneling microscope), AFM (atomic force microscope) and KFM (Kelvin force microscope).

VIII-E-1 Force Curve Measurement of Self-Assembled Organic Monolayers Bound Covalently on Silicon(111)

GRAAF, Harald; ARA, Masato¹; TADA, Hirokazu
(¹GUAS)

[*Mol. Cryst. Liq. Cryst.* **377**, 33 (2002)]

Self-assembled monolayers of alkyl chains were prepared on silicon(111) surfaces. The surface was characterized by atomic force microscopy (AFM). Atomically flat terraces were observed in topographic images of the films with contact mode AFM, indicating the formation of highly ordered monolayers. Force curve measurements showed that the adhesion force between organic films and gold cantilever was much stronger comparing to the force on hydrogen terminated

surfaces.

VIII-E-2 Atomic Force Microscope Anodization of Si(111) Covered with Alkyl Monolayers

ARA, Masato¹; GRAAF, Harald; TADA, Hirokazu
(¹GUAS)

[*Jpn. J. Appl. Phys.* **41**, 4894 (2002)]

Alkyl monolayers on Si were prepared through the reaction between 1-alkenes and hydrogen-terminated Si by heat treatment. The monolayers were characterized by atomic force microscopy (AFM), force curve and water contact angle measurements. It was found that surface properties were modified by the formation of highly ordered closely packed monolayers. The monolayers were anodized with a contact-mode AFM

by applying voltage between the conductive cantilever and surface under ambient conditions, which resulted in nanometer-scale oxidation of surfaces. After anodization, patterned areas were modified by removing the silicon oxide and terminating the surface of the grooves with hydrogen atoms by NH_4F etching, and by covering the etched surface with 1-octadecene molecules. The monolayers themselves showed high resistance to NH_4F etching and air oxidation.

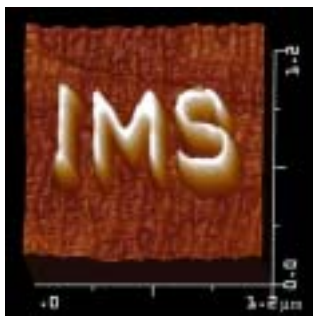


Figure 1. AFM anodization of Silicon Surfaces with AFM.

VIII-E-3 Nanopatterning of Alkyl Monolayers Covalently Bound to Si(111) with an Atomic Force Microscope

ARA, Masato¹; GRAAF, Harald; TADA, Hirokazu
(¹GUAS)

[*Appl. Phys. Lett.* **80**, 2565 (2002)]

Alkyl monolayers covalently bound to silicon were prepared through the reaction between 1-alkene molecules and hydrogen-terminated Si. The surfaces were anodized in nanometer scale with a contact-mode atomic force microscope (AFM) by applying positive bias voltage to the surface with respect to a conducting cantilever under ambient conditions. Following the anodization, patterned areas were selectively modified by chemical etching and coating with different molecules. The alkyl monolayers showed high resistance against chemical etching and protected Si surfaces from oxidation. AFM lithography of monolayers on Si was found to be useful for nanofabrication of organic/-inorganic interfaces based on the Si-C covalent bond.

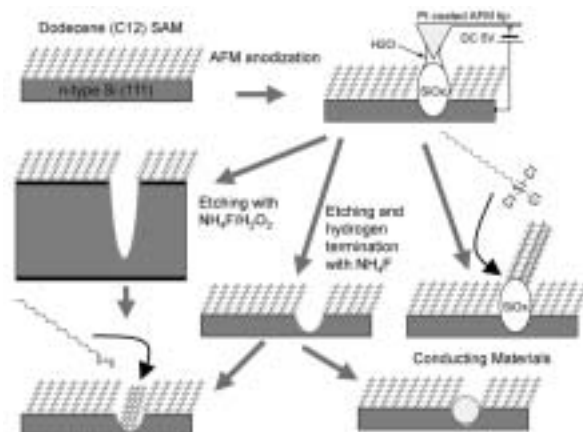


Figure 1. Nanopatterning of Silicon Surfaces with AFM.

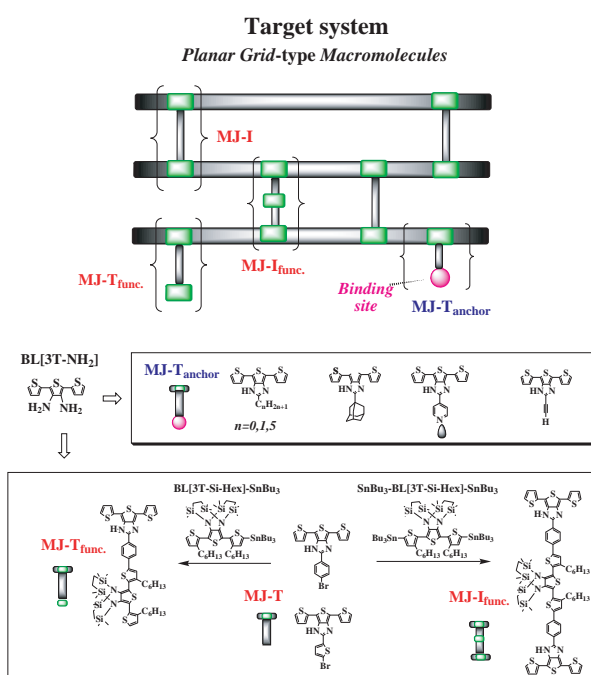
VIII-F Development of Precisely-Defined Macromolecules and their Organization on Substrate Surfaces for Molecular-Scale Electronics Circuits

The concept of molecular-scale electronics is now realized for individual components such as wire, diode, switch, and memory cell, but the fabrication of complete molecular-scale circuits remains challenging because of the difficulty of connecting molecular modules to one another. Molecular monolithic technology, which integrates the wiring, transistors and the required passive elements on a single macromolecule, has been proposed as a promising solution to this problem. In this project we have been trying to establish both the architecture of this novel class of macromolecules and the protocols for their purposive organization on metal/semiconductor substrate surfaces.

VIII-F-1 Design and Synthesis of Molecular Junction and Anchor Modules for Multi-Function Integrated Macromolecules

TANAKA, Shoji; YOKOYAMA, Takashi¹
(¹NIMS)

The design of “planar and multi-function integrated” π -conjugated macromolecules has been a subject of intensive research in the field of molecular electronics, because of their potential applications as basic components for future IT hardware such as ultra-dense molecular-scale quantum computers. In order to establish the architecture for this class of tailor-made macromolecules, we have developed various types of molecular building blocks and characterized them on substrate surfaces based on the high-resolution STM experiments combined with their bulk-level properties. Here we describe the synthesis of i) “molecule-anchor modules” for setting the molecular systems on metal/semiconductor substrate, and ii) “molecule-junction modules” for constructing planar grid-type molecular frameworks. Scheme 1 shows the synthetic pathways to these modules. Purification of these molecules was achieved by gel permeation chromatography. The purity of the obtained compounds was clearly revealed by MALDI-TOF mass spectroscopy using dithranol as matrix.



Scheme 1.

VIII-G Development of Novel Heterocyclic Compounds and their Molecular Assemblies for Advanced Materials

Heterocycles containing sulfur and/or nitrogen atoms are useful as components of functional materials since heteroatoms in their rings are helpful to stabilize ions or ion-radical species, and extended π -conjugation decreases Coulombic repulsion. In addition intermolecular interactions caused by heteroatom contacts can be expected to form novel molecular assemblies. In this project new electron acceptors, donors, and donor-acceptor compounds based on heterocycles such as 1,2,5-thiadiazole and 1,3-dithiole were synthesized and their properties including those of the charge-transfer complexes or ion-radical salts were investigated. Unique crystal structures were constructed by using weak intermolecular interactions such as hydrogen bonding or heteroatom contacts.

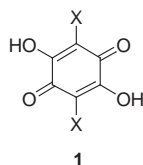
VIII-G-1 Crystal Engineering Using Anilic Acids and Dipyridyl Compounds through a New Supramolecular Synthron

ZAMAN, Md. Badruz¹; TOMURA, Masaaki;
YAMASHITA, Yoshiro²
(¹IMS and Steacie Inst. Mol. Sci.; ²IMS and Tokyo Inst.

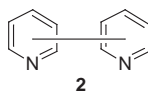
Tech.)

[*J. Org. Chem.* **66**, 5987 (2001)]

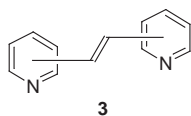
The anilic acids, 2,5-dihydroxy-1,4-benzoquinone **1a**, 2,5-dibromo-3,6-dihydroxy-1,4-benzoquinone (bromanilic acid; **1b**), 2,5-dichloro-3,6-dihydroxy-1,4-benzoquinone (chloranilic acid; **1c**), and 2,5-dicyano-3,6-dihydroxy-1,4-benzoquinone (cyananilic acid; **1d**), were cocrystallized with rigid organic ligands containing two pyridine rings, 2,4-bipyridine **2a**, 4,4'-bipyridine **2b**, 1,2-bis(2-pyridyl)ethylene **3a**, 1,2-bis(4-pyridyl)ethylene **3b**, 2,2'-dipyridylacetylene **4a**, 3,3'-dipyridylacetylene **4b**, and 4,4'-dipyridylacetylene **4c**. Fourteen complexes **5–18** were obtained as single crystals, and their crystal structures were successfully determined by X-ray analysis. All complexes except those with **2a** are 1 : 1 and are composed of an infinite linear or zigzag tape structure, the formation of which is ascribed to intermolecular O–H...N, N⁺–H...O, or N⁺–H...O[–] hydrogen bonds or a combination of these between the anilic acids and the dipyrindyl compounds. In the complexes **5** and **6**, no infinite tape structure is observed although the molecular units connected by a similar hydrogen-bonding pattern are formed. For the 1 : 1 complexes, we have found two types of stacking arrangements, segregated stacks (**7**, **9**, **12–15**, **18**) and alternated ones (**8**, **10**, **11**, **16**, **17**). In the complexes of **1c** with the series of dipyrindylacetylens **4** (**14**, **15**, **17**), the neutral, dication, and monocation states are formed depending on the nitrogen positions, which can be attributed to the different basicity of the pyridyl groups.



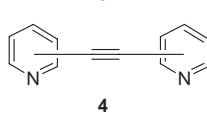
- 1a**: X = H
1b: X = Br
1c: X = Cl
1d: X = CN



- 2a**: 2,4-bipyridine
2b: 4,4'-bipyridine



- 3a**: 1,2-bis(2-pyridyl)ethylene
3b: 1,2-bis(4-pyridyl)ethylene



- 4a**: 2,2'-dipyridylacetylene
4b: 3,3'-dipyridylacetylene
4c: 4,4'-dipyridylacetylene

- 5**: complex between **1b** and **2a** **12**: complex between **1a** and **4c**
6: complex between **1c** and **2a** **13**: complex between **1b** and **4a**
7: complex between **1a** and **2b** **14**: complex between **1c** and **4a**
8: complex between **1c** and **2b** **15**: complex between **1c** and **4b**
9: complex between **1c** and **3a** **16**: complex between **1b** and **4c**
10: complex between **1b** and **3b** **17**: complex between **1c** and **4c**
11: complex between **1c** and **3b** **18**: complex between **1d** and **4c**

VIII-G-2 Bis(tetra-*n*-butylammonium) Bis(2-dicyanomethylene-4,5-dimercapto-1,3-dithiole)nickel(II)

TOMURA, Masaaki; YAMASHITA, Yoshiro¹(¹IMS and Tokyo Inst. Tech.)[*Acta Crystallogr., Sect. E* **58**, m133 (2002)]

We have carried out the X-ray crystallographic analysis of the title dithiolato-nickel complex derived from 2-dicyanomethylene-4,5-dimercapto-1,3-dithiole (dcndmdt) ligand.¹ This ligand in the nickel complex has peripheral heteroatoms and extended π -conjugated systems. In the nickel complex, [Ni(dcndmdt)₂](*n*-Bu₄N)₂, the centrosymmetric dianion is flat. The nickel atom has square-planar coordination, with Ni–S bond lengths of 2.1836(16) and 2.1940(18) Å.

Reference

- 1) M. Tomura and Y. Yamashita, *J. Mater. Chem.* **5**, 1753 (1995).

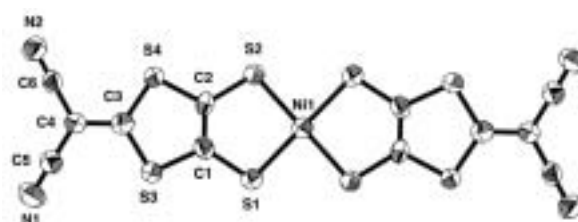


Figure 1. Molecular structure of the dianion in [Ni(dcndmdt)₂](*n*-Bu₄N)₂.

VIII-G-3 ¹H NMR Analysis and Crystal Structures of 1,1',3,3'-Tetramethyl-2,2'-bi-1*H*-Imidazolium Bis(tetraphenylborate): Ion-Associative Interactions Containing Ketone, Aldehyde, and Nitrile

ONO, Katsuhiko¹; SAITO, Katsuhiko¹; UCHIUMI, Hideki¹; TOMURA, Masaaki
 (¹Nagoya Inst. Tech.)

[*Chem. Lett.* 622 (2002)]

According to ¹H NMR analysis of 1,1',3,3'-tetramethyl-2,2'-bi-1*H*-imidazolium bis(tetraphenylborate) **1** in acetone and acetonitrile, high magnetic field shifts of the chemical shifts were observed. The facts are ascribable to ion association between the biimidazolium dication and BPh₄ anions. The crystals of **1** included some kinds of ketone, aldehyde, and nitrile as guest molecules to afford unique molecular aggregations. The biimidazolium dication is surrounded by four BPh₄ anions and is in a specific cyclic environment arising from eight phenyl groups, as shown in Figure 1. The molecular arrangements of the biimidazolium dication in the crystals can be controlled by the guest molecules.

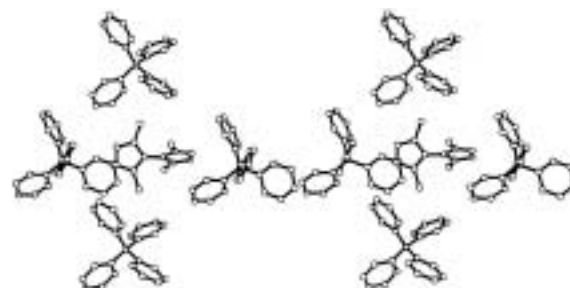


Figure 1. Stereo view of the packing mode of **1**-cyclohexanone.

VIII-G-4 4,7-Diiodo-2,1,3-Benzothiadiazole and 7,7'-Diiodo-4,4'-bis(2,1,3-benzothiadiazole)

TOMURA, Masaaki; AKHTARUZZAMAN, Md.¹; SUZUKI, Kazuharu²; YAMASHITA, Yoshiro³
(¹GUAS; ²IMS and Inst. Res. Innov.; ³IMS and Tokyo Inst. Tech.)

[*Acta Crystallogr., Sect. C: Cryst. Struct. Commun.* **58**, o373 (2002)]

The title compounds, 4,7-diiodo-2,1,3-benzothiadiazole **1** and 7,7'-diiodo-4,4'-bis(2,1,3-benzothiadiazole) **2** crystallize in the $P2_1/a$ and the noncentrosymmetric $Fdd2$ space group, respectively. In the crystal structures of **1**, a large number of short S...N and I...I contacts, and a planar I_4 square cluster are observed, as shown in Figure 1. The angle between the planes for the two 2,1,3-benzothiadiazole rings of **2** is $48.4(1)^\circ$, and short and linear N...I contacts [$3.333(8)$ Å] exist in the crystal of **2**.

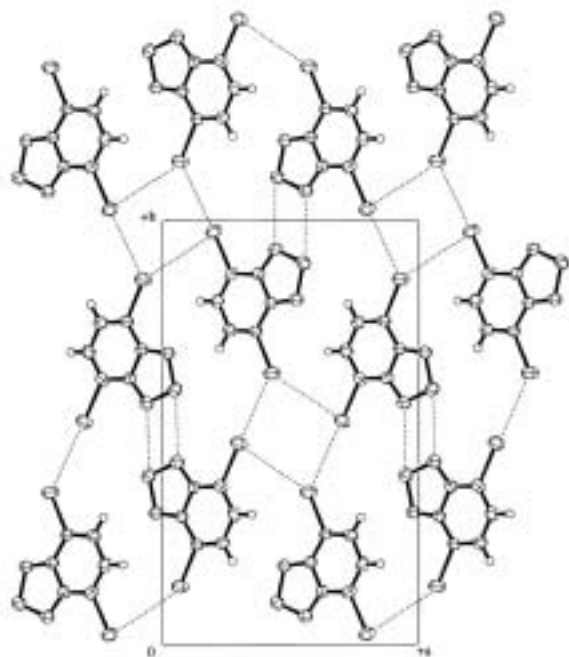


Figure 1. Packing diagram of **1** viewed along the c axis. Dotted lines show the short S...N and I...I contacts.

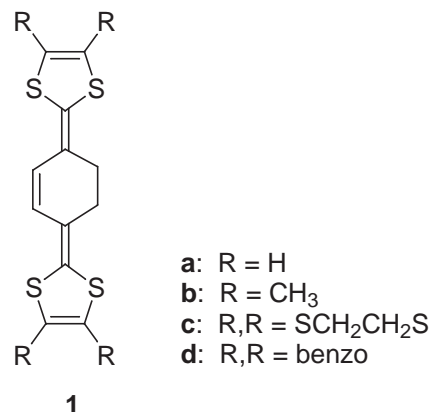
VIII-G-5 Synthesis and Properties of π -Extended TTF Analogues and Their Cation Radical and Dication Salts

YAMASHITA, Yoshiro¹; TOMURA, Masaaki; URUICHI, Mikio; YAKUSHI, Kyuya
(¹IMS and Tokyo Inst. Tech.)

[*Mol. Cryst. Liq. Cryst.* **376**, 19 (2002)]

New bis(1,3-dithole) electron donor **1** containing a cyclohexene unit were prepared using a Wittig-Honer reaction and a cycloreversion reaction. The tetramethyl

derivative afforded the highly conductive cation radical salts as single crystal whose unusual crystal structures were revealed by X-ray crystallographic analysis.



VIII-G-6 Synthesis and Structure of Bi- and Terthiophene Derivatives Having 4-Pyridylethynyl Substituents

TOMURA, Masaaki; YAMASHITA, Yoshiro¹
(¹IMS and Tokyo Inst. Tech.)

Conjugated organic oligomers are gaining increasing attention as new and promising materials in the field of molecular electronics. We have synthesized the title compounds, which are able to coordinate with metals and perform intermolecular interaction *via* hydrogen bonding, using the Sonogashira reaction. The X-ray crystallographic analyses of them revealed that the centrosymmetric bithiophene derivative has the *anti* conformation, whereas the crystallographically independent terthiophene derivative has *anti-cis* conformation. All thiophene and pyridine rings in the two derivatives are almost coplanar.

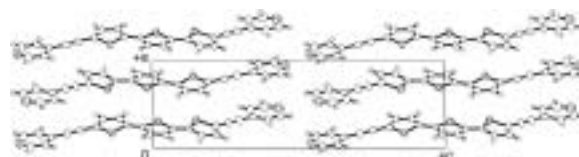


Figure 1. Molecular packing of 5,5''-bis[(4-pyridyl)ethynyl]-2,2':5',2''-terthiophene viewed along the b axis.

VIII-H Designing Artificial Photosynthesis at Molecular Dimensions

Photosynthesis is one of the finest piece of molecular machinery that Nature has ever created. Its ultrafast electron transfer and following well-organized sequence of chemical transformation have been, and will continue to be, challenging goals for molecular scientists. We are trying to mimic the function of photosynthesis by assembling molecular units that perform individual physical/chemical action. The molecular units include porphyrins, redox active organic molecules, and transition metal complexes. Our ultimate goal is to design artificial molecular systems that effect multiple chemical reactions triggered by light on the basis of molecular rationale.

VIII-H-1 Photoinduced Oxidation of Alcohols Catalyzed by Porphyrins and TEMPO

ITO, Hajime; NAGATA, Toshi

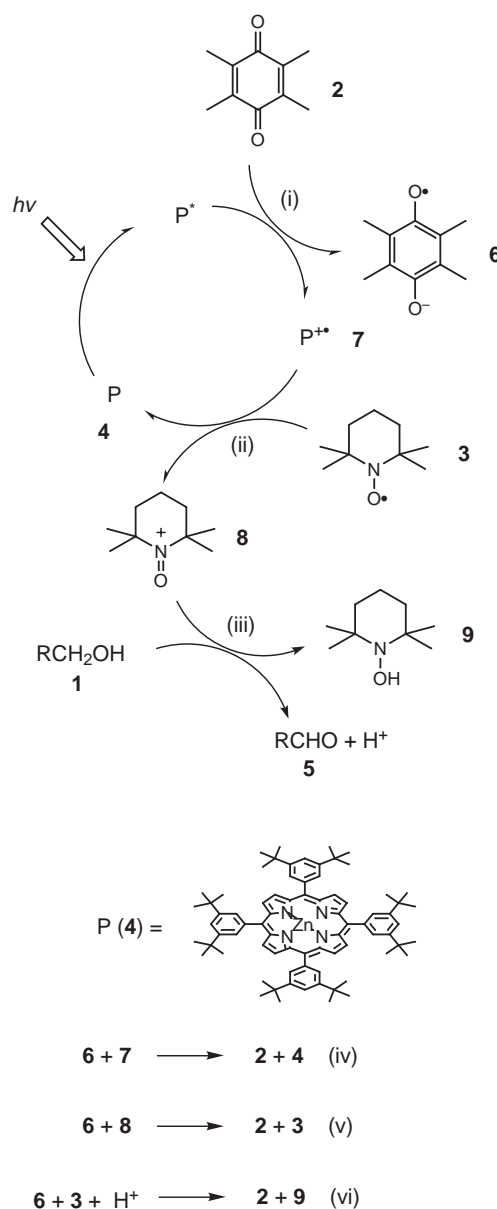
Photoinduced electron transfers involving porphyrins are widely studied, but utilizing the high-energy radical ion pairs for driving chemical reactions remains to be a great challenge. Herein we report the TEMPO-mediated oxidation of alcohols catalyzed by porphyrins under irradiation with visible light. Although there have been many reports on TEMPO-mediated oxidation of alcohols, our system is the first to utilize photoinduced electron transfer including porphyrins.

When a solution of benzyl alcohol (**1**, 0.1 mmol), duroquinone (**2**, 0.1 mmol), TEMPO (**3**, 2,2,6,6-tetramethylpiperidine N-oxide, 0.1 mmol), diisopropylethylamine (0.2 mmol) and 5,10,15,20-tetrakis(3,5-*di-t*-butylphenyl)porphinatozinc(II) (**4**, 0.001 mmol) in THF/DMF (1/1, 0.5 ml) was irradiated with visible light ($\lambda > 500$ nm, halogen lamp with a Toshiba Y-52 filter) for 10 hours, benzaldehyde (**5**) was formed in 23% yield. On addition of tetrabutylammonium perchlorate (0.1 mmol), the yield was improved to 42%. When either TEMPO, duroquinone, diisopropylethylamine or porphyrin was omitted, or in the absence of light, no benzaldehyde was detected.

As the reaction proceeded, 2,2,6,6-tetramethyl-N-hydroxypiperidine (TEMPO-H, **9**) was detected together with benzaldehyde, indicating that the oxidant was TEMPO rather than duroquinone. It is noteworthy, however, that in the absence of duroquinone the reaction did not proceed. The role of duroquinone is rationally understood by assuming photoinduced electron transfer from the porphyrin to the quinone. The tentative reaction mechanism is shown in Scheme 1; (i) the photoexcited porphyrin transfers an electron to the quinone, (ii) the cation radical of the porphyrin (**7**) oxidizes TEMPO to give the oxoammonium intermediate (**8**), (iii) the oxoammonium cation oxidizes the alcohol (**1**) with the aid of the base. The quinone anion radical (**6**) should be oxidized to regenerate the quinone either (iv) by the porphyrin cation radical, (v) by the oxoammonium cation, or (vi) by TEMPO. As the paths (iv) and (v) are non-productive, they result in the lower efficiency. Indeed, the reaction was too slow to be synthetically useful, so that we looked into the way to improve the reaction efficiency.

A moderate success was achieved by changing the electron acceptor. When 2,6-*di-t*-butyl-1,4-benzoquinone was used in place of duroquinone, benzalde-

hyde was obtained in 86% yield by use of 0.2 equivalents of TEMPO instead of the stoichiometric amount (solvent = base = pyridine, 27 hours irradiation). In this system, 2,5-*di-t*-butyl-1,4-hydroquinone accumulated instead of TEMPO-H. We assume that direct oxidation of the quinone anion radical was suppressed by the introduction of the bulky *t*-butyl groups.



VIII-I Development of New Metal Complexes as Redox Catalysts

Redox catalysis is an important field of chemistry which translates a flow of electron into chemical transformation. It is also one of the requisites for artificial photosynthesis. This project of ours aims at developing new metal complexes that perform redox catalysis at low overpotential. We have been focusing our attention to developing terdentate ligands with strong donor character, and have found that introducing a pyrrole ligand in place of pyridine leads to useful ligands.

VIII-I-1 Syntheses of a 6-(2-Pyrrolyl)-2,2'-Bipyridine Derivative and Its Ruthenium Complex

NAGATA, Toshi; TANAKA, Koji

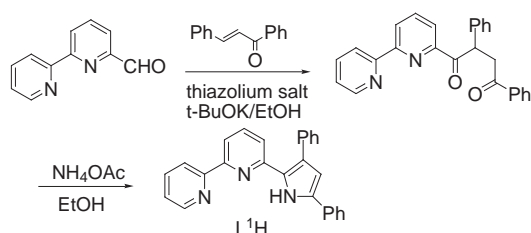
[*Bull. Chem. Soc. Jpn.* in press.]

Metal complexes of pyrroles are gathering interest as an activator of the pyrrole ring, an intermediate for synthesizing pyrrole derivatives, and as a component of conducting polymers. Herein we report the syntheses of 6-(3,5-diphenyl-2-pyrrolyl)-2,2'-bipyridine (L^1H) and its ruthenium complex $[Ru(L^1)_2]$. The compound L^1H is the first example of the "ter-aryl" ligand that has one pyrrole and two pyridine rings in this order, and it will be a useful substitute for 2,2':6',2''-terpyridine (terpy) when more electron-donating character is desirable.

The synthesis of L^1H is shown in Scheme 1. The Stetter condensation of 2,2'-bipyridine-6-carbaldehyde with chalcone was utilized, followed by ring closure of the 1,4-diketone with an ammonium salt (67% yield). By use of pyridine-2,6-dicarbaldehyde as a starting material, the compound L^2H_2 , 2,6-bis(3,5-diphenyl-2-pyrrolyl)pyridine, was also obtained (69% yield).

The ORTEP drawing of the complex $[Ru(L^1)_2]$ is shown in Figure 1. The coordination geometry around the Ru(II) center is similar to that of $[Ru(terpy)_2]X_2$, however the six pyridine/pyrrole rings are not exactly coplanar.

The cyclic voltammograms of $[Ru(L^1)_2]$ and $[Ru(terpy)_2](ClO_4)_2$ are shown in Figure 2. The Ru(III)/Ru(II) couple appeared at -0.29 V (*versus* ferrocene/ferrocenium couple) in $[Ru(L^1)_2]$, which was 1.10 V more negative than in $[Ru(terpy)_2](ClO_4)_2$, consistent with the strong donor character of the L^1 ligand. The first reduction wave (reduction of the ligand) was also negatively shifted by 0.51 V. At higher potential range ($+0.5$ – 0.7 V), $[Ru(L^1)_2]$ showed irreversible waves suggesting the oxidative degradation of the complex. Apparently the oxidation of the pyrrole rings led to the degradation of the ligand and/or the decomplexation of the metal ion.



Scheme 1. Synthesis of the ligand L^1H .

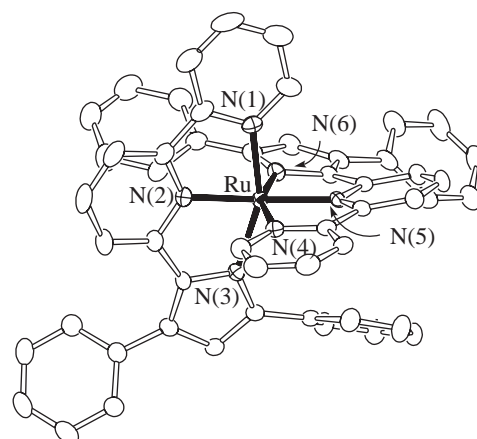


Figure 1. ORTEP view (50% probability ellipsoids) of the complex $[Ru(L^1)_2]$.

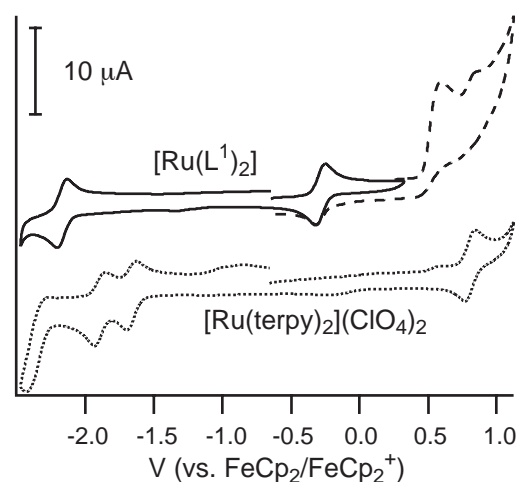


Figure 2. The cyclic voltammograms of $[Ru(L^1)_2]$ and $[Ru(terpy)_2](ClO_4)_2$.

VIII-J Electronic Properties of Monolayer-Protected Metal Clusters

Monolayer-protected metal clusters or nanoparticles have received much attention recently because their electronic and optical properties can be tuned by their sizes and shapes. The novel electronic properties of the clusters as well as their tunability are important from the viewpoint of future application as optoelectronic nanodevices. Our interests are focused on the following topics on the thiol-derivatized metal clusters and nanoparticles: (1) preparation and characterization of small clusters with core diameters of ~ 1 nm range (~ 40 atoms/cluster) which may exhibit molecular-like electronic and charging properties, (2) determination of structural dimensions (core diameters and monolayer thickness) of metal nanoparticles, and (3) development of size-selection method for the clusters and nanoparticles. Our goal is to reveal the evolution of electronic structures of the metal clusters as a function of the cluster size.

VIII-J-1 Development of Mass Spectrometer for Clusters

NEGISHI, Yuichi; TSUKUDA, Tatsuya

Mass spectrometry provides detailed informations on the chemical compositions of the metal clusters. We have constructed a time-of-flight (TOF) mass spectrometer which accommodates three types of ion sources: (1) a matrix-associated laser desorption ionization (MALDI) source for clusters obtained as solid, (2) an electrospray ionization source for clusters dispersed in aqueous phase, and (3) an electron-impact ionization source for molecular clusters. Only a brief description on the MALDI/TOF apparatus, which has been developed recently, is presented here. The specimens for mass analysis are prepared by depositing an aliquot (~ 1–5 μL) of the mix solutions of cluster samples and matrix onto a surface of a target made of stainless steel. After the solvent is evaporated at ambient atmosphere, the target is fed into the mass spectrometer through a load-lock chamber and attached to one of acceleration grids. The sample is irradiated with the third harmonic (355 nm) of a Nd:YAG laser operated at 10 Hz. The laser fluence is adjusted typically in the range of 10–40 $\mu\text{J}/\text{mm}^2/\text{pulse}$. The cluster ions thus formed are accelerated by applying a pulsed high voltage (15–20 kV) to the electrode plates. The ion beams are focused and stirred by ion optics and then detected by a MCP detector located at the end of the flight path of 1.17 m. Mass spectra of the ions of either polarity can be recorded by simply changing the polarities of the power supplies.

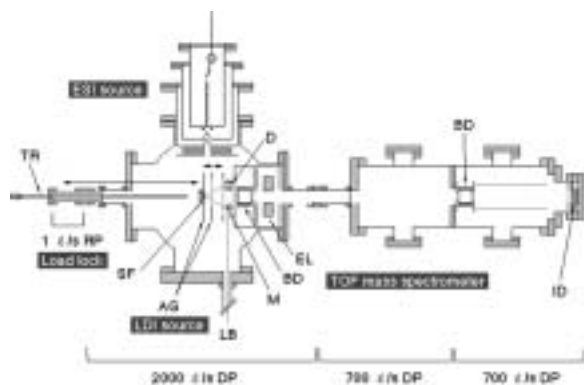


Figure 1. Schematic diagram of the apparatus: TR: transfer rod, SF: sample folder, AG: acceleration grid, LB: laser beam, M: mirror, D: damper, BD, beam deflectors, EL: einzel lens, ID: ion detector. Details of the ESI source are not described here. The EI source installed perpendicularly to the diagram is not shown.

VIII-J-2 Formation of $\text{Pd}_n(\text{SR})_m$ Clusters ($n < 60$) in the Reactions of PdCl_2 and RSH ($\text{R} = n\text{-C}_{18}\text{H}_{37}$, $n\text{-C}_{12}\text{H}_{25}$)

NEGISHI, Yuichi; MURAYAMA, Haruno; TSUKUDA, Tatsuya

[*Chem. Phys. Lett.* **366**, 561 (2002)]

Mass spectroscopic analysis revealed that Pd clusters passivated by thiolates as well as the stoichiometric thiolate complexes $\text{Pd}_n(\text{SR})_{2n}$ ($n = 5, 6$) are formed in the reactions between palladium chloride and n -alkane-thiols (RSH: $\text{R} = n\text{-C}_{18}\text{H}_{37}$, $n\text{-C}_{12}\text{H}_{25}$) in toluene. The Pd clusters thus formed are formulated as $\text{Pd}_n(\text{SR})_m$ with $m \sim 0.6n$ and the cluster size are distributed in the range of $5 \leq n \leq 60$, being consistent with core diameters of ~ 1 nm determined by TEM observations. A gap of ~ 2 eV was observed in the optical transition of the $\text{Pd}_n(\text{SR})_m$ clusters showing the emergence of non-metallic properties as a result of the size reduction.

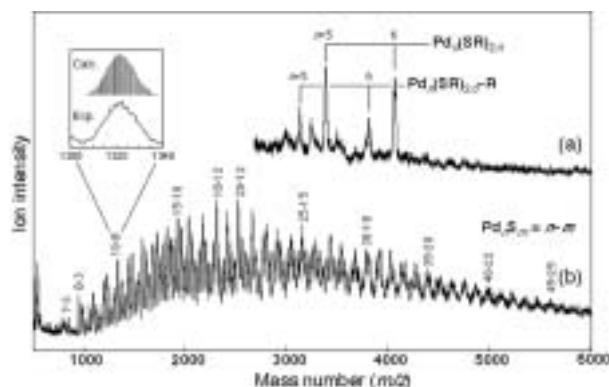


Figure 1. Typical representations of MALDI mass spectra of the mixtures of $\text{PdCl}_2/n\text{-C}_{18}\text{H}_{37}\text{SH}$ which are diluted with anthracene to (a) ~ 1 and (b) ~ 20 mol%.

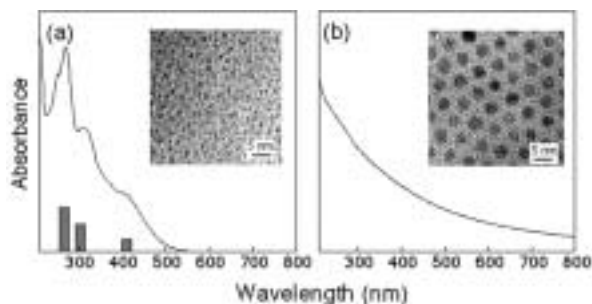


Figure 2. Optical spectra of hexane solutions of (a) PdCl₂/*n*-C₁₈H₃₇SH mixture and (b) Pd:SC₁₈H₃₇ nanoparticles. The solid bars in panel (a) represent the absorbance of the Pd_{*n*}(SC₁₈H₃₇)_{2*n*} complexes (*n* = 5 and 6).

VIII-J-3 Size-Selective Preparation of Water-Soluble Gold Clusters

NEGISHI, Yuichi; TSUKUDA, Tatsuya

Colloidal solution of gold clusters was formed upon mixing AuCl or AuCl₄⁻ and *meso*-dimercaptosuccinic acid (DMSA: HO₂CCH(SH)CH(SH)CO₂H) in water. The size distributions of the gold clusters can be controlled by simply changing the mixing ratios of the gold salts and DMSA as revealed by optical spectroscopy and TEM observations. Figure 1 shows the uv-vis spectra of the colloidal solutions prepared with different mixing ratios between AuCl and DMSA. With increase in the ratios of DMSA, the surface plasmon band at ~530 nm disappears and the onset of the optical transition shifts toward shorter wavelength, implying the reduction of the cluster sizes. The TEM measurements confirm this trend: the average sizes of the Au cores are 3.1 ± 0.7 and 1.8 ± 0.6 for the mixing ratios [DMSA]/[AuCl] of 1 and 2, respectively (Figure 2). These findings indicate the DMSA molecules act both as reducing agents against the Au(I) or Au(III) ions and stabilizing ligands for the resulting Au(0) clusters. Optimization of preparation conditions as well as purification of the clusters by polyacrylamide gel electrophoresis (PAGE) and gel permeation chromatography (GPC) is now under way in our laboratory.

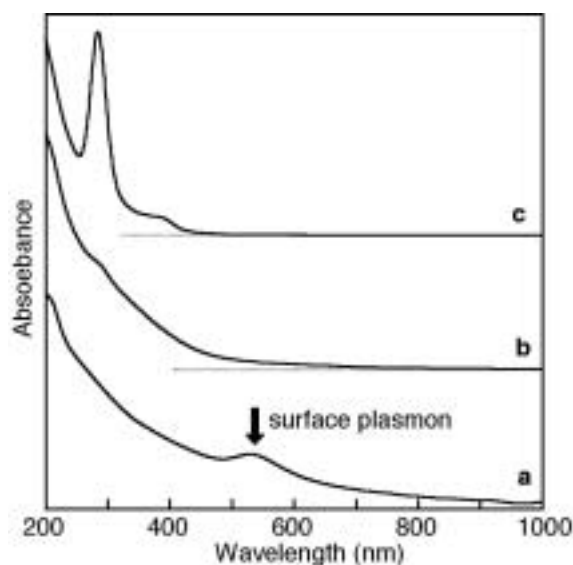


Figure 1. Optical spectra of colloidal solutions of gold clusters prepared with the mixing ratios [DMSA]/[AuCl] of (a) 0.1, (b) 0.2, and (c) 0.4.

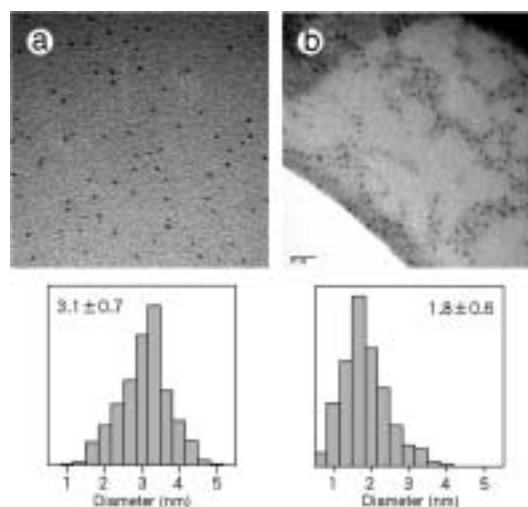


Figure 2. TEM images and size distributions of gold clusters obtained with the mixing ratios [DMSA]/[AuCl] of (a) 1 and (b) 2.

VIII-J-4 Characterization and Purification of Pd:SR Nanoparticles by Gel Permeation Chromatography

MURAYAMA, Haruno; TSUKUDA, Tatsuya

Gel permeation chromatography (GPC) and transmission electron microscopy (TEM) have been used to characterize the structures of Pd:SR (R = *n*-C₁₈H₃₇, C₁₆H₃₃, C₁₄H₂₉, C₁₂H₂₅, C₁₀H₂₁, C₆H₁₃) nanoparticles. The Pd:SR nanoparticles are prepared by ligand exchange of PVP-protected Pd nanoparticles.¹⁾ The difference between the average diameter (*D_c*) measured by TEM and hydrodynamic diameter (*D_h*) determined by GPC allows us to determine the thickness (*T*) of the monolayer of alkanethiolates. On the basis of these results together with the length of free alkanethiols, a structural model of the monolayers on the Pd clusters has been proposed. It is also demonstrated that the Pd:SR clusters which are size selected by GPC show pronounced tendency to self-assemble into two-dimensional superlattices (Figure 1). Further purification of the clusters by the GPC in a recycled mode is now in progress in our group.

Reference

- 1) T. Tsukuda, N. Kimura, T. Sasaki and T. Nagata, *Trans. Matr. Res. Soc. Jpn.* **25**, 929 (2000).

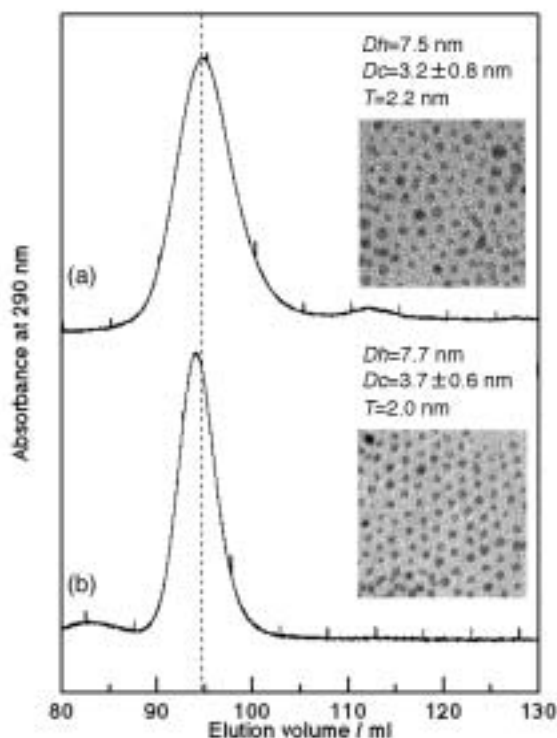


Figure 1. Chromatograms and TEM images for (a) as-prepared and (b) purified Pd:SR nanoparticles.

VIII-K Structures and Dynamics of Molecular Cluster Ions

Molecular clusters, intermediate states of matter between bulk and a molecule, provide us unique opportunities to study how the chemical and physical properties evolve with a degree of aggregation. We studied photo-induced reactions within size-selected cluster anions and evolutions of crystal structures of clusters.

VIII-K-1 Structural Evolution of Large $(\text{CO}_2)_n^-$ Clusters as Studied by Mass Spectrometry

NEGISHI, Yuichi; NAGATA, Takashi¹; TSUKUDA, Tatsuya
(¹Univ. Tokyo)

[*Chem. Phys. Lett.* **364**, 127 (2002)]

The mass distributions of $(\text{CO}_2)_n^-$ produced by electron-impact ionization of a free jet have been measured up to $n \sim 10^3$. Several intensity anomalies observed in a small size range are ascribed to the stabilities of the negative ions. In contrast, a series of humps are clearly discernible in the range of $n \geq 100$, which reflects the abundance of neutral $(\text{CO}_2)_n$. The intensity oscillations are analyzed in the context of “geometrical shell closings.” The analysis reveals that the $(\text{CO}_2)_n$ clusters with $n > \sim 80$ have truncated forms of an *fcc* crystal, most likely a cuboctahedral motif (Figure 1).

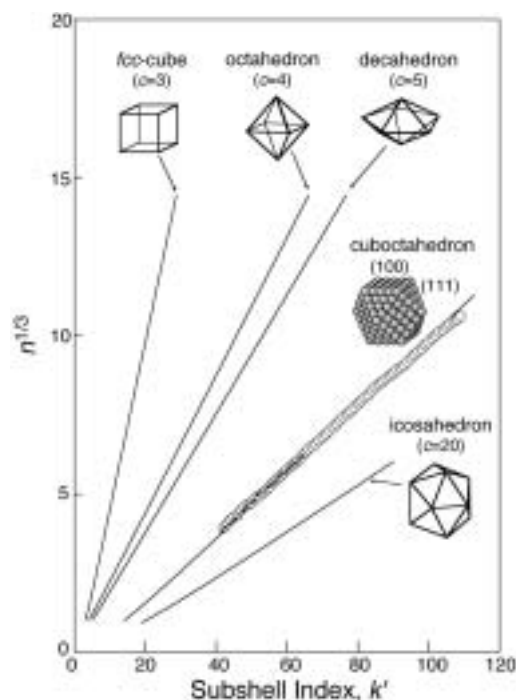


Figure 1. Plots of $n^{1/3}$ against the subshell index k' for various polyhedra. Symbols \circ and \bullet represent the experimental data for $(\text{CO}_2)_n^-$ and $(\text{CO}_2)_n^+$, respectively. Both plots are explicable in terms of cuboctahedra (CO). The spheres in the CO motif represent the CO_2 constituent molecules.

VIII-K-2 Photochemistry of $(\text{NO})_n^-$ as Studied by Photofragment Mass Spectrometry

TSUKUDA, Tatsuya; ZHU, Lei¹; SAEKI, Morihisa; NAGATA, Takashi²

(¹Data Storage Inst.; ²Univ. Tokyo)

[*Int. J. Mass Specrom.* **220**, 137 (2002)]

Photofragmentation of $(\text{NO})_n^-$ ($3 \leq n \leq 21$) in the energy range 2.7–3.6 eV (350–460 nm) results in the production of $(\text{NO})_m^-$ with $m \geq 2$ and $\text{NO}_2^-(\text{NO})_m$ with $0 \leq m \leq 2$. The photofragment yield spectra obtained for $n = 3-7$ display a broad and structureless band profile with successive blue-shift with increase in the cluster size, indicating that N_3O_3^- (reference 1) behaves as a chromophoric core in the larger $(\text{NO})_n^-$. The observed fragmentation patterns suggest that photoexcitation of the N_3O_3^- chromophore is followed by direct dissociation into $(\text{NO})_2^-$, solvent evaporation to form $(\text{NO})_m^-$, and/or intracluster reactions to produce NO_2^- .

Reference

- 1) T. Tsukuda, M. Saeki, L. Zhu and T. Nagata, *Chem. Phys. Lett.* **295**, 416 (1998).

VIII-L Rotational Echo Double Resonance (REDOR) Experiments with Overtone Adiabatic Inversion Pulses

The effect of an overtone adiabatic inversion pulse on solid-state ^{14}N spins was investigated.

VIII-L-1 The Observation of REDOR Phenomena for Solid-State ^{13}C - ^{14}N Spin Systems with the Help of Overtone Adiabatic Inversion Pulses

KUWAHARA, Daisuke

We applied overtone adiabatic inversion pulses to ^{13}C - ^{14}N spin systems in powdered *L*-alanine undergoing MAS in order to observe REDOR phenomena. The damping of ^{13}C resonance line intensities was compared with that corresponding to the REDOR experiments with normal RF pulses having a constant frequency. We tried to establish the theoretical treatment for the REDOR experiments with adiabatic inversion pulses. The computer simulations for the REDOR experiments revealed that overtone adiabatic pulses had little dependence on the offsets of rf carrier frequencies.

VIII-M Nanoscale Characterization of Heterogeneous Catalyst Surfaces

Heterogeneous catalysis occurs on a surface of a solid catalyst. Active centers for heterogeneous catalysis commonly consist of clusters of several surface atoms, and thus a long-range order of surface atoms is not normally required. Therefore, when using precious metals as catalysts, nanometer-scale superfine particles are commonly employed in order to increase its surface area and to decrease the amount of catalysts. This introduces difficulties in characterizing the catalyst surfaces and their active centers, because characterization techniques of solid surfaces at nanometer-scale are not well established. Here we mainly used scanning probe microscopes, in conjunction with other surface characterization techniques, to characterize catalytically active centers as well as the nature of catalyst-support interactions.

VIII-M-1 Determination of Extra-Framework Cation Positions and Their Occupancies on Heulandite(010) by Atomic Force Microscopy

KOMIYAMA, Masaharu; GU, Minming¹; WU, Hai-Ming²
(¹McGill Univ.; ²Res. Inst. Innovative Tech. Earth)

[*J. Phys. Chem. B* **105**, 4680 (2001)]

Atomic images of a cleaved heulandite(010) surface were obtained under an aqueous condition by atomic force microscopy (AFM). In addition to the framework oxygen atoms on the (010) plane, extra-framework cations on the surface were also imaged. An AFM imaging simulation was performed using published X-ray diffraction data to assist the assignment of the AFM-observed framework and extra-framework atoms. By comparing it with the observed AFM images, local variations of position and occupancy of individual cations were determined.

VIII-M-2 Molecular Orbital Interpretation of Thymine/Graphite NC-AFM Images

KOMIYAMA, Masaharu; UCHIHASHI, Takayuki¹; SUGAWARA, Yasuhiro^{1,2}; MORITA, Seizo²
(¹Joint Res. Center Atom Tech.; ²Osaka Univ.)

[*Surf. Interface Anal.* **29**, 53 (2001)]

Recent non-contact atomic force microscopy (nc-AFM) images of a deoxyribonucleic acid (DNA) base thymine (2,4-dioxy-5-methylpyrimidine), vacuum-deposited on a highly-oriented pyrolytic graphite (HOPG) surface, are interpreted by means of theoretical adsorption simulations, and the molecular geometry and the energetics of the adsorption system are estimated. The lowest-energy dimer configuration was found to be the one in which the respective hydrogen on number 1 nitrogen and oxygen on number 6 carbon of two thymine molecules make a hydrogen bond to each other. A surface unit cell structure was reproduced. Adsorption energy for the thymine pair on HOPG is rather small, amounting to only *ca.* 1 kcal/mol, with small variations depending on the molecular orientation with respect to the substrate surface. A possibility of having a mirrored adsorption configuration in adjacent domains is also suggested.

VIII-M-3 Partial Reduction of Si(IV) in SiO₂ Thin Film by Deposited Metal Particles—An XPS Study

KOMIYAMA, Masaharu; SHIMAGUCHI, Takemi¹
(¹Yamanashi Univ.)

[*Surf. Interface Anal.* **29**, 189 (2001)]

Metal-support interactions in the systems of dispersed metals supported on thin film silica surfaces were examined by X-ray photoelectron spectroscopy. Four metal-silica systems, Pt-, Pd-, Ag- and Au-SiO₂, all indicated the formation of partially reduced Si(IV) species by the metal deposition. The extent of the reduction varied little with the kind and the amount of deposited metal species. On the other hand, the amount of this newly formed Si(IV- δ) indicated a strong metal species dependence.

VIII-M-4 Apparent Local Structural Change Caused by Ultraviolet Light on a TiO₂ Surface Observed by Scanning Tunneling Microscopy

KOMIYAMA, Masaharu; YIN, Donghong¹
(¹Hunan Normal Univ.)

[*Jpn. J. Appl. Phys.* **40**, 4281 (2001)]

An apparent local surface structural change at nanoscale was observed by scanning tunneling microscopy on a TiO₂ surface upon irradiation with ultraviolet (UV) light. This phenomenon was reversible with UV light irradiation, and was interpreted to be due to the local accumulation of photoexcited states. This is the first real-space observation of inhomogeneous local charge distribution under UV light irradiation at nanoscale on a semiconductive photocatalyst surface, which may help identify the photocatalytic active sites and elucidate their reaction mechanisms.

VIII-M-5 Various Phases on Natural Stilbite (010) Surface Observed by Atomic Force Microscopy under Aqueous Conditions

GU, Ning¹; KOMIYAMA, Masaharu
(¹Southeast Univ.)

[*Jpn. J. Appl. Phys.* **40**, 4285 (2001)]

Various phases on a natural stilbite (010) surface were observed by atomic force microscopy (AFM) under aqueous conditions. In a wide-area observation, oriented protrusions observed on the surface differed from the “sheaflike” structure which has been found in stilbite in an aqueous NaOH solution. Narrow-area observations showed surfaces consisting of an island structure, or a structure of alternating ridges and trenches. The latter is similar to the one reported previously under ambient conditions. The atomically resolved AFM image of the stilbite confirms that its surface is in good agreement with the known crystallographic parameters of the bulk-terminated (010) surface. Defects such as dislocations and grain boundaries at the atomic level were also observed.

VIII-N Studies of Electronic Structure of Organic Thin Films and Organic/Inorganic Interfaces by Electron Spectroscopies

Electronic structures of organic film surface and organic/inorganic interface are expected to play an important role in organic-device properties. We investigated surface structures and energy alignments to clarify their electronic structures using surface sensitive spectroscopy such as photoelectron spectroscopy combined with synchrotron radiation and metastable atom electron spectroscopy.

VIII-N-1 Low Energy Electron Diffraction of the System In-[perylene-3,4,9,10-tetracarboxylic Dianhydride] on MoS₂

AZUMA, Yasushi¹; IWASAKI, Kazuaki²;
KURIHARA, Tsutomu²; OKUDAIRA K., Koji;
HARADA, Yoshiya³; UENO, Nobuo¹
(¹IMS and Chiba Univ.; ²Chiba Univ.; ³Seitoku Univ.)

[*J. Appl. Phys.* **91**, 5024 (2002)]

The system In-perylene-3,4,9,10-tetracarboxylic dianhydride ~PTCDA on MoS₂, prepared by the sequential evaporation of PTCDA and In on a cleaved MoS₂ surface, was studied by low energy electron diffraction. The result indicates that reaction products form an ordered structure on the MoS₂ surface. From the analysis of the diffraction pattern, the presence of six symmetry-equivalent domains of an oblique unit cell of In-PTCDA species results with the dimensions of 9.5 Å, 16.3 Å, and an enclosed angle of 80.2°. In addition, splitting in two domains by a mirror plane exists with the rotation angle $R5610.8^\circ$ with respect to each of the three equivalent surface crystal axes of the MoS₂ substrate. The new structure is explained by assuming that four In atoms are chemically bonded to the four carbonyl groups of the PTCDA molecules. Furthermore, it is concluded that the In₄PTCDA species become tilted after a chemical reaction between the PTCDA molecules and the In atoms, which is in agreement with results previously obtained by angle-resolved ultraviolet photoemission experiments.

VIII-N-2 Electronic Structure and Molecular Orientation at Thin Film Surfaces of Pendant-Group Polymers Studied by Outermost Surface Spectroscopy Using Metastable Atoms

OKUDAIRA K., Koji; KERA, Satoshi²;
SETOYAMA, Hiroyuki²; MORIKAWA, Eiji³;
UENO, Nobuo¹
(¹IMS and Chiba Univ.; ²Chiba Univ.; ³Louisiana State Univ.)

[*J. Electron Spectrosc. Relat. Phenom.* **121**, 225(2001)]

Metastable-atom electron spectroscopy (MAES) and ultraviolet photoelectron spectroscopy (UPS) were used to study the outermost surface of thin films of pendant group polymers: polystyrene (PSt), poly(2-vinylnaphthalene), and poly(9-vinylcarbazole). MAES is selectively sensitive to the outermost surface, and indicated that the surfaces of the polymer films were very clean,

even though they were prepared by spin-casting in a room atmosphere. In Figure 1 observed MAES and UPS of PSt are shown. By comparison with gas-phase spectra and molecular orbital calculations of model molecules with pendant groups, it was confirmed that the principal constituent at the outermost surface of these polymer films is the pendant groups. Furthermore, it was observed that the intensity for σ (C–H) states of the pendant group is stronger in MAES spectra than in UPS spectra, indicating many pendant groups are inclined at large tilt angles.

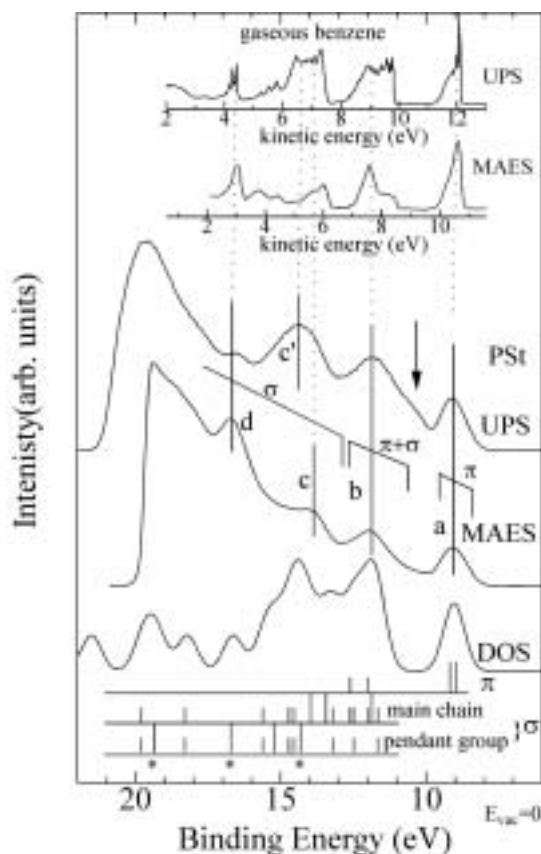


Figure 1. MAES and UPS of polystyrene (PSt) thin film. The vertical bars show the molecular orbital energies calculated by *ab initio* MO calculation (6-31G with diffuse function) for the model compound of PSt. The energy levels for the molecular orbital consisted of π orbital at pendant group and σ orbital at polymer chain are represented by the vertical bars marked by asterisk(*). The density of states (DOS) was obtained by broadening with gaussian function (width = 0.8 eV). The calculated binding energy scale was contracted by 1.35 and shifted to fit with the experimental results. The inset shows the MAES and UPS of gaseous benzene.

VIII-N-3 Photodegradation of Poly(tetrafluoroethylene) and Poly(vinylidene fluoride) Thin Films by Inner Shell Excitation

OKUDAIRA K., Koji; YAMANE, Hiroyuki²; ITO, Kazuhiko²; IMAMURA, Motoyasu³; HASEGAWA, Shinji; UENO, Nobuo¹
(¹IMS and Chiba Univ.; ²Chiba Univ.; ³AIST)

[*Surf. Rev. Lett.* **9**, 335 (2002)]

Ion time-of-flight (TOF) mass spectra of poly(tetrafluoroethylene) (PTFE) and poly(vinylidene fluoride) (PVDF) thin films near fluorine and carbon *K*-edges were observed. For PTFE thin films peaks corresponding to F^+ , CF^+ , and CF_3^+ appeared, while for PVDF F^+ and H^+ were mainly observed. They indicate that for PTFE the polymer chain (C–C bonds) as well as C–F bonds are broken by irradiation of photons near fluorine and carbon *K*-edges, while for PVDF the bond scission occurs mainly at the C–F and C–H bond. Partial ion yields (PIY) of these ions for PTFE and PVDF thin films show strong photon energy dependencies near fluorine (Figure 1) and carbon *K*-edges. The excitation from fluorine $1s$ to $\sigma(C-F)^*$ is specially efficient for F^+ ion production for both PTFE and PVDF.

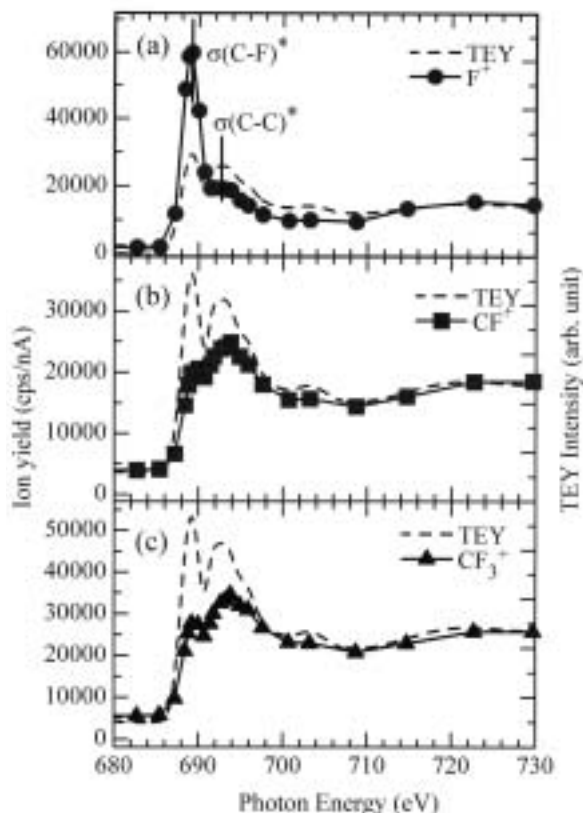


Figure 1. PIY spectra of (a) F^+ , (b) CF^+ and (c) CF_3^+ for PTFE thin film near the fluorine *K* absorption edge. TEY spectra (broken curve) are also shown for comparison. TEY spectra are renormalized at $h\nu = 682.5$ eV and at $h\nu = 730$ eV to fit PIY intensities.

VIII-N-4 Intramolecular Energy-Band Dispersion in Oriented Thin Film of n - $CF_3(CF_2)_{22}CF_3$ Observed by Angle-Resolved UV Photoemission and its Theoretical Simulation

YOSHIMURA, Daisuke¹; ISHII, Hisao²; MIYAMAE, Takayuki³; HASEGAWA, Shinji⁴; OKUDAIRA K., Koji⁵; UENO, Nobuo; SEKI, Kazuhiko¹
(¹Nagoya Univ.; ²Tohoku Univ.; ³AIST; ⁴Fuji Xerox; ⁵Chiba Univ.)

[*Surf. Rev. Lett.* **9**, 407 (2002)]

Poly(tetrafluoroethylene) (PTFE) $(CF_2)_n$ is one of the most fundamental polymers, which is the perfluorinated analogue of polyethylene $(CH_2)_n$ with a simple repeating CF_2 unit. For such a one-dimensional polymer, we can expect the formation of one-dimensional intramolecular energy-band relation along the chain direction, and the energy-band structures of PTFE have been studied theoretically. Unfortunately, however, there was no experimental result to be compared with such calculated energy-band structure. In this work, we performed angle-resolved UV photoemission spectroscopy (ARUPS) with synchrotron radiation for the oriented thin films of perfluorotetracosane (n - $CF_3(CF_2)_{22}CF_3$; PFT), which is one of the oligomer of PTFE. The sample of PFT with their long chain axis being perpendicular to the surface was prepared by in-situ vacuum evaporation. The normal-emission spectra of the PFT film show incident photon energy dependence due to the intramolecular energy-band dispersion. We also performed the theoretical simulation of the spectra by using independent-atomic-center (IAC) approximation combined with *ab initio* MO calculations. The simulations successfully reproduced the $h\nu$ -dependence of the observed ARUPS spectra. From the observed and simulated spectra, we deduced the value of inner potential V_0 , which is the parameter defining the energy origin of the free-electron-like final state, and derived reliable energy-band dispersion relation.

VIII-O Study on Compact X-Ray Sources

Electron storage rings are useful and practical devices as x-ray sources. However, these synchrotron radiation facilities which can provide intense x-rays usually occupy large area and we need many costs in order to construct and maintain the facilities. So that there have been many works to investigate compact x-ray sources. Laser undulator radiation and backward Compton scattering which are generated by interaction of electron beams from small accelerators with intense laser photons are candidates to produce hard x-rays.

X-ray sources must be shielded for radiation safety. For constructing effective shields, we need to know how many radiations are yielded from our x-ray sources. We will use high energy electrons to produce x-rays. These electrons cause radiations when they interact with beam ducts or beam dumps, so that it is useful to study radiations generated in synchrotron radiation facilities in order to estimate the yields of radiations from our x-ray sources.

VIII-O-1 Study on Radiation Shielding for Small Synchrotron Radiation Facilities

TAKASHIMA, Yoshifumi; KUWAYAMA, Shunsuke¹; KOBAYAKAWA, Hisashi¹
(¹Nagoya Univ.)

X-ray sources using high energy electrons usually generate radiations which should be shielded. In order to design effective shields, we need to estimate how many radiations are generated from a storage ring and penetrate radiation shields. Circulating electrons in a storage ring go out of their stable orbit when their energy exceeds the critical energy. These electrons are incident on the beam duct and generate electromagnetic showers around the beam duct.

We measured angular distribution of radiations around a beam duct of the storage ring of UVSOR. Figure 1 shows experimental set up. Two Photodiodes were set in tandem in a copper case and coincident signal from these two photodiodes were counted, so that we detected only charged particles. The area of the photodiodes were $7 \times 7 \text{ mm}^2$. We used 12 pairs of photodiodes installed at about 2 m upstream from the inflector. Figure 2 shows an angular distribution of the number of signal from the detectors. We notice that the stray radiations of charged particles counted at inside of the ring are more than that counted at outside, because most electrons which exceed their energy over the bucket height hit on the inside wall of the beam duct.

In order to estimate the amount of the stray radiations around compact x-ray sources, we should investigate the spatial distribution of stray radiations by comparing experimental results and theoretical calculations. We will propose a simple formula to calculate radiation dose around a small accelerator. In order to check the accuracy of the formula, we should measure the radiations at many points around UVSOR storage ring and compare the experimental results with our calculations.

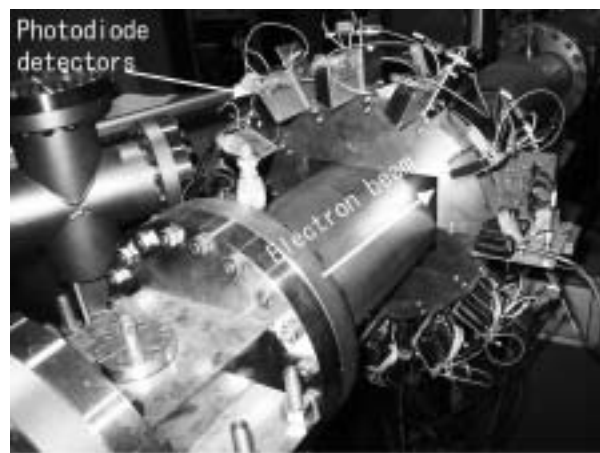


Figure 1. Experimental setup.

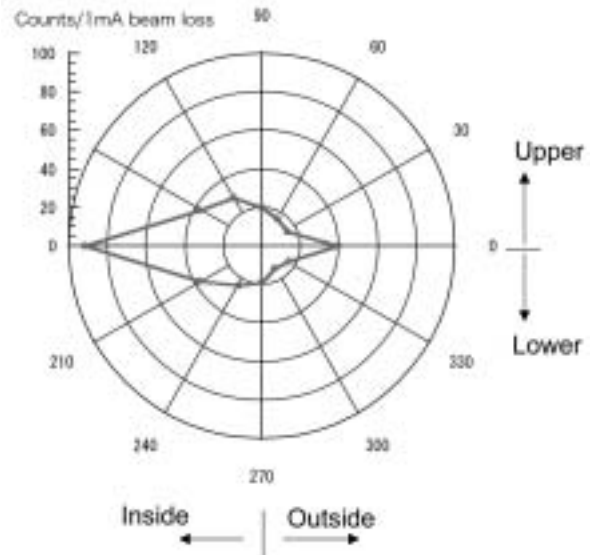


Figure 2. Angular distribution of charged particles around the beam duct of the storage ring of UVSOR.

VIII-P Syntheses of Fullerene-Based New Materials with Novel Physical Properties

Fullerene-based new materials are synthesized, and the structures and physical properties are studied in wide temperature and pressure regions. The structures and transport properties of pressure-induced superconducting fulleride, Cs_3C_{60} , are studied by X-ray powder diffraction, ESR, Raman, AC susceptibility and resistivity measurements, in order to clarify the mechanism of pressure-induced superconductivity. The structures and transport properties of metallofullerenes are also studied by X-ray diffraction and resistivity. The field-effect transistors (FET's) with thin-films of fullerenes are fabricated and their transport properties are studied in wide temperature region. STM studies on metallofullerenes adsorbed on Si(111)-(7×7) surface are performed under high vacuum condition.

VIII-P-1 Pressure and Temperature Dependences of the Structural Properties of Dy@C₈₂ Isomer I

TAKABAYASHI, Yasuhiro¹; KUBOZONO, Yoshihiro; KANBARA, Takayoshi¹; FUJIKI, Satoshi; SHIBATA, Kana²; HARUYAMA, Yusuke²; HOSOKAWA, Tomoko²; RIKIISHI, Yoshie²; KASHINO, Setuo²
(¹IMS and Okayama Univ.; ²Okayama Univ.)

[*Phys. Rev. B* **65**, 73405 (2002)]

Crystals of Dy@C₈₂ isomer I are studied by x-ray powder diffraction with synchrotron radiation in wide temperature and pressure regions. The isomer I of Dy@C₈₂ shows a simple cubic structure with lattice constant, a , of 15.85(3) Å at 298 K, while the isomer II shows a face-centered cubic structure with a of 15.75(4) Å. The structural phase transition of the second-order is indicated for the isomer I at 300–310 K by the temperature dependence of x-ray diffraction and differential scanning calorimetry. Further, the pressure dependence of the lattice constant is studied for the isomer I up to 60 kbar, which can be fitted by a Murnaghan equation of state.

VIII-P-2 Ferromagnetism and Giant Magnetoresistance in the Rare-Earth Fullerides Eu_{6-x}Sr_xC₆₀

ISHII, Kenji^{1,2}; FUJIWARA, Akihiko¹; SUEMATSU, Hiroyoshi¹; KUBOZONO, Yoshihiro
(¹Univ. Tokyo; ²JAERI)

[*Phys. Rev. B* **65**, 134431 (2002)]

We have studied crystal structure, magnetism, and electric transport properties of a europium fulleride Eu₆C₆₀ and its Sr-substituted compounds, Eu_{6-x}Sr_xC₆₀. They have a *bcc* structure, which is an isostructure of other $M_6\text{C}_{60}$ (M represents an alkali atom or an alkaline-earth atom). Magnetic measurements revealed that magnetic moment is ascribed to the divalent europium atom with $S = 7/2$ spin, and a ferromagnetic transition was observed at $T_c = 10$ –14 K. In Eu₆C₆₀, we also confirm the ferromagnetic transition by heat-capacity measurement. The striking feature in Eu_{6-x}Sr_xC₆₀ is very large negative magnetoresistance at low tempera-

ture; the resistivity ratio $\rho(H = 9 \text{ T})/\rho(H = 0 \text{ T})$ reaches almost 10^{-3} at 1 K in Eu₆C₆₀. Such large magnetoresistance is the manifestation of a strong π - f interaction between conduction carriers on C₆₀ and $4f$ electrons of Eu.

VIII-P-3 Bridging Fullerenes with Metals

CHI, Dam Hieu¹; IWASA, Yoshihiro^{1,2,3}; CHEN, X. H.⁴; TAKENOBU, Taishi²; ITO, Takayoshi¹; MITANI, Tadaoki¹; NISHIBORI, Eiji⁵; TAKATA, Masaki⁵; SAKATA, Makoto⁵; KUBOZONO, Yoshihiro
(¹JAIST; ²Tohoku Univ.; ³CREST; ⁴Univ. Sci. Tech. China; ⁵Nagoya Univ.)

[*Chem. Phys. Lett.* **359**, 177 (2002)]

The bonding nature between rare earth metals and fullerene molecules has been investigated. The electron density distribution for nominal Sm₃C₇₀, calculated by a maximum entropy method (MEM) based on the Rietveld analysis of synchrotron X-ray diffraction pattern, unambiguously demonstrated a covalent Sm...C bond, which is almost as strong as the interatomic bonding of crystal Si. Furthermore, the Sm bridges two C₇₀ molecules, producing a C₇₀...Sm...C₇₀ dimer structure.

VIII-P-4 Structure and Physical Properties of Cs_{3+α}C₆₀ (α = 0.0–1.0) under Ambient and High Pressures

FUJIKI, Satoshi; KUBOZONO, Yoshihiro; KOBAYASHI, Mototada²; KAMBE, Takashi¹; RIKIISHI, Yoshie¹; KASHINO, Setuo¹; ISHII, Kenji³; SUEMATSU, Hiroyoshi³; FUJIWARA, Akihiko⁴
(¹Okayama Univ.; ²Himeji Inst. Tech.; ³Univ. Tokyo; ⁴JAIST)

[*Phys. Rev. B* **65**, 235425 (2002)]

The intermediate phases, Cs_{3+α}C₆₀ (α = 0.0–1.0), have been prepared, and their structure and physical properties are studied by x-ray powder diffraction, Raman, ESR, electric conductivity and ac susceptibility measurements under ambient and high pressures. The x-ray powder diffraction pattern of Cs_{3+α}C₆₀ (α = 0.0–

1.0) can be indexed as a mixture of the body-centered-orthorhombic (*bco*) and cubic (A15) phases. The A15 phase diminishes above 30 kbar. The broad ESR peak due to conduction electron (*c*-ESR) is observed only for the phases around $\alpha = 0.0$ in $Cs_{3+\alpha}C_{60}$. The resistivity of the $Cs_{3+\alpha}C_{60}$ ($\alpha \neq 0$) sample follows the granular metal theory and/or Sheng model even in the sample exhibiting a broad ESR peak. No superconducting transition is observed up to 10.6 kbar in $Cs_{3+\alpha}C_{60}$ ($\alpha \neq 0$). These results present that *bco* phase of $Cs_{3+\alpha}C_{60}$ ($\alpha = 0$) is a final candidate for a pressure-induced superconductor.

VIII-P-5 Complex-Plane Impedance Study on a Hydrogen-Doped Copper Coordination Polymer: *N,N'*-bis-(2-hydroxy-ethyl)-Dithiooxamidato-Copper(II)

NAGAO, Yuki¹; IKEDA, Ryuichi¹; KANDA, Seiichi²; KUBOZONO, Yoshihiro; KITAGAWA, Hiroshi^{1,3,4}

(¹Univ. Tsukuba; ²Univ. Tokushima; ³JAIST; ⁴JST)

[*Mol. Cryst. Liq. Cryst.* **379**, 89 (2002)]

AC conductivity measurements with an impedance analyzer were carried out for a hydrogen-doped coordination polymer, *N,N'*-bis-(2-hydroxy-ethyl)-dithiooxamidato-copper(II), in order to estimate the protonic conductivity (σ_p). The $\log \sigma_p$ was linearly increased from 2.6×10^{-9} to 2.2×10^{-6} $S\text{cm}^{-1}$ with relative humidity (RH) from 45 to 100% at 300 K. A slight hysteresis of protonic conductivity was observed upon increasing and decreasing RH, which implies that H_3O^+ is generated by a reaction between water molecule and acid-base polymer near RH \sim 100%.

VIII-P-6 Crystal Structure and Electronic Transport of Dy@C₈₂

KUBOZONO, Yoshihiro; TAKABAYASHI, Yasuhiro¹; SHIBATA, Kana²; KANBARA, Takayoshi¹; FUJIKI, Satoshi; KASHINO, Setuo²; FUJIWARA, Akihiko³; EMURA, Shuichi⁴

(¹IMS and Okayama Univ.; ²Okayama Univ.; ³JAIST; ⁴Osaka Univ.)

[*Phys. Rev. B* submitted]

Crystal structure of Dy@C₈₂ isomer I at 298 K has been determined by Rietveld refinement for X-ray powder diffraction with synchrotron radiation. The isomer I shows a simple cubic structure (sc: $Pa\bar{3}$) with a lattice constant, *a*, of 15.78(1) Å. The C₂ axis of a C_{2v}-C₈₂ cage aligns along a [111] direction of this crystal lattice. The C₈₂ cage is orientationally disordered to satisfy a $\bar{3}$ symmetry along [111] which is requested in this space group. The large thermal parameter for the Dy atom estimated from the X-ray diffraction probably reflects a large disorder caused by a floating motion of the Dy atom inside the C₈₂ cage as well as a ratchet-type motion of the Dy@C₈₂ molecule. The electronic transport of thin film of Dy@C₈₂ shows a semi-conducting behavior. The energy gap, *E_g*, is estimated to

be 0.2 eV. Further, the variation of valence from Dy³⁺ to Dy²⁺ is found by metal-doping into the Dy@C₈₂ crystals.

VIII-P-7 N-Channel Field-Transistors with Thin Films of Fullerenes

KANBARA, Takayoshi²; FUJIKI, Satoshi²; SHIBATA, Kana¹; KUBOZONO, Yoshihiro¹; URISU, Tsuneo; SAKAI, Masahiro; FUJIWARA, Akihiko³

(¹Okayama Univ.; ²IMS and Okayama Univ.; ³JAIST)

[*Phys. Rev. B* submitted]

N-channel field effect transistors (FETs) are fabricated with thin films of C₆₀, C₇₀ and Dy@C₈₂, and an SiO₂ insulating layer. The transport properties of the C₆₀ and C₇₀ FET's are studied in a temperature region from 200 to 330 K. The typical FET properties are observed in C₆₀ and C₇₀ above 220 K. The hopping transport with activation energy of 0.3 eV is observed for the C₆₀ and C₇₀ FET's in this temperature region. Further, the condition of fabrication is studied in order to improve the FET property. The Dy@C₈₂ FET is first fabricated and its property is studied at 295 K.

VIII-P-8 STM Study of Dy@C₈₂ on Si(111)-(7×7) Surface

FUJIKI, Satoshi; KUBOZONO, Yoshihiro; KANBARA, Takayoshi¹; FUJIWARA, Akihiko²; HOSOKAWA, Tomoko¹; URISU, Tsuneo

(¹Okayama Univ.; ²JAIST)

[to be submitted]

Single-molecule image of Dy@C₈₂ on Si(111)-(7×7) surface is observed by STM. The Dy@C₈₂ molecules were deposited on the Si(111)-(7×7) surface under UHV chamber. The first layer of Dy@C₈₂ is disordered, and no second layer islands are found before the complete formation of the first layer of Dy@C₈₂. A single-molecule image of Dy@C₈₂ was clearly observed on the first layer. This image shows that the maximum height of the molecule is \sim 11.3 Å which corresponds to those of two long axes of Dy@C₈₂ inclusive of van der Waals radius of C atom. The STS of the multilayer of Dy@C₈₂ suggests a energy gap of 0.1 eV at 295 K, in consistent with that, 0.2 eV, determined by resistivity measurement for the Dy@C₈₂ thin film. This shows that the Dy@C₈₂ molecule is a small-gap semiconductor.

VIII-Q Effects of High Magnetic Field on Chemical Process

It is interesting to control chemical and physical process with the aid of magnetism which is one of the key properties of matter. This research group is studying the mechanisms of the interaction of matter and magnetic field in order to develop a new technique to control chemical and physical process by magnetic field. In the anodic oxidation reaction of potassium iodide, significant magnetic field effects (≤ 0.6 T) on the product yields are interpreted in terms of the Lorentz force on iodide ions. In the liquid/solid redox reaction of silver ion and copper metal, anomalous magnetic field effects (≤ 15 T) are chiefly explained by the magnetic force on generated copper ions. It is clarified that mass transportation in solution is remarkably affected by the magnetic field.

VIII-Q-1 Magnetic Field Effects on Anodic Oxidation of Potassium Iodide

UECHI, Ichiro¹; FUJIWARA, Masao¹; FUJIWARA, Yoshihisa²; YAMAMOTO, Yohsuke²; TANIMOTO, Yoshifumi¹

(¹IMS and Hiroshima Univ.; ²Hiroshima Univ.)

[*Bull. Chem. Soc. Jpn.* in press]

External magnetic fields (≤ 6 kG) significantly increase yields of I_3^- and H_2 as well as anodic currents in anodic oxidation of potassium iodide. At 0.7 V, the ratio of the current at 6 kG and at 0 kG is about 1.7, whereas that of I_3^- yield is 1.2. The ratio of the H_2 yield is 1.4 at 2 kG. The Lorentz force on ions in the solution induces convection of solution (MHD flow), resulting in acceleration of the entire reaction rate. The MHD flow of the solution is confirmed from the visual observation that reddish-brown streams of I_3^- in the solution, moving downward at zero field, undergo turbulent motion in magnetic fields. Small magnetic field effect on the I_3^- yield, compared to that on the anodic current, is attributable to the fact that the reaction of I_3^- and OH^- , generated at the cathode, is also enhanced by the MHD flow.

VIII-Q-2 High Magnetic Field Effect on the Growth of 3-Dimensional Silver Dendrites

KATSUKI, Akio¹; UECHI, Ichiro; FUJIWARA, Masao; TANIMOTO, Yoshifumi

(¹Shinshu Univ.)

[*Chem. Lett.* submitted]

A liquid/solid redox reaction between silver ion and copper metal is investigated under high vertical magnetic field (maximum field strength: 15 T). The magnetic field causes drastic changes in the color and shape of silver dendrites. At zero field, branches of metallic silver grow on the gray and cylindrical dendrites. In the presence of magnetic field, the dendrites are black in color and almost spherical in shape. The dendrites in magnetic field are denser than those at zero field. In the presence of the magnetic field, yields of silver dendrite and copper ion increase by 1.3–2. These effects are chiefly interpreted in terms of the magnetic force in copper ion in solution. As the reaction progresses, paramagnetic copper ions are generated. These ions are attracted by the magnetic force, leading to the convection of the solution.

VIII-R Theoretical and Computational Study on Gas Phase Reactions and Chromic Molecules

Quantum chemical calculations are used to produce potential energy surface (PES) to do reaction dynamics simulations. We develop the methodology to generate PES efficiently and/or automatically using quantum chemical calculation results. Another interest of our group is theoretical explanation and prediction of structural and spectral changes of photochromic and electrochromic substances.

VIII-R-1 Polycyano–Polycadmte Host Clathrates Including a Methylviologen Dication. Syntheses, Crystal Structures and Photo-Induced Reduction of Methylviologen Dication

YOSHIKAWA, Hirofumi¹; NISHIKIORI, Shin-ichi¹; WATANABE, Tokuko²; ISHIDA, Toshimasa³; WATANABE, Go³; MURAKAMI, Makoto³; SUWINSKA, Kinga⁴; LUBORADZKI, Roman⁴; LIPKOWSKI, Janusz⁴

(¹Univ. Tokyo; ²Tokyo Univ. Fisheries; ³Shizuoka Univ.; ⁴Polish Acad. Sci.)

[*J. Chem. Soc., Dalton Trans.* 1907 (2002)]

A series of polycyano-polycadmte host clathrates including a methylviologen dication (MV^{2+}), which is a photo-hemically active electron acceptor, and an organic molecule, such as alcohols, haloalkanes, ethers and small aromatics, and two complexes built of a polycyano-polycadmte and MV^{2+} were synthesized. The single crystal X-ray diffraction experiments on ten clathrates and the two complexes revealed their 3-D network polycyano-polycadmte structures built of Cd^{2+} ions and CN. bridges. The network structures are classified into five structure types. Type I, II and III were found in the clathrates, and Type IV and V were turned up in the two complexes. Type I and II have cage-like cavities and each of the cavities includes one guest, MV^{2+} or an organic molecule. Type III has a channel-like cavity where MV^{2+} ions and organic molecules are included. Type IV and V have 3-D space, which is neither a cage-like cavity nor a channel-like cavity, for embracing MV^{2+} . Although all compounds were colorless and the formation of a charge transfer complex between MV^{2+} and a neutral guest in the clathrates was not confirmed from the structural data and diffuse reflectance spectra, some of them showed a color change from colorless to blue on UV irradiation, and which arose from the reduction of MV^{2+} to a methylviologen radical MV^{+} .

VIII-R-2 IR Absorption Spectra of Electrochromic WO_3 Films

KONOSHIMA, Koji¹; GOTO, Takeshi; ISHIDA, Toshimasa¹; URABE, Kazuo¹; KITAO, Michihiko¹
(¹Shizuoka Univ.)

[*Trans. Mater. Res. Soc. Jpn.* 27, 349 (2002)]

WO_3 films were prepared by thermal evaporation. IR absorption spectra of the films were measured for

various amount of injected protons. Three peaks of $\nu(W-OH)$, $\nu(W=O)$ and $\nu(O-W-O)$ vibrations were observed. With increasing of injected protons, the intensity of peak of $\nu(W-OH)$ increased and its position shifted hugely from 3200 to 2400 cm^{-1} . We calculated various bond-patterns of OH vibrations. Then OH vibrations accompanied with hydrogen bonds are plausible for observed OH peaks. On the other hand, with increasing of injected protons the intensity of peak of $\nu(W=O)$ bond also increased, but its position shifted a little. It is considered that parts of $W-O-W-O-W$ bonds were broken by injected protons and then $W=O$ bonds were brought about.

VIII-R-3 A Local Interpolation Scheme Using No Derivatives in Potential Sampling: Application to $O(^1D) + H_2$ System

ISHIDA, Toshimasa; SCHATZ, George C.¹
(¹Northwestern Univ.)

[*J. Comput. Chem.* submitted]

We recently proposed a local interpolation scheme, in which interpolant moving least squares (IMLS) and Shepard interpolation are employed to describe potential energy surfaces. This IMLS/Shepard scheme is applicable to do potential interpolation with quantum chemical results for which analytical derivatives are not available. In this study, we apply the scheme to the highly exothermic $O(^1D) + H_2 \rightarrow H + OH$ reaction and compare it with results based on Shepard interpolation using second order Taylor expansions. An analytical surface is used to define the potential function so that errors in the interpolation function may accurately be determined. We found that the present scheme reproduces the correct reactive cross sections more accurately than the Shepard scheme, and with rms errors for energy and gradients that are significantly smaller than those from Shepard interpolation. This occurs even though the present scheme does not utilize derivative and hessian information whereas the Shepard interpolation does. The Bayesian approach proposed by Bettens and Collins does not improve the IMLS/Shepard results significantly although it does the Shepard-only approach. The accuracy in the IMLS/Shepard scheme is surprising, but can be explained by the more global nature of the interpolation.

VIII-R-4 Theoretical Study on Photoinduced Color Change and Charge Transfer of Methylviologen

ISHIDA, Toshimasa; MURAKAMI, Makoto¹;

WATANABE, Go¹; YOSHIKAWA, Hirofumi²;
NISHIKIORI, Shin-ichi²
(¹Shizuoka Univ.; ²Univ. Tokyo)

[*Internet Electron. J. Mol. Des.* submitted]

Motivation. Methylviologen dication is easily reduced to be a monocation radical, and turned to be blue, and forms a charge-transfer complex with a donor molecule. Yoshikawa *et al.* recently reported photo-induced reduction and charge transfer complexes in polycyanopolycadmate host clathrates. We study the reduction using quantum chemical calculations. The energy changes with the torsion angle of the two cations and the spectral change, solvent effect and the charge transfer between the dication and other guest molecules in the clathrates are investigated.

Method. The Hartree-Fock and CI singles, time dependent DFT calculations are carried out for the ground state and excited states of the two cations. Solvation effect is treated with the polarizable continuum model, and the charge transfer in the clathrates is modeled based on crystal structures determined experimentally.

Results. The optimized geometry of the monocation radical was found to be planar while that of the dication is twisted. These results are consistent with recent calculations for related compounds. The color change upon the photoreduction was reproduced by the calculation. The solvent effect of acetonitrile was found to be small. Charge transfer absorption was reproduced for the mesitylene-methylviologen dication complex in the clathrate host using a small model.

Conclusions. The geometrical and the color change was reproduced satisfactorily. The TDDFT scheme reproduces the observed spectra better than the CIS scheme, but the latter scheme is still valuable to evaluate qualitative feature of spectra.

VIII-R-5 Potential Energy Surface Generation Using Ab Initio Calculations and IMLS/Shepard Interpolation for the $\text{LiH} + \text{H} \rightleftharpoons \text{Li} + \text{H}_2$ Reactions

KIM, Kyoung Hoon¹; LEE, Yoon Sup¹; JEUNG, Gwang-Hi²; ISHIDA, Toshimasa³
(¹Korea Adv. Inst. Sci. Tech.; ²Univ. Paris-Sud;
³Shizuoka Univ.)

[*J. Chem. Phys.* submitted]

CASSCF following MRCI calculations are employed to generate potential energy surfaces for the reaction of $\text{LiH} + \text{H} \rightleftharpoons \text{Li} + \text{H}_2$ and analyze the reactive region for the reaction. Spectroscopic data for LiH and H_2 obtained by our scheme are in good agreement with experiment results. IMLS combined with Shepard interpolation method is used to interpolate the Potential energy surfaces. Trajectory calculations for $\text{LiH} + \text{H} \rightarrow \text{Li} + \text{H}_2$ on the interpolated potential energy surface illustrate that the initial vibrational content of LiH plays a rather minor role which is explained by the fact there is no energy barrier for the reaction $\text{LiH} + \text{H} \rightarrow \text{Li} + \text{H}_2$, and the reactive cross section has maximum value, when the initial collision energy is about 0.1 eV. Trajec-

tory calculations for $\text{Li} + \text{H}_2 \rightarrow \text{LiH} + \text{H}$ show that the reaction requires highly excited $\text{H}_2(v \geq 4)$ molecules for it to occur at low collision energy and it is more efficient to put the same amount energy into the H_2 vibration energy rather than translational energy.

VIII-S Macromolecular Self-Assembly Opens a Way to the Development of Novel Materials that Have Characteristics of Cellular Systems

In cellular systems, assembly of devices (*e.g.* enzymes) into complexes is a principle to construct supramolecular apparatuses and ensure the specificity, fidelity, and efficiency of intracellular events. Exchangeability of the components of the complex is also advantageous for adaptation to the environment and metabolism of the apparatus. For global, sustainable development, in our opinion, readiness for the adaptation and decomposition is required for any future materials and systems such as highly integrated device arrays. Utilizing elaborate macromolecular self-assemblies, we thus aimed at development of artificial systems endowed with energy- and entropy-saving properties: the system can be formed and function on demand, and are readily reusable, repairable, and bio-degradable. We attempt to fabricate the nano-systems for energy conversion and computing; for their basis, we also study on molecular mechanisms of photosynthesis and signal transduction. Our study should serve a new design concept for nano- and molecular-scale intelligent materials (see also Special Research Project (c)).

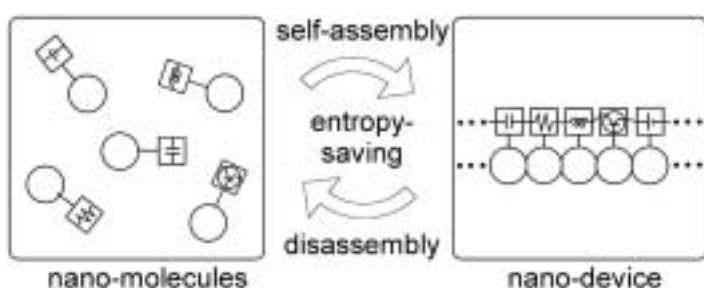


Figure 1. A concept of the “entropy-saving” nano-materials.

VIII-S-1 Fabrication of “Entropy-Saving” Nano-Solar-Cells

OBA, Toru; HANASAKI, Mitsuru¹; MINABE, Masahiro¹
(¹Utsunomiya Univ.)

Photosynthetic apparatuses in living organisms are, in common, assemblies of light-harvesting antenna parts and reaction centers (RCs) where energy conversion occur. Nano-scale order in the assembled supramolecular structure contributes efficient function. The assembly is advantageous to light adaptation and metabolism. These facts suggest that elaborate self-assembly of macromolecular components can provide solar-cells that can be formed and function on demand. We developed such device utilizing cytoskeletal nano-tubes, “microtubules” (MTs). The component protein “tubulin” (Tub) molecules assemble to form MTs at 37 °C in the presence of nucleotide, and MTs disassemble to Tubs at 0 °C. We prepared Tubs conjugated with a fluorophore for the antenna part and a photosensitizer-labeled hemoprotein for the RC, respectively. The modified Tubs were mixed and the temperature of the solution was switched simply. Only in the Tub-assembled state (MTs), solar energy absorbed by the antenna parts migrated to the sensitizer, leading to charge separation in the RC, as occurs in photosynthesis. The device reversibly functioned at each Tub-assembled state in the course of the Tub-assembly / MT-disassembly cycles.

VIII-S-2 Model Study on Signaling Behaviors of Scaffold Proteins—Toward its Application to Novel Computing Devices—

OBA, Toru; FUJIWARA, Umihito¹; MINABE, Masahiro¹
(¹Utsunomiya Univ.)

Scaffold proteins, found in postsynaptic termini, can bind several members of a signaling cascade to form a supramolecular complex, which may contribute to rapidity, fidelity, and selectivity of signal transduction.¹⁾ Such a mechanism can correlate to learning and memory formation. Due to the limitation of the experiments, however, no detailed model of scaffold action has been reported except for numerical simulations. We utilized a eukaryotic cytoskeleton ‘microtubule’ (MT) for fabrication of a model of the signaling complexes. We conjugated both glucose oxidase (GOx) and horseradish peroxidase (HRP) on the surface of an MT by use of the avidin-biotin interaction. The upstream effector (GOx) converted an input signal (*D*-glucose) into a second messenger (H₂O₂) that was diffusely supplied to the downstream effector (HRP) and converted into an output signal (Dye). It was found that sensitivity of the system to the stimulus increased with increasing density of the effectors on a MT. Further examinations of this model system may contribute to development of novel computing devices.

Reference

- 1) U. Thomas, “Modulation of synaptic signalling complexes by Homer proteins,” *J. Neurochem.* **81**, 407 (2002).

VIII-S-3 Physicochemical Studies on the Molecular Mechanism of Photosynthesis

OBA, Toru; TAMIYAKI, Hitoshi¹

(¹Ritsumeikan Univ.)

[*Photosynth. Res.* in press]

Since chlorophyll *a* and bacteriochlorophyll *a* are asymmetric molecules (Figure 1), an external ligand can coordinate to the central Mg atom either from the chlorin macrocycle side where the C13²-methoxycarbonyl moiety protrudes (denoting as the 'back' side) or from the other side (the 'face' side). We investigated which side of the macrocycle is favored for the ligand coordination, by survey of the highly resolved crystal structures of various photosynthetic proteins and theoretical model calculations. It is found that chlorophyll *a* as well as bacteriochlorophylls *a* and *b* in the photosynthetic proteins mostly bind their ligands on the 'back' sides. This finding was confirmed by the theoretical calculations for methyl chlorophyllide *a* and methyl bacteriochlorophyllide *a* as models: the 'back' type ligand-(bacterio)chlorophyll complex was more stable than the 'face' type one. The calculations predicted influence of the C13²-stereochemistry on the choice of the side of the ligand coordination, which may be correlated to the presence of the C13²-epimer of chlorophyll *a* in photosystem I reaction center.¹⁾

Reference

- 1) P. Jordan, P. Fromme, H. T. Witt, O. Klukas, W. Saenger and N. Krauß, "Three-dimensional structure of cyanobacterial photosystem I at 2.5 Å resolution," *Nature* **411**, 909 (2001).

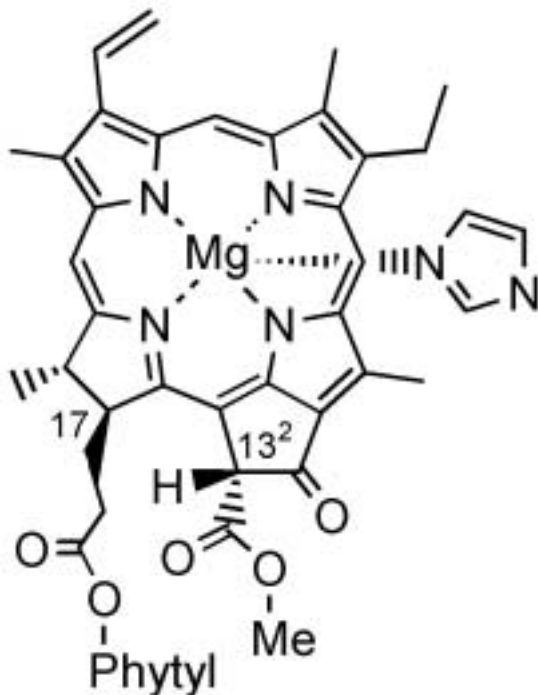


Figure 1. Molecular structure of the 'back' type chlorophyll *a*-imidazole complex.

Equipment Development Center

VIII-T Development of “Special Machine”

The technical staff of the Equipment Development Center is partly engaged in planning, researching, designing and constructing “Special machine.” This machine, is a high-tech experimental instrument, with emphasis on new technical idea and co-operative work with members inside and outside the Institute including those in industries. We collect suggestions of new instruments once every year from Professors and Associate Professors of IMS.

In this fiscal year, 2001, one project theme was adopted as Special machine.

VIII-T-1 Development of Twin-Probe Scanning Tunneling Microscope

YAMADA, Ryo; TADA, Hirokazu; YOSHIDA, Hisashi; MATSUSHITA, Kouji; SUZUI, Mitsukazu; KONDO, Takuhiko

It is important to study electrical properties of materials in nm scale for the construction of electronic devices in the same scale. Scanning probe microscopy (SPM) is one of the most powerful methods to measure local properties of solid surfaces in nm ~ atomic scales. Most of the SPM uses a single probe and, therefore, it is difficult to measure the transport properties of nanoscale structures.

We constructed a twin probe scanning tunneling microscope which has two independently driven probes. By using this instrument, it is expected to be possible to measure electrical transport properties such as resistance as a function of a distance between two probes in nano-scale.

The whole instruments were placed on a spring damper to be isolated from the mechanical vibrations. Two tube piezos which were used for the fine adjustment of the tip positions were fixed beneath steel beams. The beams were placed on commercially available microstage (Melles Griot) used for coarse adjustment of the tip positions. A current-to-voltage converter with a sensitivity of 1 nA/V was fabricated. It is used to measure a current flowing between the probe and the sample and that flowing between the each probe when the bias voltage is applied to the sample and one of the probes, respectively. The measured current was fed into the commercially available SPM controller (JEOL) and surface morphology was obtained by scanning the probe in x - y plane by the tube piezos keeping the current constant by controlling the z position of the probe.

Figure 1 shows an image of HOPG surface obtained by the instrument. Atomically flat terraces and mono-atomic steps were imaged independently by two probes at the same time. We are now optimizing the resolution and fabricating a sharper tip to get two probes closer each other.

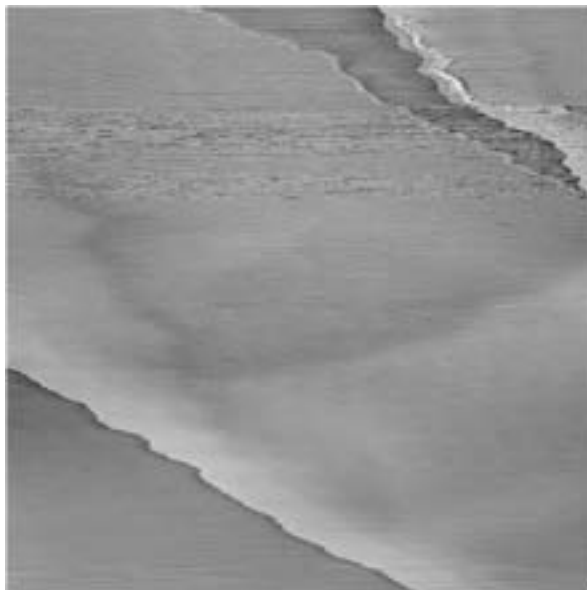


Figure 1. An STM image of HOPG surface.

Ultraviolet Synchrotron Orbital Radiation Facility

VIII-U Development of the UVSOR Light Source

VIII-U-1 Development of Lattice Components for UVSOR Upgrade Project

KATOH, Masahiro; HAYASHI, Kenji; HONDA, Toru¹; HORI, Yoichiro²; HOSAKA, Masahito; KINOSHITA, Toshio; KODA, Shigeru³; TAKASHIMA, Yoshifumi; YAMAZAKI, Jun-ichiro; KITAMURA, Hideo⁴; HARA, Toru⁴; TANAKA, Takashi⁴

(¹KEK-PF; ²IMS and KEK-PF; ³Saga Univ.; ⁴RIKEN)

We have been developing the lattice components for the UVSOR upgrade project. In this project, the original DBA lattice of the storage ring will be modified to have lower emittance and more straight sections available for insertion devices. The reconstruction will be started in March 2003 and be completed until the end of May. All the quadrupole and sextupole magnets will be replaced with combined function multi-pole magnets, which is capable of producing both quadrupole field and sextupole field. We constructed a prototype and measured the magnetic field. The results have shown that the required field strength and field quality was well realized. We have completed the design of the vacuum system. Their fabrication will be started in September 2002 and be completed until the end of February.

VIII-U-2 Storage Ring Free Electron Laser

HOSAKA, Masahito; KATOH, Masahiro; HAYASHI, Kenji; KINOSHITA, Toshio; KODA, Shigeru¹; TAKASHIMA, Yoshifumi; YAMAZAKI, Jun-ichiro

(¹Saga Univ.)

At the UVSOR, performance of the free electron lasers has been improved aiming users applications. The average output power has reached 1W level, which is the world highest record as a storage ring free electron laser (SRFEL). SRFEL have a potentiality for scientific applications as a unique light source because of variable wavelength, good coherence, temporal structure, and perfect synchronization with synchrotron radiation (SR). We started an experiment using SRFEL combined with SR. We have succeeded to observe the double-resonant excitation of Xe by using SR and SRFEL as pump and probe lights, respectively.

VIII-U-3 Ion Trapping at UVSOR

MOCHIIHASHI, Akira; KATOH, Masahiro; HAYASHI, Kenji; KINOSHITA, Toshio; HOSAKA, Masahito; TAKASHIMA, Yoshifumi; YAMAZAKI, Jun-ichiro

An ion-related vertical instability of the UVSOR electron storage ring was observed in a multi-bunch mode with empty buckets (a bunch gap). In contrast to a shorter bunch train, it was clearly seen that vertical betatron tune had step-like changes with decrease of a beam current in a longer train. The step-like change in the tune seems to be caused by sudden change in condition of stability of trapped ions. Change in amplitude of the vertical betatron oscillation along a bunch train was also observed with a bunch-by-bunch beam diagnostic system. The structure of the amplitude seems to have relation to modulation of the ion density along the train.

VIII-U-4 Design Study of Vacuum System Improvement

HORI, Yoichiro; YAMAZAKI, Jun-ichiro; KATOH, Masahiro; HAYASHI, Kenji; HOSAKA, Masahito; KINOSHITA, Toshio; MOCHIIHASHI, Akira

In the UVSOR upgrade project, vacuum beam chambers in straight sections must be replaced to new ones designed for new magnets and their arrangement, and three bending chambers need to be renewed for re-equipment of beam-lines. In the remodeling, the pumping speed distribution should be considered in order to maintain a long beam lifetime in the upgraded ring. The pump arrangement by which a required operating pressure can be achieved was searched by a simple simulation of the pressure distribution. The simulation suggests that the pump location is essential in the straight section, and that the lifetime can be expected to extend up to 10–30 % by reinforcing the pumping speed in every bend section. Also a thermal/structural analysis of the chamber has been carried out for the 500 mA storage. Though the present concept of the stainless steel with partially water-cooling will be inherited, the use of copper material is locally desirable for the parts suffered intense SR. New chambers have been designed in detail with applying above results.

VIII-V Researches by the USE of UVSOR

VIII-V-1 Non-Radiative Decay of the Core Excitons in Auger-Free Luminescence Materials, CsCl and BaF₂

KAMADA, Masao; ITOH, Minoru¹
(¹Shinshu Univ.)

[Phys. Rev. B **65**, 245104 in press]

The present work has been conducted to understand the decay processes of the Cs-5*p* and Ba-5*p* core excitons in CsCl and BaF₂, respectively, where the Auger decay process of the Cs-5*p* and Ba-5*p* core holes is energetically forbidden. The core-exciton peaks are missing in the excitation spectra for the Auger-free luminescence, which arises from a radiative decay of the valence electrons into these core holes. Resonant enhancement effects of the valence-band photoelectron spectra are observed around 13 eV for CsCl and 17 eV for BaF₂. The effects are attributed to the non-radiative decay through the direct-recombination process of an excited electron and the Cs-5*p* or Ba-5*p* core hole forming the core exciton. It is also found that the core exciton deforms its surrounding lattice with relaxation energy of about 0.3 eV in CsCl and 0.9 eV in BaF₂. The non-radiative direct-recombination probabilities of the core excitons are estimated to be about 32 and 75% for CsCl and BaF₂, respectively, by taking account of the lattice relaxation effects.

VIII-V-2 Photoelectron Spectroscopic Study on Photo-Induced Phase Transition of Spin-Crossover Complex

KAMADA, Masao; TAKAHASHI, Kazutoshi; DOI, Yo-ichiro¹; FUKUI, Kazutoshi¹; TAYAGAKI, Takeshi²; TANAKA, Ko-ichiro²
(¹Fukui Univ.; ²Kyoto Univ.)

[Phase transition **41-47**, in press]

Valence band structures in various phases of an organometal spin-crossover complex [Fe(2-pic)₃]Cl₂·EtOH have been measured by means of photoelectron spectroscopy based on the combination of synchrotron radiation and laser light. The valence band structure showed the remarkable change due to the photo-induced phase transition at low temperatures as well as the thermally induced phase transition, but the structure of the photo-induced phase was very different from that of the high-temperature phase. The DV-X α calculation based on the FeN₆ cluster was in good agreement with the photoelectron spectra. The present results indicate that the electronic structures originating from Fe and N ions are closely related to the photo-induced phase transition.

VIII-V-3 Surface-Photovoltage Effect in GaAs-GaAsP Super-Lattice Studied with Combination of Synchrotron Radiation and the Laser

TANAKA, Senku¹; MORÉ, Sam D.; TAKAHASHI, Kazutoshi; KAMADA, Masao; NISHITANI, Tomohiro²; NAKANISHI, Tsutomu²
(¹GUAS; ²Nagoya Univ.)

[SPIN2000 1000 (2001)]

Core-level photoelectron spectroscopy with the combination of synchrotron radiation (SR) and a laser was used for exploring the surface-photovoltage (SPV) effect and its temporal profiles in a GaAs/GaAsP super-lattice (SL). It was observed that the SPV value in the SL is suppressed as compared with a bulk GaAs. However, no significant difference was found in the temporal profile between the bulk and the SL. It is suggested that the suppression of the SPV in the SL is dominantly due to the small value of band bending under thermal equilibrium.

VIII-V-4 Pump/Probe Experiments with FEL and SR Pulses at UVSOR

GEJO, Tatsuo; SHIGEMASA, Eiji; NAKAMURA, Eiken; HOSAKA, Masahito; MOCHIHASHI, Akira; KATOH, Masahiro; YAMAZAKI, Jun-ichiro; HAYASHI, Kenji; TAKASHIMA, Yoshifumi; HAMA, Hiroyuki¹
(¹Tohoku Univ.)

Synchrotron radiation free electron lasers (SRFEL or FEL) has been used as a light source because of high power, high coherence and its unique temporal feature. Pump and probe experiments using FEL and synchrotron radiation (SR) pulses have been tried to perform for the last decade. This is due to the fact that the FEL pulse naturally synchronizes with the SR pulse. As the first gas-phase experiment combined FEL with SR, we have carried out the two-photon double-resonant excitation on Xe atoms, utilizing a SR pulse as a pump and an FEL pulse as a probe light.

The experiments were performed on BL7B at UVSOR, where a 3-m normal incidence monochromator is installed. The monochromatized SR from a bending magnet was used as the pump light. The estimated photon flux at BL3A1 is about 1×10^{13} photons/sec/0.1%B.W./100 mA, whereas that at BL7B is in the order of 10^9 . The FEL pulses were extracted through the backward mirror, and transported to the experimental station through a series of multi-layer mirrors. The flight path of FEL, which was adjusted to synchronize the timing between the FEL and the SR pulses, was about 30 m. Fine-tuning of the delay timing was made by using a movable optical delay system (50 cm) at the experimental station. The FEL and SR pulses introduced, coaxially crossed an effusive jet of Xe atoms from a gas nozzle. The singly charged Xe ions produced in the interaction region were detected by means of a conventional channeltron.

The first experiment on the two-photon double-resonant excitation of the Xe* 5*p*⁵*nf* autoionization states using the combination of a mode-locked laser [1]

and SR has already been successfully demonstrated by Meyer's group at LURE. The wavelength of SR was adjusted to be 10.4 eV, in order to prepare the $\text{Xe}^* 5p^5 5d$ intermediate states in a first step. The $\text{Xe}^* 5p^5 4f$ autoionization resonance can be excited within the wavelength region of FEL in a second step. Since the lifetime of the intermediate states is quite short (600 ps), the synchronization between the SR and laser pulses is essential in this experiment. The count rate for this measurement is about 200 counts/sec, which is about 1/1000 in comparison to the case when the non-monochromatized undulator radiation was used at BL3A1. Although the photon intensity of SR at BL7B is high enough to obtain total ion yield spectrum, it is found that considerable improvement on the experimental setup is required for measuring the angular distribution of photoelectrons from the same system on this beam-line.

We are planning to carry out similar experiments in the shorter wavelength region (around 400 nm) of FEL, where higher Rydberg series of the $\text{Xe}^* 5p^5 nf$ states via the $\text{Xe}^* 5p^5 5d$ intermediate state are accessible.

Reference

- 1) M. Gisselbrecht, A. Marquette and M. Meyer, *J. Phys. B* **31**, L977 (1998).

VIII-V-5 Angle-Resolved Photoion Spectra of SO_2

GEJO, Tatsuo; SHIGEMASA, Eiji; NAGASONO, Mitsuru; OJI, Hiroshi; HATSUI, Takaki; KOSUGI, Nobuhiro

The SO_2 molecule has three unoccupied valence orbitals, $3b_1^*$, $9a_1^*$ and $6b_2^*$, which can be associated with the three S $3p$ orbitals, where SO_2 has an electronic structure of $\text{S}^{4+}[(3s)^2(3p)^0] \cdot (\text{O}^{2-})_2$ in the limit of an ionic bonding picture and the $3b_1$, $9a_1$ and $6b_2$ orbitals correspond to out-of-plane $\text{S}3p \pi$ (π_{out}), in-plane $\text{S}3p \pi$ (π_{in}) and in-plane $\text{S}3p \sigma$, respectively.¹⁾ All the $\text{S}1s$ ($1a_1$) excitations to the $3b_1^*$, $9a_1^*$ and $6b_2^*$ orbitals are dipole-allowed and are found to be lying below the $\text{S}1s \rightarrow$ Rydberg excitations with the term values of 10.4, 5.7, and 4.8 eV, respectively.¹⁾ The chemical bond between S and O is not so strong, and even the excitation to the most antibonding σ^* ($6b_2$) orbital is located below the ionization threshold. The single excitations to all the unoccupied valence orbitals are observed below the ionization threshold even in the case of the O $1s$ absorption spectra assigned previously, though there are two O $1s$ orbitals, $1b_2$ and $2a_1$. The $1b_2$ - $2a_1$ splitting caused by the interaction between the two O $1s$ orbitals is expected to be negligible and does not change the situation.

The photoabsorption and angle resolved photoion spectra of SO_2 , were measured in the O K -edge region. The O $1s$ core-to-valence excited states of SO_2 were calculated by multi-reference configuration interaction including single and double excitations (MR-SDCI).

Figure 1a and 1b show the O K -edge photoabsorption and angle resolved photoion spectrum of SO_2 . The lowest photoabsorption feature A observed at 530.56 eV is well separated from the higher features. The feature A

is attributed to the O $1s\sigma(2a_1) \rightarrow \pi^*(3b_1)$ transition, considering its term value of 9.27 eV. It should be noted that the B_1 state is a dipole-allowed out-of-molecular plane (π^*) transition from the A_1 ground state, the A_1 and B_2 states are dipole-allowed in-plane transitions, and the A_2 state is dipole-forbidden; the $\pi^*(3b_1)$ orbital is not accessible from the O $1s\sigma(1b_2)$ electron. Between the lowest $1s \rightarrow \pi^*$ excitation at 530.56 eV and the O K -shell ionization threshold at 539.83 eV, the spectral feature is dominated by some broad bands labeled as B, C, and D at ~ 535 eV (term values of ~ 5 eV) arising from the $1s \rightarrow$ in-plane excitations, which consist of the O $1s \rightarrow 9a_1^*$ (dipole-allowed B_2 from $1b_2$ and A_1 from $2a_1$) and O $1s \rightarrow 6b_2^*$ (dipole-allowed A_1 from $1b_2$ and B_2 from $2a_1$) transitions. The structures E, F, and G are comparatively weak and have term values of 2.24, 1.63, and 0.75 eV, respectively; therefore, they are possibly assigned to the lowest s -type ($4s$ or $5s$) and p -type ($4p$ or $5p$) Rydberg transitions. In the continuum, two broad bands are observed around 540.80 and 542.69 eV, which are attributable to double excitations or S $3d$ -type shape resonances, because there are no other singly excited valence states than the $1s \rightarrow 3b_1^*$, $9a_1^*$ and $6b_2^*$ transitions.

References

- 1) J. Adachi *et al.*, *Chem. Phys. Lett.* **294**, 559 (1998).

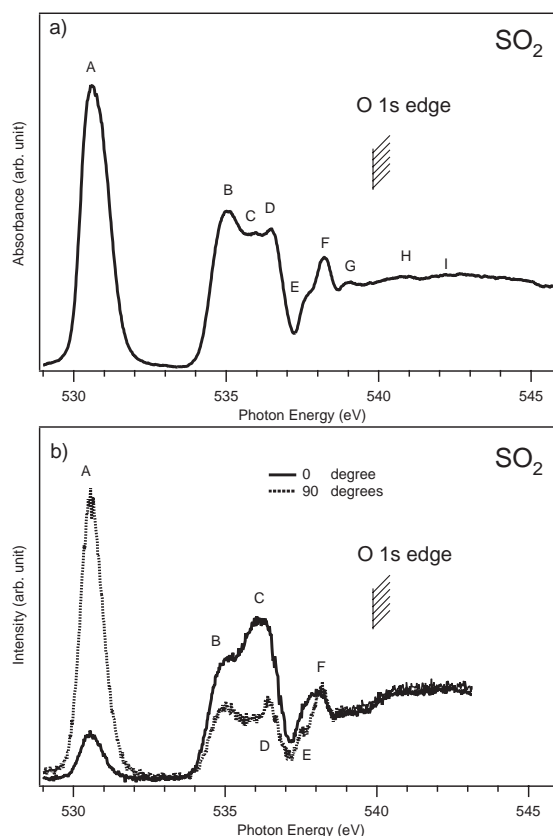


Figure 1. a) Absorption spectrum of SO_2 in the O K -edge region. b) Angle-resolved ion yield spectra of SO_2 . Dotted and solid lines denote I_{90} and I_0 ion yields, respectively.

VIII-V-6 The Measurement of Absorption Spectra of Trifluoromethyl Sulfur Pentafluoride in VUV Region

GEJO, Tatsuo; SHIGEMASA, Eiji; TAKAHASHI, Kenshi¹; MATSUMI, Yutaka¹
(¹Nagoya Univ.)

Global warming or green house effect is one of the major issues for environmental chemistry. Although CO₂, CH₄, and N₂O play a major role on the green house effect in air, some gases with much lower concentrations can contribute to the global warming because of their exceptionally large infrared absorption. For example, SF₆ has 22,200 times larger global warming potential (GWP) over a 100-year time than CO₂ although it is currently present in the atmosphere at only 4 ppt.¹⁾ Recently Sturges *et al.* detected Trifluoromethyl sulfur pentafluoride (SF₅CF₃), which is chemically close to SF₆, at Antarctic deep consolidated snow (firn).¹⁾ This Antarctic firn measurement shows that the concentration of SF₅CF₃ have increased from near zero in the late 1960s to about 0.12 ppt in 1999, whose trend matches to recent global warming tendency. They also measured a radiative forcing of SF₅CF₃, which is 0.57 watt per square meter per parts per billion.¹⁾ This is the largest radiative forcing, on a per molecule basis, of any gas found in the atmosphere up to this date. They also reported stratospheric profiles of SF₅CF₃ and suggested that it is long-lived in the atmosphere (on the order of 1000 years).¹⁾ If this is true, the irreversible accumulation of this gas may affect the green house effect drastically. In order to access this effect and lifetime of SF₅CF₃ in the stratosphere more precisely, its absorption spectra and cross sections in the VUV region are crucial.

The present photoabsorption measurement of SF₅CF₃ in the VUV region was performed at BL7B in the UVSOR facility. Synchrotron radiation at UVSOR was monochromatized by using a 3-m normal incidence monochromator. The intensity of the photon beam transmitted through a gas cell was monitored by using a silicon photodiode (IRD Inc, AXUV-100). The photoabsorption cross sections were calculated by using the Beer-Lambert expression. The data were checked to ensure there is no line saturation effect.

In the region of interest, two strong peaks in the absorption spectra of SF₅CF₃ were observed: One peak around 107 nm (A) and another one around 130 nm (B). The peak similar to A is also observed in SF₆, whereas the equivalent to the peak B was not observed. Therefore one can suggest that the peak B arises from the transition from the lone pair electron of CF₃.

Based on these data, we will estimate the lifetime of SF₅CF₃ in the stratosphere.

Reference

1) W. T. Sturges *et al.*, *Science* **289**, 613 (2000).

VIII-V-7 Symmetry-Resolved Cl 2p Photoabsorption Spectra of Cl₂

SHIGEMASA, Eiji; GEJO, Tatsuo; HATSUI, Takaki; KOSUGI, Nobuhiro

The 2p ionization spectra, or photoelectron spectra, show molecular field splittings (MFS) and spin-orbit splittings (SOS). The 2p excitation spectra, or photo-

absorption spectra, exhibit exchange splittings (EXS) in addition to MFS and SOS. We have already investigated very complicated spectral features due to EXS and SOS in the S 2p excitation region of SO₂, CS₂ and OCS, based on angle-resolved photoion spectroscopy (ARPIS) and the Breit-Pauli *ab initio* calculation. In the present work, Cl 2p ARPIS spectra of Cl₂ in comparison to HCl are reported. The lowest excited states in these molecules are the Cl 2p-π* excitation. There are three 2p orbitals, and the Cl 2p-σ* excitation involves parallel and perpendicular transitions with respect to the bond direction. We will discuss a propensity rule for the two transition directions by measuring the fragment-ion yields.

The experiments were performed on the newly constructed beamline BL4B at the UVSOR, IMS. ARPIS spectra were measured with two identical ion detectors having retarding grids, which were set at 0° and 90° relative to the electric vector of the light, by scanning the photon energy. The photon-energy resolution was set to about 50 meV for the present experiments. The Cl 2p ARPIS spectra of Cl₂ are displayed in Figure 1. The excitation energies and the nature of the structures observed will be discussed with the help of theoretical calculations.

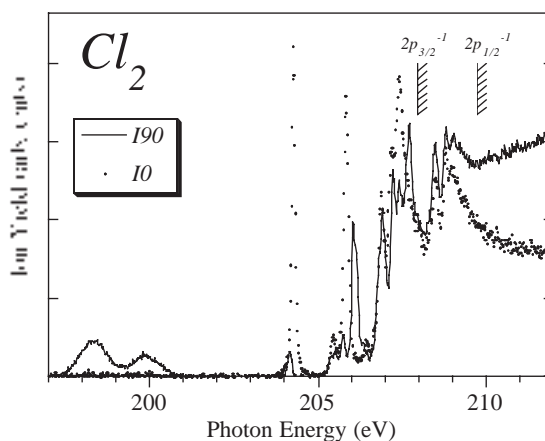


Figure 1. ARPIS spectra in the Cl 2p excitation region of Cl₂.

VIII-V-8 Dynamical Angular Correlation in Molecular Auger Decay

GUILLEMIN, Renaud¹; SHIGEMASA, Eiji; LE GUEN, Karine¹; CEOLINE, Denis¹; MIRON, Cataline¹; LECLERCQ, Nicola¹; MORIN, Paul¹; SIMON, Marc¹
(¹LURE)

[*Phys. Rev. Lett.* **87**, 203001 (2001)]

The first measurements of the angular distribution of Auger electrons from fixed-in-space molecules have been performed in the C K-shell ionization region of CO, for both parallel and perpendicular orientation of the molecular axis with respect to the light polarization vector. The ions emitted parallel or perpendicular to the electric vector of the incident radiation determine the possible Σ or Π symmetries in the ionization channels, respectively. The angular distributions obtained for the CO²⁺ B¹Σ Auger final state show dramatic spectral

variations, which also depend on the initial ionization channels, Σ or Π . The result strongly suggests the breakdown of the two-step model in which the Auger decay is treated independently of the initial photoionization process.

VIII-V-9 Nondipolar Electron Angular Distributions from Fixed-in-Space Molecules

GUILLEMIN, Renaud¹; HEMMERS, Oliver¹; LINDLE, Denis¹; SHIGEMASA, Eiji; LE GUEN, Karine²; CEOLINE, Denis²; MIRON, Cataline²; LECLERCQ, Nicola²; MORIN, Paul²; SIMON, Marc²; LANGHOFF, Peter³
(¹Univ. Nevada; ²LURE; ³Univ. California)

[*Phys. Rev. Lett.* **89**, 033002 (2002)]

The first indication of nondipole effects in the azimuthal dependence of photoelectron angular distributions emitted from fixed-in-space molecules is demonstrated in N_2 . Comparison of the results with angular distributions observed for randomly oriented molecules and theoretical derivations for the nondipole correction first order in photon momentum suggests that higher orders will be needed to describe distributions measured in the molecular frame.

VIII-V-10 Double and Triple Excitations Near the K-Shell Ionization Threshold of N_2 Revealed by Symmetry-Resolved Spectroscopy

SHIGEMASA, Eiji; GEJO, Tatsuo; NAGASONO, Mitsuru; HATSUI, Takaki; KOSUGI, Nobuhiro

[*Phys. Rev. A* **66**, 022508 (2002)]

High-resolution photoion yield spectra of N_2 are measured near the K-shell ionization threshold. Previously-unresolved multiple excitations are distinguished in the Σ - and Π -symmetry resolved spectra, which were obtained from the ion yield spectra recorded at 0° and 90° relative to the polarization direction. The three $^1\Pi_u$ and two $^1\Sigma_u^+$ doubly excited states are clearly identified. Furthermore, a weak Π -symmetry feature just at the σ^* -shape resonance position (~ 419 eV) is definitely resolved and assigned to the lowest $^1\Pi_u$ triple excitation with the help of quantum chemical calculations.

VIII-V-11 Optical and Magneto-Optical Studies on Electronic Structure of CeSb in the Magnetically Ordered States

KIMURA, Shin-ichi; OKUNO, Mitsuru¹; IWATA, Hideki¹; KITAZAWA, Hideaki²; KIDO, Giyu²; ISHIYAMA, Fumihiko³; SAKAI, Osamu⁴
(¹Kobe Univ.; ²Natl. Inst. Mater. Sci.; ³Tohoku Univ.; ⁴Tokyo Metropolitan Univ.)

[*J. Phys. Soc. Jpn.* **71**, (2002) in press]

The electronic structure of CeSb in the magnetically ordered states is examined by measuring the optical

reflectivity, the magnetic linear dichroism and the magnetic circular dichroism spectra at low temperatures under magnetic fields in the infrared region. The optical conductivity spectrum, as well as the reflectivity spectrum changes significantly with the complex magnetic phase diagram, and gives detailed information of electronic structures in the ordered states. The spectra in the ordered states cannot be explained only by the energy band folding due to the appearance of the periodic magnetic structure. By comparing with the calculated optical conductivity spectra, we found that not only the Ce4f-Sb5p mixing but also the Ce5d-Sb5p mixing mainly works in the ordered states.

VIII-V-12 Low Energy Electronic Structure of $Ce_{1-x}La_xSb$ ($x = 0, 0.1$) in the Magnetically Ordered States

KIMURA, Shin-ichi; OKUNO, Mitsuru¹; IWATA, Hideki¹; KITAZAWA, Hideaki²; KIDO, Giyu²
(¹Kobe Univ.; ²Natl. Res. Inst. Met.)

[*Physica B* **312-313**, 228 (2002)]

The anisotropy of the effect of pf mixing on the electronic structure of $Ce_{1-x}La_xSb$ ($x = 0, 0.1$) in the magnetically ordered states is examined by measuring the magnetic linear dichroism of the optical conductivity spectrum ($\sigma_{//}(\omega)$ for $E//B//[001]$, $\sigma_{\perp}(\omega)$ for $E\perp B//[001]$) in the infrared region at low temperatures under magnetic fields. The $\sigma_{\perp}(\omega)$ spectrum changes significantly with magnetic phase, whereas $\sigma_{//}(\omega)$ changes little. This result indicates that the electronic structure perpendicular to the magnetic field is more strongly modulated by pf mixing than that parallel to the field.

VIII-V-13 Temperature Dependence of Low-Energy Optical Conductivity of $Yb_4(As_{1-x}P_x)_3$ ($x = 0, 0.05, 0.15$)

KIMURA, Shin-ichi; OKUNO, Mitsuru¹; IWATA, Hideki¹; AOKI, Hidekazu²; OCHIAI, Akira³
(¹Kobe Univ.; ²Max-Planck-Inst., Germany; ³Tohoku Univ.)

[*J. Phys. Soc. Jpn.* **70**, 2829 (2001)]

To investigate the anomalous transport property and the electronic structure near the Fermi level of Yb_4As_3 , we measured the temperature dependence of the reflectivity spectra of $Yb_4(As_{1-x}P_x)_3$ ($x = 0, 0.05, 0.15$) in the photon energy range of 2 meV–1.5 eV. The optical conductivity spectrum due to carrier absorption (Drude curve) significantly changes with temperature. Above 200 K, the Drude curve with a high effective carrier density (N_{eff}) and a short relaxation time (τ) is commonly observed in all $Yb_4(As_{1-x}P_x)_3$. On the other hand, below 70 K, the Drude curve changes to one with a low N_{eff} and a long τ below 10 meV. At the same temperature, a new peak appears at 15 meV in Yb_4As_3 . The Drude curve and the new peak are considered to originate from the bare As 4p hole band and the hybridization state between the 4f and 5d bands on the

Yb³⁺ chain, respectively.

VIII-V-14 Charge Ordering Effect of Electronic Structure of Yb₄(As_{1-x}Sb_x)₃

KIMURA, Shin-ichi; NISHI, Tatsuhiko¹; OKUNO, Mitsuru¹; IWATA, Hideki¹; AOKI, Hidekazu²; OCHIAI, Akira³

(¹Kobe Univ.; ²Max-Planck-Inst., Germany; ³Tohoku Univ.)

[*J. Phys. Soc. Jpn.* **71**, 300 (2002)]

The change of the electronic structure near the Fermi level of Yb₄As₃ due to the charge ordering is examined by measuring the temperature dependence of reflectivity spectra of Yb₄(As_{1-x}Sb_x)₃ ($x = 0, 0.12, 0.24$) in the photon energy range of 2 meV–1.5 eV. In the optical conductivity spectra, a peak commonly appears at 0.4 eV below the temperature that is a little higher than the charge ordering temperature. Its intensity increases as the temperature decreases. The peak intensity indicates the ratio of the charge-ordered state for the whole because it originates from the optical transition to the Yb 5d band in the charge-ordered state.

VIII-V-15 Temperature-Induced Valence Transition of EuNi₂(Si_{0.25}Ge_{0.75})₂ Studied by Eu 4d-4f Resonant Photoemission and Optical Conductivity

KIMURA, Shin-ichi; OKUNO, Mitsuru¹; IWATA, Hideki¹; SAITOH, Tomohiko²; OKUDA, Taichi³; HARASAWA, Ayumi³; KINOSHITA, Toyohiko³; MITSUDA, Akihiro³; WADA, Hirofumi⁴; SHIGA, Masayuki⁴

(¹Kobe Univ.; ²Photon Factory; ³Univ. Tokyo; ⁴Kyoto Univ.)

[*J. Phys. Soc. Jpn.* **71**, 255 (2002)]

Eu 4d-4f resonant photoemission and optical reflectivity measurements of a temperature-induced valence transition material, EuNi₂(Si_{0.25}Ge_{0.75})₂, have been performed at several temperatures. The valence transition was observed and the mean valence was evaluated to be 2.37 ± 0.02 and 2.75 ± 0.25 below and above the valence transition temperature, respectively. The mixing between the Ni 3d conduction band and the Eu³⁺ 4f hole becomes weak as the temperature increases, showing the valence transition from Eu³⁺ to Eu²⁺.

VIII-V-16 Optical Gap in the Diluted Kondo Semiconductors Yb_{1-x}Lu_xB₁₂: Lattice and Single-Site Effects

OKAMURA, Hidekazu¹; MATSUNAMI, Masaharu¹; KIMURA, Shin-ichi; NANBA, Takao¹; IGA, Fumiroshi²; TAKABATAKE, Toshiro²

(¹Kobe Univ.; ²Hiroshima Univ.)

[*Physica B* **312-313**, 157 (2002)]

We have studied the evolution of energy gap in the

optical conductivity [$\sigma(\omega)$] of Yb_{1-x}Lu_xB₁₂ as functions of temperature (T) and non-magnetic Lu substitution (x). YbB₁₂ has a well-developed energy gap in $\sigma(\omega)$ below 20 K, with the onset of $\sigma(\omega)$ at ~ 20 meV and a shoulder at ~ 40 meV. With increasing T or x , the energy gap is rapidly filled in, which indicates the importance of coherence among the Yb 4f orbitals at different sites. The shoulder, on the other hand, remains nearly unshifted in wide ranges of T (to 70K @) and x (0–1/2), which shows that the characteristic energy for the gap is given by some single-site energy scale of Yb³⁺. Namely, both lattice and single-site effects play important roles in the gap formation of YbB₁₂.

VIII-V-17 Magneto-Optical Study of the Colossal Magnetoresistance Pyrochlore Tl₂Mn₂O₇

OKAMURA, Hidekazu¹; KORETSUNE, Toshihisa¹; MATSUNAMI, Masaharu¹; KIMURA, Shin-ichi; NANBA, Takao¹; IMAI, H.²; SHIMAKAWA, Y.²; KUBO, Y.²

(¹Kobe Univ.; ²NEC Corp.)

[*Physica B* **312-313**, 714 (2002)]

Pyrochlore Tl₂Mn₂O₇ has been found to exhibit a colossal magneto-resistance (CMR) that is comparable to that for the perovskite manganites such as La_{1-x}Sr_xMnO₃: In order to probe the microscopic electronic structures of Tl₂Mn₂O₇; we have measured its optical conductivity $\sigma(\omega)$ in wide ranges of photon energy, temperature (T), and external magnetic field (B). We have observed very strong variations of $\sigma(\omega)$ with T and B near the Curie temperature, where the CMR manifests itself. Analyses on the variations in $\sigma(\omega)$ show that both T - and B -induced evolutions of the electronic structures in Tl₂Mn₂O₇ are very similar to each other, and that they are universally related to the development of macroscopic magnetization. We have also observed a pronounced Kerr rotation at the plasma edge of the reflectivity.

VIII-V-18 Influence of Electronic Structure of CeSbNi_{0.15} on its Optical Conductivity

HONG, S. O.¹; MIN, B. H.¹; LEE, H. J.¹; KIMURA, Shin-ichi; JUNG, M. H.²; TAKABATAKE, Toshiro²; KWON, Y. S.¹

(¹SungKyunKwan Univ., Korea; ²Hiroshima Univ.)

[*Physica B* **312-313**, 251 (2002)]

The reflectivity of CeSbNi_{0.15} is measured at several temperatures in the low energy regions. The optical conductivity is obtained from the measured reflectivity. The carrier concentration and the relaxation time are evaluated by the Drude model. It is found that the pf mixing collapse takes place in CeSbNi_{0.15} and that the gap formation occurs at 7 K.

Computer Center

VIII-W Computer Simulation of Quantum Systems in Condensed Phase

VIII-W-1 Vibrational Energy Transfer from Solute to Solvent: An Analysis Based upon Path Integral Influence Functional Theory and Mixed Quantum-Classical Molecular Dynamics Method

MIKAMI, Taiji; OKAZAKI, Susumu

Path integral influence functional theory and mixed quantum-classical molecular dynamics method have been applied to the analysis of molecular mechanism of solute vibrational energy relaxation in solution. A numerical example is CN^- ion in water.

First, quantum effect of the solvent has been examined by taking a zero limit of Planck constant relevant to the solvent degrees of freedom. The effect is unexpectedly great. Classical approximation for the solvent significantly overestimates the relaxation time. The degree of the overestimation depends much upon the process, *e.g.* single-phonon, two-phonon, and three-phonon processes. However, it is interesting to find that it affects little energy dissipation path. Second, in order

to obtain a microscopic picture of the relaxation in terms of molecular motion, couplings between normal mode and the solute were divided into contributions from each water molecule. Couplings spread over the normal modes are not localized within particular modes. However, in molecular language, molecules in the first hydration shell are mostly responsible for the energy flow from the solute. Third, the couplings actually found in the solution have also been analyzed as a function of time. The solvent does not show delta-function-like coupling. This indicates that the system does not relax by collision which is usually found in the gas state. The coupling in the solution oscillates very rapidly. Then, matching of both transition frequency and phase between the interaction and the wave function of the system were found to be important. In a short time scale, we cannot find any systematic behavior of the coupling. It looks like random. However, integrating the coupling over pico second, the system shows relaxation to the ground state to a certain extent. The relaxation rate changes in hundred femto second or pico second reflecting the structural change of the hydration shell.

VIII-X Molecular Dynamics Study of Classical Complex Systems

VIII-X-1 A Molecular Dynamics Study of Water Penetration into Biomembrane

KAWAKAMI, Tomonori¹; AIZAWA, Keizo¹; HAYMET, Anthony D. J.²; OKAZAKI, Susumu (¹Tokyo Inst. Tech., ²Univ. Houston)

Free energy profile of water penetration into lipid bilayer has been evaluated based upon molecular dynamics calculations combined with thermodynamic integration method. The calculated profile for 25 arbitrarily chosen penetration paths shows that the free energy barrier height has a wide distribution, demonstrating a sort of selectivity of the path by water molecule. Structure of the path or structure of the surrounding lipid molecules was examined in order to extract a factor which determines the barrier height.

VIII-X-2 Molecular Dynamics Study of Mechanical Extension of Polyalanine by AFM Cantilever

IWAHASHI, Kensuke; MIKAMI, Taiji; MASUGATA, Kensuke¹; IKAI, Atsushi¹; OKAZAKI, Susumu

(¹Tokyo Inst. Tech.)

A series of molecular dynamics calculations have been performed mimicking the mechanical extension of α -helical polyalanine molecule in water on the AFM. Force profile has been evaluated as a function of extension. In an initial stage of the extension, $\sim 5\%$, the force was found to follow the Hooke's law up to about 140 pN. At the extension of about 10%, however, the restoring force diminishes, indicating the rupture of α -helix. Then, α -helix region and β -strand region separate from each other in one molecule. Further extension causes stepwise breakages of hydrogen bonds to give the wholly β -stranded polyalanine.

VIII-Y Theoretical Studies on Electronic Structure and Dynamics of Electronically Excited States

VIII-Y-1 Chemical Reactions in the O(¹D) + HCl System I. *Ab Initio* Global Potential Energy Surfaces for the 1¹A', 2¹A', and 1¹A'' States

NANBU, Shinkoh; KAMISAKA, Hideyuki¹; BIAN, Wensheng; AOYAGI, Mutsumi; TANAKA, Kiyoshi²; NAKAMURA, Hiroki
(¹GUAS; ²Hokkaido Univ.)

[*J. Theor. Comp. Chem.* in press]

New global *ab initio* potential energy surfaces (PES) are presented for the low-lying 1¹A', 2¹A', and 1¹A'' electronic states which are correlated to O(¹D) + HCl. These potential energy surfaces are computed by using the multi-reference configuration interaction method with the Davidson correction (MRCI + Q). The reference functions are constructed by the complete active space self-consistent field (CASSCF) calculations using the quadruple zeta + polarization basis set augmented with diffuse functions. The computations are carried out at about 5000 molecular conformations on each three-dimensional potential energy surface. The high accuracy of the computations is confirmed by a comparison with the available most accurate data for the ground state 1¹A'; thus the present work is the first report of the accurate potential energy surfaces for the two excited states. Three low-lying transition states on the excited surfaces, two (TS2 and TS4) on 1¹A'' and one (TS3) on 2¹A', are found. Since TS2 and TS3 are as low as 0.07 eV and 0.28 eV, respectively, and correlated to the OH(²Π) + Cl(²P) product, these excited surfaces are expected to play quite important roles in the reaction dynamics. Possible effects of non-adiabatic couplings among the three PESs are also briefly discussed, although the non-adiabatic couplings have not yet been estimated. The quantum reaction dynamics on these three PESs are discussed in the second and third accompanying paper.

In the present work, we have determined new global three *ab initio* potential energy surfaces accurately; and furthermore quantum wave packet dynamics calculations have been carried out to obtain the total reaction probabilities. The reaction probability for HCl(*v* = 0, *j* = 0) shows that the OH + Cl product channel *via* the 1¹A'' state should be opened at the lower collision energy than $E_{\text{coll}} = 0.529$ eV, while the channel *via* 2¹A' should be closed. Although there was the discrepancy between previous theoretical works and experimental results, it was explained by our works including the electronic excited states.

VIII-Y-2 Millimeter-Wave Spectroscopy of the Internal-Rotation Band of the He–HCN Complex and the Intermolecular Potential Energy Surface

HARADA, Kensuke¹; TANAKA, Keiichi¹; TANAKA, Takehiko¹; NANBU, Shinkoh; AOYAGI,

Mutsumi
(¹Kyusyu Univ.)

[*J. Chem. Phys.* in press]

Millimeter-wave absorption spectroscopy combined with a pulsed-jet expansion technique was applied to the measurement of the internal-rotation band of the He–HCN in the frequency region of 95–125 GHz. In total 13 rovibrational lines, split into nitrogen nuclear hyperfine structure, were observed for the fundamental internal-rotation band, *j* = 1–0. The observed transition frequencies were analyzed including their hyperfine splitting to yield an intermolecular potential energy surface, as improved from the one given by a coupled-cluster single double (triple) *ab initio* calculation. The surface obtained has a global minimum in the linear configuration (He··H–C–N) with a well depth of 30.2 cm⁻¹, and the saddle point located in the anti-linear configuration (H–C–N··He) is higher by 8.174 cm⁻¹ in energy than the global minimum. The distance R_m between the He atom and the center of mass of HCN along the minimum energy path shows a strong angular dependence; $R_m = 4.169$ Å and 4.040 Å in the linear and anti-linear forms, respectively, while it is 3.528 Å in a T-shaped configuration. In the first excited internal-rotation state (*j* = 1), levels with *l* less than 4 are bound but not for the one with *l* = 5, according to the energy level diagram calculated from the present potential energy surface, where *l* denotes the quantum number for the end-over-end rotation of the complex. The energy level diagram is consistent with the millimeter-wave observation, in which the $\Delta l = 0$ transitions with *l* = 0 ~ 4 were observed but not for those with *l* equal to or greater than 5. The band origin of the internal-rotation band, 98.70 GHz, as defined to be the same as the frequency of the *R*(0) transition, is larger by 11% than the *J* = 1–0 rotational transition frequency of the free HCN molecule.

VIII-Y-3 Determination of the Global Potential Energy Surfaces and Transition Wave Packet Dynamics for Polyatomic Systems

NANBU, Shinkoh; ISHIDA, Toshimasa¹; GRAY, Stephen K.²; GONZALEZ, Miguel³
(¹Shizuoka Univ.; ²Argonne Natl. Lab.; ³Univ. Barcelona)

Computational algorithm for the determination of the global potential energy surfaces of polyatomic systems are developed with using the interpolant moving least squares scheme, which was proposed by Ishida and Schatz [*Chem. Phys. Lett.* **314**, 369 (1999)]. In this scheme, any derivatives in quantum-chemical calculations are not required to construct the surface and in contrast with previously developed schemes based on Shepard interpolation alone. In our new algorithm, the molecular conformations are generated with the Monte

Carlo sampling, and then the *ab initio* calculations for all of the conformations are performed by parallel computing. Therefore, we have good advantage for computational time for the serial calculations. Application is made to the tetra-atomic systems, the $2\text{OH} \leftrightarrow \text{H}_2\text{O} + \text{O}$ reaction.

Regarding to the wave packet dynamics, we are also developing the program code based on the MPI-library to make a time-evolution of the wave packet for the tetra-atomic systems.

VIII-Y-4 *Ab Initio* Study of Conformers of *p*-tert-Butylcalix [4] Crown-6-Ether Complexed with Alkyl Ammonium Cations

CHOE, Jong-In¹; CHANG, Suk-Kyu¹; NANBU, Shinkoh
(¹Chung-Ang Univ.)

[*Bull. Korean Chem. Soc.* **23**, 891 (2001)]

The structures and energies of *p*-tert-butylcalix[4]-crown-6-ether (1) in various conformers and their alkyl ammonium complexes have been calculated by *ab initio* HF/6-31G quantum mechanics method. We have tried to obtain the relative affinity of partial-cone and 1,3-alternate conformers of 1 for alkyl ammonium guests by comparison with its cone-shaped analogue. We have also calculated the relative complexation efficiency of these host-guest complexes focusing on the binding sites of crown-6-ether moiety or benzene-rings pocket of the host molecule 1. These calculations revealed that the crown moiety has better complexation efficiency than upper rim part of calix[4]arene that is in similar trend to the cone-shaped complexes.

VIII-Y-5 *Ab Initio* Study of the Complexation Behavior of Calix[5]arene Derivative toward Alkyl Ammonium Cations

CHOE, Jong-In¹; CHANG, Suk-Kyu¹; MINAMINO, Satoshi; NANBU, Shinkoh
(¹Chung-Ang Univ.)

[*Bull. Korean Chem. Soc.* submitted]

The structures and complexation energies of penta-O-alkylated 1b and penta-O-tert-butyl ester 1e of *p*-tert-butylcalix[5]arene and its simplified structures (2b and 2e) toward a series of alkyl ammonium guests have been calculated by semi-empirical AM1 quantum mechanics method. For AM1 calculation, complexation efficiencies of the simplified host 2e are very similar to the values of host 1e. The complexes of simplified host 2e with alkyl ammonium ions have been also optimized by *ab initio* HF/6-31G quantum mechanics method. The calculated complexation efficiencies for 2e by *ab initio* method have been found to be bigger in magnitude than the values obtained by AM1 calculations for linear alkyl ammonium guests. Calculation results show that all of the calix [5] aryl derivatives investigated in this study have much better complexation ability toward ammonium cation without alkyl group over other alkyl ammonium guests. *Ab initio* calculations also well

duplicate the molecular discriminating behaviors of calyx [5] arene derivative 2e between butyl ammonium ions: *n*-BuNH₃⁺ > *iso*-BuNH₃⁺ > *sec*-BuNH₃⁺ > *tert*-BuNH₃⁺.

VIII-Y-6 Formation of HCl⁺(A²Σ⁺) and HBr⁺(A²Σ⁺) Resulting from He(2³S) Penning Ionization of HCl and HBr

TOKUE, Ikuo¹; TANAKA, Hiroyuki¹; YAMASAKI, Katsuyoshi¹; NANBU, Shinkoh
(¹Niigata Univ.)

[*J. Phys. Chem. A* **106**, 6068 (2002)]

He(2³S) Penning ionization of HCl and HBr leading to HCl⁺(A) and HBr⁺(A) has been studied optically by using a crossed-beam apparatus. The ratios of the vibrational population, P_v/P₁(v' = 2 and 3) of HCl⁺(A) and P₁/P₀ of HBr⁺(A), increase with the collision energy in the region of 120–200 meV. The rotational distributions of HCl⁺(A, v' = 0) and HBr⁺(A, v' = 0) can be represented by a double-Boltzmann distribution; the temperatures are 200 ± 50 and 700 ± 80 K for HCl⁺(A, v' = 0) and 250 ± 50 and 1200 ± 200 K for HBr⁺(A), and are nearly independent of the collision energy. The model potential surface for He*(Li) + HCl as the entrance channel is nearly isotropic and shows a shallow dip of about 20 meV, while the surface for He + HCl⁺(A) as the exit channel is anisotropic and shows a deep minimum of 250 meV in the He–H–Cl collinear direction. These results suggest that at least two processes contribute to formation of these ions; one is the direct Penning ionization and the other is the formation via a temporary complex [HeHCl(A)]⁺ by orbiting.

VIII-Y-7 Theoretical Study of Vibrational States for AINC/AICN

MINAMINO, Satoshi; NANBU, Shinkoh; AOYAGI, Mutsumi

The character of the low-lying electronic states of AINC strongly depends on the bond distance of Al-NC, because the covalent states are lying closely to the ionic states. Especially, due to the electronic ground state having the ionic character, the bending vibrational motion has a quite strong anharmonicity, and the motion is characterized as a large amplitude motion (LAM). Therefore, in general, the observed spectrum has the complicated vibronic structures and it is difficult to understand the molecular conformation having the LAM. In this study, we determined the global potential energy surfaces of the electronic ground state for the isomerization of AINC/AICN, and we elucidated the molecular structure of the complicated vibronic states by solving the exact Schrödinger equation for the nuclear motion.

VIII-Y-8 Boundary Expansion in Time-Dependent Nonadiabatic Problems

TAKAMI, Toshiya

Time-dependent nonadiabatic transitions were studied as an initial value problem in a finite parameter range. We introduced “boundary expansion” by expanding Schrödinger’s equation around end points of the parameter. We have shown that extra transitions emerge at the points, and are explained by the terms of the expansion. We have also shown that Berry’s superadiabatic base is naturally defined through the expansion. By the use of the superadiabatic base, we performed numerical analysis of multi-level non-adiabatic transitions in systems with a random matrix Hamiltonian.

VIII-Y-9 Optimal Control of Random Matrix Systems with a Parameter

TAKAMI, Toshiya; FUJISAKI, Hiroshi

We studied control of chaotic quantum systems by applying Optimal Control Theory (OCT) to random matrix Hamiltonian systems with a parameter. For simple two-state problems, we have shown that the optimized field obtained by OCT can be classified into several types: (i) oscillating one with a frequency which agrees with the energy split between the initial and the final state; (ii) one which mainly uses transition between diabatic states at an avoided crossing; (iii) one which can be seen as nonadiabatic transition, etc. Although the oscillating solution is always obtained even in many level systems if the final time is large enough, it is difficult to distinguish other types of solution in short time.

We have shown that the distribution of the optimized solutions for short time is affected by dynamical properties of the system. In particular, we examined influence of the strength of chaos or complexity of the system. We have also studied systems with banded random elements.

RESEARCH ACTIVITIES IX

Center for Integrative Bioscience

IX-A Molecular Mechanisms of Oxygen Activation by Heme Enzymes

By sharing a common prosthetic group, the heme enzymes such as cytochrome P450s, peroxidases, and catalases catalyze their own unique biological functions; monooxygenation, hydrogen peroxide dependent oxidation, and dismutation of hydrogen peroxide, respectively. Our efforts have been focused on the elucidation of the structure-biological function relationship of these heme enzymes by employing both enzymatic systems including mutants and their model systems.

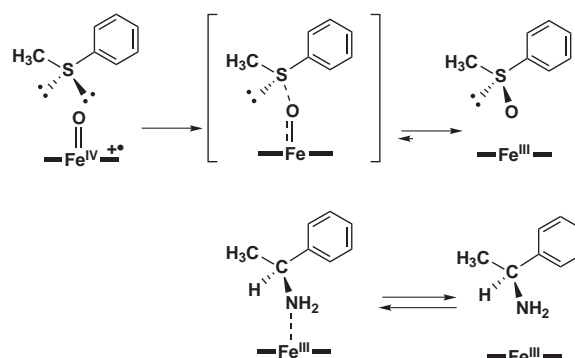
IX-A-1 Asymmetric Sulfoxidation and Amine Binding by H64D/V68A and H64D/V68S Mb: Mechanistic Insight into the Chiral Discrimination Step

KATO, Shigeru; YANG, Hui-jun; UENO, Takafumi; OZAKI, Shin-ichi¹; PHILLIPS, George N. Jr.²; FUKUZUMI, Shun-ichi³; WATANABE, Yoshihito

(¹Yamagata Univ.; ²Univ. Wisconsin; ³Osaka Univ.)

[*J. Am. Chem. Soc.* **124**, 8506 (2002)]

Myoglobin (Mb) is an oxygen transport hemoprotein that catalyzes a variety of oxidation including sulfoxidation and epoxidation in the presence of peroxides. We have recently shown that the distal histidine (His64) in sperm whale Mb is a critical residue in destabilizing a reactive intermediate, myoglobin compound I (Mb-I). The substitution of His-64 with Asp (H64D Mb) also gives Mb-I even by the reaction with H₂O₂ efficiently with the rate constant of $2.5 \times 10^4 \text{ M}^{-1}\text{s}^{-1}$. Due to the structural similarity of α -methylbenzylamine and methylphenylsulfoxide, we have examined enantioselective ligation of (*R*)- and (*S*)- α -methylbenzylamine to H64D/V68A and H64D/V68S Mbs in comparison with the sulfoxidation of thioanisole (Scheme 1). In contrast to the *R*-selective sulfoxidation by H64D/V68A and H64D/V68S, the *K* values of (*S*)- α -methylbenzylamine with H64D/V68A and H64D/V68S are 27-fold and 112-fold larger than those of the corresponding (*R*)-amine, respectively. In the case of H64D Mb, which affords almost racemic sulfoxide, however, the enantioselective binding is reversed, namely the *K* value of (*R*)-amine is about 4-fold larger than that for the (*S*) isomer.



In order to determine the chiral discrimination step in the amine binding, we have measured on rate (k_1) and off rate (k_{-1}) of amine binding to the Mb mutants by stopped-flow experiments. The on rates (k_1) of (*R*)- and (*S*)- α -methylbenzylamine to H64D/V68A and H64D/V68S are almost identical, $1.3 \times 10^4 \text{ M}^{-1}\text{s}^{-1}$ and $2.2\text{--}2.7 \times 10^4 \text{ M}^{-1}\text{s}^{-1}$, respectively. In contrast, a tremendous difference is seen for the off rate. This indicates that the chiral discrimination of the (*S*)-amine ligation over the (*R*)-amine by H64D/V68A and H64D/V68S is exclusively caused by a very small off rate of the (*S*)-amine relative to the (*R*)-amine, 1:27 for H64D/V68A and 1:92 for H64D/V68S. These selectivities would correspond to 93 and 98% ee for the amine binding, respectively. Thus, enantioselectivity in the sulfoxidation of thioanisole by H64D/V68A and H64D/V68S Mb was concluded to be determined by the off rate of sulfoxide.

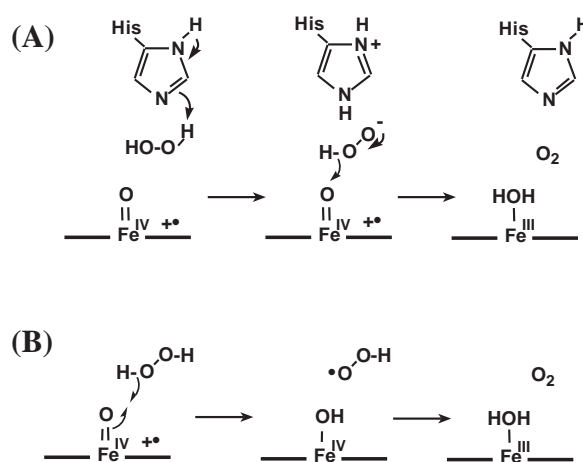
IX-A-2 Molecular Mechanism of the Catalase Reaction Studied by Myoglobin Mutants

KATO, Shigeru; UENO, Takafumi; FUKUZUMI, Shun-ichi¹; WATANABE, Yoshihito

(¹Osaka Univ.)

The catalase reaction has been studied in detail by using Mb mutants, whose compound I can be readily prepared by reaction with a nearly stoichiometric amount of *m*-chloroperbenzoic acid (*m*CPBA). Upon the addition of H₂O₂ to a Mb-I solution, Mb-I is reduced back to the ferric state without forming any intermediates. This reveals that Mb-I is capable of performing two-electron oxidation of H₂O₂ (catalatic reaction). GC-

MS analysis of the evolved O_2 from a 50:50 mixture of $H_2^{18}O_2/H_2^{16}O_2$ solution containing H64D or F43H/H64L shows two peaks for $^{18}O_2$ ($m/e = 36$) and $^{16}O_2$ ($m/e = 32$) but no indication of $^{16}O^{18}O$ ($m/e = 34$) formation. Deuterium isotope effects on rates of the catalytic reaction of Mb mutants and beef liver catalase (BLCase) suggest that the catalytic reactions of BLCase and F43H/H64L Mb proceed *via* an ionic mechanism, since the distal histidine is located at a proper position acting as a general acid-base catalyst in the ionic reaction to give a small isotope effect of less than 2.1. In contrast, other Mb mutants such as H64X (X: A, S, D) and L29H/H64L Mb oxidize H_2O_2 *via* a radical mechanism in which a hydrogen is abstracted by the ferryl species with very large isotope effects in a range of 10 to 29, due to the lack of the general acid-base catalyst. These two mechanisms are summarized in Scheme 1.



Scheme 1. Proposed mechanisms for the catalytic reaction. (A): ionic mechanism by utilizing a general acid-base catalyst. (B): Radical mechanism.

IX-B Model Studies of Non-Heme Proteins

Non-heme proteins play important roles in biological redox processes. Many reactions catalyzed by the non-heme enzymes are quite similar to those by hemoproteins. We are interested in the active intermediates responsible for oxidation and oxygenation by non-heme enzyme, especially the similarity and differences.

IX-B-1 Reactivity of Hydrogenperoxide Bound to a Mononuclear Non-Heme Iron Site

WADA, Akira¹; OGO, Seiji; NAGATOMO, Shigenori; KITAGAWA, Teizo; WATANABE, Yoshihito; JITSUKAWA, Koichiro¹; MASUDA, Hideki¹

(¹Nagoya Inst. Tech.)

[*Inorg. Chem.* **41**, 616 (2002)]

The first isolation and spectroscopic characterization of the mononuclear hydroperoxo-iron(III) complex $[Fe(H_2bppa)(OOH)]^{2+}$ (**1**) and the stoichiometric oxidation of substrates by the mononuclear iron-oxo intermediate generated by its decomposition have been described. The purple species (**1**) obtained from reaction of $[Fe(H_2bppa)(HCOO)](ClO_4)_2$ with H_2O_2 in acetone at $-50^\circ C$ gave characteristic UV-vis ($\lambda_{max} = 568$ nm, $\epsilon = 1200$ M⁻¹cm⁻¹), ESR ($g = 7.54, 5.78, \text{ and } 4.25, S = 5/2$), and ESI mass spectra (m/z 288.5 corresponding to the iron, $[Fe(bppa)(OOH)]^{2+}$), which revealed that **1** is a high-spin mononuclear iron(III) complex with a hydroperoxide in an end-on fashion. The resonance Raman spectrum of **1** in d_6 -acetone revealed two intense bands at 621 and 830 cm⁻¹, which shifted to 599 and 813 cm⁻¹, respectively, when reacted with ¹⁸O-labeled H_2O_2 . Reactions of the isolated $(bppa)Fe^{III}-OOH$ (**1**) with various substrate (single turnover oxidations) exhibited that the iron-oxo intermediate generated by decomposition of **1** is a nucleophilic species formulated as $[(H_2bppa)Fe^{III}-O\cdot]$.

IX-B-2 Synthesis, Structure, and Properties of A Novel Mononuclear Iron(III) Complex Containing Peroxocarbonate Ligand

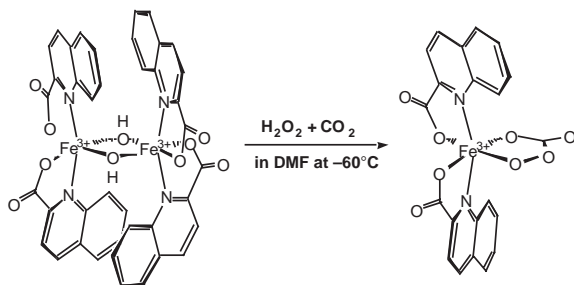
HASHIMOTO, Koji¹; NAGATOMO, Shigenori; FUJINAMI, Shuhei¹; FURUTACHI, Hideki¹; OGO, Seiji; SUZUKI, Masatatsu¹; UEHARA, Akira¹; MAEDA, Yonezo²; WATANABE, Yoshihito; KITAGAWA, Teizo

(¹Kanzawa Univ., ²Kyushu Univ.)

[*Angew. Chem. Int. Ed. Engl.* **41**, 1202 (2002)]

Mononuclear Peroxo iron(III) complexes have been proposed as a key intermediate in various oxidation reactions catalyzed by mononuclear non-heme iron enzymes and their functional model complexes. Various types of synthetic mononuclear iron(III) complexes having η^2 -peroxo, η^1 -hydroperoxo, and alkylperoxo ligand have been characterized by various spectroscopic studies. It has been shown that the structure, electronic structure, and reactivity of the peroxo complexes can be modified by the coordination environment around iron(III) center. Most of those peroxo-iron(III) complexes reported so far have nitrogen-rich coordination environments except for an edta complex. Thus it is of interest to investigate how the nature of the donor atoms and the stereochemistry of supporting ligands influence the formation, structure, and properties of such peroxo-iron(III) complexes. In this study, we have succeeded in synthesis of a mononuclear peroxocarbonate iron(III) complex with a carboxylate-rich coordination environment, $Ph_4P[Fe(qn)_2-(O_2C(O)O)] \cdot 1.5CH_3OH \cdot 0.5(CH_3)_2-$

NCHO (**1a**), derived from the reaction of a bis(μ -hydroxo)diiron(III) complex, $[\text{Fe}_2(\text{qn})_4(\text{OH})_2] \cdot 2\text{H}_2\text{O}$ (**2**) with H_2O_2 and CO_2 , where Hqn = quinaldic acid, which was characterized by X-ray, ESI-MS, EPR, UV-vis, and resonance Raman spectroscopic measurements (Scheme 1). This is the first example of a structurally characterized transition metal complex with a peroxocarbonate ligand and a mononuclear iron(III) complex having a peroxy group. We believe that the findings in this study provide an important basis for developing and expanding mononuclear iron(III) complexes having a peroxy group and are of interest to wide audience.



Scheme 1.

IX-B-3 Structural and Spectroscopic Features of a *cis* (Hydroxo)–Fe^{III}–(Carboxylato) Configuration as an Active Site Model for Lipoxigenases

OGO, Seiji¹; YAMAHARA, Ryo^{1,2}; ROACH, Mark

P.; SUENOBU, Tomoyoshi¹; AKI, Michihiko; OGURA, Takashi³; KITAGAWA, Teizo; MASUDA, Hideki²; FUKUZUMI, Shun-ichi¹; WATANABE, Yoshihito⁴

(¹Osaka Univ.; ²Nagoya Inst. Tech.; ³Univ. Tokyo; ⁴Nagoya Univ.)

[Inorg. Chem. in press]

In our preliminary communication (*Angew. Chem. Int. Ed. Engl.* **37**, 2102 (1998)), we have reported the first example of X-ray analysis of a mononuclear six-coordinate (hydroxo)iron(III) non-heme complex, $[\text{Fe}^{\text{III}}(\text{tnpa})(\text{OH})(\text{RCO}_2)]\text{ClO}_4$ {tnpa = tris(6-neopentylamino-2-pyridylmethyl)amine, **1**: $R = \text{C}_6\text{H}_5$ }, which has a characteristic *cis* (hydroxo)–Fe^{III}–(carboxylato) configuration that models the *cis* (hydroxo)–Fe^{III}–(carboxylato) moiety of the proposed (hydroxo)iron(III) species of lipoxigenases. In this full account, we report structural and spectroscopic characterization of the *cis* (hydroxo)–Fe^{III}–(carboxylato) configuration by extending the model complexes from **1** to $[\text{Fe}^{\text{III}}(\text{tnpa})(\text{OH})(\text{RCO}_2)]\text{ClO}_4$ (**2**: $R = \text{CH}_3$ and **3**: $R = \text{H}$) whose *cis* (hydroxo)–Fe^{III}–(carboxylato) moieties are isotopically labeled by $^{18}\text{OH}^-$, $^{16}\text{OD}^-$, $^{18}\text{OD}^-$, $^{12}\text{CH}_3^{12}\text{C}^{18}\text{O}_2^-$, $^{12}\text{CH}_3^{13}\text{C}^{16}\text{O}_2^-$, $^{13}\text{CH}_3^{12}\text{C}^{16}\text{O}_2^-$, $^{13}\text{CH}_3^{13}\text{C}^{16}\text{O}_2^-$, and $\text{H}^{13}\text{C}^{16}\text{O}_2^-$. Complexes **1**, **2**, and **3** are characterized by X-ray analysis, IR, EPR, and UV/Vis spectroscopy, and electrospray ionization mass spectrometry (ESI-MS).

IX-C Aqueous Organometallic Chemistry

The chemistry in aqueous media is presently undergoing very rapid growth because of many potential advantages such as alleviation of environmental problems associated with the use of organic solvents, industrial applications (*e.g.*, introduction of new biphasic processes), and reaction-specific pH selectivity. We have investigated pH-dependent reactions in aqueous media.

IX-C-1 pH-Dependent H₂-Activation Cycle Coupled to Reduction of Nitrate Ion by Cp*Ir Complexes

OGO, Seiji; NAKAI, Hidetaka; WATANABE, Yoshihito

[*J. Am. Chem. Soc.* **124**, 597 (2002)]

This paper reports a pH-dependent H₂-activation promoted by Cp*Ir complexes {Cp* = $\eta^5\text{-C}_5(\text{CH}_3)_5$ }. In a pH range of about 1 to 4, an aqueous HNO₃ solution of $[\text{Cp}^*\text{Ir}^{\text{III}}(\text{H}_2\text{O})_3]^{2+}$ (**1**) reacts with three equivalents of H₂ to yield a solution of $[(\text{Cp}^*\text{Ir}^{\text{III}})_2(\mu\text{-H})_3]^+$ (**2**) as a result of heterolytic H₂-activation. The hydrido ligands of **2** display protonic behavior and undergo H/D exchange with D⁺. Complex **2** is insoluble in a pH range of about –0.2 (1.6 M HNO₃/H₂O) to –0.8 (6.3 M HNO₃/H₂O). At pH –1 (10 M HNO₃/H₂O), a powder of **2** drastically reacts with HNO₃ to give a solution of

$[\text{Cp}^*\text{Ir}^{\text{III}}(\text{NO}_3)_2]$ (**3**) with evolution of H₂, NO, and NO₂ gases. D-labeling experiments show that the evolved H₂ is derived from the hydrido ligands of **2**. These results suggest that oxidation of the hydrido ligands of **2** couples to reduction of NO₃[–]. To complete the reaction cycle, complex **3** is transformed into **1** by increasing the pH of the solution from –1 to 1. Therefore, we are able to repeat the reaction cycle using **1**, H₂, and pH gradient between 1 and –1. A conceivable mechanism for the H₂-activation cycle with reduction of NO₃[–] is proposed.

IX-C-2 pH-Dependent Cross-Coupling Reactions of Water-Soluble Organic Halides with Organoboron Compounds Catalyzed by an Organometallic Aqua Complex $[(\text{SCS})\text{Pd}^{\text{II}}(\text{H}_2\text{O})]^+$ {SCS = C₆H₃-2,6-(CH-SBu^t)₂}

NAKAI, Hidetaka; OGO, Seiji; WATANABE, Yoshihito

[*Organometallics* **21**, 1674 (2002)]

This paper reports on the first example of pH-dependent cross-coupling reactions of water-soluble organic halides {3-*X*(C₆H₄)CO₂H, where *X* = Cl, Br, and I} with organoboron compounds {PhB(OH)₂ and Ph₄BNa} to form 3-Ph(C₆H₄)CO₂H, catalyzed by a mononuclear organometallic aqua complex [(SCS)Pd^{II}(H₂O)]₂(SO₄) {[**1**]₂·(SO₄), SCS = C₆H₃-2,6-(CH₂SBU¹)₂} in basic media (8 < pH < 13, NaHCO₃/NaOH buffers). The structure of **1**·(PF₆) was unequivocally determined by X-ray analysis. The reactions show unique pH-selectivity depending upon the organoboron compounds, *i.e.*, the rate of the reactions with PhB(OH)₂ shows a sharp maximum around pH 10, though the rate of the reactions with Ph₄BNa shows a flat maximum in a pH range of about 8 to 11. The pH-dependence is discussed on the basis of the p*K*_a values of [**1**]₂·(SO₄) and PhB(OH)₂.

IX-C-3 pH-Dependent Transfer Hydrogenation of Ketones with HCOONa as a Hydrogen Donor Promoted by (η⁶-C₆Me₆)Ru Complexes

OGO, Seiji¹; ABURA, Tsutomu; WATANABE, Yoshihito²

(¹Osaka Univ.; ²Nagoya Univ.)

[*Organometallics* **21**, 2964 (2002)]

The paper reports on the development of a new class of water-soluble organometallic catalysts for pH-dependent transfer hydrogenation. An organometallic aqua complex [(η⁶-C₆Me₆)Ru^{II}(bpy)(H₂O)]²⁺ (**1**, bpy = 2,2'-bipyridine) acts as a catalyst precursor for pH-dependent transfer hydrogenation of water-soluble and -insoluble ketones with HCOONa as a hydrogen donor in water and in biphasic media. Irrespective of the solubility of the ketones toward water, the rate of the transfer hydrogenation shows a sharp maximum around pH 4.0 (in the case of biphasic media, the pH value of the aqueous phase is adopted). In the absence of the reducible ketones, as a function of pH, complex **1** reacts with HCOONa to provide a formate complex [(η⁶-C₆Me₆)Ru^{II}(bpy)(HCOO)]⁺ (**2**) as an intermediate of β-hydrogen elimination and a hydrido complex [(η⁶-C₆Me₆)Ru^{II}(bpy)H]⁺ (**3**) as the catalyst for the transfer hydrogenation. The structures of **1**(PF₆)₂, **2**(HCOO)·HCOOH, and of [(η⁶-C₆Me₆)Ru^{II}(H₂O)₃]SO₄·3H₂O {**4**(SO₄)·3H₂O}, the starting material for the synthesis of **1**, were unequivocally determined by X-ray analysis.

IX-D Single-Molecule Physiology

A single molecule of protein (or RNA) enzyme acts as a machine which carries out a unique function in cellular activities. To elucidate the mechanisms of various molecular machines, we need to observe closely the behavior of individual molecules, because these machines, unlike man-made machines, operate stochastically and thus cannot be synchronized with each other. By attaching a tag that is huge compared to the size of a molecular machine, or a small tag such as a single fluorophore, we have been able to image the individual behaviors in real time under an optical microscope. Stepping rotation of the central subunit in a single molecule of F_1 -ATPase has been videotaped, and now we can discuss its detailed mechanism. RNA polymerase has been shown to be a helical motor that rotates DNA during transcription. Myosin V is another helical motor that moves as a left-handed spiral on the right-handed actin helix. Single-molecule physiology is an emerging field of science in which one closely watches individual, 'live' protein/RNA machines at work and examines their responses to external perturbations such as pulling and twisting. I personally believe that molecular machines operate by changing their conformations. Thus, detection of the conformational changes during function is our prime goal. Complementary use of huge and small tags is our major strategy towards this end.
<http://www.k2.ims.ac.jp/>

IX-D-1 Myosin V Is a Left-Handed Spiral Motor on the Right-Handed Actin Helix

ALI, Md. Yusuf^{1,2}; UEMURA, Sotaro³; ADACHI, Kengo¹; ITOH, Hiroyasu^{1,4}; KINOSITA, Kazuhiko, Jr.^{1,2}; ISHIWATA, Shin'ichi^{1,3}
 (¹CREST Team 13; ²Keio Univ.; ³Waseda Univ.; ⁴Hamamatsu Photonics)

[*Nature Struct. Biol.* **9**, 464 (2002)]

Myosin V is a two-headed, actin-based molecular motor implicated in organelle transport. Previously, a single myosin V molecule has been shown to move processively along an actin filament in discrete ~ 36 nm steps. However, 36 nm is the helical repeat length of actin, and the geometry of the previous experiments may have forced the heads to bind to, or halt at, sites on one side of actin that are separated by 36 nm. To observe unconstrained motion, we suspended an actin filament in solution and attached a single myosin V molecule carrying a bead duplex. The duplex moved as a left-handed spiral around the filament, disregarding the right-handed actin helix. Our results indicate a stepwise walking mechanism in which myosin V positions and orients the unbound head such that the head will land at the 11th or 13th actin subunit on the opposing strand of the actin double helix.

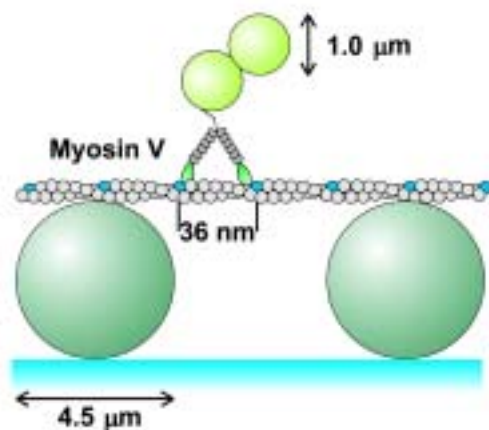


Figure 1. Experimental system for the observation of unconstrained movement of a single molecule of myosin V along an actin filament.

IX-D-2 Pause and Rotation of F_1 -ATPase during Catalysis

HIRONO-HARA, Yoko¹; NOJI, Hiroyuki^{2,3,4}; NISHIMURA, Masaya⁴; MUNAYUKI, Eiro¹; HARA, Kiyotaka Y.¹; YASUDA, Ryohei³; KINOSITA, Kazuhiko, Jr.^{3,6}; YOSHIDA, Masasuke^{1,3,5}
 (¹Tokyo Inst. Tech.; ²PRESTO; ³CREST Team 13; ⁴Univ. Tokyo; ⁵ERATO; ⁶Keio Univ.)

[*Proc. Natl. Acad. Sci. U.S.A.* **98**, 13649 (2001)]

F_1 -ATPase is a rotary motor enzyme in which a single ATP molecule drives a 120° rotation of the central γ subunit relative to the surrounding $\alpha_3\beta_3$ ring. Here, we show that the rotation of F_1 -ATPase spontaneously lapses into long (≈ 30 s) pauses during steady-state catalysis. The effects of ADP-Mg and mutation on the pauses, as well as kinetic comparison with bulk-phase catalysis, strongly indicate that the paused enzyme corresponds to the inactive state of F_1 -ATPase previously known as the ADP-Mg inhibited form in which F_1 -ATPase fails to release ADP-Mg from catalytic sites. The pausing position of the γ subunit deviates from the ATP-waiting position and is most likely the recently found intermediate 90° position.

IX-D-3 F_1 -ATPase Changes its Conformations upon Phosphate Release

MASAIKE, Tomoko¹; MUNAYUKI, Eiro¹; NOJI, Hiroyuki^{2,3}; KINOSITA, Kazuhiko, Jr.⁴; YOSHIDA, Masasuke^{1,4,5}
 (¹Tokyo Inst. Tech.; ²PRESTO; ³Univ. Tokyo; ⁴CREST Team 13; ⁵ERATO)

[*J. Biol. Chem.* **277**, 21643 (2002)]

Motor proteins, myosin, and kinesin have γ -phosphate sensors in the switch II loop that play key roles in

conformational changes that support motility. Here we report that a rotary motor, F₁-ATPase, also changes its conformations upon phosphate release. The tryptophan mutation was introduced into Arg-333 in the β subunit of F₁-ATPase from thermophilic *Bacillus* PS3 as a probe of conformational changes. This residue interacts with the switch II loop (residues 308–315) of the β subunit in a nucleotide-bound conformation. The addition of ATP to the mutant F₁ subcomplex $\alpha_3\beta$ (R333W)₃ γ caused transient increase and subsequent decay of the Trp fluorescence. The increase was caused by conformational changes on ATP binding. The rate of decay agreed well with that of phosphate release monitored by phosphate-binding protein assays. This is the first evidence that the β subunit changes its conformation upon phosphate release, which may share a common mechanism of exerting motility with other motor proteins.

IX-E Bioinorganic Chemistry of Heme-Based Sensor Proteins

Heme-based sensor proteins are a newly recognized class of heme proteins, in which the heme acts as a sensor of gaseous effector molecules such as O₂, NO, and CO. Our research interests focus on the CO-sensing transcriptional activator CooA and the O₂-sensing signal transducer HemAT. We have elucidated the structure and function relationships of CooA and HemAT by mutagenesis and some spectroscopic studies.

IX-E-1 Ligand-Switching Intermediates for the CO-Sensing Transcriptional Activator CooA Measured by Pulse Radiolysis

NAKAJIMA, Hiroshi¹; NAKAGAWA, Emi¹;
KOBAYASHI, Kazuo²; TAGAWA, Sei-ichi²;
AONO, Shigetoshi¹

(¹Japan Adv. Inst. Sci. Tech.; ²Osaka Univ.)

[*J. Biol. Chem.* **276**, 37895 (2001)]

CooA is a heme-containing and CO-sensing transcriptional activator whose activity is regulated by CO. The protoheme that acts as a CO sensor in CooA shows unique properties for its coordination structure. The Cys⁷⁵ axial ligand of the ferric heme is replaced by His⁷⁷ upon the reduction of the heme iron, and *vice versa*. In this work, the ligand-switching process induced by the reduction of the heme was investigated by the technique of pulse radiolysis. Hydrated electron reduced the heme iron in ferric CooA within 1 μs to form the first intermediate with the Soret peak at 440 nm, suggesting that a six-coordinated ferrous heme with a thiolate axial ligand was formed initially. The first intermediate was converted into the second intermediate with the time constant of 40 μs ($k = 2.5 \times 10^4 \text{ s}^{-1}$). In the second intermediate, the thiolate from Cys⁷⁵ was thought to be protonated and/or the Fe–S bond was thought to be elongated. The second intermediate was converted into the final reduced form with the time constant of 2.9 ms ($k = 3.5 \times 10^2 \text{ s}^{-1}$) for wild-type CooA. The ligand exchange between Cys⁷⁵ and His⁷⁷ took place during the conversion of the second intermediate into the final reduced form.

IX-E-2 Conformational Dynamics of the Transcriptional Regulator CooA Protein Studied by Subpicosecond Mid-Infrared Vibrational Spectroscopy

RUBTSOV, Igor V.¹; ZHANG, Tieqiao¹;
NAKAJIMA, Hiroshi¹; AONO, Shigetoshi¹;
RUBTSOV, Grigori I.²; KUMAZAKI, Shigeichi¹;
YOSHIHARA, Keitaro¹

(¹Japan Adv. Inst. Sci. Tech.; ²Lomonosov Moscow State Univ.)

[*J. Am. Chem. Soc.* **123**, 10056 (2001)]

CooA, which is a transcriptional regulator heme protein allosterically triggered by CO, is studied by femtosecond visible-pump mid-IR-probe spectroscopy. Transient bleaching upon excitation of the heme in the

Soret band is detected at approximately 1979 cm⁻¹, which is the absorption region of the CO bound to the heme. The bleach signal shows a nonexponential decay with time constants of 56 and 290 ps, caused by the rebinding of the CO to the heme. About 98% of dissociated CO recombines geminately. The geminate recombination rate in CooA is significantly faster than those in myoglobin and hemoglobin. The angle of the bound CO with respect to the porphyrin plane is calculated to be about 78 degrees on the basis of the anisotropy measurements. A shift of the bleached mid-IR spectrum of the bound CO is detected and has a characteristic time of 160 ps. It is suggested that the spectral shift is caused by a difference in the frequency of the bound CO in different protein conformations, particularly in an active conformation and in an intermediate one, which is on the way toward an inactive conformation. Thus, the biologically relevant conformation change in CooA was traced. Possible assignment of the observed conformation change is discussed.

IX-E-3 Resonance Raman and Ligand Binding Studies of the Oxygen Sensing Signal Transducer Protein HemAT from *Bacillus subtilis*

AONO, Shigetoshi¹; KATO, Toshiyuki¹; MATSUKI, Mayumi¹; NAKAJIMA, Hiroshi¹; OHTA, Takehiro;
UCHIDA, Takeshi; KITAGAWA, Teizo

(¹Japan Adv. Inst. Sci. Tech.)

[*J. Biol. Chem.* **277**, 13528 (2002)]

HemAT-Bs is a heme-containing signal transducer protein responsible for aerotaxis of *Bacillus subtilis*. The recombinant HemAT-Bs expressed in *E. coli* was purified as the oxy form in which oxygen was bound to the ferrous heme. Oxygen binding and dissociation rate constants were determined to be $k_{\text{on}} = 32 \mu\text{M}^{-1}\text{s}^{-1}$ and $k_{\text{off}} = 23 \text{ s}^{-1}$, respectively, revealing that HemAT-Bs has a moderate oxygen affinity similar to that of sperm whale Mb. The rate constant for autoxidation at 37 °C was 0.06 h⁻¹, which is also close to that of Mb. Although the electronic absorption spectra of HemAT-Bs were similar to those of Mb, HemAT-Bs showed some unique characteristics in its resonance Raman spectra. Oxygen-bound HemAT-Bs gave the $\nu(\text{Fe}-\text{O}_2)$ band at a noticeably low frequency (560 cm⁻¹), which suggests a unique hydrogen bonding between a distal amino acid residue and the proximal atom of the bound oxygen molecule. Deoxy HemAT-Bs gave the $\nu_{\text{Fe}-\text{His}}$ band at a higher frequency (225 cm⁻¹) than those of ordinary His-coordinated deoxy heme proteins. CO-bound HemAT-

Bs gave the $\nu(\text{Fe-CO})$ and $\nu(\text{C-O})$ bands at 494 and 1964 cm^{-1} , respectively, which fall on the same $\nu(\text{C-O})$ vs $\nu(\text{Fe-CO})$ correlation line as that of Mb. Based on these results, the structural and functional properties of HemAT-Bs are discussed.

IX-F Electronic Structure and Reactivity of Active Sites of Metalloproteins

Metalloproteins are a class of biologically important macromolecules that have various functions such as oxygen transport, electron transfer, oxidation, and oxygenation. These diverse functions of metalloproteins have been thought to depend on the ligands from amino acids, coordination structures, and protein structures in immediate vicinity of metal ions. In this project, we are studying the relationship between the structures of the metal active sites and functions of metalloproteins.

IX-F-1 Trigonal Bipyramidal Ferric Aqua Complex with Sterically Hindered Salen Ligand as a Model for Active Site of Protocatechuate 3,4-Dioxygenase

FUJII, Hiroshi; FUNAHASHI, Yasuhiro

[*Angew. Chem. Int. Ed. Engl.* in press]

Protocatechurate 3,4-dioxygenase (3,4-PCD) has been found in soil bacteria and is known to play a role in degrading aromatic molecules in nature. The enzyme is classified as an intradiol dioxygenase and cleaves catechol analogues bound to the iron(III) site into aliphatic products with incorporation of both atoms of molecular oxygen. It has been proposed that the enzyme does not activate an iron-bound oxygen molecule, but rather induces an iron-bound catecholate to react with O₂. Therefore, knowledge of the structure and electronic state of the iron site is essential to understanding the unique reaction of 3,4-PCD. A previous crystal structure analysis of 3,4-PCD from *Pseudomonas putida* revealed a distorted trigonal-bipyramidal ferric iron center with four endogenous protein ligands (Tyr 408, Tyr 447, His 460, and His 462) and a solvent-derived water molecule (see Figure 2). To understand the structure-function relationship of 3,4-PCD, attempts have been made over several decades to prepare inorganic model complexes of 3,4-PCD. However, no iron(III) complex that reproduces the active site of 3,4-PCD has been characterized. We report here the first example of a distorted trigonal-bipyramidal ferric aqua complex with a sterically hindered salen ligand that not only duplicates the active site but also mimics the spectral characteristics of 3,4-PCD.

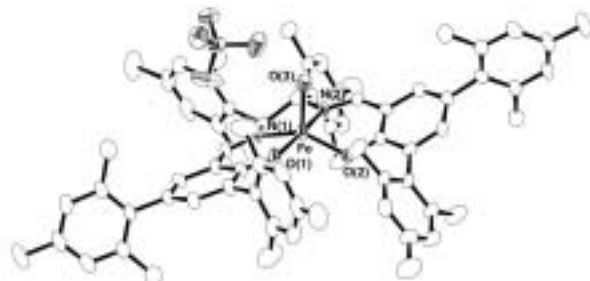


Figure 1. Structure of 3,4-PCD active site model complex prepared in this project.

IX-F-2 ¹³C-NMR Signal Detection of Iron Bound Cyanide Ions in Ferric Cyanide Complexes of Heme Proteins

FUJII, Hiroshi

[*J. Am. Chem. Soc.* **124**, 5936 (2002)]

Small molecule axial ligands potentially can serve as useful NMR probes for characterization of environment and electronic structure of prosthetic group in heme protein. In this regard, the diamagnetic ferrous states have been examined thoroughly because of easy signal detection from iron bound small molecule. The ¹³C-NMR signal of ¹³CO form of heme protein proves to be sensitive to the nature of the trans amino acid ligand. For the paramagnetic ferric state, cyanide ion would appear to have the greatest potential because of its extremely high affinity to ferric heme iron center. ¹⁵N-NMR signals of the iron bound C¹⁵N have been detected in a far-downfield region for both iron(III) porphyrin model complexes and heme proteins. However, the ¹⁵N-NMR spectroscopy remains ambiguity as a NMR probe since the ¹⁵N-NMR shift reflects the nature of both hydrogen bond in the distal side and amino acid ligand in the proximal side. On the other hand, ¹³C-NMR spectroscopy of the iron bound ¹³CN has been investigated in less detail. Although ¹³C-NMR signals of the iron bound ¹³CN are detectable in a far-upfield region (~ -2500 ppm from TMS) for bis-cyanide iron(III) porphyrin model complexes, extreme line-broadening of the signal seemed to preclude the signal detection in heme proteins and a resonance of the iron bound ¹³CN for ferric heme protein has not yet been located. During a more extensive ¹³C-NMR study, we found the ¹³C-NMR signals of the iron bound ¹³CN of ferric cyanide complexes of heme proteins and its model complexes at an unexpectedly large upfield region (~ -4000 ppm from TMS). Here, we report the first detection of ¹³C-NMR signal of the iron bound ¹³CN in heme proteins such as sperm whale myoglobin(Mb), human hemoglobin(Hb), horse heart cytochrome *c*(Cyt-*c*), and horseradish peroxidase(HRP). This study shows that the ¹³C-NMR spectroscopy of the iron bound ¹³CN provides a probe for studying nature of the proximal ligand in ferric heme protein.

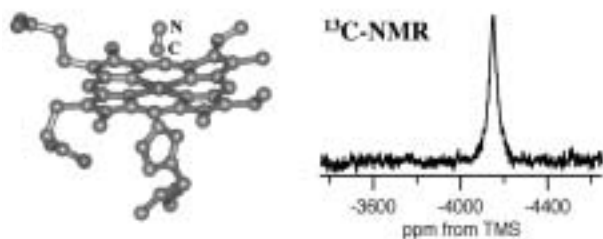


Figure 1. Active site structure of cyanide form of ferric heme protein and its ^{13}C -NMR spectrum.

IX-G Molecular Mechanism of Heme Degradation and Oxygen Activation by Heme Oxygenase

Heme oxygenase (HO), an amphipathic microsomal proteins, catalyzes the regiospecific oxidative degradation of iron protoporphyrinIX (heme) to biliverdinIX α , carbon monoxide, and iron in the presence of NADPH-cytochrome P-450 reductase, which functions as an electron donor. Heme oxygenase reaction is the biosynthesis processes of bile pigments and CO, which is a possible physiological messenger. Recent development in the bacterial expression of a soluble form of heme oxygenase has made it possible to prepare in the large quantities for structural studies. In this project, we are studying the molecular mechanism of heme degradation and the oxygen activation by heme oxygenase using various spectroscopic methods.

IX-G-1 Catalytic Mechanism of Heme Oxygenase through EPR and ENDOR of Cryoreduced Oxy-Heme Oxygenase and Asp 140 Mutants

DAVYDOV, Roman¹; KOFMAN, Viktoria¹; FUJII, Hiroshi; YOSHIDA, Tadashi²; IKEDA-SAITO, Masao³; HOFFMAN, M. Brian¹
(¹Uni. Northweatern; ²Yamagata Univ.; ³Tohoku Univ.)

annealing of wild-type oxy-HO and D140A, F mutants.

[*J. Am. Chem. Soc.* **124**, 1798 (2002)]

Heme oxygenase (HO) catalyzes the O₂- and NADPH-cytochrome P450 reductase-dependent conversion of heme to biliverdin and CO through a process in which the heme participates both as prosthetic group and substrate. It was proposed that the first mono-oxygenation step of HO catalysis is the conversion of the heme to a-meso-hydroxyheme, through a process in which an electron provided by NADPH-cytochrome P450 reductase reduces the first heme to the ferrous state and molecular of dioxygen binds to form a metastable O₂-bound complex, which then is reduced by a second electron to generate hydroperoxy ferric-HO. It was further thought that the hydroperoxy-ferric HO is the reactive hydroxylating species, rather than a high-valent ferryl active intermediate as in the case of cytochrome P450cam. However, neither the putative hydroperoxy-ferric-HO intermediate nor the a-meso-hydroxyheme product had been detected during physiological HO catalysis until our recent EPR and ENDOR study of oxy-ferrous HO cryoreduced at 77 K. In the present study we have generated a detailed reaction cycles for the first mono-oxygenation step of HO catalysis. We employed EPR and ¹H, ¹⁴N ENDOR spectroscopies to characterize the intermediates generated by 77 K radiolytic cryoreduction and subsequent

IX-H Biomolecular Science

Elucidation of a structure-function relationship of metalloproteins is a current subject of this group. The primary technique used for this project is the stationary and time-resolved resonance Raman spectroscopy excited by visible and UV lasers. The main themes that we want to explore are (1) mechanism of oxygen activation by enzymes, (2) mechanism of active proton translocation and its coupling with electron transfer, (3) coupling mechanism of proton- and electron transfers by quinones in photosynthetic reaction center, (4) higher order protein structures and their dynamics, and (5) reactions of biological NO. In category (1), we have examined a variety of terminal oxidases, cytochrome P450s, and peroxidases, and also treated their enzymatic reaction intermediates by using the mixed flow transient Raman apparatus and the Raman/absorption simultaneous measurement device. For (2) the third generation UV resonance Raman (UVR) spectrometer was constructed and we are going to apply it to a giant protein like cytochrome *c* oxidase. More recently, we succeeded in pursuing protein folding of apomyoglobin by combining UV time-resolved Raman and rapid mixing device. In (3) we succeeded in observing RR spectra of quinones A and B in bacterial photosynthetic reaction centers for the first time, but we have focused our attention on detecting tyrosine radical for the P intermediate of terminal oxidases. Some positive evidence was obtained for cytochrome *bo*. For (4) we developed a novel technique for UV resonance Raman measurements based on the combination of the first/second order dispersions of gratings and applied it successfully to 235-nm excited RR spectra of several proteins including mutant hemoglobins and myoglobins. Nowadays we can carry out time-resolved UVR experiments with nanosecond resolution to discuss protein dynamics. With the newly developed third generation UV Raman spectrometer, we have succeeded in isolating the spectrum of tyrosinate in ferric Hb M Iwate, which was protonated in the ferrous state, and the deprotonated state of Tyr244 of bovine cytochrome *c* oxidase. As a model of Tyr244, an imidazole-bound *para*-cresol was synthesized and its UV resonance Raman was investigated. For (5) we purified soluble guanylate cyclase from bovine lung and observed its RR spectra. To further investigate it, we are developing an expression system of this protein.

IX-H-1 Stationary and Time-Resolved Resonance Raman Spectra of His77 and Met95 Mutants of the Isolated Heme Domain of a Direct Oxygen Sensor from *E. coli*

SATO, Akira¹; SASAKURA, Yukie²; SUGIYAMA, Shunpei²; SAGAMI, Ikuko²; SHIMIZU, Toru²; MIZUTANI, Yasuhisa³; KITAGAWA, Teizo
(¹GUAS; ²Tohoku Univ.; ³Kobe Univ.)

[*J. Biol. Chem.* **277**, 32650 (2002)]

The heme environments of Met95 and His77 mutants of the isolated heme-bound PAS domain (*Ec* DOS PAS) of a direct oxygen sensing protein from *E. coli* (*Ec* Dos) were investigated with resonance Raman (RR) spectroscopy and compared to the wild type enzyme (WT). The RR spectra of both the reduced and oxidized WT enzyme were characteristic of six-coordinated low-spin heme complexes from pH 4 to 10. The time-resolved RR spectra of the photo-dissociated CO-WT complex had an Fe-His stretching band ($\nu_{\text{Fe-His}}$) at 214 cm^{-1} , and the $\nu_{\text{Fe-CO}}$ vs ν_{CO} plot of CO-WT *Ec* DOS PAS fell on the line of His-coordinated heme proteins. The photo-dissociated CO-His77Ala mutant complex did not yield the $\nu_{\text{Fe-His}}$ band but gave a $\nu_{\text{Fe-Im}}$ band in the presence of imidazole. The RR spectrum of the oxidized Met95Ala mutant was that of a six-coordinated low-spin complex, *i.e.* the same as that of the WT enzyme, whereas the reduced mutant appeared to contain a five-coordinated heme complex. Taken together, we suggest that the heme of the reduced WT enzyme is coordinated by His77 and Met95, and that Met95 is displaced by CO and O₂. Presumably, the protein conformational change that occurs on exchange of an unknown ligand for Met95 following heme reduction, may lead to activation of the phosphodi-

esterase domain of *Ec* Dos.

IX-H-2 Resonance Raman Studies on Xanthine Oxidase: Observation of the Mo^{VI}-Ligand Vibration

MAITI, Nakul C.¹; OKAMOTO, Ken²; NISHINO, Takeshi²; TOMITA, Takeshi³; KITAGAWA, Teizo
(¹CIB and Case Western Reserve Univ.; ²Nippon Medical School; ³CIB and Tohoku Univ.)

[*J. Biol. Inorg. Chem.* in press]

Resonance Raman spectra were investigated for the sulfo- and desulfo-forms of cow's milk xanthine oxidase with various visible excitation lines between 400 and 650 nm, and the Mo^{VI}-ligand vibrations were observed for the first time. The Mo^{VI}=S stretch was identified at 474 and 462 cm^{-1} for the ³²S and ³⁴S-sulfo-forms, respectively, but was absent in the reduced state and in the desulfo form. The Mo^{VI}=O stretch was weakly observed at 899 cm^{-1} for the sulfo-form and shifted to 892 cm^{-1} with very weak intensity for the dioxo desulfo-form. In measurements of an excitation profile, the two bands at 474 and 899 cm^{-1} showed maximum intensity at similar excitation wavelengths, suggesting that the Raman intensity of the metal-ligand modes is owed to the Mo^{VI} ← S CT transition, and that this is the origin of the intrinsically weak features of the Mo^{VI}-ligand Raman bands. When the sulfo-form was regenerated from the desulfo-form, the 899 cm^{-1} band reappeared. However, the band at 899 cm^{-1} showed no frequency shift when regeneration was conducted in H₂¹⁸O, or after several turnovers in the presence of xanthine in H₂¹⁸O. When the sulfo-form was reduced and reoxidized in H₂¹⁸O buffer, the 899 cm^{-1} band reappeared without any frequency shift. These observa-

tions suggest that the oxo oxygen in the Mo center of xanthine oxidase is not labile. Low-frequency vibrations of the Mo-center were observed together with those of the Fe₂S₂ center with some overlaps, while FAD modes were observed clearly. The absence of dithiolene modes in XO is in contrast to the Mo^V-centers of DMSO reductase and sulfite oxidase.

IX-H-3 Changes in the Abnormal α -Subunit upon CO-Binding to the Normal β -Subunit of Hb M Boston: Resonance Raman, EPR, and CD Study

NAGATOMO, Shigenori; JIN, Yayoi¹; NAGAI, Masako¹; HORI, Hiroshi²; KITAGAWA, Teizo (¹Kanazawa Univ.; ²Osaka Univ.)

[*Biophys. Chem.* **98**, 217 (2002)]

Heme-heme interaction in Hb M Boston (His α 58 \rightarrow Tyr) was investigated with visible and UV resonance Raman (RR), EPR, and CD spectroscopies. Although Hb M Boston has been believed to be frozen in the *T* quaternary state, oxygen binding exhibited appreciable cooperativity ($n = 1.4$) and the near-UV CD spectrum indicated weakening of the *T* marker at pH 9.0. Binding of CO to the normal β subunit gave no change in the EPR and visible Raman spectra of the abnormal α subunit at pH 7.5, but it caused an increase of EPR rhombicity and significant changes in the Raman coordination markers as well as the Fe(III)-tyrosine related bands of the α subunit at pH 9.0. The UVRR spectra indicated appreciable changes of Trp but not of Tyr upon CO binding to the β subunit at pH 9.0. Therefore, we conclude that the ligand binding to the β heme induces quaternary structure change at pH 9.0 and is communicated to the α heme presumably through His β 92 \rightarrow Trp β 37 \rightarrow His α 87.

IX-H-4 Coordination Geometry of Cu-Porphyrin in Cu(II)-Fe(II) Hybrid Hemoglobins Studied by Q-Band EPR and Resonance Raman Spectroscopies

VENKATESH, Balan¹; HORI, Hiroshi¹; MIYAZAKI, Gentaro¹; NAGATOMO, Shigenori; KITAGAWA, Teizo; MORIMOTO, Hideki¹ (¹Osaka Univ.)

[*J. Inorg. Biochem.* **88**, 310 (2002)]

Cu(II)-Fe(II) hybrid hemoglobins were investigated by UV-vis, Q-band (35 GHz) EPR and resonance Raman spectroscopies. EPR results indicated that Cu-porphyrin in α -subunit within hybrid hemoglobin had either 5- or 4-coordination geometry depending on the pH conditions, while Cu-porphyrin in β -subunit had only 5-coordination geometry at high and low pH values. These results were consistent with UV-vis absorption results. A new resonance Raman band appeared around 190 cm⁻¹, which was present whenever 5-coordinated Cu-porphyrin existed in Cu(II)-Fe(II) hybrid hemoglobins irrespective of the coordination number in Fe(II) subunit. This Raman band might be

assigned to Cu-His stretching mode. These results are direct demonstration of the existence of coordination changes of Cu-porphyrin in α -subunit within hybrid hemoglobin by shifting the molecular conformation from fully unliganded state to intermediately liganded state.

IX-H-5 Fine-Tuning of Copper(I)-Dioxygen Reactivity by 2-(2-Pyridyl)ethylamine Bidentate Ligands

TAKI, Masayasu¹; TERAMAE, Shinichi¹; NAGATOMO, Shigenori; TACHI, Yoshimitsu²; KITAGAWA, Teizo; ITOH, Shinobu²; FUKUZUMI, Shun-ichi¹ (¹Osaka Univ.; ²Osaka City Univ.)

[*J. Am. Chem. Soc.* **124**, 6367 (2002)]

Copper(I)-dioxygen reactivity has been examined using a series of 2-(2-pyridyl)ethylamine bidentate ligands ^{R1}Py1^{R2,R3}. The bidentate ligand with the methyl substituent on the pyridine nucleus ^{Me}Py1^{Et,Bz} (*N*-benzyl-*N*-ethyl-2-(6-methylpyridin-2-yl)ethylamine) predominantly provided a (μ - η^2 : η^2 -peroxo)dicopper(II) complex, while the bidentate ligand without the 6-methyl group ^HPy1^{Et,Bz} (*N*-benzyl-*N*-ethyl-2-(2-pyridyl)ethylamine) afforded a bis(μ -oxo)dicopper(III) complex under the same experimental conditions. Both Cu₂O₂ complexes gradually decompose, leading to oxidative *N*-dealkylation reaction of the benzyl group. Detailed kinetic analysis has revealed that the bis(μ -oxo)dicopper(III) complex is the common reactive intermediate in both cases and that O-O bond homolysis of the peroxo complex is the rate-determining step in the former case with ^{Me}Py1^{Et,Bz}. On the other hand, the copper(I) complex supported by the bidentate ligand with the smallest *N*-alkyl group (^HPy1^{Me,Me}, *N,N*-dimethyl-2-(2-pyridyl)ethylamine) reacts with molecular oxygen in a 3:1 ratio in acetone at a low temperature to give a mixed-valence trinuclear copper(II, II, III) complex with two μ_3 -oxo bridges, the UV-vis spectrum of which is very close to that of an active oxygen intermediate of lacase. Detailed spectroscopic analysis on the oxygenation reaction at different concentrations has indicated that a bis(μ -oxo)dicopper(III) complex is the precursor for the formation of trinuclear copper complex. In the reaction with 2,4-di-*tert*-butylphenol (DBP), the trinuclear copper(II, II, III) complex acts as a two-electron oxidant to produce an equimolar amount of the C-C coupling dimer of DBP (3,5,3',5'-tetra-*tert*-butyl-biphenyl-2,2'-diol) and a bis(μ -hydroxo)dicopper(II) complex. Kinetic analysis has shown that the reaction consists of two distinct steps, where the first step involves a binding of DBP to the trinuclear complex to give a certain intermediate that further reacts with the second molecule of DBP to give another intermediate, from which the final products are released. Steric and/or electronic effects of the 6-methyl group and the *N*-alkyl substituents of the bidentate ligands on the copper(I)-dioxygen reactivity have been discussed.

IX-H-6 Modulation of the Copper-Dioxygen Reactivity by Stereochemical Effect of Tetradentate Tripodal Ligands

HAYASHI, Hideki¹; UOZUMI, Kounosuke¹; FUJINAMI, Shuhei¹; NAGATOMO, Shigenori; SHIREN, Kazushi¹; FURUTACHI, Hideki¹; SUZUKI, Masatatsu¹; UEHARA, Akira¹; KITAGAWA, Teizo
(¹Kanazawa Univ.)

[*Chem. Lett.* 416 (2002)]

Dioxygen reactivity of a copper(I) complex having a sterically hindered Me-3-tpa and monooxygenase activity of its oxygenated species toward the ligand were significantly modulated by the presence of the 6-methyl group onto pyridyl group.

IX-H-7 Reactivity of Hydroperoxide Bound to a Mononuclear Non-Heme Iron Site

WADA, Akira¹; OGO, Seiji; NAGATOMO, Shigenori; KITAGAWA, Teizo; WATANABE, Yoshihito; JITSUKAWA, Koichiro¹; MASUDA, Hideki¹
(¹Nagoya Inst. Tech.)

[*Inorg. Chem.* **41**, 616 (2002)]

The first isolation and spectroscopic characterization of the mononuclear hydroperoxo-iron(III) complex [Fe(H₂bppa)(OOH)]²⁺ (**2**) and the stoichiometric oxidation of substrates by the mononuclear iron-oxo intermediate generated by its decomposition have been described. The purple species **2** obtained from reaction of [Fe(H₂bppa)(HCOO)](ClO₄)₂ with H₂O₂ in acetone at -50 °C gave characteristic UV-vis (λ_{max} = 568 nm, ϵ = 1200 M⁻¹cm⁻¹), ESR (g = 7.54, 5.78, and 4.25, S = 5/2), and ESI mass spectra (m/z 288.5 corresponding to the ion, [Fe(bppa)(OOH)]²⁺, which revealed that **2** is a high-spin mononuclear iron(III) complex with a hydroperoxide in an end-on fashion. The resonance Raman spectrum of **2** in *d*₆-acetone revealed two intense bands at 621 and 830 cm⁻¹, which shifted to 599 and 813 cm⁻¹, respectively, when reacted with ¹⁸O-labeled H₂O₂. Reactions of the isolated (bppa)Fe^{III}-OOH (**2**) with various substrates (single turnover oxidations) exhibited that the iron-oxo intermediate generated by decomposition of **2** is a nucleophilic species formulated as [(H₂bppa)Fe^{III}-O[•]].

IX-H-8 A New Mononuclear Iron(III) Complex Containing a Peroxocarbonate Ligand

HASHIMOTO, Koji¹; NAGATOMO, Shigenori; FUJINAMI, Shuhei¹; FURUTACHI, Hideki¹; OGO, Seiji; SUZUKI, Masatatsu¹; UEHARA, Akira¹; MAEDA, Yonezo²; WATANABE, Yoshihito; KITAGAWA, Teizo
(¹Kanazawa Univ.; ²Kyushu Univ.)

[*Angew. Chem. Int. Ed. Engl.* **41**, 1205 (2002)]

Stabilization of a peroxocarbonate ligand by formation of a five-membered chelate ring. The mononuclear peroxocarbonate complex **1** was prepared by the reaction of a bis(μ -hydroxo)diiron(III) complex with H₂O₂ and CO₂. Compound **1** is the first crystallography characterized transition metal complex with a peroxocarbonate ligand. Formation of the peroxocarbonate moiety in **1** proceeds by a nucleophilic addition of a peroxide anion to CO₂. Hqn = quinaldic acid.

IX-H-9 Formation, Characterization, and Reactivity of Bis(μ -oxo)dinickel(III) Complexes Supported by a Series of Bis[2-(2-pyridyl)ethyl]amine Ligands

ITOH, Shinobu¹; BANDO, Hideki²; NAKAGAWA, Motonobu²; NAGATOMO, Shigenori; KITAGAWA, Teizo; KARLIN, Kenneth D.³; FUKUZUMI, Shun-ichi²
(¹Osaka City Univ.; ²Osaka Univ.; ³Johns Hopkins Univ.)

[*J. Am. Chem. Soc.* **123**, 11168 (2001)]

Bis(μ -oxo)dinickel(III) complexes supported by a series of bis[2-(2-pyridyl)ethyl]amine ligands have been successfully generated by treating the corresponding bis(μ -hydroxo)dinickel(II) complexes or bis(μ -methoxo)dinickel(II) complex with an equimolar amount of H₂O₂ in acetone at low temperature. The bis(μ -oxo)dinickel(III) complexes exhibit a characteristic UV-vis absorption band at ~ 410 nm and a resonance Raman band at 600–610 cm⁻¹ that shifted to 570–580 cm⁻¹ upon ¹⁸O-substitution. Kinetic studies and isotope labeling experiments using ¹⁸O₂ imply the existence of intermediate(s) such as peroxo dinickel(II) in the course of formation of the bis(μ -oxo)dinickel(III) complex. The bis(μ -oxo)dinickel(III) complexes supported by the mononucleating ligands (**L1**^X = para-substituted *N,N*-bis[2-(2-pyridyl)ethyl]-2-phenylethylamine; X = OMe, Me, H, Cl) gradually decompose, leading to benzylic hydroxylation of the ligand side arm (phenethyl group). The kinetics of the ligand hydroxylation process including kinetic deuterium isotope effects (KIE), *p*-substituent effects (Hammett plot), and activation parameters ($\Delta H_{\text{H}}^{\ddagger}$ and $\Delta S_{\text{H}}^{\ddagger}$) indicate that the bis(μ -oxo)dinickel(III) complex exhibits an ability of hydrogen atom abstraction from the substrate moiety as in the case of the bis(μ -oxo)dinickel(III) complex. Such a reactivity of bis(μ -oxo)dinickel(III) complexes has also been suggested by the observed reactivity toward external substrates such as phenol derivatives and 1,4-cyclohexadiene. The thermal stability of the bis(μ -oxo)dinickel(III) complex is significantly enhanced when the dinucleating ligand with a longer alkyl strap is adopted instead of the mononucleating ligand. In the *m*-xylyl ligand system, no aromatic ligand hydroxylation occurred, showing a sharp contrast with the reactivity of the (μ - η^2 : η^2 -peroxo)dinickel(II) complex with the same ligand which induces aromatic ligand hydroxylation via an electrophilic aromatic substitution mechanism. Differences in the structure and reactivity of the active oxygen complexes between the nickel and the copper systems are discussed on the basis of the detailed

comparison of these two systems with the same ligand.

IX-H-10 UV Resonance Raman and NMR Spectroscopic Studies on the pH Dependent Metal Ion Release from Pseudoazurin

SATO, Katsuko¹; NAGATOMO, Shigenori;
DENNISON, Christopher²; NIIZEKI, Tomotake¹;
KITAGAWA, Teizo; KOHZUMA, Takamitsu¹
(¹Ibaraki Univ.; ²Univ. Newcastle upon Tyne)

[*Inorg. Chim. Acta* in press]

UV resonance Raman (UVRR) and ¹H NMR spectra are measured for native Cu(I)- and Cu(II)-pseudoazurin, its apo-protein, and a few metal-substituted derivatives. The pH titration experiments of ¹H NMR enabled us to determine the pK_a^{*} values of three His residues (His6, His40, and His81). The UVRR band characteristic of a metal coordinated histidyl imidazole was observed at 1385 cm⁻¹ for Cu(II)-pseudoazurin in D₂O but not for Cu(I)-pseudoazurin. This frequency is consistent with the N_δ coordination of His. For the Cu(I)-pseudoazurin

a characteristic band of histidyl imidazolium was detected at 1408 cm⁻¹ at acidic pH. This is assigned to protonated His81, which is deligated from Cu(I) at low pH values. The imidazolium Raman band at 1408 cm⁻¹ was also detected in the UVRR spectrum of apo-pseudoazurin at pH* = 3.9, and the acidification was accompanied by a significant change in the X-Pro bands at 1467 cm⁻¹. Pseudoazurin substituted with Zn²⁺ and Cd²⁺ gave the characteristic Raman bands of the metal coordinated imidazole at 1388 and 1384 cm⁻¹, respectively, at neutral pH, but its intensity diminished upon lowering the pH, and instead the imidazolium band at 1408 cm⁻¹ grew. The X-Pro bands of the pseudoazurins substituted with Zn²⁺ and Cd²⁺ exhibited the pH dependence very similar to that observed for apo-pseudoazurin. These findings indicate that the Zn²⁺ and Cd²⁺ ions are released from the active site at acidic pH and it is accompanied by a change in hydrogen bonding state of Pro80. This behavior is clearly absent in both the Cu(I) and Cu(II) proteins, meaning that pseudoazurin discriminates between copper and the other metal ions.

IX-I Fast Dynamics of Photoproducts in Solution Phases

Picosecond time-resolved resonance Raman (ps-TR³) spectroscopy is a promising technique to investigate ultrafast structural changes of molecules. However, this technique has not been used as widely as nanosecond TR³ spectroscopy, mainly due to the lack of light source which has suitable repetition rates of pulses and wavelength tunability. In order to obtain qualified TR³ spectra, first we need two independently tunable light sources for pump and probe pulses. Second, the repetition rate should be higher than kiloHertz to keep a moderate average laser power without making the photon density of probe pulse too high. We succeeded in developing light sources for ps-TR³ spectroscopy having wide tunability and kHz repetition, and applied them to study fast dynamics of photo-excited molecules. For carbonmonoxy myoglobin (MbCO), vibrational relaxation with the time constant of 1.9 ps was observed for CO-photodissociated heme. For Ni-octaethylporphyrin in benzene, differences in rise times of population in vibrationally excited levels among various modes were observed in the anti-Stokes spectra for the first time. This technique has been applied to identify the trans ligand of CO in the CO-bound transcriptional factor, Coo A.

On the other hand, we have constructed a nanosecond temperature-jump apparatus using a water absorption in near infrared. The new apparatus based on a Nd:YAG laser was combined with a time-resolved Raman measurement system and applied successfully to explore thermal unfolding of ribonuclease A.

IX-I-1 Time-Resolved Resonance Raman Study on Ultrafast Structural Relaxation and Vibrational Cooling of Photodissociated Carbonmonoxy Myoglobin

KITAGAWA, Teizo; HARUTA, Nami; MIZUTANI, Yasuhisa

[*Biopolymers (Biospectroscopy)* **67**, 207 (2002)]

A localized small structural change is converted to a higher order conformational change of protein and extends to a mesoscopic scale to induce a physiological function. To understand such features of protein, ultrafast dynamics of myoglobin (Mb) following CO photolysis have been investigated in this laboratory. Recent results are summarized here with a stress on

structural and vibrational energy relaxation. The core expansion of heme takes place within 2 ps but the out-of-plane displacement of the heme iron and the accompanied protein conformational change occur in ~10 and ~100 picosecond regimes, respectively. It was found from UV resonance Raman spectra that Trp7 in the N-terminal region and Tyr151 in the C-terminal region undergo appreciable structural changes upon ligand binding/dissociation and as a result, the rate of spectral change of iron-histidine (Fe-His) stretching band is influenced by viscosity of solvent. Temporal changes of the anti-Stokes Raman intensity demonstrated immediate generation of vibrationally excited heme upon photodissociation and its decay with a time constant of 1.1 ps.

IX-I-2 Vibrational Energy Relaxation of Metalloporphyrins in a Condensed Phase Probed by Time-Resolved Resonance Raman Spectroscopy

MIZUTANI, Yasuhisa; KITAGAWA, Teizo

[*Bull. Chem. Soc. Jpn.* **75**, 623 (2002)]

Recent experimental work on vibrational energy relaxation of metalloporphyrins in a condensed phase carried out in this laboratory is summarized. The formation of a vibrationally excited photoproduct of metalloporphyrins upon (π , π^*) excitation and its subsequent vibrational energy relaxation were monitored by picosecond time-resolved resonance Raman spectroscopy. Results related to intramolecular relaxation of octaethylporphyrinato nickel (NiOEP) are described. Stokes Raman bands due to a photoproduct of NiOEP instantaneously appeared upon the photoexcitation. Their intensities decayed with a time constant of ~ 300 ps, which indicates an electronic relaxation from the (d , d) excited state (B_{1g}) to the ground state (A_{1g}), being consistent with the results of transient absorption measurements. Anti-Stokes ν_4 and ν_7 bands for vibrationally excited (d , d) state of NiOEP decayed with time constants of ~ 10 and ~ 300 ps. The former is ascribed to vibrational relaxation, while the latter corresponds to the electronic relaxation from the (d , d) excited state to the electronic ground state. While the rise of anti-Stokes ν_4 intensity was instrument-limited, the rise of anti-Stokes ν_7 intensity was delayed by 2.0 ± 0.4 ps, which indicates that intramolecular vibrational energy redistribution has not been completed in the subpicosecond time regime. To study the mechanism of intermolecular energy transfer, solvent dependence of the time constants of anti-Stokes kinetics was investigated using various solvents. No significant solvent dependence of the rise and decay constants was observed for NiOEP. For an iron porphyrin, we observed two phases in intermolecular energy transfer. The fast phase was insensitive to solvent and the slow phase depended on solvents. A model of classical thermal diffusion qualitatively reproduced this behavior. For myoglobin, temporal changes of the anti-Stokes Raman intensity of the ν_4 and ν_7 bands demonstrated immediate generation of a vibrationally excited heme upon photodissociation and subsequent decays of the excited populations, whose time constants were 1.1 ± 0.6 and 1.9 ± 0.6 ps, respectively. This direct monitoring of the cooling dynamics of the heme cofactor within the protein matrix allows the characterization of the vibrational energy flow through the protein moiety and to the water bath. For solute-solvent energy transfer process, low-frequency modes of proteins seem to be less important.

IX-I-3 Mode Dependence of Vibrational Energy Redistribution in Nickel Tetraphenylporphyrin Probed by Picosecond Time-Resolved Resonance Raman Spectroscopy: Slow IVR to Phenyl Peripherals

MIZUTANI, Yasuhisa; KITAGAWA, Teizo

[*Bull. Chem. Soc. Jpn.* **75**, 965 (2002)]

The formation of the (d , d) excited state of (*meso*-tetraphenylporphyrinato)nickel (II) ([Ni(tpp)]) upon (π , π^*) excitation, and its vibrational energy relaxation were monitored by picosecond time-resolved resonance Raman spectroscopy. Stokes resonance Raman bands due the (d , d) excited state instantaneously appeared upon the photoexcitation into the (π , π^*) excited state. Their intensities decayed with a time constant of about 250 ps, which corresponds to electronic relaxation from the (d , d) excited state to the electronic ground state. This is consistent with the results of ultrafast absorption measurements reported by Eom *et al.* [H. S. Eom, S. C. Jeoung, D. Kim, J. H. Ha and Y. R. Kim, *J. Phys. Chem. A* **101**, 3661 (1997)]. Anti-Stokes ν_4 (macrocycle in-plane mode) intensities of [Ni(tpp)] in the (d , d) excited state appeared promptly and decayed with a time constant of 3.6 ± 0.6 ps. The rise and decay of anti-Stokes intensity are interpreted as vibrational excitation due to the excess energy and intermolecular vibrational energy transfer to the surrounding solvent molecules, respectively. The ϕ_4 mode, which is mainly $\nu(\text{CC})$ of the peripheral phenyl groups, gave no detectable anti-stokes intensity although the mode gave appreciable Stokes intensity. This means that the ϕ_4 mode is left vibrationally less excited than the ν_4 mode in the process of vibrational energy relaxation and that intramolecular vibrational energy redistribution is not completed in a subpicosecond time regime. These results for [Ni(tpp)] demonstrate that the vibrational modes of peripheral groups are vibrationally less excited shortly after the formation of the (d , d) excited state and that energy redistribution in the peripheral groups takes place in picoseconds, such a short time is competitive with vibrational energy transfer to the surrounding solvent molecules.

RESEARCH FACILITIES

The Institute for Molecular Science includes five research facilities. This section describes their latest equipment and activities. For further information please refer to older IMS Annual Review issues (1978–2001).

Laser Research Center for Molecular Science

This Center was established in 1997 by reorganization of a part of the Instrument Center. The new Center is composed of three research groups which are asked to develop new lasers suitable for pioneering researches in the new field of molecular science. The three groups are

1. Advanced Lasers for Chemical Reaction Studies,
2. Advanced Lasers for Synchrotron Radiation Applications
and
3. Advanced UV and IR Tunable Lasers.

The Laser Research Center are equipped with excimer lasers and all-solid-state light sources in various temporal and spectral regions, including femtosecond and nanosecond Optical Parametric Oscillators (OPO). The synchronously femtosecond OPO (OPAL; SPECTRA PHYSICS) is tunable from 1.1 μm up to 1.6 μm . The nanosecond OPO has extraordinarily wide tuning range from 420 nm up to 2.2 μm . The Laser Center also has a fluorescence analyzer (FLUOROLOG2; SPEX) which is composed of a xenon lamp house, and double and single monochromators for spectroscopy. The detector is changeable by rotating a mirror (CCD and PM). Using these instruments, one can carry out various experiments not only in the ultrafast temporal region but also in the steady-state photon-counting region.

Research Center for Molecular-scale Nanoscience

This Center was established in April 2002 after reorganization including the Research Center for Molecular Materials, the Department of Electronic Structure and the Department of Molecular Assemblies. The Center is supposed to play a principal role to integrate the innovative progress that IMS has achieved in the fields of molecular science (based on quantum chemistry and statistical mechanics) and materials science (design and synthesis of functional molecules). Its mission is to develop a new frontier of science that aims at constructing novel nanometer-scale materials, and elucidating the behavior thereof, on the basis of understanding the structure and dynamics of each molecular component.

The scientific research in this Center is carried out in the five laboratories: (A) Molecular-scale Electronics, (B) Nanocatalysis and Biomolecular Devices, (C) Nano-scale Photoscience, (D) Interface Molecular Science, and (E) Molecular Clusters, where the latter two laboratories consist of the faculty members transferred from other universities. The respective research activities of these laboratories are reported in the other sections in this Review. The Center also contains the supporting facility, which manages the instruments (EPR, SQUID, NMR, *etc.*) for inter-university use, provides liquid N_2 and He for research and machine maintenance, and takes care of the elemental analyses and the mass spectrometric measurements of chemical materials.

Equipment Development Center

A number of research instruments have been designed and constructed at the mechanical, electronic and glass work sections in this Facility. Examples of our works in this fiscal year are listed below.

- Specially designed insert for cryogen-free superconducting magnet
- Hi precision angle resolved NMR probe
- FTIR sample holder and sample exchange stage
- Equipment for production of fullerenes
- VUV light separation box
- Electron yield detector with adjustment of Z-axis
- Multi-channel Micro-ampere Constant Current Source
- Bipolar High Voltage Pulse Generator
- Ultra-Fast Rising Avalanche Transistor Switching Circuit
- High Speed Valve Controller for Molecular Beam Source
- Current-to-Voltage Converter for STM
- Thin-window X-ray cell
- Quartz cell

Development of Special Machine

Equipment Development Center is also engaged in developing Special Machine. This activity is described in detail in section "RESEARCH ACTIVITIES."

Ultraviolet Synchrotron Orbital Radiation Facility

The UVSOR accelerator complex consists of a 15 MeV injector linac, a 600 MeV booster synchrotron, and a

750 MeV storage ring. The magnet lattice of the storage ring is the so-called double-bend achromat. The double RF system is routinely operated for the user beam time, and the lifetime of the electron beam has been improved to about 6 hours at 200 mA. The storage ring is normally operated under multi-bunch mode with partial filling. The single bunch operation is also conducted about two weeks a year, which provides pulsed synchrotron radiation (SR) for time-resolved experiments. Initial beam currents stored under multi-bunch and single-bunch modes are 300 mA and 70 mA, respectively. In order to realize much smaller emittance (27 nm-rad) and create new straight sections, a new lattice for the UVSOR storage ring was designed. This upgrade project has been approved in 2002 and preparation towards the actual reconstruction for the storage ring, which includes the replacement of all the quadrupole and sextupole magnets, has begun in spring 2002. A new position monitoring system for the photon beam was smoothly installed by the end of August 2002.

Eight bending magnets and two insertion devices are available for utilizing SR. The bending magnet with its radius of 2.2 m provides SR, whose critical energy is 425 eV. There is a total of 20 beamlines operational at UVSOR, which are classified into two categories. 11 of them are so-called "Open beamlines," which are open to scientists of universities and research institutes belonging to the government, public organizations, private enterprises and those of foreign countries. The rest of the 9 beamlines are so-called "In-house beamlines," which are dedicated to the use of the research groups within IMS. We have one soft X-rays (SX) station equipped with a double-crystal monochromator, eight EUV and SX stations with a grazing incidence monochromator, four VUV stations with a normal incidence monochromator, one (far) infrared station equipped with FT interferometers, one station with a multi-layer monochromator, and four non-monochromatized stations for irradiation of white-light.

The planar undulator is composed of 24 pairs of permanent magnets, the period of which is 84 mm. This undulator will be replaced with an in-vacuum type undulator in March 2003. The helical undulator was installed in 1996, which can also be used as the helical optical klystron for free electron laser (FEL) experiments. The undulator supplies the perfect circular polarization in the photon energy range of 2–45 eV, and the elliptic polarization up to 200 eV. An in-vacuum type undulator was successfully installed at the straight section between B06 and B07, after removing the wiggler, in March 2002. A combination of the non-monochromatized undulator radiation at BL3A1 with FEL led us to the success of realizing two-photon experiments for Xe atoms last year. Further development related to the practical usability of FEL is in progress.

Discussion with users, concerning the improvements and upgrades of the beamlines at UVSOR, has been continuously made as series of UVSOR workshops. Several novel results have emerged from the beamlines that have just been constructed. Discussion for the rebuilt and rearrangement of several old beamlines has been initiated more recently, on the basis of the review and evaluation report on the present status of UVSOR in 2000. It has been settled that the reconstruction of BL3 has been given the highest priority after the upgrade of the UVSOR storage ring. The reconstruction of BL6 and introduction of high-resolution photoelectron spectrometer to BL5A have also been decided through the discussion.

In spring 2002, we had a one-month shutdown to perform periodic maintenance for the rings and beamlines and to check the incidental facilities in UVSOR. During the regular shutdown period for approximately one month in summer 2002, similar maintenance is under progress. There were a lot of trouble in one year (from September 2001 to August 2002) due mainly to the superannuated laboratory equipment, as usual, but fortunately, they did not seriously affect the user's beam time.

All uses are required to refer to the beam-line manuals and the UVSOR guidebook (latest revision in 1999), on the occasion of conducting the actual experimental procedures. Those wishing to use the open and in-house beamlines are recommended to contact with the stationmaster/supervisor and the representative, respectively. For updated information of UVSOR, <http://www.uvsor.ims.ac.jp/>.

Computer Center

Since April, 2000, Computer Center of IMS has been reorganized as Research Center for Computational Science in Okazaki National Research Institute. The main super-computers at the Center consist of a vector parallel system of Fujitsu VPP5000 and a scalar parallel system of SGI 2800. The VPP5000 system has 30 vector CPU-nodes and 256GB of main memory. The SGI system has 320 CPUs and 320GB of memory. NEC SX-5 and IBM SP2 are also installed for general-purpose computations. These computers are linked to international networks through Science Information Network (SINET).

We have two types of application categories: (a) Use-of-Facility Program is open to all the domestic scientists in molecular science and related fields; (b) Advanced Research Project is for large-scale computational projects which require resources in excess of the limit for (a) Use-of-Facility Program. The projects applying for the category (b) must be expected scientifically significant achievements. About 27% of the CPU time is used by research staffs in the Institute, while the remaining 73% is given out as research grants described above to outside scientists. As of March 2002, the number of project groups was 148 with 605 users. Some of the famous package programs in Molecular Orbital Theory, e.g. Gaussian98, Molpro2000, Hondo, etc., are kept updated as Library Programs for immediate use on the super-computers of the Center. The information for each program can be found on our Web page (<http://ccinfo.ims.ac.jp/>).

The Quantum Chemistry Literature Database (QCLDB) has been developed by the Quantum Chemistry Database Group in collaboration with staff members of the Center. The latest release, QCLDB Release 2001, contains 57,037 data. This database is accessible through the Web page (<http://qcldb.ims.ac.jp/>).

SPECIAL RESEARCH PROJECTS

IMS has special research projects supported by national funds. Three projects in progress are:

- (a) Chemical Reaction Dynamics
- (b) Molecular Photophysics and Science
- (c) Novel Material Science

These three projects are being carried out with close collaboration between research divisions and facilities. Collaborations from outside also make important contributions. Research fellows join these projects.

(a) Chemical Reaction Dynamics

Folding Mechanism of Protein Molecules Studied by Generalized-Ensemble Algorithms

OKAMOTO, Yuko; SUGITA, Yuji¹; NAGASIMA, Takehiro²; YODA, Takao; KOKUBO, Hironori³; MURATA, Katsumi³; SAKAE, Yoshitake³
(¹Univ. Tokyo; ²NIG; ³GUAS)

Proteins are the most complicated molecules that exist in nature. Since protein structures are closely related to their biological functions, the understanding of their folding mechanism from the first principles is not only very challenging but also very important. To be more specific, it is widely believed that three-dimensional structures of proteins are determined by their amino-acid sequence information. However, nobody has completely succeeded in predicting it solely from the amino-acid-sequence information (prediction from the first principles).

There are two elements for the difficulty. One element is that the inclusion of accurate solvent effects is non-trivial because the number of solvent molecules that have to be taken into account is very large. The other element for the difficulty is that there exist a huge number of local minima in the energy function, and simulations by conventional techniques will necessarily get trapped in one of the local minima without ever finding the energy global minimum. Generalized-ensemble algorithms are new simulation algorithms that can alleviate this second difficulty (for reviews, see Reference 1–3). We have been developing new generalized-ensemble algorithms. We found that the combination of multicanonical algorithm and replica-exchange method is particularly promising.³⁾

The goal of the present project is to further develop and test the effectiveness of generalize-ensemble algorithms in the protein folding problem and to succeed eventually in the prediction of tertiary structures of proteins from the first principles.

References

- 1) Y. Okamoto, *Recent Res. Devel. in Pure & Applied Chem.* **2**, 1 (1998).
- 2) U. H. E. Hansmann and Y. Okamoto, *Ann. Rev. Comput. Phys. VI D. Stauffer, Ed., World Scientific*, 129 (1999).
- 3) A. Mitsutake, Y. Sugita and Y. Okamoto, *Biopolymers (Pept. Sci.)* **60**, 96 (2001).

Nonadiabatic Chemical Dynamics

NAKAMURA, Hiroki; ZHU, Chaoyuan; MIL'NIKOV, G. V.¹; FUJISAKI, Hiroshi; KONDORSKIY, Alexey²; KAMISAKA, Hideyuki
(¹IMS and Inst. Struct. Macrokinetics, Russia; ²IMS and Lebedev Phys. Inst., Russia)

Quantum reaction dynamics of electronically non-adiabatic chemical reactions have been studied with use of the hyperspherical elliptic coordinate system. These studies have been carried out for DH_2^+ and $\text{O}(^1\text{D})\text{HCl}$ systems, although the effects of nonadiabatic transitions are not taken into account in the latter system. These are important not only by themselves to clarify the quantum dynamics, but also for developing a new semiclassical methodology.^{1),2),3)}

The semiclassical TSH (trajectory surface hopping) method for electronically nonadiabatic reactions based on the Zhu-Nakamura theory has been developed and applied to DH_2^+ system. The method has been found to work well compared to the Landau-Zener theory and is expected to be generalized to higher dimensional systems.^{4),5)} The similar type of studies are underway for conical intersection systems.

Based on the Teranishi-Nakamura theory to control molecular processes, we have developed a more practically feasible method with use of a sequence of linearly chirped pulses and applied it to selective excitation among closely lying levels and to electronic excitation of a diatomic molecule. Basic analytical theory for the nonadiabatic transition in (t,x) space is being developed, where t is time and x is a spatial coordinate.

References

- 1) H. Kamisaka, W. Bian, K. Nobusada and H. Nakamura, *J. Chem. Phys.* **116**, 654 (2002).
- 2) S. Nanbu, H. Kamisaka, W. Bian, M. Aoyagi, K. Tanaka and H. Nakamura, *J. Theor. Comp. Chem.* (in press).
- 3) H. Kamisaka, S. Nanbu, W. Bian, M. Aoyagi, K. Tanaka and H. Nakamura, *J. Theor. Comp. Chem.* (in press).
- 4) C. Zhu, H. Kamisaka and H. Nakamura, *J. Chem. Phys.* **115**, 11036 (2001).
- 5) C. Zhu, H. Kamisaka and H. Nakamura, *J. Chem. Phys.* **116**, 3234 (2002).

Imaging of Chemical Dynamics

SUZUKI, Toshinori; KOHGUCHI, Hiroshi;

KATAYANAGI, Hideki; MATSUMOTO, Yoshiteru; NISHIDE, Tatsuhiro; TSUBOUCHI, Masaaki; NISHIZAWA, Kiyoshi

Pump-probe femtosecond photoelectron imaging is employed to observe chemical reactions in isolated molecules and molecular clusters in real time. A pump pulse initiates a reaction and a probe pulse knocks out an electron from a molecule as a function of time delay. Ionization is allowed from any electronic state during the course of a reaction, so this method serves as a versatile means to explore the reaction mechanism. Rotational wave packet motion is utilized to capture the photoelectron angular distribution in the molecular frame that is one of the ultimate quantity to elucidate molecular photoionization dynamics. Photodissociation dynamics is studied by photofragment ion imaging, where vector correlation in the fragment is analyzed in detail to elucidate stereo dynamics. The result is compared with wave packet and classical trajectory calculations on *ab initio* surfaces. Full collision dynamics is studied by using a crossed beam apparatus with an ion imaging detector. Reactive species are produced by photodissociation of precursor molecules, and the scattering distributions of state-selected products are mapped out.

Stereodynamics and Active Control of Chemical Reactions by Using Electrostatic Hexapole State-Selector and Polarized Laser Excitation

CHE, Dock-Chil; HASHINOKUCHI, Mitihoro¹; SHIMIZU, Yuichiro; FUKUYAMA, Tetsuya²; KASAI, Toshio¹

(¹IMS and Osaka Univ.; ²IMS and Himeji Inst. Tech.)

Effect of molecular orientation of a target molecule with respect to a colliding reactant plays a key role in chemical reaction, and this is historically called "steric effect." It becomes more important for understanding stereodynamics of elementary reactions in the gas phase, in order to control reaction actively. To our knowledge, orientation dependences of "atom(spherical)-molecule(vector)" reactions have been studied using oriented molecules, but the steric effect of "molecule(vector)-molecule(vector)" reaction has not been studied in experiment so far. Typical examples of the "molecule-molecule" reaction are the OH + NO and the OH + CO radical reactions. These are our special research project we challenged. Our experimental strategy is to select molecular orientation by use of hexapole state-selector and/or linearly polarized laser. Thus, we have built a new crossed-beam apparatus with a 1-m long hexapole electric field and we have installed a new set of tunable YAG-dye laser system. There are two ongoing objectives of our special project as presented in the following.

(1) We investigated the reaction of oriented-OH with aligned-NO. The OH radicals are produced by a dc-discharge of H₂O seeded in He, Ar and Kr. We have developed an intense pulsed beam source and single quantum state $|J\Omega M\rangle$ of OH(X) are selected by a 1-m hexapole field. By probing each *J* state of

OH(X) with LIF spectroscopic technique, we could observe the focusing curves for $J = 3/2$ and $5/2$ states. We then state-select their orientation by the hexapole. NO is aligned by the linearly polarized UV laser. The hydrogen atom in the OH + NO → O₂ + H reaction and NH product in the OH + NO → NH + O₂ reaction are detected by REMPI and LIF, respectively. Orientation dependence of the branching ratio of the two reaction channels should provide an insight into details of stereodynamics. Experiment is now being carried out to clarify how molecular orientation affects the branching ratio of production channels.

(2) We proposed a new type of electrostatic state-selector for orienting molecules that consists of seven sets of adjacent hexapole fields to form a honeycomb field for integrating the intensities of seven oriented molecular beam lines. We employed sample gases; Ar, Kr and a polar molecule acetonitrile (CH₃CN, $\mu = 3.92$ D) seeded in those rare gases, to specify the state-selectivity of the new field. We find that the integrated beam intensity agrees very well with our theoretical estimation, while we can maintain the same beam character of each beam line, such as rotational temperature, stream velocity *etc.* for the integrated beam. We have observed the dependence of the focused CH₃CN beam intensity on the honeycomb electrode voltages, which shows ordinary normal Stark effects, confirming that the present honeycomb-type electrostatic field can be nicely used to state-select and orient molecular beams.

Monte Carlo Simulation of Chemical Gel

TAKASU, Masako¹; NOSAKA, Makoto¹

(¹IMS and Kanazawa Univ.)

The process of gelation was analyzed by Brownian dynamics simulation using modeled radical polymerization with cross-linkers. Particle densities were set near the gelation threshold determined experimentally (monomer density $d = 200$ mM 400 mM and 600 mM). We performed simulations under two conditions that did (Rule D) and did not (Rule A) prohibit the formation of intra-linkers. With Rule D, we observed gelation at $d = 600$ mM, and clustering at $d = 400$ mM. On the other hand, with Rule A, we did not observe gelation with any of the densities tested. We only observed clustering at $d = 600$ mM. Some quantities were investigated by comparing the results under the two conditions.

Electronic Structure and Decay Mechanism of Inner-Shell Excited Molecules

KOSUGI, Nobuhiro; HATSUI, Takaki

This project is being carried out at the Beamline 4B of the UVSOR facility. We have three subprojects: (A) spin-orbit, exchange, and molecular field splittings in S $2p$ and P $2p$ excited states, (B) molecules and radicals in condensed phase and in rare gas matrix, and (C) ionic fragmentations following the inner-shell resonance excitation. In (A), we have found some spin-forbidden

ionized and excited states in non-radiative (photoelectron emission) and radiative (photon emission) deexcitation spectra in collaboration with the Uppsala University. In (C), we are concentrating on theoretical interpretation of our experimental data measured for last several years.

Computational Study of Quantum Dynamics of a Solute in Solution

OKAZAKI, Susumu; MIURA, Shin-ichi;
IWAHASHI, Kensuke; TANAKA, Junji; MIKAMI,
Taiji; SATO, Masahiro

Molecular mechanism of vibrational energy relaxation of a solute molecule in solution has been analyzed based upon path integral influence functional theory. Then, solvent normal modes were transformed to each molecular motion in order to examine the couplings in terms of solvent molecules. Coupling which has large contribution to the relaxation could be attributed to a particular water molecule. Mixed quantum-classical molecular dynamics method has also been applied to the analysis of dynamic aspects of the coupling. Component which is resonant with the solute wave function was extracted from the solute-solvent interaction $\langle 0|V|1\rangle$. In a short time-scale, *i.e.* sub ps, it shows almost random behavior. However, in longer time-scale, \sim ps, it clearly shows relaxation.

Simulation method for quantum liquids has been investigated, too. A new hybrid Monte Carlo method has been developed to simulate liquid helium in super fluid state.

Photodissociation of 16 Valence Electron Systems, OCS and N₂O

NANBU, Shinkoh; MINAMINO, Satoshi; MAKI,
Jun; AOYAGI, Mutsumi

OCS and N₂O molecules have similar characters for the low-lying electronic states, because both molecules are characterized with the 16 valence electron system, and that is the reason why the electronic structures are assigned to $^1\Sigma^+$, $^1\Sigma^-$, and $^1\Delta$ symmetries in $C_{\infty v}$. And also, we can have an image of forming the similar features for the PESs of OCS and N₂O, and furthermore having the similar dynamics for the photodissociation processes, $OCS + h\nu \rightarrow CO(^1\Sigma^+) + S(^1D)$ and $N_2O + h\nu \rightarrow N_2(^1\Sigma_g^+) + O(^1D)$. Therefore, we began to study the photodissociation process with OCS, collaborating with Prof. Suzuki's group. First, the speed, angular, and alignment distributions of S atoms from the ultraviolet photodissociation have been measured by a photofragment imaging technique. From the excitation wavelength dependence of the scattering distribution of S, the excited states accessed by photoabsorption were assigned to the A' Renner-Teller component of the $^1\Delta$ and the A''($^1\Sigma^-$) states. It was found that the dissociation from the A' state gives rise to high- and low-speed fragments, while the A'' state only provides the high-speed fragment. In order to examine the bimodal speed distribution of S atoms, two-dimensional PESs of OCS and non-adiabatic coupling elements were calculated with

ab initio MO CI method, fixing the CO bond distance, and wave packet dynamics were performed including the non-adiabatic transitions. The theoretical results could qualitatively reproduce the experimental feature. However, they could not quantitatively agree with the measurements. In the present work, wave packet dynamics were performed to study the similarity due to the same 16 valence electron systems, using the newly determined three-dimensional PESs for OCS and N₂O.

Development of Single-Molecule Physiology

KINOSITA, Kazuhiko, Jr.

Our effort in this year was to establish a new lab in the newly built building of the Center for Integrative Bioscience. Our lab aims at single-molecule physiology, where we watch and manipulate individual protein/RNA molecules (molecular machines) under an optical microscope to elucidate their functions (see Research Activities). The microscopes need to be in a dust-free environment at a controlled temperature. For this purpose, we designed special chambers that would keep the sample temperature to within ± 0.1 °C. We also developed stable microscope stages and a beam homogenizer with little vibration. Software for image analysis is also being developed. I hope we are now ready for a new start.

Ultrafast Protein Dynamics Probed by Time-Resolved Resonance Raman Spectroscopy

KITAGAWA, Teizo

Ultrafast protein dynamics were examined with myoglobin (Mb) using picosecond time-resolved resonance Raman spectroscopy with a stress on structural changes and vibrational energy relaxation of heme. Studies on the structural relaxation of Mb following CO photolysis revealed that the structural change of heme itself (core expansion), caused by CO photodissociation, is completed within the instrumental response time of the time-resolved resonance Raman apparatus used (~ 2 ps). In contrast, changes in the intensity and frequency of the iron-histidine (Fe-His) stretching mode upon dissociation of the trans ligand were found to occur in the picosecond regime. The Fe-His stretching band is absent for the CO-bound form, and its appearance upon photodissociation was not instantaneous, in contrast with that observed in the vibrational modes of heme, suggesting appreciable time evolution of the Fe displacement from the heme plane. The intensity reflected the out-of-plane displacement of iron, and 80% of the movement occurred in 2 ps but the remaining 20% occurred in 40 ps. The band position of the Fe-His stretching mode changed with a time constant of about 100 ps, indicating that tertiary structural changes of the protein occurred in a 100-ps range. This rate was dependent on viscosity of solvent ($k = \eta^{-0.3}$), indicating that the small change at the Fe-His bond is communicated to the protein surface through a conformation change, and conversely the change of Fe-His bond is controlled by the surface of the protein. Temporal changes of the anti-Stokes Raman intensity of the ν_4 and ν_7 bands

demonstrated immediate generation of vibrationally excited heme upon the photodissociation and successive decay of excited populations, whose time constants were 1.1 ± 0.6 and 1.9 ± 0.6 ps, respectively. This technique has been applied to identify an axial residue of a sensor protein, *CooA*, for which geminate recombination of photodissociated CO is very fast ($\tau = 70$ ps) and therefore the Fe–His (His77) stretching Raman band could be detected only transiently with this technique.

(b) Molecular Photophysics and Science

Development of Dynamic Spectroscopy Apparatus Having Nanometer Spatial Resolution

IMURA, Kohei; NAGAHARA, Tetsuhiko;
OKAMOTO, Hiromi

Recent remarkable technological progress in scanning near-field optical microscope (SNOM) has made it possible to perform optical measurements with very high spatial resolution beyond the diffraction limit. We are constructing an apparatus for space- and time-resolved spectroscopic measurements, by combining SNOM and ultrafast time-resolved technique. With this apparatus, we have achieved ~ 100 nm spatial and ~ 100 fs temporal resolution at the same time. Various photo-physical phenomena probed under such extremely high space and time resolution can be of considerable significance not only in physics and chemistry but also in biology, and thus will open a new research activity. We plan to make use of this experimental methodology to investigate basic problems on chemical processes of mesoscopic systems. This technique also has a potential to shed a new light on nanoscale material science.

Experimental setup is schematically depicted in Figure 1. An apertured fiber probe is used to obtain spatial resolution of better than 100 nm. Radiation from a femtosecond Ti:sapphire laser or other pulsed or cw lasers are used as an excitation light source. The sample is irradiated through the fiber probe. The emission from the sample is collected through the same fiber probe tip or collected by a separate far-field optics. The preliminary experimental results are reported in II-A.

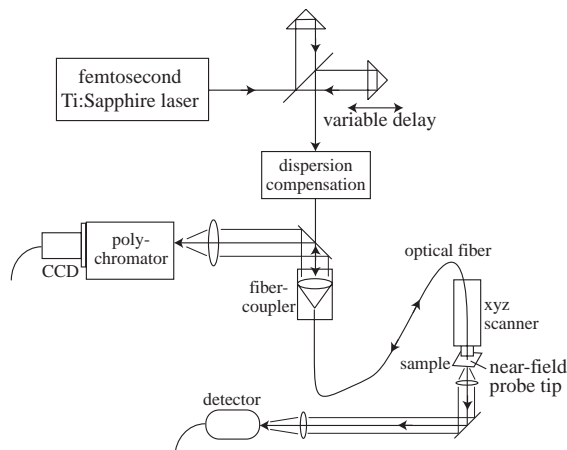


Figure 1. Schematic diagram of the experimental apparatus.

- (1) Laser Cooling and Trapping of Metastable Helium Atoms
- (2) Laser Spectroscopic Studies of Atoms and Ions in Liquid Helium

MORITA, Norio; MORIWAKI, Yoshiki¹
(¹Toyama Univ.)

In studies on “laser cooling and trapping of metastable helium atoms,” we have been still constructing a

new laser trapping apparatus for realizing the Bose-Einstein condensation of metastable He atoms. In the new apparatus, the metastable atomic beam is tightly collimated with a corner cube prism chain of totally 30 cm long, and deflected by an angle of 30 degrees after some deceleration in order to prevent the intense ground state beam from attacking the trapping region (see II-B-1). On the other hand, in “laser spectroscopic studies of atoms and ions in liquid helium,” we have experimentally observed some interesting differences between excitation spectra of Eu atoms in liquid ^4He and ^3He : sharp zero phonon lines and phonon side bands have been seen for both liquid ^4He and ^3He , but additional bands have been seen only for ^4He . These bands can be roton or maxon spectra of liquid ^4He , in which the dispersion relation is well determined, but detailed investigation is now in progress (see II-C-1).

Structure, Relaxation and Control of Reactive Cluster Studied by Two-Color Laser Spectroscopy

FUJII, Masaaki

A molecular cluster is a microscopic system of solution and/or crystal, and is thought to provide detailed information on relaxation and reaction dynamics in condensed phase. However the molecular clusters which have been studied are mainly static system which has no reaction pathway after photo-excitation, and consequently spectroscopic information which concerns the reaction mechanism has not been obtained sufficiently. In this research project started from 2000, we will apply various laser spectroscopy to the reactive clusters to reveal detailed mechanism of intracuster reaction. The originally developed spectroscopies, such as nonresonant ionization detected IR spectroscopy, UV-IR-UV ion dip spectroscopy, and the picosecond time-resolved IR dip spectroscopy, are described in the Research Activities of this group. By using these method, we have measured the IR spectra of solvated clusters, such as phenol/ammonia, naphthol/water and alcohol, carbazole/water and 7-azaindole dimers, and have discussed the relation between the structure and intracuster reactions. (see Research Activity III-E “Spectroscopy and Dynamics of Vibrationally Excited Molecules and Clusters” for detail)

Dynamics of Molecular Superexcited States Studied by Electron and Fluorescence Spectroscopy

MITSUKE, Koichiro

One of our main interests is to elucidate the spectroscopy and dynamics of molecular superexcited states. Though these states often play crucial role in photo-excitation and bimolecular reactions in the VUV and soft X-ray regions, the knowledge of their characteristics is very limited. Owing to autoionization in a very short period and strong perturbation from neighboring

neutral states, superexcited states experience various decay pathways such as neutral dissociation, internal conversion, and intramolecular vibrational redistribution. We have employed three experimental methods which serve as a means of providing insights into such processes: Photoelectron spectroscopy, dispersed fluorescence spectroscopy, and laser induced fluorescence spectroscopy. Taking maximum advantage of the tunability of synchrotron radiation, we have obtained hundreds of spectra at different primary photon energies. Assembling and comparing these one-dimensional spectra enable us to uncover novel decay pathways. For example, superexcited states are often subject to neutral dissociation into electronically excited fragments. These fragments release their internal energy by emitting fluorescence. Dispersed fluorescence spectroscopy is helpful for us in assigning the dissociation products and determining their vibrational distribution. However, this is not sufficient. If we wish to decide on which precursor state gives rise to the fragments, we should carry on excitation spectroscopy for the particular emission band with changing the primary photon energy. Namely, the fluorescence intensity should be measured as a function of two variables, the initial synchrotron radiation photon energy and final fluorescence wavelength. Two-dimensional plots thus obtained allow us to investigate involved dissociation mechanism of a superexcited state, to evaluate the magnitudes of the electronic coupling with other neutral or ionic states, and to achieve description on the potential energy surface of the relevant dissociative state.

Decay and Dissociation Dynamics of Core Excited Molecules

SHIGEMASA, Eiji; GEJO, Tatsuo

Thanks to the high performance of the newly constructed Varied-Line-Spacing Plane Grating Monochromator (VLS-PGM) at BL4B of the UVSOR facility, various spectroscopic investigations on molecular core-levels with high-resolution have become feasible. The dynamics of molecular inner-shell excitation and relaxation processes is complex even for simple molecules, and thus it is advantageous to use various experimental techniques together with such a high performance monochromator in the soft x-ray region.

The construction of apparatuses for two different types of electron-ion coincidence experiments has been started. A high luminosity double toroidal analyzer (DTA) equipped with a two-dimensional detector makes it possible to measure the angular distribution and kinetic energy of electrons/ions simultaneously. Owing to unexpected short-circuits in the electrical wiring for DTA, performance tests on it has been delayed. Threshold electron spectroscopy has proved to be very powerful in the investigation of electron correlation phenomena not only in atoms but also in molecules. In the angle-resolved photoion spectroscopy applied to the inner-shell excitations of linear molecules, the parallel and perpendicular transitions are distinguishable. Thus, it is expected that the combination between a threshold electron spectrometer and an angle-resolved photoion spectrometer can provide a rare opportunity to obtain

threshold electron spectra including the symmetry information on the excited states, which can be called as symmetry-resolved threshold electron spectra. It has been confirmed through the test experiments using VLS-PGM that the symmetry-resolved threshold electron spectra for N₂ can be measured, although the signal intensity under high-resolution condition was considerably low.

A new project towards the practical usability of the free electron laser (FEL) developed at UVSOR has been initiated in 2000. Two-photon double-resonant excitation spectrum of the autoionization Xe* $5p^54f$ resonance via the Xe* $5p^55d$ intermediate state has been successfully derived. Though similar experiments in a shorter wavelength region for FEL have been attempted, unknown strong backgrounds observed in the photoion detection system have prevented us from measuring the corresponding spectrum. A detailed inspection of the whole experimental setup is in progress.

(c) Novel Material Science

Calculations of Large Molecular Systems

ISHIMURA, Kazuya; NAGASE, Shigeru

In material science, it is of increasing interest to make reliable calculations on large molecular systems using ab initio molecular orbital or density functional methods. For this purpose, high-performance parallel calculations on PC clusters are investigated by developing computer network and effective parallel programs. Up to now, relatively good cost and speed performance are obtained.

Response of Protein Conformation to Pressure: Theoretical Study on Partial Molar Volume

HIRATA, Fumio; SATO, Hirofumi¹;
KOVALENKO, Andriy F.; IMAI, Takashi;
YAMAZAKI, Takeshi; WATANABE, Ayumi;
KINOSHITA, Masahiro¹; NISHIYAMA, Katsura²;
HARANO, Yuichi³

(¹Kyoto Univ.; ²Osaka Univ.; ³Rutgers Univ.)

Protein conformation in solution is fluctuating around its equilibrium structure, and the occurrence of the structural fluctuation is governed by its free energy. It has recently been demonstrated by Akasaka and his coworkers that pressure can be an impeccable thermodynamic parameter to realize structural fluctuations occurring in protein. Using pressure as an order parameter, Akasaka could have detected a set of NMR chemical shifts corresponding to a variety of conformations, from native to completely random states, which are supposedly the hierarchical substates appearing in the protein in the ambient condition. Since occurrence of a substate of protein with higher free energy is rare, it is difficult to detect such event by usual methods such as spectroscopy.

The thermodynamic response of protein conformation to pressure is manifested in its partial molar volume (PMV), due to the Le'Chatelier law. It is, therefore, essential to analyze PMV in order to understand conformational fluctuation of protein. The theoretical analysis of PMV is of particular importance in this respect, because there is no way to measure experimentally PMV of individual substates. If one is able to calculate PMV with theoretical method, it is not difficult task to obtain PMV of a substate of protein by producing such a conformation by, say, the multi-canonical Monte-Carlo sampling coupled with the RISM theory.

Recently, we have developed a method to calculate PMV of biomolecules in aqueous solution by combining the RISM/3D-RISM with the Kirkwood-Buff theory. In the special research project, we have carried out the theoretical treatment for PMV of a series of amino acids. The results for the twenty amino acids are not only in quantitative agreement with the experiments, but also able to discriminate the specificity each amino acid manifests in PMV.

We have also calculate the partial molar volumes and their changes associated with the coil(extended)-to-

helix transition of two types of peptide, glycine oligomer and glutamic acid oligomer, in aqueous solutions by using the Kirkwood-Buff solution theory coupled with the three-dimensional reference interaction site model (3D-RISM) theory. The calculated volume change upon the transition turn out to be small and positive in accord the experiment. The volume is analyzed by decomposing it into five contributions following the procedure proposed by Chalikian and Breslauer: the ideal volume, the van der Waals volume, the void volume, the thermal volume, and the interaction volume. The ideal volumes and the van der Waals volumes do not change appreciably upon the transition. In the both cases of glycine peptide and glutamic acid peptide, the changes in the void volumes are positive, while those in the thermal volumes are negative, and tend to balance those in the void volumes. The change in the interaction volume of glycine-peptide does not significantly contribute, while that of glutamic acid-peptide makes negative contribution.

Theory for Equilibrium and Non-Equilibrium Properties of Low-Dimensional Molecular Materials with Strong Electron Correlation

YONEMITSU, Kenji; KISHINE, Jun-ichiro;
OTSUKA, Yuichi; MIYASHITA, Naoyuki¹;
KUWABARA, Makoto²

(¹GUAS; ²Kobe Univ.)

In low-dimensional molecular materials, electron correlations are essential for the understanding of novel electronic phases. i) Mixed-stack organic charge-transfer complexes have columns of alternating donor and acceptor molecules. Neutral-ionic and dimerization phase transitions are observed in them. Since the dimerization was observed in some neutral compounds, importance of the long-range Coulomb interaction has been pointed out. We have demonstrated by the finite-temperature density-matrix renormalization-group method that transfer-modulating electron-lattice coupling also brings about dimerization in the neutral phase and that the transition becomes continuous then. The TTF-CA complex shows the discontinuous and simultaneous, neutral-ionic and dimerization phase transitions. It shows the photoinduced phase transition as well. We have solved the time-dependent Schrödinger equation to reproduce peculiarities found in time-resolved spectroscopy, such as a) the threshold intensity above which the transition takes place, b) the macroscopic coherent oscillations of neutral-ionic phase boundaries, and c) the quick loss of the second-harmonic-generation signal. ii) Among halogen-bridged binuclear metal complexes, binuclear platinum complexes are synthesized and investigated extensively. They show a variety of electronic phases owing to competing kinetic energy, Coulomb repulsion, and electron-lattice coupling. When the ligand is pop, electrons are so localized that the perturbation theory from the strong-coupling limit works very well for the ground and optically excited states. When the halogen is iodine in addition, as the

distance between the neighboring MM units increases by changing counter ions or by reducing pressure, a discontinuous transition takes place from the charge-density-wave phase to the charge-polarization phase. This can be explained by decreasing electron-lattice coupling strength compared with repulsion strength. In those materials which show the pressure-induced transition, a photo-induced transition is observed in the hysteresis loop. The transition is, however, only from the charge-density-wave to charge-polarization phases. We have clarified its mechanism. a) The lowest-energy photoexcitation brings about inter-unit charge transfer only in the former phase. b) The high-energy photoexcitation in the latter phase transfers charge so locally that the former phase never proliferates like a domino effect. iii) The dimensional crossover in excitation spectra is demonstrated by the finite-temperature density-matrix renormalization-group method. At a particular band filling that is common in organic conductors, electron correlation is so strong in the most conducting direction that electron motion is confined in this direction. The perpendicular motion takes place only incoherently. This explains the observed behavior that is reminiscent of the doped Mott insulators.

UHV System for MOKE Measurements

YOKOYAMA, Toshihiko; NAKAGAWA, Takeshi

The magnetooptical Kerr effect (MOKE) is usually the most suitable method to characterize magnetic properties of ultrathin films since the rotation angle of the electric-field vector of linearly polarized lights is nearly proportional to the magnetization of the films. Although we are planning to use x-ray magnetic circular dichroism (XMCD) in UVSOR, in-laboratory experiments is also important for several reasons. First, detailed and time-consuming characterization is required especially for the preparation of new magnetic materials. Since the beamtime in UVSOR is limited, some in-laboratory equipment is essential. Second, the measurements in the applied magnetic field is easier in MOKE since MOKE detects polarization of the reflected lights while XMCD scales emitted electrons.

We are thus constructing a new ultrahigh vacuum (UHV, $< 1 \times 10^{-8}$ Pa) system in which *in situ* MOKE can be measured. The system contains a standard UHV pumping unit, a surface cleaning system of sputtering and annealing of substrates, and a molecular beam epitaxy (MBE) system. The substrate can be cooled down to ~ 100 K using liquid nitrogen and to ~ 25 K using liquid He. A magnetic field can be applied to samples in UHV with a simple electromagnet up to 3000 Gauss. The magnetic field is not so large but is usually sufficient for ultrathin films of *3d* elements. Both the polar MOKE geometry for perpendicular magnetization and the longitudinal MOKE for in-plane magnetization are available.

Using the UHV MOKE system, we will investigate magnetic properties of ultrathin metal films, nanowires and nanodots, especially control of magnetism using surface chemical techniques such as gas deposition.

Pulsed Methods of Electron Spin Resonance Spectroscopy

KATO, Tatsuhisa; FURUKAWA, Ko

Electron spin resonance (ESR) spectroscopy has been a powerful technique for the characterization of radical species. The modern development of ESR spectroscopy enables us to investigate the transient phenomena in detail. The pulsed ESR spectroscopy gives us the prototyped demonstration of the time-dependent spectroscopy. Some time-dependent measurements were experimentally performed and compared with the theoretical model calculation. The advanced ESR method was applied to the study on the high spin state of Gd@C₈₂ described in section II-J-1 and of multi-cations of aromatic amines in section II-J-2, and to the study on the reaction mechanism in the reduction of metallofullerenes by solvation in section II-I-3.

Spectroscopic Studies of Organic Conductors

YAKUSHI, Kyuya

The low-frequency reflectivity of an organic conductor provides us with a wealth of information on the nature of charge carriers. For instance, the anisotropy of a band structure, bandwidth, effect of electron-electron correlation, and electron-molecular vibration (EMV) coupling parameters can be extracted from the analysis of the reflectivity or optical conductivity curve. For this subject, we have studied charge-transfer salts of EDOEDT-TTF, (BDTFP)₂X(PhCl)_{0.5}, (EO-TTP)₂AsF₆. In relation to this subject, we have conducted the quantum chemical study of NiPc, NiPc⁺, CoPc, and CoPc⁺. We could reproduce the intensity of the diagnostic vibrational bands, which characterize the oxidation state of NiPc and CoPc. The ring oxidation in CoPc⁺ is also very well reproduced by this calculation. This calculation including the overlap integral between the one-dimensional conductor, CoPc(AsF₆)_{0.5}, is consistent with the characteristic magnetic properties obtained by the experiment of dilute alloy with NiPc(AsF₆)_{0.5}.

Usually the molecular vibrations (local phonons) are screened by strong electronic absorption by charge carriers, and thus very few optical phonons are detected in the reflection spectrum. In this sense, Raman spectroscopy is a powerful method complementary to reflection spectroscopy for understanding molecular vibrations in a metallic state. Since some molecules have charge-sensitive vibrational modes, the Raman spectroscopic method is a powerful tool to detect the site-charge distribution (oxidation state of molecule). We are investigating the charge ordering (CO) phenomena in organic conductors using the technique of infrared and Raman spectroscopy. In the organic charge-transfer salts, CO is originated from the localization of charge carriers. Since the charge carriers in organic crystal is located at the boundary between localized and extended (delocalized) states, CO is widely found through the phase transition. The interest in CO is quickly growing, since CO is theoretically considered as being related to the charge-fluctuation-mediated superconducting mechanism. As to this subject, we have thoroughly

studied the vibrational spectrum of θ -(BEDT-TTF)₂Rb-Zn(SCN)₄ using polarized Raman and infrared spectroscopy with the aid of ¹³C-substituted isotope compound. For θ -(BDT-TTP)₂Cu(NCS)₂, We have extended the study on CO to the following charge-transfer salts, θ -(BDT-TTP)₂Cu(NCS)₂, (Me₂-DCNQI)₂Cu_xLi_{1-x} ($0 < x < 1$), and (DI-DCNQI)₂M ($M = \text{Ag, Li, Cu}$).

Broad-Line Solid State NMR Investigation of Electronic States in Molecular-Based Conductors

NAKAMURA, Toshikazu; FUJIYAMA, Shigeki

Molecular based conductors are one of the extensively studied materials. Their fundamental properties have been very well clarified. The development of the understanding of the electronic phases of these materials enables us systematic investigations of low-dimensional highly correlated electrons systems. For example, recent progress of the investigation for the charge ordering and/or charge disproportionation states in quasi-two-dimensional organic conductors, θ -type BEDT-TTF compounds, are attracting much attention in the field of solid state physics. As for quasi-one-dimensional systems, (TMTTF)₂X, have been extensively studied so far because of their various ground states such as spin-Peierls, AF, IC-SDW and superconductivity. Moreover the origin of the paramagnetic insulating states is an open question. To investigate the low temperature electronic phases, we synthesized ¹³C substituted TMTTF molecules; the two central carbon sites, of which hyperfine coupling constants are much larger than those of hydrogen sites, have been labeled with ¹³C. We investigated the charge configurations and spin dynamics in the low temperature phases of (TMTTF)₂X.

Broad-Line Solid State NMR is a powerful microscopic investigation; they are advantageous for studying the fundamental electronic properties and for understanding the detailed electronic structures of molecular based compounds. Competition of the electronic phases in molecular based conductors has attracted much attention. Investigation of such electronic phases in molecular based conductors is important to understand the unsolved fundamental problems in the field of solid state physics. The aim of this project is to clarify the electronic state (charges and spins) of molecular based compounds by microscopic point of view.

In this project, we are preparing a new NMR system under ultra-low temperatures to study more detailed electronic structure from microscopic points of view. We also try to carry out experiments with new devices under unconventional circumstance.

The following projects are also now going on.

- [1] Investigation of charge ordering States in (TMTTF)₂X
- [2] Charge and spin dynamics in organic conductors
- [3] ¹³C NMR study of two-component spins system, (BEDT-TTF)-TCNQ
- [4] Low temperature electronic phases in (EDT-TTF)₂X

Development of New Organic Conductors

KOBAYASHI, Hayao; FUJIWARA, Hideki;

TANAKA, Hisashi; ZHANG, Bin; FUJIWARA, Emiko¹; KOBAYASHI, Akiko¹
(¹Univ. Tokyo)

In order to make contribution to the progress of solid state chemistry and physics of molecular materials, we have tried to develop new types of molecular conductors and examine their physical properties. The main results obtained in the last one year are as follows. (1) We have recently reported the first example of single-component molecular metal based on the transition metal complex molecule Ni(tmdt)₂. For the development of single-component molecular metal, it is of key importance to design "anomalous π molecule" with very small HOMO-LUMO gap (< 0.5 eV) and TTF skeleton permitting to produce the sufficiently large intermolecular multi-dimensional HOMO-HOMO and LUMO-LUMO interactions. Since the single-component molecular metals have been already realized, one of the next targets may be the magnetic molecular metal based on the single-component molecules with the magnetic transition metal ions such as Cu²⁺ and Co²⁺. If the molecule has a localized magnetic moment on the central atom and the intermolecular magnetic interaction is mediated by the π conduction electrons, the large intermolecular magnetic interaction can be expected. We have recently found that the conduction electron and magnetic moments coexist in the crystal of [Cu(dmdt)₂]. (2) Under the collaboration with Dr. Uji, we found the field-induced superconductivity of λ -BETS₂FeCl₄ in 2001. Very recently, we have discovered the second example of the organic conductor exhibiting field-induced superconducting transition through the examination of the magnetoresistance of κ -BETS₂FeBr₄ up to 15 T and down to 0.58 K. These findings seem to suggest the field-induced superconductivity, which is a very rare phenomenon in inorganic conductor, can be observed in many two-dimensional magnetic organic superconductor with antiferromagnetic interaction between π conduction electrons and localized magnetic moments. (3) For the realization of molecular electronic devices, it will be necessary to develop "dual-action systems" whose conducting properties can be sharply controlled by external forces. One of the possible dual-action molecular systems will be a composite system consisting of organic layers responsible for electron conduction and inorganic layers with localized magnetic moments, whose conductivity can be controlled by tuning magnetic state of the inorganic layers. We have recently reported the first example of the novel dual-functional magnetic organic conductor whose superconducting state can be sharply switched on or off by controlling the metamagnetic transition of the anion layers.

Design and Synthesis of Organic Spin-Ladder Systems

HOSOKOSHI, Yuko; KATO, Keiichi; INOUE, Katsuya

The magnetic properties on the low-dimensional quantum spin system with an energy gap have attracted great interests in recent years. Especially the antiferro-

magnetic $S = 1/2$ spin ladder system draws much attention, since it is interesting in terms of the Haldane state and the high T_C superconductivity. The ground state of the $S = 1/2$ ladder is the resonating valence bond (RVB) state or the dimerized state. The property of the $S = 1$ antiferromagnetic ladder is also interesting. For the ground state, the Haldane state or the dimer state is expected.

Here we present organic spin ladder systems. We employed *N-tert*-butyl aminoxy as a spin source of $S = 1/2$, focusing on the stability, crystallinity and controllability of the crystal structure. We must mention that the electrostatic energy plays substantial role in controlling the molecular packing of the neutral organic crystal. The partial charges on the oxygen and nitrogen atoms on the aminoxy group prefer the intermolecular contacts between the aminoxy groups. We use the intermolecular interactions between the aminoxy groups as an antiferromagnetic leg. As an antiferromagnetic rung, we combine two $S = 1/2$ spins by intramolecular antiferromagnetic exchange coupling. As for the $S = 1$ ladder, we employed *m*-phenylenebis(*N-tert*-butylaminoxy), BNO, as an $S = 1$ unit. Intramolecular exchange coupling in BNO is reported to be $2J/k_B \sim 600$ K. Although there are several examples of $S = 1/2$ two-leg ladders, BIP-BNO (BIP-BNO = 3,5'-bis(*N-tert*-butylaminoxy)-3',5'-dibromobiphenyl) is the first example of the genuine organic system, which consists only of light elements and is ideal Heisenberg spin system. As far as the authors know, there are no example of the $S = 1$ ladder compound. The crystals of BIP-TENO (3,3',5,5'-tetrakis(*N-tert*-butyl-aminoxy)-biphenyl) form an antiferromagnetic double spin chain composed of spin dimers, in which two spins are coupled ferromagnetically. When the dimer is taken as an unit, this system can be regarded as an $S = 1$ ladder. (see V-C)

Construction of BL-7A at UVSOR for STM Observation of SR Irradiation Induced Photochemical Reaction on Si Surfaces

NONOGAKI, Youichi; URISU, Tsuneo

This beamline is constructed for STM observation of surface photochemical reaction induced by illumination of undulator radiation. The surfaces are exposed to high flux quasi-monochromatic light with varying photon energy generated by the undulator. We have been interested in photo-stimulated desorption of SiO_2 on Si surfaces due to the application of nano-fabrication by using undulator radiation.

Using bending magnet radiation, we have done many experiments of SR stimulated desorption of SiO_2 . To avoid the reduction of photon flux, the bending magnet radiation was not monochromatized. We have found that Si (111) 7×7 reconstructed surfaces appears after 2 h irradiation of SiO_2 covered Si surface even at low temperature of 700 °C. It indicates that SiO_2 desorbed completely by SR irradiation effects.

To investigate reaction mechanism of the photo-stimulated desorption of SiO_2 was an attractive target. It is necessary to observe the Si surfaces after irradiation of various excitation photon energies. Since mono-

chromatic light from bending magnet radiation is too weak, undulator radiation should be needed.

Now, we prepare construction of new BL-7A undulator beamline, which includes a plane and a toroidal mirrors as optical components. The plane mirror is used for branching the beamline and the toroidal mirror for focusing and adjusting spot position. The STM system was replaced in December 2001, which was designed so that the SR beam can illuminate the sample surface under the STM tip. Therefore, sample surfaces are observed just after the SR illumination without the sample transfer. By upgrading the beamline and the STM system, we will obtain deep knowledge about relationship between SiO_2 photo-stimulated desorption and Si core-electron transition.

Catalytic Oxidation of Alcohols in Water under Atmospheric Oxygen by Use of an Amphiphilic Resin-Dispersion of Nano-Palladium Catalyst

UOZUMI, Yasuhiro

We have previously reported that amphiphilic polystyrene-poly(ethylene glycol) (PS-PEG) resin-supported palladium-phosphine complexes catalyzed various palladium-mediated reactions smoothly in water. These observations prompted us to design and prepare the PS-PEG resin-supported palladium nanoparticles, which should have high catalytic activity owing to the large surface area of the nanoparticles and water-based reactivity provided by the amphiphilicity of the PS-PEG matrix combined in one system. Catalytic alcohol oxidation was achieved in water under atmospheric pressure of molecular oxygen by use of amphiphilic polymer-supported palladium nanoparticles.

An amphiphilic resin-dispersion of palladium nanoparticles was readily prepared by reduction of a PS-PEG resin-supported palladium(II) complex. Thus, a chelating ligand anchored on PS-PEG amino-resin was complexed to palladium by treatment with an equimolar amount of $\text{Pd}(\text{OAc})_2$ to give the stable 16-electron divalent palladium complex. The complex was treated with benzyl alcohol in refluxing water to give the desired amphiphilic PS-PEG resin-dispersion of palladium nanoparticles. Transmission electron microscopy (TEM) of the resulting palladium-resin shows that the palladium particles have a mean diameter of 9.1 nm with a narrow size distribution. The amphiphilic resin-dispersion of palladium nanoparticles exhibited high catalytic activity in aerobic oxidation of alcohols in water.

Reductive Activation of Carbon Dioxide and Oxidative Activation of Water Aimed at Energy Conversion

TANAKA, Koji

Multi-electron reduction of CO_2 affording organic compounds is much more important than two-electron reduction of CO_2 producing CO and/or HCOOH , because of the continuous decrease of free energy changes with an increase of the number of electrons participated in the reduction. Taking into account that CO_2 is smoothly converted to CO on metal complexes

through metal- η^1 -CO₂ ones, the principal factor to achieve multi-electron reduction of CO₂ is reduction of M-CO bonds without accompanying reductive cleavages of M-CO bonds due to accumulation of too much electrons in the central metals. A catalytic system, which can supply electrons to M-CO bonds through ligand localized redox reactions, may realize reduction of the M-CO bonds without evolving CO under protic conditions. Some Ru-CO complexes with mono-dentate 1,8-naphthyridine easily form a five-membered metallacycle by an attack of free nitrogen to the carbonyl carbon when the ligand undergoes one-electron reduction. We, therefore, examine the reactivity of a variety of metal-naphthyridine complexes aiming at multi-electron reduction of CO₂.

Reactivity of high valent metal-*oxo* complexes is of current interest from the viewpoints of the enzymatic activation of dioxygen on metals and oxidation or oxygenation of organics such as P-450 enzymes. Mechanistic understandings of the reactivity of O₂ on metals have, however, been limited because of the difficulty of selective cleavage of the O-O bond of O₂ on metals in artificial systems. Oxidation of Ru-OH₂ complexes causes simultaneous loss of protons to form high-valent Ru=O ones, which attract much attention to elucidate the reactivity of metal-*oxo* frameworks. Quinone is electrochemically non-innocent ligand and undergoes stepwise reduction to yield semiquinone and catecholate. Taking into account that higher oxidation states of Ru=O complexes have been obtained by sequential electron and proton loss of Ru-OH₂ ones, introduction of quinone ligands as an electron acceptor into the Ru-OH₂ framework would induce deprotonation of the aqua ligand instead of the oxidation of the central Ru ion. Along the line, we have prepared a series of metal-aqua complexes with dioxolene aimed at the smooth conversion from the aqua to hydroxy and *oxo* ligands.

Coordination Chemistry of New Multidentate Ligands and Activation of Small Molecules

KAWAGUCHI, Hiroyuki; MATSUO, Tsukasa

The efficient activation of dinitrogen under mild conditions is a challenging topic in chemistry due to its important application. Although dinitrogen complexes of almost transition metals have been prepared, there are few examples of well characterized transition metal compounds which are capable of cleaving the N≡N triple bond. As part of a research program aimed at developing new ancillary ligands to support reactive metal centers, we have found it attractive to utilize linked aryloxy ligands, in which aryloxy units are connected at *ortho* positions through methylene linkers. One of the advantages of this system is the flexible coordination modes, and the trimer can be coordinated in a U- and an S-conformation. In addition, there is the opportunity for coordinative unsaturation as compared to the calix[4]arenes. In this scenario, we have prepared titanium and niobium complexes supported by linked aryloxy trimers. In the case of niobium complexes, we found that the N≡N triple bond split took place in a mild condition. Further study to isolate an intermediate dur-

ing the course of this reaction is currently underway.

Developments and Researches of New Laser Materials

SARUKURA, Nobuhiko; OHTAKE, Hideyuki; KOZEKI, Toshimasa; ONO, Shingo¹
(¹Tokyo Univ. Sci.)

Although development of lasers is remarkable, there are no lasers which lase in ultraviolet and far infrared regions. However, it is expected that these kinds of lasers break out a great revolution in not only the molecular science but also in the industrial world.

In this project we research characters of new materials for ultraviolet and far infrared lasers, and develop new lasers by using these laser materials.

Development and Research of Advanced Tunable Solid State Lasers

TAIRA, Takunori; SHOJI, Ichiro; PAVEL, Nicolai; DASCALU, Traian; ISHIZUKI, Hideki; SATO, Yoichi; SAIKAWA, Jiro

The use of diode lasers to pump solid-state lasers opens new horizon in laser science. Diode-pumped solid-state lasers are compact, reliable, and efficient sources of coherent radiation. They can provide excellent spatial mode quality and narrow linewidths. The high spectral power brightness of these lasers has allowed high efficiency frequency extension by nonlinear frequency conversion. Moreover, the availability of new and improved nonlinear optical crystals makes these techniques more practical. Recently attention has been directed to the trivalent ytterbium ion doped YAG. The advantages of Yb:YAG lasers for a high power, high stability and wide tunability laser operation are well recognized due to its small quantum defect, long upper-state life time and wide gain width.

On the other hand, quasi phase matching (QPM) is a new technique instead of conventional birefringent phase matching for compensating phase velocity dispersion in frequency conversion. Inasmuch as the pool of mature nonlinear optical materials is limited and development of new materials takes time and cost, QPM is a useful method for extending the range of available nonlinear optical materials. The ability to pattern a QPM structure allows the nonlinear materials to be engineered for desired interactions, meaning molecular-science-specified lasers are obtainable through these artificial materials.

In this projects we research and develop new diode-pumped-solid-state lasers and new frequency conversion devices. Especially, we will focus on the combination of microchip lasers and QPM devices. These kinds of advanced tunable solid-state light, so to speak "Chroma-Chip Lasers," will assist the research of molecular science.

Synthesis of Oligonaphthalenes and Oligoanthracenes and Applications for Organic Field-Effect Transistors

ITO, Kaname; SAKAMOTO, Youichi; SUZUKI, Toshiyasu

We have synthesized 2,6-ternaphthalene (**3N**) and 2,6-quaternaphthalene (**4N**). These oligomers are colorless crystalline solids, which showed sharp melting endotherms at 287 and 351 °C, respectively. **3N** is slightly soluble in some solvents, but **4N** is insoluble in common organic solvents. 2,6-Bianthryl (**2A**) and 2,6-teranthracene (**3A**) were also synthesized by the Suzuki coupling. These oligomers are bright yellow crystalline solids, which showed sharp melting endotherms at 365 and 491 °C, respectively. **2A** and **3A** is insoluble in common organic solvents. OFETs were fabricated using anthracene oligomers as the *p*-type semiconductors. They showed the field effect with hole mobilities in the range of 10^{-3} – 10^{-2} cm²/Vs.

Field Effect Transistors of BTQBT and Its Derivatives

TAKADA, Masaki¹; YAMASHITA, Yoshiro²; TADA, Hirokazu
(¹GUAS; ²Tokyo Inst. Tech.)

[*Proc. MRS* **725**, P10.3 (2002)]

Field effect transistors (FETs) using organic semiconductor thin films as active layers have been studied intensively because they have great potential of applications to low cost electronic devices and their circuits. Most organic compounds examined so far showed rather low field effect mobilities in the range of 10^{-5} – 10^{-3} cm²/Vs. Thin films of pentacene and polythiophene are known to exhibit high mobilities and received a considerable attention.

Drift mobility of single crystals and thin films of organic semiconductors have long been investigated with a time of flight method. The components of charge transfer complexes such as tetrathiafulvalene (TTF)- and tetracyanoquinodimethane (TCNQ)-based molecules are known to show high mobilities. The introduction of sulfur and selenium into a molecule by chemical synthesis makes it possible to have strong intermolecular interaction. Among these molecules, a single crystal of bis-(1, 2, 5-thiadiazolo)-*p*-quinobis(1, 3-dithiole) (BTQBT) shows rather high hall mobility, that is 2.4–4 cm²/Vs at room temperature. We have prepared and characterized thin film field effect transistors (FETs) of BTQBT and its derivatives. Preparation and characterization of the films were carried out under ultrahigh vacuum condition. Most materials examined showed *p*-type semiconducting behaviors. Among *p*-type molecules, BTQBT films deposited at room temperature showed *p*-type semiconducting behaviors with mobility of 0.1 cm²/Vs. The on/off drain current ratio was 10⁷. The mobility and on/off ratio reached to 0.2 cm²/Vs and 10⁸, respectively, by optimizing the film growth conditions. These performances are almost comparable to those of pentacene and polythiophene thin films, indicated that BTQBT molecule is a prominent semiconducting material as a high mobility thin film. It was also found that tetracyanoquinodimethane (TCNQ) derivative showed an *n*-type semiconducting behavior

with an electron mobility of 8.9×10^{-4} cm²/Vs.

Generation of Reactive Species via Electron Transfer on Metal Complexes, as Basis of Chemical Energy Conversion Systems

NAGATA, Toshi; HINO, Takami; ITO, Hajime; KIKUZAWA, Yoshihiro

This project aims at developing redox catalysis reactions suitable for chemical energy conversion. Our current interest focuses on modeling photosynthesis, that is, driving endothermic chemical transformation by using light energy via photoinduced electron transfer. Progress has been made in the following topics during the last year:

A. Examination of various terdentate ligands as candidates for new electrocatalysis. We found that replacing one or two pyridine rings in 2,2':6',2''-terpyridine (terpy) gives new, useful terdentate ligands. The ligands are prepared by two steps from easily obtained formylpyridine derivatives. The ruthenium (II) complex of the 6-(2-pyrrolyl)-2,2'-bipyridine derivative was prepared and characterized. The redox potential of the Ru(III)/Ru(II) couple appeared 1.10 V more negative than the bis(terpyridine) complex, indicating that the higher oxidation states are more accessible for this complex.

B. Light-driven oxidation of alcohols by a TEMPO/quinone/porphyrin system was investigated. Initial survey of the reaction conditions suggested that the reaction was initiated by photoinduced electron transfer from the porphyrin to the quinone.

Electronic Structures and Reactivities of Organic/Metal Clusters

NEGISHI, Yuichi; SAKURAI, Hidehiro¹; MURAYAMA, Haruno; TSUKUDA, Tatsuya
(¹Osaka Univ.)

Metal clusters stabilized by organic molecules exhibit novel catalytic properties due to the unique geometric and electronic properties of the metallic cores and tailor-made functions of the organic molecules. However, the fabrication of the organic/metal clusters as catalysts is not trivial; stabilization by organic molecules, which is inherent to hinder coalescence of the clusters, reduces the catalytic activities of the clusters. In order to tackle such dilemma, we have employed various reagents to stabilize the clusters with minimal extent of surface poisoning. The molecules we used are dendrimers and thiol molecules with bulky functional group or cyclodextrins. The organic/metal clusters were prepared by chemical reduction of the relevant metal ions in the presence of these molecules. Geometric structures of the clusters were studied by mass spectrometry, TEM, and EXAFS measurements. In this project, we aimed to reveal the correlations between the chemical reactivities and the electronic structures of the clusters studied by photoelectron spectroscopies.

Local Distribution of Photoexcited States on a Semiconductor Surface as Observed by Scanning Tunneling Spectroscopy

KOMIYAMA, Masaharu; GU, Ning¹; LI, Yanjun; MATSUMOTO, Taki
(¹IMS and Southeast Univ.)

The photocatalytic processes occurring on a semiconductor catalyst surface may be divided into two parts: physical processes that are initiated by photo-excitation of titania electrons, and following chemical processes which are the so-called heterogeneous catalysis. The former physical processes are commonly described within the framework of band model which assumes infinite array of three-dimensional (3-D) unit cells that give rise to a periodic potential, with which the electronic band structure is defined. Thus upon UV light illumination electrons in the valence band of titania are excited to its conduction band, leaving holes in the valence band, and they migrate within each band following the energy gradient until they annihilate each other, trapped in some (defect) sites, or consumed by subsequent chemical processes. However, at the solid surfaces and in superfine particles which are the common forms of practical photocatalysts, this infinite array of unit cells in three dimensions no longer exist, and their electronic band structure are known to be quite different from that of bulk.

This very surface is where the chemical part, namely heterogeneous catalysis, occurs. It is a highly local process: individual reactant molecules adsorb on a solid catalyst surface, react in one or more steps, and the product molecules leave the surface in the process called desorption. The adsorption and/or reaction sites in heterogeneous catalysis are often very specific, in terms of their atomic and/or electronic configuration: some reactant may need particular arrangements of atoms that is present on the catalyst surface, and others may need particular electronic states of the surface atoms to provide unique adsorption or reaction sites.

Despite these vastly different descriptions between the two processes occurring in heterogeneous photocatalysis, namely the physical process that is described by infinite 3-D or 2-D array of unit cells, and the chemical process that necessitates very local description of catalyst surface, no efforts to bridge this gap are known to the authors. The present work is the first of such attempts, and examines the local electronic characters of titania surface upon UV-light illumination by means of scanning tunneling microscopy (STM).

On a single crystal titania with its (110) surface polished, we found a structure that respond to UV light irradiation.¹⁾ It was an area where there exist two islands connected by a narrow bridge whose width is about 2.5 nm. When the UV light is turned on, this bridge becomes brighter, and then goes back to the original brightness when the light is turned off. This brightness change of the bridge can be reversibly repeated. The interpretation of above results is in progress, and also an effort to detect the same effect at atomic level is in progress.

Reference

- 1) M. Komiyama and D. Yin, *Jpn. J. Appl. Phys.* **40**, 4281 (2001).

Electronic Structures and Surface Molecular Orientation of Organic Thin Films and Interfaces by Various Surface Sensitive Spectroscopies

OKUDAIRA K., Koji

Molecular orientation at the surface of organic thin films has recently gained considerable attention, since it affects electronic and optical properties of organic devices. Thin films of pendant group polymers are the most promising candidates for practical use due to their stability and facility of preparation. Furthermore, their surface properties can be easily controlled by changing the pendant chemical group. However, in general the molecules in polymer solids are not ordered due to the large molecular-weight distribution and mixed tacticity, *etc.*, and therefore it is believed that the pendant groups are also unoriented at the surface. Furthermore, since the properties of organic devices consisting of the films depend strongly on the molecular orientation at the film surfaces, determination of the surface molecular orientation such as tilt angle distribution of pendant group is very important for understanding the device properties.

The molecular orientation at the surfaces of poly(9-vinylcarbazole) (PvCz) thin films was studied by angle-resolved ultraviolet photoelectron spectroscopy and near-edge X-ray absorption fine structure (NEXAFS) spectroscopy using synchrotron radiation. The observed take-off angle (θ) dependence of photoelectron intensities from top π band peaks clearly at larger θ than the calculated one for the three-dimensional isotropic random orientation model. The results indicate that there are more pendant groups with large tilt angles than the three-dimensional isotropic random orientation model, which is in good agreement with the result obtained from NEXAFS spectroscopy. The surface electronic states of PvCz may be rather dominated by $\sigma(\text{C-H})$ states at the pendant carbazole group than π states.

Development of "Entropy-Saving" Nano-Materials

OBA, Toru; MINABE, Masahiro¹
(¹Utsunomiya Univ.)

Development and arrangement of molecular devices have been highlighted for downsizing and energy-saving in electronics and photonics. For global, sustainable development, in our opinion, such future materials should also be "entropy-saving": reusable, repairable, and bio-degradable. For development of the material system that is endowed not only with a structural order at the nano- and molecular-scale but with energy- and entropy-saving properties, we have fabricated new concept devices that utilize molecular self-assembly. The device is operated simply by mixing the functional blocks and switching external stimuli. This device, that functions only in the assembled state, can easily be decomposed into the components on demand, and the components can readily reassemble on demand to recover the function again. Exchangeability of the building blocks facilitates repair of damaged blocks, change

of the function of the device, and integration of plural functions. The present study should serve a new design principle for intelligent nano-materials (see VIII-S).

Investigation of Dynamics on Photo-Excited Solids and Surfaces by Using the Combination of Synchrotron Radiation and Laser Light

KAMADA, Masao; TAKAHASHI, Kazutoshi

Dynamics on solids and surfaces excited by photons has attracted much interest from both of basic and application sides, since it may provide new scientific fields and photo-controllable devices. We have been investigating the photo-induced phase transition using photoelectron spectroscopy based on the combination of synchrotron radiation and laser light. Core-level and valence-band photoelectron spectra of organo-metallic complex showed clearly the characteristics of the photo-induced phase transition. We have been also investigating the photo-induced phenomena on semiconductor surfaces using the combination of synchrotron radiation and laser light. Photo-induced core-level shifts observed on GaAs(100) can be interpreted in terms of surface photo-voltage effects. This work has been extended to the super-lattice systems and another semiconductors and also to the investigation of the dynamics using the experimental system for the time-response on the semiconductor surfaces. We have also conducted the two-photon excitation experiments using synchrotron radiation and laser light to understand the details of the excitonic processes in condensed matters.

Construction and Commissioning of In-Vacuum Undulator

KATOH, Masahiro; HAYASHI, Kenji; HORI, Yoichiro¹; HOSAKA, Masahito; KINOSHITA, Toshio; TAKASHIMA, Yoshifumi; YAMAZAKI, Jun-ichiro; KITAMURA, Hideo²; HARA, Toru²; TANAKA, Takashi²

(¹IMS and KEK-PF; ²RIKEN)

We have completed the construction of an in-vacuum undulator for UVSOR-BL7A until February 2002. The overall length is 1.4 m. The period length is 36 mm and the number of periods is 26. The undulator was successfully installed in the storage ring during the spring shut down as shown in Figure 1. The performance test is in progress. It has been shown that the magnetic gap could be narrowed as small as 18 mm without reducing the beam lifetime. We have not observed any heat problem nor beam instability. The synchrotron radiation spectra will be measured in this autumn.

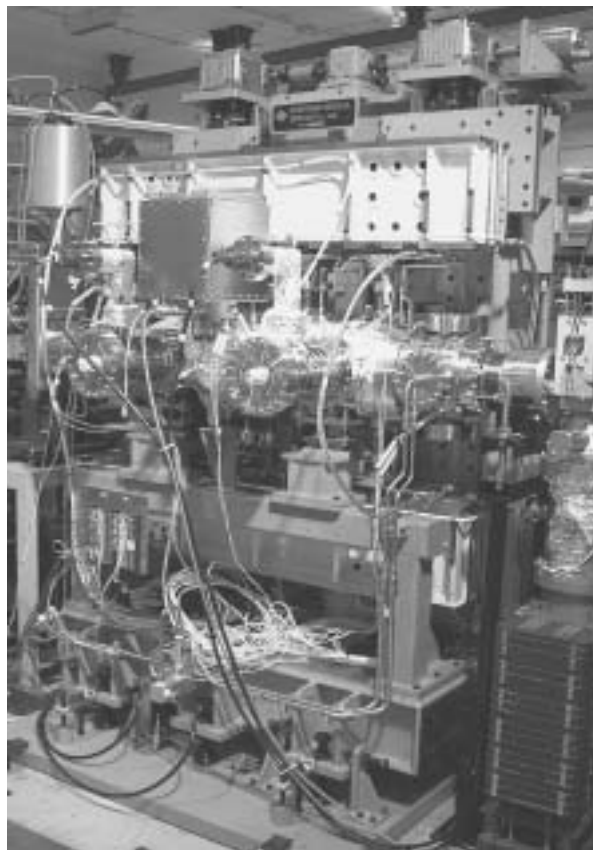


Figure 1. In-vacuum Undulator at UVSOR BL7A.

Optical Investigation on Fermiology of Strongly Correlated Electron Systems

KIMURA, Shin-ichi

Strongly correlated electron systems attract much attention because of their various physical properties. Since the origin is the interaction between the carriers and the localized magnetic moments, we are investigating the electronic structure near the Fermi level (Fermiology) by infrared and photoemission spectroscopies using synchrotron radiation. In this year, we measured optical reflectivity spectra of $\text{Yb}_4(\text{As}_{1-x}\text{Xp}_x)_3$ ($\text{Xp} = \text{P}, \text{Sb}$), $\text{CeSbNi}_{0.15}$, $\text{Yb}_{1-x}\text{Lu}_x\text{B}_{12}$, infrared magneto-optical spectra of $\text{Ce}_{1-x}\text{La}_x\text{Sb}$, $\text{Tl}_2\text{Mn}_2\text{O}_7$, $\kappa\text{-(BEDT-TTF)}_2\text{Cu-[N(CN)}_2\text{]Br}$ and resonant photoemission spectrum of $\text{EuNi}_2(\text{Si}_{0.25}\text{Ge}_{0.75})_2$. Now we are constructing a high energy resolution angle-resolved photoemission apparatus installed at BL5A of UVSOR. The apparatus will become a powerful tool for the investigation of the Fermiology of strongly correlated electron systems including organic conductors.

Preparation of Artificial Metalloenzymes by Insertion of Chromium(III) Schiff Base Complexes into Apo-Myoglobin Mutants

OHASHI, Masataka; KOSHIYAMA, Tomomi; UENO, Takafumi; YANASE, Manabu; FUJII, Hiroshi; WATANABE, Yoshihito

Construction of artificial metalloenzymes is one of

the most important subjects in bioinorganic chemistry, because metalloenzymes catalyze chemical transformation with high selectivity and reactivity under mild conditions. In this project, we have taken a novel strategy for the preparation of artificial metalloenzymes by noncovalent insertion of metal complex catalysts into protein cavities. Manganese(III) and chromium(III) Schiff base complexes are known as catalysts for various oxidations in organic solvents, thus, $[M^{III}(\text{salophen})]^+$ [$M \cdot 1$, $M = \text{Mn}$ and Cr , salophen (**1**) = N,N' -bis(salicylidene)-1,2-phenylenediamine], are employed to insert into a chiral cavity of apo-Mb. For the creation of artificial metalloenzymes, apo-Mb is an excellent candidate since reconstitution of apo-Mb with heme has been well studied. The reconstitution of apo-Mb mutants with Cr(salophen) was carried out by applying a method for modified hemes. The H_2O_2 -dependent sulfoxidation of thioanisole was examined by Cr(salophen)·apo-Mb mutants and Cr(salophen)·apo-H64D/A71GMb exhibited the highest sulfoxidation activity and Cr(salophen)·apo-H64DMb was the lowest. Figure 1 shows a preliminary crystal structure of Cr(salophen)·apo-A71GMb.

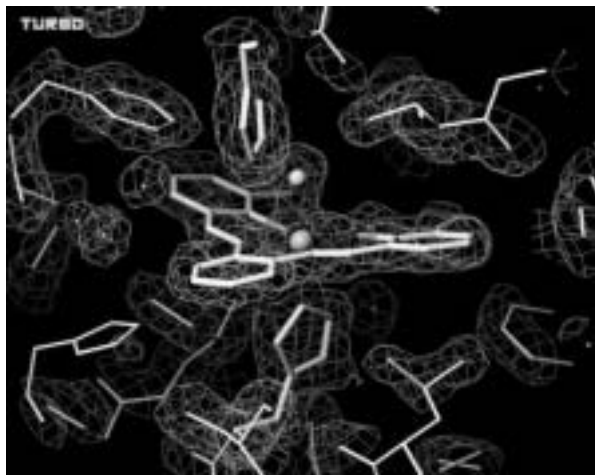


Figure 1. Preliminary crystal structure of Cr(salophen)·apo-A71GMb.

Molecular Mechanism of Oxygen Activation by Metalloenzymes

FUJII, Hiroshi; KURAHASHI, Takuya

Metalloenzymes are a class of biologically important macromolecules that have various functions such as oxygen transport, electron transfer, oxidation, and oxygenation. These diverse functions of metalloenzymes have been thought to depend on the coordination structure of the active site in the protein matrices; the ligand donors, the geometry, and the coordination mode of reactant and substrate. Furthermore, it has been thought that protein structures in immediate vicinity of active metal ion are related to enzymatic function, regio-selectivity, and stereo-selectivity. In this project, we are studying the molecular mechanism of activation of molecular oxygen mediated by metalloenzymes.

(1) To understand the structure-function relationship of 3,4-PCD, there have been attempted over several decades to prepare inorganic model complexes that

mimic the ferric iron site of 3,4-PCD, however, no ferric iron complex with the same coordination structure that in the enzyme has been characterized definitively. We have succeeded in an attainment to the ferric iron active site of 3,4-PCD by using sterically hindered salen ligand. Characterization of the model complex revealed the roles of the iron bound water ligand in the enzyme on the unique trigonal bipyramidal structure and the catechol degradation reaction.

- (2) Small molecule axial ligands potentially can serve as useful NMR probes for characterization of environment and electronic structure of prosthetic group in heme protein. In this regard, the diamagnetic ferrous states have been examined thoroughly because of easy signal detection from iron bound small molecule. We reported the first detection of ^{13}C -NMR signal of the iron bound ^{13}CN in heme proteins such as sperm whale myoglobin(Mb), human hemoglobin(Hb), horse heart cytochrome *c*(Cyt-*c*), and horseradish peroxidase(HRP). This study showed that the ^{13}C -NMR spectroscopy of the iron bound ^{13}CN provides a probe for studying nature of the proximal ligand in ferric heme protein.
- (3) Heme oxygenase (HO) catalyzes the O_2 - and NADPH-cytochrome P450 reductase-dependent conversion of heme to biliverdin and CO through a process in which the heme participates both as prosthetic group and substrate. To investigate the functionality of highly conserved polar amino acids in the distal helix of HO-1, we have generated a detailed reaction cycles for the first mono-oxygenation step of HO catalysis. We employed EPR and ^1H , ^{14}N ENDOR spectroscopies to characterize the intermediates generated by 77 K radiolytic cryoreduction and subsequent annealing of wild-type oxy-HO and D140A, F mutants.

OKAZAKI CONFERENCE

Okazaki COE Conference

Reactions in Aqueous Media

(October 2–3, 2001)

Organizing members:

UOZUMI, Yasuhiro (Chairperson); WATANABE, Yoshihito; HIRATA, Fumio

The International Center of Excellence (COE) Symposium of Institute Molecular Science (IMS) of the 2001 fiscal year was held on October 2 and 3, 2001 at Okazaki Conference Center. This symposium was organized by 3 members of IMS.

The objective of this COE symposium was to overview the frontier of chemical reactions in water from viewpoints of synthetic organic, bioorganic, theoretical chemistry. The symposium also emphasized recent major developments in the fields of process chemistry, green chemistry, spectroscopic study, and the various related fields in aqueous media.

Since development of water-based chemical transformations is rapidly becoming an of importance area of chemistry, this COE symposium was very timely and successful. Fourteen topics were given by invited speakers including 5 leading scientists from abroad. The titles of invited papers are as follows: *Designing New Recoverable/Reusable Catalysts Using Polymer Supports* [Prof. David E. Bergbreiter (Texas A & M University)]; *Structure and Dynamics of Phenol/Naphthol Aqueous Cluster Studied by Laser Spectroscopy* [Prof. Masaaki Fujii (IMS)]; *Chemical Transformations within Aqueous Coordination Nanocages* [Prof. Makoto Fujita (Nagoya University)]; *Dynamics, Pathways, and Tunneling in Enzymatic Reactions* [Prof. Jiali Gao (University of Minnesota)]; *Molecular Theory for Solvent Effect on Organic Reactions in Aqueous Environment* [Prof. Fumio Hirata (IMS)]; *New Dimensions of Organic Transformations in Water* [Prof. Shu Kobayashi (Tokyo University)]; *Developing catalytic reactions in air and water* [Prof. Chao-Jun Li (Tulane University)]; *pH-Dependent Activation Cycle of Dihydrogen* [Prof. Seiji Ogo (IMS)]; *Transition Metal-Catalyzed Enantioselective Reactions in Water Using Water-Soluble Chiral Ligands Derived from Natural Sugars* [Prof. Kouichi Ohe (Kyoto University)]; *Water Dynamics; Fluctuations and Reactions* [Prof. Iwao Ohmine (Nagoya University)]; *Radical Reaction in Water* [Prof. Koichiro Oshima (Kyoto University)]; *Catalytic Functionalization of Methane in Aqueous Solution* [Prof. Georg Suess-Fink (Institute de Chimie, Universite de Neuchatel)]; *Palladium Catalysis in Water* [Prof. Yasuhiro Uozumi (IMS)]; *Molecular Clusters as Probes of Solvent Effects: The influence of water on the conformational preferences of flexible molecules* [Prof. Timothy S. Zwier (Purdue University)].

JOINT STUDIES PROGRAMS

As one of the important functions of an inter-university research institute, IMS undertakes joint studies programs for which funds are available to cover research expenses as well as travel and living expenses of individuals. The proposals from domestic scientists are reviewed and controlled by an inter-university committee.

The programs are carried out under one of the following categories:

- (1) Joint Studies on Special Projects (a special project of significant relevance to the advancement of molecular science can be carried out by a team of several groups of scientists).
- (2) Research Symposia (a symposium on timely topics organized by collaboration between outside and IMS scientists).
- (3) Cooperative Research (a research program carried out by outside scientists with collaboration from an IMS scientist).
- (4) Use of Facility (a research program carried out by outside scientists at the research facilities of IMS except the UVSOR facility).
- (5) Invited Research Project
- (6) Joint Studies Programs using beam lines of UVSOR Facility.
- (7) Use of Facility Program of the Computer Center (research programs carried out by outside scientists at research facilities in Computer Center).

In the fiscal year 2001, the numbers of joint studies programs accepted for the categories (1)–(7) were 5, 6, 112, 58, 3, 163, and 128, respectively.

(1) Special Projects

A. Studies on Excited State Dynamics by Time-Resolved Photoelectron Imaging

SUZUKI, Toshinori; DE LANGE, Cornelis¹;
TAKATSUKA, Kazuo²; MCKOY, Vincent³
(¹Univ. Amsterdam; ²Univ. Tokyo; ³Caltech)

One of the dreams for molecular scientists is to observe chemical reactions in real time. As electrons move much faster than nuclei in a molecule, chemical reactions are governed by electronic motions (Born-Oppenheimer approximation). Real-time observation of (non-stationary) electronic states of a molecule is the key for understanding reaction mechanism. Note that an electron has a spin angular momentum and the electronic states with different spin multiplicity come into play in reactions. Previous experimental methods based on optical transitions between the bound states were unable to observe both singlet and triplet states simultaneously with the same wavelength. In 1999, IMS research group has developed a novel experimental means, femtosecond photoelectron imaging where a pump pulse initiates a reaction, and a probe pulse knocks out a valence electron to form a scattering distribution of photoelectrons. The distributions are visualized by two-dimensional position sensitive detection of electrons. The distribution reflects the shape of molecular orbital and nuclear motions that rapidly change during the course of reactions. Since photoionization is allowed from any electronic state, the method probes all the electronic states involved in the reaction. Independently with this experimental research, Tokyo-Caltech research group has been developing a theory for pump-probe photoelectron spectroscopy, in particular photoelectron energy and angular distributions, for exploring non-adiabatic dynamics. This special research program

for one and half years was launched to stimulate discussions between experimental and theoretical groups at the frontier.

The laser system is a standard one consisting of an oscillator, an amplifier, and optical parametric amplifiers (OPAs). The output from the oscillator, 80 MHz, 300 mW is introduced into a hybrid chirped pulse amplifier pumped by a Nd:YLF laser. The amplified pulse is a 1 kHz pulse train of ~ 2.5 mJ/pulse⁻¹ light centered at ~ 800 nm with a band width of 13 nm. This amplified light is split into two equal intensity beams to pump two OPAs. Each OPA system has a computer controlled motor drive that adjusts the angles of crystals and a grating to maximize the OPA efficiency at each wavelength. Depending on the experiment, the second, the third, and the fourth harmonics of Ti:sapphire fundamental are also used. The cross-correlation of the pump and probe beams is typically 150–200 fs. The probe beam is optically delayed with respect to the pump beam using a hollow corner cube on a computer-controlled delay stage. The pump and probe laser beams are crossed with a molecular beam in the static electric field in the velocity mapping mode. A pump laser excites molecules in the beam to an electronically excited state, then a probe pulse ionizes the ensemble of molecules. The generated photoelectrons are accelerated parallel to the molecular beam and projected onto a position sensitive imaging detector. The detector consists of a 40 mm diameter dual MCP backed by a phosphor screen. Light from the phosphor is coupled out of the vacuum chamber by means of a fiber bundle where it was recorded by a CCD camera with 512×512 pixels. The field-free region of the electron flight path was shielded with a μ -metal tube against stray magnetic fields.

The $S_1(1B_{3u})$ state of pyrazine has been the best-known example of an intermediate case in molecular radiationless transition theory. Coherent excitation of an intermediate case molecule exhibits a bi-exponential fluorescence decay, where the fast decay is due to the ultrafast dephasing of the optically prepared singlet state

into a mixed singlet-triplet state and the slow decay is the depopulation of this mixed state. This classic problem was revisited by femtosecond TRPEI to shed light on the dark triplet manifold. Figure 1 shows a series of photoelectron images observed by (1+1') REMPI using 324 nm pump and 200 nm probe light at different time delays. These correspond to the 2D sections of the 3D photoelectron scattering distributions: pyrazine molecules are located in the middle of each image, and outgoing photoelectrons are visualized at the point proportional to their scattering velocity vectors. The images observed at short time delays consist of a number of sharp rings. This structure disappears with a lifetime of 110 ps. Correspondingly, a low energy electron signal due to ionization from the triplet manifold grows in the inner part of the image: the triplet levels isoenergetic with the initially photoexcited singlet 0^0 level have large vibrational energies, 4055 cm^{-1} , and the Franck-Condon overlap favors ionization to highly vibrationally excited states in the cation. The sharp rings are transitions to overtone and combination levels of totally symmetric vibrational modes in the cation, and their intensity distribution follows the Franck-Condon factors between the $S_1\ 0^0$ level and the cation. The pump and probe polarization directions are parallel to each other in the vertical direction in the figure. The angular anisotropy does exist, yet is rather weak ($\beta \sim 0.3$), reflecting the complex spatial structure of a π^* valence orbital from which an electron is ejected by the probe light. As a conventional way of presentation, the PEDs were extracted from these images by integrating the angular part of the 2D photoelectron scattering distributions, as shown in Figure 2. All the spectra cross at the same energy (isosbestic point), indicating that the spectra consist of two components in dynamic equilibrium. The ionization from the triplet manifold peaks at zero kinetic energy indicating that 200 nm is not a sufficiently short wavelength to ionize the entire vibrational wave-packet in the triplet manifold, making the sensitivity of the experiment to the triplet character relatively less than that for the singlet. Similarly, we have excited pyrazine to various vibronic levels in S_1 ($E_{\text{vib}} < 2000\text{ cm}^{-1}$) and observed the photoelectron images. In all cases, the singlet signal decayed without changing its structure, meaning that IVR in the S_1 manifold does not occur prior to electronic dephasing due to the lack of sufficient vibrational state density. The same result has been obtained for deuterated pyrazine.

In addition to the electronic and vibrational dynamics, coherent excitation of the $P(\Delta J = -1)$, $Q(0)$, and $R(+1)$ branch lines creates a superposition of molecular rotational eigenstates, *i.e.* a rotational wave-packet. The constructive and destructive interferences between different J components create a time-dependent molecular axis alignment that revives with characteristic time periods determined by rotational constants. Figure 4 shows the rotational revival feature observed for pyrazine S_1 and T_1 states after coherent excitation.

For further detailed examination of rotational wave-packet and its possible use for the study of stereodynamics of molecules, we explored (1+1') and (2+1') REMPI of NO via the $A(^2\Sigma^+) 3s$ Rydberg state. Figure 3 shows the anisotropy parameters of the time-dependent PAD. The rotational temperature in the beam was esti-

mated to be about 20 K, so the NO molecules were populated in the lowest few rotational levels in $^2\Pi_{1/2}$. Since the geometry of a Rydberg state is almost the same as that of a cation, the Franck-Condon propensity upon ionization is $\Delta v = 0$. The photoelectron energy distribution was essentially a single Gaussian function with a width determined by the energy resolution of TRPEI. Although variations of the anisotropy parameters against the time delay were only within 0.1, they were well reproducible and in excellent agreement with the expected time dependence of molecular axis alignment parameter. We have approximated the photoelectron outgoing wave from NO with p and f waves, and determined their transition dipole and phase shifts by analyzing time-dependent photoelectron angular distributions. This is the first report of photoelectron angular distribution in the molecular frame determined by using a rotational wave packet. The result was compared with theoretical prediction by Professor McKoy and co-workers.

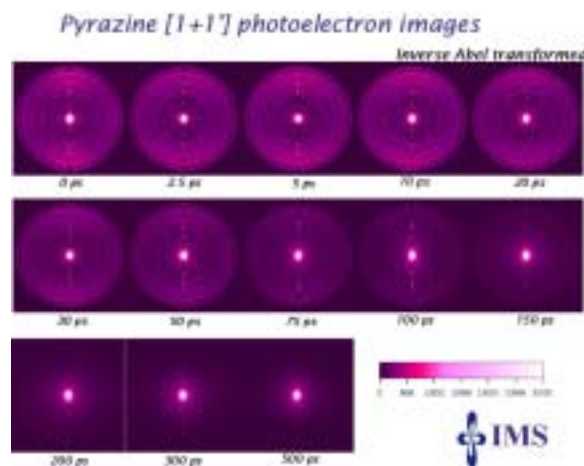


Figure 1. Time-resolved photoelectron images in (1+1') REMPI of pyrazine via $S_1\ 0^0$ level by pump at 324 nm and probe at 197 nm. The images are inverse Abel transforms of the raw data. The pump and probe laser polarization directions are vertical in the figure.

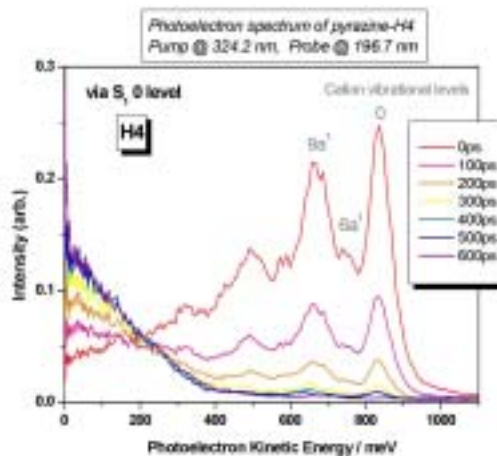


Figure 2. Photoelectron kinetic energy distribution extracted from the images shown in Figure 1.

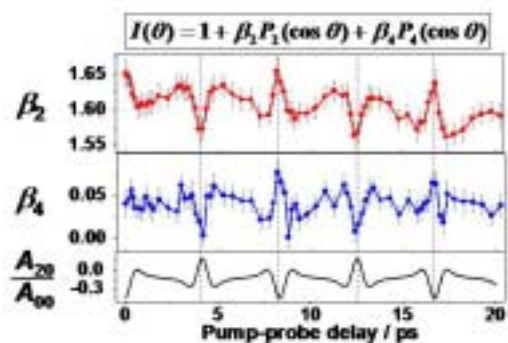


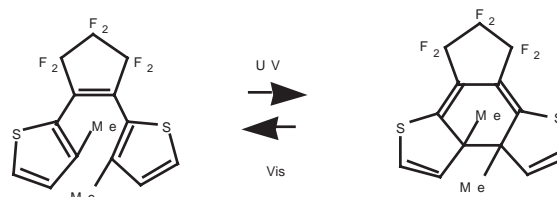
Figure 3. Time-dependent photoelectron anisotropy parameters determined for $(1+1')$ REMPI of NO via A ($2\Sigma^+$) state.

B. Ultrafast Time-Resolved Study on Photochromic Reactions in the Isolated State and Condensed Phase

SEKIYA, Hiroshi¹; IRIE, Masahiro¹; SAKURAGI, Hirochika²; OKABE, Chie¹; TANAKA, Nobuyuki¹; NAKABAYASHI, Takakazu; NISHI, Nobuyuki
(¹Kyushu Univ.; ²Univ. Tsukuba)

Organic photochromic molecules have been of considerable interests in its potential for the applications to optical memory and light switches. Various types of organic photochromic molecules have been studied. Spiropyran derivatives^{1,2)} and azobenzene derivatives^{3,4)} are thermally unstable and return to the initial isomers in the dark. In contrast, furylfulgide derivatives^{5,6)} and diarylethene derivatives^{7,8)} are thermally irreversible photochromic molecules. Among these molecules diarylethene derivatives are the most promising material for applications to optical devices because of their excellent thermal stability, rapid response, and high sensitivity.^{7,8)}

A lot of reports have been presented on the photochromic reactions of diarylethene derivatives, and some studies are concentrated on the quantum yields in the cyclization and cycloreversion reactions. The quantum yield must strongly depend on the potential energy surfaces (PES) on which reaction proceeds. However, PES's of diarylethene derivatives have not been well understood. Thus, in this project, we have introduced spectroscopic techniques, which have not been used to investigate photochromic reactions of diarylethene derivatives so far. FT-Raman spectroscopy has been successfully applied to distinguish the open-ring and closed-ring isomers of 1,2-bis(3-methyl-2-thienyl)perfluorocyclopentene (BMTF) in solution (Scheme 1).⁹⁾ Picosecond time-resolved Raman spectroscopy has been used to investigate structural changes of the molecule in the photochromic reaction process.¹⁰⁾ Electronic spectroscopy is applied to explore the excited-state potential of the open-ring isomer of BMTF in the isolated state.¹¹⁾ Now, we are measuring the rates for photochromic reactions of the diarylethenes by time-resolved femtosecond spectroscopy under isolated jet-cooled conditions. We will report on picosecond time-resolved study of diarylethene derivatives in solution and femtosecond time-resolved study of *N*-salicylideneaniline (SA) in the isolated state. Photochromic reaction of SA is originated from excited-state intramolecular proton transfer.



Scheme 1.

B-1 FT-Raman Spectrum of BMTF

Photochromic reaction of BMTF has been studied by FT-Raman spectroscopy.⁹⁾ The Raman bands in the 1400–1600 cm^{-1} region of the open-ring isomer of BMTF are clearly distinguished from those of the closed-ring isomer. The vibrational assignment has been made by measuring the polarized Raman spectrum and density functional theory calculations at the B3LYP/6-31G** level. Two anti-parallel and four parallel conformers are obtained for the open-ring isomer. Among these conformers only the most stable anti-parallel conformer may undergo the cyclization. The FT-Raman spectroscopic study suggests that time-resolved Raman spectroscopy is a promising method to investigate structural change of the molecule during the reaction process.

B-2 Picosecond Time-Resolved Study of Cyclization Reaction of DMTF

The cyclization reaction of 1,2-bis(2,5-dimethyl-3-thienyl)perfluorocyclopentene (DMTF) was investigated by picosecond time-resolved Raman spectroscopy. The UV pulse at 310 nm was used to excite the open-ring isomer, and the visible pulse at 568 nm was used to detect the resonance Raman spectra of the generated closed-ring isomer in the S_0 state. The time-resolved Raman spectra of DMTF in 1-butanol are shown in Figure 1A. Immediately after the photoexcitation, two Raman bands at 1551 and 1592 cm^{-1} were observed. They are attributable to the closed-ring isomer of DMTF in the electronic ground state (S_0). Figure 1B shows the time-developments of the Raman intensity at 1551 cm^{-1} exhibiting the experimentally limited rise (< 4 ps). This result indicates that the cyclization reaction of BMTF occurs within 4 ps.¹⁰⁾

The time-dependence of the peak position of the band at 1551 cm^{-1} is shown in Figure 1C. With increasing the delay time between the pump and probe pulses, its peak position shifts to a higher wavenumber and its bandwidth becomes narrow. This change is associated with intermolecular vibrational relaxation of the closed-ring isomer of the vibrational excited state.

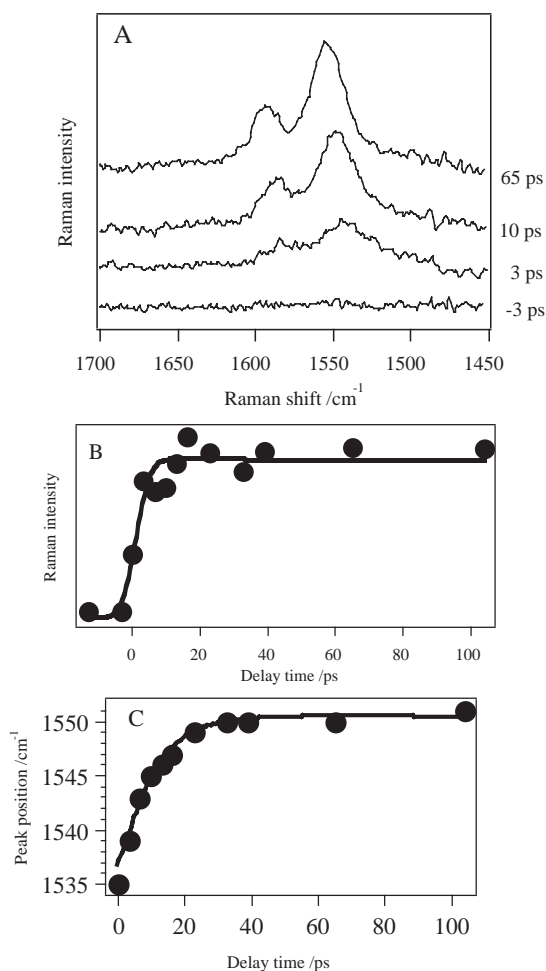


Figure 1. Picosecond time-resolved Raman spectra of DMTF in 1-butanol (A), Plots of the Raman intensity of DMTF at 1551 cm^{-1} against the delay time (B), and temporal change of the frequency of the band around 1550 cm^{-1} of BMTF against the delay time (C).

B-3 Picosecond Time-Resolved Study of Cycloreversion Reaction of BMPTF

The cycloreversion reaction has been studied with 2-bis(3-methyl-5-phenyl-2-thienyl)perfluorocyclopentene (BMPTF) by using picosecond time-resolved anti-Stokes Raman spectroscopy. The pump and probe wavelengths were 480 and 395 nm, respectively. These wavelengths correspond to the absorption regions of the closed-ring and open-ring forms of BMPTF, respectively.

Figure 1 shows the anti-Stokes Raman spectra of BMPTF at 2 and 8 ps. The intensity scale is normalized for the peak intensity at 1610 cm^{-1} , which is assigned to the C=C stretching mode of the cyclopentene moiety. The change in the relative intensity of the anti-Stokes Raman bands was observed. It has been shown that a part of excess energy generated via the cycloreversion reaction is localized on the C=C stretching mode of the cyclopentene moiety. This means that the C=C stretching mode is one of the accepting modes in the cycloreversion process.

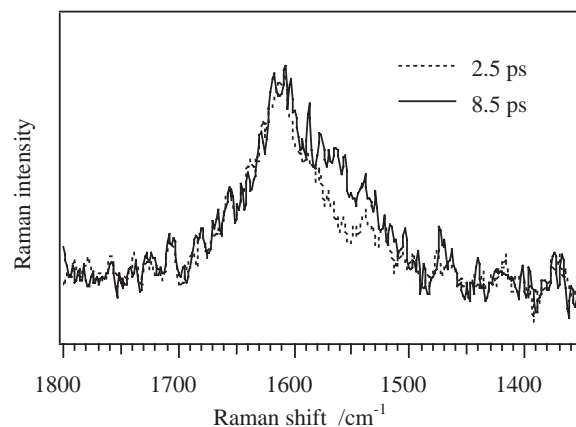


Figure 1. Picosecond time-resolved anti-Stokes Raman spectra of BMPTF in acetonitrile. The intensity of each spectrum is normalized by reference to the intensity of the band at 1610 cm^{-1} .

B-4 Femtosecond Time-Resolved Study of *N*-Salicylideneaniline in the Isolated State

The excitation of the enol-form of *N*-salicylideneaniline (SA) produces the keto-form through excited-state intramolecular proton transfer (Scheme 1). The laser induced fluorescence excitation and dispersed fluorescence spectra of jet-cooled SA have been observed in a supersonic free jet for the first time. The spectrum shows a very broad feature with no vibronic structure in the $24800\text{--}29000\text{ cm}^{-1}$ region except for a broad peak at 28200 cm^{-1} . The broad feature of the spectrum has been ascribed to the homogeneous broadening of vibronic bands due to very fast internal conversion from the ${}^1\pi\pi^*$ to ${}^1n\pi^*$ state which is located below the ${}^1\pi\pi^*$ state as well as to the excited-state intramolecular proton transfer reaction.¹²⁾ No resonance emission has been detected following the excitation of the ${}^1\pi\pi^*$ state of the enol form, while anomaly Stokes-shifted fluorescence was observed at $15000\text{--}20500\text{ cm}^{-1}$. The dispersed fluorescence spectra show two broad maxima separated by $700\text{--}1000\text{ cm}^{-1}$, suggesting that two keto tautomers are produced via the excited-state intramolecular proton transfer reaction. The existence of the corresponding two cis-keto tautomers with similar energies has been suggested by density functional theory calculations at the B3LYP/6-31G** level and ab initio calculations at the HF/6-31G** level.

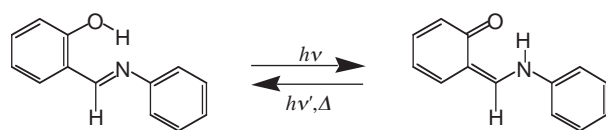
In order to examine the above conclusion obtained from the electronic spectroscopy of jet-cooled SA the pump and probe technique with the detection of ion signal generated by multi-photon ionization has been applied to determine the decay rate of the excited state of the enol-form. Figure 1 shows a typical decay curve. The decay curve is fitted by bi-exponential function with two decay rate constants: fast decay is less than 250 fs and slow decay is 1.7 ps. The fast component is ascribed to the decay of initially photoexcited ${}^1\pi\pi^*$ state due to excited-state proton transfer and fast internal conversion to the ${}^1n\pi^*$ state, while the slow component to the decay of the ${}^1n\pi^*$ state. These results are in good agreement with the conclusion derived from the electronic spectroscopy.

We have observed the fluorescence and dispersed fluorescence spectra of jet-cooled BMTF. It has been

shown that the initially photoexcited electronic state is not the S_1 state but the S_2 state and fast internal conversion occurs from the S_2 state.¹¹⁾ The experiment of ultrafast time-resolved spectroscopy is in progress to investigate the fast internal conversion process and to determine the photochromic reaction rates of diarylethene derivatives. A very close similarity exists in the excited state potential of SA and diarylethene derivatives. Femtosecond time-resolved study may provide consistent results with those obtained from the fluorescence spectroscopy.

References

- 1) M. Hirano, A. Miyashita and H. Nohira, *Chem. Lett.* 209 (1991).
- 2) O. Pieroni, A. Fissi, N. Angelini and F. Lenci, *Acc. Chem. Res.* **34**, 9 (2001).
- 3) E. Sackmann, *J. Am. Chem. Soc.* **93**, 7088 (1971).
- 4) H. Rav and E. Luddecke, *J. Am. Chem. Soc.* **104**, 1616 (1982).
- 5) P. J. Darcy, H. G. Heller, P. J. Strydom and J. Whittall, *J. Chem. Soc. Perkin I* 202 (1981).
- 6) Y. Yokoyama, *Chem. Rev.* **100**, 1717 (2000).
- 7) M. Irie and M. Mohri, *J. Org. Chem.* **53**, 803 (1988).
- 8) M. Irie, *Chem. Rev.* **100**, 1685 (2000).
- 9) C. Okabe, N. Tanaka, T. Fukaminato, T. Kawai, M. Irie, Y. Nibu, H. Shimada, A. Goldberg, S. Nakamura and H. Sekiya, *Chem. Phys. Lett.* **357**, 113 (2002).
- 10) C. Okabe, T. Nakabayashi, N. Nishi, T. Fukaminato, T. Kawai, M. Irie and H. Sekiya, The First Symposium on "Understanding of Nonequilibrium-Nonstationary Characteristics Specific to Chemical-Reacting Phenomena—Reconsideration of Statistical Theory from the Viewpoint of Modern Chemistry," (March 8–10, Okazaki).
- 11) N. Tanaka, C. Okabe, K. Sakota, T. Fukaminato, T. Kawai, M. Irie, A. Goldberg, S. Nakamura and H. Sekiya, *J. Mol. Struct.* **616**, 113 (2002).
- 12) N. Otsubo, C. Okabe, H. Mori, K. Sakota, K. Amimoto, T. Kawato and H. Sekiya, *J. Photochem. Photobiol. A (Chemistry)*, Special Issue on Photo-induced Proton Transfer, in press.



Scheme 1.

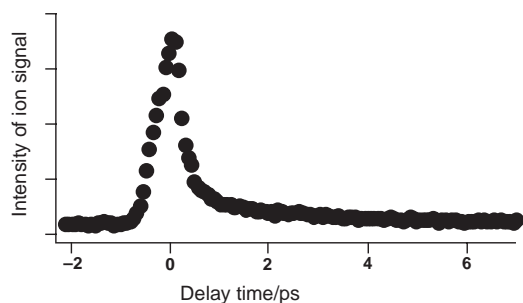


Figure 1. Decay curve obtained by exciting the enol tautomer of *N*-salicylideneaniline in the isolated jet-cooled conditions. Ion signal was detected as a function of the delay time of the ionization pulse.

C. Development of Effective Generalized-Ensemble Algorithms for Complex Systems with Many Degrees of Freedom

OKAMOTO, Yuko; SUGITA, Yuji; NAGASIMA, Takehiro; MITSUTAKE, Ayori¹; NAKAZAWA, Takashi²; YUMINAGA, Hiroko²; BERG, Bernd A.³ (¹Keio Univ.; ²Nara Women's Univ.; ³Florida State Univ.)

Complex systems with many degrees of freedom such as spin glasses and biopolymers have a huge number of local minima in potential energy. Conventional constant-temperature simulations based on canonical ensemble will thus tend to get trapped in states of energy local minima. Generalized-ensemble algorithms, which are based on artificial non-Boltzmann weight factors, alleviate this multiple-minima problem by performing random walks in potential energy space, allowing the simulation to explore a much wider range of the configurational space than by conventional methods. The advantage of generalized-ensemble algorithms lies in the fact that from only one simulation run, one can obtain not only the global-minimum state in potential energy but also various thermodynamic quantities as a function of temperature. Multicanonical algorithm, simulated tempering, and replica-exchange method are well-known examples of generalized-ensemble algorithms and have been widely used in simulations of spin systems and protein systems. However, as the system becomes complex, the application of these algorithms faces technical difficulties. In the first two methods, the determination of the non-Boltzmann weight factors becomes very time-consuming. In the third method, on the other hand, the weight factor determination is trivial, but much more simulation time is required for the production run than in the first two methods. Recently, we have developed new effective generalized-ensemble algorithms that combine the merits of these three generalized-ensemble algorithms (for a recent review, see A. Mitsutake, Y. Sugita and Y. Okamoto, *Biopolymers (Peptide Science)* **60**, 96 (2001)). The purpose of the present project is to further test the effectiveness of these new methods by performing simulations of spin systems and protein systems and to develop even more powerful generalized-ensemble algorithms.

C-1 Generalized-Ensemble Simulations of Spin Systems and Protein Systems

[*Comput. Phys. Commun.* **146**, 69 (2002)]

We test the effectiveness of the recently proposed generalized-ensemble algorithms that combine the merits of multicanonical algorithm and replica-exchange method, namely, replica-exchange multicanonical algorithm (REMUCA) and multicanonical replica-exchange method (MUCAREM). A spin system and protein systems were used for the test. For the former, two-dimensional 10-state Potts model was simulated. For the latter, various short peptide systems both in gas phase and in aqueous solution were simulated. REMUCA and MUCAREM present new methods for the multicanonical weight factor determination. It was shown for the

Potts model case that these methods are at least as powerful as the most effective method that was known previously.

D. Study on the Magnetization of the Supramolecule Built by Fullerenes

KATO, Tatsuhisa; TOYAMA, Namiki; TASHIRO, Kentaro¹; AKASAKA, Takeshi²; AIDA, Takuzo¹; YAMAUCHI, Seigo³; DINSE, Klaus-Peter⁴
(¹Univ. Tokyo; ²Univ. Tsukuba; ³Tohoku Univ.; ⁴Darmstadt Univ. Tech.)

An endohedral metallofullerene is the building-block molecule for the nano-scaled structure with ferromagnetism. On the other hand an association of a porphyrin with C₆₀ is well known, and an inclusion through π -electron donor-acceptor interaction is highly interesting in view of the construction of a supramolecule. Moreover the system composed of a metalloporphyrin with a metallofullerene leads to other attention of the parallel alignment of spins via spin exchange interaction, which is the key issue of the ferromagnetism. Tokyo group synthesized a face-to-face cyclic dimer of metalloporphyrin and reported that a cyclic dimer of zinc-porphyrin (Zn-PD) forms an inclusion complex with C₆₀ (Zn-PD+C₆₀), of which the association constant K_{assoc} of $6.7 \times 10^5 \text{ M}^{-1}$ is much higher than those of organic media reported to date. If a copper-porphyrin dimer (Cu-PD) is used as a host molecule, there are two radical sites in the system, and a question arises as to whether the two radical sites couple or not. When a spin-labeled fullerene of La@C₈₂ is introduced between the two radical sites of Cu-PD, the assignment of the resultant spin state of the inclusion complex (Cu-PD+La@C₈₂) comes into the final question.

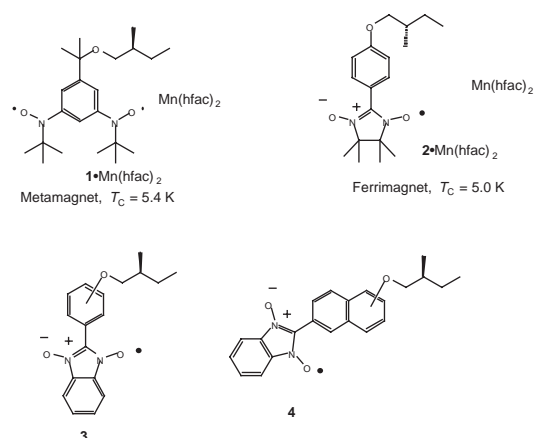
E. Magnetic Anisotropy and Magnetic Viscosity of Chiral Molecule-Based Magnets

INOUE, Katsuya; HOSOKOSHI, Yuko; BARANOV, Nikolai¹; NAKAMURA, Nobuo²; ISHIZUKA, Keita²; SAKAGUCHI, Takahiro²
(¹IMS and Ural State Univ.; ²Housei Univ.)

Magnetic anisotropy is an important characteristic feature of magnets. Molecule-based magnets can control the dimensionality of magnetic structure of spins. These magnets show clear magnetic anisotropy and easy to analyze by the magnetic single crystal measurements. Recently, we designed and synthesized many chiral molecule-based magnets. In the chiral magnets, the magnetic moments located in asymmetrical position and the magnetic dipole fields are also asymmetric. The magnetic anisotropy of these materials is great interesting. In the program, we planned to make new low dimensional chiral magnets and study for magnetic anisotropy and magnetic viscosity of these magnets.

E-1 Synthesis and Structural Studies of New One-Dimensional Chiral Molecule-Based Magnets

In 1999, we have already made a chiral metamagnet with a $T_N = 5.5 \text{ K}$ (**1**•Mn(hfac)₂) and a ferrimagnet with a $T_C = 4.5 \text{ K}$ (**2**•Mn(hfac)₂). These magnets are small brown and blue single crystals, respectively. The sizes of these crystals are less than ca. 0.5 mm, this size crystal is too small for single crystal magnetic measurements. The crystallizability of materials depends on the solubility and/or molecular shapes. Usually, planer molecules have good crystallizability than the bulky molecules. Then we design new organic radicals to make large single crystals.



The synthetic route of the new chiral bidendate monoradicals radical **3** is illustrated in Figure 1. *p*- and *m*- isomer were obtained as green solid and green oil, respectively. Complexation with bis(hexafluoroacetyl)acetate manganese are now in progress.

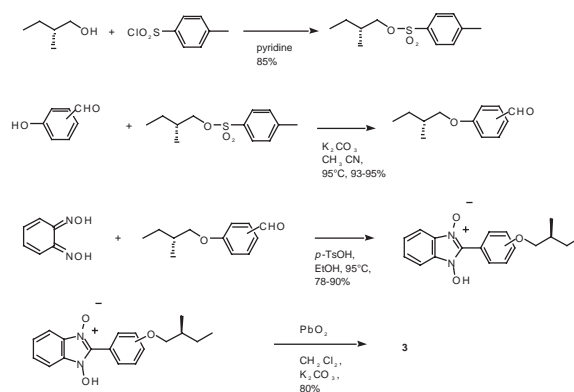


Figure 1.

F. Thermal and Optical Switching of Spin-Crossover Compounds

HAYAMI, Shinya¹; HOSOKOSHI, Yuko; INOUE, Katsuya; SATO, Osamu²; MAEDA, Yonezo¹
(¹Kyushu Univ.; ²KAST)

The design of molecules, which can be utilized for information processing and information storage, is one of the main challenges in molecular materials science. The molecules for such purpose must exhibit bistability, which may be defined as the property of a molecular

system being able to exist in two different electronic states in a certain range of external perturbation. Typical example of molecular species exhibiting such molecular bistability is spin crossover complexes. Since the discovery of the first spin-crossover complex, a variety of d^n ($n = 4-7$) transition metal compounds exhibiting bistability between high-spin (HS) and low-spin (LS) states have been reported. Usually, the spin transition phenomena can be induced by a variation of temperature or of pressure. On the other hand, Decurtine et al. show that the spin transition can be induced by illumination in 1984. This finding shows that the spin-crossover compounds have potential applications for optical switches and data storage devices. Here we purpose to develop the optical switching molecular devices.

F-1 Photo-Induced Spin Transition for Iron(III) Compounds with π - π Interactions

JUHASZ, Gergely¹; HAYAMI, Shinya¹; SATO, Osamu²; MAEDA, Yonezo¹
(¹Kyushu Univ.; ²KAST)

[Chem. Phys. Lett. in press]

The magnetic susceptibilities of the spin-crossover compound $[\text{Fe}(\text{pap})_2]\text{PF}_6 \cdot \text{MeOH}$ (**1**) have been measured and compared with that of the previously reported compound $[\text{Fe}(\text{pap})_2]\text{ClO}_4 \cdot \text{H}_2\text{O}$ (**2**). Compound **1** is a spin-crossover compound with spin transition temperature $T_{1/2} = 288$ K, and does not show a hysteresis loop around the spin transition temperature, in contrast with compound **2**. Magnetic susceptibilities measured after illumination prove that **1** exhibits the LIESST effect, so does compound **2**. The crystallographic data on the molecular packing show the presence of π stacking between the aromatic rings of pap ligands, which appears to be responsible for the LIESST effect.

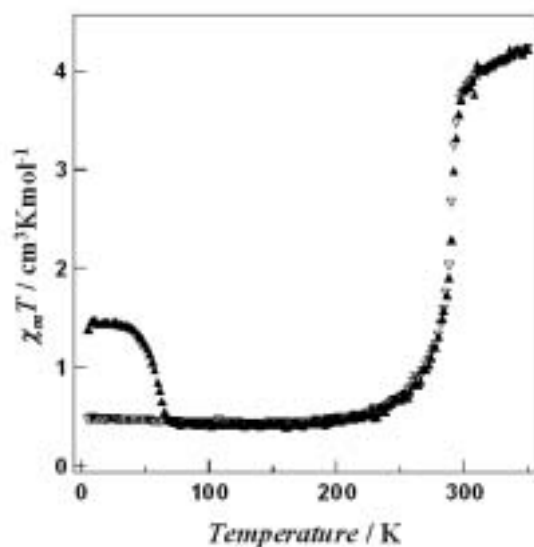


Figure 1. Photomagnetic behavior: $\chi_m T$ of $[\text{Fe}(\text{pap})_2]\text{PF}_6 \cdot \text{MeOH}$ (**1**) as a function of temperature on cooling (∇), after irradiated at 5 K and warming up (\blacktriangle).

F-2 Crystal Structure of a Molecular Building Block with π - π Intermolecular Interaction

HAYAMI, Shinya¹; KAWAMURA, Kazunori¹; JUHASZ, Gergely¹; KAWAHARA, Takayoshi¹; UEHASHI, Keigo¹; MAEDA, Yonezo¹
(¹Kyushu Univ.)

[Mol. Cryst. Liq. Cryst. **379**, 371 (2002)]

Mononuclear iron(II) compound $[\text{Fe}(\text{4tpt})_2(\text{NCS})_2 \cdot (\text{MeOH})_2] \cdot \text{MeOH}$ (**1**) (4tpt = 2,4,6-tri(4-pyridyl)-1,3,5-triazine) was synthesized and characterized by X-ray single crystal diffraction, Mössbauer spectra, magnetic susceptibilities, electronic spectra and IR spectra. The crystal structure of **1** was determined. Crystal data for **1**: $\text{C}_{42}\text{H}_{40}\text{O}_4\text{N}_{14}\text{S}_2\text{Fe}_1$, space group $P-1$, $Z = 2$, $a = 7.091(1)$, $b = 10.630(2)$, $c = 28.251(7)$ Å, $\alpha = 89.77(1)^\circ$, $\beta = 90.072(9)^\circ$, $\gamma = 84.45(1)^\circ$, $V = 2119.5(7)$ Å³, $R1 = 0.069$. The compound **1** has two 4tpt ligands, and forms π - π stacking between the 4tpt ligands in the neighboring complexes along the b axis. The assembly of the constituent complexes forms 1-D zigzag chains because of the strong π - π stacking between the neighboring complexes. Two methanol molecules are contained in the space between the 1-D zigzag chains.

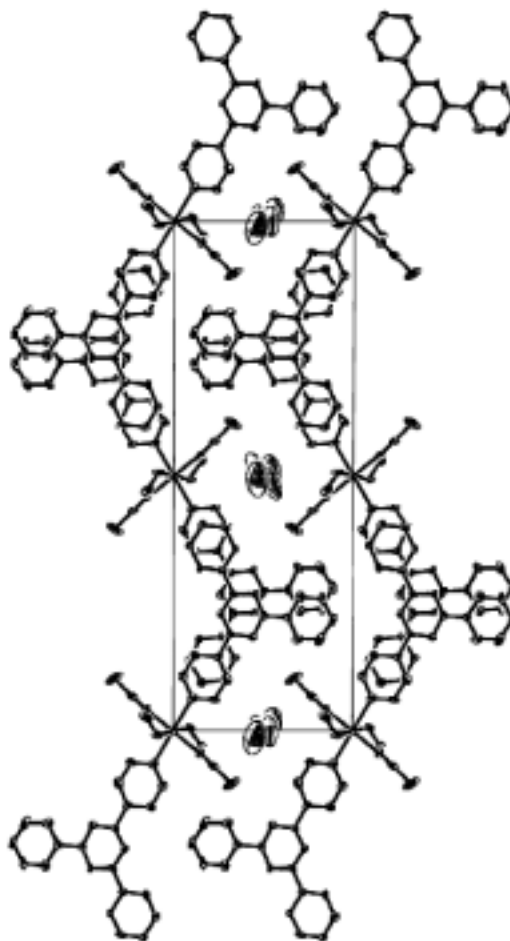


Figure 1. Crystal packing view of $[\text{Fe}(\text{4tpt})_2(\text{NCS})_2 \cdot (\text{MeOH})_2] \cdot \text{MeOH}$ (**1**) with π - π stacking between complexes.

F-3 Study of Intermolecular Interaction for the Spin-Crossover Iron(II) Compounds

HAYAMI, Shinya¹; KAWAJIRI, Ryo¹; JUHASZ, Gergely¹; KAWAHARA, Takayoshi¹; SATO, Osamu²; MAEDA, Yonezo¹
(¹Kyushu Univ.; ²KAST)

[submitted]

In the iron(II) spin-crossover compounds [Fe(PM-iPA)₂(NCS)₂] (**1**) and [Fe(PM-iPA)₂(NCSe)₂] (**2**) (PM-iPA = *N*-2'-pyridylmethylene-isopropylamine) with ligand having bulky substitute, the thermal spin transition have occurred at $T_{1/2} = 267$ K and 376 K without thermal hysteresis, respectively. The compounds **1** and **2** could not be observed light-induced excited spin state trapping (LIESST) effect even at 5 K. On the other hand, Létard *et al.* have reported that the iron(II) spin-crossover compounds [Fe(PM-L)₂(NCX)₂] (L = A, BiA, TeA, PEA and AzA; X = S and Se) with ligands having π system exhibited thermal spin transition, respectively. The iron(II) compounds have exhibited LIESST effect, and the critical LIESST temperature, $T_c(\text{LIESST})$, has been observed. The structure of **1** and **2** are crystallized at *Pnma* and *C2/c* at room temperature, respectively, and structure of low-spin state are also same space group without structural change. The structures of the iron(II) compounds with π system ligands also have been reported in the high-spin state, and the structure in the low-spin state remain if the compounds occurred spin transition. It has been found that the compound **1** and **2** have not form any intermolecular interactions between the complexes, while the compounds with π system ligands form π - π intra- and intermolecular interactions in the ligands. It is thought that the intermolecular interactions play an important role in the trapping a light-induced metastable state.

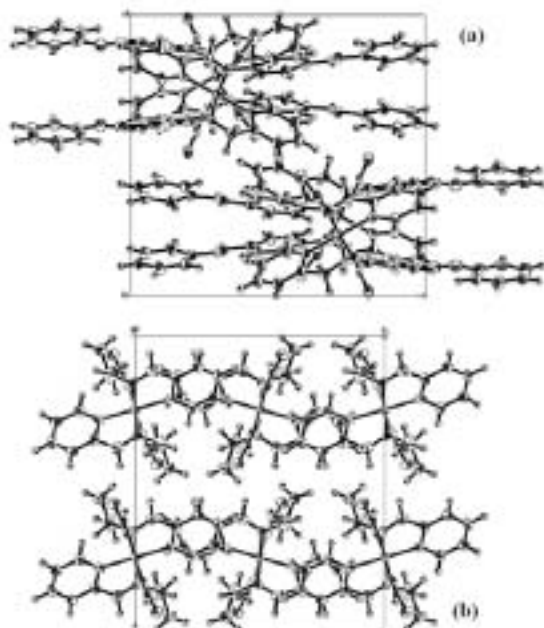


Figure 1. Crystal packings of (a) [Fe(PM-iPA)₂(NCS)₂](**1**) and (b)[Fe(PM-AzA)₂(NCS)₂](**3**) in the low-spin state.

F-4 The High-Spin \rightarrow Low-Spin States Relaxation in Iron(III) Compounds

HAYAMI, Shinya¹; HOSOKOSHI, Yuko; INOUE, Katsuya; SATO, Osamu²; MAEDA, Yonezo¹
(¹Kyushu Univ.; ²KAST)

During the past years many studies have been performed on the dynamics of the HS \rightarrow LS relaxation, especially for iron(II) spin-crossover compounds in solution and at ambient temperatures. Different experimental methods were used to determine the rate constants k_{HL} of the HS \rightarrow LS relaxation. After the studies of McGarvey and Lawthers, however, pulsed laser excitation has become the most common technique. For iron(II) spin-crossover complexes, HS \rightarrow LS relaxation rates and activation parameters determined with line shape analysis of Mössbauer spectra in the solid state around room temperature were similar to those in solution. This technique, however, is restricted to systems with transition temperature $T_{1/2}$ around room temperature, because at temperatures where the rate constants k_{HL} fit into the Mössbauer time window of $10^6 \text{ s}^{-1} \leq k_{\text{HL}} \leq 10^8 \text{ s}^{-1}$, HS and LS species must be simultaneously present in sufficient concentrations. With the discovery of LIESST and the elucidation of the mechanism of light-induced population of metastable HS states, new possibilities to study HS \rightarrow LS relaxation in the solid and at low temperatures were opened. Here we show the HS \rightarrow LS relaxation and the rate constants k_{HL} for iron(III) LIESST complex.

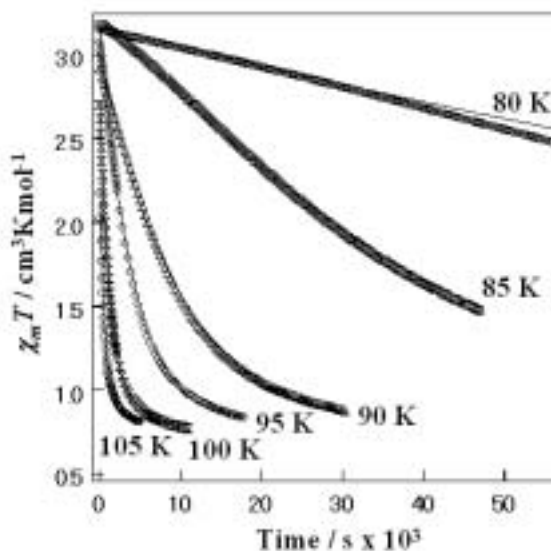


Figure 1. Dependence of $\chi_m T$ on time for the HS \rightarrow LS transformation in quenched-in [Fe(pap)₂]ClO₄.

(2) Research Symposia

(from September 2001 to August 2002)

1. New Developments in Molecular Science Research using Scanning Probe Microscopy (February 14-15, 2002)
Chair: KOMIYAMA, Masaharu

2. Atomic and Molecular Dynamics on Valence Excitation and Ionization
(February 18-19, 2002)
Chair: **KOUCHI, Noriyuki**
3. Water and Biomolecules Cooperate in Chemistry of Life
(May 15-17, 2002)
Chair: **HIRATA, Fumio**
4. Symposium of Molecular Science
(May 17-18, 2002)
Chair: **KAJIMOTO, Okitsugu**
5. Symposium on Physical Chemistry for Young Researchers of Molecular Science
(June 5, 2002)
Chair: **KATO, Hajime**
6. Current Status and Future Prospect of Dynamics of Photon, Electron and Heavy-particle Collisions
(July 25-26, 2002)
Chair: **TAKAHASHI, Masahiko**

(3) Cooperative Research

This is one of the most important categories that IMS undertakes for conducting its own research of the common interest to both outside and IMS scientists by using the facilities at IMS. During the first half of the fiscal year of 2001 ending on September 30, 99 outside scientists from 47 research groups joined the Cooperative Research programs, and during the second half, 107 outside scientists from 65 research groups joined the programs. The names and affiliations of those collaborations are found in the Research Activities sections in this Review.

(4) Use of Facility

The numbers of projects accepted for the Use-of-Facility program during the first half and the second half of the fiscal year of 2001 amounted to 2 and 5 for the Laser Research Center for Molecular Science, 24 and 27 for the Research Center for Molecular Materials (the Research Center for Molecular-scale Nanoscience from April 1, 2002), and 0 and 0 for Equipment Development Center, respectively.

(5) Invited Research

Under this joint-study program, several scientists were invited from other institutions of help for construction and improvement of instruments in IMS. The total number of the projects in this category was 3 (2 for the

first half and 1 for the second half) in the fiscal year of 2001.

(6) Use of UVSOR Projects

In the UVSOR Facility with the 750 MeV electron storage ring, there are twenty beam lines available for synchrotron radiation research (see UVSOR ACTIVITY REPORT 2001). Under the Use of UVSOR Projects, many synchrotron radiation experiments have been carried out by outside scientists on eleven beam lines in close cooperation with the UVSOR staff. The total number of the projects in this category was 163 (82 for the first half and 81 for the second half) in the fiscal year of 2001.

(7) Use of Facility Program of the Computer Center

Computer Center provides three types of research programs for outside scientists: (a) Use-of-Facility Program; (b) Cooperative Research Program; (c) Advanced Research Program. The numbers of projects accepted for each programs during the fiscal year of 2001 were (a) 124 with 499 users, (b) 4 with 6 users (2 projects for the first half and 2 projects for the second half) and (c) 0 with 0 users. Computer time distributed to these projects amounted to 73% of the total annual CPU time.

FOREIGN SCHOLARS

Visitors from abroad are always welcome at IMS and they have always played an important role in the research activities of the Institute. The foreign scientists who visited IMS during the past year (September 2000–August 2001) are listed below.

*¹ indicates attendance at an Okazaki Conference; *² a MONBUSHO (the Ministry of Education, Science, Sports and Culture, Japan) or JSPS (the Japan Society for the Promotion of Science) Invited Fellow; *³ an IMS councillor; *⁴ an IMS visiting professor or associate professor from abroad (period of stay from 6 to 12 months); *⁵ a JSPS Post-Doctoral or Ronpaku Fellow; *⁶ an IMS visiting scientist and *⁷ a visitor to IMS.

Scientists who would like to visit IMS under programs *² and *⁴ are invited to make contact with IMS staff in their relevant field.

Dr. Traian Dascalu ^{*6}	Inst. of Atomic Physics	(Rumania)	Apr. '01–
Prof. Bin Zhang ^{*2*4}	Inst. of Chemistry Chinese Academy of Sci.	(China)	Jun. '02–
Dr. Harald Graaf ^{*5}	Univ. of Bremen	(Germany)	–Sep. '01
Prof. Voicu Lupei ^{*2}	Inst. of Atomic Physics	(Rumania)	–Sep. '01
Dr. Yulin Lam ^{*6}	National Univ. of Singapore	(Singapore)	Sep.–Oct. '01
Prof. Ludwik Adamowicz ^{*6}	Univ. of Arizona	(U.S.A.)	Sep.–Dec. '01
Dr. Wojciecowski Roman ^{*5}	Technical Univ. of Lodz	(Poland)	Sep. '01–Sep. '02
Prof. Jing Lu ^{*5}	Beijing Univ.	(China)	Sep. '01–Sep. '03
Prof. Jiali Gao ^{*7}	Univ. of Minnesota	(U.S.A.)	Oct '01
Prof. Chao-Jun Li ^{*7}	Tulane Univ.	(U.S.A.)	Oct '01
Prof. Timothy S. Zwier ^{*7}	Purdue Univ.	(U.S.A.)	Oct '01
Prof. Georg Süss-Fink ^{*7}	Univ. de Neuchatel	(Switzerland)	Oct '01
Prof. David E. Bergbreiter ^{*7}	Texas A&M Univ.	(U.S.A.)	Oct '01
Mr. Richard Bonneau ^{*7}	Univ. of Washington	(U.S.A.)	Oct '01
Dr. Justin Mansell ^{*7}	Intellite	(U.S.A.)	Oct '01
Prof. Stephen Meech ^{*5}	East Anglia Univ.	(U.K.)	Oct.–Dec. '01
Dr. Bicolai Pavel	Inst. of Atomic Physics	(Rumania)	–Nov. '01
Prof. Arnold Hoff ^{*6}	Leiden Univ.	(Holland)	Nov. '01
Dr. Olga Drozdova ^{*6}	Florida Univ.	(U.S.A.)	Nov.–Dec. '01
Dr. Biswajit Pal ^{*5}	Univ. of Alabama	(India)	Nov. '01–Nov. '03
Dr. Alexey Kondorskiy ^{*5}	P.N.Lebedev Inst.	(Russia)	Nov. '01–Nov. '03
Prof. Wolfgang Domcke ^{*7}	Technical Univ. of Munich	(Germany)	Dec. '01
Prof. Sason Shaik ^{*7}	Hebrew Univ.	(Israel)	Dec. '01
Dr. David E. Manolopoulos ^{*7}	Univ. of Oxford	(U.K.)	Dec. '01
Dr. Marc Benard ^{*7}	CNRS	(France)	Dec. '01
Prof. Martin Quack ^{*7}	Swiss Federal Inst. of Technology	(Switzerland)	Dec. '01
Prof. Peter Taylor ^{*7}	Univ. of California	(U.S.A.)	Dec. '01
Prof. Yundong Wu ^{*7}	The Hong Kong Univ. of Sci. and Tech.	(China)	Dec. '01
Prof. Dennis Salahub ^{*7}	Steacie Inst. for Molecular Sciences	(Canada)	Dec. '01
Prof. Weston T. Borden ^{*7}	Univ. of Washington	(U.S.A.)	Dec. '01
Prof. Kwang Soo Kim ^{*7}	Pohang Univ. of Science and Tech.	(Korea)	Dec. '01
Prof. Jape Olsen ^{*7}	Univ. of Aarhus	(Denmark)	Dec. '01
Prof. Peter Pulay ^{*7}	Univ. of Arkansas	(U.S.A.)	Dec. '01
Prof. Kristoffer Andersson ^{*7}	Univ. of Oslo	(Norway)	Dec. '01
Prof. Eok Kyun Lee ^{*2}	KAIST	(Korea)	Dec. '01–Feb. '02
Prof. Won Kweon Jang ^{*2}	Hanseu Univ.	(Korea)	Dec. '01–Feb. '02
Prof. Younk Yoo Kim ^{*6}	Hankuk Univ.	(Korea)	Dec. '01–Feb. '02
Prof. Chun-Woo Lee ^{*2}	Ajou Univ.	(Korea)	Dec. '01–Mar. '02
Prof. Myroslav F. Holovko ^{*2}	Ukrainian Academy of Science	(Ukraine)	Dec. '01–Mar. '02
Prof. Wensheng Bian ^{*5}	Shandong Univ.	(China)	–Jan. '02
Prof. Kankan Bhattacharyya ^{*7}	Indian Association for the Cultivation of Sci.	(India)	Jan. '02
Prof. Yuri Belokon ^{*7}		(Russia)	Jan. '02
Prof. Yuxiang Mo ^{*6}	Tsinghua Univ.	(China)	Jan.–Mar. '02
Prof. Ning Gu ^{*2}	Southeast Univ.	(China)	Jan.–Jul. '02
Prof. Yoshitaka Koga ^{*7}	Univ. of British Columbia	(Canada)	Feb. '02
Dr. Byeong-seun Min ^{*6}	Sungkyunkwan Univ.	(Korea)	Feb. '02
Dr. Eun-Duk Moon ^{*6}	Sungkyunkwan Univ.	(Korea)	Feb. '02
Prof. Yeong Sik Kim ^{*7}	Dankook Univ.	(Korea)	Feb. '02
Prof. Hong Jin Kong ^{*7}	KAIST	(Korea)	Feb. '02
Prof. Roman Sweitlik ^{*2*4}	Inst. of Molecular Phys. Polish Academy of Sci.	(Poland)	Feb. '02
Prof. Yong-seung Kwon ^{*6}	Sungkyunkwan Univ.	(Korea)	Feb. '02
Prof. Karl Wieghardt ^{*7}	Max-Plank Inst.	(Germany)	Feb. '02

Dr. Vincenzo Carravetta ^{*2}	Inst. of Quantum Chem. and Molecular Energetics (Italy)	Feb.–Aug. '02
Dr. Debabrata Mandal ^{*5}	S.A.jaipuria College (India)	–Mar. '02
Dr. Gennady Mil'nikov ^{*6}	Inst. of Structural Macrokinetics (Russia)	–Mar. '02
Prof. Charles L. Brooks ^{*7}	Scripps Research Inst. (U.S.A.)	Mar. '02
Dr. Konstantin Kostov ^{*7}	Univ. of Chicago (U.S.A.)	Mar. '02
Dr. G. Rajagopal ^{*7}	Madras Univ. (India)	Mar. '02
Prof. Peter G. Wolynes ^{*7}	Univ. California (U.S.A.)	Mar. '02
Dr. Andrij Baumketner ^{*7}	Kanazawa Univ. (Japan)	Mar. '02
Dr. Chee Chin Liew ^{*7}	National Inst. of Advanced Science and Tech. (Japan)	Mar. '02
Dr. Kuo-Kan Liang ^{*7}	Inst. of Atomic and Molecular Sciences (Taiwan)	Mar. '02
Dr. Feng-Yin Li ^{*7}	Natl. Center for High-Performance Computing (Taiwan)	Mar. '02
Dr. Jun-Ho Choi ^{*7}	Korea Univ. (Korea)	Mar. '02
Dr. Kijeong Kwac ^{*7}	Korea Univ. (Korea)	Mar. '02
Dr. Sihyun Ham ^{*7}	Korea Univ. (Korea)	Mar. '02
Dr. Jae-Weon Lee ^{*7}	KAIST (Korea)	Mar. '02
Dr. Kasi Nehru ^{*7}	Inha Univ. (Korea)	Mar. '02
Dr. Daniel Thangadurai ^{*7}	KAIST (Korea)	Mar. '02
Dr. Udom Robkob ^{*7}	Mahidol Univ. (Thailand)	Mar. '02
Dr. Samuel Selvaraj ^{*7}	Bharathidasan Univ. (India)	Mar. '02
Dr. Soonmin Jang ^{*7}	Soul National Univ. (Korea)	Mar. '02
Dr. Jinhyuk Lee ^{*7}	Soul National Univ. (Korea)	Mar. '02
Prof. Seokmin Shin ^{*7}	Soul National Univ. (Korea)	Mar. '02
Prof. Ronald Brudler ^{*7}	Scripps Res. Inst. (U.S.A.)	Mar. '02
Prof. Baranov Nikolai Viktorovich ^{*2}	Ural State Univ. (Russia)	Mar.–Jul'02
Prof. Side Du	Fudan Univ. (China)	–Apr. '02
Prof. Robert Byer ^{*7}	Stanford Univ. (U.S.A.)	Apr. '02
Dr. Mikhail Vener ^{*7}	Karpov Inst. of Physical Chemistry (Russia)	Apr. '02
Prof. Bernd A. Berg ^{*2}	Florida State Univ. (U.S.A.)	Apr.–Jun. '02
Dr. Nicolaie Pavel ^{*5}	Inst. of Atomic Physics (Rumania)	Apr. '02–Feb. '03
Dr. Olga Drozdova ^{*6}	A.F.Ioff Physico-Technical Inst. (Russia)	Apr. '02–Mar. '03
Prof. Changshun Wang ^{*6}	Henan Univ. (China)	Apr. '02–Mar. '03
Prof. Jiri Hudecek ^{*6}	Charles Univ. (Czech)	–Mar. '02
Dr. Giovanni La Penna ^{*6}	Natural Research Council (Italy)	May '02
Dr. Jörg Sichelschmit ^{*6}	Max-Planck Inst. für Chem. Phys. fester Strabe (Germany)	May '02
Prof. Oleg Tolstikhin ^{*7}	National Inst. for Fusion Science (Japan)	May '02
Prof. Tadeusz Michal Luty ^{*5}	Technical Univ. of Wroclaw (Poland)	May–Aug. '02
Dr. Gennady V. Mil'nikov ^{*6}	Russian Academy of Science (Russia)	May–Oct. '02
Prof. Herve Cailleau ^{*7}	Univ. of Rennes (France)	Jun. '02
Prof. Marie-Helene Lemee-Cailleau ^{*7}	Univ. of Rennes (France)	Jun. '02
Prof. Edward I. Solomon ^{*7}	Stanford Univ. (U.S.A.)	Jun. '02
Prof. James P. Collman ^{*7}	Stanford Univ. (U.S.A.)	Jun. '02
Dr. Ha Jin Lee ^{*2}	Hanyang Univ. (Korea)	Jun. '02–
Mr. Eirik F. Da Silva ^{*6}	Norwegian Univ. of Science and Technology (Norway)	Jul. '02
Prof. Yugal Khajuria ^{*7}	Tohoku Univ. (Japan)	Jul. '02
Prof. John Eland ^{*7}	Tohoku Univ. (Japan)	Jul. '02
Dr. Richard Hall ^{*7}	Inst. of Materials Structure Science (Japan)	Jul. '02
Prof. Young-Kyu Choi ^{*7}	Silla Univ. (Korea)	Jul. '02
Prof. Martin Fejer ^{*7}	Stanford Univ. (U.S.A.)	Jul. '02
Prof. Jiri Hudecek ^{*6}	Charles Univ. (Czech)	Jul. '02
Dr. Gina Marie Florio ^{*7}	Purdue Univ. (U.S.A.)	Jul.–Aug. '02
Prof. Sangkyu Kim ^{*2}	Inha Univ. (Korea)	Jul.–Aug. '02
Mr. Olivier Porcherie ^{*2}	Univ. of Montpellier (France)	Jul.–Aug. '02
Mr. Yong Hoon Kim ^{*6}	Yonsei Univ. (Korea)	Jul.–Sep. '02
Prof. Zheng-Qiang Li ^{*6}	Jilin Univ. (China)	Jul.–Sep. '02
Prof. Pawel Kozlowski ^{*2}	Univ. of Louisville (U.S.A.)	Jul.–Dec. '02
Prof. Pawel Kozlowski ^{*2}	Univ. of Louisville (U.S.A.)	Jul.–Dec. '02
Prof. Zhe-Ming Wang ^{*2}	Peking Univ. (China)	Jul.'02–Jul. '03
Prof. Ranga Rao Gangavarapu ^{*2}	Indian Inst. of Technology (India)	Jul.'02–Nov. '03
Prof. Klaus Peter Dinse ^{*2}	Univ. Darmstadt (Germany)	Aug.–Nov. '02
Dr. Maurice Janssen ^{*7}	Vrije Univ. (Holland)	Aug. '02
Prof. John Hepburn ^{*7}	Univ. of British Columbia (Canada)	Aug. '02
Prof. Lars Pettersson ^{*7}	Stockholm Univ. (Sweden)	Aug. '02
Prof. Stacey Sorensen ^{*7}	Lund Univ. (Sweden)	Aug. '02
Dr. Christian Alcaraz ^{*6}	LURE (France)	Aug. '02

Prof. Faris Gelmukhanov ^{*7}	Royal Inst. of Technology	(Sweden)	Aug. '02
Prof. Eckart Ruehl ^{*7}	Osnabrueck Univ.	(Germany)	Aug.-Sep. '02
Dr. Marc Simon ^{*7}	LURE	(France)	Aug.-Sep. '02
Dr. Renaud Guillemin ^{*6}	LBL	(U.S.A.)	Aug.-Sep. '02

AWARDS

Professor Inokuchi's Achievement

Professor Hiroo Inokuchi, Professor Emeritus of Institute for Molecular Science (IMS), received the Order of Culture in 2001 for his contribution to "Discovery and Development of Organic Semiconductor." He was a Faculty member of IMS (1975–1987), and acceded the Director-General of IMS (1987–1993) and President of Okazaki National Research Institutes (1993–1995). Professor Inokuchi opened a new scientific field "Organic Semiconductor." His academic achievements are summarized as follows.

- 1. Discovery and Verification of Electronic Conduction in Conjugated π -Electron Molecular Solids.*

Through physicochemical studies on carbon and graphite, Professor Hiroo Inokuchi initiated measurements of electrical conductivity in condensed polycyclic aromatic (π -electron) compounds such as violanthrone, isoviolanthrone and pyranthron, and verified in a most convincing way that intermolecular electron transfer is mediated by intermolecular overlap of the π -electrons. The electronic conductivity was found to clearly increase by applying high pressure, and to decrease by removing the π -electrons through hydrogenation. He named these polycyclic π -electron compounds 'organic semiconductors' since their conductivities increase with temperature. Professor Inokuchi extended his π -electron materials to include charge-transfer complexes, and discovered extraordinarily high conductivity in a perylene-bromine complex. This was a great breakthrough from organic semiconductors to organic conductors, which finally lead to organic superconductors. Along this line, the first successful organic metal was TTF-TCNQ studied by Heeger *et al.*, but due to the 1-dimensional (1D) nature of this compound, the metal-insulator (M-I) transition at low temperatures presented a crucial obstacle for realizing a superconducting state in these materials. Professor Inokuchi tackled and overcame this difficulty by ingenious molecular design to elevate the dimensionality to 2-D to suppress the M-I transition. He measured confirmed a persistent metallic nature in (BEDT-TTF)₂ClO₄ for the first time, and finally succeeded in realizing superconductors based on BEDT-TTF salts which now comprise the largest family of organic superconductors. Professor Inokuchi was also influential in the area of single component molecular materials, where he proposed the idea of the 'molecular fastener effect,' which involves the enhancement of intermolecular interactions due to the additivity of van der Waals interactions between long hydrocarbon chains. This idea was successfully realized in various compounds.
- 2. Catalytic Activity of Some Organic Materials.*

Professor Inokuchi was also able to exploit π -electron functionality, to design molecular catalysts. He first observed that the *ortho-para* hydrogen conversion reaction proceeded very rapidly on polycyclic aromatic hydrocarbon-alkali metal charge-transfer complex, and reached the conclusion that the catalytic activity is mediated through charge transfer. In fact, this important discovery started an explosion of studies on the catalysis of charge-transfer complexes. Charge-transfer complexes, including graphite intercalation compounds, chloranil-alkali metal complexes, and cytochrome *c*₃-alkali metal complexes were investigated intensively. These studies established that reactivity is closely related to the electric and magnetic properties of the molecular catalyst such that, once again, the charge transfer plays a vital role. In particular, Professor Inokuchi observed high metallic conductivity of cytochrome *c*₃ thin film under a hydrogen atmosphere over a certain temperature range. This anomalous behavior suggests the possible superconductivity in the biological systems.
- 3. U. V. Photoelectron Spectroscopy for Organic Solids.*

Beginning in 1963, Professor Inokuchi developed U. V. photoelectron spectroscopy for organic thin films. By analyzing the kinetic energy of photoelectrons emitted from the films, he provided key information on the electronic structures of more than 100 organic compounds. Information such as the ionization potentials, the polarization energies, and the band gap energies provides a very useful powerful guide for the characterization of typical organic solids (including polymers) as well as enabling a systematic search for molecular functionality materials.
- 4. Fundamental Aspects of Molecular Electronics.*

Professor Inokuchi reached the concept of "molecular electronics" through the study of organic materials with π -electron functionality. He identified three important functions in molecular devices: transport, storage and regulation of electrons in molecular materials. Over the past 40 years, his studies on the electron transport properties of molecular conductors have set the standard for the field he largely created. In addition to this work, he also studied graphite intercalation compounds as a means for the storage of electrons and several photochromic as regulators of electrons. As mentioned above, Professor Inokuchi is the pioneer and the leader in the field of molecular electronics.
- 5. Administrative Contributions to the Fields of Molecular Sciences and Solid State Chemistry.*

Professor Inokuchi was a primary founding member of the Institute for Molecular Science, Okazaki, Japan, which has been one of the brightest centers of molecular science in the world. He also contributed to the development of the Institute as a faculty member and the Director-General for 17 years. His contribution to molecular science and solid-state chemistry through the activities in this Institute is enormous.

Professor Kitagawa's Scientific Achievements

Prof. Teizo Kitagawa of the Center for Integrative Bioscience received a Chemical Society of Japan Award in 2001 for his contributions to "The Elucidation of Structures and Dynamics of Heme Proteins by Time-resolved Resonance Raman Spectroscopy." By utilizing advantages of vibrational spectroscopy, Professor Kitagawa has studied molecular mechanisms of various hemoproteins including the allosteric effect of hemoglobin, molecular dynamics of myoglobin, and oxygen activation mechanisms of peroxidases and cytochrome oxidase. The followings are the summary of his scientific achievements related to the award.

- 1) Molecular structural studies on the allosteric effect of hemoglobin: hemoglobin, a tetramer protein consisting of two α and two β subunits, binds molecular oxygen with an allosteric effect. On the basis of the assignment and monitoring of the Fe(II)-Histidine stretching mode, Professor Kitagawa demonstrated how the binding affinity of molecular oxygen is controlled.
- 2) Studies on the molecular mechanism of cytochrome oxidase: the catalytic cycle of cytochrome oxidase consists of at least 6 intermediates and completes in 5 msec. Prof. Kitagawa successfully characterized all the intermediates including O=Fe(V) species, which had been considered to be Fe(III)-O-O-Cu(II) for more than 30 years.
- 3) Direct observation of cooling of heme upon photodissociation of carbonmonoxy myoglobin: the formation of vibrationally excited heme upon photodissociation of carbonmonoxy myoglobin and its subsequent vibrational energy relaxation were monitored by picosecond anti-Stokes resonance Raman spectroscopy. This direct monitoring of the cooling dynamics of the heme cofactor within the globin matrix allowed discussion on the thermal energy flow through the protein moiety and to the water bath.
- 4) Application of ultraviolet resonance Raman spectroscopy for higher order structural changes of proteins and their dynamics: a Raman spectrum of one specific amino acid residue such as tyrosine, tryptophan, phenylalanine, and histidine in a protein as large as 200,000 dalton was selectively observed by ultraviolet resonance Raman spectroscopy with the use of 200–240 nm Raman-excitation. The observation for a change of one particular amino acid enables us to understand a communication pathway between different subunits upon oxygen binding to a heme.

Associate Professor Taira's Scientific Achievements

Associate professor Takunori Taira of Laser Research Center for Molecular Science received the Technology Development Award of Japan Fine Ceramics Association in 2001 for his contribution to "Fabrication of extremely low-scattering-loss Nd:YAG ceramics and development of high-performance ceramic lasers." This award is given to the persons who invented new product or technology which made a big impact on the technology development for fine ceramics industries. He and his co-winner, Dr. Akio Ikesue of Japan Fine Ceramics Center and Professor Kunio Yoshida of Osaka Institute of Technology, developed quite a new technique to fabricate highly transparent Nd:YAG ceramics and succeeded in laser oscillation with much higher efficiency than using conventional Nd:YAG single crystals. YAG ceramics can be doped with much more Nd ions than YAG single crystals, which increases the absorption efficiency for the pump beam. This advantage is expected to realize high-power and highly efficient microchip (the thickness of laser medium is less than 1 mm) lasers which emit blue or green as well as 1 μ m light. His achievements broke the preconception that ceramics are always opaque, opening the door to new applications of ceramics as "optical materials."

Associate Professor Kinoshita's Scientific Achievement

Prof. Masahiro Kinoshita at Kyoto University, a former visiting professor of our institute, has been awarded the "good paper prize" for 2001 from the Society of Chemical Engineers, Japan. The prize is awarded every year to about four distinguished papers that were published in the Japanese Journal of Chemical Engineering. Professor Kinoshita's paper to which the prize has been awarded is entitled "Statistical-Mechanical Analysis on Entropically Driven Formation of Ordered Structure" (*Kagaku Kogaku Ronbunshu* Vol. 27, No.6, pp. 683–689 (2001)). The paper was written during his stay at IMS as a visiting professor. Professor Kinoshita has been involved in a variety of collaborative projects in our institute. The outline of the paper is given below.

The paper sheds light on roles of the entropic excluded volumes in biological systems by a microscopic theory. It deals with the process that a surface and large particles immersed in small particles form ordered structure with the result of increase in the system entropy. More specific, major conclusions drawn for the entropically driven contact of large particles with a surface are as follows: Great specificity arises between the diameter of the large particle and the surface curvature, and high selectivity is provided for the lock and key steric interaction between macromolecules. It would be possible to control the motion of a large particle by adjustment of the surface geometry: the study could be extended to nano-technology such as control of particle arrays. Further development is described in the following: M. Kinoshita, "Spatial Distribution of a Depletion Potential between a Big Solute of

Arbitrary Geometry and a Big Sphere Immersed in Small Spheres," *J. Chem. Phys.* **116**(8), 3493–3501 (2002).

Research Associate Sato's Scientific Achievement

Dr. Hirofumi Sato in Kyoto University won the "The Chemical Society of Japan Award for Young Chemists for 2001."

Sato had been a research associate in our institute until this April, and the prize is awarded to the research he has carried out in the institute.

Chemical reaction is not only a central issue in the material science, but also an essential problem to understand what going on in biological system. In the mean time, Chemical reactions in our real life is always taking place in some solvent environment, not in vacuo, which is true especially in our living systems. The prize is awarded to Sato for his contribution to establish a molecular theory with respect to the solvent effect on chemical reactions. Sato's accomplishments are classified roughly into two. The first is concerned with the methodological development of the RISM-SCF theory. The RISM-SCF theory is a theory first proposed by Tenno, Kato, and Hirata in 1993, which combines the statistical mechanics of molecular liquid (RISM) with the ab initio MO theory to determine the electronic structure of a solute molecule and solvent structure self-consistently. Sato has given an alternative formulation of the theory based on the variational principle, which at the same time has established a method of calculating the energy derivatives. The latter is of particular importance, for example, to optimize geometry of a molecule and to calculate the vibrational spectrum of a molecule in solution, and provides a new tool to explore chemical processes in solution. In fact, the theory of NMR chemical shift in solution, which has been developed by Dr. Yamazaki, is based on Sato's variational formalism and on the method of energy derivatives. With respect to methodological aspect, Sato has also made important contribution concerning coupling of the ab initio electronic structure theory with the 3D-RISM theory. The 3D-RISM theory has been developed by Dr. Kovalenko in our group during last few years, which provides detailed three dimensional structure of solvent around a solute. Sato has combined the theory with the ab initio method to study the electronic structure and solubility of a CO in water.

Dr. Sato's another contribution is to explore a wide variety of chemical reaction in solution, from inorganic to organic, by means of the RISM-SCF theory, and to give a microscopic explanation to reaction mechanisms which have long stayed in phenomenological levels. Among many interesting studies Sato has done, I would like to introduce just one example which concerns the acidity of hydrogen halides in water, a problem in high school text book. All the hydrogen halides except for hydrogen fluoride show strong acidity, while the fluoride exhibits weak acidity. The phenomena is paradoxical if one considers the fluoride has the largest electronegativity. The problem attracted attention from theoretical chemists including L. Pauling. The key to solve the puzzle is to take account for the solvent effect. In fact, Pauling has shown based on the experimental free energy of solvation that the non-dissociated form of HF has lower free energy than the dissociated form. However, Pauling could not answer the question why it happens, because his analysis was phenomenological. Based on the RISM-SCF method, Sato first has shown that HF is in fact a weak acid. Moreover, he could have successfully explain the reason. According to the explanation, HF makes two types of hydrogen-bonds with water molecules, ($\text{H}_2\text{O}\cdots\text{H-F}$) and ($\text{FH}\cdots\text{H-O-H}$), while all other hydrogen halides form only one type of hydrogen-bonds ($\text{H}_2\text{O}\cdots\text{H-X}$). The extra hydrogen-bond gives extra stability to the non-dissociated form of HF.

Research Associate Shoji's Achievements

Research Associate Dr. Ichiro Shoji of Laser Research Center for Molecular Science received "Young Scientist Award for the Presentation of an Excellent Paper," in 2002, from the Japan Society of Applied Physics (JSAP) with the paper "Reduction of Depolarization Induced by Thermal Birefringence Using a (100)-cut YAG Crystal." This award was given to young scientists who have presented excellent papers at the JSAP annual meetings.

Dr. Shoji studied at the Tokyo University, there he investigated on the nonlinear optical phenomena and, together with Prof. Ito, he built the way to measure the absolute nonlinear constants. After moved to Taira group of the Institute for Molecular Science, and he becomes interested in the ceramic YAG lasers. The ceramic YAG is an attractive and strange material as the laser medium. He was bewildered by this new material and found the mistakes in the solid-state laser theory. In the Solid-State Laser field, many efforts were done toward the high-power and high-quality laser system by the compensation of thermally induced problems risen from the pump quantum defects. The solutions, which are complicated and not perfect are, based on (111)-cut YAG material. Every compensation method based on (111)-cut YAG because Drs. Koechner and Rice have built a beautiful theory about thermal effect in laser rod. Lately, Dr. Shoji found the mistakes in Koechner's theory by the experiments and built the new model. With detail measurement of thermally induced birefringence in Nd:YAG single crystal of (111), (100), and (110)-cut we discovered new way to reduce it drastically. This novel solution to reduce the thermal problems should apply to any solid-state optical devices.

His result makes it clear that, sometimes, we have to reconsider a problem from its basics in order to solve the complicated high technology and/or practical situations.

Mr. Hayashi's Scientific Achievements

Our Colleague Mr. Naoki Hayashi, Department of Molecular Structure, received the Award for young researcher of the Liquid Crystal Society of Japan in 2001 for his contribution to "Investigations of Molecular Orientational Ordering in Liquid Crystals by Polarized Raman Scattering." Since the discovery of V-shape switching of liquid crystals, the mechanism of the switching has been open to dispute. Especially a random switching mechanism has interested people, however, a clear evidence for the random switching mechanism has not been reported. Mr. Hayashi could give the experimental evidence proving the random switching mechanism of V-shape phenomena of liquid crystal by using the polarized Raman scattering measurement. Moreover, he has found the breaking out of the uniaxiality in the molecular orientational distribution in ferroelectric phase of liquid crystal. His works have been published in the journals, *Phys. Rev. E*, *Phys. Rev. Lett.*, and *etc.*

Dr. Hisashi Tanaka's Scientific Achievement

Dr. Tanaka, a JSPS postdoctoral fellow in Kobayashi Group at the department of Molecular Assemblies, received the first "Synthetic Metal Young Award" at the International Conference of Synthetic Metals held in Shanghai (ICSM2002)(June 29-July 5, 2002). This newly started award will be given every two years at ICSM meetings. The ICSM2002 had more than 2000 participants, from which four young participants (one student, two postdoctoral fellows and one young independent researcher) were selected. Dr. Tanaka received the post-doc award for his contribution to the recent two remarkable achievements in the field of synthetic metals: (1) the development of single-component molecular metals and (2) the discovery of the field-induced superconductivity of organic conducting system.

Mr. Zhi-Hong Wang's Scientific Achievement

Mr. Zhi-Hong Wang in Urisu group, a third year Student of the Graduate University for Advanced Studies received the Award for Most Impressive Presentation in 2001 Microprocess and Nanotechnology Conference for his contribution "Hydrogen Diffusion and Chemical Reactivity with Water on Nearly Ideally H-terminated Si(100) Surface." He has observed the hydrogen atoms in the Si bulk spectroscopically for the first time by using BML-IRRAS (infrared reflection absorption spectroscopy using a buried metal layer substrate).

LIST OF PUBLICATIONS

Department of Theoretical Studies

- K. KOBAYASHI, Y. SANO and S. NAGASE**, "Theoretical Study of Endohedral Metallofullerenes: $\text{Sc}_{3-n}\text{La}_n\text{N}@C_{80}$ ($n = 0-3$)," *J. Comput. Chem.* **22**, 1353 (2001).
- M. ICHINOHE, Y. ARAI, A. SEKIGHUCHI, N. TAKAGI and S. NAGASE**, "A New Approach to the Synthesis of Unsymmetrical Disilenes and Germanasilene: Unusual ^{29}Si NMR Chemical Shifts and Regiospecific Methanol Addition," *Organometallics* **20**, 4141 (2001).
- N. TAKAGI and S. NAGASE**, "A Silicon-Silicon Triple Bond Surrounded by Bulky Terphenyl Groups," *Chem. Lett.* 966 (2001).
- A. HAN, T. WAKAHARA, Y. MAEDA, Y. NIINO, T. AKASAKA, K. YAMAMOTO, M. KAKO, Y. NAKADAIRA, K. KOBAYASHI and S. NAGASE**, "Photochemical Cycloaddition of C_{78} with Disilirane," *Chem. Lett.* 974 (2001).
- M. KIMURA and S. NAGASE**, "The Quest of Stable Silanones. Substituent Effects," *Chem. Lett.* 1098 (2001).
- N. TAKAGI and S. NAGASE**, "Substituent Effects on Germanium-Germanium and Tin-Tin Triple Bonds," *Organometallics* **20**, 5498 (2001).
- K. GOTO, Y. HINO, Y. TAKAHASHI, T. KAWASHIMA, G. YAMAMOTO, N. TAKAGI and S. NAGASE**, "Synthesis, Structure, and Reactions of the First Stable Aromatic S-Nitrosothiol Bearing a Novel Dendrimer-Type Steric Protection Group," *Chem. Lett.* 1204 (2001).
- A. SEKIGUCHI, Y. ISHIDA, N. FUKAYA, M. ICHINOHE, N. TAKAGI and S. NAGASE**, "The First Halogen-Substituted Cyclotrimerenes: A Unique Halogen Walk over the Three-Membered Ring Skeleton and Facial Stereoselectivity in the Diels-Alder Reaction," *J. Am. Chem. Soc.* **124**, 1158 (2002).
- T. SASAMORI, N. TAKEDA, M. FUJIO, M. KIMURA, S. NAGASE and N. TOKITOH**, "Synthesis and Structure of the First Stable Phosphabismuthene," *Angew. Chem. Int. Ed.* **41**, 139 (2002).
- J. KOBAYASHI, K. GOTO, T. KAWASHIMA, M. W. SCHMIDT and S. NAGASE**, "Synthesis, Structure, and Bonding Properties of 5-Carbaphosphatranes: A New Class of Main Group Atrane," *J. Am. Chem. Soc.* **124**, 3703 (2002).
- T. SASAMORI, Y. ARAI, N. TAKEDA, R. OKAZAKI, Y. FURUKAWA, M. KIMURA, S. NAGASE and N. TOKITOH**, "Syntheses, Structures and Properties of Kinetically Stabilized Distibenes and Dibismuthenes, Novel Doubly Bonded Systems between Heavier Group 15 Elements," *Bull. Chem. Soc. Jpn.* **75**, 661 (2002).
- T. WAKAHARA, A. HAN, Y. NIINO, Y. MAEDA, T. AKASAKA, T. SUZUKI, K. YAMAMOTO, M. KAKO, Y. NAKADAIRA, K. KOBAYASHI and S. NAGASE**, "Silylation of Higher Fullerenes," *J. Mater. Chem.* **12**, 2061 (2002).
- T. WAKAHARA, S. OKUBO, M. KONDO, Y. MAEDA, T. AKASAKA, M. WAELCHLI, M. KAKO, K. KOBAYASHI, S. NAGASE, T. KATO, K. YAMAMOTO, X. GAO, E. V. CAEMELBECKE and K. M. KADISH**, "Ionization and Structural Determination of the Major Isomer of $\text{Pr}@C_{82}$," *Chem. Phys. Lett.* **360**, 235 (2002).
- T. WAKAHARA, Y. NIINO, T. KATO, Y. MAEDA, T. AKASAKA, M. T. H. LIU, K. KOBAYASHI and S. NAGASE**, "A Non-Spectroscopic Method to Determine the Photolytic Decomposition Pathways of 3-Chloro-3-Alkyldiazirine; Carbene, Diazo and Rearrangement in Excited State," *J. Am. Chem. Soc.* **124**, 9465 (2002).
- K. -Y. AKIBA, S. MATSUKAWA, T. ADACHI, Y. YAMAMOTO, S. Y. RE and S. NAGASE**, "Effect of $\sigma^*_{\text{P-O}}$ Orbital on Structure, Stereomutation, and Reactivity of C-Apical O-Equatorial Spirophosphoranes," *Phosphorus, Sulfur Silicon Relat. Elem.* **177**, 1671 (2002).
- T. NAKAZAWA, S. BAN, Y. OKUDA, M. MASUYA, A. MITSUTAKE and Y. OKAMOTO**, "A PH-Dependent Variation in α -Helix Structure of the S-Peptide of Ribonuclease A Studied by Monte Carlo Simulated Annealing," *Biopolymers* **63**, 273 (2002).
- T. NAGASIMA, Y. SUGITA, A. MITSUTAKE and Y. OKAMOTO**, "Generalized-Ensemble Simulations of Spin Systems and Protein Systems," *Comput. Phys. Commun.* **146**, 69 (2002).
- G. V. MIL'NIKOV and H. NAKAMURA**, "Use of Diabatic Basis in the Adiabatic-by-Sector R-Matrix Propagation Method in Time-Independent Reactive Scattering Calculations," *Comput. Phys. Commun.* **140**, 381 (2001).
- G. V. MIL'NIKOV and H. NAKAMURA**, "Practical Implementation of the Instanton Theory for the Ground State Tunneling Splitting," *J. Chem. Phys.* **115**, 6881 (2001).
- C. ZHU, H. KAMISAKA and H. NAKAMURA**, "Significant Improvement of the Trajectory Surface Hopping Method by the Zhu-Nakamura Theory," *J. Chem. Phys.* **115**, 11036 (2001).
- G. V. MIL'NIKOV and H. NAKAMURA**, "Regularization of Scattering Calculations at R-Matrix Poles," *J. Phys. B: At. Mol. Opt. Phys.* **34**, L791 (2001).
- H. KAMISAKA, W. BIAN, K. NOBUSADA and H. NAKAMURA**, "Accurate Quantum Dynamics of Electronically Nonadiabatic Chemical Reactions in the DH_2^+ System," *J. Chem. Phys.* **116**, 654 (2002).
- C. ZHU, H. KAMISAKA and H. NAKAMURA**, "New Implementation of the Trajectory Surface Hopping Method with Use of the Zhu-Nakamura Theory. II. Application to the Charge Transfer Processes in the 3D DH_2^+

System," *J. Chem. Phys.* **116**, 3234 (2002).

P. KOLORENC, M. CÍZEK, J. HORÁČEK, G. V. MIL'NIKOV and H. NAKAMURA, "Study of Dissociative Electron Attachment to HI Molecule by using R-matrix Representation for Green's Function," *Physica Scripta* **65**, 328 (2002).

Y. SUZUKI and Y. TANIMURA, "Probing a Colored-Noise Induced Peak of a Strongly Damped Brownian System by One- and Two-Dimensional Spectroscopy," *Chem. Phys. Lett.* **358**, 51 (2002).

Y. TANIMURA, V. B. P. LEITE and J. N. ONUCHIC, "The Energy Landscape for Solvent Dynamics in Electron Transfer Reactions: a Minimalist Model," *J. Chem. Phys.* **117**, 2172 (2002).

O. HINO, Y. TANIMURA and S. TEN-NO, "Biorthogonal Approach for Explicitly Correlated Calculations Using the Transcorrelated Hamiltonian," *J. Chem. Phys.* **115**, 7865 (2001).

O. HINO, Y. TANIMURA and S. TEN-NO, "Application of the Transcorrelated Hamiltonian to the Linearized Coupled Cluster Singles and Doubles Model," *Chem. Phys. Lett.* **353**, 317 (2002).

A. MASUHARA, H. KASAI, T. KATO, S. OKADA, H. OIKAWA, Y. NOZUE, S.K. TRIPATHY and H. NAKANISHI, "Hetero-Multilayered Thin Films Made Up of Polydiacetylene Microcrystals and Metal Fine Particles," *J. Macromol. Sci.-Pure appl. Chem. A* **38**, 1371 (2002).

S. SAITO, "Electronic Properties of Nanotube Based Materials," *Tours 2000 Symposium on Nuclear Physics IV*, M. Amould, *et al.*, Eds., American Institute of Physics Conference Proceedings **561**, 214 (2001).

N. HAMADA, M. YAMAJI, S. OKADA and S. SAITO, "Dielectric Function of C₆₀-Encapsulating Nanotube," *Proc. International Symposium on Nanonetwork Materials: Fullerenes, Nanotubes, and Related Systems* (Kamakura, 15–18 January 2001), S. Saito *et al.*, Eds., American Institute of Physics Conference Proceedings **590**, 201 (2001).

S. OKADA, S. SAITO, A. OSHIYAMA and Y. MIYAMOTO, "Electronic Structure and Energetics of Carbon Nanotubes Encapsulating C₆₀," *Proc. International Symposium on Nanonetwork Materials: Fullerenes, Nanotubes, and Related Systems* (Kamakura, 15–18 January 2001), S. Saito *et al.*, Eds., American Institute of Physics Conference Proceedings **590**, 173 (2001).

S. OKADA, S. SAITO and A. OSHIYAMA, "Semiconducting Form of the First-Row Elements: C₆₀ Chain Encapsulated in BN Nanotubes," *Phys. Rev. B* **64**, 20130 (2001).

K. UMEMOTO, S. SAITO, S. BERBER and D. TOMANEK, "Carbon Foam: Spanning the Phase Space between Graphite and Diamond," *Physical Review B* **64**, 193409-1 (2001).

Y. MIYAMOTO, S. SAITO and D. TOMANEK, "Electronic Interwall Interactions and Charge Redistribution in Multiwall Nanotubes," *Phys. Rev. B* **65**, 041402-1 (2001).

K. UMEMOTO and S. SAITO, "Electronic Structure of Ba₄C₆₀ and Cs₄C₆₀," *Proc. International Symposium on Nanonetwork Materials: Fullerenes, Nanotubes, and Related Systems* (Kamakura, 15–18 January 2001), S. Saito *et al.*, Eds., American Institute of Physics Conference Proceedings **590**, 305 (2001).

A. Oshiyama, S. Okada and S. Saito, "Prediction of Electroic Properties of Carbon-Based Nanotstructures," *Physica B* **323**, 21 (2002).

T. MIYAKE and S. SAITO, "Electronic Structure of Potassium-Doped Carbon Nanotubes," *Physica B* **323**, 219 (2002).

S. OKADA, S. SAITO and A. OSHIYAMA, "Electronic and Geometric Structures of Multi-Walled BN Nanotubes," *Physica B* **323**, 224 (2002).

K. KANAMITSU and S. SAITO, "Geometries, Electronic Properties, and Energetics of Isolated Single Walled Carbon Nanotubes," *J. Phys. Soc. Jpn.* **71**, 483 (2002).

S. OKADA, S. SAITO and A. OSHIYAMA, "Interwall Interaction and Electronic Structure of Double-Walled BN Nanotubes," *Phys. Rev. B* **65**, 165410 (2002).

T. MIYAKE and S. SAITO, "Electronic Structure of Potassium-Doped Carbon Nanotubes," *Phys. Rev. B* **65**, 165419 (2002).

M. KAMIYA, T. TSUNEDA and K. HIRAO, "A Density Functional Study of van der Waals Interactions," *J. Chem. Phys.* **117**, 6010 (2002).

W. LIE, D. G. FEDROV and K. HIRAO, "Theoretical Study of the Reaction XY₄ = XY₃ + Y, where X = C, Si, Ge, Sn, Pb and Y = CH₃, C₂H₅," *J. Phys. Chem. A* **106**, 7057 (2002).

J. PAULOVIC, T. NAKAJIMA, K. HIRAO and L. SELJO, "Third-Order Douglas-Kroll Ab Initio Model Potential for Actinides," *J. Chem. Phys.* **117**, 3597 (2002).

M. DUPUIS, Y. KAWASHIMA and K. HIRAO, "The QM/MM-pol-vib/CAV Solvation Model with Polarizable MM for Excited States: II. Application to the Blue Shift in H₂CO ¹(π* ← n) Excitation," *J. Chem. Phys.* **117**, 1255 (2002).

M. DUPUIS, M. AIDA, Y. KAWASHIMA and K. HIRAO, "The QM/MM-pol-vib/CAV Solvation Model With Polarizable MM for Excited States: I. Energy and Gradients Formulation and Implementation," *J. Chem. Phys.* **117**, 1242 (2002).

Y. KAWASHIMA, M. DUPUIS and K. HIRAO, "The QM/MM-pol-vib/CAV Solvation Model Extended to the Monte Carlo Method: Application to the Blue Shift of the H₂CO ¹(π* ← n) Excitation," *J. Chem. Phys.* **117**, 248 (2002).

- T. TSUCHIYA, T. NAKAJIMA, K. HIRAO and L. SEIJO**, "A Third-Order Douglas-Kroll Ab Initio Model Potential for Lanthanides," *Chem. Phys. Lett.* **361**, 334 (2002).
- T. YANAI, T. NAKAJIMA, Y. ISHIKAWA, and K. HIRAO**, "Highly Efficient Algorithm for Electron Repulsion Integrals over Relativistic Four-Component Gaussian-Type Spinors," *J. Chem. Phys.* **116**, 10122 (2002).
- H. A. WITEK, D. G. FEDOROV, A. VIEL, P-O. WIDMARK and K. HIRAO**, "Theoretical Study of the Unusual Potential Energy Curve of the $A^1\Sigma^+$ State of AgH," *J. Chem. Phys.* **116**, 8396 (2002).
- T. NAKAJIMA and K. HIRAO**, "Accurate Relativistic Gaussian Basis Sets Determined by the Third-Order Douglas-Kroll Approximation with a Finite-Nucleus Model," *J. Chem. Phys.* **116**, 8270 (2002)
- K. YAGI, T. TAKETSUGU and K. HIRAO**, "A New Analytic Form of Ab Initio Potential Energy Function: An Application to H_2O ," *J. Chem. Phys.* **116**, 3963 (2002).
- H. NAKANO, R. UCHIYAMA and K. HIRAO**, "Quasi-Degenerate Perturbation Theory with General Multiconfiguration Self-Consistent Field Reference Functions," *J. Comput. Chem.* **23**, 1166 (2002).
- Y. NAKAO, Y. K. CHOE and K. HIRAO**, "A CASCI-MRMP Method Based on Kohn-Sham Orbitals," *Mol. Phys. (Davidson Special Issue)* **100**, 729 (2002).
- R. C. DEKA and K. HIRAO**, "Lewis Acidity and Basicity of Cation-Exchanged Zeolites: QM/MM and Density Functional Studies," *J. Mol. Catal. A-Chem.* **181**, 275 (2002).
- H. A. WITEK, Y. -K. CHOE, J. P. FINLEY and K. HIRAO**, "Intruder-State Avoidance Multireference Møller-Plesset Perturbation Theory," *J. Comput. Chem.* **23**, 957 (2002).
- K. YAGI, T. TAKETSUGU and K. HIRAO**, "Generation of Full-Dimensional Potential Energy Surface of Intramolecular Hydrogen Atom Transfer in Malonaldehyde and Tunneling Dynamics," *J. Chem. Phys.* **115**, 10647 (2001).
- D. AJITHA and K. HIRAO**, "Dipole Moments of $^2\Sigma$ and $^2\Pi$ Ktates of CN Radical at Different Internuclear Distances *via* Fock Space Multi-Reference Coupled Cluster Linear Response Approach," *Chem. Phys. Lett.* **347**, 121 (2001).
- T. NAKAJIMA and K. HIRAO**, "Relativistic Effects for Polarizabilities and Hyperpolarizabilities of Rare Gas Atoms," *Chem. Lett.* 766 (2001).
- Y. KUROSAKI and T. TAKAYANAGI**, "Ab initio Molecular Orbital Study of $O(^1D)$ Insertion into C–C Bond in Cyclopropane and Ethane," *Chem. Phys. Lett.* **355**, 424 (2002).
- T. TAKAYANAGI**, "Quantum Scattering Calculations of the $O(^1D) + N_2(X^1\Sigma_g^+) \rightarrow O(^3P) + N_2(X^1\Sigma_g^+)$ Spin-Forbidden Electronic Quenching Collision," *J. Phys. Chem. A* **106**, 4914 (2002).
- T. TAKAYANAGI and H. AKAGI**, "Translational Energy Dependence of $NO + NO / N_2 + O_2$ Product Branching in the $O(^1D) + N_2O$ Reaction: a Classical Trajectory Study on a New Global Potential Energy Surface for the Lowest $^1A'$ State," *Chem. Phys. Lett.* **363**, 298 (2002).
- T. TAKAYANAGI and M. SHIGA**, "Path Integral Molecular Dynamics Combined with Discrete-Variable-Representation Approach: the Effect of Solvation Structures on Vibrational Spectra of Cl_2 in Helium Clusters," *Chem. Phys. Lett.* **362**, 504 (2002).
- A. KOVALENKO and F. HIRATA**, "A Replica Reference Interaction Site Model Theory for a Polar Molecular Liquid Sorbed in a Disordered Microporous Material with Polar Chemical Groups," *J. Chem. Phys.* **115**, 8620 (2001).
- H. SATO and F. HIRATA**, "Realization of Three-Dimensional Solvation-Structure from Site-Site Radial Distribution Functions in Liquids," *Bull. Chem. Soc. Jpn.* **74**, 1831 (2001).
- T. IMAI, Y. HARANO, A. KOVALENKO and F. HIRATA**, "Theoretical Study for Volume Changes Associated with the Helix-Coil Transition of Polypeptides," *Biopolymers* **59**, 512 (2001).
- T. SUMI, T. IMAI and F. HIRATA**, "Integral Equations for Molecular Fluids Based on Interaction Site Model: Density-Functional Formulation," *J. Chem. Phys.* **115**, 6653 (2001).
- T. YAMAZAKI, H. SATO and F. HIRATA**, "Solvent Effect on the Nuclear Magnetic Shielding: Ab Initio Study by the Combined Reference Interaction Site Model and Electronic Structure Theories," *J. Chem. Phys.* **115**, 8949 (2001).
- F. HIRATA and S-H. CHONG**, "Collective Density Fluctuations and Dynamics of Ions in Water Studied by the Interaction-Site Model of Liquids," *Cond. Matter Phys.* **4**, 261 (2001).
- T. YAMAGUCHI and F. HIRATA**, "Site-Site Mode-Coupling Theory for the Shear Viscosity of Molecular Liquids," *J. Chem. Phys.* **115**, 9340 (2001).
- A. KOVALENKO and F. HIRATA**, "First Principle Realization of a van der Waals-Maxwell Theory for Water," *Chem. Phys. Lett.* **349**, 496 (2001).
- A. KOVALENKO and F. HIRATA**, "Description of a Polar Molecular Liquid in a Disordered Microporous Material with Activating Chemical Groups by a Replica RISM Theory," *Cond. Matter Phys.* **4**, 643 (2001).
- M. KINOSHITA, T. IMAI, A. KOVALENKO and F. HIRATA**, "Improvement of the Reference Interaction Site Model Theory for Calculating the Partial Molar Volume of Amino Acids and Polypeptides," *Chem. Phys. Lett.* **348**, 337 (2001).
- T. YAMAGUCHI and F. HIRATA**, "Translational Diffusion and Reorientational Relaxation of Water Analyzed by Site-Site Generalized Langevin Theory," *J. Chem. Phys.* **116**, 2502 (2002).
- H. SATO and F. HIRATA**, "Equilibrium and Nonequilibrium Solvation Structure of Hexaamineruthenium (II,III)

in Aqueous Solution: Ab Initio RISM-SCF Study," *J. Phys. Chem. A* **106**, 2300 (2002).

K. YOSHIDA, KOVALENKO, T. YAMAGUCHI and F. HIRATA, "Structure of *tert*-Butyl Alcohol-Water Mixtures Studied by the RISM Theory," *J. Phys. Chem. B* **106**, 5042 (2002).

T. IMAI, H. NOMURA, M. KINOSHITA and F. HIRATA, "Partial Molar Volumes and Compressibilities of Alkali-Halide Ions in Aqueous Solution: Hydration Shell Analysis with an Integral Equation Theory of Molecular Liquids," *J. Phys. Chem.* **106**, 7308 (2002).

T. YAMAGUCHI and F. HIRATA, "Interaction-Site Model Description of the Reorientational Relaxation of Molecular Liquids: Incorporation of the Interaxial Coupling into the Site-Site Generalized Langevin/Mode-Coupling Theory," *J. Chem. Phys.* **117**, 2216 (2002).

M. KUWABARA and K. YONEMITSU, "Ground State Phases and Optical Properties in Extended Peierls-Hubbard Models for Halogen-Bridged Binuclear Metal Complexes," *J. Mater. Chem.* **11**, 2163 (2001).

X. SUN, R. L. FU, K. YONEMITSU and K. NASU, "Photoinduced Phenomenon in Polymers," *Phys. Rev. A* **64**, 032504 (2001).

K. YONEMITSU, "Intra- and Inter-Chain Excitations near a Quantum Phase Transition in Quasi-One-Dimensional Conductors," *Mol. Cryst. Liq. Cryst.* **376**, 53 (2002).

M. MORI and K. YONEMITSU, "Optical Conductivity for Possible Ground States of Dimerized Two-Band Pd(dmit)₂ Salts," *Mol. Cryst. Liq. Cryst.* **376**, 141 (2002).

M. KUWABARA and K. YONEMITSU, "Optical Excitations in XMMX Monomers and MMX Chains," *Mol. Cryst. Liq. Cryst.* **376**, 251 (2002).

J. KISHINE, P. A. LEE and X. G. WEN, "Signature of the Staggered Flux State around a Superconducting Vortex in Underdoped Cuprates," *Phys. Rev. B* **65**, 064526 (2002).

K. YONEMITSU, "Quantum and Thermal Charge-Transfer Fluctuations for Neutral-Ionic Phase Transitions in the One-Dimensional Extended Hubbard Model with Alternating Potentials," *Phys. Rev. B* **65**, 085105 (2002).

K. YONEMITSU, "Finite-Temperature Phase Diagram of Mixed-Stack Charge-Transfer Complexes," *J. Phys. Chem. Solids* **63**, 1495 (2002).

J. KISHINE, "Underlying SU(2) Gauge Structure and Hidden Staggered Flux State in the Lightly Doped Spin Liquid," *J. Phys. Chem. Solids* **63**, 1559 (2002).

J. KISHINE and K. YONEMITSU, "Dimensional Crossovers and Phase Transitions in Strongly Correlated Low-Dimensional Electron Systems: Renormalization-Group Study," *Int. J. Mod. Phys. B* **16**, 711 (2002).

K. YONEMITSU, "Lattice and Magnetic Instabilities near the Neutral-Ionic Phase Transition of the One-Dimensional Extended Hubbard Model with Alternating Potentials in the Thermodynamic Limit," *Phys. Rev. B* **65**, 205105 (2002).

K. YONEMITSU, M. KUWABARA and N. MIYASHITA, "Variation Mechanisms of Ground-State and Optical-Excitation Properties in Quasi-One-Dimensional Two-Band Electron Systems," *Mol. Cryst. Liq. Cryst.* **379**, 467 (2002).

K. YONEMITSU, "Collective Excitations and Confinement in the Excitation Spectra of the Spinless Fermion Model on a Ladder," *Phys. Rev. B* **66**, 035121 (2002).

Department of Molecular Structure

H. OKAMOTO and M. KINOSHITA, "Picosecond Infrared Spectrum of 4-(Pyrrol-1-yl)benzoxazole: Structure of the Excited Charge-Transfer States of Donor-Acceptor Systems," *J. Phys. Chem. A* **106**, 3485 (2002).

H. OKAMOTO, M. KINOSHITA, S. KOHTANI, R. NAKAGAKI and K. A. ZACHARIASSE, "Picosecond Infrared Spectra and Structure of Locally Excited and Charge Transfer Excited States of Isotope-Labeled 4-(Dimethylamino)benzoxazoles," *Bull. Chem. Soc. Jpn.* **75**, 957 (2002).

T. YAMAZAKI, N. MORITA, R. S. HAYANO, E. WIDMANN and J. EADES, "Antiprotonic Helium," *Phys. Rep.* **366**, 183 (2002).

K. TOZAWA, H. YAGI, K. HISAMATSU, K. OZAWA, M. YOSHIDA and H. AKUTSU, "Functions and ATP-Binding Responses of the Twelve Histidine Residues in the TF₁-ATPase β Subunit," *J. Biochem.* **130**, 527 (2001).

K. SUGASE, Y. OYAMA, K. KITANO, T. IWASHITA, T. FUJIWARA, H. AKUTSU and M. ISHIGURO, "Designing Analogs of Mini Atrial Natriuretic Peptide Based on Structural Analysis by NMR and Restrained Molecular Dynamics," *J. Med. Chem.* **45**, 881 (2002).

E. HARADA, Y. FUKUOKA, T. OHMURA, A. FUKUNISHI, G. KAWAI, T. FUJIWARA and H. AKUTSU, "Redox-Coupled Conformational Alternations in Cytochrome *c*₃ from *D. vulgaris* Miyazaki F on the Basis of its Reduced Solution Structure," *J. Mol. Biol.* **319**, 767 (2002).

A. BANDARA, S. S. KANO, K. ONDA, S. KATANO, J. KUBOTA, K. DOMEN, C. HIROSE and A. WADA, "SFG Spectroscopy of CO/Ni(111): UV Pumping and Transient Hot Band Transition of Adsorbed CO," *Bull. Chem. Soc. Jpn.* **75**, 1125 (2002).

K. ONDA, M. NAKAGAWA, T. ASAKAI, R. WATASE, A. WADA, K. ICHIMURA and C. HIROSE,

“Controlling Packing Structure of Hydrophobic Alkyl Tails of Monolayered Films of Ion-Paired Macrocyclic Amphiphiles as Studied by Sum-Frequency Generation Spectroscopy,” *J. Phys. Chem. B* **106**, 3855 (2002).

A. FURUBE, T. SHIOZAWA, A. ISHIKAWA, A. WADA, K. DOMEN and C. HIROSE, “Femtosecond Transient Absorption Spectroscopy on Photocatalysts, $K_4Nb_6O_{17}$ and $Ru(bpy)_3^{2+}$ Intercalated $K_4Nb_6O_{17}$ Thin Films,” *J. Phys. Chem. B* **106**, 3065 (2002).

K. KUSAFUKA, H. NOGUCHI, K. ONDA, C. HIROSE, K. DOMEN and A. WADA, “Time-Resolved Study of Formate/Ni(111) Surface by Picosecond SFG Spectroscopy,” *Surf. Sci.* **502/503**, 313 (2002).

K. ONDA, A. WADA, K. DOMEN and C. HIROSE, “Realtime Observation of Desorption Process of Isobutene in Zeolite Using Picosecond Infrared Lasers,” *Surf. Sci.* **502/503**, 319 (2002).

H. TAKABA, K. KUSAFUKA, M. N. GAMO, Y. SATO, T. ANDO, J. KUBOTA, A. WADA and C. HIROSE, “Vibrational Sum-Frequency Observation of Synthetic Diamonds,” *Diam. Rel. Mater.* **10**, 1643 (2001).

K. ONDA, K. TANABE, H. NOGUCHI, A. WADA, T. SHIDO, A. YAMAGUCHI and Y. IWASAWA, “Surface Hydroxyl Group and Adsorbed Water on γ - Al_2O_3 Studied by Picosecond Infrared Pump-Probe Experiment,” *J. Phys. Chem. B* **105**, 11456 (2001).

D. MATSUMURA, T. YOKOYAMA, K. AMEMIYA, S. KITAGAWA and T. OHTA, “X-Ray Magnetic Circular Dichroism Study on Spin Reorientation Transition of Magnetic Thin Films Induced by Surface Chemisorption,” *Phys. Rev. B* **66**, 024402 (2002).

S. OKUBO, T. KATO, M. INAKUMA and H. SHINOHARA, “Separation and Characterization of ESR-Active Lanthanum Endohedral Fullerenes,” *New Diamond and Frontier Carbon Technology* **11**, 285 (2001).

S. S. SEOMUN, J. K. VIJI, N. HAYASHI, T. KATO and A. FUKUDA, “Surface Molecular Alignment by In-Plane Anchoring in the Cell Showing the V-Shaped Switching,” *Appl. Phys. Lett.* **79**, 940 (2001).

T. IKOMA, Q. ZHANG, F. SAITO, K. AKIYAMA, S. TERO-KUBOTA and T. KATO, “Radicals in the Mechanochemical Dechlorination of Hazardous Organochlorine Using CaO Nanoparticles,” *Bull. Chem. Soc. Jpn.* **74**, 2303 (2001).

A. ITO, H. INO, K. TANAKA, K. KANEMOTO and T. KATO, “Facile Synthesis, Crystal Structures, and High-Spin Cationic States of All-para-Brominated Oligo(*N*-phenyl-*m*-aniline)s,” *J. Org. Chem.* **67**, 491 (2002).

T. KATO, S. OKUBO, M. INAKUMA and H. SHINOHARA, “Electronic State of Scandium Trimer Encapsulated in C_{82} Cage,” *Phys. Solid State* **44**, 410 (2002).

Department of Electronic Structure

K. HINO, Y. INOKUCHI, K. KOSUGI, H. SEKIYA, Y. HOSOKOSHI, K. INOUE and N. NISHI, “Photochemical Generation of High Spin Clusters in Solution: Cyclopentadienyl-Vanadium $_mO_n$,” *J. Phys. Chem. B* **106**, 1290 (2002).

H. MORI, H. KUGISAKI, Y. INOKUCHI, N. NISHI, E. MIYOSHI, K. SAKOTA, K. OHASHI and H. SEKIYA, “Structure and Intermolecular Hydrogen Bond of Jet-Cooled *p*-Aminophenol-(H_2O) $_1$ Studied by Electronic and IR-Dip Spectroscopy and Density Functional Theory Calculations,” *Chem. Phys.* **277**, 105 (2002).

T. NAKABAYASHI and N. NISHI, “States of Molecular Associates in Binary Mixtures of Acetic Acid with Protic and Aprotic Polar Solvents: A Raman Spectroscopic Study,” *J. Phys. Chem. A* **106**, 3491 (2002).

Y. INOKUCHI and N. NISHI, “Infrared Photodissociation Spectroscopy of Protonated Formic Acid-Water Binary Clusters, $H^+(HCOOH)_nH_2O$ ($n = 1-5$). Spectroscopic Study of Ion Core Switch Model and Magic Number,” *J. Phys. Chem. A* **106**, 4529 (2002).

T. NAKABAYASHI, S. KAMO, K. WATANABE, H. SAKURAGI and N. NISHI, “Observation of Formation Dynamics of Solvated Aromatic Cation Radicals Following Photoionization,” *Chem. Phys. Lett.* **355**, 241 (2002).

H. MORI, H. KUGISAKI, Y. INOKUCHI, N. NISHI, E. MIYOSHI, K. SAKOTA, K. OHASHI and H. SEKIYA, “LIF and IR Dip Spectra of Jet-Cooled *p*-Aminophenol- M ($M = CO, N_2$): Hydrogen-Bonded or van der Waals-Bonded Structure?” *J. Phys. Chem. A* **106**, 4886 (2002).

K. OHASHI, Y. INOKUCHI, N. NISHI and H. SEKIYA, “Intermolecular Interaction in Aniline-Benzene Hetero-Trimer and Aniline Homo-Trimer Ions,” *Chem. Phys. Lett.* **357**, 223 (2002).

Y. INOKUCHI, K. OHASHI, H. SEKIYA and N. NISHI, “Intracluster Proton Transfer in Aniline-Amine Complex Ions,” *Chem. Phys. Lett.* **359**, 288 (2002).

Y. HONKAWA, Y. INOKUCHI, K. OHASHI, N. NISHI and H. SEKIYA, “Infrared Photodissociation Spectroscopy of Aniline $^+$ -(water) $_{1,2}$ and Aniline $^+$ -(methanol) $_{1,2}$,” *Chem. Phys. Lett.* **358**, 419 (2002).

M. SAKAI, K. DAIGOKU, S. ISHIUCHI, M. SAEKI, K. HASHIMOTO and M. FUJII, “Structures of Carbazole-(H_2O) $_n$ ($n = 1-3$) Clusters Studied by IR Dip Spectroscopy and a Quantum Chemical Calculation,” *J. Phys. Chem. A* **105**, 8651 (2001).

H. YOKOYAMA, H. WATANABE, T. OMI, S. ISHIUCHI and M. FUJII, “Structure of Hydrogen-Bonded Clusters of 7-Azaindole Studied by IR Dip Spectroscopy and Ab Initio Molecular Orbital Calculation,” *J. Phys. Chem. A* **105**, 9366 (2001).

S. ISHIUCHI, M. SAKAI, K. DAIGOKU, T. UEDA, T. YAMANAKA, K. HASHIMOTO and M. FUJII,

“Picosecond Time-Resolved Infrared Spectra of Photo-Excited Phenol-(NH₃)₃ Cluster,” *Chem. Phys. Lett.* **347**, 87 (2001).

M. SAEKI, S. ISHIUCHI, M. SAKAI and M. FUJII, “Structure of 1-Naphthol/Alcohol Clusters Studied by IR Dip Spectroscopy and Ab Initio Molecular Orbital Calculations,” *J. Phys. Chem. A* **105**, 10045 (2001).

S. KINOSHITA, H. KOJIMA, T. SUZUKI, T. ICHIMURA, K. YOSHIDA, M. SAKAI and M. FUJII, “Pulsed Field Ionization Zero Kinetic Energy Photoelectron Study on Methylanisole Molecules in a Supersonic Jet,” *Phys. Chem. Chem. Phys.* **3**, 4889 (2001).

H. G. KJAERGAARD, D. L. HOWARD, D. P. SCHOFIELD, T. W. ROBINSON, S. ISHIUCHI and M. FUJII, “OH- and CH-Stretching Overtone Spectra of Catechol,” *J. Phys. Chem. A* **106**, 258 (2002).

K. YOSIDA, K. SUZUKI, S. ISHIUCHI, M. SAKAI, M. FUJII, C. E. H. DESSENT and K. MÜLLER-DETHLEFS, “The PFI-ZEKE Photoelectron Spectrum of m-Fluorophenol and its Aqueous Complexes: Comparing Intermolecular Vibrations in Rotational Isomers,” *Phys. Chem. Chem. Phys.* **4**, 2534 (2002).

H. KATAYANAGI and T. SUZUKI, “Non-Adiabatic Bending Dissociation of OCS: The Effect of Bending Excitation on the Transition Probability,” *Chem. Phys. Lett.* **360**, 104 (2002).

B. BOTAR, T. YAMASE and E. ISHIKAWA, “Synthesis and Structure of a Novel Vanadium-Containing Tungstobismustate(III) K₁₂[(VO)₃(BiW₉O₃₃)₂].30H₂O,” *Inorg. Chem. Commun.* **4**, 551 (2001).

H. NARUKE and T. YAMASE, “Crystallization and Structural Characterization of Two Europium Molybdates, Eu₄Mo₇O₂₇ and Eu₆Mo₁₀O₃₉,” *J. Solid State Chem.* **160**, 85 (2001).

H. MURAKAMI, T. KOZEKI, Y. SUZUKI, S. ONO, H. OHTAKE, N. SARUKURA, E. ISHIKAWA and T. YAMASE, “Nanocluster Crystals of Lacunary Polyoxometalates: Novel application as Structure Design-Flexible, Inorganic Nonlinear Materials,” *Appl. Phys. Lett.* **79**, 3564 (2001).

L. YANG, H. NARUKE and T. YAMASE, “A 3-D Inorganic/Organic Hybrid Vanadium Oxide with Pentacoordinate Co(II) Complex, [Co(4,4'-bipy)V₂O₆],” *Acta Crystallogr., Sect. C: Cryst. Struct. Commun.* **57**, 1378 (2001).

H. NARUKE and T. YAMASE, “Tb₂Mo₄O₁₅,” *Acta Crystallogr., Sect. E* **57**, i106 (2001).

F. GAO, T. YAMASE and H. SUZUKI, “H₂O₂-Based Epoxidation of Bridged-Cyclic Alkenes with [P{Ti(O₂)₂W₁₀O₃₈}⁷⁻ in Monophasic Systems: Active Site and Kinetics,” *J. Mol. Catal., A* **180**, 97 (2002).

T. YAMASE and P. PROKOP, “Photochemical Formation of Tire-Shaped Molybdenum Blues: Topology of a Defect Anion, [Mo₁₄₂O₄₃₂H₂₈(H₂O)₅₈]¹²⁻,” *Angew. Chem. Int. Ed. Engl.* **41**, 466 (2002).

H. NARUKE and T. YAMASE, “Size-Dependent Population of Trivalent Rare Earth (RE³⁺) in [RE₂(H₂O)₂(SbW₉O₃₃)(W₅O₁₈)₂]¹⁵⁻, and Structural Characterization of a Lanthanum-Polyoxotungstate Complex [Lu₃(H₂O)₄(SbW₉O₃₃)₂(W₅O₁₈)₂]²¹⁻,” *Bull. Chem. Soc. Jpn.* **75**, 1275 (2002).

H. NARUKE and T. YAMASE, “Gd₄Mo₇O₂₇, a Novel Phase in the Gd₂O₃-MoO₃ System,” *Acta Crystallogr., Sect. E* **58**, i62 (2002).

T. IIMORI and Y. OHSHIMA, “S₁-S₀ Vibronic Spectra of Benzene Clusters Revisited: I. The Tetramer,” *J. Chem. Phys.* **117**, 3656 (2002).

T. IIMORI, Y. AOKI and Y. OHSHIMA, “S₁-S₀ Vibronic Spectra of Benzene Clusters Revisited: II. The Trimer,” *J. Chem. Phys.* **117**, 3675 (2002).

Department of Molecular Assemblies

I. SHIROTANI, J. HAYASHI, K. YAKUSHI, K. TAKEDA, T. YOKOTA, K. SHIMIZU, K. AMAYA, A. NAKAYAMA and K. AOKI, “Pressure-Induced Insulator-to-Metal Transition and Superconductivity in Iodanil, C₆I₄O₂,” *Physica B* **304**, 6 (2001).

M. MAKSIMUK, K. YAKUSHI, H. TANIGUCHI, K. KANODA and A. KAWAMOTO, “The C=C Stretching Vibrations of κ-(BEDT-TTF)₂Cu[N(CN)₂]Br and its Deuterated Analogues,” *J. Phys. Soc. Jpn.* **70**, 3728 (2001).

K. YAMAMOTO, K. YAKUSHI, K. MIYAGAWA, K. KANODA and A. KAWAMOTO, “Charge Ordering in θ-(BEDT-TTF)₂RbZn(SCN)₄ Studied by Vibration Spectroscopy,” *Phys. Rev. B* **65**, 85110 (2002).

J. OUYANG, K. YAKUSHI, T. KINOSHITA, N. NANBU, M. AOYAGI, Y. MISAKI and K. TANAKA, “The Assignment of the In-Plane Molecular Vibrations of the BDT-TTP Electron-Donor Molecule Based on the Polarized Raman and Infrared Spectra, where BDT-TTP is 2,5-bis(1,3-dithiol-2-ylidene)-1,3,4,6-Tetrathiapentalene,” *Spectrochim. Acta, Part A* **58**, 1643 (2002).

T. NAKAMURA, K. TAKAHASHI, T. ISE, T. SHIRAHATA, M. URUICHI, K. YAKUSHI and T. MORI, “Magnetic Properties of Organic Spin-Ladder Systems, (BDTFP)₂X(PhCl)_{0.5},” *Mol. Cryst. Liq. Cryst.* **376**, 95 (2002).

O. DROZDOVA, H. YAMOCHI, K. YAKUSHI, M. URUICHI and G. SAITO, “Charge Transfer Degree of BO Complexes,” *Mol. Cryst. Liq. Cryst.* **376**, 135 (2002).

Y. YAMASHITA, M. TOMURA, M. URUICHI and K. YAKUSHI, “Synthesis and Properties of π-Extended TTF Analogues and their Cation Radical and Dication Salts,” *Mol. Cryst. Liq. Cryst.* **376**, 19 (2002).

K. YAKUSHI, J. OUYANG, M. SIMONYAN, Y. MISAKI and K. TANAKA, “Charge Order in θ-(BDT-

- TTP)₂Cu(NCS)₂,” *Mol. Cryst. Liq. Cryst.* **380**, 53 (2002).
- Y. DING, M. SIMONYAN, Y. YONEHARA, M. URUICHI and K. YAKUSHI**, “Formation of Mixed Crystal System Co_xNi_{1-x}Pc(AsF₆)_{0.5},” *Mol. Cryst. Liq. Cryst.* **380**, 283 (2002).
- K. YAMAMOTO, K. YAKUSHI, M. INOKUCHI, M. KINOSHITA and G. SAITO**, “Charge Disproportionation and its Ordering Pattern in θ and α Types of BEDT-TTF Salts Studied by Raman and Infrared Spectroscopy,” *Mol. Cryst. Liq. Cryst.* **380**, 221 (2002).
- G. SAITO, H. SASAKI, T. AOKI, Y. YOSHIDA, A. OTSUKA, H. YAMOCHI, O. O. DROZDOVA, K. YAKUSHI, H. KITAGAWA and T. MITANI**, “Complex Formation of Ethylenedioxyethylenedithio-tetrathiafulvalene (EDOEDT-TTF: EOET) and its Self-Assembling Ability,” *J. Mater. Chem.* **12**, 1640 (2002).
- T. YAMAMOTO, H. TAJIMA, R. KATO, M. URUICHI and K. YAKUSHI**, “Raman Spectra of (Me₂-DCNQI)₂Cu_xLi_{1-x} ($0 < x < 1$). The Evidence of Charge Separation at Room Temperature in a One-Dimensional Conductor Having a Quarter-Filled Band,” *J. Phys. Soc. Jpn.* **71**, 1956 (2002).
- T. NAKAMURA, K. TAKAHASHI, T. SHIRAHATA, M. URUICHI, K. YAKUSHI and T. MORI**, “Magnetic Investigation of Possible Quasi-One-Dimensional Two-Leg Ladder Systems, (BDTFP)₂X(PhCl)_{0.5} (X = PF₆, AsF₆),” *J. Phys. Soc. Jpn.* **71**, 2022 (2002).
- M. URUICHI, K. YAKUSHI, T. SHIRAHATA, K. TAKAHASHI, T. MORI and T. NAKAMURA**, “Structural Phase Transition in Quasi-1D Conductors, (BDTFP)₂X(PhCl)_{0.5} (X = PF₆, AsF₆) [BDTFP = 5,7-bis(1,3-dithiol-2-ylidene)-5,7-dihydrofuro[3,4-*b*]pyrazine],” *J. Mater. Chem.* **12**, 2696 (2002).
- T. NAKAMURA, T. TAKAHASHI, S. AONUMA and R. KATO**, “EPR Investigation of the Electronic States in β' -Type [Pd(dmit)₂]₂ Compounds (Where dmit is the 1,3-Dithia-2-Thione-4,5-Dithiolato),” *J. Mater. Chem.* **11**, 2159 (2001).
- T. NAKAMURA, K. TAKAHASHI, T. ISE, T. SHIRAHATA, M. URUICHI, K. YAKUSHI and T. MORI**, “Magnetic Properties of Organic Spin-Ladder Systems, (BDTFP)₂X(PhCl)_{0.5},” *Mol. Cryst. Liq. Cryst.* **376**, 95 (2002).
- S. FUJIYAMA and T. NAKAMURA**, “NMR Study of Charge Localized States of (TMTTF)₂Br,” *J. Phys. Chem. Solids* **63**, 1259 (2002).
- S. FUJIYAMA, M. TAKIGAWA, S. HORII, N. MOTOYAMA, H. EISAKI and S. UCHIDA**, “NMR Observation of Charge Fluctuations in Quasi-One-Dimensional Cuprates,” *J. Phys. Chem. Solids* **63**, 1119 (2002).
- T. NAKAMURA, K. TAKAHASHI, T. SHIRAHATA, M. URUICHI, K. YAKUSHI and T. MORI**, “Magnetic Investigation of Possible Quasi-One-Dimensional Two-Leg Ladder Systems, (BDTFP)₂X(PhCl)_{0.5} (X = PF₆, AsF₆),” *J. Phys. Soc. Jpn.* **71**, 2022 (2002).
- T. NAITO, T. INABE, H. KOBAYASHI and A. KOBAYASHI**, “A New Molecular Metal Based on Pd(dmit)₂: Synthesis, Structure and Electrical Properties of (C₇H₁₃NH)[Pd(dmit)₂]₂ (dmit²⁻ = 2-thioxo-1,3-dithiole-4,5-dithiolate),” *J. Mater. Chem.* **11**, 2199 (2001).
- V. GRITSENKO, H. TANAKA, H. KOBAYASHI and A. KOBAYASHI**, “A New Molecular Superconductor, κ -(BETS)₂TiCl₄ (BETS = bis(ethylenedithio)tetraselenafulvalene),” *J. Mater. Chem.* **11**, 2410 (2001).
- R. B. LYUBOVSKII, S. I. PESOTSKII, S. V. KONOVALIKHIN, G. V. SHILOV, A. KOBAYASHI, H. KOBAYASHI, V. I. NIZHANKOVSKII, J. A. A. J. PERENBOOM, O. A. BOGDANOVA, E. I. ZHILYAEVA and R. N. LYUBOVSKAYA**, “Crystal Structure, Electrical Transport, Electronic Band structure and Quantum Oscillations Studies of the Organic Conducting Salt, θ -(BETS)₄HgBr₄(C₆H₅Cl),” *Synth. Met.* **123**, 149 (2001).
- H. MORIYAMA, S. NAGAYAMA, T. MOCHIDA and H. KOBAYASHI**, “Nickel Complexes with Extended Tetrathiafulvalene Dithiolate Ligands,” *Synth. Met.* **120**, 973 (2001).
- C. PALASSIS, M. MOLA, J. TRITZ, S. HILL, S. UJI, K. KAWANO, M. TAMURA, T. NAITO and H. KOBAYASHI**, “Periodic Orbit Resonances in κ -ET₂I₃,” *Synth. Met.* **120**, 999 (2001).
- H. SHINAGAWA, S. UJI, T. TERASHIMA, H. TANAKA, H. KOBAYASHI, A. KOBAYASHI and M. TOKUMOTO**, “Phase Transition in Magnetic Field Parallel to the Conducting Plane for λ -(BETS)₂FeCl₄,” *Synth. Met.* **120**, 929 (2001).
- E. ZHILYAEVA, O. BOGDANOVA, R. LYUBOVSKAYA, S. PESOTSKII, J. PERENBOOM, S. KONOVALIKHIN, G. SHILOV, A. KOBAYASHI and H. KOBAYASHI**, “New BETS Based Molecular Conductors with Bromomercurate Anions,” *Synth. Met.* **120**, 1089 (2001).
- T. I. MAKAROVA, P. SCHARFF, B. SUNDQVIST, B. NARYMBETOV, H. KOBAYASHI, M. TOKUMOTO, V. A. DAVYDOV, A. V. RAKHMANINA and L. S. KASHEEVAROVA**, “Anisotropic Metallic Properties of Highly-Oriented Rhombohedral C₆₀ Polymer,” *Synth. Met.* **121**, 1099 (2001).
- B. NARYMBETOV, A. OMERZU, V. V. KABANOV, M. TOKUMOTO, H. KOBAYASHI and D. MIHAJLOVIC**, “C₆₀ Molecular Configurations Leading Ferromagnetic Exchange Interactions in TDAE-C₆₀,” *Trans. Mater. Res. Soc. Jpn.* **26**, 1143 (2001).
- D. Z. KURMAEV, A. MOEWES, U. SCHWINGENSCHLOGL, R. CLAESSEN, M. I. KATSNELSON, H. KOBAYASHI, S. KAGOSHIMA, Y. MISAKI, D. L. EDERER, K. ENDO and M. YANAGIHARA**, “Electronic Structure of Charge Transfer Salts,” *Phys. Rev. B* **64**, 233107-1 (2001).
- S. UJI, H. KOBAYASHI, L. BALICAS and J. S. BROOKS**, “Superconductivity in an Organic Conductor Stabilized by a High Magnetic Field,” *Adv. Mater.* **14**, 243 (2002).

- S. UJI, C. TERAKURA, T. TERASHIMA, T. YAKABE, Y. TERAJ, M. TOKUMOTO, A. KOBAYASHI, F. SAKAI, H. TANAKA and H. KOBAYASHI, "Fermi Surface and Internal Magnetic Field of Organic Conductors λ -(BETS)₂Fe_xGa_{1-x}Cl₄," *Phys. Rev. B* **65**, 113101 (2002).
- B. NARYMBETOV, A. OMERZU, V. KAVANOV, M. TOKUMOTO, H. KOBAYASHI and D. MIHAJLOVIC, "C₆₀ Molecular Configurations Leading to Ferromagnetic Exchange Interactions in TDAE·C₆₀," *Russian, J. Solid. State Phys.* **44**, 422 (2002).
- E. FUJIWARA, V. GRITSENKO, H. FUJIWARA, I. TAMURA, H. KOBAYASHI, M. TOKUMOTO and A. KOBAYASHI, "Magnetic Molecular Conductors Based on BETS Molecules and Divalent Magnetic Anions [BETS = Bis(ethylenedithio)tetraselenafulvalene]," *Inorg. Chem.* **41**, 3230 (2002).
- H. FUJIWARA, H. KOBAYASHI, E. FUJIWARA and A. KOBAYASHI, "An indication of Magnetic-Field-Induced Superconductivity in a Bi-Functional Layered Organic Conductor, κ -(BETS)₂FeBr₄," *J. Am. Chem. Soc.* **124**, 6816 (2002).
- B. ZHANG, H. TANAKA, H. FUJIWARA, H. KOBAYASHI, E. FUJIWARA and A. KOBAYASHI, "Dual-Action Molecular Superconductors with Magnetic Anions," *J. Am. Chem. Soc.* **124**, 9982 (2002).
- H. TANAKA, H. KOBAYASHI and A. KOBAYASHI, "A Conducting Crystal Based on A Single-Component Paramagnetic Molecule, [Cu(dmdt)₂] (dmdt = dimethyltetrathiafulvalenedithiolate)," *J. Am. Chem. Soc.* **124**, 10002 (2002).
- V. GRITSENKO, E. FUJIWARA, H. FUJIWARA and H. KOBAYASHI, "Stable Molecular Metals Based on Bis(ethylenedithio)tetraselenafulvalene and Halogen Ions: κ -(BETS)₂X·C₂H₄(OH)₂ (X = Br, Cl)," *Synth. Met.* **128**, 273 (2002).
- H. KOBAYASHI, E. FUJIWARA, H. FUJIWARA, H. TANAKA, H. AKUTSU, I. TAMURA, T. OTSUKA, A. KOBAYASHI, M. TOKUMOTO and P. CASSOUX, "Development and Physical Properties of Magnetic Organic Superconductors Based on BETS Molecules [BETS = bis(ethylenedithio)tetraselenafulvalene]," *J. Phys. Chem. Solids* **63**, 1235 (2002).
- I. TAMURA, H. KOBAYASHI and A. KOBAYASHI, "X-Ray Diffraction Study of α -(BEDT-TTF)₂I₃ Single Crystal under High Pressure," *J. Phys. Chem. Solids* **63**, 1255 (2002).
- S. I. PESOTSKII, R. B. LYUBOVSKII, W. BIEBERRACHER, M. V. KARTSOVNIK, V. I. NIZHANKOPVSKII, N. D. KUSHCH, H. KOBAYASHI and A. KOBAYASHI, "On the Possibility of a Radical Decrease in the Strength of Many-Body Interactions in the Organic Metal α -(BETS)₂KHg(SCN)₄," *J. Exp. Theor. Phys.* **94**, 431 (2002).
- H. KOBAYASHI, E. FUJIWARA, H. FUJIWARA, H. TANAKA, I. TAMURA, B. ZHANG, V. GRITSENKO, T. OTSUKA, A. KOBAYASHI, M. TOKUMOTO and P. CASSOUX, "Magnetic Organic Superconductor—Interplay of Conductivity and Magnetism," *Mol. Cryst. Liq. Cryst.* **379**, 9 (2002).
- A. KOBAYASHI, W. SUZUKI, E. FUJIWARA, T. OTSUKA, H. TANAKA, Y. OKANO and H. KOBAYASHI, "Molecular Design and Development of Single-Component Molecular Metals with Extended TTF Ligands," *Mol. Cryst. Liq. Cryst.* **379**, 19 (2002).
- H. KOBAYASHI, E. FUJIWARA, H. FUJIWARA, H. TANAKA, T. OTSUKA, A. KOBAYASHI, M. TOKUMOTO and P. CASSOUX, "Antiferromagnetic Organic Superconductors, BETS₂FeX₄ (X = Br, Cl)," *Mol. Cryst. Liq. Cryst.* **380**, 139 (2002).
- E. OJIMA, H. FUJIWARA, H. TOKUMOTO and A. KOBAYASHI, "New Organic Conductors Based on Tellurium-Containing Dobor Molecules," *Mol. Cryst. Liq. Cryst.* **380**, 175 (2002).
- H. FUJIWARA, E. FUJIWARA and H. KOBAYASHI, "Synthesis, Structures and Physical Properties of the Cation Radical Salts Based on Tempo Radical Containong Electron Donors," *Mol. Cryst. Liq. Cryst.* **380**, 269 (2002).
- W. SUZUKI, E. FUJIWARA, A. KOBAYASHI, A. HASAGAWA, T. MIYAMOTO and H. KOBAYASHI, "Syntheses, Structure and Physical Properties of Palladium Complexes with an Extended-TTF Dithiolate Ligand, Bis(di-n-propylthiotetrathiafulvalenedithiolato)palladate," *Chem. Lett.* 936 (2002).
- S. UJI, C. TERAKURA, T. TERASHIMA, Y. OKANO and R. KATO, "Anisotropic Superconductivity and Dimensional Crossover in (TMET-STF)₂BF₄," *Phys. Rev. B* **64**, 214517 (2001).
- E. WATANABE, M. FUJIWARA, J. -I. YAMAURA and R. KATO, "Synthesis and Properties of Novel Donor-Type Metal-Dithiolene Complexes Based on 5,6-dihydro-1,4-dioxine-2,3-dithiol (edo) Ligand," *J. Mater. Chem.* **11**, 2131 (2001).
- T. NAKAMURA, T. TAKAHASHI, S. AONUMA and R. KATO, "EPR Investigation of the Electronic States in β' -Type [Pd(dmit)₂] Compounds (where dmit is 2-thioxo-1,3-dithiole-4,5-dithiolate)," *J. Mater. Chem.* **11**, 2159 (2001).
- K. OSHIMA, T. SASAKI, M. MOTOKAWA and R. KATO, "Quantized Hall Effect-Like Behavior in (DMET-TSeF)₂AuI₂," *Synth. Met.* **120**, 943 (2001).
- M. TAMURA, K. YAMANAKA, Y. MORI, Y. NISHIO, K. KAJITA, H. MORI, S. TANAKA, J. -I. YAMAURA, T. IMAKUBO, R. KATO, Y. MISAKI and K. TANAKA, " π -f Composite Metals," *Synth. Met.* **120**, 1041 (2001).
- M. TAMURA, T. IMAKUBO, K. YAMANAKA, Y. MORI, Y. NISHIO, K. KAJITA, Y. MISAKI, K. TANAKA, H. MORI, S. TANAKA, J. -I. YAMAURA and R. KATO, "Preparation, Structure and Electronic Properties of Some Organic Donor Salts of Rare-Earth Complex Anions: Novel 4f- π Composite Conductors," *Mol.*

Cryst. Liq. Cryst. **379**, 35 (2002).

S. OHIRA, M. TAMURA and R. KATO, "Superconductivity of [Pd(dmit)₂] Salts under Pressure Studied by an RF Technique," *Mol. Cryst. Liq. Cryst.* **379**, 41 (2002).

J. -I. YAMAURA and R. KATO, "High Pressure X-Ray Crystal Structure Analysis of Pd(dmit)₂ Salts," *Mol. Cryst. Liq. Cryst.* **379**, 47 (2002).

T. NAKAMURA, T. TAKAHASHI, S. AONUMA and R. KATO, "g-Tensor Analyses of β'-Type Pd(dmit)₂ Metal Complexes," *Mol. Cryst. Liq. Cryst.* **379**, 53 (2002).

T. IMAKUBO, N. TAJIMA, M. TAMURA, R. KATO, Y. NISHIO and K. KAJITA, "A Supramolecular Superconductor θ-(DIETS)₂[Au(CN)₄]," *J. Mater. Chem.* **12**, 159 (2002).

T. KAWAMOTO, M. ASHIZAWA, T. MORI, J. -I. YAMAURA, R. KATO, Y. MISAKI and K. TANAKA, "Dimerization Effect on the Physical Properties in New One-Dimensional Organic Conductors: (ChTM-TTP)₂AuBr₂, (ChTM-TTP)₂GaCl₄, and (ChTM-TTP)ReO₄," *Bull. Chem. Soc. Jpn.* **75**, 435 (2002).

Y. SHIMOJO, M. A. TANATAR, T. ISHIGURO and R. KATO, "Superconductivity and Magnetoresistance Oscillations in Weakly Pressurized Quasi One-Dimensional Superconductor (DMET-TSeF)₂AuI₂," *J. Phys. Soc. Jpn.* **71**, 393 (2002).

Y. OSHIMA, H. OHTA, K. KOYAMA, M. MOTOKAWA, H. M. YAMAMOTO and R. KATO, "Observation of High-Order Harmonic Resonances in Magneto-optical Measurement of (BEDT-TTF)₂Br(DIA)," *J. Phys. Soc. Jpn.* **71**, 1031 (2002).

Department of Applied Molecular Science

K. INOUE, H. IMAI, P. S. GHALSASI, K. KIKUCHI, M. OHBA, H. OKAWA and J. V. YAKHMI, "A Three-Dimensional Ferrimagnet with High Magnetic Transition Temperature (T_C) of 53 K Based on a Chiral Molecule," *Angew. Chem. Int. Ed. Engl.* **40**, 4242 (2001).

N. V. BARANOV, T. GOTO, Y. HOSOKOSHI, K. INOUE, F. IWAHORI and N. V. MUSHNIKOV, "Magnetic Viscosity at the Metamagnetic Phase Transition in Organic Mn^{II}(hfac)₂ Compound with the One-Dimensional Chain Structure," *Mater. Sci. Forum* **373-376**, 441 (2001).

K. INOUE, A. S. MARKOSYAN, H. KUMAGAI and P. S. GHALSASI, "Synthesis and Magnetic Properties of Chiral Molecule Based Magnets," *Mater. Sci. Forum* **373-376**, 449 (2001).

I. S. DUBENCO, I. YU. GAIDUKOVA, K. INOUE, ASHOT S. MARKOSYAN and V. E. RODIMIN, "Instability of Co Magnetism and Magnetoelastic Properties of the (Ho, Y)Co₃ Compounds," *Mater. Sci. Forum* **373-376**, 633 (2001).

K. SUZUKI, Y. HOSOKOSHI and K. INOUE, "Pressure-induced Metamagnetic Behavior in a Quasi-One-Dimensional Molecule-Based Ferrimagnet," *Chem. Lett.* 316 (2002).

K. SUZUKI, Y. HOSOKOSHI and K. INOUE, "Pressure Effects on Molecular Magnets of Mn Complexes with Bisaminoxylbenzene Derivatives," *Mol. Cryst. Liq. Cryst.* **379**, 247 (2001).

N. AZUMA, N. SENBA, K. OKUDA, K. OHARA, Y. HOSOKOSHI, K. INOUE and K. MUKAI, "Synthesis and Magnetic Property of the Salts of Positively Charged Verdazyl Radicals and TCNQF₄⁻ Anion Radical," *Mol. Cryst. Liq. Cryst.* **376**, 341 (2001).

M. INOKUCHI, K. SUZUKI, M. KINOSHITA, Y. HOSOKOSHI and K. INOUE, "Magnetic Properties of Cs and N(CH₃)₄ Salts of TCNQ," *Mol. Cryst. Liq. Cryst.* **376**, 507 (2001).

K. MUKAI, M. YANAGIMOTO, Y. SHIMOBÉ, K. KINDO and T. HAMAMOTO, "High-Field Magnetization and Magnetic Susceptibility Studies of the Doping Effect of Nonmagnetic Impurities on the Organic Spin-Peierls System: p-CyDOV Radical Crystal," *J. Phys. Chem. B* **106**, 3687 (2002).

H. KUMAGAI, K. INOUE and M. KURMOO, "Self-Organized Metallo-Helicates and -Ladder with 2,2'-Biphenyldicarboxylate (C₁₄H₈O₄)₂⁻: Synthesis, Crstal Structures, and Magnetic Properties," *Bull. Chem. Soc. Jpn.* **75**, 1283 (2002).

K. KATOH, Y. HOSOKOSHI, K. INOUE, M. I. BARTASHEVICH, H. NAKANO and T. GOTO, "Magnetic Properties of Organic Two-Leg Spin-Ladder Systems with $S = 1/2$ and $S = 1$," *J. Phys. Chem. Solids* **63**, 1277 (2002).

H. KUMAGAI, N. KYRITSAKAS, Y. OKA, K. INOUE and M. KURMOO, "Hydrothermal Synthesis and Structural and Magnetic Characterization of the Coordination Bonding Network Co^{II}(H₂O)₂Carboxy-Cinnamate," *Mol. Cryst. Liq. Cryst.* **379**, 217 (2002).

Y. OKA, H. KUMAGAI, K. INOUE and M. KURMOO, "Hydrothermal Synthesis and Characterization of a Two-Dimensional Cobalt (II) Complex Containing Cinnamate Anion," *Mol. Cryst. Liq. Cryst.* **379**, 265 (2002).

S. HAYAMI, Y. HOSOKOSHI, K. INOUE, Y. EINAGA, O. SATO and Y. MAEDA, "Pressure-Stabilized Low-Spin State for Binuclear Iron(III) Spin-Crossover Compounds," *Bull. Chem. Soc. Jpn.* **74**, 2361 (2001).

M. TANAKA, Y. HOSOKOSHI, A. S. MARKOSYAN, K. INOUE and H. IWAMURA, "Metal (3d)-Organic (2p)-Hybrid Magnets Made of Mn(II) Ions with Tris(aminoxyl) Radicals (R) as Bridging Ligands. 2D Complexes [Mn(hfac)₂]₃•R₂," *Synth. Met.* **122**, 463 (2001).

H. KUMAGAI, Y. OKA, M. AKITA-TANAKA and K. INOUE, "Hydrothermal Synthesis and Characterization of a Two-Dimensional Nickel(II) Complex Containing Benzenehexacarboxylic Acid(mellitic acid)," *Inorg. Chim. Acta* **332**, 176 (2002).

K. HINO, Y. INOKUCHI, K. KOSUGI, H. SEKIYA, Y. HOSOKOSHI, K. INOUE and N. NISHI,

“Photochemical Generation of High Spin Clusters in Solution: (Cyclopentadienyl-Vanadium)_mO_n,” *J. Phys. Chem. B* **106**, 1290 (2002).

S. AONUMA, H. CASELLAS, B. GARREAU De BONNEVAL, I. MALFANT, C. FAULMAN, P. CASSOUX, Y. HOSOKOSHI and K. INOUE, “Structure and Property of M(dmit)₂ Salt with Trimethylammonio-TEMPO and Related Magnetic Organic Cations,” *Mol. Cryst. Liq. Cryst.* **130**, 263 (2002).

K. JITSUKAWA, T. IRISA, H. EINAGA and H. MASUDA, “A Substrate-Specific α -Hydroxylation of Dipeptides Mediated upon a Co(III)-Terpyridine Complex: A Functional Model for Peptidylglycine α -Hydroxylating Monooxygenase,” *Chem. Lett.* **30** (2001).

H. KUMITA, T. MORIOKA, T. OZAWA, K. JITSUKAWA, H. EINAGA and H. MASUDA, “Site-Selective Recognition of Amino Acids by The Co(III) Complexes Containing (N)(O)₃-Type Tripodal Tetradentate Ligand,” *Bull. Chem. Soc. Jpn.* **74**, 1035 (2001).

K. MATSUMOTO, T. OZAWA, K. JITSUKAWA, H. EINAGA and H. MASUDA, “Crystal Structure and Redox Behavior of a Novel Siderophore Model System: A Trihydroxamate-Iron(III) Complex with Intra- and Interstrand Hydrogen Bonding Networks,” *Inorg. Chem.* **40**, 190 (2001).

H. KUMITA, K. JITSUKAWA, H. EINAGA and H. MASUDA, “Characterization of an NH- π Interaction in Co(III) Ternary Complexes with Aromatic Amino Acids,” *Inorg. Chem.* **40**, 3936 (2001).

K. JITSUKAWA, Y. OKA, H. EINAGA and H. MASUDA, “Reverse Reactivity in Hydroxylation of Adamantane and Epoxidation of Cyclohexene Catalyzed by the Mononuclear Ruthenium-oxo Complexes with 6-Substituted Tripodal Polypyridine Ligands,” *Tetrahedron Lett.* **42**, 3467 (2001).

K. MATSUMOTO, T. OZAWA, K. JITSUKAWA, H. EINAGA and H. MASUDA, “A Structural Model of the Ferrichrome Type Siderophore: Chiral Preference Induced by Intramolecular Hydrogen Bonding Networks in Ferric Trihydroxamate,” *Chem. Commun.* 978 (2001).

K. MATSUMOTO, N. SUZUKI, T. OZAWA, K. JITSUKAWA and H. MASUDA, “Crystal Structure and Solution Behavior of the Iron(III) Complex of the Artificial Trihydroxamate Siderophore with Tris(3-aminopropyl)-Amine Backbone,” *Eur. J. Inorg. Chem.* **10**, 2481 (2001).

K. JITSUKAWA, M. HARATA, H. ARII, H. SAKURAI and H. MASUDA, “SOD Activities of the Copper Complexes with Tripodal Polypyridylamine Ligands Having a Hydrogen Bonding Site,” *Inorg. Chim. Acta* **324**, 108 (2001).

S. OGO, R. YAMAHARA, T. FUNABIKI, H. MASUDA and Y. WATANABE, “Biomimetic Intradiol-Cleavage of Catechols with Incorporation of Both Atoms of O₂: The Role of the Vacant Coordination Site on the Iron Center,” *Chem. Lett.* 1062 (2001).

M. ISHIDA, M. Takai, H. Okabayashi, H. Masuda, M. Furusaka, and C. J. O’Connor, “Supramolecular Aggregates formed by L-Glutamic Acid-Oligomers: SANS and SAXS Studies of the Hydrogen Bonded Self-Assembly,” *Phys. Chem. Chem. Phys.* **3**, 3140 (2001).

M. ISHIDA, M. TAKAI, H. OKABAYASHI, H. MASUDA, M. FURUSAKA and C. J. O’CONNOR, “Micellar Structure of an Oligopeptide Surfactant “Trimeric *N*-Dodecanoyl-L-Proline Potassium Salt” in Aqueous Solution—Small-Angle Neutron Scattering Study,” *Colloid Polym. Sci.* **279**, 1034 (2001).

A. YOSHINO, M. ISHIDA, H. YUKI, H. OKABAYASHI, H. MASUDA and C. J. O’CONNOR, “Structure of Liquid-Crystalline Phases Formed by *N*-Acetyl-L-Glutamic Acid Oligomeric Benzyl Esters—²H NMR Study,” *Colloid Polym. Sci.* **279**, 1144 (2001).

M. ISHIDA, M. TAKAI, H. OKABAYASHI, H. MASUDA, E. NISHIO and C. J. O’CONNOR, “FTIR Evidence for Antiparallel β -Sheet Structures of Long Oligomeric *N*-Acetyl-L-Glutamic Acid Benzyl Esters,” *Vibrational Spectroscopy* **27**, 135 (2001).

M. ISHIDA, M. TAKAI, H. OKABAYASHI, H. MASUDA, E. NISHIO and C. J. O’CONNOR, “Long Acyl Chain Induces Conformational Changes in Oligomeric *N*-Acyl-L-Proline Anions: a FTIR Study,” *Vibrational Spectroscopy* **27**, 109 (2001).

K. IZAWA, T. OGASAWARA, H. MASUDA, H. OKABAYASHI and I. NODA, “Application of Generalized Two-Dimension Correlation Theory to Gel Permeation Chromatographic Analysis,” *Phys. Chem. Commun.* **12**, 1 (2001).

K. IZAWA, T. OGASAWARA, H. MASUDA, H. OKABAYASHI and I. NODA, “Two-Dimensional Correlation Gel Permeation Chromatography Study of Octyltriethoxysilane Sol-Gel Polymerization Process,” *Macromolecules* **35**, 92 (2002).

H. OKABAYASHI, K. IZAWA, T. YAMAMOTO, H. MASUDA, E. NISHIO and C. J. O’CONNOR, “Surface Structure of Silica Gel Reacted with 3-Mercaptopropyltriethoxysilane and 3-Aminotriethoxysilane: Formation of the S-S Bridge Structure and its Characterization by Raman Scattering and Diffuse Reflectance Fourier Transform Spectroscopic Studies,” *Colloid Polym. Sci.* **280**, 135 (2002).

M. TAKANI, T. YAJIMA, H. MASUDA and O. YAMAUCHI, “Spectroscopic and Structural Characterization of Copper(II) and Palladium(II) Complexes of a Lichen Substance Usnic Acid and its Derivatives. Possible Forms of Environmental Metals Retained in Lichens,” *J. Inorg. Biochem.* **91**, 139 (2002).

K. JITSUKAWA, H. SHIOZAKI and H. MASUDA, “Epoxidation Activities of Mononuclear Ruthenium-oxo Complexes with a Square Planar 6,6’-bis(benzoylamino)-2,2’-bipyridine and Axial Ligands,” *Tetrahedron Lett.* **43**, 1491 (2002).

A. WADA, S. OGO, S. NAGATOMO, T. KITAGAWA, Y. WATANABE, K. JITSUKAWA and H.

MASUDA, "Reactivity for a Hydroperoxide Bound to Mononuclear Non-Heme Iron Site," *Inorg. Chem.* **41**, 616 (2002).

K. IZAWA, T. OGASAWARA, H. MASUDA, H. OKABAYASHI, C. J. O'CONNOR and I. NODA, "Two-Dimensional Correlation Gel Permeation Chromatography (2D GPC) Study of 1H,1H,2H,2H-Perfluorooctyltriethoxysilane Sol-Gel Polymerization Process," *J. Phys. Chem. B* **106**, 2867 (2002).

K. IZAWA, T. OGASAWARA, H. MASUDA, H. OKABAYASHI, C. J. O'CONNOR and I. NODA, "Growth Process of Polymer Aggregates Formed by Perfluorooctyltriethoxysilane. -Resolved Near-IR and Two-Dimensional Near-IR Correlation Studies," *Colloid Polym. Sci.* **280**, 380 (2002).

R. YAMAHARA, S. OGO, H. MASUDA and Y. WATANABE, "(Catecholato)iron(III) Complexes: Structural and Functional Models for the Catechol-Bound Iron(III) Form of Catechol Dioxygenases," *J. Inorg. Biochem.* **88**, 284 (2002).

K. IZAWA, T. OGASAWARA, H. MASUDA, H. OKABAYASHI, C. J. O'CONNOR and I. NODA, "2D Gel Permeation Chromatography (2D GPC) Correlation Studies of the Growth Process for Perfluorooctyltriethoxysilane Polymer Aggregates," *Phys. Chem. Chem. Phys.* **4**, 1053 (2002).

K. IZAWA, T. OGASAWARA, H. MASUDA, H. OKABAYASHI, C. J. O'CONNOR and I. NODA, "TWO-Dimensional Correlation Gel Permeation Chromatography (2D correlation GPC) Study of the Sol-Gel Polymerization of Octyltriethoxysilane. HCl-Concentration Dependence," *Phys. Chem. Commun. [online computer file]* No. 2 (2002).

H. OKABAYASHI, M. ISHIDA, H. YUKI, N. HATTORI, H. MASUDA and C. J. O'CONNOR, "Phase Structures of the *N*-Acetyl-L-Glutamic Acid Oligomeric Benzyl Esters (Exact Residue Numbers 4, 6, 8, and 12)-Dioxane Systems and their Optical Properties," *Colloid Polym. Sci.* **280**, 599 (2002).

K. IWATA and H. TAKAHASHI, "Photoinduced Cl Transfer Reaction between Biphenyl and Carbon Tetrachloride Studied by Nanosecond Time-Resolved Infrared Spectroscopy and Picosecond Time-Resolved Fluorescence Spectroscopy," *J. Mol. Struct.* **598**, 97 (2001).

K. IWATA, S. TAKEUCHI and T. TAHARA, "Photochemical Bimolecular Reaction between Biphenyl and Carbon Tetrachloride: Observed Ultrafast Kinetics and Diffusion-Controlled Reaction Model," *Chem. Phys. Lett.* **347**, 331 (2001).

H. ISHIKAWA, K. IWATA and H. HAMAGUCHI, "Picosecond Dynamics of Stepwise Double Proton Transfer Reaction in the Excited State of the 2-Aminopyridine/Acetic Acid System," *J. Phys. Chem. A* **106**, 2305 (2002).

K. IWATA, R. OZAWA and H. HAMAGUCHI, "Analysis of the Solvent- and Temperature-Dependent Raman Spectral Changes of *S*₁ *Trans*-Stilbene and the Mechanism of the *Trans* to *Cis* Isomerization: Dynamic Polarization Model of Vibrational Dephasing and the C=C Double-Bond Rotation," *J. Phys. Chem. A* **106**, 3614 (2002).

K. IWATA, "Effects of Pump and Probe Light Field on Picosecond Time-Resolved Resonance Raman Spectra of *S*₁ *Trans*-Stilbene. Disagreement between Stokes- and Anti-Stokes Scattering Frequencies," *Bull. Chem. Soc. Jpn.* **75**, 1075 (2002).

J. YAMADA, T. TOITA, H. AKUTSU, S. NAKATSUJI, H. NISHIKAWA, I. IKEMOTO and K. KIKUCHI, "The Crystal Structure and Physical Properties of β-(BDA-TTP)₂FeCl₄ [BDA-TTP = 2,5-bis(1,3-dithian-2-ylidene)-1,3,4,6-tetrathiapentalene]," *Chem. Commun.* 2538 (2001).

T. KODAMA, M. KUSUDA, N. OZAWA, R. FUJII, K. SAKAGUCHI, H. NISHIKAWA, I. IKEMOTO, K. KIKUCHI, Y. MIYAKE and Y. ACHIBA, "Spectroscopic Studies of Endohedral Metallofullerenes," *New diamond and Frontier Carbon Technology* **11**, 367 (2001).

K. INOUE, H. IMAI, P. S. GHALSASI, K. KIKUCHI, M. OHBA, H. KAWA, and J. V. YAKHMI, "A Three-Dimensional Ferrimagnet with a High Magnetic Transition Temperature (*T*_C) of 53 K Based on a Chiral Molecule," *Angew. Chem., Int. Ed. Engl.* **40**, 4242 (2001).

T. ISHII, R. KANEHAMA, N. AIZAWA, M. YAMASHITA, H. MATSUZAKA, K. SUGIURA, H. MIYASAKA, T. KODAMA, K. KIKUCHI, I. IKEMOTO, H. TANAKA, K. MARUMOTO and S. KURODA, "Fullerene C₆₀ Exhibiting a Strong Intermolecular Interaction in a Cocrystallite with C₄ Symmetrical Cobalt Tetrakis(di-*tert*-butylphenyl)porphyrin," *J. Chem. Soc., Dalton Trans.* 2975 (2001).

H. NISHIKAWA, T. MORIMOTO, T. KODAMA, I. IKEMOTO, K. KIKUCHI, J. YAMADA, H. YOSHINO and K. MURATA, "New Organic Superconductors Consisting of an Unprecedented π-Electron Donor," *J. Am. Chem. Soc.* **124**, 730 (2002).

T. KODAMA, N. OZAWA, Y. MIYAKE, K. SAKAGUCHI, H. NISHIKAWA, I. IKEMOTO, K. KIKUCHI and Y. ACHIBA, "Structural Study of Three Isomers of Tm@C₈₂ by ¹³C NMR Spectroscopy," *J. Am. Chem. Soc.* **124**, 1452 (2002).

J. YAMADA, M. WATANABE, T. TOITA, H. AKUTSU, S. NAKATSUJI, H. NISHIKAWA, I. IKEMOTO and K. KIKUCHI, "2-(1,3-Dithiolan-2-ylidene)-5-(1,3-dithian-2-ylidene)-1,3,4,6-Tetrathiapentalene (DHDA-TTP), a Hybrid of BDH-TTP and BDA-TTP, and Its Metallic Cation-Radical Salts," *Chem. Commun.* 1118 (2002).

S. OKADA, H. OHOYAMA and T. KASAI, "Stereo-Selectivity in the Penning Ionization Reaction of CH₃X (X = Cl, Br, I) + Ar(³P) → CH₃X⁺ + Ar + e⁻," *Chem. Phys. Lett.* **355**, 77 (2002).

A. OKANO, H. OHOYAMA and T. KASAI, "Focusing and Selecting the Linear Type HBr-N₂O by Using a 2 m Long Electrostatic Hexapole Field," *J. Chem. Phys.* **116**, 1325 (2002).

M. HASHINOKUCHI, R. KOUMURA, D. -C. CHE and T. KASAI, "A New Channel of Hydrogen Elimination in the 121.6-nm Photodissociation of Formic Acid Detected by a Doppler-Selected TOF Mass Spectrometry," *J. Mass Spectrom. Soc. Jpn.* **50**, 7 (2002).

D. -C. CHE, M. HASHINOKUCHI, Y. SHIMIZU, H. OHOYAMA and T. KASAI, "Photodissociation of DCl Dimer Selected by an Electrostatic Hexapole Field Combined with a Doppler-Selected Time-of-Flight Technique: Observation of [CIDCl] Transient Species," *Phys. Chem. Chem. Phys.* **3**, 4979 (2001).

K. MORITANI, M. OKADA, M. NAKAMURA, T. KASAI and Y. MURATA, "Hydrogen-Exchange Reactions via Hot Hydrogen Atoms Produced in the Dissociation Process of Molecular Hydrogen on Ir{100}," *J. Chem. Phys.* **115**, 9947 (2001).

K. IMURA, H. OHOYAMA and T. KASAI, "Evidence for the HCl⁺(A) Formation in the Reaction of Ne(³P) with the Size-Selected HCl Dimer Using an Electrostatic Hexapole field," *Chem. Lett.* 1136 (2001).

M. NOSAKA, M. TAKASU and K. KATOH, "Characterization of Gels by Monte Carlo Method Using a Model of Radical Polymerization with Cross Linkers," *J. Chem. Phys.* **115**, 11333 (2001).

H. NOGUCHI and M. TAKASU, "Self-Assembly of Amphiphiles into Vesicles: a Brownian Dynamics Simulation," *Phys. Rev. E* **64**, 041913 (2001).

H. NOGUCHI and M. TAKASU, "Fusion Pathways of Vesicles, a Brownian Dynamics Simulation," *J. Chem. Phys.* **115**, 9547 (2001).

H. NOGUCHI and M. TAKASU, "Adhesion of Nanoparticles to Vesicles: a Brownian Dynamics Simulation," *Biophys. J.* **83**, 299 (2002).

H. NOGUCHI and M. TAKASU, "Structural Changes of Pulled Vesicles: a Brownian Dynamics Simulation," *Phys. Rev. E* **65**, 051907 (2002).

Department of Vacuum UV Photoscience

T. KINOSHITA, H. GUNASEKARA, Y. TAKATA, S. KIMURA, M. OKUNO, Y. HARUYAMA, N. KOSUGI, K. G. NATH, H. WADA, A. MITSUDA, M. SHIGA, T. OKUDA, A. HARASAWA, H. OGASAWARA and A. KOTANI, "Spectroscopy Studies of Temperature-Induced Valence Transition on Eu₂(Si_{1-x}Ge_x)₂ around Eu 3d-4f, 4d-4f and Ni 2p-3d Excitation Regions," *J. Phys. Soc. Jpn.* **71**, 148 (2002).

E. RÜHL, R. FLESCHE, W. TAPPE, D. NOVIKOV and N. KOSUGI, "Sulfur 1s Excitation of S-2 and S-8: Core-Valence- and Valence- Valence-Exchange Interaction and Geometry-Specific Transitions," *J. Chem. Phys.* **116**, 3316 (2002).

M. MIZUNO, H. HAMAGUCHI and T. TAHARA, "Observation of Resonance Hyper-Raman Scattering from *all-trans*-Retinal," *J. Phys. Chem. A* **106**, 3599 (2002).

T. FUJINO, S. Yu. ARZHANTSEV and T. TAHARA, "Femtosecond/picosecond Time-Resolved Spectroscopy of *Trans*-Azobenzene: Isomerization Mechanism Following S₂ (ππ*) ← S₀ Photoexcitation," *Bull. Chem. Soc. Jpn.* **75**, 1031 (2002).

D. MANDAL, T. TAHARA, N. M. WEBBER and S. R. MEECH, "Ultrafast Fluorescence of the Chromophore of the Green Fluorescent Protein in Alcohol Solutions," *Chem. Phys. Lett.* **358**, 495 (2002).

D. MANDAL, S. SOHBAN, T. TAHARA and K. BHATTACHARYA, "Femtosecond Study of Solvation Dynamics of DCM in Micelles," *Chem. Phys. Lett.* **359**, 77 (2002).

Z. WANG, H. NODA, Y. NONOGAKI, N. YABUMOTO and T. URISU, "IR Line Width Broadening at Nearly Ideal H-Terminationregion on Si(100)-(2×1) Surfaces," *Surf. Sci.* **502**, 86 (2002).

Z. WANG, H. NODA, Y. NONOGAKI, N. YABUMOTO and T. URISU, "Hydrogen Diffusion and Chemical Reactivity with Water on Nearly Ideally H-terminated Si(100) Surface," *Jpn. J. Appl. Phys.* **41**, 4275 (2002).

Y. TAKABAYASHI, Y. KUBOZONO, T. KANBARA, S. FUJIKI, K. SHIBATA, Y. HARUYAMA, T. HOSOKAWA, Y. RIKIISHI and S. KASHINO, "Pressure and Temperature Dependences of the Structural Properties of Dy@C₈₂ Isomer I," *Phys. Rev. B* **65**, 73405 (2002).

S. FUJIKI, Y. KUBOZONO, M. KOBAYASHI, Y. RIKIISHI, S. KASHINO, K. ISHII, H. SUEMATSU and A. FUJIWARA, "Structure and Physical Properties of Cs_{3+α}C₆₀ (α = 0.0–1.0) under Ambient and High Pressures," *Phys. Rev. B* **65**, 235425 (2002).

S. D. MORE, H. GRAAF, M. BAUNE, C. WANG and T. URISU, "Influence of Substrate Roughness on the Formation of Aliphatic Self-Assembled Monolayers (SAM) on Silicon(100)," *Jpn. J. Appl. Phys.* **41**, 4390 (2002).

S. MORE, W. BERNDT, A. SEITSONNEN and A. M. BRADSHAW, "Adsorption of Pt(111) (√3 × √3)R30° and (2×2)-Na: Experiment and Theory," *Phys. Rev. B* **63**, 075406 (2001).

S. TANAKA, S. D. MORE, J. MURAKAMI, M. ITOH and M. KAMADA, "Surface Photovoltage Effects on p-GaAs (100) from Core-Level Photoelectron Spectroscopy Using Synchrotron Radiation and a Laser," *Phys. Rev. B* **64**, 155308 (2001).

S. MIYAKE, I. SHIMIZU, R. MANORY, T. MORI and G. KIMMEL, "Structural Modifications of Hafnium Oxide Films Prepared by Ion Beam Assisted Deposition under High Energy Oxygen Irradiation," *Surf. Coat. Technol.* **146-147**, 237 (2001).

- S. SAKABE, K. NISHIHARA, N. NAKASHIMA, J. KOU, S. SHIMIZU, V. ZHAKHOVSKII, H. AMITANI and F. SATO**, "The Interactions of Ultra-Short High-Intensity Laser Pulses with Large Molecules and Clusters: Experimental and Computational Studies," *Physics of Plasmas* **8**, 2517 (2001).
- Y. HIKOSAKA and K. MITSUKE**, "Formation and Autoionization of a Dipole-Forbidden Superexcited State of CS₂," *J. Phys. Chem. A* **105**, 8130 (2001).
- H. NAKANO, T. MORI, T. HORIKUBI and N. KAMEGASHIRA**, "Structural Analysis of a New Layered Compound: La_{0.05}Sr_{0.95}MnO₃," *J. Am. Ceram. Soc.* **85**, 1576 (2002).
- T. MORI, N. KAMEGASHIRA, K. AOKI, T. SHISHIDO and T. FUKUDA**, "Crystal Growth and Crystal Structures of the LnMnO₃ Perovskites: Ln = Nd, Sm, Eu and Gd," *Mater. Lett.* **54**, 238 (2002).
- R. MANORY, T. MORI, I. SHIMIZU, S. MIYAKE and G. KIMMEL**, "Growth and Structure Control of HfO_{2-x} Films with Cubic and Tetragonal Structures Obtained by Ion Beam Assisted Deposition," *J. Vac. Sci. Technol., A* **20**, 549 (2002).
- K. IWASAKI and K. MITSUKE**, "Development of a Conical Energy Analyzer for Angle-Resolved Photoelectron Spectroscopy," *Surf. Rev. Lett.* **9**, 583 (2002).

Coordination Chemistry Laboratories

- Y. UOZUMI, M. KAWATSURA and T. HAYASHI**, "(R)-2-Diphenylphosphino-2'-methoxy-1,1'-binaphthyl," *Org. Syn.* **78**, 1 (2002).
- Y. UOZUMI and M. NAKAZONO**, "Amphiphilic Resin-Supported Rhodium-Phosphine Catalysts for C-C Bond Forming Reactions in Water," *Adv. Synth. Catal.* **344**, 274 (2002).
- S. NAGAI, S. TAKEMOTO, T. UEDA, K. MIZUTANI, Y. UOZUMI and H. TOKUDA**, "Studies on the Chemical Transformations of Rotenoids. 6 Synthesis and Antitumor-Promoting Activity of [1]Benzofuro[2,3-d]pyridazines Fused with 1,2,4-Triazole, 1,2,4-Triazine and 1,2,4-Triazepine," *J. Heterocyclic Chem.* **38**, 1097 (2001).
- S. NAGAI, T. MIYACHI, T. NAKANE, T. UEDA and Y. UOZUMI**, "Synthesis and Potential Central Nervous System Stimulant Activity of 5,8-Methanoquinazolines and Bornano[1,2,4]triazines Fused with Imidazole and Pyrimidine," *J. Heterocyclic Chem.* **38**, 379 (2001).
- Y. UOZUMI, T. ARII and T. WATANABE**, "Double Carbonylation of Aryl Iodides with Primary Amines under Atmospheric Pressure Conditions Using Pd/PPh₃/DABCO/THF System," *J. Org. Chem.* **66**, 5272 (2001).
- T. HAYASHI, J. W. HAN, A. TAKEDA, J. TANG, K. NOHMI, K. MUKAIDE, H. TSUJI and Y. UOZUMI**, "Modification of Chiral Monodentate Phosphine Ligands (MOP) for Palladium-Catalyzed Asymmetric Hydrosilylation of Cyclic 1,3-Dienes," *Adv. Synth. Catal.* **343**, 279 (2001).
- T. HAYASHI, S. HIRATE, K. KITAYAMA, H. TSUJI, A. TORII and Y. UOZUMI**, "Asymmetric Hydrosilylation of Styrenes Catalyzed by Palladium-MOP Complexes: Ligand Modification and Mechanistic Studies," *J. Org. Chem.* **66**, 1441 (2001).
- K. NISHIYAMA, A. KUBO, I. TANIGUCHI, M. YAMADA and H. NISHIHARA**, "Effects of Alkyl Chain as a Spacer on Electrochemical Reaction and SEIRA Spectra for Self-Assembled Monolayer Having Anthraquinone Redox Center," *Electrochemistry* **69**, 980 (2001).
- I. TANIGUCHI**, "Analysis of Biological Functions of Metalloproteins Using Biocompatible Modified Electrodes," *Anal. Sci.* **17**, 1355 (2001).
- T. SAWAGUCHI, F. MIZUTANI and I. TANIGUCHI**, "Interfacial Structures of Self-Assembled Monolayers of 2-pyridinethiol on Au(111) Studied by In Situ Tunneling Microscopy," *Anal. Sci.* **17**, 1383 (2001).
- K. NISHIYAMA, H. IKEBE, Y. HOSHIDE, H. NAGAI and I. TANIGUCHI**, "NADP⁺ Sensor on *Chrorella* Ferredoxin/Ferredoxin-NADP⁺-Reductase Modified Indium Oxides," *Chem. Sens.* **17**, 92 (2001).
- K. NISHIYAMA, A. KUBO, A. UEDA and I. TANIGUCHI**, "Surface pK_a of Amine-Terminated Self-Assembled Monolayers Evaluated by Direct Observation of Counter Anion by FT-Surface Enhanced Raman Spectroscopy," *Chem. Lett.* **80** (2002).
- I. TANIGUCHI, K. HARA, H. ISHIMOTO, M. IWAI and S. RANGARAJAN**, "Ion Selectivity for Electrode Reactions on Functionalized Monolayer Modified Electrode," *Chem. Sens.* **18**, 133 (2002).
- S. UEMURA, M. SAKATA, I. TANIGUCHI, C. HIRAYAMA and M. KUNITAKE**, "In-Situ STM Observation of Coronene Epitaxial Adlayers on Au(111) Surfaces Prepared by the Transfer of Langmuir Films," *Thin Solid Films* **409**, 206 (2002).
- G. P. -J. HAREAU, S. NEYA, N. FUNASAKI and I. TANIGUCHI**, "New Route to Protoporphyrins III and XIII from Common Starting Pyrroles," *Tetrahedron Lett.* **43**, 3109 (2002).
- M. YAMASHITA, K. YOKOYAMA, S. FURUKAWA, T. MANABE, T. ONO, K. NAKATA, C. KACHI-TERAJIMA, F. IWAHORI, T. ISHII, H. MIYASAKA, K. SUGIURA, H. MATSUZAKI, H. KISHIDA, H. OKAMOTO, H. TANAKA, Y. HASEGAWA, K. MARUMOTO, H. ITO and S. KURODA**, "Tuning of Electronic Structures of Quasi-One-Dimensional Bromo-Bridged Ni(III) Complexes with Strong Electron-Correlation by Doping of Co(III) Ions, [Ni_{1-x}Co_x(chxn)₂Br]Br₂," *Inorg. Chem.* **41**, 1998 (2002).
- S. FUJIMORI, A. INO, T. OKANE, A. FUJIMORI, K. OKADA, T. MANABE, M. YAMASHITA, H. KISHIDA and H. OKAMOTO**, "Angle-Resolved Photoemission Study of Halogen-Bridged MX-Chain

Compound $[\text{Ni}(\text{chxn})_2\text{Br}]_2\text{Br}_2$," *Phys. Rev. Lett.* **88**, 247601-1(2002).

H. TANAKA, K. MARUMOTO, S. KURODA, T. MANABE and M. YAMASHITA, "ESR Detection of Induced Spin Moments in Halogen-Bridged Mixed-Metal Complexes $\text{Ni}_{1-x}\text{Pd}_x(\text{chxn})_2\text{Br}_3$," *J. Phys. Soc. Jpn.* **71**, 1370 (2002).

K. NAKATA, H. MIYASAKA, K. SUGIMOTO, T. ISHII, K. SUGIURA and M. YAMASHITA, "Construction of a One-Dimensional Chain Composed of Mn_6 Clusters and 4,4'-bipyridine Linkers: The First Step for Creating of "Nano-Dots-Wires," *Chem. Lett.* 658 (2002).

T. KURODA-SOWA, S. FUKUDA, S. MIYOSHI, M. MAEKAWA, M. MUNAKATA, H. MIYASAKA and M. YAMASHITA, "A Chemical Modification of a Mn_{12} Single-Molecule Magnet by Replacing Carboxylate Anion with Diphenylphosphate Anions," *Chem. Lett.* 682 (2002).

S. NORO, R. KITaura, M. KONDO, S. KITAGAWA, T. ISHII, H. MATSUZAKA and M. YAMASHITA, "Framework Engineering by Anions and Porous Functionalities of $\text{Cu}(\text{II})/4,4'$ -bpy Coordination Polymers," *J. Am. Chem. Soc.* **124**, 2568 (2002).

H. TANAKA, K. MARUMOTO, S. KURODA, T. ISHII, R. KANEHAMA, N. AIZAWA, H. MATUZAKA, K. SUGIURA, H. MIYASAKA, T. KODAMA, K. KIKUCHI, I. IKEMOTO and M. YAMASHITA, "ESR Studies of $\text{Co}(\text{tbp})_2\text{C}_{60}$ Single Crystal," *J. Phys.: Condens. Matter* **14**, 3993 (2002).

S. NORO, S. KITAGAWA, M. YAMASHITA and T. WADA, "New Microporous Coordination Polymer Affording Guest-Coordination Sites at Channel Walls," *Chem. Commun.* 222 (2002).

F. KAKIUCHI, H. OHTAKI, M. SONODA, N. CHATANI and S. MURAI, "Mechanistic Study of the $\text{Ru}(\text{H})_2(\text{CO})(\text{PPh}_3)_3$ -Catalyzed Addition of C-H Bonds in Aromatic Esters to Olefins," *Chem. Lett.* 918 (2001).

N. CHATANI, T. ASAUMI, S. YORIMITSU, T. IKEDA, F. KAKIUCHI and S. MURAI, " $\text{Ru}_3(\text{CO})_{12}$ -Catalyzed Coupling Reaction of sp^3 C-H Bonds Adjacent to a Nitrogen Atom in Alkylamines with Alkenes," *J. Am. Chem. Soc.* **123**, 10935 (2001).

N. CHATANI, A. KAMITANI, M. OSHITA, Y. FUKUMOTO and S. MURAI, "Catalytic Carbonylation Reactions of Benzyne Derivatives," *J. Am. Chem. Soc.* **123**, 12686 (2001).

H. INOUE, N. CHATANI and S. MURAI, "Cycloisomerization of ω -Aryl-1-Alkynes: GaCl_3 as a Highly Electrophilic Catalyst for Alkyne Activation," *J. Org. Chem.* **67**, 1414 (2002).

F. KAKIUCHI, K. IGI, M. MATSUMOTO, T. HAYAMIZU, N. CHATANI and S. MURAI, "A New Chelation-Assistance Mode for a Ruthenium-Catalyzed Silylation at the C-H Bond in Aromatic Ring with Hydrosilanes," *Chem. Lett.* 396 (2002).

F. FUKUMOTO, K. SAWADA, N. CHATANI and S. MURAI, " $\text{Ir}_4(\text{CO})_{12}$ -Catalyzed Coupling Reaction of Imidazoles with Aldehydes in the Presence of a Hydrosilane to Give 2-Substituted Imidazoles," *Angew. Chem., Int. Ed. Engl.* **41**, 2779 (2002).

T. WADA, K. TSUGE and K. TANAKA, "Synthesis and Redox Properties of Bis(ruthenium-hydroxo)complexes with Quinone and Bipyridine Ligand as a Water-Oxidation Catalysts," *Inorg. Chem.* **40**, 329 (2001).

H. SUGIMOTO and K. TANAKA, "Ruthenium Terpyridine Complexes with Mono- and Bidentate Dithiolene Ligands," *J. Chem. Soc., Dalton Trans.* 57 (2001).

T. TOMON, D. OYAMA, T. WADA, S. KAZUSHI and K. TANAKA, "A Ru-Carbene Complex with a Metallacycle Involving a 1,8-naphthylidene Framework," *Chem. Commun.* 1100 (2001).

K. ITO, T. NAGATA and K. TANAKA, "Synthesis and Electrochemical Properties of Transition Metal Complexes of 2,2':6',2''-Terpyridine 1,1''-Dioxide," *Inorg. Chem.* **40**, 6331 (2001).

H. SUGIMOTO and K. TANAKA, "Synthesis of New Ruthenium Carbonyl Terpyridine *o*-Phenylene Complexes: Strong Interaction between carbonyl and *o*-Phenylene Ligands," *J. Organomet. Chem.* **622**, 280 (2001).

K. KOBAYASHI, H. OHTSU, T. WADA and K. TANAKA, "Ruthenium Oxy Radical Complex Containing *o*-Quinone Ligand Detected by ESR Measurements of Spin Trapping Technique," *Chem. Lett.* 868 (2002).

Y. SUNADA, Y. HAYASHI, H. KAWAGUCHI and K. TATSUMI, "Alkynethiolato and Alkyneselenolato Ruthenium Half-Sandwich Complexes: Synthesis, Structures, and Reactions with $(\eta^5\text{-C}_5\text{H}_5)_2\text{Zr}$," *Inorg. Chem.* **40**, 7072 (2001).

Y. ARIKAWA, H. KAWAGUCHI, K. KASHIWABARA and K. TATSUMI, "Trithiotungsten(VI) Complexes Having Phosphine-Thiolate Hybrid Ligands: Synthesis and Cluster Forming Reactions with CuBr , FeCl_2 , and $[\text{Fe}(\text{CH}_3\text{CN})_6](\text{ClO}_4)_2$," *Inorg. Chem.* **41**, 513 (2002).

H. KAWAGUCHI and T. MATSUO, "Binuclear Iron(II) Complex from a Linked-bis(amidinate) Ligand: Synthesis and its Reaction with Carbon Monoxide," *Chem. Commun.* 958 (2002).

T. KOMURO, T. MATSUO, H. KAWAGUCHI and K. TATSUMI, "Palladium Dimethylsilanedithiolato Complex: a Precursor for Ti-Pd and Ti-Pd₂ Heterometallic Complexes," *Chem. Commun.* 988 (2002).

T. MATSUO, H. KAWAGUCHI and M. SAKAI, "Synthesis and Structures of Ti(III) and Ti(IV) Complexes Supported by a Tridentate Aryloxy Ligand," *J. Chem. Soc., Dalton Trans.* 2536 (2002).

J. -P. LANG, H. KAWAGUCHI and K. TATSUMI, "Reactions of Tetrathiotungstate and Tetrathiomolybdate with Substituted Haloalkanes," *J. Chem. Soc., Dalton Trans.* 2573 (2002).

H. KAWAGUCHI and T. MATSUO, "Dinitrogen-Bond Cleavage in a Niobium Complex Supported by a Tridentate Aryloxy Ligand," *Angew. Chem., Int. Ed. Engl.* **41**, 2792 (2002).

- N. NAKATA, N. TAKEDA and N. TOKITOH**, "Synthesis and Structure of a Kinetically Stabilized 2-Germanaphthalene: the First Stable Neutral Germaaromatic Compound," *Organometallics* **20**, 5507 (2001).
- S. YASUI, K. ITOH, A. OHNO and N. TOKITOH**, "Kinetic Deuterium Isotope Effect in Single-Electron Transfer Occurring from Tributylphosphine to Viologens," *Chem. Lett.* 1056 (2001).
- N. TAKEDA, T. KAJIWARA and N. TOKITOH**, "Reaction of Stable Silylene-Isocyanide Complexes with Boranes: Synthesis and Properties of the First Stable Silylborane-Isocyanide Complexes," *Chem. Lett.* 1076 (2001).
- M. ITOH, K. TAKENAKA, R. OKAZAKI, N. TAKEDA and N. TOKITOH**, "The First Stable Aromatic S-Nitrosothiol: Synthesis, Structure and Reactivity," *Chem. Lett.* 1206 (2001).
- K. NAGATA, N. TAKEDA and N. TOKITOH**, "Syntheses and Crystal Structures of the First Disulfur and Diselenium Complexes of Platinum," *Angew. Chem. Int. Ed. Engl.* **41**, 136 (2002).
- T. SASAMORI, N. TAKEDA, M. FUJIO, M. KIMURA, S. NAGASE and N. TOKITOH**, "Synthesis and Structure of the First Stable Phosphabismuthene," *Angew. Chem. Int. Ed. Engl.* **41**, 139 (2002).
- N. TOKITOH, T. SADAHIRO, K. HATANO, T. SASAKI, N. TAKEDA and R. OKAZAKI**, "Synthesis of Kinetically Stabilized Silaneselone and Silanetellone," *Chem. Lett.* 34 (2002).
- N. TAKEDA, A. SHINOHARA and N. TOKITOH**, "The First Stable 9-Silaanthracene," *Organometallics* **21**, 256 (2002).
- N. TOKITOH, K. KISHIKAWA, R. OKAZAKI, T. SASAMORI, N. NAKATA and N. TAKEDA**, "Synthesis and Characterization of an Extremely Hindered Tetraaryl-Substituted Digermene and Its Unique Properties in the Solid State and in Solution," *Polyhedron* **21**, 563 (2002).
- T. SASAMORI, Y. ARAI, N. TAKEDA, R. OKAZAKI, Y. FURUKAWA, M. KIMURA, S. NAGASE and N. TOKITOH**, "Syntheses, Structures and Properties of Kinetically Stabilized Distibenes and Dibismuthenes, Novel Doubly Bonded Systems between Heavier Group 15 Elements," *Bull. Chem. Soc. Jpn.* **75**, 661 (2002).
- N. NAKATA, N. TAKEDA and N. TOKITOH**, "Synthesis and Properties of the First Stable Germabenzene," *J. Am. Chem. Soc.* **124**, 6914 (2002).
- N. TOKITOH, T. SASAMORI, N. TAKEDA and S. NAGASE**, "Systematic Studies on Homo- and Heteronuclear Doubly Bonded Compounds of Heavier Group 15 Elements," *Phosphorus, Sulfur Silicon Relat. Elem.* **177**, 1473 (2002).
- K. NAGATA, N. TAKEDA and N. TOKITOH**, "Synthesis of Novel Platinum Dichalcogenido-Complexes by Taking Advantage of Bulky Phosphine Ligands," *Phosphorus, Sulfur Silicon Relat. Elem.* **177**, 1859 (2002).
- S. YASUI, K. ITOH, A. OHNO and N. TOKITOH**, "Reaction of Trivalent Phosphorus Compounds with Viologens," *Phosphorus, Sulfur Silicon Relat. Elem.* **177**, 2001 (2002).
- T. SASAMORI, N. TAKEDA and N. TOKITOH**, "Synthesis and Reaction of the First Stable Phosphabismuthene, a Novel Compound with Phosphorus-Bismuth Double Bond," *Phosphorus, Sulfur Silicon Relat. Elem.* **177**, 2003 (2002).
- N. NAKATA, N. TAKEDA and N. TOKITOH**, "Reactions of 2-Germanaphthalene with Elemental Sulfur and Selenium: Synthesis of Novel Cyclic Polychalcogenides Containing a Germanium, Trichalcogenagermolanes," *Chem. Lett.* 818 (2002).
- F. TAKEI, H. HAYASHI, K. ONITSUKA and S. TAKAHASHI**, "Helical Poly(aryl isocyanide)s Possessing Chiral Alkoxy carbonyl Groups," *Polym. J.* **33**, 310 (2001).
- F. FENG, T. MIYASHITA, F. TAKEI, K. ONITSUKA and S. TAKAHASHI**, "Formation of an Optically Active Helical Polyisocyanide Langmuir-Blodgett Film," *Chem. Lett.* 764 (2001).
- F. TAKEI, H. HAYASHI, K. ONITSUKA, N. KOBAYASHI and S. TAKAHASHI**, "Helical Chiral Polyisocyanides Possessing Porphyrin Pendants: Determination of Helicity by Exciton Coupled Circular Dichroism," *Angew. Chem., Int. Ed.* **40**, 4092 (2001).

Laser Research Center for Molecular Science

- Z. LIU, T. KOZEKI, Y. SUZUKI, N. SARUKURA, K. SHIMAMURA, T. FUKUDA, M. HIRANO and H. HOSONO**, "Ce³⁺:LiCaAlF₆ Crystal for High-Gain or High-Peak-Power Amplification of Ultraviolet Femtosecond Pulses and New Potential Ultraviolet Gain Medium: Ce³⁺:LiSr_{0.8}Ca_{0.2}AlF₆," *IEEE J. Sel. Top. Quantum Electron.* **7**, 542 (2001).
- M. OTO, S. KIKUGAWA, N. SARUKURA, M. HIRANO and H. HOSONO**, "Optical Fiber for Deep Ultraviolet Light," *IEEE Photonics Technol. Lett.* **13**, 978 (2001).
- K. SHIMAMURA, H. SATO, A. BENSALAH, V. SUDESH, H. MACHIDA, N. SARUKURA and T. FUKUDA**, "Crystal Growth of Fluorides for Optical Applications," *Cryst. Res. Technol.* **36**, 801 (2001).
- H. MURAKAMI, T. KOZEKI, Y. SUZUKI, S. ONO, H. OHTAKE, N. SARUKURA, E. ISHIKAWA and T. YAMASE**, "Nanocluster Crystals of Lacunary Polyoxometalates as Structure-Design-Flexible, Inorganic Nonlinear Materials," *Appl. Phys. Lett.* **79**, 3564 (2001).
- H. OHTAKE, Y. SUZUKI, N. SARUKURA, S. ONO, T. TSUKAMOTO, A. NAKANISHI, S. NISHIZAWA, M. L. STOCK, M. YOSHIDA and H. ENDERT**, "THz-Radiation Emitter and Receiver System Based on a 2T Permanent Magnet, 1040 nm Compact Fiber Laser and Pyroelectric Thermal Receiver," *Jpn. J. Appl. Phys., Part 2* **40**, L1223 (2001).

- K. SHIMAMURA, H. SATO, A. BENSALAH, H. MACHIDA, N. SARUKURA and T. FUKUDA**, "Growth of Ce-Doped Colquiriite- and Scheelite-Type Single Crystals for UV Laser Applications," *Opt. Mater.* **19**, 109 (2002).
- Z. LIU, K. SHIMAMURA, T. FUKUDA, T. KOZEKI, Y. SUZUKI and N. SARUKURA**, "High-Energy Pulse Generation from Solid-State Ultraviolet Lasers Using Large Ce:Fluoride Crystals," *Opt. Mater.* **19**, 123 (2002).
- K. KAWAMURA, N. ITO, N. SARUKURA, M. HIRANO and H. HOSONO**, "New Adjustment Technique for Time Coincidence of Femtosecond Laser Pulses Using Third Harmonic Generation in Air and its Application to Holograph Encoding System," *Rev. Sci. Instrum.* **73**, 1711 (2002).
- Y. SUZUKI, T. KOZEKI, S. ONO, H. MURAKAMI, H. OHTAKE, N. SARUKURA, T. NAKAJYO, F. SAKAI and Y. AOKI**, "Hybrid Time-Resolved Spectroscopic System for Evaluating Laser Material Using a Table-Top-Sized, Low-Jitter, 3-MeV Picosecond Electron-Beam Source with a Photocathode," *Appl. Phys. Lett.* **80**, 3280 (2002).
- H. OHTAKE, Y. SUZUKI, S. ONO, N. SARUKURA, T. HIROSUMI and T. OKADA**, "Simultaneous Measurement of Thickness and Water Content of Thin Black Ink Films for the Printing Using THz Radiation," *Jpn. J. Appl. Phys., Part 2* **41**, L475 (2002).
- K. YAMAMOTO, K. TOMINAGA, H. SASAKAWA, A. TAMURA, H. MURAKAMI, H. OHTAKE and N. SARUKURA**, "Far-Infrared Absorption Measurements of Polypeptides and Cytochrome *c* by THz Radiation," *Bull. Chem. Soc. Jpn.* **75**, 1083 (2002).
- Y. SUZUKI, S. ONO, H. MURAKAMI, T. KOZEKI, H. OHTAKE, N. SARUKURA, G. MASADA, H. SHIRAIISHI and I. SEKINE**, "0.43 J, 10 Hz Fourth Harmonic Generation of Nd:YAG Laser Using Large Li₂B₄O₇ Crystals," *Jpn. J. Appl. Phys., Part 2* **41**, L823 (2002).
- T. KOZEKI, Y. SUZUKI, M. SAKAI, H. OHTAKE, N. SARUKURA, K. SHIMAMURA, T. FUKUDA, T. NAKAJYO, F. SAKAI and Y. AOKI**, "Electron-Beam Excitation of a Ce³⁺:LiCaAlF₆ Crystal for Future High-Peak-Power UV lasers," *Appl. Phys. B* **74**, S185 (2002).
- V. LUPEI, A. LUPEI, S. GEORGESCU, T. TAIRA, Y. SATO and A. IKESUE**, "The Effect of Nd Concentration on the Spectroscopic and Emission Decay Properties of Highly Doped Nd:YAG Ceramics," *Phys. Rev. B* **64**, 092102 (2001).
- V. LUPEI, N. PAVEL and T. TAIRA**, "Laser Emission in Highly-Doped Nd:YAG Crystals under ⁴F_{5/2} and ⁴F_{3/2} Pumping," *Opt. Lett.* **26**, 1678 (2001).
- V. LUPEI, A. LUPEI, N. PAVEL, T. TAIRA and A. IKESUE**, "Comparative Investigation of Spectroscopic and Laser Emission Characteristics under Direct 885-nm Pump of Concentrated Nd:YAG Ceramics and Crystals," *Appl. Phys. B* **73**, 757 (2001).
- V. LUPEI, N. PAVEL and T. TAIRA**, "Highly Efficient Laser Emission in Concentrated Nd:YVO₄ Components under Direct Pumping into the Emitting Level," *Opt. Commun.* **201**, 431 (2002).
- J. SAIKAWA, S. KURIMURA, I. SHOJI and T. TAIRA**, "Tunable Frequency-Doubled Yb:YAG Microchip Lasers," *Opt. Mater.* **19**, 169 (2002).
- I. SHOJI, Y. SATO, S. KURIMURA, V. LUPEI, T. TAIRA, A. IKESUE and K. YOSHIDA**, "Thermal-Birefringence-Induced Depolarization in Nd:YAG Ceramics," *Opt. Lett.* **27**, 234 (2002).
- V. LUPEI, N. PAVEL and T. TAIRA**, "Efficient Laser Emission in Concentrated Nd Laser Materials under Pumping into the Emitting Level," *IEEE J. Quantum Electron.* **38**, 240 (2002).
- V. LUPEI, A. LUPEI, S. GEORGESCU, B. DIACONESCU, T. TAIRA, Y. SATO, S. KURIMURA and A. IKESUE**, "High-Resolution Spectroscopy and Emission Decay in Concentrated Nd:YAG Ceramics," *J. Opt. Soc. Am. B* **19**, 360 (2002).
- I. SHOJI and T. TAIRA**, "Intrinsic Reduction of the Depolarization Loss in Solid-State Lasers by Use of a (110)-cut Y₃Al₅O₁₂ Crystal," *Appl. Phys. Lett.* **80**, 3048 (2002).
- V. LUPEI, N. PAVEL and T. TAIRA**, "1064-nm Laser Emission of Highly Doped Nd: Yttrium Aluminum Garnet under 885-nm Diode Laser Pumping," *Appl. Phys. Lett.* **80**, 4309 (2002).
- N. E. YU, J. H. RO, M. CHA, S. KURIMURA and T. TAIRA**, "Broadband Quasi-Phase-Matched Second Harmonic Generation in MgO-Doped Periodically Poled LiNbO₃ at the Communications Band," *Opt. Lett.* **27**, 1046 (2002).
- T. DASCALU, T. TAIRA and N. PAVEL**, "Diode Edge-Pumped Microchip Composite Yb:YAG Laser," *Jpn. J. Appl. Phys.* **41**, L606 (2002).

Research Center for Molecular-scale Nanoscience

- N. TROMBACH, H. TADA, S. HILLER, D. SCHLETTWEIN and D. WOHRLE**, "Photovoltaic Junction Properties of Ultrathin Films of Phthalocyaninatooxovanadium (PcVO) on H-Terminated N-Si(111)," *Thin Solid Films* **396**, 109 (2001).
- K. OKAMOTO, T. TOJO, H. TADA, M. TERAZIMA and K. MATSUSIGE**, "Microscopic Patterning on The Polysilane Films by The Laser Induced Grating Technique," *Mol. Cryst. Liq. Cryst.* **370**, 379 (2001).
- M. TAKADA, H. YOSHIOKA, H. TADA and K. MATSUSHIGE**, "Electrical Characteristics of Phthalocyanine Films Prepared by Electrophoretic Deposition," *Jpn. J. Appl. Phys.* **41**, L73 (2002).
- M. TAKADA, H. GRAAF, Y. YAMASHITA and H. TADA**, "BTQBT (bis-(1, 2, 5-thiadiazolo)-p-quinobis(1, 3-dithiole)) Thin Films; A Promising Candidate for High Mobility Organic Transistors," *Jpn. J. Appl. Phys.* **41**, L4

(2002).

M. ARA, H. GRAAF and H. TADA, "Nanopatterning of Alkyl Monolayers Covalently Bound to Si(111) with An Atomic Force Microscope," *Appl. Phys. Lett.* **80**, 2565 (2002).

M. ARA, H. GRAAF and H. TADA, "Atomic Force Microscope Anodization of Si(111) Covered with Alkyl," *Jpn. J. Appl. Phys.* **41**, 4894 (2002).

H. GRAAF, M. ARA and H. TADA, "Force Curve Measurement of Self-Assembled Organic Monolayers Bound Covalently on Silicon (111)," *Mol. Cryst. Liq. Cryst.* **377**, 33 (2002).

M. TACHIBANA, S. TANAKA, Y. YAMASHITA and K. YOSHIKAWA, "Small Bandgap Polymers Involving Tricyclic Nonclassical Thiophene as a Building Block," *J. Phys. Chem. B* **106**, 3549 (2002).

M. B. ZAMAN, M. TOMURA and Y. YAMASHITA, "Crystal Engineering Using Anilic Acids and Dipyridyl Compounds through a New Supramolecular Synthon," *J. Org. Chem.* **66**, 5987 (2001).

M. TOMURA and Y. YAMASHITA, "Bis(tetra-n-butylammonium) Bis(2-dicyanomethylene-4,5-dimercapto-1,3-dithiole)nickel(II)," *Acta Crystallogr., Sect. E* **58**, m133 (2002).

K. ONO, K. SAITO, H. UCHIUMI and M. TOMURA, "¹H NMR Analysis and Crystal Structures of 1,1',3,3'-Tetramethyl-2,2'-bi-1*H*-Imidazolium Bis(tetraphenylborate): Ion-Associative Interactions Containing Ketone, Aldehyde, and Nitrile," *Chem. Lett.* 622 (2002).

M. TOMURA, M. AKHTARUZZAMAN, K. SUZUKI and Y. YAMASHITA, "4,7-Diiodo-2,1,3-benzothiadiazole and 7,7'-Diiodo-4,4'-bis(2,1,3-benzothiadiazole)," *Acta Crystallogr., Sect. C: Cryst. Struct. Commun.* **58**, o373 (2002).

Y. YAMASHITA, M. TOMURA, M. URUICHI and K. YAKUSHI, "Synthesis and Properties of π -Extended TTF Analogues and Their Cation Radical and Dication Salts," *Mol. Cryst. Liq. Cryst.* **376**, 19 (2002).

K. ITO, T. NAGATA and K. TANAKA, "Synthesis and Electrochemical Properties of Transition Metal Complexes of 2,2':6',2''-Terpyridine 1,1''-Dioxide," *Inorg. Chem.* **40**, 6331 (2001).

M. SAEKI, T. TSUKUDA and T. NAGATA, "Ab initio Study of $\text{CO}_2^- \cdot \text{CO}_2 \leftrightarrow \text{C}_2\text{O}_4^-$ Isomerization," *Chem. Phys. Lett.* **348**, 461 (2001).

L. ZHU, K. TAKAHASHI, M. SAEKI, T. TSUKUDA and T. NAGATA, "Photodissociation of Gas-Phase I_3^- : Product Branching in the Visible and UV Regions," *Chem. Phys. Lett.* **350**, 233 (2001).

T. TSUKUDA, L. ZHU, M. SAEKI and T. NAGATA, "Photochemistry of $(\text{NO})_n^-$ as Studied by Photofragment Mass Spectrometry," *Int. J. Mass Spectrom.* **220**, 137 (2002).

H. SAKURAI, T. TSUKUDA and T. HIRAO, "Pd/C as a Reusable Catalyst for the Coupling Reaction of Halophenols and Arylboronic Acids in Aqueous Media," *J. Org. Chem.* **67**, 2721 (2002).

H. SAKURAI, T. HIRAO, Y. NEGISHI, H. TSUNAKAWA and T. TSUKUDA, "Palladium Clusters Stabilized by Cyclodextrins Catalyze Suzuki-Miyaura Coupling Reactions in Water," *Trans. Mater. Res. Soc. Jpn.* **27**, 185 (2002).

D. KUWAHARA, T. NAKAI, J. ASHIDA and S. MIYAJIMA, "Novel Structure Discovered on Two-Dimensional Spin-Echo NMR Spectra for a Homonuclear Two-Spins System in Rotating Solids," *Proceedings of 14th Conference of the International Society of Magnetic Resonance* 130 (2001).

M. KOMIYAMA, M. GU and H.-M. WU, "Determination of Extra-framework Cation Positions and Their Occupancies on Heulandite(010) by Atomic Force Microscopy," *J. Phys. Chem. B* **105**, 4680 (2001).

M. KOMIYAMA, T. UCHIHASHI, Y. SUGAWARA and S. MORITA, "Molecular Orbital Interpretation of Thymine/graphite NC-AFM Images," *Surf. Interface Anal.* **29**, 53 (2001).

M. KOMIYAMA and D. YIN, "Apparent Local Structural Change Caused by Ultraviolet Light on a TiO_2 Surface Observed by Scanning Tunneling Microscopy," *Jpn. J. Appl. Phys.* **40**, 4281 (2001).

M. KOMIYAMA and T. SHIMAGUCHI, "Partial Reduction of Si(IV) in SiO_2 Thin Film by Deposited Metal Particles - An XPS Study," *Surf. Interface Anal.* **29**, 189 (2001).

N. GU and M. KOMIYAMA, "Various Phases on Natural Stilbite (010) Surface Observed by Atomic Force Microscopy under Aqueous Conditions," *Jpn. J. Appl. Phys.* **40**, 4285 (2001).

S. HASEGAWA, K. YAKUSHI, H. INOKUCHI, K. K. OKUDAIRA, N. UENO, K. SEKI, E. MORIKAWA and V. SAILE, "Calculated Photoelectron Angular Distributions of ω -(*n*-pyrrolyl)alkanethiol Self-Assembled Monolayers for Distinguishing Between Different Arrangements of Pyrrole Groups," *J. Electron Spectrosc. Relat. Phenom.* **120**, 121 (2001).

S. HASEGAWA, T. HORIGOME, K. YAKUSHI, H. INOKUCHI, K. K. OKUDAIRA, N. UENO, K. SEKI, R. J. WILLCUT, R. L. McCARLEY, E. MORIKAWA and V. SAILE, "Angle-Resolved Photoemission Measurements of ν -(*n*-pyrrolyl)alkanethiol Self-Assembled Monolayers Using In-Situ Sample Preparation Apparatus," *J. Electron Spectrosc. Relat. Phenom.* **113**, 101 (2001).

K. K. OKUDAIRA, E. MORIKAWA, S. HASEGAWA, H. ISHII, Y. AZUMA, M. IMAMURA, H. SHIMADA, K. SEKI and N. UENO, "Surface Electronic Structure and Molecular Orientation of Poly(9-vinylcarbazole) Thin Film: ARUPS and NEXAFS," *Nucl. Instrum. Methods Phys. Res., Sect. A* **467-468**, 1233

(2001).

K. K. OKUDAIRA, S. KERA, H. SETOYAMA, E. MORIKAWA and N. UENO, "Electronic Structure and Molecular Orientation at Thin Film Surfaces of Pendant-Group Polymers Studied by Outermost Surface Spectroscopy Using Metastable Atoms," *J. Electron Spectrosc. Relat. Phenom.* **121**, 225 (2001).

H. YAMANE, H. SETOYAMA, S. KERA, K. K. OKUDAIRA and N. UENO, "Low-Energy Electron Transmission Experiments on Graphite," *Phys. Rev. B* **64**, 113407 (2001).

Y. AZUMA, K. IWASAWA, T. KURIHARA, K. K. OKUDAIRA, Y. HARADA and N. UENO, "Low Energy Electron Diffraction of the System In-[perylene-3,4,9, 10-tetracarboxylic Dianhydride] on MoS₂," *J. Appl. Phys.* **91**, 5024 (2002).

D. YOSHIMURA, H. ISHII, T. MIYAMAE, S. HASEGAWA, K. K. OKUDAIRA, N. UENO and K. SEKI, "Intramolecular Energy-Band Dispersion in Oriented Thin Film of n-CF₃(CF₂)₂₂CF₃ Observed by Angle-Resolved UV Photoemission and its Theoretical Simulation," *Surf. Rev. Lett.* **9**, 407 (2002).

Y. TAKABAYASHI, Y. KUBOZONO, T. KANBARA, S. FUJIKI, K. SHIBATA, Y. HARUYAMA, T. HOSOKAWA, Y. RIKIISHI and S. KASHINO, "Pressure and Temperature Dependences of the Structural Properties of Dy@C₈₂ Isomer I," *Phys. Rev. B* **65**, 73405 (2002).

K. ISHII, A. FUJIWARA, H. SUEMATSU and Y. KUBOZONO, "Ferromagnetism and Giant Magnetoresistance in the Rare-Earth Fullerides Eu_{6-x}Sr_xC₆₀," *Phys. Rev. B* **65**, 134431 (2002).

D. H. CHI, Y. IWASA, X. H. CHEN, T. TAKENOBŪ, T. ITO, T. MITANI, E. NISHIBORI, M. TAKATA, M. SAKATA and Y. KUBOZONO, "Bridging Fullerenes with Metals," *Chem. Phys. Lett.* **359**, 177 (2002).

S. FUJIKI, Y. KUBOZONO, M. KOBAYASHI, T. KAMBE, Y. RIKIISHI, S. KASHINO, K. ISHII, H. SUEMATSU and A. FUJIWARA, "Structure and Physical Properties of Cs_{3+α}C₆₀ (α = 0.0–1.0) under Ambient and High Pressures," *Phys. Rev. B* **65**, 235425 (2002).

Y. NAGAO, R. IKEDA, S. KANDA, Y. KUBOZONO and H. KITAGAWA, "Complex-Plane Impedance Study on a Hydrogen-Doped Copper Coordination Polymer: *N,N'*-bis-(2-hydroxy-ethyl)-Dithiooxamidato-Copper(II)," *Mol. Cryst. Liq. Cryst.* **379**, 89 (2002).

Y. TANIMOTO, Y. AKIMOTO, Y. FUJIWARA, M. MUKAI, T. TAKUI, T. KINOSHITA and K. ITOH, "Magnetic Field Effect on the Fluorescence of *m*-Phenylenebis(phenylmethylene) in a Rigid Glass at 77 K," *Bull. Chem. Soc. Jpn.* **74**, 2325 (2001).

Y. TANIMOTO, R. YAMAGUCHI, Y. KANAZAWA and M. FUJIWARA, "Magnetic Orientation of *Lysozyme* Crystals," *Bull. Chem. Soc. Jpn.* **75**, 1133 (2002).

S. KOHTANI, M. SUGIYAMA, Y. FUJIWARA, Y. TANIMOTO and R. NAKAGAKI, "Asymmetric Photolysis of 2-Phenylcycloalkanones with Circularly Polarized Light: A Kinetic Model for Magnetic Field Effects," *Bull. Chem. Soc. Jpn.* **75**, 1223 (2002).

Y. FUJIWARA, J. HAMADA, T. AOKI, T. SHIMIZU, Y. TANIMOTO, H. YONEMURA, S. YAMADA, T. UJIE and H. NAKAMURA, "Chain Length Dependence of High Magnetic Field Effects on Lifetimes of Radical Ions Pairs Linked by a Methylene Chain: Interpretation by both Spin-Lattice and Spin-Spin Relaxations," *Mol. Phys.* **100**, 1405 (2002).

M. FUJIWARA, K. KAWAKAMI and Y. TANIMOTO, "Magnetic Orientation of Carbon Nanotubes at Temperatures of 231 K and 314 K," *Mol. Phys.* **100**, 1085 (2002).

H. YOSHIKAWA, S. NISHIKIORI, T. WATANABE, T. ISHIDA, G. WATANABE, M. MURAKAMI, K. SUWINSKA, R. LUBORADZKI and J. LIPKOWSKI, "Polycyano-Polycadmate Host Clathrates Including a Methylviologen Dication. Syntheses, Crystal Structures and Photo-Induced Reduction of Methylviologen Dication," *J. Chem. Soc., Dalton Trans.* 1907 (2002).

K. KONOSHIMA, T. GOTO, T. ISHIDA, K. URABE and M. KITAO, "IR Absorption Spectra of Electrochromic WO₃ Films," *Trans. Mater. Res. Soc. Jpn.* **27**, 349 (2002).

UVSOR (Ultraviolet Synchrotron Orbital Radiation) Facility

S. ASAKA, M. ITOH and M. KAMADA, "Ultraviolet Light Amplification within a Nanometer-Sized Layer," *Phys. Rev. B* **63**, 81104 (2001).

S. TANAKA, S. D. MORÉ, J. MURAKAMI, M. ITOH, Y. FUJII and M. KAMADA, "Surface Photovoltage Effects on p-GaAs(100) from Core-Level Photoelectron Spectroscopy Using Synchrotron Radiation and a Laser," *Phys. Rev. B* **64**, 155308 (2001).

M. ITOH and M. KAMADA, "Comparative Study of Auger-Free Luminescence and Valence-Band Photoemission in Wide-Gap Materials," *J. Phys. Soc. Jpn.* **70**, 3446 (2001).

M. KAMADA and M. ITOH, "Nonradiative Decay of Core Excitons in the Auger-Free Luminescence Materials CsCl and BaF₂," *Phys. Rev. B* **65**, 245104 (2002).

T. TSUJIBAYASHI, K. TOYODA, S. SAKURAGI, M. KAMADA, and M. ITOH, "Spectral Profile of the Two-Photon Absorption Coefficients in CaF₂," *Appl. Phys. Lett.* **80**, 2883 (2002).

K. KANDA, T. KITAGAWA, Y. SHIMIZUGAWA, Y. HARUYAMA, S. MATSUI, M. TERASAWA, H. TSUBAKINO, I. YAMADA, T. GEJO and M. KAMADA, "Characterization of Hard Diamond-Like Carbon

- Films Formed by Ar-Gas Cluster Ion Beam-Assisted Fullerene Deposition," *Jpn. J. Appl. Phys.* **41**, 4295 (2002).
- M. KAMADA, S. TANAKA, K. TAKAHASHI, Y. DOI, K. FUKUI, T. KINOSHITA, Y. HARUYAMA, S. ASAKA, Y. FUJII and M. ITOH**, "Beam-line Systems for Pump-Probe Photoelectron Spectroscopy Using SR and Laser," *Nucl. Instrum. Methods Phys. Res., Sect. A* **467/468**, 1441 (2001).
- S. ASAKA, J. AZUMA, T. TSUJIBAYASHI, M. ITOH, M. WATANABE, O. ARIMOTO, S. NAKANISHI, H. ITOH and M. KAMADA**, "Optical Detection System Using Time Structure of UVSOR for Combined Laser-SR Experiments," *Nucl. Instrum. Methods Phys. Res., Sect. A* **467/468**, 1455 (2001).
- M. KAMADA**, "Experiments with Combined Laser and SR at the UVSOR Facility," *LSWAVE Proceedings* 11 (2001).
- S. D. MORÉ, S. TANAKA, T. NISHITANI, T. NAKANISHI and M. KAMADA**, "Cesiumoxide-GaAs Interface and Layer Thickness in NEA Surface Formation," *SPIN2000* 916 (2001).
- S. TANAKA, K. TAKAHASHI, S. D. MORÉ, T. NISHITANI, T. NAKANISHI, and M. KAMADA**, "Surface Photo-Voltage Effect on Clean and NEA Surfaces of GaAs and Its Superlattice," *SPIN2000* 1000 (2001).
- M. KAMADA, K. TAKAHASHI, Y. DOI, F. FUKUI, T. TAYAGAKI and K. TANAKA**, "Photoelectron Spectroscopic Study on Photo-Induced Phase Transition of Spin-Crossover Complex," *Phase Transition* **41** (2002).
- S. TANAKA, K. TAKAHASHI, J. AZUMA, K. HAYAKAWA, M. ITOH and M. KAMADA**, "New Spectroscopy for Photo-Induced Phenomena Using Combination of Synchrotron Radiation and Laser," *Phase Transition* **51** (2002).
- K. TAKAHASHI, M. KAMADA, Y. DOI, K. FUKUI, T. TAYAGAKI and K. TANAKA**, "Photo-Induced Phase Transition of Spin-Crossover Complex Studied with the Combination of SR and Laser," *Surf. Rev. Lett.* **9**, 319 (2002).
- S. TANAKA, S. D. MORÉ, T. NISHITANI, K. TAKAHASHI, T. NAKANISHI and M. KAMADA**, "Surface-Photovoltage Effect on GaAs-GaAsP Super-Lattice Studied with Combination of Synchrotron Radiation and Laser," *Surf. Rev. Lett.* **9**, 1297 (2002).
- R. GUILLEMIN, E. SHIGEMASA, K. LE GUEN, D. CEOLIN, C. MIRON, N. LECLERCQ, P. MORIN and M. SIMON**, "Dynamical Angular Correlation in Molecular Auger Decay," *Phys. Rev. Lett.* **87**, 203001 (2001).
- R. GUILLEMIN, O. HEMMERS, D. W. LINDLE, E. SHIGEMASA, K. LE GUEN, D. CEOLIN, C. MIRON, N. LECLERCQ, P. MORIN, M. SIMON and P. W. LANGHOFF**, "Nondipolar Electron Angular Distributions from Fixed-in-Space Molecules," *Phys. Rev. Lett.* **89**, 033002 (2002).
- E. SHIGEMASA, T. GEJO, M. NAGASONO, T. HATSUI and N. KOSUGI**, "Double and Triple Excitations near the K-Shell Ionization Threshold of N₂ Revealed by Symmetry-Resolved Spectroscopy," *Phys. Rev. A* **66**, 022508 (2002).
- S. KODA, M. HOSAKA, J. YAMAZAKI, M. KATOH and H. HAMA**, "Development of Longitudinal Feedback System for a Storage Ring Free Electron Laser," *Nucl. Instrum. Methods Phys. Res., Sect. A* **475**, 211 (2001).
- M. HOSAKA, S. KODA, M. KATOH, J. YAMAZAKI and H. HAMA**, "FEL Induced Electron Bunch Heating Observed by a Method Based on Synchronous Phase Detection," *Nucl. Instrum. Methods Phys. Res., Sect. A* **475**, 217 (2002).
- M. HOSAKA, S. KODA, M. KATOH, J. YAMAZAKI, K. HAYASHI, K. TAKASHIMA, T. GEJO and H. HAMA**, "From the Operation of an SRFEL to a User Facility," *Nucl. Instrum. Methods Phys. Res., Sect. A* **483**, 146 (2002).
- S. KIMURA, T. NISHI, M. OKUNO, H. IWATA, H. AOKI and A. OCHIAI**, "Charge Ordering Effect of Electronic Structure of Yb₄(As_{1-x}Sb_x)₃," *J. Phys. Soc. Jpn.* **71**, 300 (2002).
- S. KIMURA, M. OKUNO, H. IWATA, T. SAITOH, T. OKUDA, A. HARASAWA, T. KINOSHITA, A. MITSUDA, H. WADA and M. SHIGA**, "Temperature-Induced Valence Transition of EuNi₂(Si_{0.25}Ge_{0.75})₂ Studied by Eu 4d-4f Resonant Photoemission and Optical Conductivity," *J. Phys. Soc. Jpn.* **71**, 255 (2002).
- H. OKAMURA, M. MATSUNAMI, S. KIMURA, T. NANBA, F. IGA and T. TAKABATAKE**, "Optical Conductivity of Diluted Kondo Semiconductors Yb_{1-x}Lu_xB₁₂," *J. Phys. Soc. Jpn.* **71**, 303 (2002).
- S. O. HONG, B. H. MIN, H. J. LEE, S. KIMURA, M. H. JUNG, T. TAKABATAKE and Y. S. KWON**, "Influence of Electronic Structure of CeSbNi_{0.15} on its Optical Conductivity," *Physica B* **312-313**, 251 (2002).
- H. OKAMURA, M. MATSUNAMI, S. KIMURA, T. NANBA, F. IGA and T. TAKABATAKE**, "Optical Gap in the Diluted Kondo Semiconductors Yb_{1-x}Lu_xB₁₂: Lattice and Single-Site Effects," *Physica B* **312-313**, 157 (2002).
- H. OKAMURA, T. KORETSUNE, M. MATSUNAMI, S. KIMURA, T. NANBA, H. IMAI, Y. SHIMAKAWA and Y. KUBO**, "Magneto-Optical Study of the Colossal Magnetoresistance Pyrochlore Tl₂Mn₂O₇," *Physica B* **312-313**, 714 (2002).
- S. KIMURA, M. OKUNO, H. IWATA, H. KITAZAWA and G. KIDO**, "Low-Energy Electronic Structure of Ce_{1-x}La_xSb (x = 0, 0.1) in the Magnetically Ordered States," *Physica B* **312-313**, 228 (2002).
- S. KIMURA, M. OKUNO, H. IWATA, T. NISHI, H. AOKI and A. OCHIAI**, "Low-Energy Optical Conductivity of Yb₄As₃," *Physica B* **312-313**, 356 (2002).
- T. KINOSHITA, H. P. N. J. GUNASEKARA, Y. TAKATA, S. KIMURA, M. OKUNO, Y. HARUYAMA, N. KOSUGI, K. G. NATH, H. WADA, A. MITSUDA, M. SHIGA, T. OKUDA, A. HARASAWA, H. OGASAWARA and A. KOTANI**, "Spectroscopy Studies of Temperature-Induced Valence Transition Material

- EuNi₂(Si_{1-x}Ge_x)₂ around Eu 3d-4f, Eu 4d-4f and Ni 2p-3d Excitation Regions,” *J. Phys. Soc. Jpn.* **71**, 148 (2002).
H. OKAMURA, T. KORETSUNE, M. MATSUNAMI, S. KIMURA, T. NANBA, H. IMAI, Y. SHIMAKAWA and Y. KUBO, “Charge Dynamics in the Colossal Magneto-Resistance Pyrochlore Ti₂Mn₂O₇,” *Phys. Rev. B* **64**, 180409(R) (2001).
S. KIMURA, M. OKUNO, H. IWATA, H. AOKI and A. OCHIAI, “Temperature Dependence of Low-Energy Optical Conductivity of Yb₄(As_{1-x}P_x)₃ (x = 0, 0.05, 0.15),” *J. Phys. Soc. Jpn.* **70**, 2829 (2001).

Computer Center

- I. TOKUE, H. TANAKA, K. YAMASAKI and S. NANBU**, “Formation of HCl⁺(A²Σ⁺) and HBr⁺(A²Σ⁺) Resulting from He(2³S) Penning Ionization of HCl and HBr,” *J. Phys. Chem. A* **106**, 6068 (2002).
J. -I. CHOE, S. -K. CHANG and S. NANBU, “Ab Initio Study of Conformers of p-tert-Butylcalix[4]crown-6-Ether Complexed with Alkyl Ammonium Cations,” *Bull. Korean Chem. Soc.* **23**, 891 (2002).
J. OUYANG, K. YAKUSHI, T. KINOSHITA, S. NANBU, M. AOYAGI, Y. MISAKI and K. TANAKA, “The Assignment of the In-Plane Molecular Vibrations of the BDT-TTP Electron-Donor Molecule Based on the Polarized Raman and Infrared Spectra, where BDT-TTP is 2,5-bis(1,3-dithiol-2-ylidene)-1,3,4,6-Tetrathiapentalene,” *Spectrochim. Acta, Part A* **58**, 1643 (2002).

Center for Integrative Bioscience

- S. OGO, S. MAKIHARA, Y. KANEKO and Y. WATANABE**, “pH-Dependent Transfer Hydrogenation, Reductive Amination, and Dehalogenation of Water-Soluble Carbonyl Compounds and Alkyl Halides Promoted by Cp*Ir Complexes,” *Organometallic* **20**, 4903 (2001).
S. OGO, R. YAMAHARA, T. FUNABIKI, H. MASUDA and Y. WATANABE, “Biomimetic Intradiol-Cleavage of Catechols with Incorporation of Both Atoms of O₂: The Role of the Vacant Coordination Site on the Iron Center,” *Chem. Lett.* 1062 (2001).
T. TOMITA, S. OGO, T. EGAWA, H. SHIMADA, N. OKAMOTO, Y. IMAI, Y. WATANABE, Y. ISHIMURA and T. KITAGAWA, “Elucidation of the Differences between the 430 and 455-nm Absorbing Forms of P450-Isocyanide Adducts by Resonance Raman Spectroscopy,” *J. Biol. Chem.* **276**, 36261 (2001).
I. HARA, T. UENO, S. OZAKI, S. ITOH, K. LEE, N. UEYAMA and Y. WATANABE, “Oxidative Modification of Tryptophan-43 in the Heme Vicinity of the F43W/H64L Myoglobin Mutant,” *J. Biol. Chem.* **276**, 36067 (2001).
S. OGO, T. ABURA and Y. WATANABE, “pH-Dependent Transfer Hydrogenation of Ketones with HCOONa as a Hydrogen Donor Promoted by (η⁶-C₆Me₆)Ru Complexes,” *Organometallics* **21**, 2964 (2002).
S. OGO, H. NAKAI and Y. WATANABE, “pH-Dependent H₂-Activation Cycle to Reduction of Nitrate Ion by Metal Complexes,” *J. Am. Chem. Soc.* **124**, 597 (2002).
H. NAKAI, S. OGO and Y. WATANABE, “pH-Dependent Cross-Coupling Reactions of Water-Soluble Organic Halides with Organoboron Compounds Catalyzed by an Organometallic Aqua Complex [(SCS)Pd^{II}(H₂O)]⁺ {SCS = C₆H₃-2,6-(CH₂SBu^t)₂},” *Organometallics* **21**, 1674 (2002).
A. WADA, S. OGO, S. NAGATOMO, T. KITAGAWA, Y. WATANABE, K. JITSUKAWA and H. MASUDA, “Reactivity of Hydrogen Peroxide Bound to a Mononuclear Non-Heme iron Site,” *Inorg. Chem.* **41**, 616 (2002).
K. HASHIMOTO, S. NAGATOMO, S. FUJINAMI, H. FURUTACHI, S. OGO, M. SUZUKI, A. UEHARA, Y. MAEDA, Y. WATANABE and T. KITAGAWA, “A New Mononuclear Iron(III) Complex Containing a Peroxocarbonate Ligand,” *Angew. Chem. Int. Ed. Engl.* **41**, 1201 (2002).
S. KATO, H. -J. YANG, T. UENO, S. OZAKI, G. N. PHILLIPS, Jr., S. FUKUZUMI and Y. WATANABE, “Asymmetric Sulfoxidation and Amine Binding by H64D/V68A and H64D/V68S Mb: Mechanistic Insight into the Chiral Discrimination Step,” *J. Am. Chem. Soc.* **124**, 8506 (2002).
K. OHKUBO, R. TAYLOR, O. V. BOLTALINA, S. OGO and S. FUKUZUMI, “Electron Transfer Reduction of a Highly Electron-Deficient Fullerene, C₆₀F₁₈,” *Chem. Commun.* **41**, 1202 (2002).
M. Y. ALI, S. UEMURA, K. ADACHI, H. ITOH, K. KINOSITA, Jr. and S. ISHIWATA, “Myosin V is a Left-Handed Spiral Motor on the Right-Handed Actin Helix,” *Nature Struct. Biol.* **9**, 464 (2002).
T. MASAIKE, E. MUNAYUKI, H. NOJI, K. KINOSITA, Jr. and M. YOSHIDA, “F₁-ATPase Changes its Conformations upon Phosphate Release,” *J. Biol. Chem.* **277**, 21643 (2002).
Y. HIRONO-HARA, H. NOJI, M. NISHIMURA, E. MUNAYUKI, K. Y. HARA, R. YASUDA, K. KINOSITA, Jr. and M. YOSHIDA, “Pause and Rotation of F₁-ATPase during Catalysis,” *Proc. Natl. Acad. Sci. U.S.A.* **98**, 13649 (2001).
H. NAKAJIMA, E. NAKAGAWA, K. KOBAYASHI, S. TAGAWA and S. AONO, “Ligand-Switching Intermediates for the CO-Sensing Transcriptional Activator CooA Measured by Pulse Radiolysis,” *J. Biol. Chem.* **276**, 37895 (2001).
V. RUBTSOV, T. ZHANG, H. NAKAJIMA, S. AONO, G. I. RUBTSOV, S. KUMAZAKI and K. YOSHIHARA, “Conformational Dynamics of Transcriptional Regulator CooA Protein Studied by Subpicosecond

Mid-Infrared Vibrational Spectroscopy," *J. Am. Chem. Soc.* **123**, 10056 (2001).

S. AONO, T. KATO, M. MATSUKI, H. NAKAJIMA, T. OHTA, T. UCHIDA and T. KITAGAWA, "Resonance Raman and Ligand Binding Studies of the Oxygen Sensing Signal Transducer Protein HemAT from *Bacillus subtilis*," *J. Biol. Chem.* **277**, 13528 (2002).

R. DAVYDOV, V. KOFMAN, H. FUJII, T. YOSHIDA, M. IKEDA SAITO and B. M. HOFFMAN, "Catalytic Mechanism of Heme Oxygenase Through EPR and ENDOR of Cryoreduced Oxy-Heme Oxygenase and its Asp140 Mutants," *J. Am. Chem. Soc.* **124**, 1798 (2002).

H. FUJII, "¹³C-NMR Signal Detection of Iron Bound Cyanide Ions in Ferric Cyanide Complexes of Heme Proteins," *J. Am. Chem. Soc.* **124**, 5936 (2002).

N. OKISHIO, T. TANAKA, M. NAGAI, R. FUKUDA, S. NAGATOMO and T. KITAGAWA, "Identification of Tyrosine Residues Involved in Ligand Recognition by the Phosphatidylinositol 3-Kinase Src Homology 3 Domain: Circular Dichroism and UV Resonance Raman Studies," *Biochemistry* **40**, 15797 (2001).

S. ITOH, H. BANDO, M. NAKAGAWA, S. NAGATOMO, T. KITAGAWA, K. D. KARLIN and S. FUKUZUMI, "Formation, Characterization, and Reactivity of Bis(μ -oxo)dinickel(III) Complexes Supported by A Series of Bis[2-(2-pyridyl)ethyl]amine Ligands," *J. Am. Chem. Soc.* **123**, 11168 (2001).

S. ITOH, H. KUMEI, M. TAKI, S. NAGATOMO, T. KITAGAWA and S. FUKUZUMI, "Oxygenation of Phenols to Catechols by A (μ - η^2 : η^2 -Peroxo)dinickel(II) Complex: Mechanistic Insight into the Phenolase Activity of Tyrosinase," *J. Am. Chem. Soc.* **123**, 6708 (2001).

Y. MIZUTANI and T. KITAGAWA, "Ultrafast Structural Relaxation of Myoglobin Following Photodissociation of Carbon Monoxide Probed by Time-Resolved Resonance Raman Spectroscopy," *J. Phys. Chem. B* **105**, 10992 (2001).

Y. MIZUTANI and T. KITAGAWA, "Ultrafast Dynamics of Myoglobin Probed by Time-Resolved Resonance Raman Spectroscopy," *Chem. Records* **1**, 258 (2001).

T. TOMITA, S. OGO, T. EGAWA, H. SHIMADA, N. OKAMOTO, Y. IMAI, Y. WATANABE, Y. ISHIMURA and T. KITAGAWA, "Elucidation of the Differences between the 430- and 455-nm Absorbing Forms of P450-Isocyanide Adducts by Resonance Raman Spectroscopy," *J. Biol. Chem.* **276**, 36261 (2001).

A. WADA, S. OGO, S. NAGATOMO, T. KITAGAWA, Y. WATANABE, K. JITSUKAWA and H. MASUDA, "Reactivity of Hydroperoxide Bound to a Mononuclear Non-Heme Iron Site," *Inorg. Chem.* **41**, 616 (2002).

S. AONO, T. KATO, M. MATSUKI, H. NAKAJIMA, T. OHTA, T. UCHIDA and T. KITAGAWA, "Resonance Raman and Ligand Binding Studies of the Oxygen-Sensing Signal Transducer Protein HemAT from *Bacillus Subtilis*," *J. Biol. Chem.* **277**, 13528 (2002).

M. AKI, T. OGURA, Y. NARUTA, T. H. LE, T. SATO and T. KITAGAWA, "UV Resonance Raman Characterization of Model Compounds of Tyr244 of Bovine Cytochrome *c* Oxidase in Its Neutral, Deprotonated Anionic, and Deprotonated Neutral Radical Forms: Effects of Covalent Binding between Tyrosine and Histidine," *J. Phys. Chem. A* **106**, 3436 (2002).

N. HARUTA and T. KITAGAWA, "Time-Resolved UV Resonance Raman Investigation of Protein Folding Using a Rapid Mixer: Characterization of Kinetic Folding Intermediates of Apomyoglobin," *Biochemistry* **41**, 6595 (2002).

K. HASHIMOTO, S. NAGATOMO, S. FUJINAMI, H. FURUTACHI, S. OGO, S. SUZUKI, A. UEHARA, Y. MAEDA, Y. WATANABE and T. KITAGAWA, "A New Mononuclear Iron(III) Complex Containing a Peroxocarbonate Ligand," *Angew. Chem. Int. Ed. Engl.* **41**, 1202 (2002).

H. HAYASHI, K. UOZUMI, S. FUJINAMI, S. NAGATOMO, K. SHIREN, H. FURUTACHI, M. SUZUKI, A. UEHARA and T. KITAGAWA, "Modulation of the Copper-Dioxygen Reactivity by Stereochemical Effect of Tetradentate Tripodal Ligands," *Chem. Lett.* 416 (2002).

S. HIROTA, Y. MIZOGUCHI, O. YAMAUCHI and T. KITAGAWA, "Observation of an Isotope-Sensitive Low-Frequency Raman Band Specific to Metmyoglobin," *J. Biol. Inorg. Chem.* **7**, 217 (2002).

T. KITAGAWA, N. HARUTA and Y. MIZUTANI, "Time-Resolved Resonance Raman Study on Ultrafast Structural Relaxation and Vibrational Cooling of Photodissociated Carbonmonoxy Myoglobin," *Biopolymers* **67**, 207 (2002).

Y. MIZUTANI and T. KITAGAWA, "Mode Dependence of Vibrational Energy Redistribution in Nickel Tetraphenylporphyrin Probed by Picosecond Time-Resolved Resonance Raman Spectroscopy: Slow IVR to Phenyl Peripherals," *Bull. Chem. Soc. Jpn.* **75**, 965 (2002).

S. NAGATOMO, Y. JIN, M. NAGAI, H. HORI and T. KITAGAWA, "Changes in the Abnormal α -Subunit upon CO-Binding to the Normal β -Subunit of Hb M Boston: Resonance Raman, EPR and CD Study," *Biophys. Chem.* **98**, 217 (2002).

S. NAGATOMO, M. NAGAI, N. SHIBAYAMA and T. KITAGAWA, "Differences in Changes of the α 1- β 2 Subunit Contacts between Ligand Binding to the α and β Subunits of Hemoglobin A: UV Resonance Raman Analysis Using Ni-Fe Hybrid Hemoglobin," *Biochemistry* **41**, 10010 (2002).

A. SATO, Y. SASAKURA, S. SUGIYAMA, I. SAGAMI, T. SHIMIZU, Y. MIZUTANI and T. KITAGAWA, "Stationary and Time-Resolved Resonance Raman Spectra of His77 and Met95 Mutants of the Isolated Heme Domain of a Direct Oxygen Sensor from *E. coli*," *J. Biol. Chem.* **277**, 32650 (2002).

M. TAKI, S. TERAMAE, S. NAGATOMO, Y. TACHI, T. KITAGAWA, S. ITOH and S. FUKUZUMI, "Fine-

Tuning of Copper(I)-Dioxygen Reactivity by 2-(2-Pyridyl)ethylamine Bidentate Ligands," *J. Am. Chem. Soc.* **124**, 6367 (2002).

B. VENKATESH, H. HORI, G. MIYAZAKI, S. NAGATOMO, T. KITAGAWA and H. MORIMOTO, "Coordination Geometry of Cu-Porphyrin in Cu(II)-Fe(II) Hybrid Hemoglobins Studied by Q-Band EPR and Resonance Raman Spectroscopies," *J. Inorg. Biochem.* **88**, 310 (2002).

REVIEW ARTICLES AND TEXTBOOKS

Department of Theoretical Studies

S. NAGASE and K. HIRAO, *Advance in Molecular Theory. Introduction to Modern Chemistry* (in Japanese), Iwanami; Tokyo (2002).

K. KOBAYASHI, "Theoretical Prediction and Design of Endohedral Metallofullerenes," *Chemical Industry* (in Japanese) **53**, 617 (2002).

Y. SUGITA and Y. OKAMOTO, "Free-Energy Calculations in Protein Folding by Generalized-Ensemble Algorithms," *Lecture Notes in Computational Science and Engineering*, T. Schlick and H. H. Gan, Eds. Springer-Verlag; Berlin, 304 (2002).

Y. OKAMOTO, "Computer Simulations of Protein Folding," *Computational Science* (in Japanese), *Japanese Scientific Monthly (GAKUJUTSU GEPPU)* **55**, 28 (2002).

K. NAGAYA, Y. TERANISHI and H. NAKAMURA, "Selective Excitation Among Closely Lying Multi-Levels," in *Laser Control and Manipulation of Molecules*, A. Bandrauk, R. J. Gordon and Y. Fujimura, Eds., ACS Symposium Series 821, American Chemical Society (2002).

H. NAKAMURA, *Nonadiabatic Transition: Concepts, Basic Theories and Applications*, World Scientific/Imperial College Press; Singapore (2002).

T. NAKAJIMA, T. TSUNEDA, H. NAKANO and K. HIRAO, "Recent Advances in Electronic Structure Theory," *J.Theor.Comput.Chem.* **1**, 109 (2002).

H. NAKANO, K. SORAKUBO, K. NAKAYAMA and K. HIRAO, "Complete Active Space Valence Bond (CASVB) Method and its Application to Chemical Reactions," *Valence Bond Theory*, David Cooper, Ed., Elsevier, 55 (2002).

T. NAKAJIMA, T. YANAI and K. HIRAO, "Relativistic Electronic Structure Theory," *J. Comput. Chem.* **23**, 847 (2002).

Department of Molecular Structure

T. YOKOYAMA, "Theory of XAFS," in *X-ray Absorption Spectroscopy: XAFS and its Applications* (in Japanese), T. Ohta, Ed., IPC Inc.; Tokyo, 7 (2002).

T. KATO, T. AKASAKA, K. TASHIRO and T. AIDA, "An Inclusion Complex of a Cyclic Dimer of Metalloporphyrin with La@C₈₂," *Proceedings of the International Symposium on Fullerenes, Nanotubes, and Carbon Nanoclusters*, P. V. Kamat, D. M. Guldi and K. M. Kadish, Eds., The Electrochemical Society, Inc.; Pennington, **11**, 354 (2001).

S. OKUBO and T. KATO, "Spin Dynamics of Lanthanum Metallofullerenes," *The Proceedings of the International Symposium on Nanonetwork Materials, Fullerenes, Nanotubes, and Related Systems*, S. Saito et al., Eds., AIP Conference Proceedings, **590**, 469 (2001).

Department of Electronic Structure

T. SUZUKI, L. WANG and H. KOHGUCHI, "Femtosecond Time-Resolved Photoelectron Imaging," in *Imaging in Chemical Dynamics*, ACS Symposium Series 770 (2001).

T. SUZUKI and B. J. WHITAKER, "Non-Adiabatic Dynamics Effects in Chemistry Revealed by Time-Resolved Charged Particle Imaging," *International Reviews of Physical Chemistry* **20**, 313 (2001).

H. KOHGUCHI and T. SUZUKI, "Rotational Inelastic Scattering of Free Radicals," *Annual Report on the Progress of Chemistry* (2002).

T. SUZUKI, "Femtosecond Time-Resolved Photoelectron Imaging," in *Advances in Physical Chemistry*, World Scientific; Singapore (2002).

T. SUZUKI and S. NANBU, "Non-Adiabatic Bending Dissociation of OCS," in *Low-Lying Potential Energy Surfaces*, ACS Symposium Series 828 (2002).

T. YAMASE, "Current Topics on Antiviral Drugs, Topics 4: Antiviral Activity of Polyoxometalates for a Novel Typed Inorganic Drug," *J. Clinical & Experimental Medicine* **201**, 262 (2002).

T. YAMASE, "Time-Resolved ESR-Spectroscopic Investigation of Polyoxometalate Photochemistry," *Catalysts & Catalysis* **44**, 340 (2002).

Department of Molecular Assemblies

T. NAKAMURA, M. TANIGUCHI, Y. MISAKI, K. TANAKA and Y. NOGAMI, "ESR Investigation of Organic Conductor with Itinerant and Local Spins, (CHTM-TTP)₂TCNQ," in *EPR in the 21st Century*, A.

Kawamori, J. Yamauchi and H. Ohta, Eds., Elsevier Science; Amsterdam, 192 (2002).

Department of Applied Molecular Science

H. IWAMURA and K. INOUE, "Magnetic Ordering in Metal Coordination Complexes with Aminoxyl Radicals," *Magnetism: Molecules to Materials II, Molecule-Based Materials*, J. S. Miller and M. Drillon, Eds., 61 (2001).

K. INOUE, "Nitroxide Radical-Metal-Based Molecular Magnets," *π -Electron Magnetism-From Molecules to Magnetic Materials-, Structure & Bonding*, J. Veciana Ed., Springer-Verlag; Heidelberg, **100**, 61 (2001).

M. HASHIMOTO, T. YUZAWA, C. KATO, K. IWATA and H. HAMAGUCHI, "Fast Time-Resolved Mid-Infrared Spectroscopy Using Grating Spectrometers," in *Handbook of Vibrational Spectroscopy*, J. M. Chalmers and P. R. Griffiths Eds., John Wiley & Sons; West Sussex, **1**, 666 (2002).

H. HAMAGUCHI and K. IWATA, "Physics and Chemistry of S_1 *trans*-Stilbene in Solution as Studied by Time-Resolved Raman Spectroscopy," *Bull. Chem. Soc. Jpn.* **75**, 883 (2002).

H. KATAURA, T. KODAMA, K. KIKUCHI, H. HIRAHARA, S. IJIMA, S. SUZUKI, W. KRÄTSCHMER and Y. ACHIBA, "Optical Properties of Fullerene-Peapods," in *Nanonetwork Materials: Fullerenes, Nanotubes, and Related Systems*, S. Saito, T. Ando, Y. Iwasa, K. Kikuchi, M. Kobayashi and Y. Saito, Eds., American Institute of Physics Conference Proceedings; Melville, N. Y., **590**, 165 (2001).

K. SUEKI, K. AKIYAMA, C. KURATA, K. OOGAMA, Y. L. ZHAO, M. KATADA, S. ENOMOTO, S. AMBE, F. AMBE, H. NAKAHARA and K. KIKUCHI, "Behaviors of Metals in Production of Nanonetwork Materials Investigated by Radiochemical Technique," in *Nanonetwork Materials: Fullerenes, Nanotubes, and Related Systems*, S. Saito, T. Ando, Y. Iwasa, K. Kikuchi, M. Kobayashi and Y. Saito, Eds., American Institute of Physics Conference Proceedings; Melville, N. Y., **590**, 313 (2001).

T. ISHII, R. KANEHAMA, N. AIZAWA, M. YAMASHITA, H. MATSUZAKA, H. MIYASAKA, T. KODAMA, K. KIKUCHI, I. IKEMOTO, Y. IWASA and M. SHIRO, "Synthesis and Crystal Structure of Cocrystallite with Silver Octaethylporphyrin and C_{70} ," in *Nanonetwork Materials: Fullerenes, Nanotubes, and Related Systems*, S. Saito, T. Ando, Y. Iwasa, K. Kikuchi, M. Kobayashi and Y. Saito, Eds., American Institute of Physics Conference Proceedings; Melville, N. Y., **590**, 409 (2001).

K. AKIYAMA, K. SUEKI, Y. L. ZHAO, H. HABA, K. TSUKADA, T. KODAMA, K. KIKUCHI, T. OHTSUKI, Y. NAGAME, H. NAKAHARA and M. KATADA, "Characterization of Actinide Metallofullerenes," in *Nanonetwork Materials: Fullerenes, Nanotubes, and Related Systems*, S. Saito, T. Ando, Y. Iwasa, K. Kikuchi, M. Kobayashi and Y. Saito, Eds., American Institute of Physics Conference Proceedings; Melville, N. Y., **590**, 437 (2001).

M. CHIKAMATSU, K. KIKUCHI, T. KODAMA, H. NISHIKAWA, I. IKEMOTO, N. YOSHIMOTO, T. HANADA, Y. YOSHICA, N. TANIGAKI and K. YASE, "Out-of-Plane and In-Plane Structure of the Cast Films of Long Alkyl Chain-Linked C_{60} via Phenyl Ring," in *Nanonetwork Materials: Fullerenes, Nanotubes, and Related Systems*, S. Saito, T. Ando, Y. Iwasa, K. Kikuchi, M. Kobayashi and Y. Saito, Eds., American Institute of Physics Conference Proceedings; Melville, N. Y., **590**, 455 (2001).

K. KIKUCHI, K. SAKAGUCHI, N. OZAWA, T. KODAMA, H. NISHIKAWA, I. IKEMOTO, K. KOHDATE, D. MATSUMURA, T. YOKOYAMA and T. OHTA, "Valence Change of Tm Atom in Metallofullerene," in *Nanonetwork Materials: Fullerenes, Nanotubes, and Related Systems*, S. Saito, T. Ando, Y. Iwasa, K. Kikuchi, M. Kobayashi and Y. Saito, Eds., American Institute of Physics Conference Proceedings; Melville, N. Y., **590**, 473 (2001).

Coordination Chemistry Laboratories

Y. UOZUMI, K. SHIBATOMI, "Preparation of Optically Active Phosphines as Catalysts for Asymmetric Synthesis," *Jpn. Kokai Tokkyo Koho* **7** (2001).

Y. UOZUMI, "Palladium Catalysis in Water," in *My Favorite Organic Synthesis*, The Society of Synthetic Organic Chemistry; Japan, 242 (2002).

Y. UOZUMI, "Combinatorial Approaches towards Organic Synthetic Catalysts," *J. Soc. Synth. Org.* **60**, 434 (2002).

Y. UOZUMI and T. HAYASHI, "Solid-Phase Palladium Catalysis for High-Throughput Organic Synthesis," in *Combinatorial Chemistry-A Practical Handbook*, R. Hanco, P. Göllitz and K. C. Nicolaou, Eds., Wiley-VCH; Weinheim, Germany (2002).

N. TOKITOH, "New Aspects in the Chemistry of Silaaromatic Compounds," *Organometallic News* (in Japanese) **6** (2002).

K. ONITSUKA, F. TAKEI and S. TAKAHASHI, "Syntheses and Properties of Helical Chiral Polyisocyanides," *Kobunshi Kako* (in Japanese) **50**, 122 (2001).

F. TAKEI, K. ONITSUKA and S. TAKAHASHI, "Screw-Sense-Selective Polymerization of Isocyanides," *Jasco Report* (in Japanese) **43**, 47 (2001).

S. TAKAHASHI and K. ONITSUKA, "Precise Synthesis of Organometallic Macromolecules," *Kagaku Kogyo* (in Japanese) **52**, 919 (2001).

K. ONITSUKA and S. TAKAHASHI, "Precise Synthesis of Helical Chiral Polymers Catalyzed by Transition Metal Complexes," *Syokubai* (in Japanese) **44**, 334 (2002).

Laser Research Center for Molecular Science

Z. LIU, N. SARUKURA and M. A. DUBINSKII, "All-Solid-State, Short-Pulse, Tunable, Ultraviolet Laser Sources Based on Ce³⁺ Activated Fluoride Crystals," in *Ultraviolet Spectroscopy and UV Lasers*, P. Misra and M. A. Dubinskii, Eds., Marcel Dekker; New York (2002).

I. SHOJI, T. TAIRA and A. IKESUE, "Ceramic Lasers," *The Transactions of the Institute of Electronics, Information and Communication Engineers C* **J84-C**, 918 (2001).

T. TAIRA, et al., "Optical Society in Future," *CD-ROM, Kagaku* (in Japanese) **31**, (2002).

A. IKESUE, T. TAIRA and K. YOSHIDA, "The Fabrication of Nd:YAG Ceramics with Extremely Low Optical Scattering and the Development of High Performance Ceramic Laser," *Fine Ceramics Report* (in Japanese) **20**, 192 (2002).

Research Center for Molecular-scale Nanoscience

H. TADA and S. TANAKA, "Electrical Measurement in Molecular-Scale," in *Molecular Nanotechnology* (in Japanese), K. Matsushige and K. Tanaka, Eds., Kagaku Dojin; Kyoto (2002).

Y. NEGISHI and T. TSUKUDA, "Synthesis and Mass Spectroscopic Characterization of Metal Clusters," *Aerosol Kenkyu* (in Japanese) **17**, 9 (2002).

M. KOMIYAMA, *Handbook of Interfaces*, Y. Iwasawa, Y. Umezawa, T. Sawada and K. Tsujii, Eds., NTS; Tokyo (2001).

N. UENO, K. K. OKUDAIRA, Y. AZUMA, S. KERA and S. HASEGAWA, "Studies of Organic Thin Films and Interfaces by Various Electron Spectroscopies: Molecular Orientation, Electronic States and Reactions," in *Conjugated Polymer and Molecular Interfaces: Science and Technology for Photonic and Optoelectronic Applications*, Salaneck, Seki, Kahn and Pireaux, Eds., Marcel Dekker Inc; NY, **6** 153 (2001).

Y. KUBOZONO, "Preparation of Fullerene-Based Hybrid Materials," *Kagaku Kogyo* **53**, 13 (2002).

Computer Center

T. SUZUKI and S. NANBU, "Non-Adiabatic Bending Dissociation of OCS Induced by Orbital Unlocking," in *Symposium Series No. 828/Low-Lying Potential Energy Surfaces*, American Chemical Society Books (2002).

Center for Integrative Bioscience

Y. WATANABE, "Constriction of Heme Enzymes: Four Approaches," *Curr. Opin. Chem. Biol.* **6**, 208 (2002).

R. YAMAHARA, S. OGO, H. MASUDA and Y. WATANABE, "(Catecholato)iron(III) Complexes: Structural and Functional Models for the Catechol-Bound Iron(III) Form of Catechol Dioxygenases," *J. Inorg. Biochem.* **88**, 284 (2002).

Y. WATANABE, "Two-Electron Oxidized Derivatives of Fe(III) Porphyrins," *J. Biol. Inorg. Chem.* **6**, 846 (2001).

S. AONO, "Gene Regulation by CO: Structure and Function of the CO-Sensing Transcriptional Regulator CooA," *Kagaku to Seibutsu* (in Japanese) **40**, 206 (2002).

S. AONO, "CO Receptor System in a Microorganism," *Igaku no Ayumi* (in Japanese) **201**, 533 (2002).

H. FUJII, "Electronic Structure and Reactivity of High-Valent Oxo Iron Porphyrins," *Coord. Chem. Rev.* **226**, 51 (2002).

H. FUJII, "Oxygen Activation Mechanism of Heme Oxygenase," *Chemical Industry* (in Japanese) **53**, 18 (2002).

T. KITAGAWA and S. HIROTA, "Raman Spectroscopy of Proteins," in *The Handbook of Vibrational Spectroscopy*, J. M., Chalmers and P. R. Griffiths, Eds., John Wiley & Sons; Chichester (2002).

Y. MIZUTANI and T. KITAGAWA, "Vibrational Energy Relaxation of Metalloporphyrins in a Condensed Phase Probed by Time-Resolved Resonance Raman Spectroscopy," *Bull. Chem. Soc. Jpn.* **75**, 623 (2002).

Y. MIZUTANI, K. YAMAMOTO and T. KITAGAWA, "Studies on Dynamics of Protein Folding/Unfolding by Using the Laser-Induced Temperature Jump Technique," *Tanpakusitsu Kakusan Kouso* (in Japanese) **47**, 670 (2002).

AUTHOR INDEX

to "Research Activities" and "Special Research Projects"

A

ABURA, Tsutomu 218
 ACHIBA, Yohji 114
 ADACHI, Kengo 219
 ADACHI, Takahiro 18
 AIZAWA, Keizo 211
 AKAGI, Hiroshi 35
 AKAI, Yoshio 33
 AKASAKA, Takeshi 19, 59
 AKHTARUZZAMAN, Md. 184
 AKI, Michihiko 217
 AKIBA, Kin-ya 18
 AKUTSU, Hideo 52
 AKUTSU, Hiroki 115
 ALI, Md. Yusuf 219
 AMEMIYA, Kenta 56
 ANDO, Tomohiro 61
 AOKI, Hidekazu 209–210
 AOKI, Yasuhito 81
 AOKI, Yasushi 165–166
 AONO, Shigetoshi 221
 AONUMA, Shuji 91
 AOYAGI, Mutsumi
 24–25, 132, 212–213, 235
 ARA, Masato 180–181
 ARAI, Yoshimitsu 158
 ARII, Hidekazu 110
 ARII, Taro 142
 ARZHANTSEV, Sergei, Yu. 128
 ASAUMI, Taku 149
 AZUMA, Yasushi 194

B

BABA, Miyuki 102
 BAER, Andrew J. 148
 BANDARA, Athula 55
 BANDO, Hideki 227
 BARTASHEVICH, M. I. 104
 BAUNE, Micheal 134
 BENSALAH, Amina 163–164
 BERBER, Savas 33

BHATTACHARYYA, Kankan 128
 BIAN, Wensheng 24–25, 212
 BOTAR, Bogdan 78

C

CEOLINE, Denis 208–209
 CHANG, Suk-Kyu 213
 CHATANI, Naoto 149
 CHE, Dock-Chil 117, 234
 CHEN, X. H. 197
 CHI, Dam Hieu 197
 CHOE, Jong-In 213
 CHOE, Yoong-Kee 19
 CHONG, Song-Ho 38
 CUI, HengBo 99
 CUSANOVICH, Michael A. 52
 CÔTE, Adrien P. 148
 ČÍŽEK, M. 27

D

DAIGOKU, Kota 72–73
 DASCALU, Traian 175, 243
 DAVIDSON, Gerg J. E. 148
 DAVYDOV, Roman 224
 DENNISON, Christopher 228
 DESSENT, Caroline E. H. 74
 DOI, Yo-ichiro 206
 DOMEN, Kazunari 55
 DROZDOVA, Olga 90

E

EINAGA, Hisahiko 109–110
 EMURA, Shuichi 198
 ENDO, Hiroaki 102
 ENOKI Toshiaki 87

F

FENG, Fei 162

FUJII, Hiroshi 223–224, 246–247
 FUJII, Masaaki 72–74, 237
 FUJII, Ryosuke 114
 FUJIKI, Satoshi 197–198
 FUJIMORI, Atsushi 145
 FUJIMORI, Shin-ichi 145
 FUJINAMI, Shuhei 216–227
 FUJINO, Tatsuya 128
 FUJIO, Mizue 156
 FUJISAKI, Hiroshi 25, 214, 233
 FUJIWARA, Akihiko 197–198
 FUJIWARA, Emiko 94–99, 241
 FUJIWARA, Hideki
 94–96, 98–99, 241
 FUJIWARA, Masahiro 100
 FUJIWARA, Masao 199
 FUJIWARA, Toshimichi 52
 FUJIWARA, Umihito 202
 FUJIWARA, Yoshihisa 199
 FUJIYAMA, Shigeki 91, 241
 FUJIYOSHI, Satoru 127
 FUKAMINATO, Tuyoshi 67
 FUKAYA, Norihisa 18
 FUKUDA, Atsuo 61
 FUKUDA, Satoshi 146
 FUKUDA, Tsuguo 163–164, 166
 FUKUI, Kazutoshi 206
 FUKUMOTO, Yoshiya 149
 FUKUNISHI, Arima 52
 FUKUOKA, Yuki 52
 FUKUSHIMA, Nobuhiro 107
 FUKUYAMA, Tetsuya 234
 FUKUZUMI, Shun-ichi
 215, 217, 226–227
 FUNAHASHI, Yasuhiro 107, 223
 FUNASAKI, Noriaki 144
 FURUKAWA, Ko 59, 240
 FURUKAWA, Sachie 145
 FURUKAWA, Yukio 158
 FURUTACHI, Hideki 216, 227

G

GAO, Feixue 79
 GEJO, Tatsuo 206–209, 238
 GEORGESCU, Serban 169
 GONZALEZ, Miguel 212
 GOTO, Takeshi 200
 GOTO, Tsuneaki 104
 GRAAF, Harald 134, 179–181
 GRAY, Stephen K. 212
 GRITSENKO, Victor 95
 GU, Minming 192
 GU, Ning 192, 245
 GUILLEMIN, Renaud 208–209
 GUILLEVIC, J. 87
 GUO, Jinghua 124

H

HAMA, Hiroyuki 206
 HAMAGUCHI, Hiro-o 112–113, 129
 HAN, Jin Wook 141
 HAN, Rushan 19
 HANAN, Gerry S. 148
 HANASAKI, Mitsuru 202
 HARA, Kazunori 144
 HARA, Kiyotaka Y. 219
 HARA, Toru 205, 246
 HARADA, Erisa 52
 HARADA, Kensuke 212
 HARADA, Yoshiya 194
 HARANO, Yuichi 239
 HARASAWA, Ayumi 210
 HARATA, Manabu 110
 HAREAU, G. P. -J 144
 HARUTA, Nami 228
 HARUYAMA, Yusuke 139, 197
 HASEGAWA, Shinji 126, 195
 HASHIMOTO, Kazuhito 57
 HASHIMOTO, Kenro 72–73
 HASHIMOTO, Koji 216, 227
 HASHINOKUCHI, Mitihiro 117, 234
 HATANO, Ken 157, 160
 HATSUI, Takaki 123–124, 207–209, 234
 HAYASHI, Hideki 227
 HAYASHI, Hiroko 162
 HAYASHI, Kenji 205–206, 246
 HAYASHI, Naoki 61
 HAYASHI, Tamio 141
 HAYMET, Anthony D. J. 211
 HEMMERS, Oliver 209
 HIGUCHI, Yoshiki 52
 HIKOSAKA, Yasumasa 135
 HINO, Kazuyuki 63–64
 HINO, Osamu 31
 HINO, Takami 244
 HIRAKI, Koichi 88–89
 HIRANO, Masahiro 163, 165
 HIRAO, Kimihiko 34
 HIRATA, Fumio 21, 36–39, 239
 HIRATE, Seiji 141

HIRAYAMA, Chuichi 144
 HIRONO-HARA, Yoko 219
 HIROSE, Chiaki 55
 HIROSUMI, Tomoya 165
 HIYAMA, Miyabi 27
 HOFFMAN, M. Brian 224
 HONDA, Toru 205
 HONG, S. O. 210
 HONKAWA, Yoshiki 68–69
 HORI, Hiroshi 226
 HORI, Yoichiro 205, 246
 HORÁČEK, J. 27
 HOSAKA, Masahito 205–206, 246
 HOSHIDE, Yasuhiro 144
 HOSOKAWA, Tomoko 197–198
 HOSOKOSHI, Yuko 104–106, 241
 HOSONO, Hideo 163, 165
 HOWARD, Daryl L. 74
 HUDECECK, Jiri 133

I

ICHIKAWA, Shinji 121
 ICHIMURA, Teijiro 73
 ICHINOHE, Masaki 18
 IGA, Fumiroshi 210
 IIMORI, Toshifumi 81
 IKAI, Atsushi 211
 IKEBE, Hisami 144
 IKEDA, Ryuichi 198
 IKEDA, Tsutomu 149
 IKEDA-SAITO, Masao 224
 IKEMOTO, Isao 114–115
 IKESUE, Akio 168–169, 171
 IMABAYASHI, Shinichiro 52
 IMAI, H. 210
 IMAI, Takashi 37, 39, 239
 IMAMURA, Motoyasu 195
 IMURA, Kohei 47–48, 116, 237
 INO, Akihiro 145
 INO, Haruhiro 60
 INOKUCHI, Makoto 86
 INOKUCHI, Yoshiya 64, 66, 68–69
 INOUE, Hiroki 149
 INOUE, Katsuya 103–106, 241
 IRIE, Masahiro 67
 ISE, Toshihiro 92
 ISHIDA, Toshimasa 200–201, 212
 ISHIDA, Yutaka 18
 ISHII, Hisao 195
 ISHII, Kenji 197
 ISHII, Tomohiko 145, 147
 ISHIKAWA, Eri 78
 ISHIKAWA, Hironori 113
 ISHIKAWA, Yasuyuki 34
 ISHIMOTO, Hitoshi 144
 ISHIMURA, Kazuya 239
 ISHIUCHI, Shun-ichi 72–74
 ISHIWATA, Shin'ichi 219
 ISHIYAMA, Fumihiko 209

ISHIZUKI, Hideki 243
 ITO, Akihiro 60
 ITO, Hajime 185, 244
 ITO, Hiroshi 145
 ITO, Kaname 244
 ITO, Kazuhiko 195
 ITO, Naoko 165
 ITO, Takayoshi 197
 ITOH, Hiroyasu 219
 ITOH, Minoru 206
 ITOH, Shinobu 226–227
 IWAHASHI, Kensuke 211, 235
 IWAHORI, Fumiyasu 145
 IWAI, Mitsuru 144
 IWASA, Yoshihiro 197
 IWASAKI, Kazuaki 194
 IWASAWA, Yasuhiro 55
 IWATA, Hideki 209–210
 IWATA, Koichi 111–113

J

JEUNG, Gwang-Hi 201
 JIN, Yayoi 226
 JITSUKAWA, Koichiro 107–110, 216, 227
 JUNG, M. H. 210

K

KACHI-TERAJIMA, Chihiro 145
 KAKIUCHI, Fumitoshi 149
 KAMADA, Masao 206, 246
 KAMBE, Takashi 197
 KAMISAKA, Hideyuki 23–25, 212, 233
 KAMITANI, Akihito 149
 KAMIYA, Muneaki 34
 KANBARA, Takayoshi 197–198
 KANDA, Seiichi 198
 KANEMOTO, Katsuichi 60
 KANO, Satoru S. 55
 KANODA, Kazushi 88–89
 KANYA, Reika 82
 KARLIN, Kenneth D. 227
 KASAI, Toshio 116–118, 132, 234
 KASHINO, Setuo 197–198
 KATANO, Satoshi 55
 KATAYANAGI, Hideki 76–77, 234
 KATO, Reizo 91, 100
 KATO, Shigeru 215
 KATO, Takashi 19, 109
 KATO, Tatsuhisa 58–61, 240
 KATO, Toshiyuki 221
 KATO, Tsuyoshi 29
 KATOH, Keiichi 104–105, 241
 KATOH, Kouichi 119
 KATOH, Masahiro 205–206, 246
 KATSUKI, Akio 199
 KAWAGUCHI, Hiroyuki 154–155, 243
 KAWAI, Gota 52

- KAWAI, Tsuyoshi 67
 KAWAKAMI, Tomonori 211
 KAWAMOTO, Atsushi I 85
 KAWAMOTO, Tadashi 88
 KAWAMURA, Ken-ichi 165
 KAWATSURA, Motoi 141
 KERA, Satoshi 194
 KIDO, Giyu 209
 KIKUCHI, Koichi 103, 114–115
 KIKUGAWA, Shinya 163
 KIKUZAWA, Yoshihiro 244
 KIM, Kyoung Hoon 201
 KIM, Sang Kyu 76
 KIMURA, Masahiro 17, 156, 158
 KIMURA, Shin-ichi 209–210, 246
 KINOSHITA, Masahiro 21, 37, 39, 239
 KINOSHITA, Shin-ichi 73
 KINOSHITA, Toshio 205, 246
 KINOSHITA, Toyohiko 210
 KINOSHITA, Kazuhiko, Jr. 219, 235
 KIRITA, Keizo 105
 KISHIDA, Hideo 145, 146
 KISHIKAWA, Kuniyuki 158
 KISHINE, Jun-ichiro 42, 44–45, 239
 KITAGAWA, Hiroshi 198
 KITAGAWA, Soichiro 56
 KITAGAWA, Susumu 147
 KITAGAWA, Teizo 108, 216–217, 221, 225–229, 235
 KITAMURA, Hideo 205, 246
 KITAO, Michihiko 200
 KITAURA, Kazuo 19
 KITAURA, Ryo 147
 KITAYAMA, Kenji 141
 KITAZAWA, Hideaki 209
 KJAERGAARD, Henrik G. 74
 KOBAYAKAWA, Hisashi 196
 KOBAYASHI, Akiko 94–99, 241
 KOBAYASHI, Hayao 94–99, 241
 KOBAYASHI, Kaoru 18–19
 KOBAYASHI, Katsuaki 152
 KOBAYASHI, Kazuo 221
 KOBAYASHI, Mototada 197
 KODA, Shigeru 205
 KODAMA, Takeshi 114
 KOFMAN, Viktoria 224
 KOHGUCHI, Hiroshi 77, 233
 KOHZUMA, Takamitsu 228
 KOJIMA, Hiroshi 73
 KOKUBO, Hironori 233
 KOLORENC', P. 27
 KOMATSU, Shingo 177
 KOMIYAMA, Masaharu 192, 245
 KOMURO, Takashi 154
 KONDO, Mituru 147
 KONDO, Takuhiko 204
 KONDORSKIY, Alexey 26, 233
 KONOSHIMA, Koji 200
 KORETSUNE, Toshihisa 210
 KOSHIYAMA, Tomomi 246
 KOSUGI, Kentaroh 63–64
 KOSUGI, Nobuhiro 123–126, 207–209, 234
 KOU, Junkei 139
 KOUMURA, Ryouji 117
 KOVALENKO, Andriy 39, 239
 KOZEKI, Toshimasa 78, 163–166, 243
 KUBO, Atsushi 121–122, 143–144
 KUBO, Y. 210
 KUBOTA, Jun 55
 KUBOZONO, Yoshihiro 139, 197–198
 KUGISAKI, Hitomi 68–69
 KUMAGAI, Hitoshi 104
 KUMAGAI, Jiro 52
 KUMAZAKI, Shigeichi 221
 KUMITA, Hideyuki 109–110
 KUNIMOTO, Takashi 105
 KUNITAKE, Masashi 144
 KURAHASHI, Takuya 247
 KURIHARA, Tsutomu 194
 KURIMURA, Sunao 168
 KURMOO, Mohamedally 104
 KURODA, Shin-ichi 145–146
 KURODA-SOWA, Takayoshi 146
 KUSAFUKA, Koji 55
 KUSUDA, Masaya 114
 KUWABARA, Makoto 42–43, 239
 KUWAHARA, Daisuke 191
 KUWAYAMA, Shunsuke 196
 KWON, Y. S. 210
L
 LANG, Roy 83
 LANGHOFF, Peter 209
 LE GUEN, Karine 208–209
 LECLERCQ, Nicola 208–209
 LEE, H. J. 210
 LEE, Patrick A. 45
 LEE, Yoon Sup 201
 LEITE, Vitor B. P. 31
 LI, Yanjun 245
 LINDLE, Denis 209
 LIPKOWSKI, Janusz 200
 LIU, Michael T. H. 19
 LIU, Zhenlin 163–164
 LU, Jing 19
 LUBORADZKI, Roman 200
 LUPEI, Aurelia 169, 171
 LUPEI, Voicu 168–169, 171–172, 174
 LUTY, Tadeusz 42
M
 MACHIDA, Hiroshi 163–164
 MAEDA, Yonezo 216, 227
 MAEDA, Yutaka 19, 59
 MAEKAWA, Masahiko 146
 MAITI, Nakul C. 225
 MAKI, Jun 132, 235
 MANABE, Toshio 145–146
 MANDAL, Debabrata 128
 MARUMOTO, Kazuhiro 145–146
 MASADA, Genta 166
 MASAIKE, Tomoko 219
 MASUDA, Hideki 107–110, 216–217, 227
 MASUDA, Suomi 123
 MASUGATA, Kensuke 211
 MATSUDA, Isao 83
 MATSUI, Yuki 60
 MATSUKAWA, Shiro 18
 MATSUKI, Mayumi 221
 MATSUMI, Yutaka 208
 MATSUMOTO, Kenji 107, 109
 MATSUMOTO, Takanori 33
 MATSUMOTO, Taki 245
 MATSUMOTO, Yoshiteru 76, 234
 MATSUMURA, Daiju 56
 MATSUMURA, Hisashi 137
 MATSUNAMI, Masaharu 210
 MATSUO, Tsukasa 154–155, 243
 MATSUSHIGE, Kazumi 179
 MATSUSHITA, Kouji 204
 MATSUZAKA, Hiroyuki 147
 MATSUZAKI, Hiroyuki 145
 MAYER, Bodo 18
 MEECH, S. R. 128
 MENEGHETTI, Moreno 88–89
 MEYER, Terrance E. 52
 MIKAMI, Masuhiro 21
 MIKAMI, Taiji 211, 235
 MIL'NIKOV, G. V. 23–27, 233
 MIN, B. H. 210
 MINABE, Masahiro 202, 245
 MINAMINO, Satoshi 213, 235
 MIRON, Cataline 208–209
 MISAKI, Yohji 87–88, 90, 92, 99
 MISAWA, Kazuhiko 83
 MITANI, Tadaoki 197
 MITSUDA, Akihiro 210
 MITSUKE, Koichiro 135–139, 237
 MITSUTAKE, Ayori 21
 MIURA, Shin-ichi 235
 MIWA, Satoshi 107
 MIYAKE, Yoko 114
 MIYAMAE, Takayuki 195
 MIYASAKA, Hitoshi 145–146
 MIYASHITA, Naoyuki 42–43, 239
 MIYASHITA, Seiji 105
 MIYASHITA, Tokuji 162
 MIYAZAKI, Gentaro 226
 MIYOSHI, Eisaku 68–69
 MIZUNO, Misao 129
 MIZUTANI, Fumio 143
 MIZUTANI, Mamoru 107
 MIZUTANI, Yasuhisa 225, 228–229
 MOCHIHASHI, Akira 205–206
 MORI, Hirotoshi 68–69
 MORI, Takanori 139
 MORI, Takehiko 88, 92
 MORIKAWA, Eiji 194
 MORIMOTO, Hideki 226

- MORIMOTO, Takanobu 114
MORIN, Paul 208–209
MORIOKA, Taiju 110
MORISHIMA, Yuji 108
MORITA, Yoshifumi 45
MORITA, Norio 50, 237
MORITA, Seizo 192
MORITANI, Kousuke 118
MORIWAKI, Yoshiki 50, 237
MORÉ, Sam D. 131, 133–134, 206
MUGURUMA, Chizuru 21
MUKAIDE, Kotaro 141
MUNAKATA, Megumu 146
MUNEYUKI, Eiro 219
MURAI, Shinji 149
MURAKAMI, Hidetoshi 78, 165–166
MURAKAMI, Makoto 200
MURATA, Katsumi 233
MURATA, Keizo 114
MURATA, Yoshitada 118
MURAYAMA, Haruno 187–188, 244
MÜLLER-DETHLEFS, Klaus 74
- N**
- NAGAHARA, Tetsuhiko 48, 237
NAGAI, Hidenori 144
NAGAI, Masako 226
NAGAO, Yuki 198
NAGASE, Shigeru 17–19, 156, 158, 160, 239
NAGASIMA, Takehiro 233
NAGASONO, Mitsuru 123–124, 207, 209
NAGATA, Kazuto 156
NAGATA, Takashi 66, 189–190
NAGATA, Toshi 185–186, 244
NAGATOMO, Shigenori 108, 216, 226–228
NAGAYA, Kuninobu 25–26
NAGAYOSHI, Kanade 19
NAKABAYASHI, Takakazu 65–67
NAKAGAWA, Emi 221
NAKAGAWA, Motonobu 227
NAKAGAWA, Takeshi 240
NAKAI, Hidetaka 217
NAKAJIMA, Hiroshi 221
NAKAJIMA, Takahito 34
NAKAJYO, Terunobu 165–166
NAKAMURA, Eiken 206
NAKAMURA, Hiroki 23–27, 212, 233
NAKAMURA, Mamiko 118
NAKAMURA, Toshikazu 91–93, 241
NAKANISHI, Tsutomu 206
NAKANO, Chikako 86–87
NAKANO, Haruyuki 34
NAKANO, Hiroki 104
NAKATA, Kazuya 145, 147
NAKATA, Norio 158–159
NAKATSUJI, Shin-ichi 115
NAKAZONO, Maki 142
NANBA, Takao 210
NANBU, Shinkoh 24–25, 132, 212–213, 235
NARUKE, Haruo 78–79
NEALSON, Kenneth H. 52
NEGISHI, Yuichi 187–189, 244
NEYA, Saburo 144
NIINO, Yasuyuki 19
NIIZEKI, Tomotake 228
NISHI, Nobuyuki 63–69
NISHI, Tatsuhiko 210
NISHIBORI, Eiji 197
NISHIDE, Tatsuhiko 77, 234
NISHIHARA, Hiroshi 143
NISHIKAWA, Hiroyuki 114–115
NISHIKIORI, Shin-ichi 200–201
NISHIMURA, Masaya 219
NISHINO, Takeshi 225
NISHITANI, Tomohiro 206
NISHIYAMA, Katsuhiko 143–144
NISHIYAMA, Katsura 239
NISHIZAWA, Kiyoshi 234
NOBUSADA, Katsuyuki 24
NODA, Hideyuki 132
NOGAMI, Yoshio 92
NOGUCHI, Hidenori 55
NOGUCHI, Hiroshi 119–120
NOHMI, Kenji 141
NOJI, Hiroyuki 219
NOMURA, Hiroyasu 37
NONOGAKI, Youichi 131–132, 242
NORDGREN, Joseph 124
NORO, Shin-ichiro 147
NOSAKA, Makoto 119, 234
- O**
- OBA, Toru 202, 245
OCHIAI, Akira 209–210
OGASAWARA, Akira 105
OGATA, Hideaki 52
OGAWA, Takuji 102
OGO, Seiji 108, 216–218, 227
OGURA, Takashi 217
OHASHI, Kazuhiko 68–69
OHASHI, Masataka 246
OHKOSHI, Shin-ichi 57
OHMURA, Tomoaki 52
OHOYAMA, Hiroshi 116–117
OHSHIMA, Yasuhiro 81–82
OHSHIMO, Keiji 66
OHTA, Hiroshi 43
OHTA, Hitoshi 105
OHTA, Takehiro 221
OHTA, Toshiaki 56–57
OHTAKE, Hideyuki 78, 165–166, 243
OHTSU, Hideki 152
OISHI, Osamu 180
OJI, Hiroshi 124–126, 207
OKA, Yoshiyuki 108–109
OKABE, Chie 66–67
OKADA, Kozo 145
OKADA, Michio 118
OKADA, Seiki 116
OKADA, Tomoaki 165
OKAMOTO, Hiromi 47–48, 237
OKAMOTO, Hiroshi 145–146
OKAMOTO, Kaoru 57
OKAMOTO, Ken 225
OKAMOTO, Yuko 21, 233
OKAMURA, Hidekazu 210
OKANE, Tetsuo 145
OKANO, Akihiko 117
OKANO, Yoshinori 97
OKAZAKI, Renji 17, 157–158
OKAZAKI, Susumu 211, 235
OKUBO, Shingo 58–59
OKUBO, Suzumu 105
OKUDA, Taichi 210
OKUDAIRA K., Koji 194–195, 245
OKUMURA, Ko 30
OKUNISHI, Eiji 63
OKUNO, Mitsuru 209–210
OMI, Takuichiro 73
ONDA, Ken 55
ONITSUKA, Kiyotaka 162
ONO, Katsuhiko 183
ONO, Masaki 138–139
ONO, Shingo 78, 165–166, 243
ONO, Takashi 145
ONUCHIC, Jose' Nelson 31
OOI, Kenta 132
OOYAMA, Dai 152–153
OSHITA, Masayuki 149
OTO, Masanori 163
OTSUKA, Takeo 95, 99
OTSUKA, Yuichi 239
OUAHAB, Laurence 87
OUYANG, Jianyon 87
OZAKI, Shin-ichi 215
OZAWA, Hiroaki 102
OZAWA, Kiyoshi 52
OZAWA, Norio 114
OZAWA, Ryosuke 112
OZAWA, Tomohiro 107, 109–110
- P**
- PAVEL, Nicolaie 171–172, 174–175, 243
PECILE, C. 89
PENG, Lianmao 19
PHILLIPS, George N. Jr. 215
PICHL, Lukas 27
PROKOP, Petra 79
- R**
- RANGARAJAN, Srinivasan 144
RE, Suyong 18–19
RIKIISHI, Yoshie 197
ROACH, Mark P. 217
ROBINSON, Timothy W. 74

- RUBTSOV, Grigorii I. 221
 RUBTSOV, Igor V. 221
- S**
- SADAHIRO, Tomoyuki 157
 SAEKI, Morihisa 72–73, 190
 SAGAMI, Ikuko 225
 SAIKAWA, Jiro 243
 SAITO, Katsuhiko 183
 SAITO, Susumu 33
 SAITOH, Tomohiko 210
 SAKAE, Yoshitake 233
 SAKAGUCHI, Koichi 114
 SAKAI, Fumio 165–166
 SAKAI, Makoto 72–74
 SAKAI, Masahiro 155, 166, 198
 SAKAI, Osamu 209
 SAKAMOTO, Youichi 177, 244
 SAKATA, Makoto 197
 SAKATA, Masayo 144
 SAKOTA, Kenji 68–69
 SAKURAI, Hidehiro 244
 SAKURAI, Hiromu 110
 SARUKURA, Nobuhiko 78, 163–166, 243
 SASADA, Hiroyuki 54
 SASAKAWA, Hiroaki 166
 SASAKI, Takayo 157, 160
 SASAKURA, Yukie 225
 SASAMORI, Takahiro 17, 156, 158, 160
 SATO, Akira 225
 SATO, Hirofumi 36, 239
 SATO, Hiroki 163–164
 SATO, Katsuko 228
 SATO, Masahiro 235
 SATO, Yoichi 168–169, 243
 SAWAGUCHI, Takahiro 143
 SCHATZ, George C. 200
 SCHOFIELD, Daniel P. 74
 SEKI, Kazuhiko 195
 SEKIGUCHI, Akira 18
 SEKINE, Ichiro 166
 SEKIYA, Hiroshi 63, 66–69
 SETOYAMA, Hiroyuki 194
 SHIBATA, Kana 197–198
 SHIDO, Takahumi 55
 SHIGA, Masayuki 210
 SHIGEMASA, Eiji 123–124, 206–209, 238
 SHIMAGUCHI, Takemi 192
 SHIMAKAWA, Y. 210
 SHIMAMURA, Kiyoshi 163–164, 166
 SHIMIZU, Toru 225
 SHIMIZU, Yuichiro 117, 234
 SHINOHARA, Akihiro 157, 160
 SHINOHARA, Hisanori 58
 SHIOZAKI, Hiroyoshi 108
 SHIRAHATA, Takashi 92
 SHIRAIISHI, Hiroyuki 166
 SHIRASAWA, Nobuhiko 177
 SHIREN, Kazushi 152, 227
- SHOJI, Ichiro 168–169, 171, 243
 SIMON, Marc 208–209
 SIMONYAN, Mkhital 87
 SOBHAN, Sen 128
 SUDESH, Vikas 163
 SUEMATSU, Hiroyoshi 197
 SUENOBU, Tomoyoshi 217
 SUGAWARA, Yasuhiro 192
 SUGIMOTO, Hideki 151–152
 SUGIMOTO, Kunihisa 147
 SUGITA, Yuji 21, 233
 SUGIURA, Ken-ichi 145, 147
 SUGIYAMA, Shunpei 225
 SUWINSKA, Kinga 200
 SUZUI, Mitsukazu 204
 SUZUKI, Hideo 79
 SUZUKI, Kazuharu 184
 SUZUKI, Kazunari 74
 SUZUKI, Kazuya 126
 SUZUKI, Kenji 86, 88
 SUZUKI, Kentaro 106
 SUZUKI, Masatatsu 216, 227
 SUZUKI, Naomi 109
 SUZUKI, Norihiro 56
 SUZUKI, Tadashi 73
 SUZUKI, Toshinori 75–77, 233
 SUZUKI, Toshiyasu 177, 244
 SUZUKI, Wakako 97
 SUZUKI, Yoko 29–30
 SUZUKI, Yuji 78, 163–166
 SWIETLIK, Roman 87–88
- T**
- TABE, Michiharu 132
 TACHI, Yoshimitsu 226
 TADA, Hirokazu 179–181, 204, 244
 TAGAWA, Sei-ichi 221
 TAHARA, Tahei 111, 127–129
 TAIRA, Takunori 168–169, 171–172, 174–175, 243
 TAJIMA, Naoya 100
 TAKABATAKE, Toshiro 210
 TAKABAYASHI, Yasuhiro 197–198
 TAKADA, Masaki 179–180, 244
 TAKAGI, Nozomi 17–18, 160
 TAKAHASHI, Hiroaki 112
 TAKAHASHI, Kazuko 92
 TAKAHASHI, Kazutoshi 206, 246
 TAKAHASHI, Kenshi 208
 TAKAHASHI, Shigetoshi 162
 TAKAHASHI, Toshihiro 88–89, 91
 TAKAMI, Toshiya 213–214
 TAKASHIMA, Yoshifumi 196, 205–206, 246
 TAKASU, Masako 119–120, 234
 TAKATA, Masaki 197
 TAKAYAMA, Yuki 52
 TAKAYANAGI, Toshiyuki 35
 TAKEDA, Akira 141
 TAKEDA, Nobuhiro 17, 156–160
- TAKEI, Fumie 162
 TAKENOBU, Taishi 197
 TAKEUCHI, Satoshi 111, 127
 TAKI, Chiyoie 107
 TAKI, Masayasu 226
 TAMIYAKI, Hitoshi 202
 TAMURA, Atsuo 166
 TAMURA, Itaru 95
 TAMURA, Masafumi 100
 TANABE, Kinuka 55
 TANAKA, Hiroyuki 213
 TANAKA, Hisaaki 145–146
 TANAKA, Hisashi 94, 96, –98, 241
 TANAKA, Junji 235
 TANAKA, Kazuyoshi 60, 87–88, 92
 TANAKA, Keiichi 212
 TANAKA, Kiyoshi 24–25, 212
 TANAKA, Ko-ichiro 206
 TANAKA, Koji 90, 151–153, 186, 242
 TANAKA, Senku 206
 TANAKA, Shoji 182
 TANAKA, Takashi 205, 246
 TANAKA, Takehiko 212
 TANAKA, Yasutaka 148
 TANG, Jun 141
 TANIGUCHI, Isao 143–144
 TANIGUCHI, Masateru 92
 TANIMOTO, Yoshifumi 199
 TANIMURA, Yoshitaka 29–31
 TATSUMI, Kazuyuki 154
 TAYAGAKI, Takeshi 206
 TAYLOR, Nicholas J. 148
 TEN-NO, Seiichiro 31
 TERAMAE, Shinichi 226
 TERANISHI, Yoshiaki 25–26
 TOITA, Takashi 115
 TOKITO, Shizuo 177
 TOKITOH, Norihiro 17, 156–160
 TOKORO, Hiroko 57
 TOKUE, Ikuo 213
 TOKUMOTO, Madoka 95
 Tomimoto, Yusuke 52
 TOMINAGA, Keisuke 166
 TOMITA, Takeshi 225
 TOMON, Takashi 152
 TOMURA, Masaaki 182–184
 TOMÁNEK, David 33
 TORII, Akira 141
 TOYAMA, Namiki 59
 TSAPIN, Alexandre S. 52
 TSUBOUCHI, Masaaki 75, 77, 234
 TSUGE, Kiyoshi 151–152
 TSUJI, Hayato 141
 TSUKUDA, Tatsuya 187–190, 244
 TSUNEDA, Takao 34
 TSUZUKI, Toshimitsu 177
- U**
- UCHIDA, Takeshi 221

- UCHIHASHI, Takayuki 192
 UCHIUMI, Hideki 183
 UCHIYAMA, Ryoma 34
 UECHI, Ichiro 199
 UEDA, Akihiro 144
 UEDA, Tadashi 72
 UEHARA, Akira 216, 227
 UEMURA, Shinobu 144
 UEMURA, Sotaro 219
 UENO, Nobuo 194–195
 UENO, Takafumi 215, 246
 UMEMOTO, Koichiro 33
 UOZUMI, Kounosuke 227
 UOZUMI, Yasuhiro 141–142, 242
 URABE, Kazuo 200
 URISU, Tsuneo 131–134, 198, 242
 URUICHI, Mikio 92, 184
- V**
- VENKATESH, Balan 226
- W**
- WADA, Akihideo 55
 WADA, Akira 108, 110, 216–227
 WADA, Hirofumi 210
 WADA, Tatsuo 147
 WADA, Tohru 151–152
 WAKAHARA, Takatsugu 19
 WANG, Changshun 131, 134
 WANG, Zheming 96–97
 WANG, Zhihong 131–132
 WATANABE, Ayumi 239
 WATANABE, Go 200–201
 WATANABE, Hidekazu 73, 132
 WATANABE, Kazuo 66
 WATANABE, Masashi 148
 WATANABE, Satoru 132
 WATANABE, Tokuko 200
 WATANABE, Toshihiro 142
 WATANABE, Yoshihito 108, 215–218, 227, 246
 WEBBER, N. M. 128
 WEN, Xiao-Gang 45
 WHITAKER, Benjamin J. 75
 WOJCIECHOWSKI, Roman 85–86, 88
 WU, Hai-Ming 192
- Y**
- YABUMOTO, Norikuni 132
 YAKUSHI, Kyuya 85–90, 92, 184, 240
 YAMADA, Jun-ichi 114–115
 YAMADA, Mami 143
 YAMADA, Ryo 180, 204
 YAMAGUCHI, Aritomo 55
 YAMAGUCHI, Toshio 39
 YAMAGUCHI, Tsuyoshi 38
 YAMAHARA, Ryo 217
 YAMAMOTO, Kaoru 85–90
 YAMAMOTO, Kohji 166
 YAMAMOTO, Yohsuke 18, 199
 YAMAMURA, Shusaku 131–132
 YAMANAKA, Takaya 72
 YAMANE, Hiroyuki 195
 YAMASAKI, Katsuyoshi 213
 YAMASE, Toshihiro 78–79
 YAMASHITA, Masahiro 145–147
 YAMASHITA, Yoshiro 179, 182–184, 244
 YAMAUCHI, Shouichi 132
 YAMAURA, Jun-ichi 87, 100
 YAMAZAKI, Jun-ichiro 205–206, 246
 YAMAZAKI, Takeshi 239
 YANAI, Takeshi 34
 YANASE, Manabu 246
 YANG, Hui-jun 215
 YANG, Lan 78
 YASUDA, Ryohei 219
 YASUKAWA, Fumiko 52
 YIN, Donghong 192
 YODA, Takao 21, 233
 YOKOYAMA, Hiroshi 73
 YOKOYAMA, Kohei 145
 YOKOYAMA, Takashi 182
 YOKOYAMA, Toshihiko 56–57, 63–64, 240
 YONEDA, Atsuro 107
 YONEMITSU, Kenji 41–44, 239
 YORIMITSU, Shuhei 149
 YOSHIDA, Hisashi 122, 204
 YOSHIDA, Keigo 73–74
 YOSHIDA, Koji 39
 YOSHIDA, Kunio 168
 YOSHIDA, Masasuke 219
 YOSHIDA, Tadashi 224
 YOSHIHARA, Keitaro 221
 YOSHIKAWA, Hirofumi 200–201
 YOSHIMURA, Daisuke 195
 YOSHINO, Harukazu 114
 YOSHIOKA, Hirokazu 179
- Z**
- ZAMAN, Md. Badruz 182
 ZHANG, Bin 94, 96–97, 241
 ZHANG, Tieqiao 221
 ZHANG, Xinwei 19
 ZHAO, Xiangeng 19
 ZHOU, Yunsong 19
 ZHU, Chaoyuan 23–24, 233
 ZHU, Daoben 96–97
 ZHU, Lei 190